BINDING SERVICES
Tel +44 (0)29 2087 4949
Fax.+44 (0)29 2037 1921
E-Mail Bindery@Cardiff.ac.uk

The tectonomagmatic evolution of the Caribbean plate: insights from igneous rocks on Jamaica

Alan Robert Hastie

Submitted in partial fulfilment of the requirements for the degree of Ph.D.

Cardiff University

July 2007

ProQuest LLC
789 East Eisenhower Parkway
P.O. Box 1346
Ann Arbor, MI 48106-1346

Abstract

The identification of post-Jurassic arc and plateau rocks in Jamaica has helped constrain the tectonic evolution of the Caribbean plate by identifying when, where and how the different volcanic rocks formed. This research therefore not only evaluates the existing models of Caribbean plate evolution, it also presents for the first time, a detailed geochemical and geochronolgical analysis of the igneous rocks on Jamaica.

This study has focussed on the igneous rocks of the Blue Mountains, Central, Above Rocks and Benbow Cretaceous Inliers and the Tertiary Wagwater belt. Major and trace element data, Sr, Nd, Pb and Hf isotope analysis and argon radiometric ages have confirmed the presence of a Cretaceous oceanic plateau section within the Blue Mountains inlier and a number of primitive and evolved Cretaceous island arc sequences in the remaining inliers. Rare high-Nb basalts (HNB) and adakites have also been discovered in the Tertiary Wagwater belt.

Many elements have been mobilised because of intense tropical weathering, and so the tectonic setting and petrogenesis of most of the analysed samples were interpreted using immobile trace elements which has led to the development of the Co-Th, Th/Zr-La/Yb, Ce/Lu-Sm/Yb, La/Hf-Sm/Y and Th/Hf-Sm/Yb discrimination diagrams. These diagrams have been used to classify the Jamaican volcanic arc rocks and thus identify their extent of fractionation and incompatible trace element enrichment.

Immobile trace element and isotope geochemistry has identified at least 5 mantle wedge components and 8 slab components in the Jamaican island arc rocks. Additionally, the Bath-Dunrobin plateau lavas, the adakites and the HNBs represent at least three other chemically distinct source regions. The Bath-Dunrobin plateau lavas are derived from a ~ 90 Ma heterogeneous mantle plume source region which is distinct from the source regions for other Caribbean oceanic plateau lavas as it contains a larger HIMU component giving it more radiogenic Pb isotope ratios.

The adakites have been derived from the combination of complex post-eruptive alteration, partial melting, fractional crystallisation and hybridisation processes. Rather than being related to a melt from a subducting slab, the Jamaican adakites appear to be derived from a melt of lower crustal garnet amphibolite with inter-bedded sedimentary material. The HNBs are derived from a HIMU-type source, which contained garnet and amphibole and so is distinct from the source region of the oceanic plateau.

Using the new geochemical and geochronological data, together with the stratigraphic information and temporal location of the Jamaican igneous rocks, it is possible to place Jamaica in the Pacific model of Caribbean plate evolution. From 120-75 Ma Jamaica formed the northernmost part of the Great Arc of the Antilles and erupted bimodal tholeiitic and calcalkaline magmas, which eventually evolved into calcalkaline and shoshonitic lavas after the collision of the Caribbean oceanic plateau ~90 Ma. From ~55 Ma Jamaica collided with the Yucatan peninsula and was subsequently tectonically transported to the east by transtensional opening of the Cayman Trough. This extension enabled decompression melting of the underlying asthenosphere to form the HNBs and adakites.

Acknowledgements

I would firstly like to give huge thanks to Andrew Kerr for not only devising this project but for also being available when I needed him for geochemical advice on rocks from any tectonic environment and persistent discussions on the evolution of the Caribbean plate. Additional appreciation must also go to Julian Pearce for his in-depth knowledge and help with constructing the immobile element diagrams and his sound advice with regards to island arc volcanics. Thanks to Ian McDonald for allowing me to run so many samples on the ICP-MS and OES when my samples kept on failing. I am also grateful to Ian Miller and Dan Barfod who are responsible for me obtaining all of my Sr-Pb-Nd-Hf radiogenic data and my $^{39}Ar/^{40}Ar$ data.

I'd like to thank everyone on the sunny island of Jamaica who helped me in the field and in the night clubs of Kingston; these include Simon Mitchell, Trevor Jackson, Arnott Jones, Ryan Ramsook, Vencott Adams and Toto. I am especially grateful to Arnott, Simon and Ryan for all their help in the field and in finding me a place to rest my head at night.

Many, many thanks to all the PhD students at Cardiff University (past and present) for being there when a beer was needed. I would like to especially thank, Bryan Hatton, David Holwell, Kevin Jones, Rich Lilly and Martin Wolstencroft for the persistently excellent banter which has kept us all sane over the years. Thanks also to Cat Baudon, Rhodri Davis, Helena Evans, Paivi Heinio, Sarah Dare, Cathal Linnane, Elizabeth Molyneux and Julia Sas for their friendship. Many more thanks to my Mum and Dad who supported me (morally and financially) throughout my academic career and will hopefully continue to do so!

My last thanks go to Ruth Liley, my wonderful partner, and my best friend who, for some reason, has chosen to stay with me through good and bad.

For

Gwyneth Bedford

Supplementary material

This study deals with the complex geochemistry of several island arc, OIB and oceanic plateau successions. There are a large number of rock units which are compared to one another, as such, there are a number of instances where sections in one chapter will utilise the figures of a previous chapter. Consequently, to aid the reader, loose copies of a number of important diagrams are enclosed in the envelope overleaf. Additionally a glossary is inserted to aid the reader with understanding the large number of abbreviations and Jamaican rock types.

Glossary

Geological abbreviations

IAT – Island Arc Tholeiite

CA – Calc-alkaline

HK – High K calc-alkaline

SHC – Shoshonite

ICT – IAT to CA transitional composition

N-MORB – Normal Mid-Ocean Ridge Basalt

ME-MORB – More enriched Mid-Ocean Ridge Basalt

E-MORB – Enriched Mid-Ocean Ridge Basalt

DMM – Depleted MORB Mantle

EM – Enriched Mantle

OIB – Ocean Island Basalt

NHRL – Northern Hemisphere Reference Line

LILE – Large Ion Lithophile Elements

LREE – Light Rare Earth Elements

MREE – Middle Rare Earth Elements

HREE – Heavy Rare Earth Elements

REE - Rare Earth Elements

HFSE – High Field Strength Elements

Jamaican rock units

	Location	Age	Rock type	Rock series
Bath-Dunrobin Formation	Blue Mountain Inlier	Turonian-Coniacian (~ 90 Ma)	Basaltic oceanic plateau lavas	tholeiitic
Lower Devils Racecourse Formation	Benbow Inlier	Upper Hauterivian to lower Barremian (~132-128Ma)	Acidic island arc lavas	IAT
Upper Devils Racecourse Formation	Benbow Inlier	Upper Barremian to upper Aptian (~125-115Ma)	Basic and intermediate island arc lavas	CA
Mt Charles Formation	Above Rocks Inlier	Lower Maastrichtian (70.5 Ma)	Intermediate and acidic island arc lavas	CA
Border Formation	Above Rocks Inlier	Lower Maastrichtian (70.5 Ma)	Basic and intermediate island arc lavas	CA and SHC
Sunning Hill lavas	Sunning Hill Inlier	Lower Maastrichtian (70.5 Ma)	Intermediate and acidic island arc lavas	SHC
Bath-Dunrobin tuffs	Blue Mountain Inlier	Turonian-Coniacian (~ 90 Ma)	Acidic tuff layers	CA
IAT group	Central Inlier	?	Basic island arc lava	IAT
ICT group	Central Inlier	?	Intermediate island arc lava	ICT
CA group 1 (CA1)	Central Inlier	Campanian (79.5 Ma)	Basic to acidic island arc lavas	CA
CA group 2 (CA2)	Central Inlier	?	Basic to acidic island arc lavas	CA
SHC group	Central Inlier	Lower Eocene (55.3 Ma)	Intermediate island arc lavas and ignimbrites	SHC
Newcastle Volcanics	Wagwater Basin	Lower Eocene (51.65 Ma)	Adakites	CA/SHC
Halberstadt Volcanics	Wagwater Basin	Lower Eocene (51.65 Ma)	High-Nb basalts	Alkali basalts

List of Contents

Appendix E – Major and trace element data for the Cretaceous and Tertiary Jamaican igneous rocks and their variation diagrams

Appendix F - References for data sources used in the discrimination diagrams in Chapters 6 and 7.

Chapter 1

Introduction

1.1 Rationale of the Project

The complex question of Caribbean plate tectonic evolution requires a multidisciplinary approach involving volcanology, igneous petrology, structural geology and palaeontology. Plate tectonic models of Caribbean plate evolution are widely debated, and this study on the Cretaceous-Tertiary igneous rocks of Jamaica aims to help clarify the existing models.

There have been few geochemical and geochronological studies on the igneous rocks on Jamaica. Some of the volcanic rocks have been identified petrographically, but their mode of formation and petrogenesis are still unclear i.e. did they originate in a subduction-related setting, a mid-ocean ridge or an oceanic plateau? The temporal and spatial identification of arc and plateau rocks in Jamaica will be valuable in determining plate evolution by identifying when, where and how the different volcanic rocks formed.

This study will therefore not only evaluate the existing models of Caribbean plate evolution, it will also present, for the first time, a detailed geochemical and geochronolgical analysis of the igneous rocks on Jamaica.

1.2 Aims of the Project

1.2.1 The controversial aspects with the Caribbean evolutionary model

The Pacific model for Caribbean plate evolution is at present the favoured hypothesis (Chapter 2). It is thought that the Caribbean plate is made up of an

oceanic plateau that originated in the Pacific. A heterogeneous plume composed of both relatively depleted and enriched material was responsible for forming the plateau (e.g. Sinton *et al.*, 1998; Hauff *et al.*, 2000a; Kerr *et al.*, 2002b). However, it is still debated whether or not the Caribbean oceanic plateau originated from the Galapagos hotspot. Many authors regard the Galapagos hotspot to be the prime candidate for the eruption of the plateau (e.g. Révillon *et al.*, 1999; White *et al.*, 1999; Hoernle *et al.*, 2004; Kerr and Tarney, 2005); conversely, Pindell and Kennan (2001) propose that the plateau was not far enough west relative to North America to be formed by the Galapagos hotspot.

The timing of a subduction polarity reversal, which occurred when the Caribbean oceanic plateau was emplaced between North and South America, is still controversial. Some authors suggest that it occurred in the Aptian/Albian (e.g. Pindell and Barrett, 1990; Lebron and Perfit, 1993; Draper *et al.*, 1996; Pindell and Kennan, 2001), while others support a Campanian reversal (e.g. Duncan and Hargraves, 1984; Burke, 1988; Kerr *et al.*, 1999; White *et al.*, 1999; Kerr and Tarney, 2005). A 124.5 – 97 Ma unconformity in Hispaniola, Puerto Rico and possibly Cuba has been suggested as proof of an Aptian/Albian reversal (Kerr *et al.*, 2003). However, it is doubtful that this localised event can be interpreted as a Caribbean wide subduction polarity reversal.

A Campanian reversal is now becoming favoured by many workers in the Caribbean (e.g. White *et al.*, 1999; Kerr and Tarney, 2005). This is because the Cretaceous Caribbean oceanic plateau and Jurassic mid-ocean ridge basalt (MORB) continued to accrete on to the Great Arc of the Antilles until ~ 80 Ma from the southwest thus indicating that northeasterly subduction had to have occurred until this time (Montgomery *et al.*, 1994; Hauff *et al.*, 2000a; Kerr *et al*, 2003). Also, the plateau is mostly ~ 90 Ma, therefore, assuming that the plateau is responsible for the subduction polarity reversal, it could not have occurred in the Aptian/Albian because in this case the reversal would pre-date the eruption of the plateau (Sinton *et al.*, 1998; Kerr *et al.*, 1999; Kerr *et al.*, 2003).

An island arc tholeiite (IAT) to calcalkaline (CA) transition within the extensive volcanic island arc sequences around the Caribbean margin is also controversial. It is debated whether the transition occurred due to subduction polarity reversal or simply due to a changing source composition over time without the need

for a polarity reversal (Kerr *et al.*, 2003). The latter theory is becoming increasingly favoured (e.g. Thompson, 2002).

Consequently, the evolution of the Caribbean plate is an extremely complex problem that still requires extensive study. More detailed geochemical, geochronological, structural and palaeontological studies have to be carried out to support, refine or discount models of Caribbean plate evolution (Chapter 2).

1.2.2 The aims of this study

Jamaica is a relatively large island in the Caribbean region which contains numerous Cretaceous inliers and Tertiary grabens with a wide variety of poorly understood igneous rocks (Chapter 3). These large sections of unstudied igneous rocks may hold important information on the evolution of Jamaica and on the Caribbean region. The primary aims of this study are therefore to:

1. Construct a detailed geochemical and temporal study of post Jurassic igneous rocks on Jamaica.
2. Determine if the Galapagos hotspot is a viable source for the Caribbean oceanic plateau.
3. Further constrain the timing of the subduction polarity reversal.
4. Determine the timing and cause of the IAT to CA change in the island arc chemistry. Was it due to a subduction polarity reversal or due to a changing source composition over time?

As such, a geochemical and geochronological study of the Jamaican igneous rocks will enable existing models of Caribbean plate evolution to be supported and/or refined.

In addition, recent studies within the Caribbean (e.g. Thompson *et al.*, 2004) have highlighted the intense alteration of volcanic rocks due to tropical weathering and hydrothermal alteration. Geochemical interpretation of volcanic rocks from the Caribbean region is thus complicated since many geochemical discrimination diagrams rely on mobile elements and oxides e.g. the total alkali silica diagram (TAS). Therefore, a further aim of this project is to develop discrimination diagrams that utilise immobile elements to classify altered island arc lavas based on their

degree of fractionation and large ion lithophile element (LILE), light rare earth element (LREE) and actinide enrichment.

Chapter 2

The Caribbean Plate

2.1 Introduction

The aim of this chapter is to present a multidisciplinary overview of the geology of the Caribbean region in order to place the igneous rocks of Jamaica into the tectonic framework of Caribbean plate evolution. The geochemistry and geochronology of the igneous rocks in the Caribbean region will be discussed and used, in conjunction with structural and palaeontological data, to outline the two major models of Caribbean plate evolution.

2.2 The Caribbean Region

The Caribbean is a relatively small plate, with a total area of 6×10^5 km^2 (Fig. 2.1). The plate margins are important in understanding the past and present tectonic evolution of the plate (e.g. Révillon *et al.*, 1999; 2000). To the east and west there are subduction zones with the Cocos plate in the west subducting under the Central American arc to produce recent volcanism (Costa Rica and Panama), and in the east the Atlantic oceanic crust is subducting under the Caribbean plate to form the active Lesser Antilles island arc (Wadge and Burke, 1983; Pindell and Barrett, 1990; Pindell and Kennan, 2001). In addition to the presently active Central American and the Lesser Antilles arcs, there are also the Greater Antilles islands in the north (Cuba, Hispaniola, Puerto Rico, Jamaica and the Virgin islands) and the Dutch Antilles in the south. The Greater Antilles represent extinct early Cretaceous to Early Tertiary island arcs and the Dutch Antilles (Bonaire, Aruba and Curaçao) consist of both

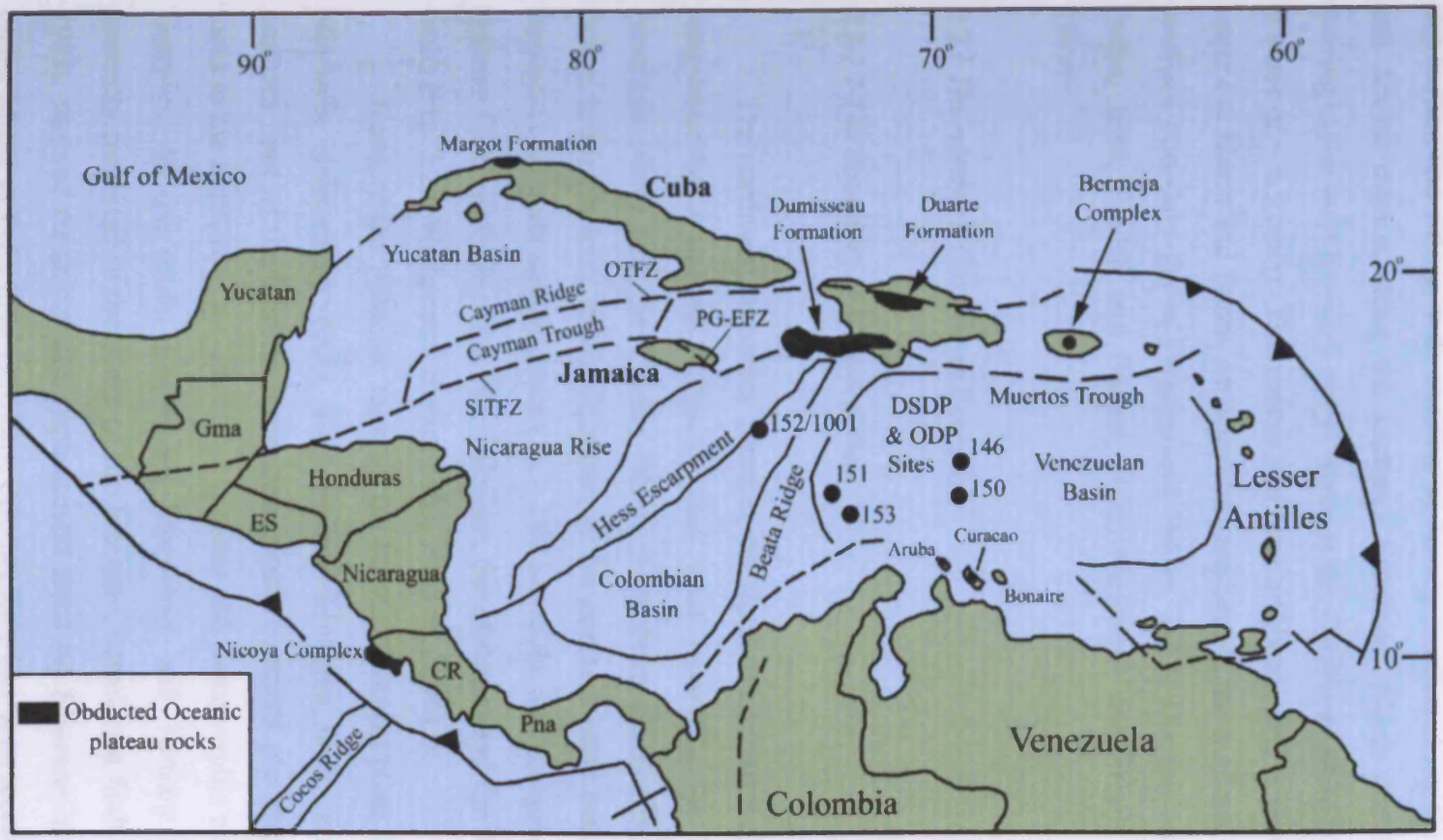

Figure 2.1 – Map of the Caribbean and Central American region. Guatemala (Gma), El Salvador (ES), Costa Rica (CR), Panama (Pna), Swan Islands Transform Fault Zone (SITFZ), Oriente Transform Fault Zone (OTFZ), Plantain Garden-Enriquillo Fault zone (PG-EFZ) (modified from Sinton *et al.*, 1998).

Cretaceous arc and oceanic plateau sequences (Fig. 2.1) (Duncan and Hargraves, 1984; Burke, 1988; Pindell and Barrett, 1990; Kerr *et al.*, 1999; White *et al.*, 1999).

The northern and southern boundaries of the plate are complex areas of strike-slip motion and rifting, with sinistral strike slip motion along the northern boundary and dextral motion along the southern boundary. North and South America are moving to the west by ~ 2-3 cm/yr whereas the Caribbean plate is moving to the west at a rate of ~ 1.9 cm/yr. This means that the Caribbean plate is moving to the east with respect to North and South America thus explaining the motions on the northern and southern boundary zones (Wadge and Burke, 1983; Duncan and Hargraves, 1984; Burke, 1988; Pindell and Barrett, 1990; Meschede and Frisch, 1998; Kerr *et al.*, 1999).

2.2.1 The northern Caribbean boundary

2.2.1.1 The boundary in the northwest

The northwest boundary between the North American and Caribbean plates is represented by a sinistral strike-slip fault zone separating the Maya Block (North American plate) and the Chortis Block (Caribbean plate) (Fig. 2.2) (Wadge and Burke, 1983; Harlow, 2004). This part of the northern plate boundary can be traced through Guatemala and Honduras, is ~ 100 km wide, and comprises three major fault systems from north to south: the Polochic, the Motagua and the Jocotan-Chamelecon faults (Fig. 2.2) (Wadge and Burke, 1983; Harlow, 2004).

North of the Polochic fault on the North American plate, Late Palaeozoic and Mesozoic sedimentary rocks outcrop. The Motagua fault, which is the present northern limit of the Chortis continental block, contrasts pre-Mesozoic metamorphic rocks to the north with pre-Mesozoic igneous and metamorphic rocks (the Las Ovejas Complex) to the south. Cretaceous limestones and Tertiary volcanic rocks are generally restricted to the south of the Jocotan-Chamelecon fault (Wadge and Burke, 1983). Most of the strike-slip displacement since the Miocene has been concentrated on the Motagua fault, although some displacement has been recorded on the Polochic fault. There is no known Quarternary displacement across the Jocotan-Chamelecon fault (Fig. 2.2) (Wadge and Burke, 1983).

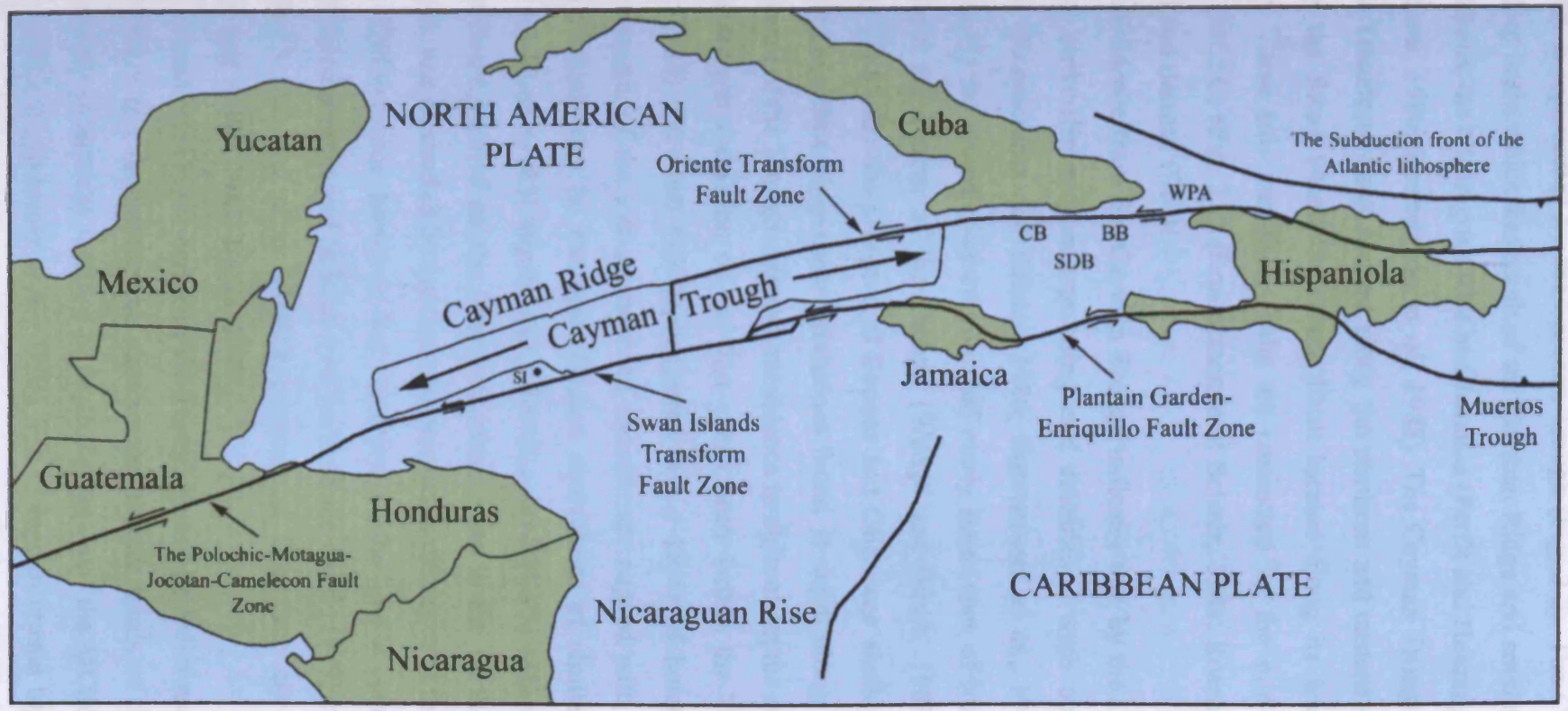

Figure 2.2 – Diagram of the northern Caribbean plate boundary from Guatemala to Hispaniola. Baitiquiri Basin (BB), Chivirico Basin (CB), Santiago Deformed Belt (SDB), Swan Islands (SI), Windward Passage Area (WPA).

To the east of the Central American fault system the northern Caribbean plate boundary is represented by the Cayman Trough (Fig. 2.2). The Cayman Trough is a long, deep basin which lies south of the Cayman Ridge and southern Cuba, and north of Honduras, the Nicaraguan Rise and Jamaica (Perfit and Heezen, 1978; Rosencrantz and Sclater, 1986; Rosencrantz *et al.*, 1988). The Cayman Trough is bounded by the Oriente Transform Fault located along the northern and eastern edge of the Trough and by the Swan Island Transform Fault located along its southern and western margin. These two transform faults are connected by the mid-Cayman spreading centre (MCSC) (Fig. 2.2) (Rosencrantz and Sclater, 1986; Rosencrantz *et al.*, 1988; Pindell and Barrett, 1990).

Evidence from the Cayman Trough indicates that by the Late Oligocene (25-33 Ma) strike-slip motion, spreading and subsidence were occurring within the Trough (Rosencrantz and Sclater, 1986; Rosencrantz *et al.*, 1988). This evidence includes (1) the recovery of micritic and marly limestones of Miocene and younger ages from the bottom of the Trough (Wadge and Burke, 1983; Rosencrantz and Sclater, 1986). (2) the presence of Eocene and Oligocene shallow-water limestones and late Oligocene deep-water limestones found at depth along the north (Cayman Ridge) wall of the Trough suggests subsidence to abyssal depths during the Oligocene and subsequent formation of the first ocean crust within the Trough (Wadge and Burke, 1983). (3) Land (1979) suggested that a series of horst-like blocks at the eastern margin of the Trough north of Jamaica are capped with Eocene age clastic deposits which may be the down-faulted equivalents of similar nearby Jamaican rocks. (4) Mann (1983) argued that Late Oligocene clastic sedimentation within the Tabera Basin, located on the Hispaniola fault zone in the north-central Dominican Republic, was controlled by fault movements along the edges of the basin.

This evidence, however, does not constrain the time of opening of the Cayman Trough (Rosencrantz and Sclater, 1986) for which Land (1979) proposed an Eocene age (38-55 Ma) and other workers propose an Oligocene age of initial opening (Wadge and Burke, 1983; Burke, 1988).

Ocean crust in the centre of the Trough has a high relief and slopes away from the MCSC. Crust underlying the western and eastern thirds of the Trough has less relief and no substantial increase in depth further from the MCSC (Rosencrantz and Sclater, 1986; Rosencrantz *et al.*, 1988).This change in crustal topography coincides with an increase in width of the Cayman Trough from 70-80 km across its outer

sections to 100-110 km across its central section (Rosencrantz and Sclater, 1986; Rosencrantz *et al.*, 1988). This suggests that spreading occurred in two episodes and that the lack of subsidence in the outer crust indicates that the early phase of spreading was faster than the present phase (Rosencrantz and Sclater, 1986; Rosencrantz *et al.*, 1988).

Rosencrantz and Sclater (1986) modelled the opening of the Cayman Trough and proposed that the spreading rate over the past 30 Ma is ~ 15 mm/yr but the faster, earlier stage of rifting would have had a spreading rate of ~ 40 mm/yr. Rosencrantz *et al* (1988) calculated Cayman Trough crustal ages based on subsidence curves, which accommodate lateral as well as vertical cooling of the oceanic lithosphere, and a re-evaluation of the marine magnetic anomaly sequence. They concluded that between 44 Ma and a ridge jump at 31 Ma the Trough opened at a rate of ~ 25-40 mm/yr. The width of the Trough at this period was ~ 80 km. The Swan Island Transform Fault lay to the north of the Swan Islands. At 31 Ma the spreading axis moved westwards by ~ 30 km. Spreading continued at this new axis until ~ 26 Ma when the axis again moved 30 km to the east. At 26 Ma spreading in the Cayman Trough underwent a major change. The rate of opening slows to between 15-16 mm/yr. The spreading axis lengthens to the south and the width of the Trough increases from 80 to 110 km. The Swan Island Transform Fault now lies to the south of the Swan Islands. Slow spreading continues to the present. A ridge jump also occurred at anomaly 3A (5.5 Ma) when the axis moved to the east by ~ 35-40 km (Rosencrantz *et al.*, 1988).

The total length of oceanic crust within the Cayman Trough is ~ 950-1000 km. However, because the opening of the Cayman Trough included an early episode of crustal stretching and rifting, the total extension is greater than the spreading distance and is estimated to be around 1100 km (Fig. 2.2) (Rosencrantz and Sclater, 1986; Pindell and Barrett, 1990).

Northeast-southwest trending rift related block faulting has been recognised at the eastern and western ends of the Trough (Rosencrantz and Sclater, 1986). This is in contrast with the east northeast-west southwest trend of the spreading direction of the Cayman Trough (Rosencrantz and Sclater, 1986). Rifting oblique to the trend of the block faulting is characteristic of pull-apart basins within strike-slip fault systems (Rosencrantz and Sclater, 1986). As such the Cayman Trough is considered to be an extended pull apart basin that records ~ 1100 km of sinistral offset between the North

American and Caribbean plates since the Eocene/Oligocene (Rosencrantz and Sclater, 1986; Burke, 1988; Pindell and Barrett, 1990).

2.2.1.2 The boundary in the northeast

The tectonic setting of the northeastern Caribbean boundary is still not fully understood. From Cuba to Hispaniola the Caribbean and North American plate boundary is represented by the sinistral strike-slip Oriente Transform Fault Zone, which extends from the northern Cayman Trench boundary, to the south of Cuba and then through northern Hispaniola (Fig. 2.2) (Calais and Lepinay, 1991; Calais *et al.*, 1992). However there is no continuity, in the Windward Passage area, between the Oriente fault and the subduction front of the Atlantic oceanic lithosphere beneath Puerto Rico and Hispaniola. Therefore, the nature of the northern Caribbean boundary to the east of Hispaniola is still essentially unknown (Fig. 2.2) (Calais and Lepinay, 1991; Calais *et al.*, 1992).

The plate boundary in the northeast shows active regional transpression and local transtension (Calais and Lepinay, 1991). The Santiago Deformed Belt (SDB), a succession of deformed sediments, shows clear compressional features and the Oriente transform fault displays strike-slip movements. It is therefore logical to relate the structure of the SDB to an active transpressional tectonic regime occurring along the southern Cuban margin (Calais and Lepinay, 1991; Calais *et al.*, 1992). The transpressive structure of the SDB must be related to regional oblique relative motion along the Oriente transform fault. Additionally, while the southern Cuban margin undergoes this regional transpression it is also subject to local transtension as seen in the Chivirico and the Baitiquiri basins (Fig. 2.2). This transtension is restricted to well deliminated basins always located at the tensioned dextral offsets of the Oriente fault (Calais and Lepinay, 1991; Calais *et al.*, 1992).

To the south of the Oriente fault system the Swan Island Transform-Plantain Garden-Enriquillo Fault Zone extends from the southern Cayman Trough boundary, through eastern Jamaica and southern Hispaniola to eventually form the Muertos Trough (Pindell and Barrett, 1990; Calais and Lepinay, 1991; Calais *et al.*, 1992). It has been suggested that the Caribbean plate (Venezuelan basin) is thrusting under the Atlantic lithosphere to create the Muertos Trough, possibly forming a pseudo-

subduction zone (Fig 2.2) (Müller *et al.*, 1999). Conversely, Calais *et al.* (1992) propose, using seismic data, that there is no northward subduction of the Venezuelan basin beneath the Muertos trough.

Calais *et al.* (1992) reported deep (> 50 km) earthquakes beneath eastern Hispaniola and explained them by invoking the existence of a lithospheric slab under the northeastern corner of the Caribbean plate, which was derived from the frontal subduction of the Atlantic oceanic crust beneath the active Lesser Antilles arc. The absence of volcanism in Puerto Rico and Hispaniola related to this subducted slab could be explained by the fact that it has already been dehydrated to produce the magmatism of the northern Lesser Antilles (Calais *et al.*, 1992).

Byrne *et al.* (1985) have suggested that the Muertos Trough is a plate boundary and that based on seismic evidence other plate boundaries can be recognised. This may indicate that the northern Caribbean boundary is composed of a number of different microplates. This idea is supported by Leroy and Mauffret (1996); however, more work has to be carried out on the northeast Caribbean plate boundary in order to determine the relationship of the Muertos Trough and the Oriente fault with the subduction front of the Atlantic lithosphere beneath Puerto Rico, Hispaniola and the Lesser Antilles (Fig. 2.2) (Pindell and Barrett, 1990; Calais and Lepinay, 1991; Calais *et al.*, 1992).

2.2.2 The southern Caribbean boundary

The southern boundary of the plate is also a complex area of deformation within the Caribbean region. The Caribbean/South American plate boundary is one of the most oblique convergent margins in the world (Ave Lallemant, 1997). The boundary is spilt into several east-west trending orogenic belts of which the Cordillera de la Costa is the main belt (Van der Hilst, 1994; Ave Lallemant, 1997; Thompson, 2002). The Cordillera de la Costa is composed of oceanic (serpentinites, eclogites, blueschists and amphibolites) and continental (gneisses, schists, quartzites and marbles) rocks. The oceanic rocks have a high grade of metamorphism (amphibolite grade) and are generally found in the north and were metamorphosed in the late Cretaceous (Ave Lallemant, 1997). The oceanic rocks are also chemically similar to

MORB. The lower grade (greenschist grade) continental rocks occur in the south and were metamorphosed in the Tertiary (Fig. 2.3) (Ave Lallemant, 1997).

The formation of the Cordillera de la Costa Belt and the structural development of the region are crucial in understanding the evolution of the southern Caribbean region. It is thought that the Cordillera de la Costa Belt was formed just after a subduction polarity reversal (Ave Lallemant, 1997). The Proto-Caribbean lithosphere subducted under a Caribbean oceanic plateau to form dextral oblique motion on the northern margin of the Great Arc of the Antilles (Section 2.5) (Ave Lallemant, 1997). Arc parallel dextral shear and extension occurred due to the curvature of the arc and this extension thinned the arc and the accretionary wedge allowing the uplift of deeply buried high-grade metamorphic rocks (Ave Lallemant, 1997). During this process the southern tip of the arc was colliding with the NW margin of South America allowing imbricated continental rocks to enter the subduction zone and "mix" with the oceanic rocks. This accounts for the oceanic and continental origin of the rocks of the Cordillera de la Costa and the presence of the high pressure-low temperature rocks (Burke, 1988; Pindell and Barrett, 1990; Ave Lallemant, 1997; Müller *et al.*, 1999; Pindell and Kennan, 2001).

The Cordillera de la Costa Belt was then transported to the east along the Caribbean/South American plate boundary. When the Cordillera de la Costa Belt was near its present longitudinal position in the Oligocene/Miocene the North and South American continents began to converge (Ave Lallemant, 1997; Müller *et al.*, 1999). This resulted in Caribbean material, along with the Cordillera de la Costa Belt, to overthrust the South American continent in southwest verging thrusts (Fig. 2.3). These numerous Late Cretaceous and pre-Miocene, southwest-verging, thrust faults are seen along with major dextral strike-slip lineaments (Fig. 2.3) (Ave Lallemant, 1997).

These two deformational events resulted in the formation of the Cordillera de la Costa Belt, the exhumation of the high pressure-low temperature rocks and the structural morphology of the northern South American continent (Ave Lallemant, 1997). This suggests that from the late Cretaceous to the Miocene the Caribbean plate was transported to the east, relative to the Americas, and from the Eocene was thrust onto the South American continent. However, since the Miocene the Caribbean plate has been underthrusting the South American plate with the South Caribbean

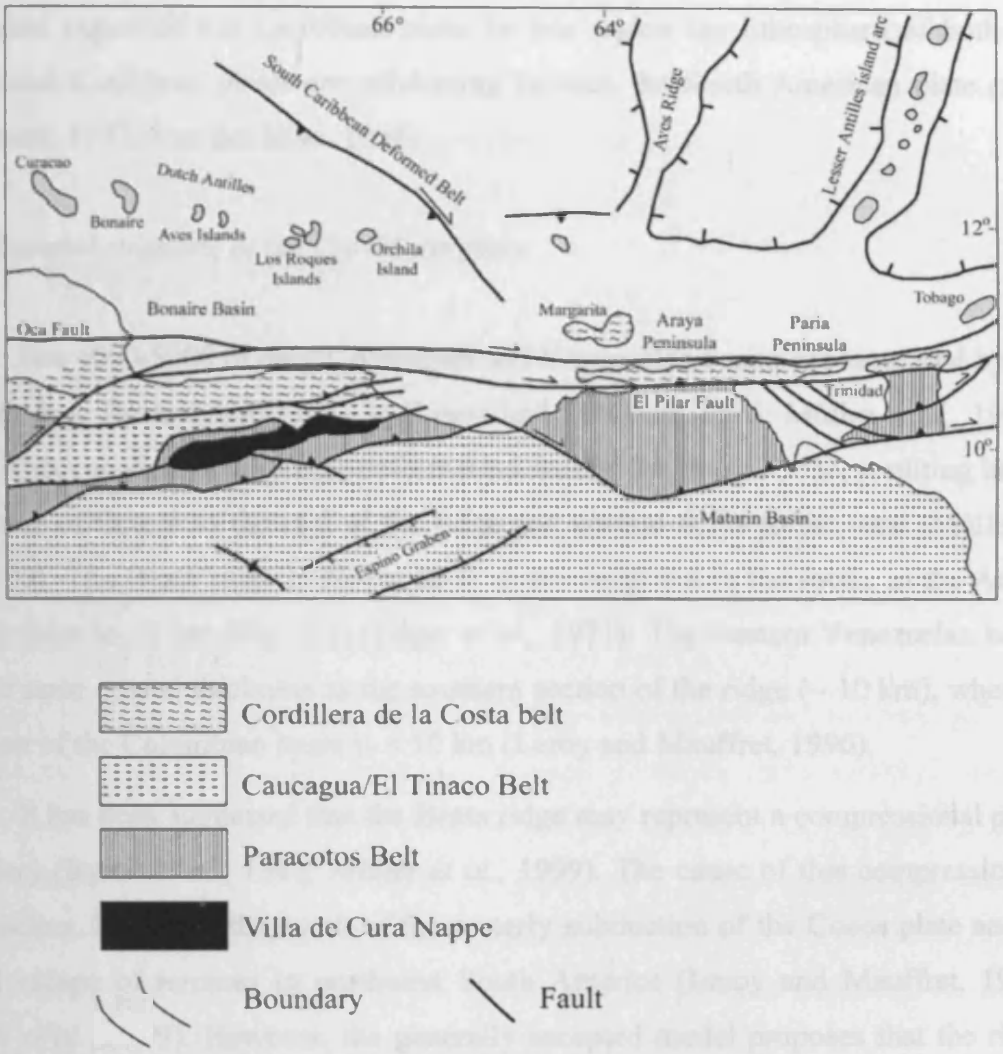

Figure 2.3 – Diagram showing the location of the complexes on the southern Caribbean boundary and its associated structural geology (after Ave Lallemant, 1997).

Deformed Belt representing the new plate boundary (Fig. 2.3) (Van der Hilst, 1994). Further evidence of this can be seen with seismic tomographic studies in the southwest region of the Caribbean plate. In this region the lithosphere of both the Nazca and Caribbean plates are subducting beneath the South American plate (Ave Lallemant, 1997; Van der Hilst, 1994).

2.2.3 Internal structure of the Caribbean plate

The 4000-5000 m deep Colombian and Venezuelan basins are separated by the 2000 m deep Beata ridge (Fig. 2.1) (Leroy and Mauffret, 1996; Müller *et al.*, 1999). In the Miocene there was intense deformation around the Beata Ridge, resulting in the formation of thrusts to the east of the ridge and normal faults to the west (Müller *et al.*, 1999). The Beata ridge is 20 km thick in the north but in the south, in the Aruba Gap, it thins to 10 km (Fig. 2.1) (Edgar *et al.*, 1971). The western Venezuelan basin has the same crustal thickness as the southern section of the ridge (~ 10 km), whereas the crust of the Colombian basin is < 10 km (Leroy and Mauffret, 1996).

It has been suggested that the Beata ridge may represent a compressional plate boundary (Byrne *et al.*, 1985; Müller *et al.*, 1999). The cause of this compression is still unclear. It may be the result of the easterly subduction of the Cocos plate and/or lateral escape of terranes in northwest South America (Leroy and Mauffret, 1996; Müller *et al.*, 1999). However, the generally accepted model proposes that the ridge and its associated deformation were caused by the clockwise rotation of the "Colombian microplate", which then overthrust the "Venezuelan microplate". This suggests that north-south American convergence in the Miocene increased in magnitude to the west thus squeezing the Colombian microplate to the east (Fig. 2.1) (Wadge and Burke, 1983; Leroy and Mauffret, 1996; Müller *et al.*, 1999). This east-west movement is supported by present-day GPS plate motion studies (Müller *et al.*, 1999).

The Nicaraguan Rise has a northeast-southwest trend and lies to the southwest of Jamaica (Fig. 2.1). It has been described by Robinson (1971) as a "submerged belt of crustal thickness" due to its indeterminate affinity. Draper (1986), Pindell and Barrett (1990) and Meschede and Frisch (1998) consider the Nicaraguan Rise to be an extinct island arc section. However they also note that no fore-arc or accretionary

prism material has been found, and therefore the Nicaraguan Rise-Jamaican arc could have been part of the Chortis block in front of southern Mexico. Conversely, Wadge *et al.* (1982) and Dunham (1996) have argued that the Nicaraguan Rise has the same crustal thickness as the Colombian basin and that it could represent oceanic crust. The origin and age of the Nicaraguan Rise thus remains unclear.

2.3 The Caribbean Oceanic Crust

Normal oceanic crust is 6-8 km thick; however, the Caribbean oceanic crust varies in thickness from 8-20 km (Edgar *et al.*, 1971; Leroy and Mauffret, 1996). This thicker oceanic crust has been observed on seismic refraction and reflection surveys and is responsible for the sea floor lying at a depth of ~ 4 km, which is 1 km shallower than expected for Cretaceous oceanic crust of normal thickness (Edgar *et al.*, 1971; Leroy and Mauffret, 1997; Burke, 1988). The Caribbean oceanic crust also lacks any convincing magnetic anomalies (Burke, 1988; Pindell and Kennan, 2001). It is for these reasons, together with geochemical evidence from accreted oceanic plateau sections from around the Caribbean margins and from DSDP/ODP drilling, that the Caribbean plate is considered to represent a submerged oceanic plateau (Donnelly *et al.*, 1990; Sinton *et al.*, 1998; Révillon *et al.*, 1999; White *et al.*, 1999; Pindell and Kennan, 2001; Kerr *et al.*, 2003). Oceanic plateau rocks can be easily distinguished from igneous rocks from other tectonic settings (Table 2.1).

The obducted plateau sequences around the Caribbean (Fig. 2.1) and on the northwestern coast of South America provide igneous petrologists with a unique opportunity to study these originally sub-aqueous geological features (Donnelly *et al.*, 1990; Kerr *et al.*, 1998ab; 2002ab). Additionall y, as noted above, the Caribbean oceanic plateau has been drilled during DSDP leg 15 and ODP Leg 165 (Fig. 2.1) (Sinton *et al.*, 1998).

It is thought that oceanic plateau/MORB rocks in and around the Caribbean-Colombian region are composed of material of at least four, and possibly five, different ages (Sinton *et al.*, 1998; Révillon *et al.*, 2000; Kerr *et al.*, 2003; Hoernle *et al.*, 2002; 2004). The Aptian (124-112 Ma) phase is represented by the obduction of Jurassic MORB onto the Great Arc of the Antilles to form the Duarte (Hispaniola) and Bermeja (Puerto Rico) complexes (Donnelly *et al.*, 1990; Montgomery *et al.*,

1994; Lapierre *et al.*, 1997). Based on evidence from intercalated cherts which contain Jurassic radiolaria Montgomery *et al.* (1994) proposed that the Bermeja and parts of the Duarte Complex are Pacific Jurassic oceanic fragments. It has also been suggested that a small plateau may have obducted at this time because of the discovery of Aptian plateau fragments on Cuba (Kerr *et al.*, 1999). Consequently, a local 97-124.5 Ma unconformity on Cuba, Hispaniola and Puerto Rico could have been produced by the obduction of this Jurassic MORB and/or plateau material. Additionally, it is uncertain as to whether this obduction could have induced a subduction polarity reversal as suggested by Pindell and Barrett, (1990) and Pindell and Kennan, (2001) (Section 2.5).

The second phase (89-93 Ma) makes up the majority of the Caribbean plate, including the obducted sections on the northwestern coast of South America, and represents the Cretaceous Caribbean oceanic plateau (Duncan and Hargraves, 1984; Burke, 1988; Sinton *et al.*, 1998; Révillon *et al.*, 1999; Kerr *et al.*, 2003).

The third phase consists of a period of MORB and plateau magmatism at ~ 80-72 Ma (Kerr *et al.*, 2003) and continued plume magmatism at the Galapagos hotspot over the past 90 Ma (Hoernle *et al.*, 2002; 2004). Plateau magmas have been discovered accreted to the trailing edge of the plateau and the western seaboard of the Americas (Costa Rica and Panama) (Hoernle *et al.*, 2002). These magmas were created by the continuing eruption of the Galapagos hot spot over the past 90 Ma (Donnelly *et al.*, 1990; Spadea and Espinosa, 1996; Sinton *et al.*, 1998; Hoernle, *et al.*, 2002; Kerr *et al.*, 2002; Hoernle, *et al.*, 2004).

The MORB magmatism could have formed by extension during the emplacement of the Caribbean plateau between the American continents. An example of this magmatism has been found on the Hess Rise drilled during DSDP Leg 15 Site 152 (Section 2.4.1) (Sinton *et al.*, 1998). Additionally, recent work on the Beata Ridge has also discovered basalts, dolerites and gabbros with plume like geochemistry e.g. enriched Ni and Cr, flat to enriched REE patterns, εNd ratios from + 5 to + 9.5 and high MgO contents (Révillon *et al.*, 2000). These plateau rocks have been dated by $^{40}Ar/^{39}Ar$ at ~ 76 Ma and are therefore part of the third phase (Révillon *et al.*, 2000).

The last phase of oceanic igneous activity consists of extensional magmas formed at ~ 55 Ma on the Beata ridge. These magmas are not thought to be related to

Tectonic setting	High-MgO lavas (>14%)	$(La/Nb)_{pmn}$	$(REE)_{cn}$ pattern	Pillow lavas	Tephra layers	subaerial eruption
Oceanic plateau	yes	≤1	predominantly flat	yes	very few	occasionally
Mid-ocean ridge	rare	≤1	LREE-depleted	yes	very few	no
Marginal basin	no	≤1	predominantly flat	yes	very common	no
Oceanic island basalt	rare	≤1	predominantly LREE-enriched	yes	very few	frequently
Continent-ocean margin plateau	yes	contain sequences with ≤1 & >>1	Flat to LREE-enriched	yes	occasional	common
Arc (continental & oceanic)	rare	>>1	LREE-enriched	yes	very common	frequently
Continental flood basalt	yes	mostly >>1 < 10% of flows ≤1	Flat to LREE-enriched	no	occasional	always

Table 2.1 – Summarising some of the field and geochemical characteristics used to distinguish igneous rocks from different tectonic environments (after Kerr *et al.*, 2000). Primitive mantle normalised = pmn.

an additional mantle plume due to their localised occurrence (Révillon *et al.*, 2000). They have a similar plume chemistry to the 76 Ma lavas and are thought to have developed by extensional tectonics. Therefore, it is feasible to assume that the 76 Ma plateau rocks on the Beata Ridge came about by similar extensional processes, thus negating the need for two hotspots/plateaus to be involved in the Caribbean oceanic plateau formation (Hoernle *et al.*, 2004; Révillon *et al.*, 2000).

Hoernle *et al.* (2004) also found plateau rocks in the Nicoya Peninsula (Costa Rica) that had an $^{40}Ar/^{39}Ar$ age of ~ 130-140 Ma. It is still uncertain whether these lavas are part of Caribbean plateau or are a separate plateau/seamount that collided with the Chortis block (Section 2.5).

2.4 The Caribbean Oceanic Plateau

2.4.1 The identification of the Caribbean oceanic plateau

The Caribbean plate is principally composed of two large basins; the Venezuelan and Colombian basins, which are separated by several ridges (Section 2.2.3 and Fig. 2.1) (Sinton *et al.*, 1998). The B" reflector horizon is a seismic term used to describe the top of the oceanic plateau (Ewing *et al.*, 1967). The reflector horizon is mostly smooth, apart from parts of the Venezuelan and Colombian basins where it is rough and deeper (similar to normal oceanic crust) (Ludwig *et al.*, 1975; Diebold *et al.*, 1981). The relationship between the smooth and the rough reflectors has been interpreted to be that of normal, older extended oceanic crust (rough B") overlain by younger flows and sills of the Caribbean oceanic plateau (smooth B") (Diebold *et al.*, 1981; Bowland and Rosencrantz, 1988). An exception to this may be the crust between the Beata Ridge and the Hess escarpment that appears to have been produced by extension that post-dates the plateau (Diebold *et al.*, 1981; Meschede and Frisch, 1998; Sinton *et al.*, 1998; Révillon *et al.*, 2000).

Five sites were drilled during DSDP Leg 15, four in smooth B" regions (all in the Venezuelan basin and the Beata Ridge) and one in a rough B" region (DSDP-152) (Figure 2.1) (Donnelly, 1973; Sinton *et al.*, 1998). DSDP Leg 15 geochemical data indicate the presence of oceanic plateau material within the Venezuelan basin and on the Beata Ridge. However, no widespread geochemical study has been carried out in

the Colombian Basin. Samples were drilled on the Hess Escarpment as part of DSDP Leg 15 (Site 152) and ODP Leg 165 (Site 1001), where the rocks are younger (~ 80 Ma) than the plateau lavas and have a MORB-type chemistry (Sinton *et al.*, 1998). Therefore, is it possible that the Caribbean oceanic plateau is only represented by the Venezuelan basin and that the rest of the Caribbean plate (including the Colombian Basin) is composed of MORB-type and arc material (Sinton *et al.*, 1998; Müller *et al.*, 1999).

The oceanic plateau rocks that make up most of the Caribbean plate meet the criteria set out in Table 2.1. The Caribbean plate is 8-20 km thick, much thicker than average oceanic crust (Edgar *et al.*, 1971; Leroy and Mauffret, 1996). The only known Phanerozoic spinifex textured komatiites (high-MgO) are found on Gorgona Island, Colombia where they may represent part of the Caribbean plateau (e.g. Kerr *et al.*, 1996c). Picrites are also found, and are more abundant, with exposures in Colombia, Curaçao, Hispaniola and Venezuela (Kerr *et al.*, 1996abc; 2002; 2003; Arndt *et al.*, 1997).

Most of the rocks are clearly submarine with abundant hyaloclastites and pillow lavas, which lack tephra layers e.g. the ~ 5 km thick section of obducted plateau pillow basalts and picrites on Curaçao (Kerr *et al.*, 1996b). The plateau volcanics also have flat, depleted and enriched rare earth element (REE) patterns and higher Ni and Cr concentrations (Chapters 6 and 7) (e.g. Donnelly *et al.*, 1990; Kerr *et al.*, 2003). Other trace elements and isotopes (e.g. Nb and εNd(i)) can also be used to classify a rock as having an oceanic plateau origin as opposed to a MORB or arc affinity (Table 2.1). All of these elements and isotopes will be utilised in Chapters 6 and 7 of this study to determine the petrogenesis of the arc and plateau rocks on Jamaica.

2.4.2 The origin of oceanic plateaux

It is thought that oceanic plateaux such as the Ontong Java and the Caribbean oceanic plateaux are formed by decompression melting of ascending hot mantle plumes (e.g. Arndt, 2002; Kerr *et al.*, 2003). A plume is composed of a hot axial tail capped by a relatively larger, cooler head, which inevitably entrains surrounding material as in ascends through the mantle (Campbell *et al.*, 1989; Richards *et al.*,

1989; Campbell and Griffiths, 1990; Arndt, 2002). Mantle plumes are thought to be 200-300°C hotter than normal ambient mantle according to petrological and seismic modelling (e.g. Campbell *et al.*, 1989; Campbell and Griffiths, 1990; Herzberg and O'Hara, 2002). These temperatures are necessary to produce enough melt to form the thickened oceanic crust of oceanic plateaux and to give MgO rich melts that are common in large igneous provinces (e.g. Campbell *et al.*, 1989; Campbell and Griffiths, 1990; Herzberg and O'Hara, 2002; Campbell, 2007).

Plumes originate at thermal boundary layers, such as the core-mantle boundary or the 670 km discontinuity, and buoyantly rise until they meet the lithosphere (e.g. Campbell and Griffiths, 1990; Courtillot *et al.*, 2003). As a mantle plume collides with the base of the lithosphere decompression melting will rapidly produce large amounts of melt that will eventually form an oceanic plateau or continental flood basalt (Campbell *et al.*, 1989; Campbell and Griffiths, 1990; Campbell, 2007). The volumes of magma produced as a result of this decompression melting can be vast. For example, the Ontong Java oceanic plateau has an estimated melt volume of 44-50×10^6 km^3 (Saunders *et al.*, 1996; Eldholm and Coffin, 2000) whereas the estimated original melt volume of the Caribbean oceanic plateau is ~ 4×10^6 km^3 (Kerr, 1998a).

2.4.3 The age of the Caribbean oceanic plateau material

Of the four phases of volcanism that formed the Caribbean plate the most volumous phase consists of the ~ 89-93 Ma Caribbean oceanic plateau (Alvarado *et al.*, 1997; Sinton *et al.*, 1998; White *et al.*, 1999; Kerr *et al.*, 2003). The age of the plateau has been determined with both relative and absolute dating methods. Most of the modern reliable dates come from $^{40}Ar/^{39}Ar$ studies; however other isotopic dating methods e.g. Re-Os and palaeontological evidence have also been used to constrain the age of the plateau (Table 2.2) (Kerr *et al.*, 2003).

Location	Age (Ma)	Dating method	Reference(s)
DSDP Leg 15 Site 146	90.6-92.1	$^{40}Ar/^{39}Ar$ plateau age	Sinton *et al.*, 1998
DSDP Leg 15 Site 150	94.3	$^{40}Ar/^{39}Ar$ plateau age	Sinton *et al.*, 1998
Beata Ridge	76	$^{40}Ar/^{39}Ar$ plateau age	Révillon *et al.*, 2000
ODP Leg 165 Site 1001	80.8-81.3	$^{40}Ar/^{39}Ar$ plateau age	Sinton *et al.*, 2000
Curaçao Lava Formation	88-89.5	$^{40}Ar/^{39}Ar$ plateau age	Sinton *et al.*, 1998
Curaçao Lava Formation	85.6 ± 8.1	Re-Os	Walker *et al.*, 1999
Aruba Lava Formation	90.5-88.5	Ammonites	Beets *et al.*, 1984
Dumisseau Formation	88.7-92	$^{40}Ar/^{39}Ar$ plateau age	Sinton *et al.*, 1998
Duarte Complex	86.1 and 86.7	$^{40}Ar/^{39}Ar$ plateau age	Lapierre *et al.*, 1999
Bath-Dunrobin Formation	87.5-91	Radiolarian chert	Montgomery and Pessagno, 1999
Nicoya Complex	94.7-87.5	$^{40}Ar/^{39}Ar$ plateau age	Sinton *et al.*, 1997
Nicoya Complex	83	$^{40}Ar/^{39}Ar$ isochron age	Hauff *et al.*, 2000
Nicoya Complex	~ 130	$^{40}Ar/^{39}Ar$ plateau age	Hoernle *et al.*, 2002
Tortugal Complex	89.7	$^{40}Ar/^{39}Ar$ plateau age	Alvarado *et al.*, 1997
Quepos Complex	59	$^{40}Ar/^{39}Ar$ isochron age	Hauff *et al.*, 2000
Quepos Complex	63.9	$^{40}Ar/^{39}Ar$ plateau age	Sinton *et al.*, 1997
Osa Complex	62.1	$^{40}Ar/^{39}Ar$ isochron age	Hauff *et al.*, 2000
Central Cordillera, Colombia	82.6 and 84.7	$^{40}Ar/^{39}Ar$ plateau age	Kerr *et al.*, 2002
Western Cordillera, Colombia	91.7	$^{40}Ar/^{39}Ar$ plateau age	Kerr *et al.*, 1997
Western Cordillera, Colombia	76.3	$^{40}Ar/^{39}Ar$ plateau age	Sinton *et al.*, 1998
Serrania de Baudo, Colombia	77.9-72.5	$^{40}Ar/^{39}Ar$ plateau age	Kerr *et al.*, 1997
Pinon Unit, Ecuador	90.5-88.5	$^{40}Ar/^{39}Ar$ plateau age	Jaillard *et al.*, 1995
Pallatanga Unit, Ecuador	86.5-83	$^{40}Ar/^{39}Ar$ plateau age	Wilkinson, 1998

Table 2.2 – Summary of the isotopic and palaeontological ages on ophiolitic sequences from the Caribbean and South American region (From Kerr *et al.* 2003).

2.5 Models of Caribbean plate evolution

2.5.1 Evolutionary models

At present there are two general models for the evolution of the Caribbean plate. The first of these is the in-situ model, which suggests that the Caribbean oceanic crust may represent an oceanic plateau that formed in-situ in the proto-Caribbean region along a proto-Caribbean spreading axis (Beccaluva *et al.*, 1996; Meschede and Frisch, 1998; Giunta *et al.*, 2002). Most Caribbean workers, however, prefer the Pacific model (Duncan and Hargraves, 1984; Burke, 1988; Pindell and Barrett, 1990; Sinton *et al.*, 1998; Kerr *et al.*, 1999; 2002ab; White *et al.*, 1999; Hauff *et al.*, 2000ab; Pindell and Kennan, 2001; Thompson, 2002; Thompson *et al.*, 2003; 2004).

In this preferred model the Caribbean oceanic plateau forms in the Pacific on the Farallon plate. The northern part of the plateau is then tectonically emplaced between the North and South American continents, which had begun to separate in the early Jurassic, whereas the southern part of the plateau collided and accreted to the northwestern margin of South America forming the significant ophiolite sequences in Colombia and Ecuador (Fig. 2.1) (Duncan and Hargraves, 1984; Burke, 1988; Pindell and Barrett, 1990; Sinton *et al.*, 1998; Kerr *et al.*, 1999; 2002ab; White *et al.*, 1999; Hauff *et al.*, 2000ab; Pindell and Kennan, 2001; Thompson, 2002; Thompson *et al.*, 2003; 2004). A general overview of the Pacific model of Caribbean plate evolution, based on a compilation of existing tectonic models, is shown in Figure 2.4.

2.5.2 Caribbean evolutionary discussion

The palaeopositions of the North American, African and South American plates were determined by Pindell and Barrett (1990) with the use of finite difference solutions. Plate rotations that fit magnetic anomaly pairs together were used to determine the palaeoposition of Africa relative to North America. The palaeoposition of South America can then be constructed relative to Africa. The palaeopositions of South America with regard to North America can then be calculated with a finite difference

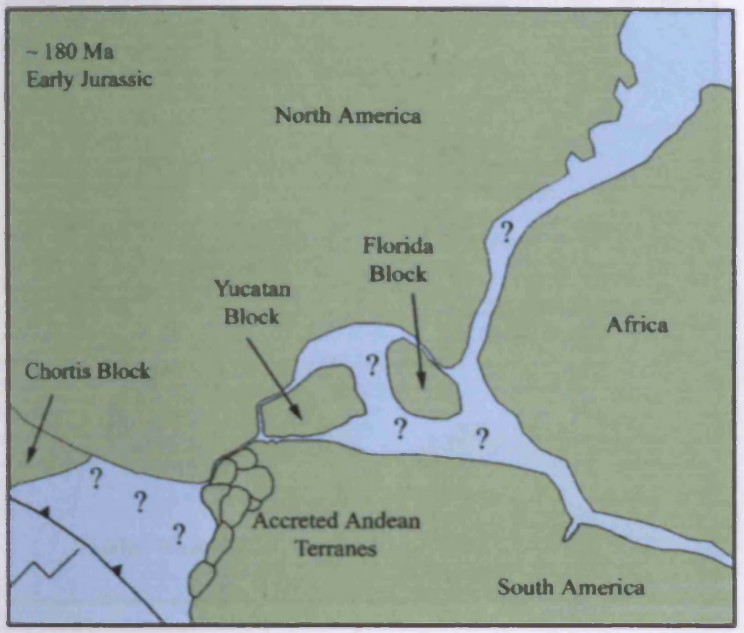

• **~ 180 Ma** - The paleopositions of the American and African plates are calculated by finite difference solutions (using magnetic anomalies). The fit of the plates is determined by using palaeomagnetic poles/bands, fracture and marginal zones from opposing continents, the 1000 fathom isobaths, removing younger accreted terranes and by restoring post-rift offsets and extension within the rifted basins (Pindell and Barrett, 1990; Muller et al., 1999; Pindell and Kennan, 2001).

•The Yucatan Block was located in-between the three continents (Burke, 1988).

•According to palaeontological evidence the oldest section of the MORB-like Bermeja Complex of Puerto Rico was formed at this time in the Pacific region (Montgomery et al., 1994).

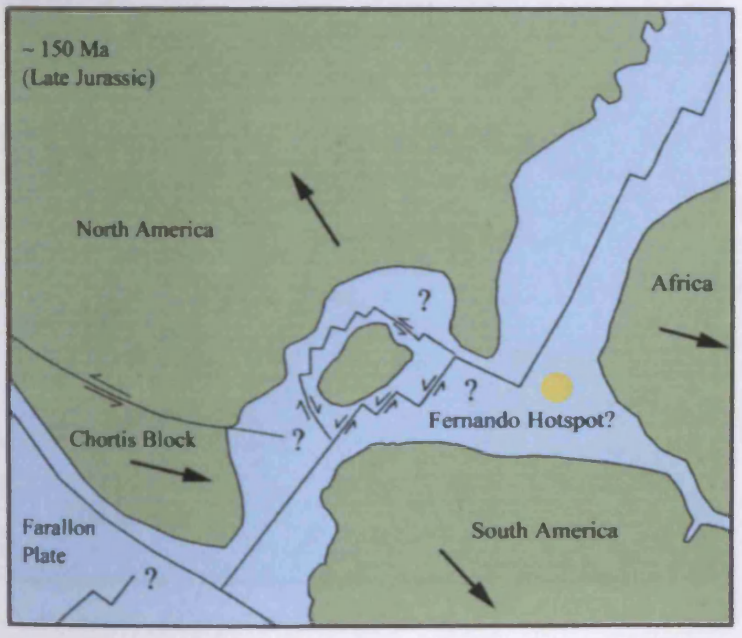

• **~ 150 Ma** - The Central Atlantic started to open, this was accompanied by spreading in the Gulf of Mexico that led to the separation of North and South America. Sedimentation in the area verifies the Jurassic age of sea floor spreading (Burke, 1988; Meschede and Frisch, 1998; Pindell and Kennan, 2001). The rate at which the American plates diverged can be determined using the finite difference solutions (Pindell and Barrett, 1990; Muller et al., 1999). At the same time the Yucatan block swung in an anti-clockwise direction and the Chortis block moved to the east (Burke, 1988; Meschede and Frisch, 1998; Pindell and Kennan, 2001). The Fernando hotspot began to erupt to form the Bahamas Platform (Duncan and Hargraves, 1984).

•Palaeontological evidence shows that the MORB of the Duarte Complex of Hispaniola and the middle section of the Bermeja Complex formed in the Pacific region (Montgomery et al., 1994).

Figure 2.4 - Schematic diagrams reconstructing the evolution of the Caribbean plate from the early Jurassic to the present day.

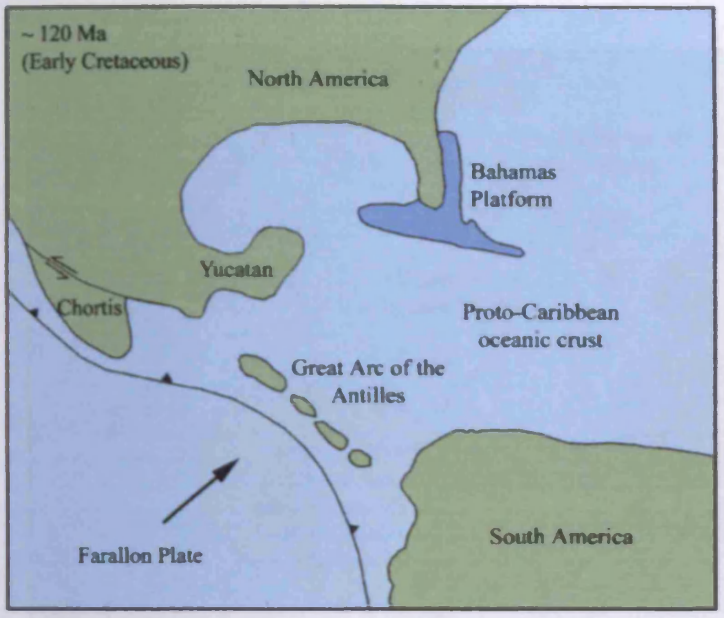

• **~ 120 Ma** - The opening of the South Atlantic formed a triple junction north of South America, which led to the cessation of sea floor spreading in the Gulf of Mexico (Duncan and Hargraves, 1984; Muller et al., 1999).

•The subduction of the Farallon plate resulted in the growth of a large island arc chain (The Great Arc of the Antilles) (Duncan and Hargraves, 1984; Burke, 1988; Pindell and Kennan, 2001). The arc probably nucleated on an existing fracture zone of the Proto Caribbean or Farallon spreading system (Burke, 1988). The arc at this time was erupting volcanic rocks with a tholeiitic chemistry (Donnelly et al., 1990; Kerr et al., 1999).

•The Yucatan Block rotated counter clockwise and collided with the North American continent (Burke, 1988). Blue schists in Mexico were uplifted and exposed due to southeasterly movement of the Chortis Block (Harlow, 2004).

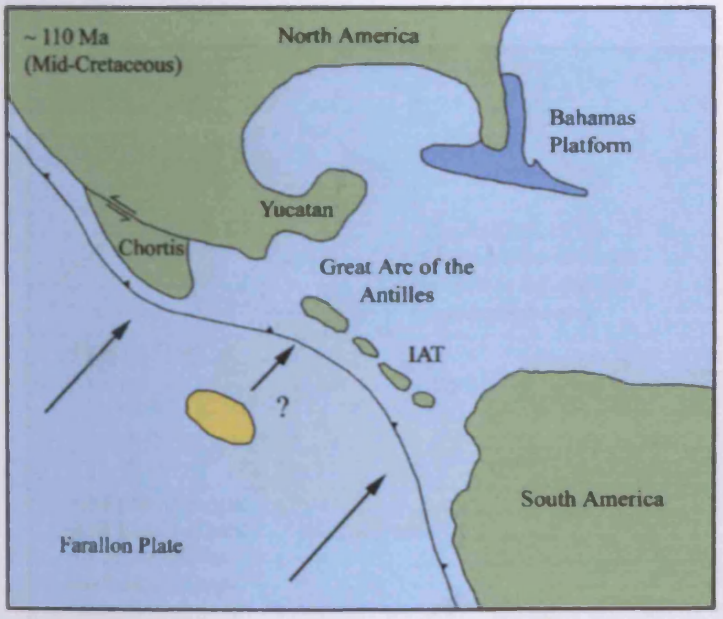

• **~ 110 Ma** - A localised unconformity found in Hispaniola and possibly Cuba at ~ 124.5-97 Ma may have formed due to: (1) the obduction of Jurassic MORB to form the Duarte and Bermaja complexes or (2) the collision of a small Aptian oceanic plateau (Aptian plateau fragments are found in Cuba) (Kerr et al., 1999; Kerr and Tarney, 2005).

•It is debated to whether the chemistry of the arc magmas changed from IAT to CA at this time. Lebron and Perfit (1993) suggest that the unconformity represents the change from IAT to CA. However Kerr et al (2003) suggest that the change from IAT to CA occurred before the unconformity and that the collision of the plateau and/or MORB fragments did not alter arc chemistry. The change is more likely to be due to a different or evolving source region for the island arc magmas.

•The Fernando hotspot has ceased activity.

Figure 2.4 - continued.

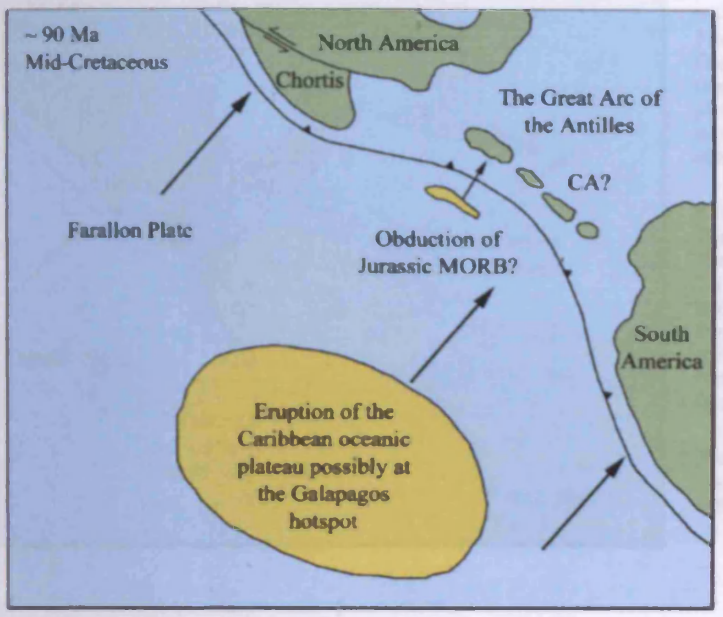

• **~ 90 Ma** – The Caribbean oceanic plateau is erupted onto the Farallon oceanic crust. Most Caribbean workers propose that the plateau originated from the Galapagos hotspot (Duncan and Hargraves, 1984; Kerr et al., 1999; Revillon et al., 1999; White et al., 1999; Kerr and Tarney, 2005). Pindell and Kennan (2001) argue that the plateau has not been far enough to the west relative to North America to encounter the Galapagos hotspot.

•The Great Arc of the Antilles was now erupting subaerial CA volcanic rocks along with their intrusive equivalents (Donnelly et al., 1990; Kerr et al., 1999).

•The last section of Jurassic MORB was obducted onto the Great Arc of the Antilles to become the youngest section of the Bermeja Complex, Puerto Rico (Montgomery et al., 1994).

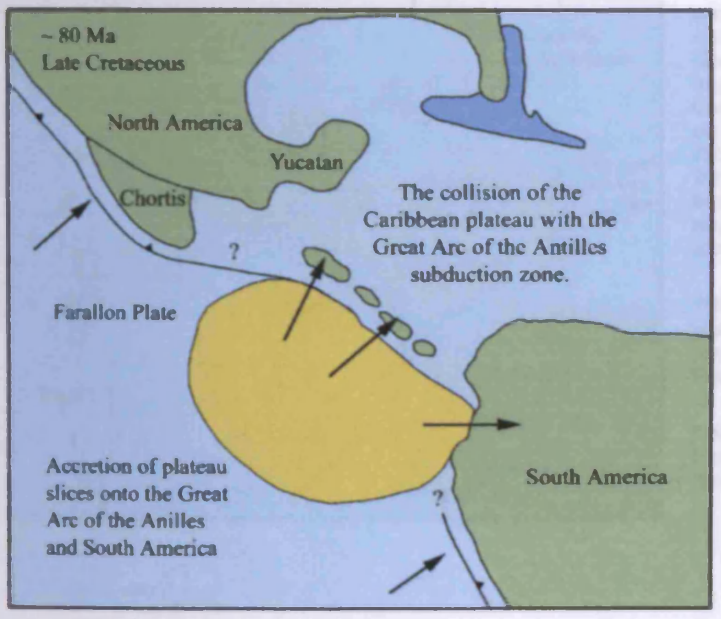

• **~ 80 Ma** - The southern portion of the Caribbean plateau collided with the northwestern South American margin. This resulted in plateau material (basalts, picrites and gabbros) being accreted in Colombia and Ecuador (Kimura and Ludden, 1995; Kerr et al., 1998; 2002; 2003).

•The northern portion of the plateau continued to move to the northeast on the Farallon plate. Shortly after the southern collisions, the northern portion collided with the Great Arc of the Antilles. Evidence of collision can be seen with plateau thrust slices being present on Hispaniola, Puerto Rico and Jamaica (Burke, 1988; White et al., 1999; Kerr and Tarney, 2005).

•When the plateau collided it was too thick, hot and buoyant to subduct. This inevitably lead to subduction polarity reversal and subduction back-step (Saunders et al., 1996; Kerr et al., 2003).

Figure 2.4 - continued.

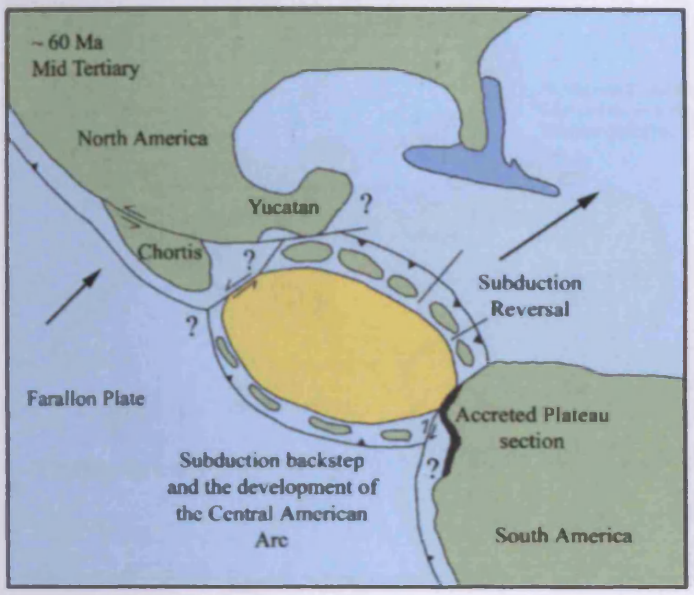

• **~ 60 Ma** – Subduction polarity reversal resulted in the Proto-Caribbean oceanic crust being consumed under the Great Arc of the Antilles (Lebron and Perfit, 1993; Kerr et al., 2003). Subduction back step behind the oceanic plateau formed the Central American arc that would subsequently form the Costa Rica-Panama isthmus (Kerr et al., 2003).

•The Great Arc of the Antilles split into three sections. The western end of the northern portion collided with the Yucatan block in the Late Cretaceous-Early Tertiary and the eastern end collided with the Bahamas platform in the Paleocene-Oligocene. The Central segment formed the Aves Swell and later formed the Lesser Antilles. The southern portion collided and accreted with the NW corner of South America (Duncan and Hargraves, 1984; Burke, 1988; Pindell and Kennan, 2001).

•Strike-slip motion to the north and south of the plateau has now begun (Duncan and Hargraves, 1984; Burke, 1988).

• **~ 40 Ma** – Although the timing is uncertain, the northern part of the Central American arc probably collided with the Chortis Block in the mid-Tertiary (Pindell and Kennan, 2001, Harlow, 2004). Jamaica began to collide with the Yucatan Block from the late Cretaceous-early Tertiary (Burke, 1988). Cuba started to collide with the Bahamas Platform by the end of the Paleocene-Eocene (Burke, 1988; Pindell and Kennan, 2001) and Hispaniola and Puerto Rico collided with the Bahamas platform in the Oligocene thus ending arc magmatism in the Greater Antilles (Burke, 1988; Montgomery and Pessagno; 1999).

•Strike-slip fault zones to the north and south of the plateau begin to accommodate 1100-1400 km of displacement (Wadge and Burke, 1983; Burke, 1988; Pindell and Barrett, 1990).

•An anomalous plateau fragment found in Equador (the Pinon Unit) may indicate a third plateau colliding with South America (Kerr et al., 2002)?

Figure 2.4 - continued.

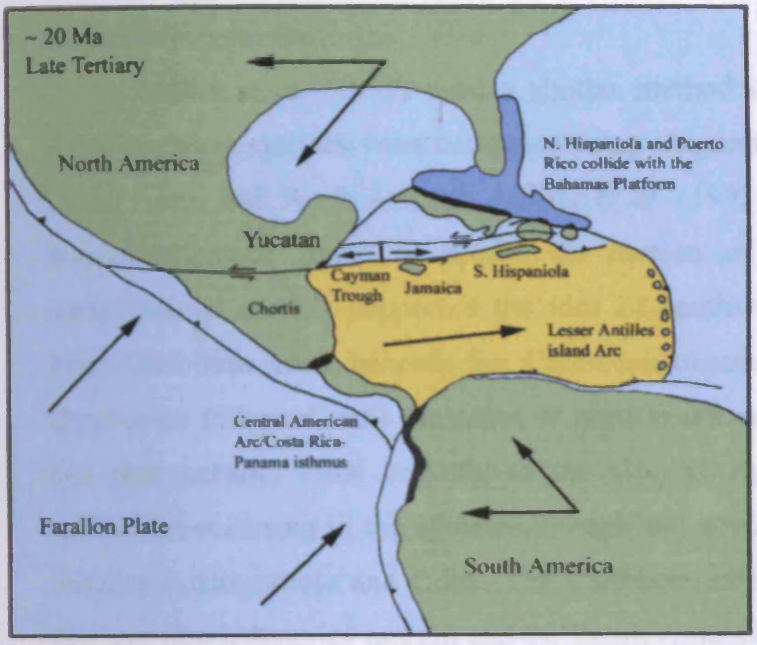

- **~ 20 Ma** - The Chortis block has been translated to the east by ~ 1050 km. This movement was accommodated on the Motagua-Polochic fault system (Wadge and Burke, 1983; Harlow et al., 2004). As the Chortis block moved around the southern tip of the Yucatan block the immense strain in the area, formed the now extinct rifts in the Nicaraguan Rise (Burke, 1988). Harlow et al (2004) and Lebron and Perfit (1993) propose that the Nicaraguan Rise is part of the Chortis Block.

- The southern portion of Hispaniola collides with the northern portion in the Miocene (Lewis and Draper, 1990). The Central American Arc/Costa Rica-Panama isthmus collides with South America in the mid to late Miocene (Burke, 1988; Pindell and Barrett, 1990; Muller et al., 1999).

- Relative eastward motion of the Caribbean plate formed the Cayman Trough in the Eocene-Oligocene, which subsequently translated Jamaica to the east (Rosencrantz and Sclater, 1986).

Figure 2.4 - continued.

circuit. This method is then used to calculate the relative motions of the plates with respect to one another.

Müller *et al.* (1999) used a similar method in which the North and South American plate motions were computed using magnetic anomalies and fracture zones in the North and South Atlantic. Müller *et al.* (1993) also used the Atlantic-Indian hotspot reference frame to model the motion of the American plates. These computational models supported the idea of southwest directed subduction of the Proto-Caribbean crust beneath the Caribbean oceanic plateau within the Tertiary. Quiescence followed until the onset of north-south convergence in the Miocene. At this time oceanic crust underthrust the Greater Antilles with possible localised subduction occurring in the Muertos Trough and southwest verging thrusts and folds forming in Hispaniola and Cuba. The Caribbean oceanic crust also underthrust the northern South America margin and the South American plate collided with the Costa Rica-Panama arc in the Miocene – Pliocene (Byrne *et al.*, 1985; Müller *et al.*, 1999; Hoernle *et al.*, 2002).

According to the Atlantic-Indian hotspot reference frame studies of Müller *et al.* (1999) the Caribbean plate, since the Oligocene, appears to have remained stationary (in a mantle reference frame), therefore the plate is "*not being driven*" by constructive or destructive plate tectonics. Consequently, Müller *et al.* (1999) suggest that there are no forces associated with subduction or ridge push occurring on the Caribbean plate. Therefore, the Caribbean plate is stationary and, as such, the strike-slip motions along the northern and southern Caribbean plate boundaries are driven by westward movement of both North and South America only. Thus, the Caribbean plate is not moving to the east because of its collision with the Bahamas platform and the lack of space caused by North and South American convergence (Müller *et al.*, 1993; 1999). This is contrary to the view of Meschede and Frisch (1998) who have proposed that the Caribbean plate is moving to the west but at a slower rate than the American plates thus producing the observed strike-slip motions on the northern and southern Caribbean margins.

2.5.3 Problems associated with the in-situ model

As noted in the previous section, the Pacific model is now favoured by most Caribbean workers. This is largely because the in-situ model does not explain a

number of problems associated with the evolution of the Caribbean plate. Palaeomagnetic data deduced that the plateau basalts lay 10-15° further to the south of their present latitudes in the Campanian (Pindell and Kennan, 2001) and this is only possible if these basalts have been transported into the Proto-Caribbean region from the southwest.

Palaeontological evidence also supports the Pacific model with radiolaria of equatorial Pacific faunal affinities being found in Puerto Rico and Hispaniola in Jurassic MORB thrust slices (Montgomery *et al.*, 1994). These radiolaria are older than the proposed opening of the Proto-Caribbean and thus require large scale lateral transport to the northeast to lie in their present location. The third piece of evidence comes from the accreted ~ 89-93 Ma oceanic plateau terranes in northwest South America (Table 2.2). The Caribbean plateau must have been transported from the west to the east in relation to North and South America so that part of it could have accreted onto the South American continent (Duncan and Hargraves, 1984; Burke, 1988; Révillon *et al.*, 1999; Kerr *et al.*, 2002ab).

In addition, the in-situ models are inconsistent with one another, with each model being significantly different, principally in terms of time scales and various subduction zones trending in several different directions. (cf. Beccaluva *et al.*, 1996; Meschede and Frisch, 1998; Giunta *et al.*, 2002). Proponents of the in-situ model have not addressed these problems; instead they simply argue that the Pacific model is unfeasible. One of their main arguments is that the Proto-Caribbean region would not have been wide enough to accommodate the plateau and that the Chortis block and its smaller associated blocks would not be able to rotate behind the advancing plateau and so encircle it (Beccaluva *et al.*, 1996; Meschede and Frisch, 1998; Giunta *et al.*, 2002). Conversely, workers such as Pindell and Kennan (2001) have argued that the Proto-Caribbean gap was wide enough and that the Chortis block was capable of encircling the western side of the Caribbean plateau.

2.5.4 Problems associated with the Pacific Model

The biggest problem associated with the Pacific model is the timing of the subduction polarity reversal and its effect on the chemistry of the island arc magmas. Geochemical studies suggest that the chemistry of the arc lavas changes from an island arc tholeiite (IAT) to calc-alkaline (CA) affinity (e.g. Donnelly *et al.*, 1990;

Kerr *et al.*, 2003). This compositional change could be the result of a collision of oceanic material (Jurassic MORB or a plateau fragment) with the Great Arc of the Antilles in the Aptian/Albian or Campanian thus forming a subduction polarity reversal.

An unconformity separating the IAT and CA rocks has been linked to a subduction reversal, and has been dated at 124.5-97 Ma by a fossiliferous limestone in Hispaniola (Donnelly *et al.*, 1990; Kerr *et al.*, 2003). However, it should be noted that the unconformity is only found on Hispaniola, Puerto Rico and possibly Cuba. Therefore it is doubtful that this localised event can be interpreted as evidence for a Caribbean-wide subduction polarity reversal. Recent studies also indicate that many CA rocks pre-date the Aptian/Albian thus implying that a subduction reversal could not have been the cause for an IAT to CA transition (Donnelly *et al.*, 1990; Kerr *et al.*, 1999; Hauff *et al.*, 2000a; Kerr *et al.*, 2003).

In addition, the subduction polarity reversal is now thought to have occurred in the Campanian and not the Aptian/Albian (Duncan and Hargraves, 1984; Burke, 1988; Stockhert *et al.*, 1995; Sinton *et al.*, 1998; Révillon *et al.*, 1999; Kerr *et al.*, 2003). The Cretaceous Caribbean oceanic plateau and Jurassic MORB continued to accrete on to the Great arc of the Antilles from the southwest until ~ 80 Ma, thus, suggesting that northeasterly subduction continued until this time (e.g. Montgomery *et al.*, 1994; Hauff *et al.*, 2000; Kerr *et al.*, 2003). Furthermore, the plateau is ~ 90 Ma; therefore, the reversal could not have occurred in the Aptian/Albian because the reversal would pre-date the eruption of the plateau (e.g. Sinton *et al.*, 1998; Kerr *et al.*, 1999; Kerr *et al.*, 2003). Conversely, it should be noted that other researchers e.g. Pindell and Barrett, (1990) and Pindell and Kennan, (2001) still support an Aptian/Albian subduction polarity reversal and propose that it is the mechanism for IAT-CA transition.

Nevertheless, the existence of a subduction polarity reversal in either the Campanian or the Albian/Aptian does not prove that it was the cause of the change in island arc chemistry. The composition of intra-oceanic island arc lavas can change because of many other factors e.g. differing sediment input into the subduction zone or thickening of the arc resulting in smaller amounts of partial melting (e.g. Pearce and Peate, 1995).

Donnelly *et al.* (1971) suggested that the change from IAT to CA compositions is due to an increasing amount of chemically different sediment being

subducted and incorporated into the island-arc source region e.g. evidence for this is found on Cuba and Puerto Rico. However, the lack of geochemical and geochronological evidence means that this hypothesis has not been thoroughly tested. (Donnelly and Rogers, 1978; Donnelly *et al.*, 1990; Spadea and Espinosa, 1996; Sinton *et al.*, 1998; Kerr *et al.*, 1999; Kerr *et al.*, 2003).

The final un-resolved problem with the Pacific model is the origin of the Caribbean oceanic plateau. Many authors e.g. Duncan and Hargraves (1984) and Sinton *et al.* (1998), regard the Galapagos hotspot to be the prime candidate for the source of the plateau. One argument against this is the apparent lack of magmatism ~ from 72-15Ma. However, data has been collected from Malpelo Island (south of Panama) and accreted complexes in Central America that indicate that the hotspot was active from 16 to 71 Ma (Hauff *et al.*, 2000b; Hoernle *et al.*, 2002; 2004).

Hoernle *et al.* (2002) presented trace element and isotopic data from the Galapagos Islands, accreted complexes and from the Caribbean plateau. The isotopic ratios are all similar and suggest that the Galapagos hotspot is a possible candidate for generating the Caribbean oceanic plateau. Conversely, Pindell and Kennan (2001) have demonstrated that the plateau was not far enough west relative to North America to encounter the Galapagos hotspot. Consequently, the origin of the Caribbean oceanic plateau is still problematic and more multi-disciplinary studies are required in order to resolve the problem (Sinton *et al.*, 1998; Révillon *et al.*, 1999; Pindell and Kennan, 2001).

2.5.5 Arc sequences

In addition to the oceanic plateau material, the evolution of the Caribbean region from the early Cretaceous to the present-day involves the formation of at least four island arc chains. These include the Great Arc of the Antilles, the Aves, the Lesser Antilles and the Central American arcs (Figs. 2.1 and 2.4) (Duncan and Hargraves, 1984; Burke, 1988; Pindell and Barrett, 1990; Kerr *et al.*, 1999). Consequently, the islands in the Caribbean region are made up of many island arc successions which require further study in order to constrain the evolution of the Caribbean plate (e.g. Donnelly *et al.*, 1990).

Island arc rocks have a characteristic chemistry which enables them to be easily distinguished from igneous rocks from other tectonic settings (Table 2.1, Chapters 5, 6 and 7). Plateau and arc successions have been studied on several islands around the Caribbean and have been used with structural, stratigraphical and palaeontological studies to constrain the current Pacific model of Caribbean evolution (Fig. 2.4) (e.g. Donnelly *et al.*, 1990; Kerr *et al.*, 2003).

2.5.6 Two oceanic plateaux?

Kerr and Tarney (2005) have suggested that two separate oceanic plateau accretion events occurred in northwestern South America: one in the early Campanian (83-80 Ma) and one in the mid-Eocene (~ 45 Ma). These two plateau sequences are both ~ 90 Ma yet they are separated by a late Cretaceous to early Tertiary island arc sequence in Ecuador and Colombia. The Campanian accretion has been confirmed with radiometric ages on tonalities that intrude the older plateau, whereas the younger accretion event is thought to include the plateau fragments on the western margin of South America and possibly the island of Gorgona (Kerr and Tarney, 2005).

Palaeomagnetic data on Gorgona plateau lavas suggest that they are derived from a latitude of 26-30°S, and suggests that Gorgona did not originate from an equatorial region and hence is not derived from the Galapagos hotspot (Kerr and Tarney, 2005). Other data from oceanic plateau sequences in Colombia and Ecuador show that there are two distinct palaeolatitudes: one equatorial and one more southerly (Kerr and Tarney, 2005). Therefore, assuming a 45 Ma gap between formation and accretion, of the second 90 Ma plateau in northwestern South America a possible location for the "Gorgona plateau", taking into account the NNE directed, ~ 5-10 cm/yr Farallon plate, could be the Sala y Gomez hot spot (Kerr *et al.*, 2002 and Kerr and Tarney, 2005).

2.6 Overview of oceanic plateau and associated arc sequences in the Caribbean-Colombian region

2.6.1. Curaçao

The island is located in the southern Caribbean Sea (Fig. 2.1) and is part of the Dutch Antilles (Kerr *et al.*, 1996b). It is mainly composed of the ~ 5 km thick Curaçao Lava Formation which is comprised of picrites at the base that evolve into tholeiitic pillow basalts, dolerites and hyaloclastites nearer the top (Kerr *et al.*, 1996b; Révillon *et al.*, 1999). The 88-90 Ma Curaçao Lava Formation has been interpreted as being part of the Caribbean oceanic plateau (Table 2.2) (Kerr *et al.*, 1996b; Révillon *et al.*, 1999).

2.6.2 Aruba

The island is located in the Dutch Antilles (White *et al.*, 1999). The Aruba Lava Formation (ALF) is a ~ 3 km thick succession of mafic volcanic rocks with a lack of interbedded terrestrial sedimentation, suggesting that the magmas were erupted away from a continental landmass. The formation is composed of pillowed and massive basalts with some dolerite dykes and rare pyroclastics (Donnelly *et al.*, 1990; White *et al.*, 1999; Kerr *et al.*, 2003). The interbedded sediments contain Turonian ammonites that give an age of ~ 88.5 – 90.5 Ma, which is the same age as the oceanic plateau (White *et al.*, 1999). The rocks have flat REE patterns, lack a Nb and Ta anomaly and have similar trace element ratios and εNd values (~ 7) to the Curaçao lavas that are geographically close to Aruba.

The chemical and palaeontological evidence suggests that the Aruba lavas have an oceanic plateau origin and may have been derived from the same or a similar source region as the Curaçao lavas (Donnelly *et al.*, 1990; White *et al.*, 1999; Kerr *et al.*, 2003). A tonalitic batholith on the island intrudes the ALF and has an age of ~85 – 82 Ma. The pluton has transitional chemistry from IAT to CA signatures. The batholith represents a subduction related melt that intruded the ALF after the

Caribbean oceanic plateau collided with the Great Arc of the Antilles (White *et al.*, 1999).

2.6.3 Bonaire

The Washikemba Formation (WF) is split into two separate units (Thompson, 2002). There is a 5 km thick succession of Cretaceous igneous rocks in the north and a 3 km succession of pillow basalts and rhyolitic domes in the south. Geochemical data shows that the WF is part of the island arc tholeiite series (Donnelly *et al.*, 1990; Kerr *et al.*, 2003; Thompson, 2002).

2.6.4 Trinidad and Tobago

The Sans Souci Formation (SSF) is found on the island of Trinidad. It is a ~ 1 km thick succession of basalts, basaltic pyroclastics, gabbros and rare inter-bedded layers of terrigenous sediments. The chemistry of the volcanics are similar to Curaçao lavas and a K-Ar date by Wadge and McDonald, (1985) gave an age of ~ 87 Ma. Consequently, the succession may be an obducted slice of the Caribbean oceanic plateau (Donnelly *et al.*, 1990; Kerr *et al.*, 2003). The island of Tobago consists of a poorly understood island arc succession composed predominantly of andesitic pyroclastic rocks and a dioritic plutonic complex. These volcanics and the pluton have an IAT affinity (Donnelly *et al.*, 1990; Kerr *et al.*, 2003).

2.6.5 Puerto Rico

In addition to the Jurassic Bermeja Complex (Section 2.3), Puerto Rico also contains a complex tectonic regime of accreted arc terranes with IAT, CA and shoshonitic (SHC) affinities. Kerr *et al.* (2003) suggests that the IAT gradually evolve into CA rocks; however, they also propose that there is evidence that the two series were coeval at times. Conversely, Donnelly *et al.* (1990) suggests that the transition from IAT to CA rocks is marked by a well defined unconformable boundary between the pre-Robles (IAT) and the Robles-Rio Orocovis Formations. Both authors, however, seem to agree that the transition occurred in the Albian (~ 100 Ma) (Donnelly *et al.*, 1990; Kerr *et al.*, 2003).

2.6.6 Hispaniola

The island is composed of oceanic plateau rocks and up to 11 different arc terranes of IAT and CA affinities (Donnelly *et al.*, 1990; Kerr *et al.*, 2003). The Dumisseau Formation (DF) is a 1.5 km thick succession of pillowed and massive basalts, dolerite sills, minor picrites and pelagic sediments. Fossils from the base of the formation give ages of 86–90 Ma and $^{40}Ar/^{39}Ar$ plateau ages of the basalts range from 88–92 Ma (Donnelly *et al.*, 1990; Kerr *et al.*, 2003). The chemistry of the DF lavas are similar to the chemistry of the DSDP leg 15 lavas e.g. they have flat to LREE enriched REE patterns. The trace element ratios and the isotopic analysis indicate that the rocks could be from a heterogeneous plume source, similar to plateau lavas in Colombia and Gorgona (Sections 2.6.9 and 2.6.10). The chemical and chronological evidence suggests that the DF is an obducted section of the Caribbean oceanic plateau (Donnelly *et al.*, 1990; Kerr *et al.*, 2003).

The Duarte Complex (DC) is divided into two units; the lower unit is at least 10 km thick and is composed of picrites, basalts and schists. The upper unit is ~ 3–4 km thick and is further divided into 3 fault bounded sections (Donnelly *et al.*, 1990; Lapierre, 1997; Kerr *et al.*, 2003). The first section contains amphibolites and epidote-amphibolite gneisses; the second has pillow basalts with upper Jurassic sediments; and the last has serpentinized peridotites. The latter two sections have typical MORB chemistry. Conversely, the picrites and basalts of the lower unit have flat and LREE enriched REE patterns and have a similar geochemistry to the rocks from site 151 (DSDP leg 15) and the DF (Donnelly *et al.*, 1990; Lapierre, 1997; Kerr *et al.*, 2003). The amphibolites in the upper unit have an age of ~ 86 Ma (Table 2.2). The aforementioned data suggests that the lower DC unit and the lower section of the upper unit have an oceanic plateau origin.

A succession of Cretaceous to Eocene volcanic arc rocks are found in the north of Hispaniola. The Maimaon Formation (MF) is a northwest trending band of metamorphosed volcanic arc rocks composed of a basaltic–keratophyre suite (Donnelly *et al.*, 1990; Kerr *et al.*, 2003). It is early Cretaceous in age and has been interpreted to be part of the IAT suite in the Caribbean region. The Amina schists, which are found to the northwest of the MF have a similar chemistry. The Los Ranchos Formation (LRF) is a 1 km thick unit composed of basalts to rhyolites and like the MF represents an early Cretaceous succession of IAT affinity (Donnelly *et al.*,

1990; Kerr *et al.*, 2003). To the east, the succession is overlain by the Loma La Vega and the Las Guajabas volcanics that have characteristic CA chemistry. Tertiary igneous rocks are also found on Hispaniola. However, it is uncertain to whether these volcanics are subduction related or were formed due to the collision of Southern Hispaniola with North Hispaniola in the Miocene (Donnelly *et al.*, 1990; Lewis and Draper, 1990; Kerr *et al.*, 2003).

2.6.7 Cuba

The Margot Formation (MF) in the northwest of the country has a typical oceanic plateau chemistry i.e. flat REE patterns and has intercalated sediments with fossils giving an age of 124 – 90 Ma (Donnelly *et al.*, 1990; Kerr *et al.*, 1999; Kerr *et al.*, 2003). Other ophiolitic sequences are found on Cuba; however, they are Jurassic in age and formed in a rift related continental margin between the Yucatan and South America. Extensive island arc terranes with IAT, CA and SHC chemistry are also found on the island. The IAT and CA rocks indicate that the chemical change between the two is more gradual than was previously thought (Donnelly *et al.*, 1990; Kerr *et al.*, 1999; Kerr *et al.*, 2003).

2.6.8 Costa Rica

Eight igneous complexes are found in Costa Rica, the best studied of these are the Nicoya Peninsula (NP) and Tortugal Complex (TC). The NP has been dated by $^{40}Ar/^{39}Ar$ to give ages of 83-95 Ma. The TC has been dated at ~ 89.7 Ma and has tholeiitic rocks with flat REE patterns and high Ni and Cr values (Alvarado *et al.*, 1997). Most of the complexes are interpreted to be obducted oceanic plateau-type fragments. Two of the complexes, the Quepos and the Osa give younger ages of 59 – 65 and 62 Ma respectively, have plateau type chemistry and have been linked to the accretion of the Galapagos-derived seamounts after the formation of the Caribbean plate. The oldest complex, the Santa Elena has an IAT signature (Donnelly *et al.*, 1990; Alvarado *et al.*, 1997; Hauff *et al.*, 2000; Hoernle *et al.*, 2002; 2004; Kerr *et al.*, 2003).

2.6.9 Colombia

In Colombia oceanic rocks are found in three main regions, the western Central Cordillera, the Western Cordillera and the Serrania de Baudo (Kerr *et al.*, 2002b). The volcanic rocks include picrites and basalts and most have an age of ~ 90 Ma (Table 2.2). The geochemistry of the picrites and basalts suggests an oceanic plateau affinity derived from a heterogeneous mantle plume (Kerr *et al.*, 2002b). Cretaceous and Tertiary island arc rocks are also found accreted to the Colombian margin. The intermediate to basic volcano-sedimentary Quebradagrande Complex in the Central Cordillera is of Valanginian-Albian (140-97 Ma) age and shows clear subduction related geochemical signatures. The Western Cordillera contains terranes of IAT and CA rocks of Campanian age with La/Yb ratios of between 4 and 10, LREE enrichment and relative depletions of Nb and other HFSE (Spadea and Espinosa, 1996; Kerr *et al.*, 2003).

2.6.10 Gorgona, Colombia

Gorgona Island is 8 km long, 2.5 km wide and lies ~ 50 km off of the west of Colombia (Fig. 2.1) (Kerr *et al.*, 1996c). The island is mostly composed of mafic and ultramafic volcanic and intrusive rocks, which also include the only known Phanerozoic spinifex textured komatiites (Kerr *et al.*, 1996c). It is still debated to whether or not the igneous rocks represent a part of the Caribbean oceanic plateau (Section 2.5.7). The igneous rocks comprise four groups which include, enriched basalts, depleted basalts, LREE depleted komatiites and LREE depleted picrites. It is thought that these lavas were derived from partial melting of a heterogeneous mantle plume source region (Arndt *et al.*, 1997; Hauff *et al.*, 2000; Kerr *et al.*, 1996c; Révillon *et al.*, 2002). The komatiites and picrites are the result of melting from the hot axis of a mantle plume that has previously undergone melt extraction (Arndt *et al.*, 1997; Kerr, 2005).

2.6.11 Venezuela

Metamorphosed basaltic and ultramafic volcanic rocks are found in northern Venezuela (Donnelly *et al.*, 1990; Kerr *et al.*, 2003). Their age has not been

constrained due to the lack of fossils and their high metamorphic grade. The Villa de Cura Group is located in the north of the country it is 4 - 5 km thick and trends east – west. It is composed of arc and plateau rocks, with the plateau rocks having La/Nb = 1, flat REE patterns and having similar chemistries to the plateau rocks on Curaçao and Aruba. The island arc rocks display typical IAT signatures (Donnelly *et al.*, 1990; Kerr *et al.*, 2003).

2.6.12 Ecuador

Ecuador is composed of a number of accreted plateau and arc terranes. The arc terranes include the Machuci, the Naranjal, the Rio Cala, the Las Orquideas and the San Lorenzo units (Kerr *et al.*, 2002a). The plateau terranes consist of the Pinon, the Naranjal, the Pallatanga and the San Juan units. The Naranjal unit is composed of both plateau and island arc material (Kerr *et al.*, 2002a).

A detailed study by Kerr *et al.* (2002a) suggested that the Pinon and the Pallatanga units are separated from each other by the Macuchi and the Naranjal units, therefore the Pinon and the Pallatanga represent two separate plateaux (Section 2.5.7). They propose that the Pallatanga Unit can be correlated with the same plateau sequences in Colombia and the rest of the Caribbean and that the Pinon Unit is a second plateau that accreted to the northwest of South America after the emplacement of the Caribbean plateau and the obduction of the Pallatanga Unit.

2.7 Summary

1. Although there are a minimum of four oceanic crustal phases in the Caribbean region, the Caribbean plate is mostly composed of a plume-derived 89-93 Ma oceanic plateau.
2. The Caribbean oceanic plateau was formed by melting of the initial phase of a hotspot, possibly Galapagos, and then transported to the northeast on the Farallon plate. At ~ 80 Ma the southern portion of the plateau was accreted to the northwestern margin of the South American continent and the northern portion was emplaced between the North and South American continents.
3. Collision of the plateau with the Great Arc of the Antilles induced subduction polarity reversal and subduction back step. Subsequent development of

sinistral and dextral transcurrent faults on the plateaus northern and southern boundaries respectively isolated the plateau forming the Caribbean plate.

4. Subduction polarity reversal is thought to have occurred in either the Albian/Aptian or the Campanian.
5. The subduction zone magmas change from a tholeiitic to a calcalkaline - shoshonite chemistry. The cause of this geochemical change is still controversial but may well represent changing source characteristics over time.

Chapter 3

Jamaican Geology

3.1 Introduction

The island of Jamaica has an area of ~ 11,425 km^2 and is situated on the northwestern Caribbean plate margin southeast of the Cayman Trough, west of Hispaniola and south of Cuba (which is now part of the American plate) (Figs. 2.1, 3.1 and 3.2) (Robinson *et al.*, 1971; Jackson and Smith, 1978).

Two thirds of Jamaica is covered with Tertiary limestone that overlies Cretaceous volcanic and sedimentary rocks (Draper, 1986). The island can be divided into two major structural blocks. The main block encompasses most of the island, is located to the west and is known as the Cornwall – Middlesex Block (Figs. 3.1 and 3.2). To the east lies the smaller Blue Mountain Block that is separated from the latter by the fault bounded Wagwater basin (Figs. 3.1 and 3.2) (Robinson *et al.*, 1971; Jackson and Smith, 1978). The lower lying Cornwall – Middlesex block can be further subdivided into an eastern shelf area, the Clarendon block and the western Hanover block. These are separated from each other by another graben structure known as the Montpelier-Newmarket Zone (Figs. 3.1 and 3.2) (Robinson *et al.*, 1971; Draper, 1986; Robinson, 1988; Lewis and Draper, 1990).

3.2 Blue Mountain Block

The Blue Mountain inlier contains the ophiolitic Bath-Dunrobin Formation in the south, and extensive andesitic and dacitic magmatism in the central and northern areas of the inlier (Figs. 3.1 and 3.2). These andesites and dacites belong to the

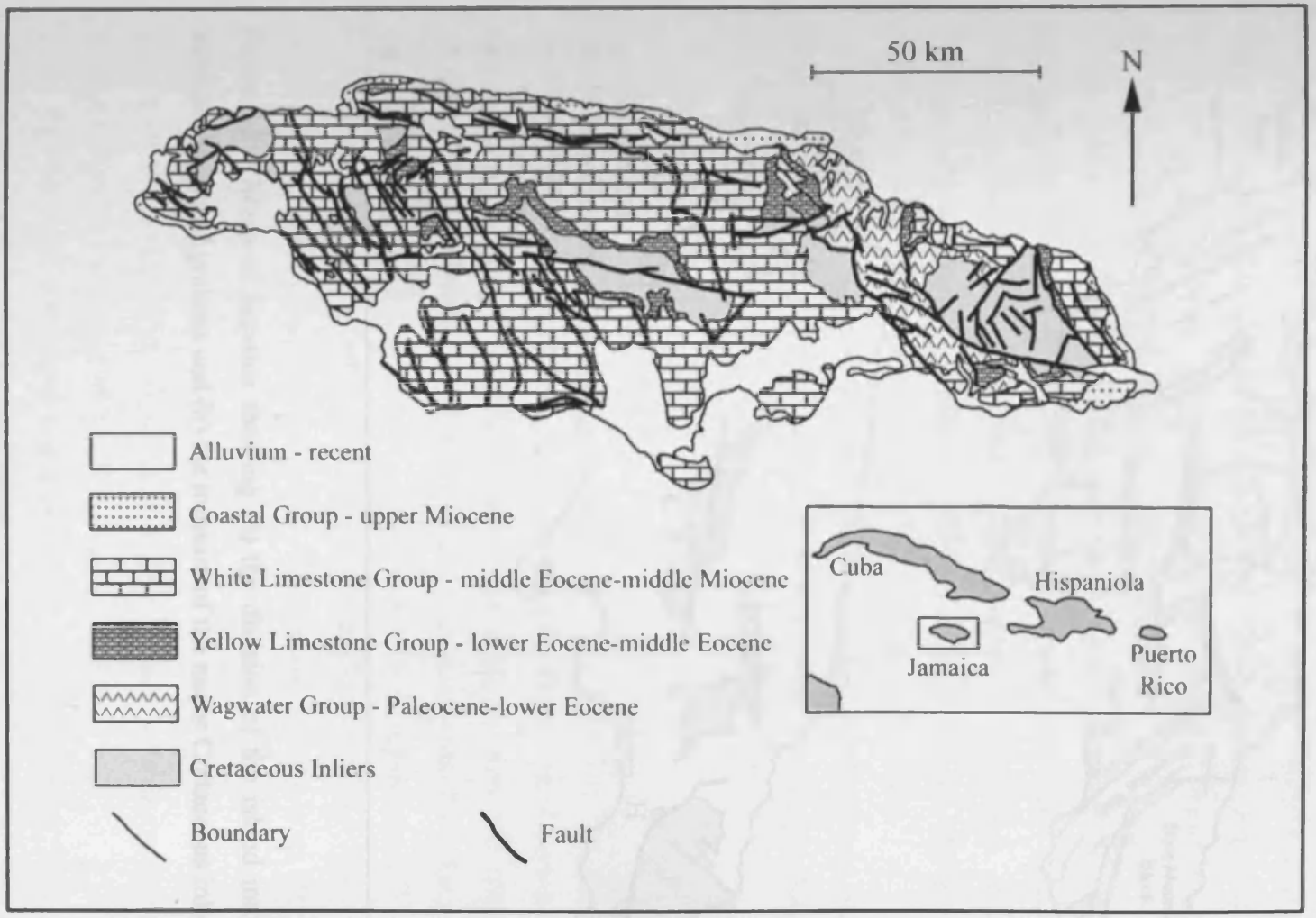

Figure 3.1 – Geological map of Jamaica (modified from Lewis and Draper, 1990).

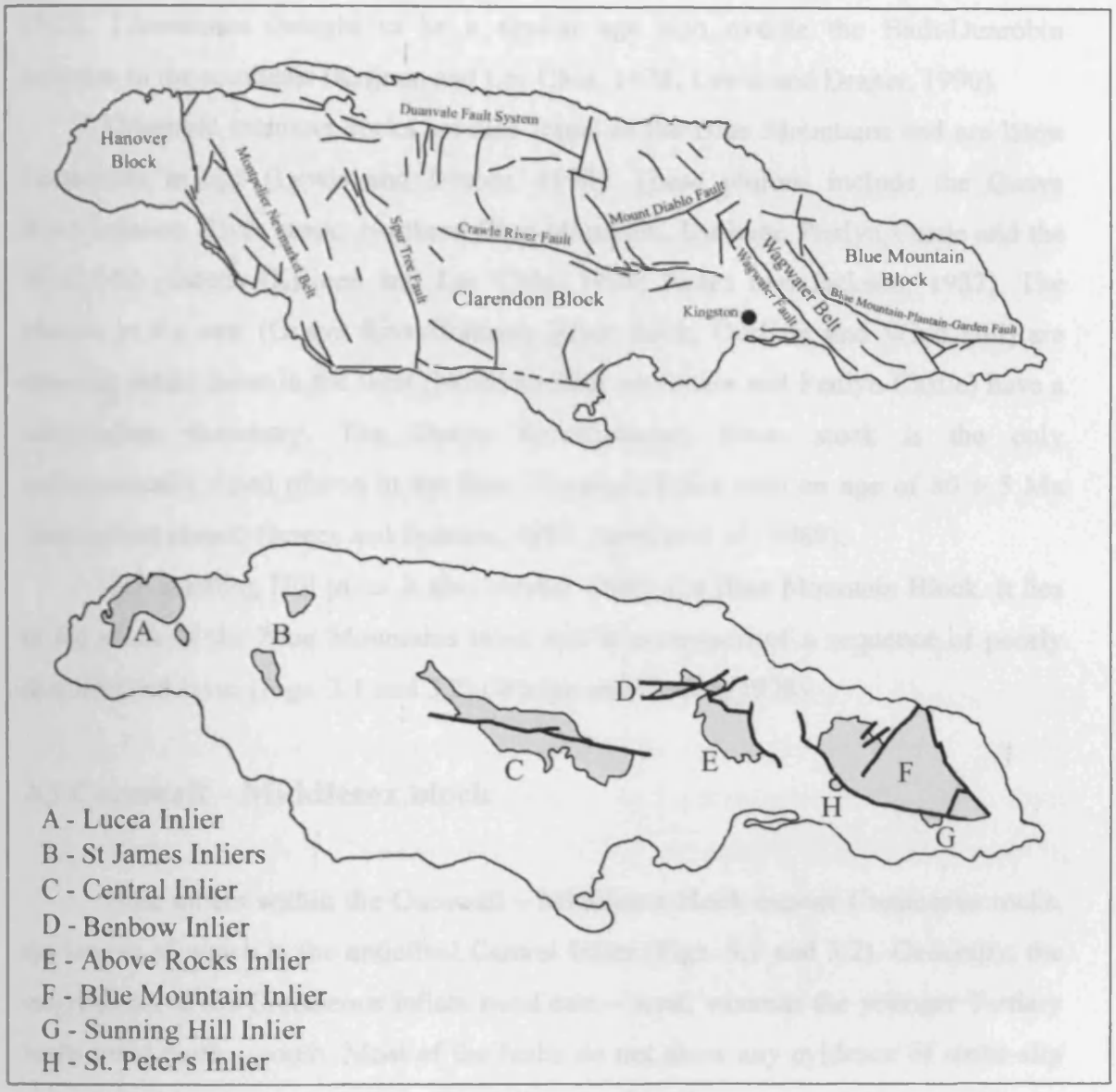

Figure 3.2 – Maps of Jamaica showing (a) the division of the island into different tectonic blocks and grabens and (b) the location of the major Cretaceous inliers.

Bellevue and Bonnie View Formations, have calcalkaline affinities and are overlain by limestones of late Campanian/Maastrichtian age (Wadge *et al.*, 1982; Jackson, 1987). Limestones thought to be a similar age also overlie the Bath-Dunrobin complex in the southeast (Krijnen and Lee Chin, 1978; Lewis and Draper, 1990).

Granitoid intrusive rocks are also found in the Blue Mountains and are latest Cretaceous in age (Lewis and Draper, 1990). These plutons include the Guava River/Johnson River stock, Northern Blue Mountain, Durham, Penlyn Castle and the Wind Hill plutons (Krijnen and Lee Chin, 1978; Isaacs and Jackson, 1987). The plutons in the east (Guava River/Johnson River stock, Durham and Wind Hill) are tholeiitic while those in the west (Northern Blue Mountain and Penlyn Castle) have a calcalkaline chemistry. The Guava River/Johnson River stock is the only radiometrically dated pluton in the Blue Mountain Inlier with an age of 80 ± 5 Ma (method not stated) (Isaacs and Jackson, 1987; Jackson *et al.*, 1989).

The Sunning Hill inlier is also located within the Blue Mountain Block. It lies to the south of the Blue Mountains inlier and is composed of a sequence of poorly characterised lavas (Figs. 3.1 and 3.2) (Wadge and Draper, 1978).

3.3 Cornwall – Middlesex block

Nine inliers within the Cornwall – Middlesex block expose Cretaceous rocks, the largest of which is the anticlinal Central Inlier (Figs. 3.1 and 3.2). Generally, the major faults in the Cretaceous inliers trend east – west, whereas the younger Tertiary faults trend north – south. Most of the faults do not show any evidence of strike-slip motion (Robinson *et al.*, 1971). The inliers in the Clarendon and Hanover Blocks mostly contain sedimentary and igneous rocks of Barremian to early Tertiary ages (Jackson, 1987). The largest of the Cretaceous inliers in the Cornwall-Middlesex block include the Benbow, Central and Above Rocks inliers. Unlike many of the other smaller inliers in the block, these latter inliers contain significant successions of igneous rocks (e.g. Jackson, 1987).

The Benbow inlier is composed of volcanic and sedimentary rocks (the oldest of which are Barremian; 130-125Ma); the volcanic rocks have been reported to be dominantly andesitic in composition (Burke *et al.*, 1969; Jackson, 1987). The Central and Above Rocks inliers are also composed of volcanic and sedimentary formations.

The rocks of the Central inlier are of upper Cretaceous ages (Mitchell, 2003); however, the age of the Above Rocks Formations has not been determined.

3.4 Cretaceous and Tertiary volcanic rocks – an overview

The Cretaceous volcanic rocks are unimodal with predominant andesitic volcanism whereas the Tertiary lavas are bimodal with basalts and dacites (Roobol, 1972; Jackson, 1987). The Benbow Inlier is the only locality where Lower Cretaceous island arc rocks have been found (Jackson *et al.*, 1989). In this inlier the volcanic and sedimentary rocks are undeformed and form the Devils Racecourse Formation. The Devils Racecourse is Barremian in age, includes pillow basalts and dacite lava flows and the limited available geochemistry suggests that they have a tholeiitic and calcalkaline affinity (Jackson, 1987; Jackson *et al.*, 1989).

Upper Cretaceous rocks are much more widespread in Jamaica, with basalt, andesite and dacite lava flows being found in the Blue Mountain, Giblatore and Central inliers (Jackson, 1987; Jackson *et al.*, 1989; Mitchell, 2003). The dominant Jamaican volcanic group of upper Cretaceous age belongs to a poorly-dated series of mafic pyroclastic deposits, minor flows and unfossiliferous sedimentary rocks of the Central Inlier. The oldest of these units may belong to the tholeiitic and the younger to the calcalkaline series. There is also a similar series of Santonian-Campanian volcanic rocks in the small Lucea inlier in western Jamaica (Donnelly *et al.*, 1990; Mitchell, 2003). The igneous and sedimentary rocks in the Above Rocks inlier are of an uncertain age (Jackson *et al.*, 1989).

Eocene bimodal volcanics have also been discovered in the Wagwater basin (Jackson and Smith, 1978; Jackson and Smith, 1979) and unimodal Tertiary ignimbrites are present in the Summerfield Group of the Central inlier.

3.5 The Blue Mountain Inlier: the Bath-Dunrobin Formation

The volcanic and sedimentary rocks in the Blue Mountain Inlier have an E–NE dip and three fault trends of NE, E and SE, with the NE trend being dominant (Wadge and Draper, 1978; Jackson and Smith, 1979; Jackson *et al.*, 1980; Wadge *et al.*, 1982). The stratigraphy and structure of the Blue Mountain inlier has been studied

by Krijnen and Lee Chin (1978), Wadge and Draper (1978) and Wadge *et al.* (1982). Krijnen and Lee Chin (1978) were the first to give a full description of the main lithological units within the inlier; these units are described below (Fig. 3.3).

3.5.1 The Back Rio Grande Formation

The Back Rio Grande Formation is the oldest formation found in the inlier. The sequence consists of a submarine succession with a basal volcaniclastic conglomerate member which is conformably overlain by the 8-10 m thick Back Rio Grande Limestone Member of Campanian age (based on rudist bivalves) (Krijnen and Lee Chin, 1978).

3.5.2 The Bellevue Formation

The formation is a ~ 600-1500 m thick, predominantly submarine volcanic island arc succession with volcaniclastic conglomerates capped by a ~ 20-80 m thick limestone unit of Campanian/Maastrichtian age (Krijnen and Lee Chin, 1978). In detail the formation is composed of four members that can be found in the northern and central part of the inlier:

1. The basal unit is the Guava River Member, which consists of a 50-100 m thick succession of grey calcareous mud and siltstone that conformably overlays the Back Rio Grande Limestone Member (Krijnen and Lee Chin, 1978).
2. The Guava River Member is in faulted contact with porphyries of the overlying Bellevue Porphyry Member. The Bellevue Porphyry consists of a ~ 600 m thick succession of submarine volcanic basalts, andesites and dacites which are found in only one locality. The rocks are extremely altered due to intense tropical weathering, hydrothermal processes and possible regional metamorphism (Krijnen and Lee Chin, 1978).
3. The base of The Ginger House Member is not seen but it is composed of purple-to-grey polymict conglomerates with a sandy tuffaceous matrix and clasts of andesitic porphyry and bright green chloritised

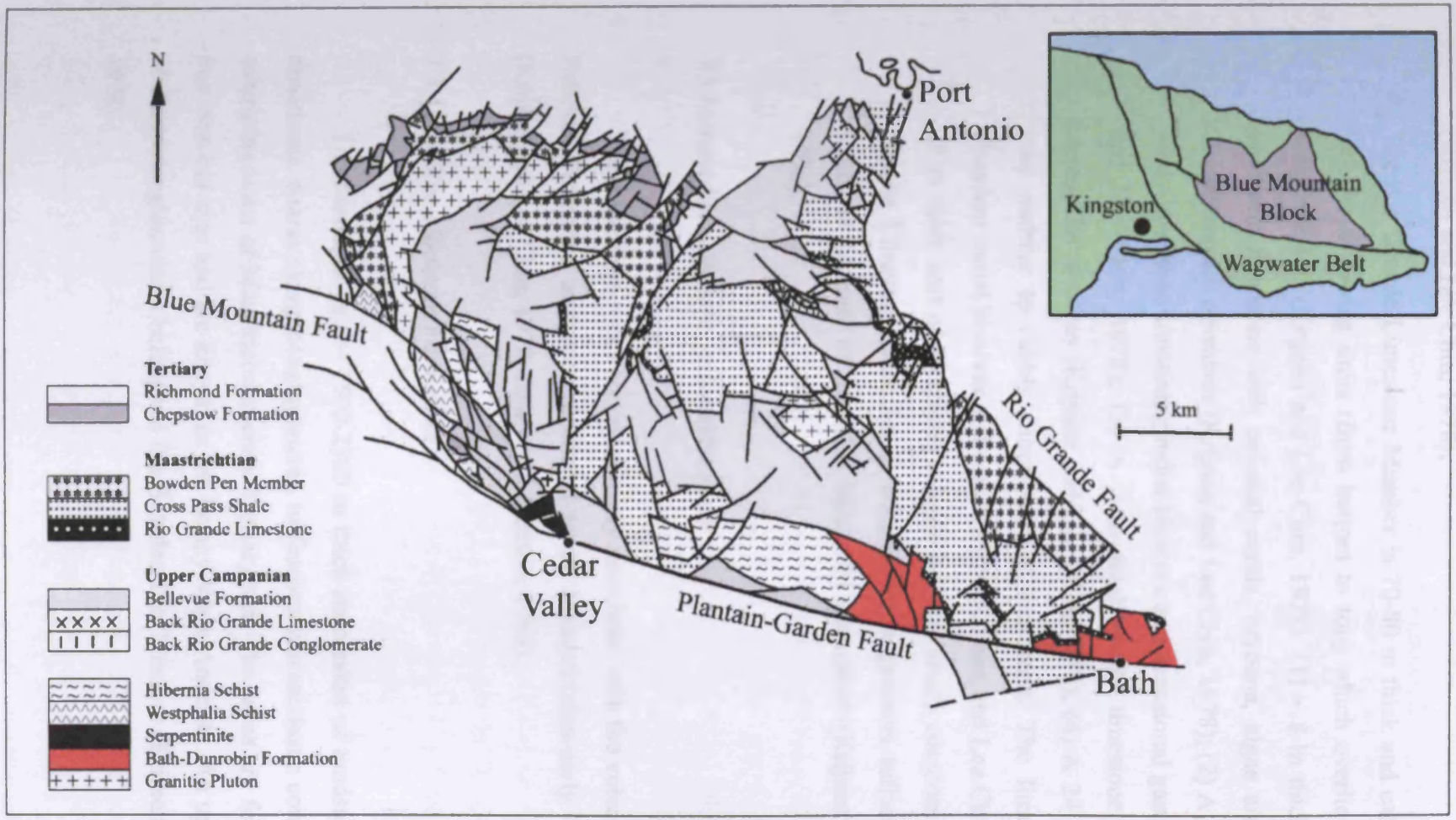

Figure 3.3 – Geological map of the Blue Mountain Inlier (modified from Krijnen and Lee Chin, 1978).

pelitic rock. This succession grades into the Rio Grande Limestone Member (Krijnen and Lee Chin, 1978).

4. The Rio Grande Limestone Member is 70-80 m thick and can be subdivided into the following units (from bottom to top) which overlie a basal rubbly conglomerate (Krijnen and Lee Chin, 1978): (1) ~ 8 m thick grey compact bioclastic limestone with colonial corals, bryozoa, algae and fragments of *Titanosarcolites* bivalves (Krijnen and Lee Chin, 1978); (2) A 19 m thick grey sandy limestone containing rudist bivalves and occasional gastropods (Krijnen and Lee Chin, 1978); (3) A 2 m thick sandy limestone with abundant *Acteonella* bivalves (Krijnen and Lee Chin, 1978); (4) A 24 m thick unit of grey nodular to rubbly limestone and sandstone. The limestone contains abundant rudist bivalves and coral fossils (Krijnen and Lee Chin, 1978); (5) A 12 m thick unit of bioclastic calcarenites and sandy conglomerates. The Rio Grande Limestone Member is overlain by a greenish tuffaceous sandstone which is the base of the Blue Mountain Formation (Krijnen and Lee Chin, 1978).

3.5.3 Granodiorite-tonalite-adamellite rocks

These intrusive rocks are consistently associated with the volcanic series of the Bellevue Formation and are considered to be Maastrichtian-early Tertiary in age (Krijnen and Lee Chin, 1978; Issacs and Jackson, 1987).

3.5.4 The Blue Mountain Formation

The formation is a ~ 1500-2500 m thick succession of mudstones, siltstones, sandstones, coarse slump conglomerates, tuffaceous volcaniclastic conglomerates and submarine lavas of Maastrichtian-early Tertiary age. The lavas are found around the Port Antonio area and are known as the Bonny View Andesite. An upper succession of slump conglomerates belongs to the Bowden Pen Member (Krijnen and Lee Chin, 1978).

3.5.5 The Chepstow Limestone

The Chepstow Limestone is a ~ 35 m thick impure bioclastic limestone unit of probable Palaeocene-Early Eocene age that overlays the Bonny View Andesite and Blue Mountain Formation (Krijnen and Lee Chin, 1978).

3.5.6 The Richmond Formation

The formation is a 500-1500 m thick succession of conglomerates, siltstones and shales of early Eocene age. It is transgressive over the Chepstow Limestone (Krijnen and Lee Chin, 1978).

3.5.7 The Bath-Dunrobin Formation

In the southeast of the Blue Mountain Inlier, in the Bath area, Krijnen and Lee Chin (1978) proposed that the Bellevue Formation was represented by a volcanic unit composed of spilitic basalts. Close to the top of the volcanic unit, finer grained, often un-fossiliferous calcareous sediments are present (Krijnen *et al.*, 1993). Krijnen and Lee Chin (1978) named this the Bath limestone, which they considered to be a lateral equivalent of the late Campanian Rio Grande Limestone Member.

Subsequent fieldwork in the area has demonstrated that the Bath limestone is in faulted contact with the volcanic rocks and no evidence can be found to indicate that the Bath and Rio Grande limestones are lateral equivalents (Simon Mitchell pers. comm. 2006). Additionally the Back Rio Grande Limestone is also represented in the region, but only as fault slices and is never seen in stratigraphic contact with the volcanic lavas, thus, preventing it from also being used to date the igneous rocks (Simon Mitchell pers. comm. 2006).

The volcanic unit was originally named the Bath Volcanics by Bateson (1974), and was then re-named the Dunrobin Volcanic member by Jackson and Smith, (1979) and Bath-Dunrobin Formation by Wadge and Draper, (1978). In this thesis the volcanics will be referred too as the "Bath-Dunrobin Formation" due to the name being consistently used since the late 1970's (Figs. 3.3 and 3.4).

The Bath Dunrobin Formation occurs as fault-bounded blocks within a 2-3 km wide fault zone, to the north of the sinistral Blue Mountains-Plantain Garden fault and covers an area of ~11 km^2 around Bath, and ~18 km^2 around Dunrobin hill (Wadge *et al.*, 1982) (Fig. 3.4).

The Wild Cane Complex occupies a fault bounded block in the middle of the Dunrobin area (Fig. 3.4). The complex consists of basalts, which are intruded by dolerites and gabbros and is considered to be the lowest stratigraphical section of the Bath-Dunrobin Formation (Fig. 3.4) (Wadge *et al.*, 1982).

The Bath-Dunrobin Formation consists of a thick sequence of late Cretaceous extrusive, tholeiitic, massive basalts, which are black or dark green when fresh and purple or brown when highly altered. The rocks are non-vesicular and aphyric. Pillow lavas occur, but are generally obscured by weathering; no sheeted dykes have been observed (Wadge and Draper, 1978; Wadge *et al.*, 1982). Some layers of red mudstone and chert occur inter-bedded with the basaltic lavas (Montgomery and Pessagno, 1999).

Horsfield and Roobol (1974) suggested that the Plantain Garden fault was responsible for bringing oceanic rocks to the surface; an idea which is supported by the study of Wadge *et al.* (1982) who showed that the Blue Mountain Inlier has a major positive Bouguer anomaly of 155 mgal. Wadge *et al.* (1982) suggest that the dense rocks that make up the Bath-Dunrobin Formation, and the metamorphic rocks along the Plantain Garden fault, are found at shallower depths to the north of the fault than to the south. Consequently, the Bath-Dunrobin Formation may represent an exhumed portion of dense oceanic material.

Low grade metamorphism and hydrothermal alteration has affected most of the formation; the secondary minerals present are calcite, chlorite, prehnite, quartz and zeolites. This alteration and spilitization has increased the volatile and sodium contents of the rocks (Wadge *et al.*, 1982), however, the immobile elements can still be used for classification.

It has been proposed on the basis of major elements and limited trace elements that the Bath-Dunrobin lavas display a MORB affinity (Jackson *et al.*, 1980; Jackson, 1987). However, others have argued that the geochemistry of the Bath-Dunrobin basalts is similar to DSDP Leg 15 basalts drilled in the Venezuelan basin (Wadge and Draper, 1978; Wadge *et al.*, 1982) and so are more likely to represent an accreted tectonic slice of the Caribbean oceanic plateau (Donnelly *et al.*, 1990; Kerr *et al.*,

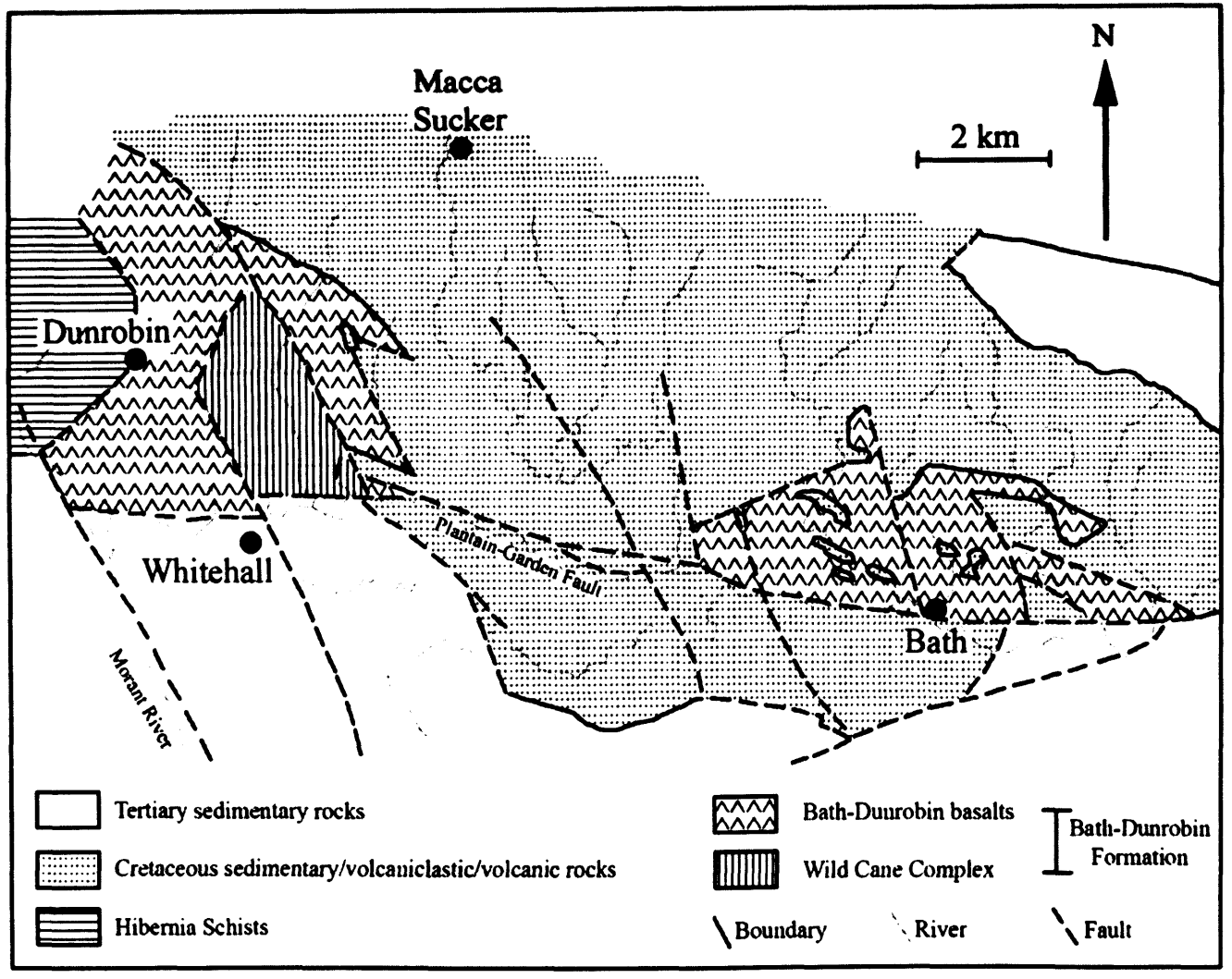

Figure 3.4 - Location of the Bath-Dunrobin Formation (modified from Wadge *et al.*, 1982).

2003). Consequently, the petrogenesis of the Bath-Dunrobin Formation remains unclear.

3.5.8 The age of the Bath-Dunrobin Formation

Previous work on the Blue Mountains (Krijnen and Lee Chin, 1978; Wadge and Draper, 1978), have interpreted the whole inlier in simplistic terms using two 'marker limestone' horizons: the Back Rio Grande Limestone and the Rio Grande Limestone (Fig. 3.3). The Back Rio Grande Limestone yields Campanian rudists (*Barrettia monilifera* Woodward) and foraminifers (*Pseudorbitoides trechamnni* Douvillé), whereas the Rio Grande limestone (supposedly equivalent to the 'Bath Limestone' of Krijnen and Lee Chin, 1978) yields Maastrichtian rudists (*Titanosarcolites*) (Krijnen and Lee Chin, 1978).

Krijnen and Lee Chin (1978) thought that these two limestones in the southern Blue Mountains bounded the Bath-Dunrobin Formation, and consequently interpreted the volcanic succession as being late Campanian in age and equivalent to the Bellevue Volcanics of the northeastern Blue Mountains (Fig. 3.3). More recently, Montgomery and Pessagno (1999) studied radiolarian assemblages from two samples (mudstones and cherts) collected in situ in the Bath area and found Late Turonian to Coniacian radiolarian assemblages. These results are clearly not in agreement.

A K-Ar age from a basalt collected from the Bath-Dunrobin Formation in the Island River near Bath gives an age of 47 ± 2 Ma (Wadge *et al.*, 1982). However, this age is likely to be unreliable due to the mobility of K during intense tropical weathering, hydrothermal alteration and low grade metamorphism.

Recent geological mapping has shed considerable light on the age and relationships of the Bath-Dunrobin lavas (Fig. 3.4). They occur as fault-bounded blocks within a 2-3 km- wide fault zone on the southern side of the Blue Mountain Inlier (Figs. 3.3 and 3.4). Boundaries between lithologies are invariably faulted, so that age relationships are difficult to ascertain. The Back Rio Grande Limestone is represented in the region, but only as fault slices and is never observed in stratigraphic contact with the Bath-Dunrobin lavas. All the available evidence points to the fact that the Back Rio Grande Limestone is considerably younger than the Bath-Dunrobin Formation. The 'Bath Limestone' is represented by a dense micritic limestone with stylolites and is completely devoid of fossils (see Krijnen *et al.*, 1993); it may have

normal stratigraphic contacts with the Bath-Dunrobin lavas, although most contacts appear faulted (Mitchell. pers. comm. 2006). The lack of fossils means that a correlation of the 'Bath Limestone' with the Rio Grande Limestone is unlikely. It is therefore clear that neither limestone aids in the age determination of the Bath-Dunrobin Formation.

The location of the radiolarian assemblage reported by Montgomery and Pessagno (1999) from Churchill's Vineyard was located in the field. It is clear that these radiolarians were not collected from the Wild Cane Complex of Wadge *et al.* (1978) as reported by Montgomery and Pessagno (1999), but from a thin sequence of inter-bedded red cherts and mudstones within the Bath-Dunrobin lava succession. The radiolarian assemblage from this level indicates a Middle Turonian to Late Coniacian age (92-86 Ma), similar to other samples within the area (Montgomery and Pessagno, 1999). The Bath-Dunrobin lavas, therefore, represent a Turonian-Coniacian suite of basaltic volcanics, and are significantly older that the basalts of the Bellevue Formation in the northern part of the inlier.

3.5.9 Summary of the Bath-Dunrobin Formation

The Turonian-Coniacian age and the possible similar geochemistry of the Bath-Dunrobin basalts to the plateau basalts in Curaçao, Aruba and drilled during DSDP Leg 15 in the Venezuela Basin, suggests that the Bath-Dunrobin Formation could be a tectonic slice from the Caribbean oceanic plateau (Wadge, 1982; Draper, 1986; Donnelly *et al.*, 1990; Lewis and Draper, 1990; Kerr *et al.* 2003). However, Jackson (1987) and Jackson *et al.* (1980) propose that the Bath-Dunrobin lavas have a MORB composition. Consequently, this project aims to perform a full geochemical study on the Bath-Dunrobin Formation to unequivocally determine the affinity of the basalts.

3.6 The Central Inlier

The Central Inlier is the second largest inlier of Cretaceous rocks in Jamaica, after the Blue Mountains, and is composed of lava flows, minor intrusives, extensive volcaniclastic sediments and carbonates (Fig. 3.5) (Mitchell and Blissett, 2001). The

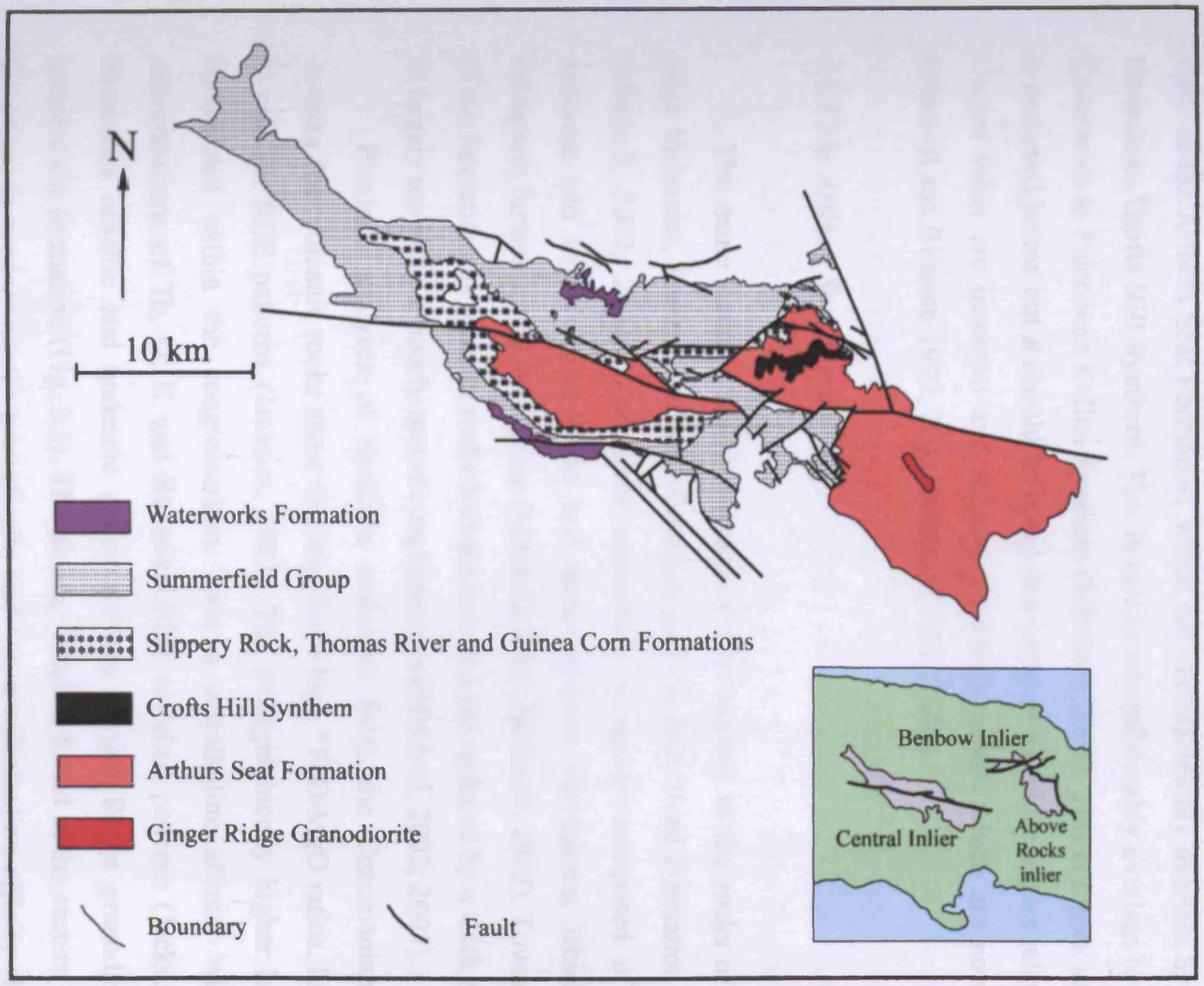

Figure 3.5 – Simple stratigraphic and structural geological map of the Central inlier (modified from Mitchell, 2002).

Central Inlier is the only inlier in Jamaica that has been mapped extensively and, as such, a detailed stratigraphy can be constructed based on palaeontological ages (Mitchell and Blissett, 1999; 2001; Mitchell, 2000; 2002; 2003). The igneous rocks in this inlier can also be placed within a temporal and spatial framework. The stratigraphy of the inlier can be split into three main blocks:

The oldest block is the lower/upper Cretaceous igneous and volcaniclastic rocks of the Arthurs Seat Formation, which are unconformably overlain by the upper Cretaceous Crofts Hill Synthem. This in turn is unconformably overlain by the upper Cretaceous to Paleocene Kellits Synthem (Mitchell, 2003). This complex stratigraphy is reviewed below but it should be noted that some of the older papers relating to the Central inlier are incorrect and refer to formation names which are now obsolete (Mitchell and Blissett, 1999; 2001; Mitchell, 2002; 2003).

3.6.1 The Arthurs Seat Formation

The name Arthurs Seat Formation is now applied to the rocks of the Main ridge Volcanics, Eastern Volcanic Complex and the Bull Head Formation (Fig. 3.5) (Mitchell, 2002; 2003). The lower succession is mainly composed of tholeiitic andesitic and basaltic lava flows and their intrusive equivalents, which become infrequent further up the succession (Mitchell, 2002; Mitchell, 2003). Towards the top of the formation the igneous rocks become rare and are replaced by a thick succession of largely un-bedded, poorly sorted conglomerates (Mitchell, 2002; 2003).

Previous analyses of tholeiitic andesites from the Cenomanian-Turonian Arthurs Seat volcanic rocks show that they have high *FeO/MgO ratios, low Th and U and flat REE patterns (Jackson, 1987). The stratigraphically higher lava flows, intercalated within the conglomerates, have a calcalkaline affinity with higher concentrations of Th, U, K and Rb and LREE enriched patterns (Jackson, 1987). Numerous basaltic and andesitic dykes and the Ginger Ridge granodiorite have intruded the formation (Fig. 3.5). The pluton, which is found in the eastern section of the inlier, is predominantly granodiorite and has a calcalkaline affinity (Isaacs and Jackson, 1987).

The overlying Peters Hill limestone yields Santonian (83 - 87.5 Ma) fossil ages and the Ginger Ridge granodiorite has a K-Ar isochron age of 85 ± 9 Ma (Turonian to Campanian) (Lewis *et al.*, 1972). The presence of an unconformity

between the Arthurs Seat Volcanics and the overlying material and the occurrence of dykes within the Arthurs Seat Formation and their absence in the overlying formations suggests a significant time gap with associated erosion (Fig. 3.5) (Mitchell and Blissett, 2001; Mitchell, 2002; 2003). Nevertheless, although there is an unconformity, and although the K-Ar may not be reliable due to element mobility, the Arthurs Seat Formation is tentatively attributed to the late Cretaceous.

3.6.2 Crofts Hill Synthem.

The Crofts Hill Synthem consists of three formations:

1. Peters Hill Formation – The formation rests unconformably on top of the conglomerates, andesites and basalts of the Arthurs Seat formation. It is 25 m thick and is composed of a lower conglomerate and an upper rudist-bearing limestone, which also contains echinoids and corals. The rudist bivalve *Barrettia coatesi* gives a late Santonian age for the formation (Mitchell, 2003).
2. Black River Formation – Rests conformably on the Peters Hill formation and consists of a coarsening upward sequence of mudstones to sandstones. The fossil rudist bivalves *I. balticus* and *I. balticus kunimiensis* suggest a Campanian age (Mitchell, 2003).
3. Dawburn Content Formation – Rests conformably on the Black River Formation and consists of a succession of alternating sandstones and shales. The top of the formation terminates against a thrust (Mitchell, 2003).

3.6.3 Kellits Synthem.

The Kellits Synthem consists of four formations:

1. Slippery Rock Formation – The formation is 150-175 m thick and rests unconformably on older Cretaceous rocks of the Arthurs Seat Formation and the Crofts Hill Synthem. It is predominantly composed of red/brown/grey conglomerates and sandstones in thick beds of tens of centimetres to several metres. The matrix-supported conglomerates are interpreted to be debris flow deposits whereas the clast supported conglomerates and sandstones are

thought to be braided stream deposits. The top of the succession is marked by marine rocks containing fossils which include bivalves, gastropods and trace fossils. The presence of Charophyte gyrogonites together with certain nannofossils suggests a Campanian to Maastrichtian age for the formation (Robinson, 1988; Mitchell and Blissett, 2001; Mitchell, 2000; 2002; 2003).

2. Thomas River Formation – The 175 m thick unit rests conformably on the Slippery Rock formation and is composed of distinctive thin beds of mudstone, sandstone and rare limestones. Maastrichtian fossils have been found in the grey mudstones, calcareous sandstones and limestones and include charophytes, rudist bivalves, gastropods, foraminifera and ostracods. Based on the fossil evidence the formation is interpreted as an estuary deposit with a number of marine transgressions (Mitchell, 2002; 2003).
3. Guinea Corn Formation – It is the main rudist bearing limestone in the late Cretaceous succession and is ~ 180 to 210 m thick. The lower part is composed of interbedded greenish-grey mudstone, siltstone and rubbly limestone, which is then succeeded by massive rubbly limestone with few siltstone layers. The upper part of the succession consists of mudstones with graded sandstones similar to the succeeding Green River Formation (Robinson, 1988; Mitchell, 2000; 2002; 2003). Fossils within the formation include rudist bivalves (*Praebarrettia, Bournonia, Biradiolites, Antillocaprina, Thyrastylon* and *Titanosarcolites*), other molluscs, corals, echinoids, foraminifera (*Kathina* and *Chubbina*) and ostracodes. These fossils, especially the rudists, suggest a late Maastrichtian age for the formation. (Robinson, 1988; Mitchell, 2000; 2002; 2003). The evolutionary change from *Bournonia cancellata* to *Bournonia barretti*, and the first appearance of *Biradiolites jamaicensis* are useful biostratigraphic markers of the Upper Maastrichtian (Mitchell, 2003). Underwood and Mitchell (2000) discovered the shark, *Serratolamna serrata*, and Steuber *et al.* (2002) used Sr-isotope geochronology, both of which also suggest a late Maastrichtian age for the Guinea Corn Formation.
4. The Summerfield Group – Originally this Group was mistakenly mapped as a formation due to the structural complexity within the area (Fig. 3.5) (Mitchell and Blissett, 2001). However, recent work in the region has enabled workers at the University of the West Indies to raise the Summerfield's status from

formation to group and recognise four distinct formations within it (Mitchell and Blissett, 1999; 2001 Mitchell, 2000; 2002; 2003). The four formations in the Summerfield group can be mapped from the north to the south of the anticlinal structure representing the Central inlier (Fig. 3.5) and include:

a) The Green River Formation – is composed of thinly-bedded (~ 40 cm), fine-coarse grained sandstones interbedded with mudstones. The formation is ~ 60 m thick and overlies the Guinea Corn and Slippery Rock Formations (Mitchell and Blissett, 1999; 2001; Mitchell, 2002; 2003).
b) The Peckham Formation – is ~ 150 m thick, sits conformably on the Green River Formation and is composed of massive sandstones with intercalated mudstones. (Mitchell and Blissett, 1999; 2001; Mitchell, 2002; 2003).
c) The Mahoe River Formation – is a succession of conglomerates and interbedded sandstones 210 m thick which lie conformably over the Peckham Formation (Mitchell and Blissett, 1999; 2001; Mitchell, 2002; 2003).
d) The Waterworks (Tuff) Formation – is composed of a hornblende pumice ignimbrite with mudrock accidentals and no associated fallout deposit. The ignimbrite is derived from a distant volcanic vent because there is a lack of lava flows associated with it. The andesitic accidental clasts are also well rounded suggesting that they have been transported for a considerable distance. Apart from the lower section, which shows some cross bedding, large scale ripples and dunes, the ignimbrite is massive (Mitchell and Blissett, 1999; 2001; Mitchell, 2002; 2003; Robinson, 1988). Ahmad *et al.* (1987a) obtained a fission track date of 55.3 ± 2.8 Ma from apatites separated from the ignimbrite giving the deposit a late Paleocene (55-65 Ma) age.

The Summerfield Group is interpreted as a shallowing upwards succession, passing from offshore, relatively deep water to shallow water marine (the Green River and Peckham Formations). This is subsequently overlain by terrestrial braided stream deposits (the Mahoe River Formation) (Mitchell, 2000). The succession is, therefore, interpreted as the progradation of a volcaniclastic apron around an active subaerial

volcanic cone with the Summerfield Group representing a distal rather than a proximal position on the volcanic apron (Mitchell, 2000).

3.6.4 The Yellow Limestone Group

This laterally extensive succession rests unconformably on the numerous Cretaceous and Tertiary formations of the Central inlier. Foraminiferal evidence shows that the base of the group was deposited in the lower middle Eocene (Robinson, 1988; Mitchell and Blissett, 1999; 2001; Mitchell, 2002; 2003).

3.6.5 Summary

The detailed stratigraphy that has been determined in the Central Inlier enables the volcanic and intrusive rocks of the Arthurs Seat Formation and the Waterworks Formation to be placed in their stratigraphic context (Fig. 3.5). A geochemical study of these igneous rocks is now required in order to determine their petrogenesis. A temporal study is important, especially in conjunction with future compositional data, since it will constrain the tholeiitic and calcalkaline chemical transition of any arc rocks and possibly shed new light on the timing of the subduction polarity reversal within the Caribbean region.

3.7 The Benbow Inlier

This inlier is small compared to the Central Inlier and only contains one succession of Cretaceous igneous rocks (the Devils Racecourse Formation) along with the small Flint River granodiorite (Burke *et al.*, 1969; Isaacs and Jackson, 1987). The Devils Racecourse Formation is considered to be the oldest sequence of igneous rocks on Jamaica. The formation can be dated using conformable overlying sedimentary sequences and inter-bedded limestones containing abundant Barremian and Aptian (125-113 Ma) rudists and Nerineid gastropods (Burke *et al.*, 1969). However, no absolute dating has been carried out on the Devils Racecourse lavas or the Flint River intrusion (Fig. 3.6). The northward dipping Cretaceous igneous and sedimentary rocks are stratigraphically conformable but the lower Eocene sediments unconformably overlie the Cretaceous rocks (Fig. 3.6 and Table 3.1) (Burke *et al.*, 1969).

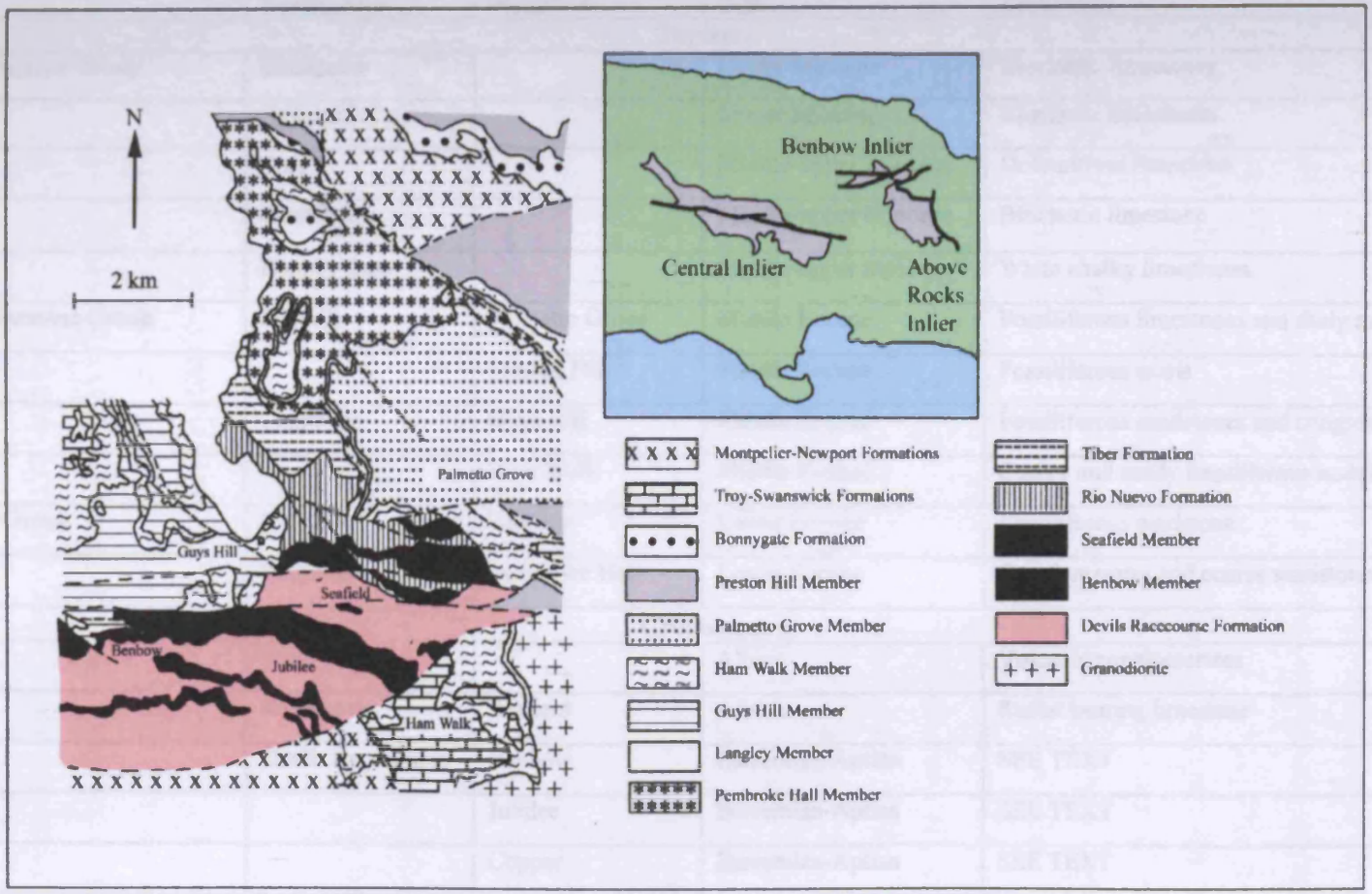

Figure 3.6 – Geological map of the Benbow Inlier (modified from Burke *et al.*, 1969).

Group	Formation	Member	Age	Lithology
Tertiary				
White Limestone Group	Montpelier		Lower Miocene	Bioclastic limestones
	Newport		Lower Miocene	Bioclastic limestones
	Troy		Middle-upper Miocene	Dolomitised limestone
	Swanswick		Middle-upper Miocene	Bioclastic limestone
	Bonney Gate		Middle-upper Miocene	White chalky limestones
Yellow Limestone Group	Fonthill	Palmetto Grove	Middle Eocene	Fossiliferous limestones and shaly marls
		Preston Hill	Middle Eocene	Fossiliferous marls
	Chapelton	Guys Hill	Middle Eocene	Fossiliferous sandstones and conglomerates
		Ham Walk	Middle Eocene	Clayey and sandy fossiliferous nodular limestone
Wagwater Group	Richmond	Langley	Lower Eocene	Fossiliferous mudstone
	Wagwater	Pembroke Hall	Lower Eocene	Conglomerates and coarse sandstones
Cretaceous				
	Tiber		Albian	Volcanic conglomerates
	Rio Nuevo	Seafield	Albian	Rudist bearing limestone
	Devils Racecourse	Benbow	Barremian-Aptian	SEE TEXT
		Jubilee	Barremian-Aptian	SEE TEXT
		Copper	Barremian-Aptian	SEE TEXT
		Phillipsburg	Barremian-Aptian	SEE TEXT

Table 3.1 – Stratigraphy and lithology of the Benbow Inlier (modified from Burke *et al.*, 1969).

The Devils Racecourse Formation is composed of ~1000 m of mafic and felsic lavas, volcaniclastics and four inter-bedded limestone members (Burke *et al.*, 1969). The oldest limestone member is the Copper member, although it is unclear whether the Phillipsburg limestone member is older or stratigraphically related to the Copper member (Fig. 3.6 and Table 3.1) (Burke *et al.*, 1969; Robinson *et al.*, 1971; Jackson and Smith, 1989). The next youngest is the Jubilee member and the top most unit is the Benbow member.

The Devils Racecourse Formation can therefore be split into lower, middle and upper units. The lower section lies below the Copper member, the middle section is between the Copper and the Benbow members and the upper unit is above the Benbow member (Burke *et al.*, 1969). The lower section is at least ~ 400 m thick; however, its base is not exposed. The rocks have been considerably altered with low grade regional metamorphism and an episode of hydrothermal alteration, which is confined to the rocks south of the Copper member (Burke *et al.*, 1969). The lower 300 m are fine-grained dark rocks, which display flow-banding in some sections indicating that they are flows and not intrusives. However, some of the rocks may be intrusive; the extensive weathering and vegetation cover makes identification difficult (Burke *et al.*, 1969). The top-most 100 m of the lower unit consists of volcanic conglomerates (Burke *et al.*, 1969; Robinson *et al.*, 1971).

The middle section consists of more volcaniclastic rocks inter-bedded with the Jubilee limestone. The upper Devils Racecourse is mostly composed of pillow lavas and rare volcaniclastic rocks (Roobol, 1972). Jackson (1987) and Donnelly *et al.* (1990) suggested that the lavas of the Devils Racecourse Formation evolve from a tholeiitic chemistry at the base to a calcalkaline composition in the lavas at the top of the sequence.

The Rio Nuevo Formation overlies the Devils Racecourse Formation; the contact is assumed to be conformable but this is not clear in the field. The formation consists of siltstones, shales and carbonates that have been heavily faulted. The fossil evidence in the Rio Nuevo gives an Albian age (Fig. 3.6) (Burke *et al.*, 1969).

The Flint River granodiorite intrudes the late Cretaceous rocks in the east of the inlier and like the other Cretaceous rocks it is also unconformably overlain by Eocene sediments (Fig. 3.6) (Burke *et al.*, 1969; Issacs and Jackson, 1987).

3.8 The Above Rocks Inlier

Covering an area of 118 km^2 the Above Rocks is one of the larger Cretaceous inliers in Jamaica and contains a sequence of sedimentary and volcanic rocks known as the Mt Charles and Border Volcanic Formations (Fig. 3.7) (Manning and McCain, 1989). The age of these formations is not known but Robinson (1994) suggests that they may be the oldest rocks in Jamaica and possibly be Valanginian (136-140 Ma) in age. This contradicts the majority of the work carried out on Jamaica that suggests that the Devils Racecourse Formation in the Benbow Inlier is the oldest (e.g. Donnelly *et al.*, 1990). In the late Cretaceous to early Paleocene these formations under went two episodes of intrusive activity, resulting in the emplacement of the Above Rocks granodiorite and its associated dykes (Jackson, 1987; Manning and McCain, 1989; Jackson *et al.*, 1998).

The oldest rocks in the inlier belong to the Cretaceous Mt Charles Formation. This formation is overlain by the Border Volcanic Formation (Manning and McCain, 1989). Most of the contacts are faulted however in the Lucky Hill area (Appendix A, Fig. A.1) the contact seems to be gradational indicating that the formations could be conformable. In the south, Tertiary limestones unconformably overlie the Cretaceous rocks in the inlier (Fig. 3.7) (Manning and McCain, 1989; Jackson *et al.*, 1998).

3.8.1 Mt Charles Formation

The formation consists of metamorphosed conglomerates, banded cherts and mudstones with intercalated andesitic tuffs and lavas, which dip to the west. Moderately good exposures are seen in-between Lucky Hill and Freetown (Appendix A, Fig. A.1) (Manning and McCain, 1989).

3.8.2 Border Volcanic Formation

The formation consists of andesitic lavas, tuffs, agglomerates, conglomerates, sandstones and siltstones, which again dip to the west. The volcanics are purple, porphyritic and aphanitic (aphyric) andesites (Manning and McCain, 1989).

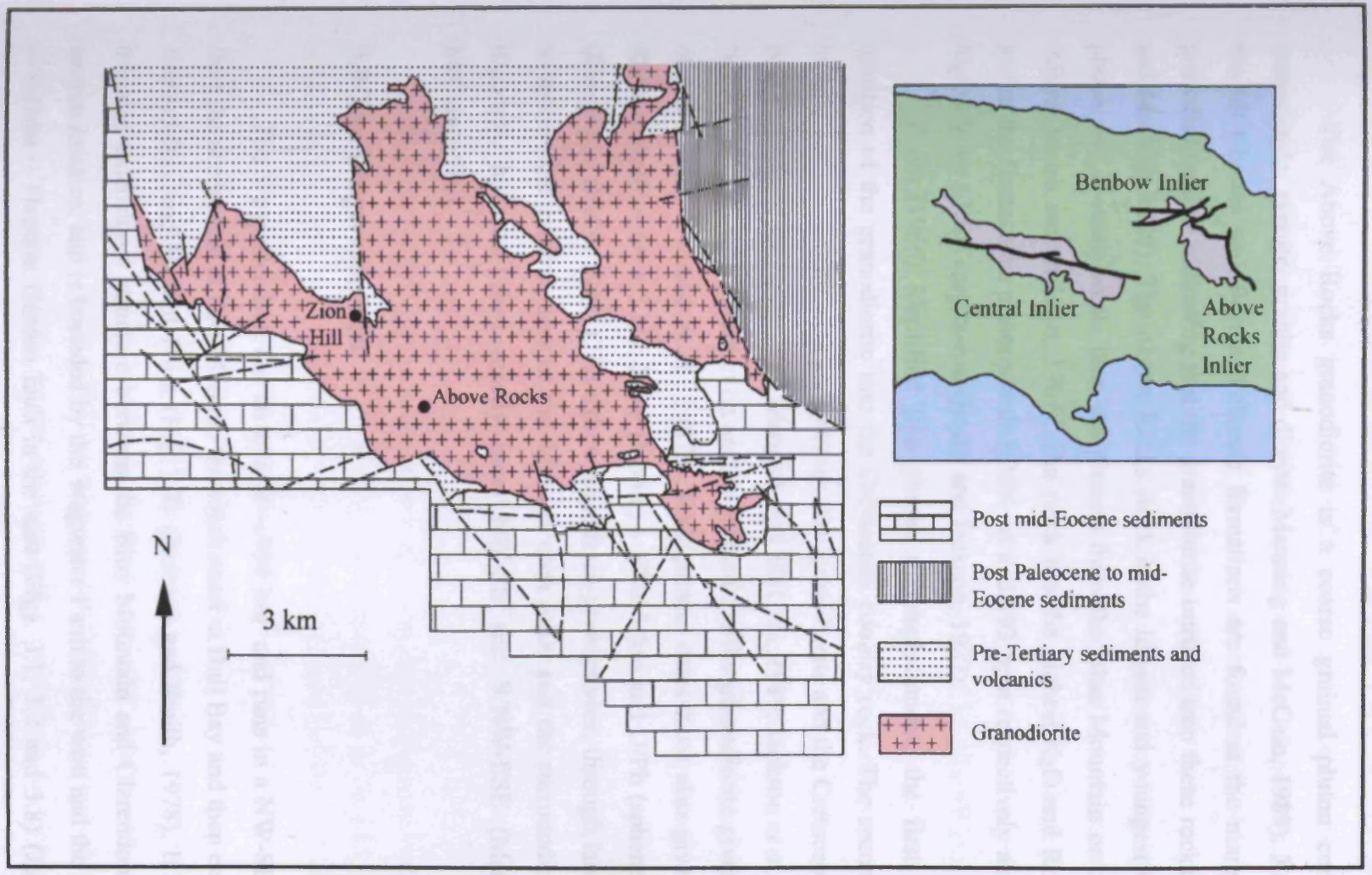

Figure 3.7 – Geological map of the Above Rocks Inlier (modified from Manning and McCain, 1989).

3.8.3 The Above Rocks Granodiorite

The Above Rocks granodiorite is a coarse grained pluton composed of granodiorite, syenite, granite and diorite (Manning and McCain, 1989). Xenoliths of the Mt Charles and Border Volcanic formations are found at the margins of the granodiorite, thus indicating that the granodiorite intruded into these rocks (Manning and McCain, 1989). The Above Rocks stock is the largest and youngest Cretaceous pluton and is more acidic than the plutons from the Blue Mountain or the Central inliers (Issacs and Jackson, 1987). The stock has the highest K_2O and Rb values of any of the Cretaceous plutons with 5.36% wt and 193 ppm respectively and has very high relative LREE enrichment (Issacs and Jackson, 1987).

Reed (1966) identified two phases of emplacement, the first being the intrusion of the granodiorite into the Cretaceous country rock. The second was the intrusion of numerous dykes and sills into the granodiorite and the Cretaceous country rock (Issacs and Jackson, 1987; Manning and McCain, 1989; Jackson *et al.*, 1998). A fission track age determination on apatite grains from the granodiorite gives an age of 60.4 ± 3.4 Ma (Ahmad *et al.*, 1987b). Radiometric dates have also given ages of: Rb/Sr (biotite) – 64 ± 5 Ma, K/Ar (biotite) – 67 ± 5 Ma and U/Pb (sphene) – 64 Ma (Chubb and Burke, 1963). The dykes range from granophyres, through lamprophyres to aplites. The relative ages of the dykes to each other and the surrounding rocks is uncertain, however, they mostly trend NW-SE and WNW-ESE (Manning and McCain, 1989).

3.9 The Wagwater Belt

The Wagwater Belt has an area of ~ 950 km^2 and runs in a NW-SE direction from the north coast at Port Maria to the south coast at Bull Bay and then eastwards to Holland Bay and Morant Point (Fig. 3.8) (Jackson and Smith, 1978). It is a fault-bounded extensional structure between the Blue Mountain and Clarendon blocks in eastern Jamaica, and is bounded by the Wagwater Fault to the west and the Silver Hill – Yallahs – Plantain Garden fault in the east (Figs. 3.1, 3.2 and 3.8) (Jackson and Smith, 1979; Jackson *et al.*, 1989).

Horsfield (1974) suggests that these faults became active in the early Tertiary and, during this period, downthrow on the Wagwater Fault was to the east and downthrow on the Yallahs-Plantain Garden Fault was to the south and west. On either side of these faults two Cretaceous blocks, represented by the Blue Mountains Block to the east and the Cornwall-Middlesex Block to the west, were uplifted and provided a sedimentary source to fill the newly formed basin (Fig. 3.8).

A sequence of approximately 3700 m of strongly folded and faulted Paleocene to lower Eocene sedimentary and volcanic rocks are exposed in the basin and make up the Wagwater group (Jackson and Smith, 1978). This group is separated into a lower, middle and an upper subgroup (Jackson and Smith, 1979). The lower and upper subgroups consist of sedimentary rocks only, whereas the middle subgroup contains sedimentary and volcanic rocks. The Wagwater group is overlain by the mid-Eocene Yellow and White limestone Groups to the north and south respectively (Jackson and Smith, 1979).

The middle subgroup contains the Halberstadt and Newcastle Volcanic Formations that only occur in the northern and central portions of the Wagwater belt (Fig. 3.8). The Halberstadt volcanics are composed of extrusive basalts and spilites and the Newcastle volcanics consist of extrusive dacites, quartz keratophyres and associated pyroclastic rocks (Jackson and Smith, 1978; 1979; Jackson *et al.*, 1989; Jackson and Scott, 1997). The Halberstadt Volcanics have a smaller volume than the Newcastle volcanics. Roobol (1972) proposed that the Halberstadt lavas erupted under 300 m of water.

The spilites and quartz keratophyres are the metasomatized equivalents of the basalts and dacites respectively. Hydrothermal fluids enriched in Na and CO_2 and at temperatures below 400°C converted the high temperature primary minerals of the basalts and dacites into low temperature alteration minerals (e.g. clay minerals) (Jackson and Smith, 1978; 1979; Jackson *et al.*, 1989).

Both the basalts and the dacites are subalkaline but they do not belong to the same volcanic series. The basalts are tholeiitic and the dacites are calcalkaline (Jackson and Smith, 1978; 1979; Jackson *et al.*, 1989). The geochemistry of the Halberstadt basalts is similar to that of the tholeiitic rocks from the Colombia River Basalts and the Deccan Traps with LREE enrichment and similar Ti – Zr – Y concentrations (Jackson and Smith, 1978; 1979). However, more recently, it has been

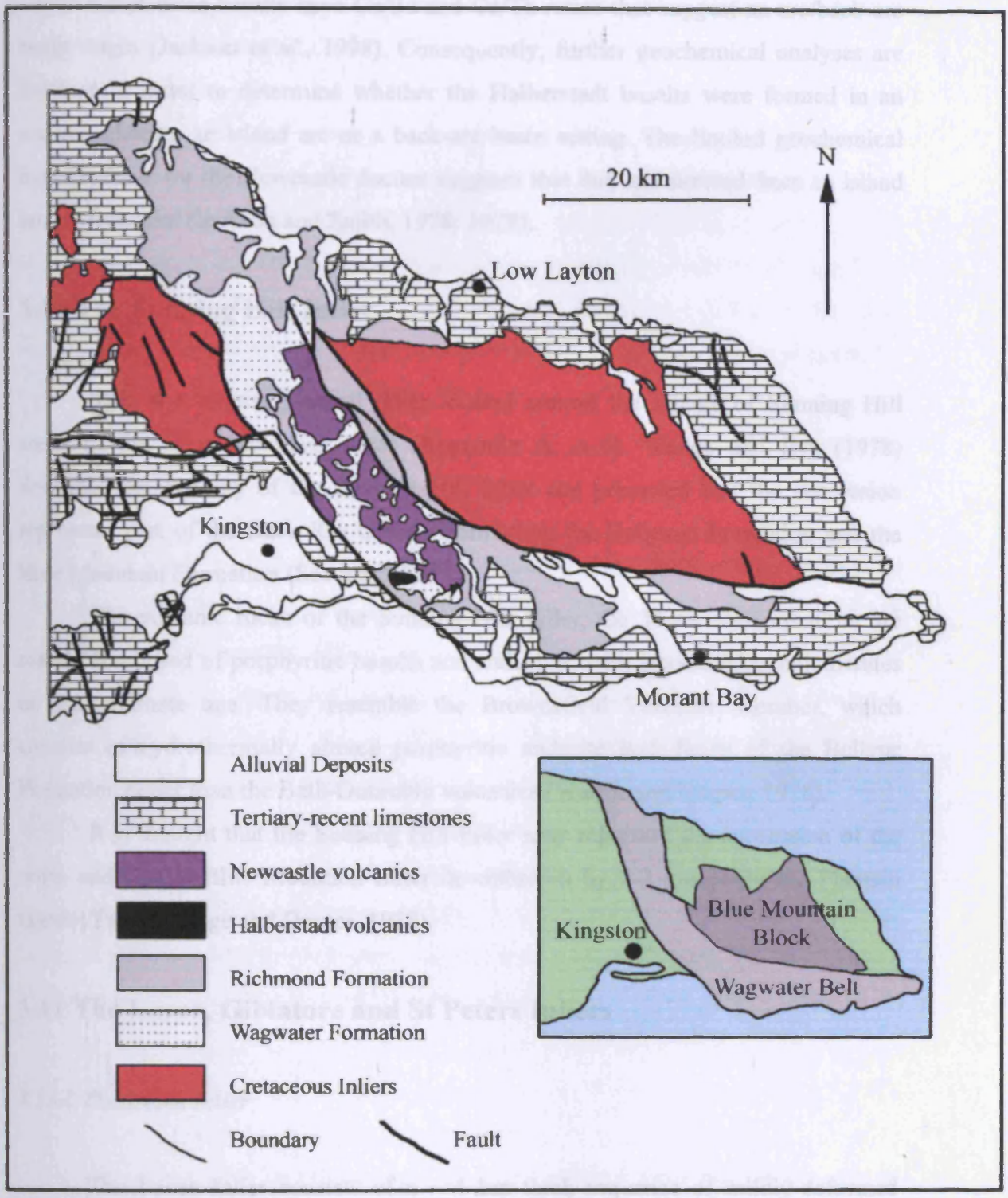

Figure 3.8 – Geological map of the Wagwater Basin (modified from Jackson and Smith, 1978).

reported that these basalts have Ce/Ba and Ce/Th ratios that suggest an arc/back-arc basin origin (Jackson *et al.*, 1998). Consequently, further geochemical analyses are required in order to determine whether the Halberstadt basalts were formed in an oceanic plateau, an island arc or a back-arc basin setting. The limited geochemical data available for the Newcastle dacites suggests that they are derived from an island arc environment (Jackson and Smith, 1978; 1979).

3.10 The Sunning Hill Inlier

This is a relatively small inlier located around the village of Sunning Hill south of the Blue Mountain Inlier (Appendix A, A.4). Wadge and Eva (1978) described the geology of the Sunning Hill inlier and proposed that the succession represents part of the Back Rio Grande Formation, the Bellevue Formation and the Blue Mountain Formation (Section 3.5).

The volcanic rocks of the Sunning Hill Inlier, the Thornton Formation, are mainly composed of porphyritic basalts and andesites, with associated conglomerates of indeterminate age. They resemble the Brownsfield Volcanic Member, which consists of h ydrothermally altered porphyritic andesite lava flows of the Bellvue Formation rather than the Bath-Dunrobin volcanics (Wadge and Draper, 1978).

It is thought that the Sunning Hill Inlier may represent the succession of the north and central Blue Mountain Inlier downthrown by 2-3 km along the Plantain Garden Fault (Wadge and Draper, 1978).

3.11 The Lucea, Giblatore and St Peters Inliers

3.11.1 The Lucea Inlier

The Lucea Inlier consists of a ~ 4 km thick sequence of mildly-deformed volcaniclastic sediments and limestones of Santonian to Campanian age (Delong *et al.*, 1983; Schmidt, 1988). The inlier also has a small number of igneous sills, dykes and lava flows (Delong *et al.*, 1983; Schmidt, 1988). In addition, the conglomerates can contain a significant number of mafic to acidic igneous clasts (Delong *et al.*, 1983; Schmidt, 1988). A limited geochemical study by Delong *et al.* (1983) proposed

that the igneous rocks have an island arc affinity; however, the rocks require further investigation to confirm this finding.

3.11.2 The Giblatore Inlier

The small Giblatore Inlier lies between the Central and Above Rocks Inliers (Fig. 3.1). Little is known about this inlier; however, Jackson *et al.* (1989) noted that Campanian-Maastrichtian age basaltic, andesitic and dacitic lava flows can be found in the inlier. Analysis of an andesite lava flow from the Giblatore Inlier suggested a calcalkaline island arc affinity (Jackson, 1987).

3.11.3 The St. Peter's Inlier

The rocks around St. Peter's were mapped as part of a Basal Complex (Jackson, 1985). The Complex is a ~ 5.5 km long lenticular body, which is located in the Wagwater Belt between Tertiary strata (Fig. 3.2). In 1974 the basal complex was renamed "the Green Volcanics" and was thought to be Cretaceous in age (Jackson, 1985). The rocks in the St. Peter's Inlier include basalts, felsic volcanics, diorites, sandstones, mudstones and re-crystallised limestones. The basalts have a fine grained aphyric texture and have been significantly altered (Jackson, 1985).

Preliminary geochemical data suggests that the basalts at St. Peter's belong to the Halberstadt Volcanic Formation (Jackson, 1985). Consequently, the igneous rocks in the St Peter's Inlier may represent a melange of rocks belonging to the Wagwater Group which have been altered and mylonitized along the Yallahs fault?

3.12 Low Layton

A small section of pillow lavas and hyaloclastites have been discovered at Low Layton, which is located on the northeast coast of Jamaica (Fig. 3.8) (Jackson, 1987). The section is thought to be an uplifted submarine volcano which erupted along a series of ENE trending fissures above the trace of the E-W trending Duanvale fault zone (Fig. 3.2). The lavas have been interpreted as intra-plate alkali basalts of

Miocene age (Wadge and Wooden, 1982; Jackson, 1987). The lavas have high alkali, P_2O_5, Rb and Ba contents and low Y/Nb ratios (Jackson, 1987).

Similar rocks to these have been discovered on a small seamount in the Jamaica Passage which is located to the east of Jamaica (Roobol and Horsfield, 1976). These rocks lie to the north of an offshore extension of the Plantain Garden fault. Both the Duanvale and Plantain Garden fault zones are Cenozoic and are related to the opening of the Cayman Trough to the north.

3.13 Associated metamorphic rocks

Metamorphic rocks are found adjacent to the north and south of the Silver Hill – Yallahs – Plantain Garden fault (Fig. 3.3). To the south the Westphalia Schists display amphibolite facies metamorphism, while to the north the Hibernia schists have blueschist and greenschist facies mineralogies (Jackson and Smith, 1979; Draper, 1986). A third group of metamorphic rocks known as the Green Bay schists are found in the Kingston area and are similar in character and mineralogy to the Westphalia schists (Fig. 3.3) (Jackson and Smith, 1979; Draper, 1986).

The Hibernia schists are ultramafic to mafic in composition whereas the Westphalia schists are dominantly intermediate (Draper, 1986). The Hibernia schists, when plotted on a total alkali silica (TAS) diagram show tholeiitic affinities whereas the Westphalia schists are more calcalkaline in nature (Draper, 1986). Nevertheless, although the chemistry is unreliable, due to element mobility with metamorphism, Draper (1986) suggested an ocean floor affinity for the Hibernia schists.

The Westphalia schists are thought to be derived from a sedimentary or volcaniclastic protolith of lavas and sedimentary rocks (Draper, 1986). The calcalkaline affinity of the schist could suggest that it is a metamorphic product of the dacites and sediments found within the Wagwater basin. However, this theory is complicated by the fact that a study of the closure temperature of hornblende within the schist gives an age of ~ 76.5 Ma (Draper, 1986); therefore, the rocks would have been buried before this time. The schists were exhumed at ~ 65 Ma as they are overlain by the Paleocene Black Limestone Formation (Draper, 1986). This is supported with closure temperature studies of biotites giving an age of ~ 50 Ma (Draper, 1986).

Together with the 65 Ma exhumation age it would have taken 20 to 75 Ma (assuming 0.14 to 0.04 cm/yr erosion rates) to exhume the schists. Therefore the rocks could be up to ~ 85 – 140 Ma, thus suggesting that the volcanic rocks that make up the schist are Cretaceous arc rocks and not metamorphic equivalents of the younger Tertiary dacites (Jackson and Smith, 1979; Draper, 1986). The Westphalia schists have typical amphibolite facies mineralogy. The amphibolite metamorphism is thought to have been formed by local compressional tectonics due to the Yallahs-Blue Mountain faults representing a restraining bend. (Jackson and Smith 1979; Draper, 1986; Mitchell, 2003).

The greenschist portion of the Hibernia schist is interpreted to be a section of metasedimentary rocks, whereas the blueschists are thought to be metabasic rocks from an obducted ophiolite that has been exhumed by normal faulting in the Wagwater belt (Draper, 1986).

The Bath-Dunrobin Formation (with a possible plateau affinity) and the blueschists have a very similar chemistry (Draper, 1986). Consequently, the Hibernia schist could represent a metamorphosed, exhumed portion of oceanic plateau material.

3.14 Summary

1. Jamaica is situated on the northern Caribbean plate margin with the Cayman trough to the north and the Nicaraguan Rise to the south.
2. Two thirds of Jamaica is covered with Tertiary limestone that overlies Cretaceous volcanic and sedimentary rocks. The island can be divided into two major structural blocks. The main block encompasses most of the island, is located to the west and is known as the Cornwall – Middlesex Block. To the east lies the smaller Blue Mountain Block that is separated from the latter by the fault bounded Wagwater basin. The lower lying Cornwall – Middlesex block can be further subdivided into an eastern shelf area, the Clarendon block and the western Hanover block. These are separated from each other by another graben structure known as the Montpelier- Newmarket Zone.
3. The Bath-Dunrobin Formation (Blue Mountains Inlier) is a thick sequence of late Cretaceous tholeiitic basalts with a controversial affinity. It has been

suggested that the basalts have a plateau (Kerr *et al.*, 2003) or a MORB origin (Jackson, 1987).

4. The Central inlier contains the Cenomanian-Turonian island arc Arthurs Seat Formation and the Ginger Ridge granodiorite. It has been proposed that the lower volcanics have tholeiitic characteristics and the upper lavas have calcalkaline affinities.
5. The Benbow inlier consists of the Barremian-Aptian Devils Racecourse arc lavas and the Flint River granodiorite. Inter-bedded limestone members clearly constrain the age of the Devils Racecourse Formation. The lavas are thought to have a tholeiitic and calcalkaline affinity.
6. The Mt Charles Formation, the Border Volcanic Formation and the Above Rocks granodiorite are the igneous rocks found within the Above Rocks inlier. The Mt Charles and Border Volcanic Formations are composed of sedimentary and volcanic successions with an indeterminate age and composition.
7. The Wagwater Belt is a fault-bounded extensional structure between the Blue Mountain and Clarendon blocks in east Jamaica. A sequence of Paleocene to lower Eocene sedimentary and volcanic rocks, which are exposed in the basin, make up the Wagwater group. The volcanics are separated into the Newcastle and Halberstadt Formations. The Halberstadt volcanics are composed of extrusive basalts and spilites and the Newcastle volcanics consist of extrusive dacites, quartz keratophyres and associated pyroclastic rocks. The origin of both the Newcastle and Halberstadt volcanics is unclear.
8. The small Sunning Hill Inlier exposes porphyritic basalts and andesites whose tectonic affinity is also unknown.
9. Mafic island arc lavas have been identified in the Lucea Inlier but more analyses are needed to determine the petrogenesis of the lavas. Similarly more analyses and field mapping need to be completed in the Giblatore Inlier and especially the St. Peter's inlier to deduce whether the St. Peter's lavas are related to the Halberstadt volcanics.
10. The Westphalia schists are thought to be derived from a sedimentary or volcaniclastic protolith. The Hibernia schists have a blueschist and greenschist facies. The greenschist portion of the Hibernia schist is interpreted to be a section of metasedimentary rocks, where as the blueschists are thought to be

metabasic rocks from an obducted ophiolite that has been exhumed by normal faulting in the Wagwater belt.

Chapter 4

Field geology and petrography of the Jamaican igneous rocks

4.1 Introduction

Approximately 3 months of fieldwork were completed in Jamaica during two field seasons in the summer of 2004 and 2005. Fieldwork was conducted with the assistance of members of the Department of Geography and Geology at the University of the West Indies (UWI). The UWI provided crucial logistical support and access to recent stratigraphical maps of Jamaica.

The objectives of the fieldwork were to identify igneous rocks in the Cretaceous inliers and the Tertiary Wagwater belt and subsequently determine their identity and petrogenesis. These findings would be combined with present geological information on the Caribbean region to study the evolution of the Caribbean island arcs and the Caribbean oceanic plateau from the early Cretaceous. These objectives would be achieved through the following specific aims:

- Investigate the Cretaceous inliers, where igneous rocks have been reported, and the Tertiary Wagwater belt to locate the igneous rocks.
- Carry out extensive sampling of the igneous rocks so they can be subsequently analysed to determine their identity, petrogenesis and age.
- Use field relationships and previous palaeontological and stratigraphical work to back up the radiometric ages.

Stratigraphical information, provided by UWI, was used to help locate the igneous rocks. This was often difficult due to (a) the difficulty in identifying altered igneous rocks, (b) the fact that many of the ordinance survey and geological maps are not accurate and (c) the general lack of geological mapping carried out in Jamaica. Moreover, it was beyond the scope of this study to undertake detailed mapping of the Cretaceous inliers due to their large size (e.g. the Central inlier is larger than the islands of Bonaire and Aruba, Dutch Antilles). Consequently, igneous rocks were located using available published geological maps and limited small scale mapping along with locality information from UWI staff (mainly Dr Simon Mitchell).

4.1.1 Problems in the field

There are a number of problems associated with fieldwork in tropical climates, which had to be overcome, mainly related to the extent of chemical weathering. Many of the sedimentary and igneous rocks have been altered due to intense tropical weathering and hydrothermal and metamorphic processes. The least-altered igneous rocks can be easily identified, but when the surrounding sedimentary (predominantly limestone) and igneous rocks have been substantially altered they can be difficult to distinguish from one another in the field unless the limestone is fossiliferous.

It was noted that altered igneous rocks are more resistant to weathering than limestones and, as such, when they are heavily altered they have an orange "sandstone appearance" whereas the limestones have a "grey/orange conglomerate appearance". Other sedimentary rocks, e.g. sandstones and shales, are easily identified by the presence of bedding and sedimentary structures. Some igneous rock outcrops were relatively fresh and volcanic structures such as pillow lavas could be readily observed, however, subsequent petrographic analysis found that these rocks were still substantially altered. Nevertheless, it was the igneous rocks from these relatively fresh outcrops that were sampled and analysed.

Fieldwork and sampling was also hampered by a lack of outcrop (Fig. 4.1 and 4.2). The Cretaceous inliers and Tertiary Wagwater Belt of Jamaica consist of many high mountains and are mostly covered with dense tropical forests (e.g. Blue Mountain Peak in the Blue Mountains inlier is 2254 m high) (Fig. 4.1). The density of the vegetation resulted in most outcrops being found along road cuttings and river

beds (Fig. 4.2). These outcrops are often small and can only be traced laterally, with any degree of confidence, with detailed mapping. Cannabis plantations in the Jamaican interior meant that certain outcrops along river banks and off road were inaccessible. Farmers drying and preparing their "harvest" on the river banks meant that outcrops in that immediate area were sometimes not accessible (Fig. 4.2).

Fieldwork was also disrupted by the weather. A small number of tropical storms and hurricanes prevented fieldwork on a number of occasions. Five days were to be spent collecting igneous rocks in the western Lucea Inlier, however, tropical storms brought down a large number of power lines and trees thus blocking and flooding most of the roads. After three days of flooding, fieldwork in the Lucea Inlier was abandoned (Fig. 4.1). Hurricane Emily on the 17th July, 2005 caused a huge amount of damage to infrastructure in eastern Jamaica. Large landslides covered many outcrops and washed away numerous bridges and sections of road thus preventing access to some important igneous outcrops (Fig. 4.1). One objective in the 2005 field season was to sample more of the oceanic plateau rocks found in the Bath-Dunrobin Formation, however, Emily washed away the roads on the mountains leading to the outcrop, consequently, no further samples of the Bath-Dunrobin Formation could be collected (Fig. 4.1).

4.1.2 Alteration of the igneous rocks

Many outcrops (~ 90%) in the Cretaceous inliers and in the Wagwater belt consist of substantially altered igneous rocks. It is clear from petrography that they have been highly altered by tropical weathering and hydrothermal and metamorphic processes. Tropical weathering chemically alters rocks at a faster rate than weathering in temperate climates (Summerfield, 1997). In temperate climates carbonic acid is the main reactant; however, in humid tropical climates the amount of water available for weathering is higher, this results in the production of silicic acids (Summerfield, 1997). Larger amounts of vegetation contribute organic acids, and when these acids are combined with carbonic acid, silicic acid and higher temperatures, it leads to intense tropical weathering (Summerfield, 1997).

Chemically, elements that are readily mobilised during weathering and

Figure 4.1 – (a) Tropical storm over the Central Inlier; (b) Landslide in the Central Inlier caused by a tropical storm, such landslides cover outcrops (c-d) Roads were washed away by torrential rain brought by hurricane Emily on the 17th July, 2005. These two examples were found whilst attempting to reach outcrops of the Bath-Dunrobin Formation in 2005; (e) Most of the interior of the island is made up of dense forests and hills; (f) On foot it is apparent how thick the vegetation can be in many places.

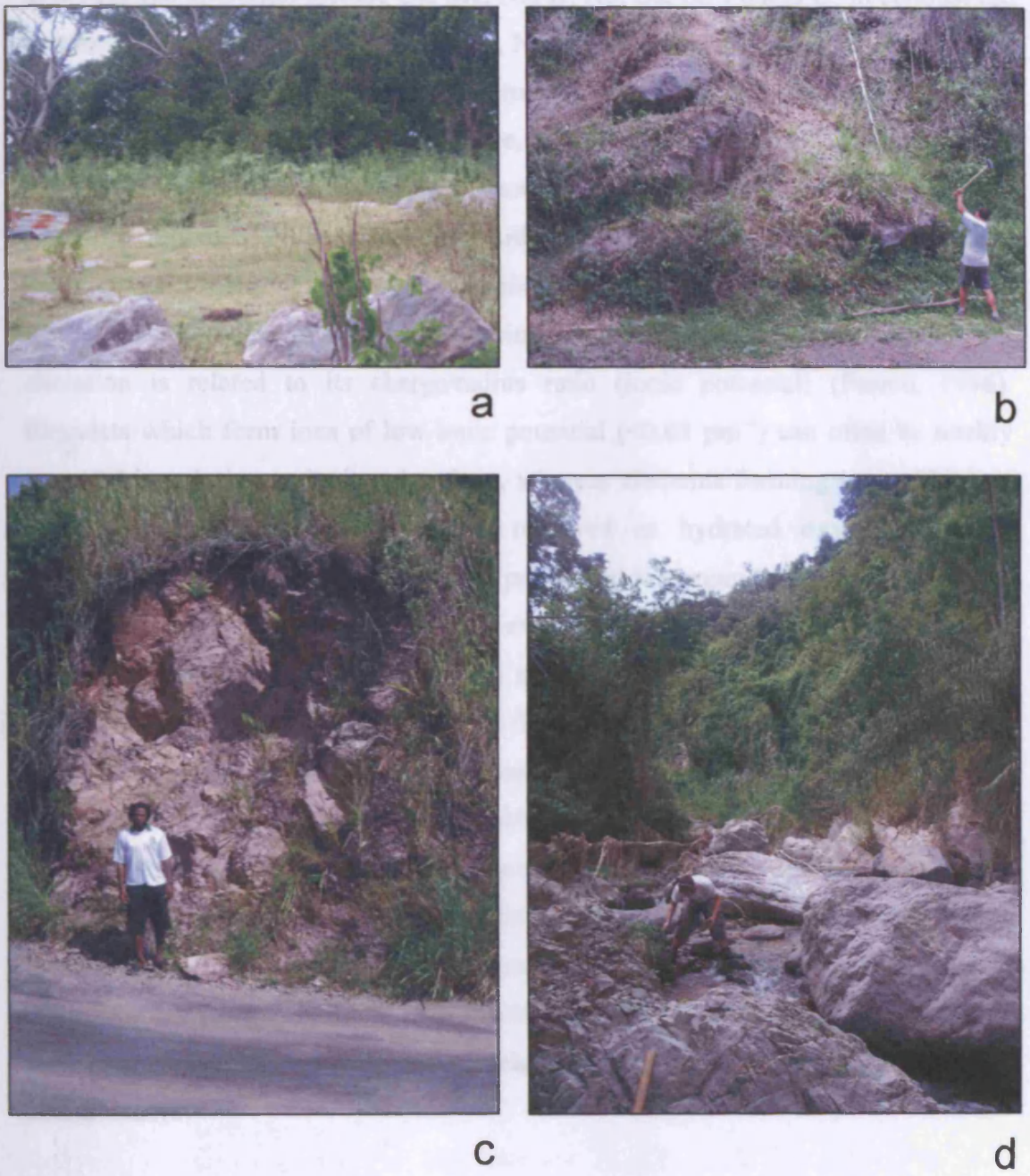

Figure 4.2 – (a) Illegal cannabis plantation near Dry Hill, Central Inlier; (b-c) examples of outcrop found along road cuttings; (b) is an exposure of the Waterworks ignimbrite on the road between Ritchies and Coffee Piece, Central Inlier; (c) is an exposure of the upper Devils Racecourse Formation on the road between Golden Grove and Top Hill, Benbow Inlier; (d) Collecting lava samples in a river section near Connors, Central Inlier.

hydrothermal alteration include Ca, Mg, Na, K, Rb, Ba, Sr, Pb and U. In contrast the elements Zr, Hf, Nb, Ta, Y, Ti, Cr, Co, P, Ni, the Rare Earth Elements (REE), Th, Ga and Sc are considered to be relatively immobile (Floyd and Winchester, 1975, 1978; Winchester and Floyd, 1976, 1977; Pearce, 1982, 1996; Arculus, 1987; Summerfield, 1997; Polat *et al.*, 2002). The order of mobility from most mobile to least mobile is generally regarded to be Large Ion Lithophile Elements (LILE) > Rare Earth Elements REE > High Field Strength Elements (HFSE) (Arculus, 1987).

The behaviour of an element during subaerial weathering and hydrothermal alteration is related to its charge/radius ratio (ionic potential) (Pearce, 1996). Elements which form ions of low ionic potential (<0.03 pm^{-1}) can often be readily removed in solution as hydrated cations, whereas elements forming ions of highest ionic potential (>0.10 pm^{-1}) can be removed as hydrated oxyions. Ions of intermediate ionic potential (0.03 – 0.10 pm^{-1}) tend to remain in the solid product of weathering and are usually immobile even at greenschist grade metamorphism (Pearce, 1996). Recent experiments also show that this may be true for submarine weathering as well, however a change in fluid composition from H_2O-rich to a CO_2- or SiO_2- rich partial melt and/or an increase in temperature, may mobilise otherwise immobile elements (McCulloch and Gamble, 1991; Pearce, 1996).

Therefore, humid tropical weathering combined with hydrothermal alteration and metamorphic processes has substantially altered igneous rocks in Jamaica which leads to problems of (1) identifying them in the field (Section 4.1.1), (2) locating fresh samples for geochemical and geochronological analysis and (3) determining their petrogenesis due to many mobile elements and oxides being used in igneous classification.

4.2 Sample localities, field geology and petrography

4.2.1 Classification by a mineral mode analysis

The primary method of classifying both plutonic and volcanic igneous rocks is based upon their mineral modal proportions. Unfortunately the igneous rocks collected in this study have all suffered variable degrees of alteration. The alteration has resulted in the primary mineralogy in all the samples being partially replaced by

secondary minerals such as clays, sericite, chlorite, epidote, pumpellyite, calcite and quartz. Consequently, these rocks can not be classified based on their mineral proportions. This change in mineralogy has also altered the chemistry of the rocks, thus preventing a normative classification to be obtained. The following sections summarise the main petrographic features of each of the sample groups; however, a more comprehensive thin section description of each sample can be found in Table A.1 of Appendix A. The classification of the igneous rocks is based on immobile element geochemical criteria, which are described in Chapter 6 and 7.

4.2.2 The Central Inlier

4.2.2.1 Sampling and field observations

Recent stratigraphical mapping of the Central Inlier located many outcrops of igneous rock (e.g. Mitchell and Blissett, 1999; 2001; Mitchell, 2002; 2003). As a result, 80 samples were collected from the Arthurs Seat Formation, the Ginger Ridge granodiorite and the Waterworks Formation. AHCI01-08, 10, 11, 14-37, 39-60, 62-80 were collected from the Arthurs Seat Formation, AHCI61 is a sample from the Ginger Ridge granodiorite and AHCI09, 09a, 12, 13 and 38 are ignimbrite samples from the Waterworks Formation. Although the mapping of the inlier is quite detailed, the upper and lower sections of the Arthurs Seat Formation have only been identified in a number of localities. The igneous rocks in the Thomas River and Crooked River section are part of the lower and upper Arthurs Seat Formation respectively (Fig. A.5, Appendix A). The position of the other igneous rocks in the stratigraphic sequence is unknown; e.g. the lavas around Connors and Dry Hill (Fig. A.5, Appendix A).

The igneous rocks of the Arthurs Seat are, petrographically, highly variable and the reader is directed to Table A.1, Appendix A for a detailed analysis of many of the collected samples. In general, the igneous rocks of the Arthurs Seat Formation are lavas or dykes, are phyric and aphyric and have basaltic to dacitic compositions. Although most of the outcrops are not identifiable as dykes or flows, because of the intense weathering and heavy vegetation cover. Nevertheless, in a few cases field relations and igneous structures are well developed (Fig. 4.3 and 4.4). AHCI14 is an excellent example of a cross cutting dyke with abundant internal vesicles. Other

examples of cross cutting dykes include: AHCI10-12a, 16, 18, 21, 23, 25, 27, 29 and 44 (Fig. 4.4). Most of these dykes are found in the Thomas River section (Figs A.5 and A.6, Appendix A) and can be seen cross-cutting a large body of fine grained mafic/intermediate igneous rock. The dykes can be spilt into two groups, a mafic group that trends NW-SE and a felsic group that trends N/NE-S/SW (Fig. 4.4). At the western end of the Thomas River section there is a complex interaction of igneous rock (Fig. A.6) where samples AHCI45, 47-54 were collected. Various contacts and chilled margins can be seen, however, the contacts do not seem to be continuous and this, coupled with the heavily eroded nature of the rock, meant that the structure of the area is still unclear.

AHCI33 and AHCI72 are the only igneous rocks found during this study in the Central Inlier that have vesicles and amygdales on their upper surface, thus suggesting that they are flows and not intrusives (Fig. 4.4). The only pillow lavas discovered in the Central Inlier were found on Dry Hill (AHCI76-78) (Fig. 4.3). The pillows are badly weathered and can be identified on the southern slope of the hill (Fig. A.5).

The Ginger Ridge granodiorite has been altered to such a degree that the rocks at some of the outcrops have been completely replaced by clay minerals. AHCI61 was from one of the few relatively fresher outcrops and is the only sample to be collected. The ignimbrite outcrops, which make up the Waterworks Formation, were all relatively fresh but were mostly concealed by large amounts of vegetation (Fig. 4.2). The ignimbrites are massive and contain abundant pumice and accidental fragments. The pumice represents the juvenile material and it is these pumice that were drilled-out and geochemically analysed.

4.2.2.2 Petrographic observations

In thin section, the Arthurs Seat lavas and dykes are basaltic to dacitic, phyric or aphyric and are composed of a variety of minerals which have been variably altered to secondary minerals; the most altered samples have not been considered for analysis (Fig. 4.5) (Table A.1, Appendix A). The Ginger Ridge sample is a coarse grained plagioclase-hornblende adcumulate with sericite, chlorite and pumpellyite alteration.

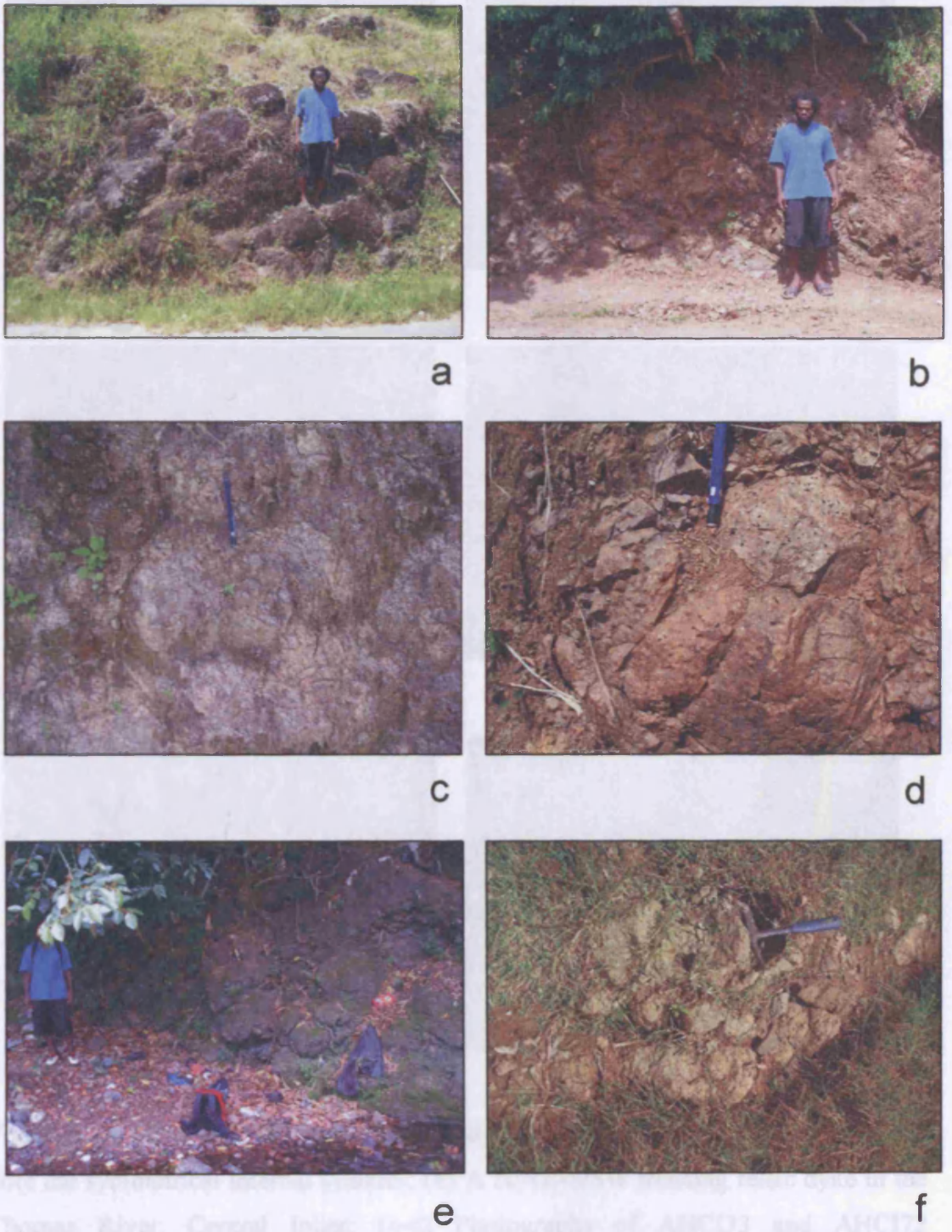

Figure 4.3 – Examples of pillow lavas found in Jamaica; (a-d) The upper Devils Racecourse Formation along the road around Golden Grove, Benbow Inlier; (e) Pillow lavas found in the Island River whilst sampling the Bath-Dunrobin Formation, Blue Mountain Inlier; (f) Pillow structures on the southern slope of Dry Hill, Central Inlier.

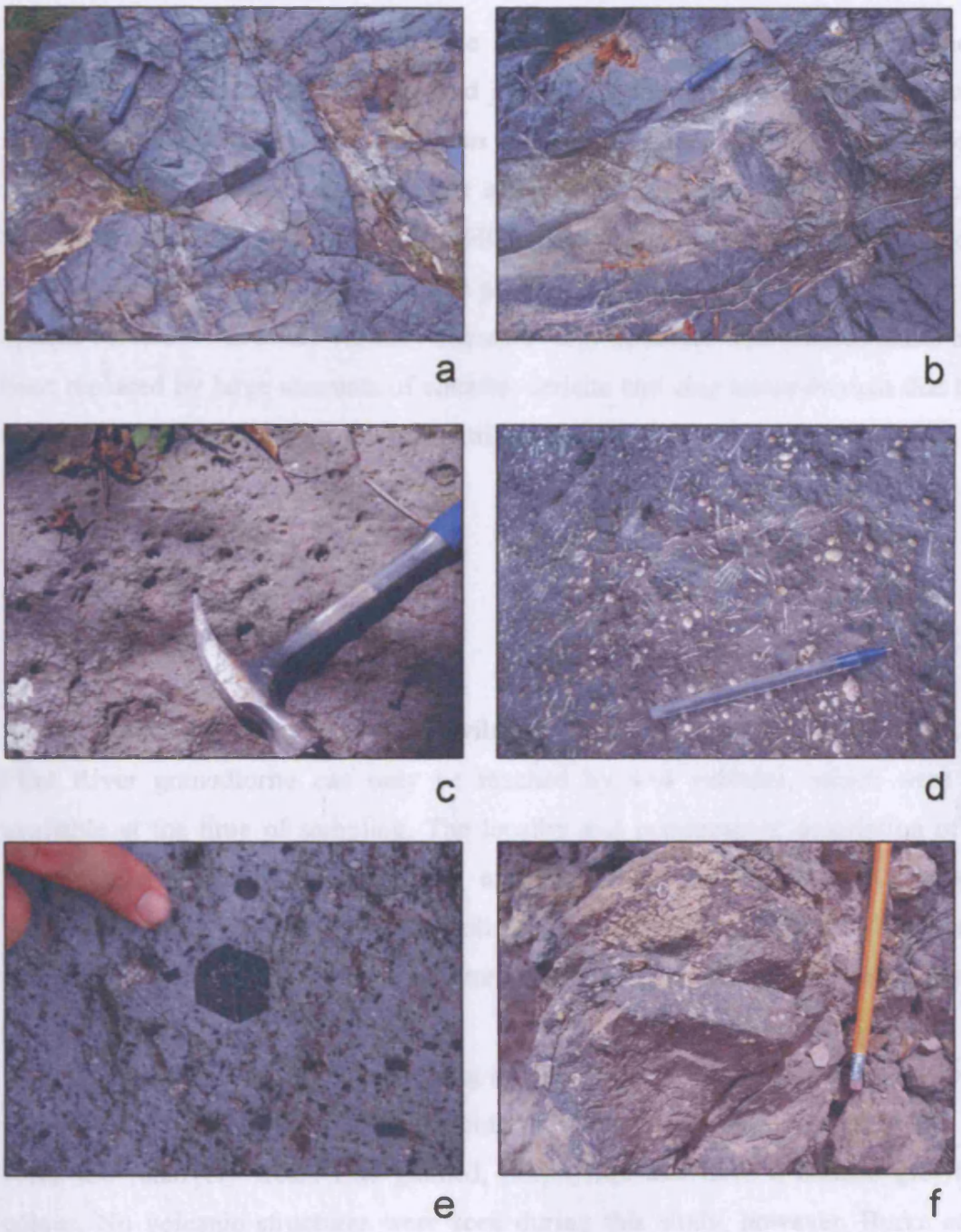

Figure 4.4 – (a) A NW-SE trending mafic dyke in the Thomas River, Central Inlier, note the symmetrical internal vesicles; (b) A N/NE-S/SW trending felsic dyke in the Thomas River, Central Inlier; (c-d) Photographs of AHCI33 and AHCI72 respectively showing their upper surface vesicles and amygdales. Note that AHCI72 also contains large feldspar phenocrysts; (e) Large amphibole phenocrysts in AHCI10 further demonstrating that although the majority of igneous rocks are badly weathered, some are still relatively fresh; (f) Amygdales in the Halberstadt lavas in Bito Quarry.

In thin section fresh ignimbrite samples have isotropic pumice fragments surrounded by abundant accidental and juvenile phenocrysts/rock fragments and a similarly isotropic matrix with a fibrous fabric. The samples from the Waterworks Formation differ from fresh ignimbrite samples because they have been subject to tropical weathering. In thin section, AHCI09, 09a, 12, 13 and 38 are composed of pumice fragments, lithic fragments and plagioclase feldspar, quartz, hornblende and opaque minerals which are variably altered to clay minerals. The pumice clasts have been replaced by large amounts of chlorite, sericite and clay minerals such that they can be easily distinguished from the matrix (Fig. 4.6).

4.2.3 The Benbow Inlier

4.2.3.1 Sampling and field observations

Within this inlier only the Devils Racecourse Formation was sampled, the Flint River granodiorite can only be reached by 4×4 vehicles, which were un-available at the time of sampling. The locality and petrographic description of the samples can be found in Table A.1 and Figure A.3 of Appendix A. Samples AHBI01-07 and AHBI16-30 were collected from the lower Devils Racecourse Formation, whereas AHBI09-15 are from the upper Devils Racecourse Formation (Section 3.6, Chapter 3).

AHBI01-07 were collected along the Devils Racecourse road where the lower Devils Racecourse Formation is represented by 5-8 m tall cliffs of igneous rock. The rocks are relatively fresh, fine grained, porphyritic and have a darkish grey/blue colour. No volcanic structures were seen during this study, however, Burke *et al.* (1965) described flow banding from these rocks and proposed that they are lava flows. Conversely, flow banding can also develop in sills and dykes (Kerr, pers. comm. 2006).

AHBI16-30 were collected from outcrops that were substantially altered and/or mostly covered with vegetation. It is assumed that they represent laterally equivalent outcrops to the lavas along the Devils Racecourse road (Fig. A.3). The rocks are fine grained, mostly porphyritic and have a darkish blue/grey/brown colour

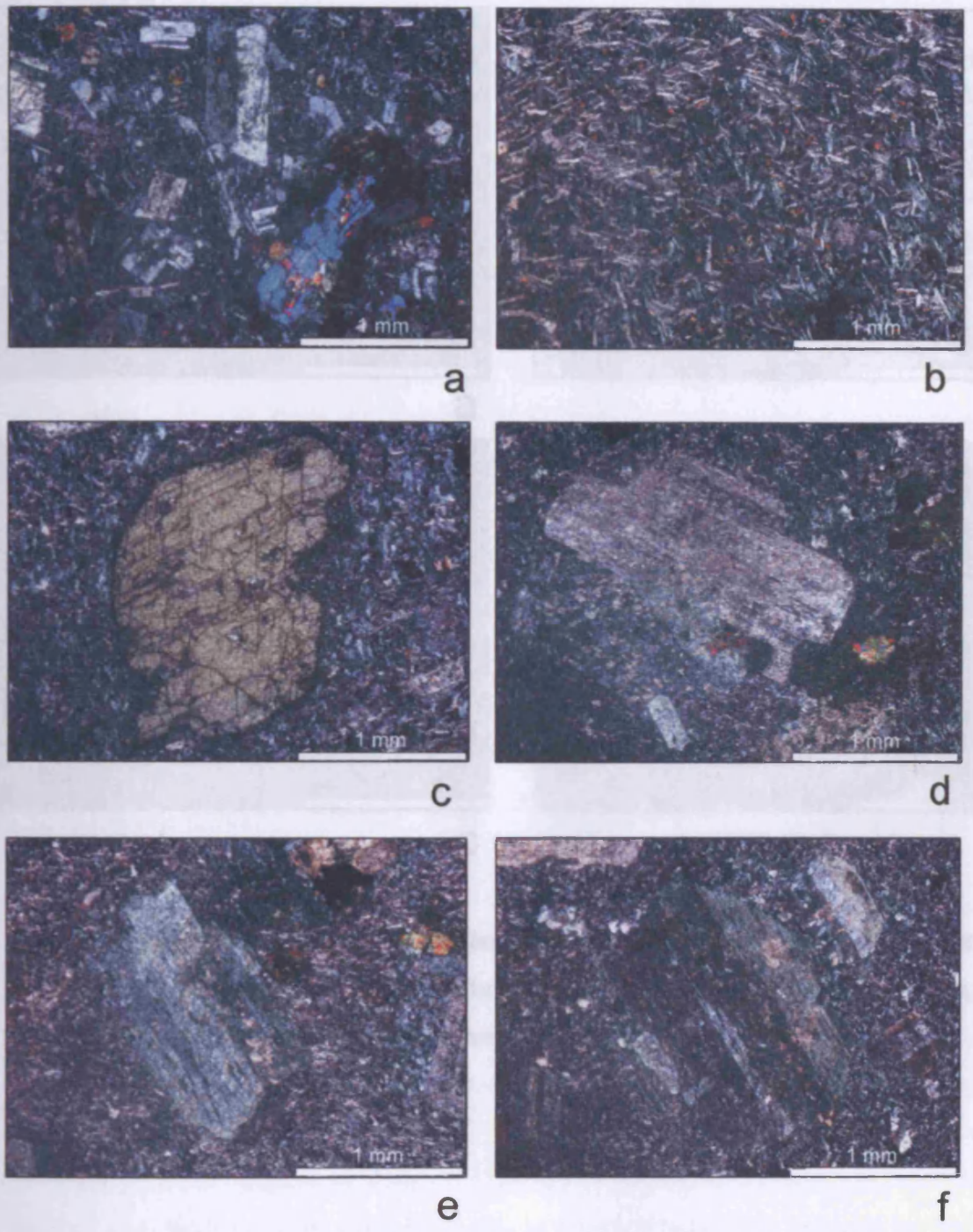

Figure 4.5 – (a-b) Photomicrographs from the Central Inlier igneous rocks showing typical textures. (a) Sample AHCI37 with phenocrysts of K-feldspar, plagioclase feldspar, biotite and clinopyroxene (blue birefringence); (b) Sample AHCI21 is aphyric and composed of aligned plagioclase feldspar and clinopyroxene; (c) AHCI10 showing a large amphibole phenocryst; (d-f) AHCI28-AHCI30 respectively showing the common replacement of plagioclase feldspar with sericite, chlorite and epidote.

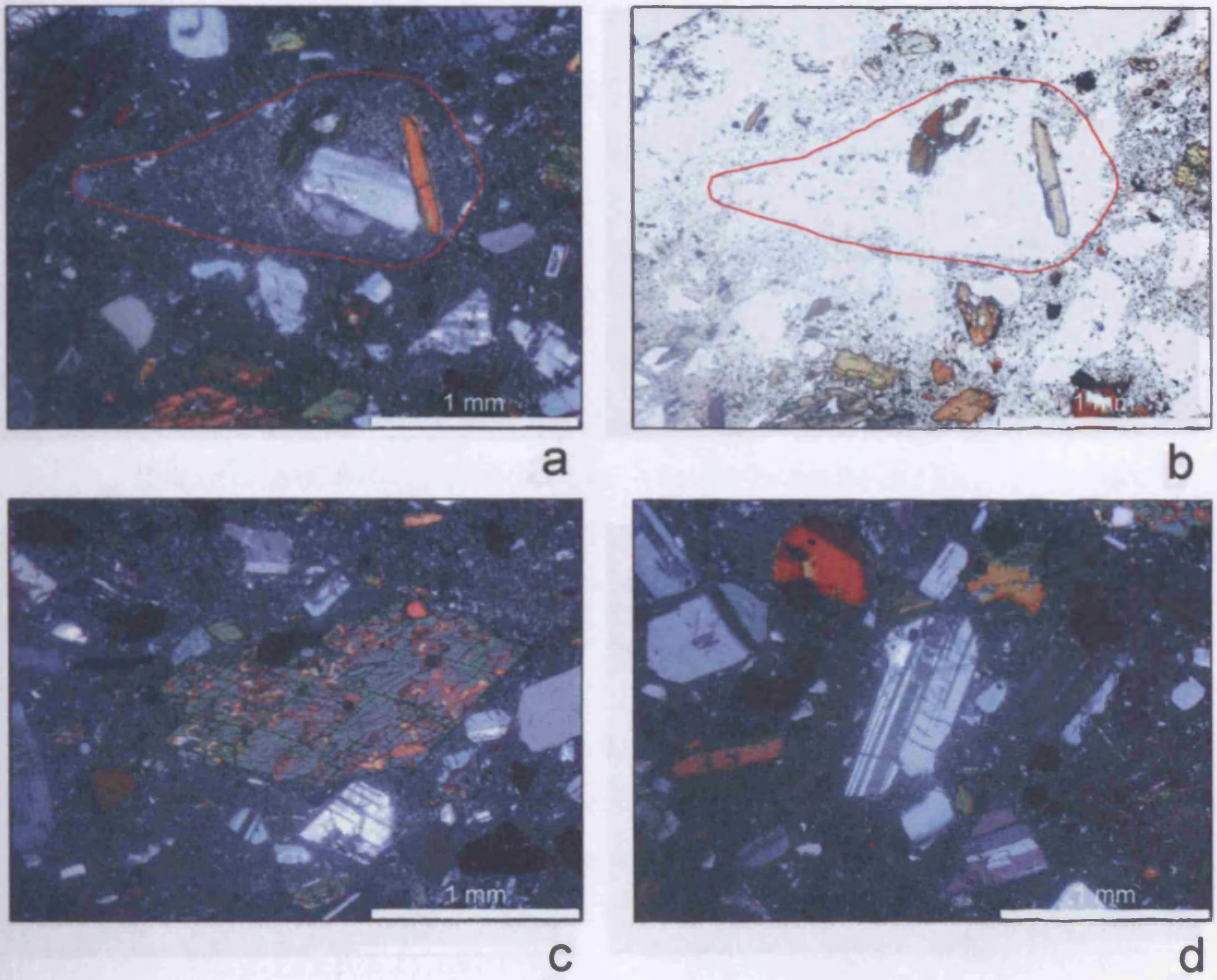

Figure 4.6 – (a-b) Cross polarised and plane polarised images of a pumice fragment in AHCI09. The red outline marks its boundary; (c-d) Show the feldspar, quartz, amphibole and opaque crystals in the altered glassy matrix of AHCI09.

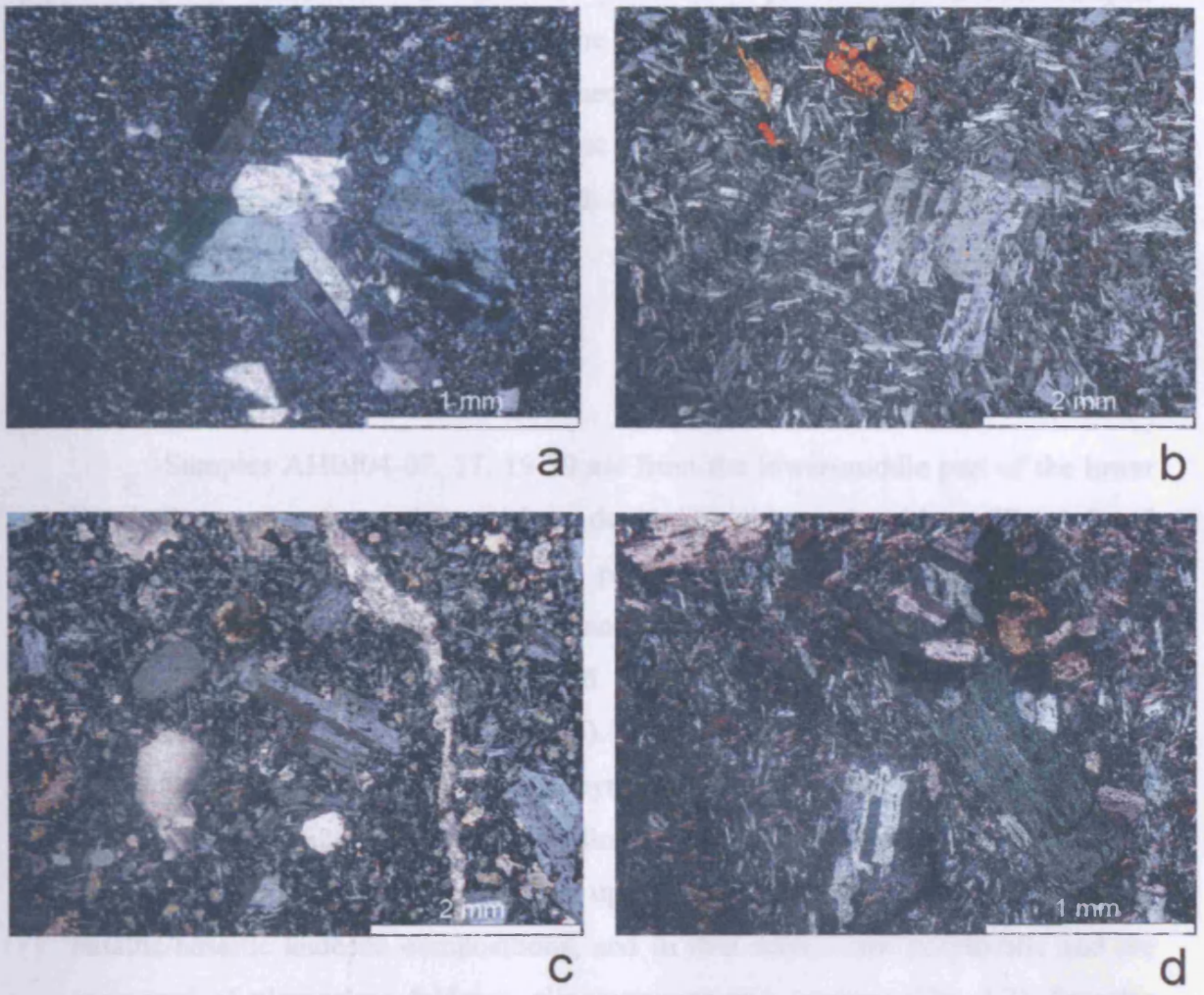

Figure 4.7 – (a) Cross polarised photomicrograph of AHBI05 showing the relatively fresh feldspar phenocrysts set in a feldspar, quartz and opaque groundmass; (b) AHBI01 showing feldspar and clinopyroxene phenocrysts in a groundmass of feldspar, clinopyroxene and opaques; (c) AHBI10 (upper Devils Racecourse pillow lava) composed of plagioclase feldspar phenocrysts that are within a groundmass of feldspar and opaques. Most of the minerals in the rock have been replaced by clay minerals, sericite, chlorite and calcite; (d) AHBI19 is a lava from the more altered lower Devils Racecourse section to the west of the Devils Racecourse road. The rock is porphyritic with phenocrysts of plagioclase feldspar and K-feldspar set in a groundmass of feldspars, quartz and opaques.

which occasionally has a green tint because of the presence of chlorite. Samples AHBI09-15 were collected from near the village of Golden Grove where the upper Devils Racecourse Formation is composed of vesicular pillow lavas, thus indicating that the igneous rocks are lava flows that erupted in a submarine environment (Fig. 4.3). The lavas are substantially altered, fine grained, porphyritic and have a dark grey/brown colour.

4.2.3.2 Petrographic observations

Samples AHBI04-07, 17, 19-30 are from the lower-middle part of the lower Devils Racecourse Formation and have dacitic/rhyolitic compositions (Fig. A.3 and Chapter 6). In thin section they are phyric or aphyric and are composed of plagioclase feldspar, K-feldspar, quartz and opaques (Fig. 4.7). The uppermost lavas in the lower section, AHBI01, 03, 16 and 18, have basaltic andesite/andesitic compositions (Fig. A.3 and Chapter 6). In thin section they are phyric and are composed of plagioclase feldspar, clinopyroxene and opaques (Fig. 4.7). AHBI09-15 were sampled from the interior of the pillow lavas due to the rims being very heavily weathered (Fig. 4.3 and A.3). The upper Devils Racecourse lavas all have basaltic/basaltic andesite compositions, and in thin section are porphyritic and are composed of plagioclase feldspar, clinopyroxene and opaques (Fig. 4.7). Samples AHBI12-15 contain fine needle shaped opaques in the groundmass.

All of the Devils Racecourse samples have been altered by weathering, hydrothermal and low grade regional metamorphic processes. The grade of alteration varies with individual samples (Table A.1, Appendix A). However, the primary mineralogy of all the rocks has been partially or extensively replaced with secondary minerals such as sericite, chlorite, epidote, calcite and clay minerals (Fig. 4.7).

4.2.4 The Above Rocks Inlier

4.2.4.1 Sampling and field observations

Samples were collected from the Above Rocks granodiorite (AHAR01-03, 05-11), the xenoliths in the granodiorite (AHAR04 and 12), the Mt Charles Formation (AHAR13 and 19) and the Border Volcanic Formation (AHAR14-18). All

but one of the granodiorite samples were collected along the well exposed river section from Zion Hill to St Faiths (Fig. A.1, Appendix A). The granodiorite is not layered and does not appear to be a cumulate. Sedimentary structures, occasionally visible in large plutons, are also absent. Shear zones through the pluton are occasionally seen and are the site of chalcopyrite mineralisation.

At Zion Hill the granodiorite is coarse grained, massive and has abundant xenoliths, however, it then grades into a medium grained massive porphyritic granodiorite before grading back into a massive coarse grained rock towards St Faiths (Fig. 4.8). The mineralogy (Table A.1, Appendix A.1) and the geochemistry (Chapter 6) of all the granodiorite samples are very similar and thus the change in grain size is not a result of mixing/mingling of differing magma or a residual late-stage fluid.

It is possible that a portion of the surrounding Mt Charles or Border Volcanic Formations may have been faulted into the region and that the medium grained samples (AHAR07-10) may be rocks from one of these volcanic formations. This is not thought to be the case because, as mentioned above, the medium grained samples have the same mineralogy as the coarse granodiorite e.g. biotite, amphibole, K-feldspar, plagioclase feldspar and quartz. Conversely the volcanic rocks are made up of plagioclase feldspar and opaques and only a few samples have either amphibole or biotite (Fig. 4.8). The medium grained granodiorite samples also have a more enriched geochemistry than the volcanic rocks (Chapter 6). Consequently, the geochemical and mineralogical similarity of the medium grained samples to the coarse grained pluton suggests that the former may represent the chilled margin of the Above Rocks granodiorite.

With regard to the xenoliths, AHAR04 was collected under Zion Bridge and AHAR12 was collected near St Faiths along the river section (Fig. A.1). The Mt Charles and Border Volcanic lavas were collected north of Glengoffe, around Brainard and at Cavalier. Outcrop for both of the volcanic formations was very limited. Figure A.2 shows a detailed map of where AHAR13-15 were collected, however, the outcrop in the area is nearly non-existent and it is questionable how Manning and McCain (1989) managed to produce such a detailed map. Exposure from Brainard to Platfield was adequate, although many outcrops are substantially altered; consequently, only 3 samples (AHAR16-18) were collected.

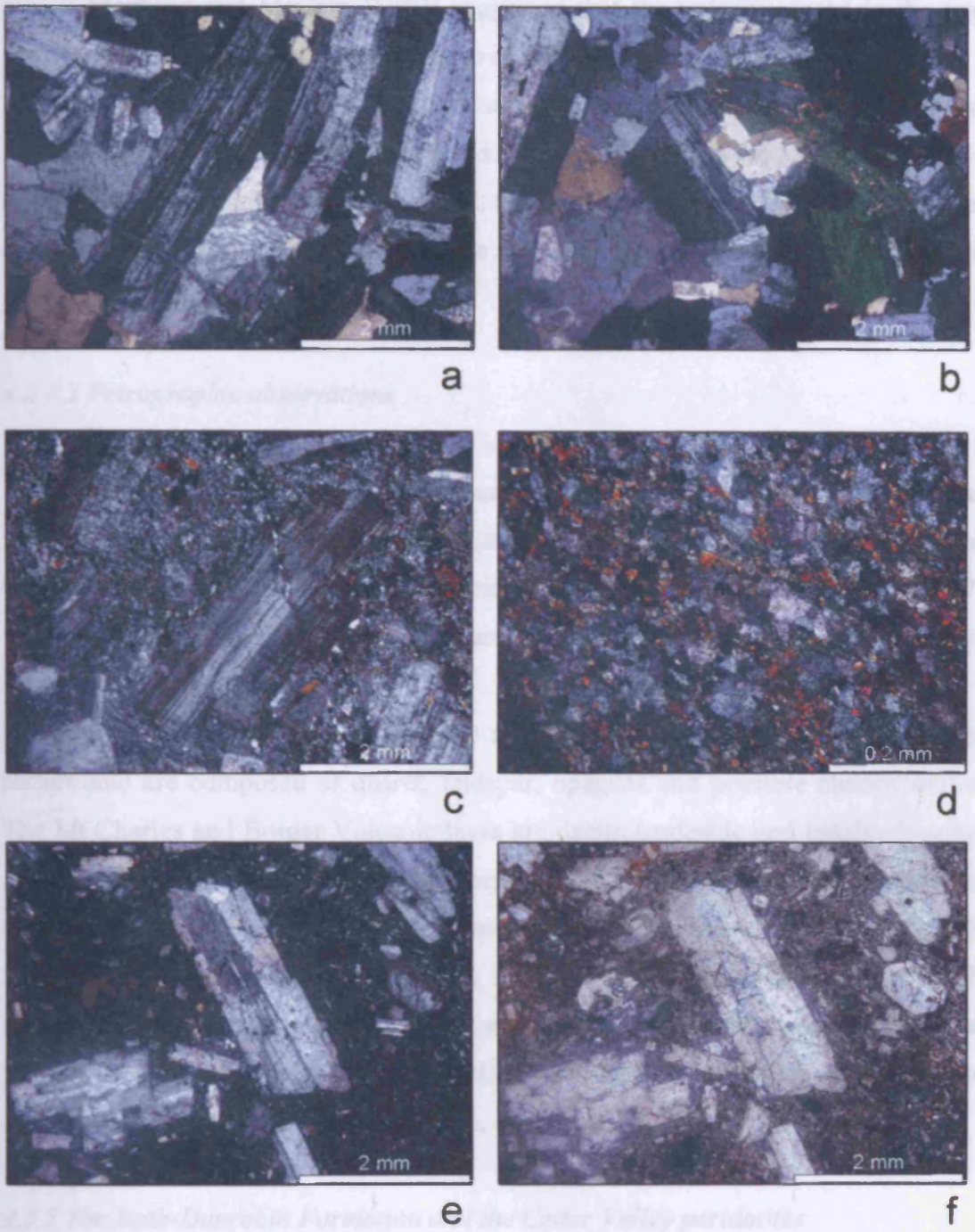

Figure 4.8 – (a-b) Cross polarised photomicrographs of AHAR02 showing examples of the coarse grained granodiorite, composed of plagioclase feldspar, K-feldspar, biotite mica, hornblende, quartz and opaques; (c) AHAR10 showing an example of the porphyritic granodiorite; (d) Xenolith with a seriate texture of quartz, feldspar, opagues and clinopyroxene?; (e-f) Cross and plane polarised images of AHAR14 (Border lava) showing that the lava is porphyritic and is moderately altered. The groundmass is composed of a significant amount of clay minerals and sericite.

Manning and McCain (1989) suggested that the volcanic rocks in the two formations were lavas due to the presence of aligned plagioclase phenocryst flow textures. Unfortunately, no flow structures were discovered during this study, nevertheless, these rocks are considered to be lavas based on the fieldwork by Manning and McCain (1989). In the field, the lavas of the Mt Charles and the Border formations are substantially altered, fine grained, porphyritic and range in colour from dark brown/grey to light blue/grey.

4.2.4.2 Petrographic observations

In thin section, the granodiorite samples are composed of quartz, plagioclase feldspar, K-feldspar (sometimes microcline), amphibole, biotite and opaques, all of which have been variably replaced by sericite and clay minerals. Samples AHAR07-10 are composed of these minerals but are porphyritic, see Fig. 4.8 and Table A.1, for further information.

The xenoliths (AHAR04 and 12) are extremely fine grained, have a seriate texture and are composed of quartz, feldspar, opagues and possible clinopyroxene. The Mt Charles and Border Volcanic lavas are dacitic/andesitic and basaltic/basaltic andesites respectively. They are all porphyritic with phenocrysts of plagioclase feldspar set in a groundmass of plagioclase and opaques (some identified as sphene). Amphibole is present as a phenocryst and matrix phase in AHAR14 and 17. AHAR13 contains microcline and quartz as phenocryst and groundmass phases. The primary mineralogy of all the lavas is replaced to a variable extent by calcite, sericite and clay minerals (Fig. 4.8 and Table A.1, Appendix A).

4.2.5 The Bath-Dunrobin Formation and the Cedar Valley peridotites

The Cedar Valley peridotite is found to the north of Newcastle (Fig. A.7, Appendix A). Although not enough time was available to examine the geochemistry of the peridotites, it is useful for the reader to note that a large unstudied section of peridotite exists in eastern Jamaica. The peridotites (AHBD02-06, 08) are coarse grained and are mostly composed of olivine with ~ 5-10% orthopyroxene and up to ~ 5% clinopyroxene and opaques. These mineral proportions suggest that the peridotites are harzburgites. In thin section, the olivine and pyroxene are partly

replaced by serpentine minerals, however, the alteration is not extensive and so primary mineral proportions can be identified (Fig. 4.9).

A micro-granite dyke (AHBD07) was discovered cross-cutting one of the peridotite outcrops. In thin section, the dyke is un-altered, porphyritic and is composed of plagioclase feldspar, K-feldspar, hornblende and quartz (Table A.1, Appendix A). The geochemistry shows that it has an island arc affinity (Chapter 6). The age and affinity of the dyke and its relationship to the peridotite could be an important factor in any tectonic model of Jamaica (Chapter 7).

The Bath-Dunrobin lavas were collected east of Bath (Fig. A.4) along the Island River (samples AHBD09-26) and one of its eastern tributaries (samples AHBD27-30). The exposure in both river sections was good, but many of the rocks were heavily altered and weathered. AHBD09-11, 13, 14, 16-21, 23-30 are all altered, fine grained, dark grey/black basaltic rocks whereas AHBD12, 15 and 22 are fine grained, porphyritic, black, acidic tuff layers intercalated within the basalts. The basalts are phyric and aphyric and commonly have a greenish tint due to the presence of chlorite. Pillow lavas are occasionally found along the Island River section (Fig. 4.3).

In thin section, the basalts are composed of plagioclase feldspar, clinopyroxene and opaques that are variably replaced with sericite, calcite, clay minerals and serpentine (Fig. 4.9). Quartz and calcite veins are common in many of the samples. The tuffs are made up of a glassy fragmented matrix with larger quartz and zeolite crystals (Fig. 4.9).

4.2.6 The Newcastle Volcanic Formation, Wagwater Group

4.2.6.1 Sampling and field observations

The lavas of the Newcastle Volcanic Formation are Tertiary in age and were collected from the central Wagwater basin (Table A.1, Fig. A.7 and A.8, Appendix A). The majority of the samples (AHWG11-34) were collected along road cuttings from Irish Town to Freetown and from Happy Gate to Woodford (Fig. A.7, Appendix A). AHWG01-05 were collected in a network of quarries located to the south of Bito (Fig. A.8, Appendix A).

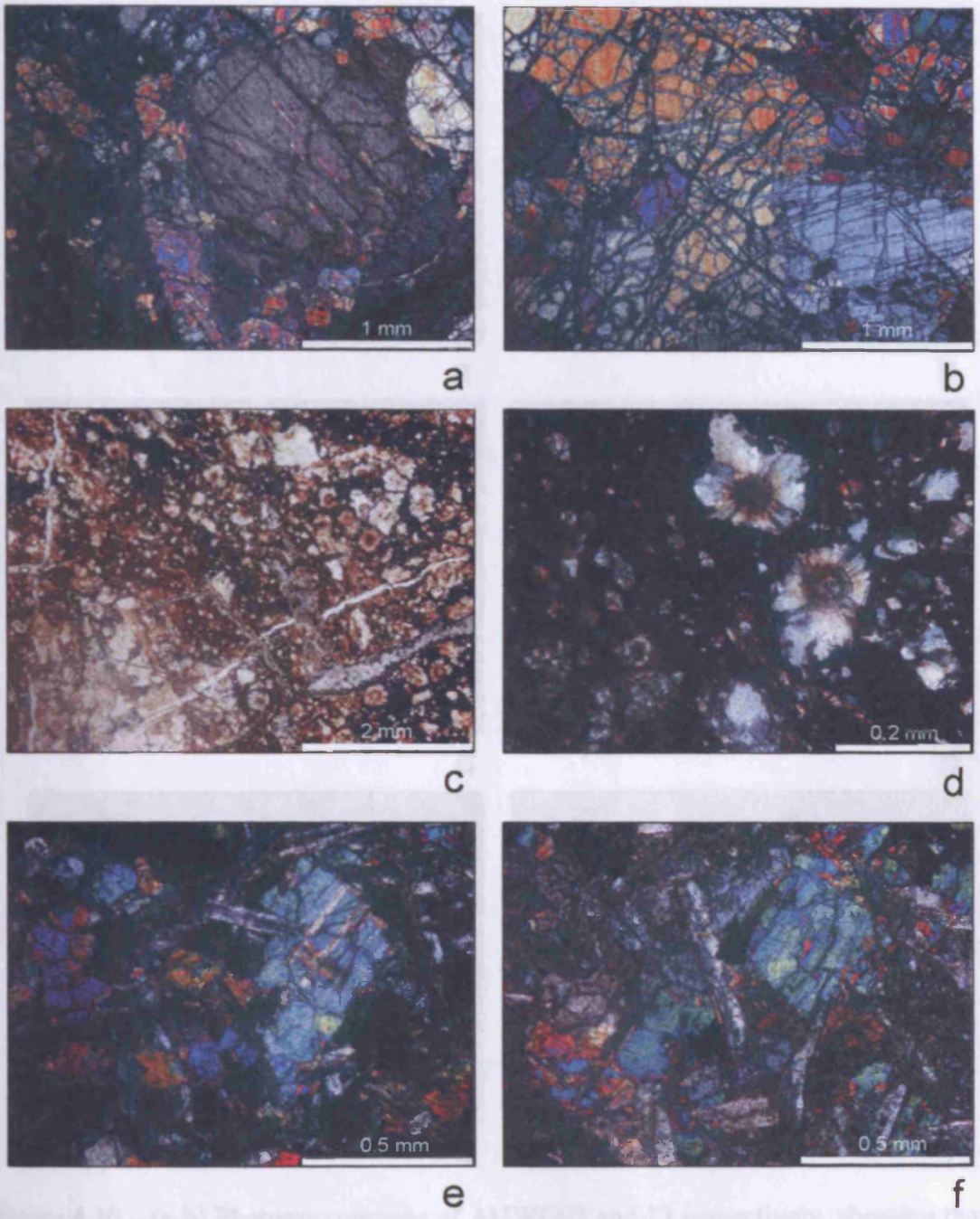

Figure 4.9 – (a-b) Photomicrographs of AHBD05, and 04 respectively; (a) Clinopyroxene crystal surrounded by and enclosing olivine crystals; (b) Serpentinised olivine and clinopyroxene; (c) Plane polarised image of the AHBD15 tuff which is composed of quartz and zeolites and has a very fragmented appearance; (d) Cross polarised image of the zeolites in AHBD15; (e-f) AHBD13 and 16 respectively show the typical texture and mineralogy of the Bath-Dunrobin lavas. The rocks are aphyric and are composed of plagioclase feldspar, clinopyroxene, olivine and opaques that have been extensively replaced by serpentine, clay minerals and sericite.

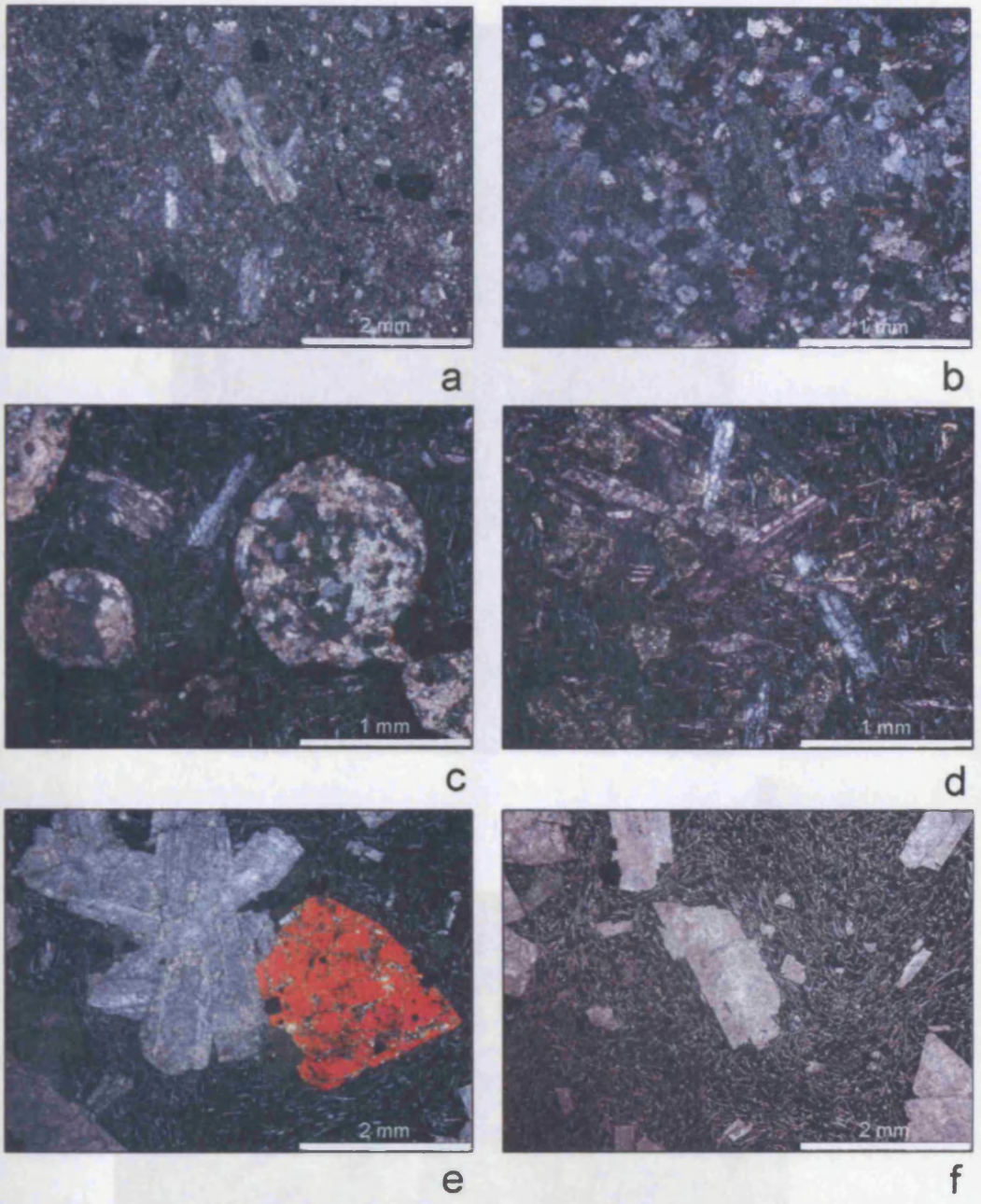

Figure 4.10 – (a-b) Photomicrographs of AHWG03 and 13 respectively, showing that the Newcastle lavas are porphyritic and have a seriate texture. The rocks are composed of variably altered plagioclase feldspar, K-feldspar, quartz and opaques; (c) Photomicrograph of a calcite, quartz and chlorite filled amygdale from AHHB01; (d) Cross polarised image of AHHB02 showing that the Halberstadt lavas are porphyritic and are composed of plagioclase feldspar and opaques which are partially replaced by sericite, clay minerals and chlorite; (e-f) Cross and plane polarised images of AHSUN105. The rock contains phenocrysts of plagioclase feldspar and amphibole. The groundmass is composed of needle-like feldspar and opague crystals that show extensive clay mineral, chlorite and calcite alteration.

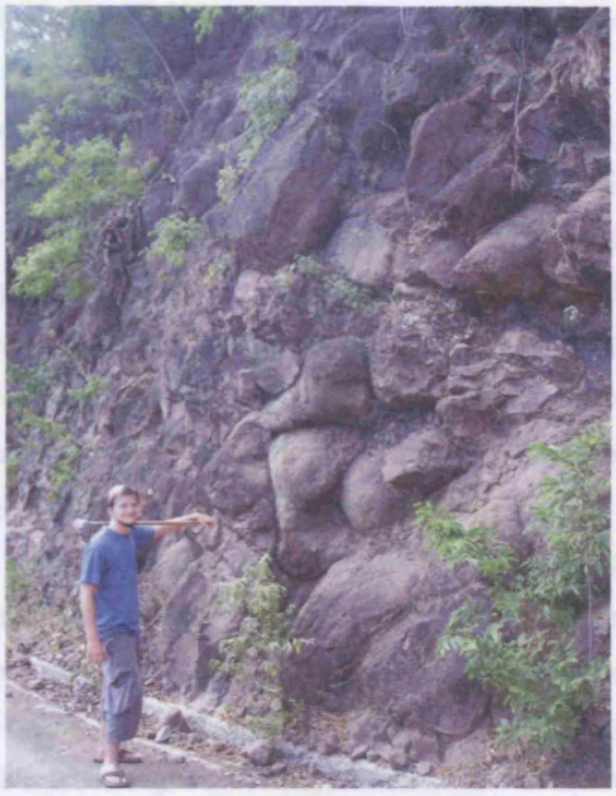

a

b

Figure 4.11 – (a) Pillow structures of the Halberstadt Volcanic Formation along the road between Newstead and Bito; (b) Examples of the ~ 1.5 m long and ~ 50 cm wide tube structures related to the pillow lavas. These are also found along the road between Newstead and Bito.

An exact location is not given because; firstly the GPS was not functioning correctly at the quarry and secondly, the AHWG01-05 outcrops were being worked; consequently the outcrops will no longer exist.

The exposure along the road sections was quite extensive and although many of the outcrops were substantially weathered and covered with abundant vegetation there was enough exposure to locate and collect relatively fresh samples (AHWG11-34). The samples collected in the quarry came from small blasted sections of benches. The Newcastle lavas are renowned for their auto-brecciation and high levels of jointing, and this, coupled with the damage caused by the blasting made identifying original layering impossible.

Jackson and Smith (1979) considered the igneous rocks in the Newcastle Volcanic Formation to be lava flows and not intrusives. In the course of this study the outcrops were found to be massive and did not show any flow textures. However, this thesis will continue to use the interpretation of Jackson and Smith (1979) and will regard the Newcastle igneous rocks as flows. The lavas are porphyritic and have a light or dark grey/blue colour with a greenish tint due to the presence of chlorite.

4.2.6.2 Petrographic observations

In thin section AHWG01-05 are phyric and are made up of plagioclase feldspar, K-feldspar, amphibole, quartz and opaques that have undergone variable degrees of alteration to replace some of the primary mineralogy with sericite and clay minerals (Fig. 4.10). AHWG11-34 are phyric, or have a seriate texture, and are also composed of plagioclase feldspar, K-feldspar, amphibole, quartz and opaques (Fig. 4.10). The primary mineralogy of these samples has been partially replaced with clay minerals, sericite and chlorite. In some of the samples the chlorite replacement can be relatively extensive e.g. AHWG21 (Table A.1).

4.2.7 The Halberstadt Volcanic Formation, Wagwater Group

The samples from the Halberstadt Volcanic Formation, like the Newcastle lavas, were collected from the central Wagwater basin. AHHB01-09 were collected along the road section from Newstead to Bito (Table A.1 and Fig. A.8, Appendix A). AHWG06-10 were sampled in the same quarry complex from where the Newcastle

lavas AHWG01-05 were collected. Like these Newcastle lavas, exact locations for AHWG06-10 are not given due to the complexities outlined in Section 4.2.6.1.

AHHB01-09 are greenish-grey, porphyritic amygdoidal/vesicular pillow lavas. These pillows are up to ~ 1.5 m wide and are found extensively in many of the outcrops (Fig. 4.11). Halberstadt pillows generally form the classic "pillow" shape but also form long tube structures that are ~ 1.5 m long and ~ 50 cm wide (Fig. 4.11). In thin section, the lavas are porphyritic and are composed of plagioclase feldspar and opaques which are partially replaced by clay minerals, chlorite and sericite. The amygdales range in size from < 1 mm to ~ 5 mm and are composed of quartz, calcite and chlorite (Fig. 4.10). The rocks also have abundant calcite veins.

The Halberstadt lavas in the quarry can be intensely altered due to hydrothermal, weathering and possible metamorphic processes. AHWG06 and 07 came from large outcrops that were so altered the rock disintegrated by lightly touching it. The samples were too altered to be analysed, and in thin section the original mineralogy of the rock has been completely replaced by quartz, chlorite, clay minerals and opaques. AHWG06 and 07 contain so much chlorite that in hand specimen the rock is green and very fragile.

AHWG08-10 were collected from relatively fresh outcrops, which formed massive, porphyritic amygdoidal/vesicular basaltic flows which have a dark grey colour. These flows lack the pillow structures seen in the road section but in thin section the samples are similar to AHHB01-09. They are composed of plagioclase feldspar and opaques that are partially replaced by clay minerals, chlorite and sericite. The rocks also have abundant calcite veins. The amygdales range in size from < 1 mm to ~ 5 mm and are made up of quartz, calcite and chlorite.

4.2.8 The Sunning Hill Inlier

The Sunning Hill Inlier samples were collected along a road cutting to the west of Sunning Hill by Dr Simon Mitchell of the UWI (Fig. A.4, Appendix A). AHSUN101-105 were sampled from outcrops of pillow basalts at the stratigraphic base of the inlier. In hand specimen AHSUN101, 103-104 are extensively altered and were not considered for further analysis. The primary mineralogy of AHSUN101, 103-104 has been replaced by clay minerals and chlorite; they are also heavily fractured with numerous quartz and calcite veins.

AHSUN102 and 105 are altered, porphyritic, grey/blue lavas. AHSUN102 has undergone more intense alteration than AHSUN105 but it is still fresh enough to analyse. In thin section AHSUN105 is porphyritic and is composed of plagioclase feldspar, amphibole and opaques that are altered to clay minerals, chlorite and calcite (Table A.1 and Fig. 4.10). AHSUN102 is more altered, porphyritic and composed of plagioclase feldspar and opaques which are being replaced with clay minerals, sericite and chlorite (Table A.1).

4.3 Summary

Extensive igneous successions have been found and sampled in most of the Cretaceous inliers and in the Tertiary Wagwater belt. The Devils Racecourse, Mt Charles, Border Volcanic, Newcastle Volcanic, Halberstadt Volcanic and the Sunning Hill samples are made up of solely extrusive lavas. The Arthurs Seat Formation is composed of lava flows, porphyrys and dykes. The Bath-Dunrobin Formation consists mostly of lavas but it also has a small number of intercalated tuff layers. Granodiorites and xenoliths were sampled from the Central and Above Rocks Inliers. The Waterworks Formation is represented by ignimbrites that were collected so that their juvenile pumice clasts could be analysed.

The outcrops were usually sparse and small, due to the density of vegetation in the Jamaican interior. This resulted in the vast majority of the rocks being sampled from road cuttings and river sections. Tropical weathering and hydrothermal and metamorphic processes are responsible for altering all of the igneous rocks throughout the island. Consequently, all the igneous rocks collected during this study were variably altered to some degree.

Chapter 5

Classification of altered volcanic island arc rocks using immobile trace elements: Development of the Co-Th, Th/Zr-La/Yb, Ce/Lu-Sm/Yb, La/Hf-Sm/Y and Th/Hf-Sm/Yb discrimination diagrams

5.1 Introduction

A significant aim of this study was to develop a method of classifying altered island arc lavas using immobile trace elements. The first part of this chapter describes the development of a new Co-Th discrimination diagram, which successfully discriminates altered island arc rocks on the basis of their degree of fractionation and LILE, LREE and actinide enrichment. The Co-Th section of this chapter has been formulated as a separate paper and has been accepted by the Journal of Petrology.

The second part of the Chapter describes the development of the Th/Zr-La/Yb, Ce/Lu-Sm/Yb, La/Hf-Sm/Y and Th/Hf-Sm/Yb discrimination diagrams. These are constructed to classify altered arc rocks based on their level of LILE, LREE and actinide enrichment only. The diagrams are necessary, in conjunction with the Co-Th diagram, to accurately classify the Jamaican igneous rocks as having island arc tholeiite (IAT), calcalkaline (CA) or shoshonitic (SHC) affinities. The identification of the lavas as either IAT or CA is crucial in determining the tectonic evolution of Jamaica and of the Caribbean plate (e.g. Chapter 2.5.4).

A limited amount of geochemical data and interpretation of the Devils Racecourse lavas is presented in this Chapter to demonstrate the usefulness of the

new discrimination diagrams. However, the full geochemical and petrogenetic study of these rocks is discussed in detail in Chapters 6 and 7.

5.2 Development of the Co-Th discrimination diagram

5.2.1 Rationale for development

One of the main methods of classifying igneous rocks is based on the degree of silica and alkali enrichment. The first division of igneous rocks into subalkaline and alkaline types resulted from work by petrologists around a hundred years ago (e.g. Iddings, 1892). This division is still used today, but has evolved into the total alkali-silica diagram (TAS) (Fig. 5.1) (Le Bas *et al.*, 1986; 1992). Although the TAS diagram is used to distinguish alkaline and subalkaline lavas it is mainly used for classifying how fractionated a rock is, based on its silica concentration.

The first alkali discrimination plot used for volcanic rocks was that of Peacock (1931) (Fig. 5.1). This diagram uses the enrichment of K_2O + Na_2O and depletion of CaO with increasing differentiation of a given volcanic suite to classify rocks as alkalic, alkali-calcic, calc-alkalic or calcic. This diagram is now rarely used by modern petrologists but it is important to note that many misleading terms used today have their origin in this discrimination plot e.g. alkali olivine basalts (Arculus, 2003).

The majority of volcanic arc lavas plot in the subalkaline field on the TAS diagram. These arc lavas are further classified on the basis of the enrichment of other oxide concentrations. The common diagrams used by geochemists include the total Fe as FeO (i.e. FeO*)/MgO vs SiO_2 plot (Miyashiro, 1974; Arculus, 2003), the (Na_2O + K_2O) vs MgO vs FeO* (AFM) discrimination plot with boundaries from Kuno (1968) and the K_2O vs SiO_2 diagram, which also discriminates rocks based on the extent of fractionation (Peccerillo and Taylor, 1976; Rickwood, 1989). These diagrams classify volcanic arc lavas as being IAT or CA based upon the degree of K_2O, FeO or FeO*/MgO enrichment. The K_2O vs SiO_2 diagram has the advantage of classifying lavas as high-K calcalkaline (HK) and SHC based on K_2O enrichment and it also has SiO_2 divisions enabling the extent of fractionation to be determined.

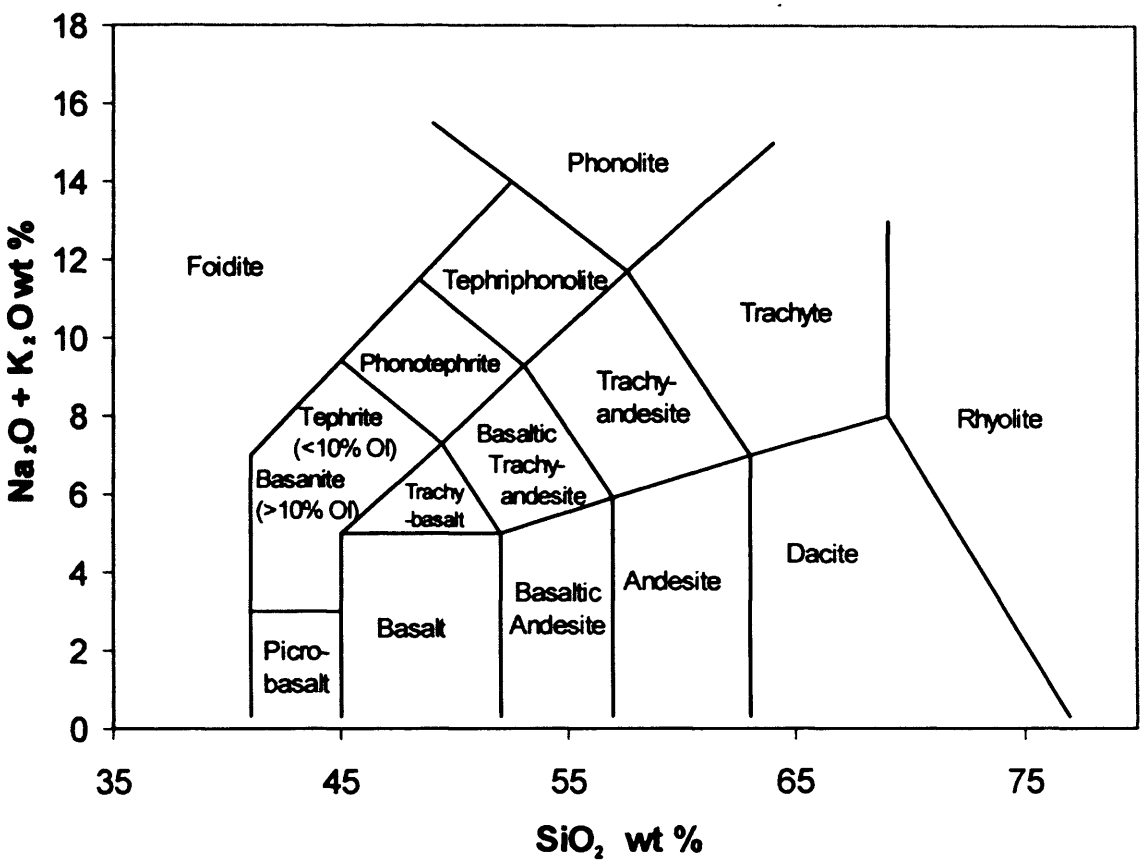

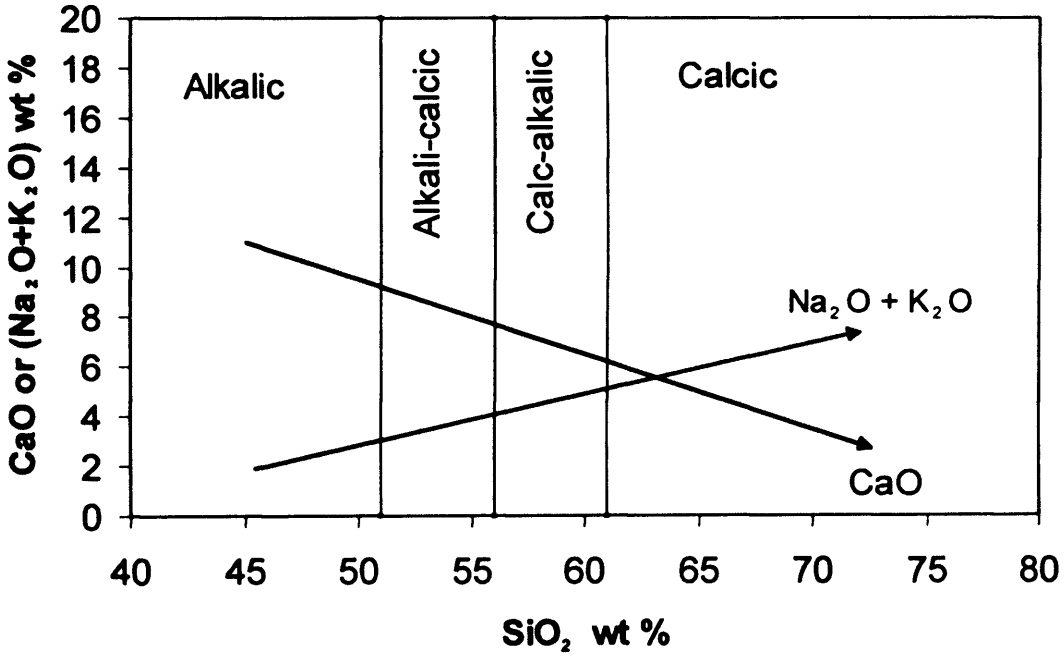

Figure 5.1 – (a) The total alkali silica diagram (Le Bas *et al.*, 1986; 1992); (b) The alkali discrimination plot of Peacock (1931).

Chapter 4 has highlighted the problem of classifying altered Jamaican arc rocks using the diagrams described above. Cretaceous and Tertiary volcanic arc samples collected from Jamaica have undergone intense tropical weathering and hydrothermal alteration, which has mobilised many of the elements (Chapter 6). Most common discrimination diagrams for arc lavas use predominantly mobile elements and oxides, which renders these diagrams unreliable for classifying highly altered samples. Therefore a new classification diagram has to be constructed to identify altered island arc lavas based upon their degree of fractionation and K_2O enrichment using immobile trace elements.

5.2.2 Previous immobile trace element diagrams

Immobile trace element classification diagrams were pioneered by Pearce and Cann (1973), Floyd and Winchester, (1975, 1978) and Winchester and Floyd, (1976, 1977). Many of the discrimination plots were designed to discriminate between different magma series and their fractionation products and not their tectonic environment, although tectonic discrimination diagrams have also been produced.

The SiO_2 vs Zr/TiO_2 plot was intended to give an indication of the degree of fractionation and alkalinity for altered lavas. TiO_2 decreases with fractionation and this decrease is greater within the alkaline rocks due to their higher Zr concentrations. Therefore, an increase in Zr/TiO_2 ratios in relation to SiO_2 can give an indication of the alkalinity and fractionation of a magmatic suite (Winchester and Floyd, 1977).

Additionally, Winchester and Floyd (1977) proposed that a SiO_2-Nb/Y diagram would show the alkalinity of a particular igneous rock. They based this on the fact that Nb/Y ratios will not change markedly with differing amounts of fractionation but alkaline rocks will have greater abundances of Nb. The two diagrams of Winchester and Floyd (1977) have been combined into a single Zr/TiO_2-Nb/Y discrimination plot that has been subsequently updated by Pearce (1996; Fig. 7).

The work by Floyd and Winchester, (1975, 1978) and Winchester and Floyd, (1976, 1977) has, however, limitations with regard to island arc rocks, since the diagrams were constructed using all types of igneous rocks *except* for island arc lavas. The diagrams classify volcanic rocks on the basis of their subalkaline and

alkaline nature but do not subdivide rocks into more specific IAT, CA, HK and SHC fields. This was due to the lack of analyses of these rocks in the late 1970's.

The updated diagram (Pearce, 1996) uses island arc data but it raises another problem; namely the large overlap displayed by island arc basalts, basaltic andesites, andesites and dacites (Pearce, 1996; Fig. 7). This overlap is due to island arc lavas fractionating accessory minerals earlier in their crystallisation sequence than magmas from other tectonic environments e.g. Fe–Ti oxides crystallise more rapidly due to oxidation from the incorporation of water during their petrogenesis. Consequently, the use of the Zr/TiO_2-Nb/Y diagram for the classification of island arc lavas is not recommended because (i) the fields for basalts, basaltic andesites, andesites and dacites overlap and (ii) the diagram does not subdivide the arc lavas into IAT, CA, HK and SHC affinities.

5.2.3 The subduction zone process

For a new discrimination diagram to be constructed, the mobile elements K and, to a lesser extent Si, have to be replaced with immobile elements that behave in a similar way during subduction zone processes but subsequently remain immobile during surface weathering. The selection of suitable proxy elements requires a detailed knowledge of how these elements behave during subduction zone processes.

Island arc lavas generally have normal mid-ocean ridge basalt (N-MORB)-like abundances of HFSE e.g. Nb, Ta, Zr, Hf and Y and heavy rare earth elements (HREE) and are relatively enriched in LILE e.g. K, Rb and Ba, light rare earth elements (LREE) and certain actinides e.g. Th and U. However, the abundances of HFSE and HREE can be depleted relative to N-MORB if the mantle peridotite wedge above the subducting plate has been subjected to previous melt extraction such as in a back arc basin (Ewart, 1982; McCulloch and Gamble, 1991; Pearce, 1982, 1996; Tatsumi *et al.*, 1992; Pearce and Peate, 1995; Tatsumi and Kogiso, 1997).

Many models of arc magmatism have suggested that a single component is transported from the subducting slab to the arc source to account for the composition of arc volcanics (McCulloch and Gamble, 1991; Pearce, 1982, 1996; Tatsumi *et al.*, 1992; Pearce and Peate, 1995; Tatsumi and Kogiso, 1997). The LILE, LREE and actinide enrichment occurs due to the addition of a hydrous fluid or melt component into the mantle wedge during the formation of arc magmas. Hydrothermally altered

MORB and oceanic sediments are regarded as the main source of subducted slab-derived aqueous fluids (McCulloch and Gamble, 1991; Pearce and Peate, 1995; Tatsumi and Kogiso, 1997).

It is now thought that 1.0 – 2.0 wt % of water is extracted from the basaltic oceanic crust during the amphibolite/eclogite transition, but, more water will be added to the overlying mantle wedge if the slab has a sedimentary cover. The heterogeneous nature of sedimentary successions means a sedimentary cover can drastically alter the composition of a fluid output from the subducting slab (Tatsumi and Kogiso, 1997; Plank & Langmuir, 1998).

Most fluid release occurs under the fore-arc, which then migrates upward and reacts with the overlying peridotite to produce hydrous phases such as phlogopite, amphibole (pargasite) and serpentine. The elements added to the peridotite from the slab derived fluid are largely partitioned into amphibole and phlogopite. The modified peridotite above the slab descends with the plate and undergoes three fluid release stages at ~ 2.7 GPa (under the fore-arc), 3.5 GPa and 6 GPa (Table 5.1). These reactions represent the change in mineralogy with increasing pressure and temperature (Pearce and Peate; 1995, Tatsumi and Kogiso, 1997).

Serpentine, which breaks down at 2.7 GPa, contains a very small quantity of mobile trace elements compared to amphibole and phlogopite, and so the fluid release at this pressure will be mostly water (Tatsumi and Kogiso, 1997). Most of the trace element budget is released with the breakdown of amphibole at 3.5 GPa (Tatsumi and Kogiso, 1997). This amphibole-derived fluid would ascend forming further hydrous peridotites again with amphibole and phlogopite. If the solidus temperature of this hydrous peridotite is exceeded at a particular depth, initial partial melting can take place (Tatsumi *et al.*, 1986; Pearce and Peate, 1995; Tatsumi and Kogiso, 1997). In addition, new data presented in Tatsumi (2003) suggests that the main fluid release at 3.5 GPa could also be the result of chlorite breakdown as well as amphibole decomposition. Tatsumi and Kogiso (1997) and Pearce and Peate (1995) estimated that the amount of this partial melting could be as high as 20-30%, thus producing the tholeiitic chemistry of lavas in many volcanic arc fronts.

As the modified peridotite above the slab further descends phlogopite breaks down at 6 GPa to cause smaller amounts of partial melting. This could explain the CA chemistry and fewer volcanoes found in back arc regions (Tatsumi *et al.*, 1986).

Pressure/Temperature	Reactants	Products
600 °C (2.7 GPa)	serpentine	olivine + opx + H_2O
3.5GPa	pargasite + opx	phlogopite + cpx + olivine + garnet + H_2O
6GPa	phlogopite + opx + cpx	K-amphibole + garnet + olivine + K_2O + H_2O

Table 5.1 – Dehydration reactions in the down drawn peridotite layer after Tatsumi (1997).

The uncertainty of forming CA magmas by this process is that the island arc source (the modified peridotite) should be heavily depleted in incompatible elements due to the dehydration of amphibole at 3.5 GPa (Tatsumi *et al.*, 1986). Conversely, Stern *et al.* (1993) suggest that lower degrees of partial melting beneath the back arc region are due to the decreasing proportion of slab derived water due to the greater distance from the volcanic front.

Many other studies have suggested that a single component from the slab is too simplistic and does not explain many trace element and isotopic signatures (e.g. Miller *et al.*, 1994; Brenan *et al.*, 1995; Regelous *et al.*, 1997; Class *et al.*, 2000; Elliott, 2003). These studies have identified several components: (a) aqueous fluid from altered oceanic crust and sediment and (b) silicate melts from the oceanic basalt and sediment, which are transported from the subducting slab to the arc source region (e.g. Miller *et al.*, 1994; Brenan *et al.*, 1995; Regelous *et al.*, 1997; Class *et al.*, 2000; Elliott, 2003).

The transport of some elements, such as Th and La, is also controversial. Large ions with low charges, such as K^+, are more easily mobilised by super-critical aqueous slab-derived fluids than the smaller highly charged ions, such as Zr^{4+}. However, the mobility of elements such as the LREE (La^{3+}) and the actinides (Th^{4+}), which are moderately charged and have relatively large ionic radii is less clear (Elliott, 2003). At low temperatures LREE and Th do not readily partition into aqueous fluids but at higher temperatures there is contradictory evidence (Elliott, 2003).

Elliott (2003) proposes that at low temperatures the LREE and the actinides are not mobilised by supercritical aqueous fluids. However, experimental evidence has produced conflicting results at higher temperatures (Elliott, 2003). It has been suggested that Th is only transported into the wedge by a sedimentary melt from the subducting slab. Conversely, Keppler (1996) presents convincing evidence to suggest that both a "normal" and a chloride-rich fluid from a subducted slab would readily transport Th into the overlying mantle wedge.

Consequently, it is clear that the number of subduction components involved in arc genesis and the transport of certain elements by aqueous fluids and silicate melts derived from the slab is controversial. However, for the purpose of this study the subduction component(s) are characterised as one entity that enriches the sub-arc mantle. It is also assumed that elements such as the LREE and Th are mobile in slab derived aqueous fluids and behave in a similar manner to the LILE (evidence for this is presented in Sections 5.2.4 and 5.2.5.1). This suggests that elements such as the LREE and Th could be used as proxies for K enrichment in arc lavas.

5.2.4 Element mobility using trace elements

Some elements will remain in the slab and are described as "conservative" while others are removed by the fluid/melt and are "non-conservative" (Pearce and Peate, 1995). Conservative elements can be identified by using an "X"/Yb vs Ta/Yb plot, where "X" is the element being studied. If "X" is conservative the volcanic arc data will fall within a MORB array but if it is non-conservative the "X"/Yb ratio will be increased. Some care is necessary with this classification as some conservative elements behave non-conservatively when crust and/or subducted sediment undergoes melting rather than dehydration e.g. Zr and Nb (Pearce and Peate, 1995).

The conservative nature of any given element is principally determined by bulk distribution coefficients between:

1. The slab/fluid (aqueous & melt) at 2.7, 3.5 and 6GPa.
2. The mantle/fluid (aqueous & melt).
3. The mantle/melt within the wedge melting column.

Conservative elements include Zr, Hf, Nb, Ta, Y, Ti and the HREE and these remain in the slab due to the low solubility of minerals such as rutile, zircon, apatite, monazite and garnet (Pearce and Peate, 1995). Melts are more effective than aqueous fluids in transferring elements from slab to wedge and it is thought that higher temperature melts can have substantial concentrations of certain HFSE and HREE (Tatsumi *et al.*, 1986; McCulloch and Gamble, 1991; Pearce and Peate, 1995). Non-conservative elements include K, Ba, Rb, Sr, U, Th, and the LREE, and are incompatible elements, found in large quantities along crystal boundaries and not in the crystal structure of the various slab minerals (Tatsumi *et al.*, 1986). Non-conservative elements are easily removed and transported by hot percolating aqueous fluids, thus, concentrating them in any fluid flux from the subducting slab (Tatsumi *et al.*, 1986; Keppler, 1996). It is for these reasons that the "X"/Yb vs Ta/Yb diagram is utilised for the study of the subduction component in arc lavas and can classify the rocks on the basis of their LILE, LREE and actinide enrichment (Pearce, 1982).

The distinction between conservative and non-conservative behaviour has enabled geochemists to use a number of other immobile trace element diagrams to study altered island arc lavas. Similar to the "X"/Yb vs Ta/Yb diagram, m ulti-element and REE plots are also useful in separating IAT, CA and SHC lavas. This is demonstrated in Figure 5.2, which shows that the lower and upper Devils Racecourse lavas have IAT and CA compositions respectively (see Chapter 6 for more information). The Benbow Th/Yb-Ta/Yb diagram also indicates that the Th is non-conservative.

SHC and CA volcanic rocks may have formed by smaller amounts of partial melting and consequently they will be relatively more enriched in LILE, LREE, U and Th compared to HFSE than IAT lavas, which have formed by larger degrees of partial melting. The chemical heterogeneity of the slab and associated sedimentary cover may also contribute to the more enriched nature of SHC and CA lavas relative to IAT lavas.

Trace element ratio plots that utilise the relationship between non-conservative and conservative elements, e.g. "X"/Yb-Ta/Yb plot (Fig. 5.2), have helped determine the range of enrichment of elements, such as Ba, Sr and Th, in arc rocks (Pearce, 1982). Similar trace element diagrams can be used for the same purpose, provided they highlight the more enriched nature of SHC and CA relative to IAT lavas. The obvious problem with all of the diagrams discussed above is that

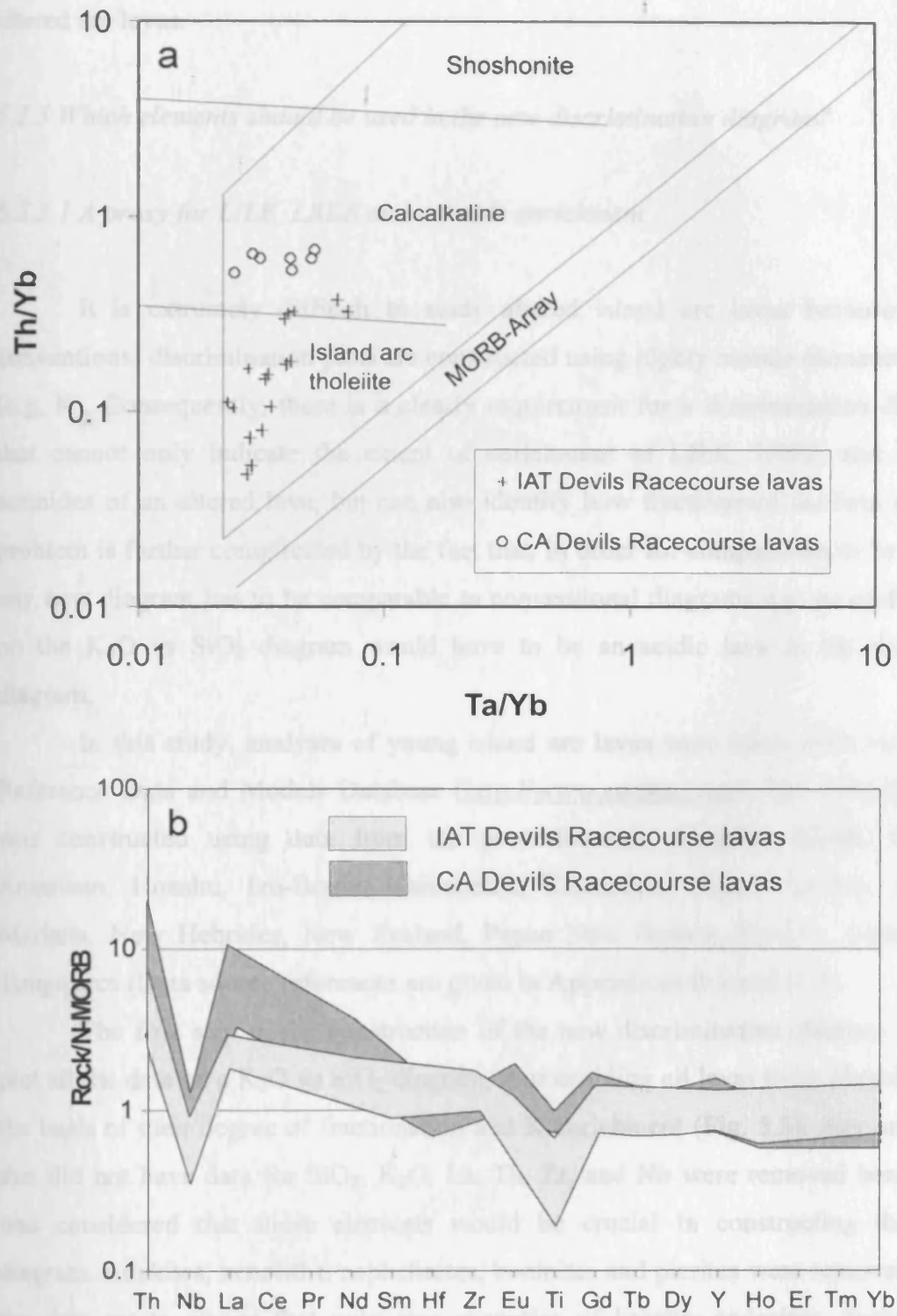

Figure 5.2 – (a) Th/Yb vs Ta/Yb trace element ratio plot and (b) A Multielement diagram showing island arc tholeiite (IAT) and calcalkaline (CA) lavas of the Devils Racecourse Formation. Normalising values in (b) are from Sun and McDonough (1989).

none of them are suitable for identifying and classifying the extent of fractionation of altered arc lavas.

5.2.5 Which elements should be used in the new discrimination diagram?

5.2.5.1 A proxy for LILE, LREE and actinide enrichment

It is extremely difficult to study altered island arc lavas because many conventional discrimination plots are constructed using highly mobile elements (e.g. K). Consequently, there is a clearly requirement for a discrimination diagram that cannot only indicate the extent of enrichment of LILE, LREE and certain actinides of an altered lava, but can also identify how fractionated the lava is. The problem is further complicated by the fact that, in order for comparisons to be made, any new diagram has to be comparable to conventional diagrams e.g. an acidic lava on the K_2O vs SiO_2 diagram would have to be an acidic lava in the proposed diagram.

In this study, analyses of young island arc lavas were taken from the Earth Reference Data and Models Database (http://www.earthref.org). The new diagram was constructed using data from the post-Mesozoic Aleutian, Banda, Central American, Honshu, Izu-Bonin, Kamchatka, Kermadec, Lesser Antilles, Luzon, Mariana, New Hebrides, New Zealand, Papua New Guinea, Ryukyu, Sunda and Tonga arcs (Data source references are given in Appendices B.1 and B.2).

The first step in the construction of the new discrimination diagram was to plot all the data on a K_2O vs SiO_2 diagram, thus enabling all lavas to be identified on the basis of their degree of fractionation and K enrichment (Fig. 5.3). Any analyses that did not have data for SiO_2, K_2O, La, Th, Zr, and Nb were removed because it was considered that these elements would be crucial in constructing the new diagram. Adakites, xenoliths, nephelinites, boninites and picrites were removed from the data set to ensure that only *type* examples of basalts, andesites, dacites and rhyolites were used to construct the new discrimination plot (Fig. 5.3).

All samples designated in the database as being weathered or metamorphosed were also removed. Finally, K vs Zr variation diagrams were constructed to ensure that the remaining data consisted of relatively unaltered samples. The K-Zr variation diagrams in Figures 5.4a and 5.4b display representative data from the Aleutian and

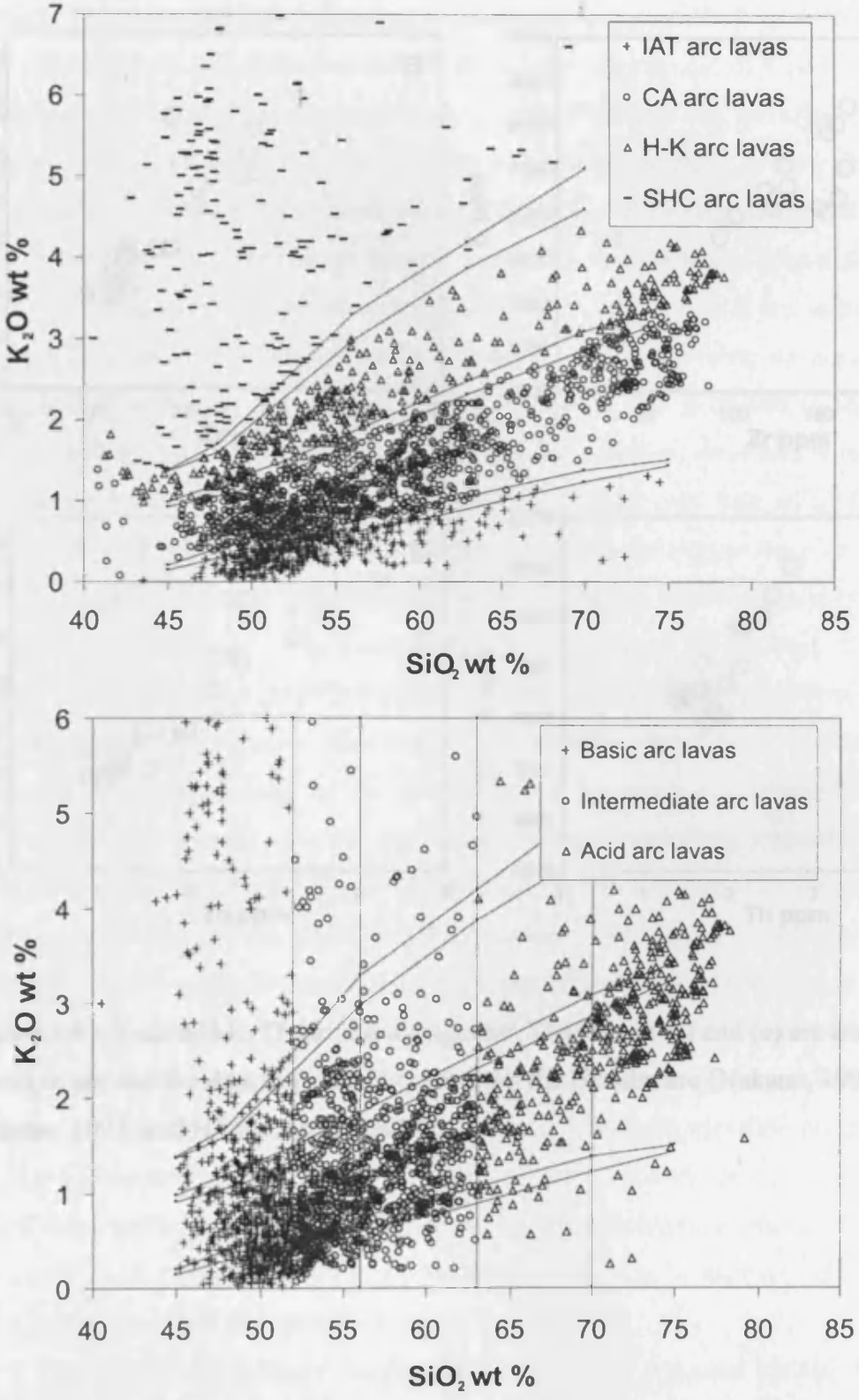

Figure 5.3 – Plot of 2492 island arc analyses on K_2O vs SiO_2 discrimination diagrams (Appendix B.1). Compositional fields and boundaries for K_2O vs SiO_2 diagram are from Peccerillo and Taylor 1976; Rickwood, 1989).

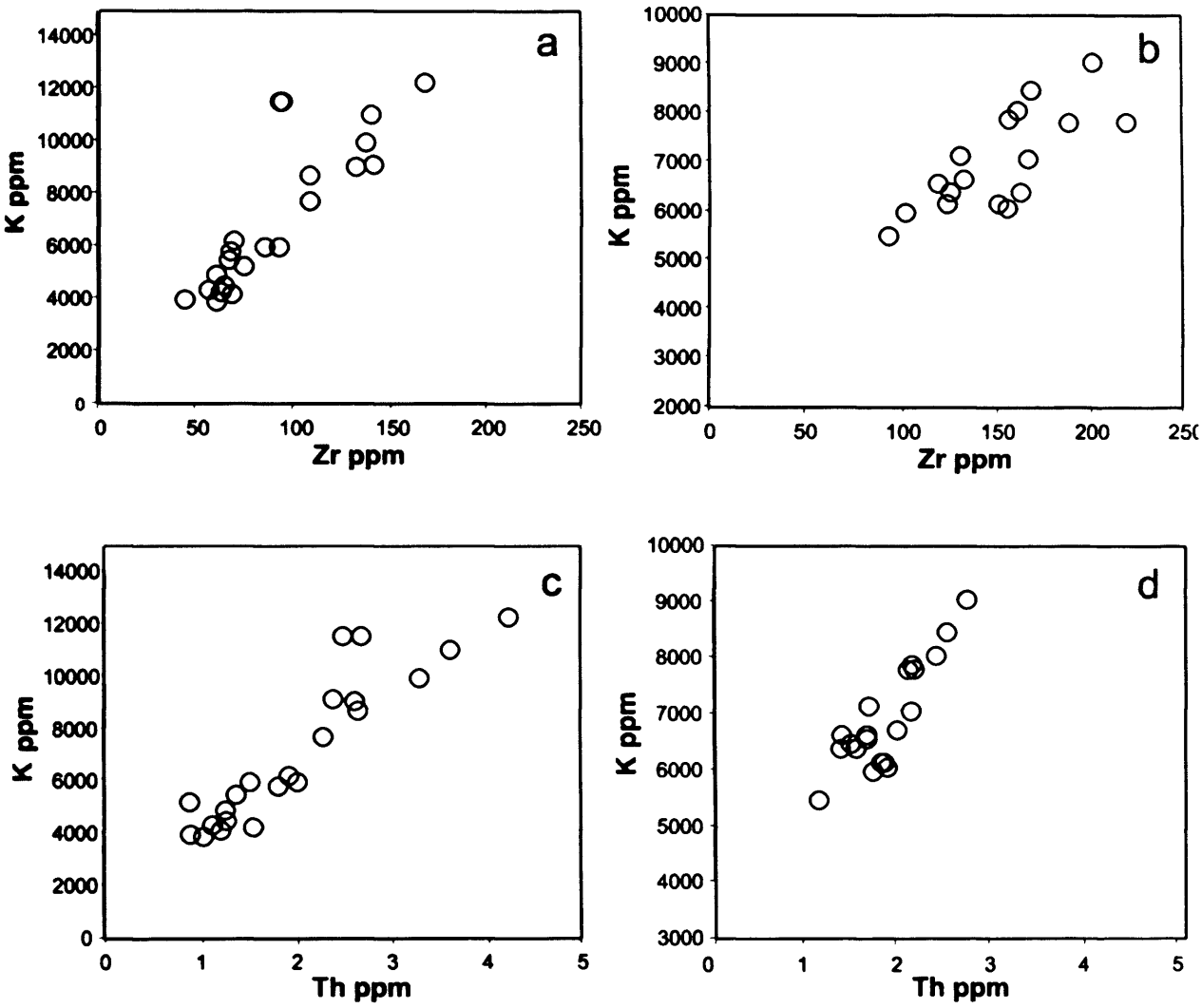

Figure 5.4 – K-Zr and K-Th variation diagrams. The data in (a) and (c) are from the Aleutian arc and the data in (b) and (d) are from the Honshu arc (Nakano, 1993; Nakano, 1994; and Hildreth *et al.*, 2004).

Honshu arcs respectively (Nakano, 1993; Nakano 1994 and Hildreth *et al.*, 2004). The data forms linear trends indicating (i) K has not been mobilised by weathering or hydrothermal alteration processes and (ii) the relative enrichment of K and Zr during fractional crystallisation demonstrates that both elements are incompatible. For comparison, the variation diagrams in Chapter 6 and Appendix E show that K in rocks that have undergone extensive weathering does not form liquid lines of descent when plotted against an immobile element, indicating that the K has been mobilised.

An assessment of the relative enrichment of LILE, LREE and actinides in altered island arc lavas requires that an element immobile during weathering and hydrothermal alteration processes is used to replace K. Th is chosen to replace K because it behaves in a similar manner to K in a subduction zone and is relatively immobile (Pearce, 1996). K-Th variation diagrams in Figures 5.4c and 5.4d show linear trends for the Aleutian and Honshu arcs respectively suggesting (i) K and Th have not been mobilised by weathering or hydrothermal alteration processes, (ii) relative enrichment, and so incompatibility of K and Th during fractional crystallisation and (iii) K and Th behave in a similar manner during subduction zone and partial melting processes. Figure 5.5a also shows that, unlike K, Th displays a relatively good linear trend for the altered Devils Racecourse arc lavas and so is relatively immobile during weathering and hydrothermal alteration processes.

However, the immobility of Th results in it not entering slab derived fluids until the temperature of the subducting slab reaches ~ 450°C (Pearce pers. comm.). K does enter slab fluids below this temperature; therefore, an arc magma produced at a shallow depth would have a high K content relative to the Th abundance i.e. the rock would plot as CA on a K_2O-SiO_2 diagram and IAT on a discrimination plot based on Th. As such, the data used in this study were plotted on K-Th variation diagrams, N-MORB normalised multi-element and "X"/Yb-Ta/Yb trace element ratio diagrams. These diagrams reveal that very few samples display relative enrichments of K while Th remains at N-MORB abundances. Consequently Th can be used as a close proxy for K in the new discrimination diagram.

In constructing the new diagram, Th concentration was used instead of Th/Yb for quantifying the LILE, LREE and actinide enrichment of island arc lavas. It has already been shown by Pearce (1982) that this latter ratio can be used to discriminate between IAT, CA and SHC compositions; however, the ratio is less affected by differentiation processes. This is contrary to the K_2O-SiO_2 diagram, where the K_2O

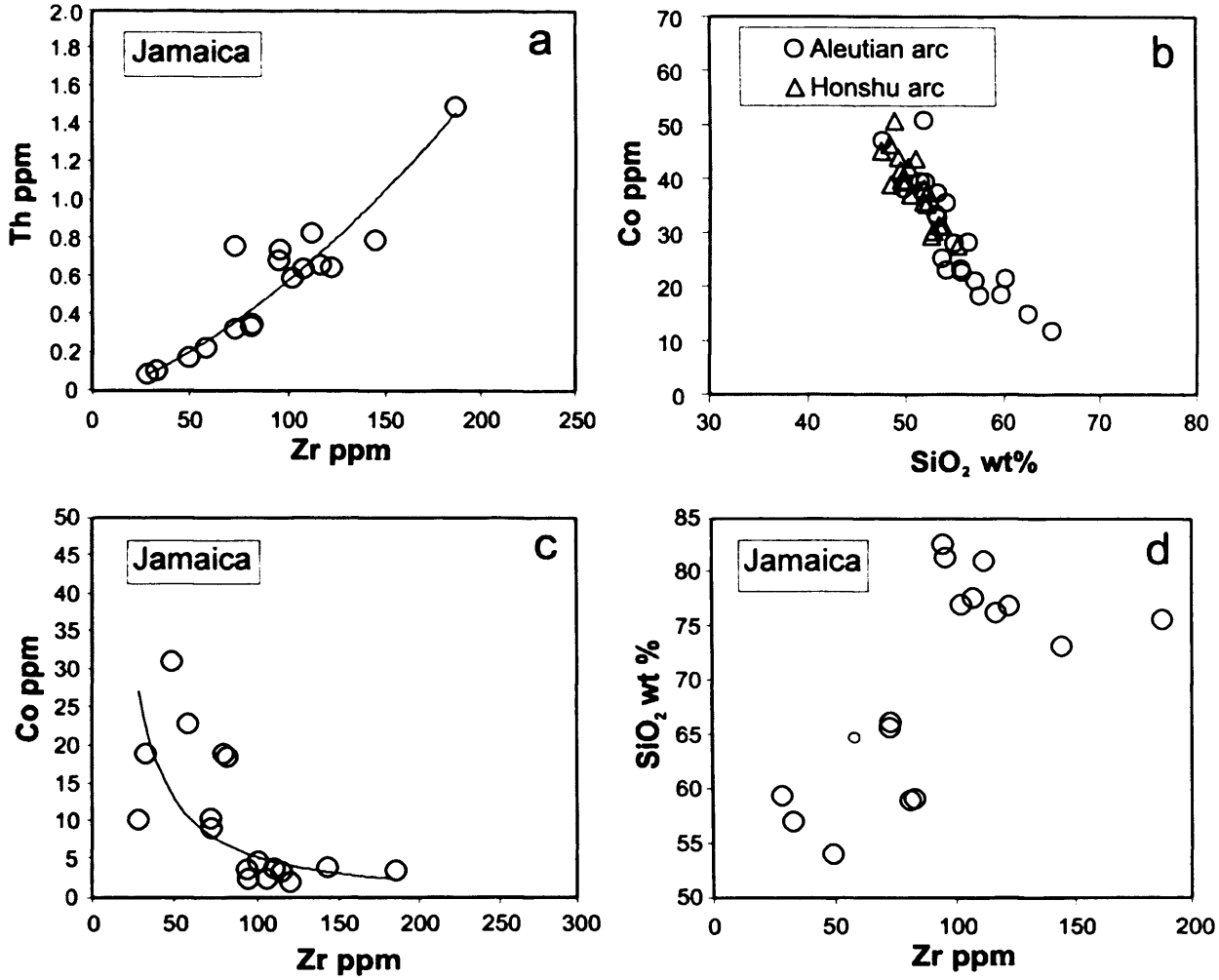

Figure 5.5 – Th-Zr, Co-SiO_2, Co-Zr and SiO_2-Zr variation diagrams. Diagrams a-c display clear liquid lines of decent for: (a) Th-Zr data for altered Jamaican samples, (b) Co-SiO_2 data from the Aleutian and Honshu arcs (Nakano, 1993; Nakano, 1994; and Hildreth *et al.*, 2004) and (c) Co-Zr data for altered Jamaican samples. (d) shows that SiO_2-Zr data from the Jamaican samples does not form a clear liquid line of descent thus indicating that the Si, unlike the Th and Co in the Jamaican lavas, has been mobilised.

abundances are affected by differentiation processes. Therefore, for the new diagram to be comparable to the K_2O-SiO_2 plot of Peccerillo and Taylor (1976) the Th concentration has be used because the LILE (e.g. K), LREE and actinide (e.g. Th) concentrations will increase and decrease in the melt with variable degrees of fractional crystallisation and partial melting.

5.2.5.2 A proxy for the extent of fractionation

In order to assess the relative extent of fractionation, many previous discrimination plots use an essentially incompatible element that is then taken up by a minor phase during the later stages of fractional crystallisation. This means that a ratio containing that particular element will be substantially changed during fractionation so that the rock can be classified e.g. the SiO_2 vs Zr/TiO_2 plot of Winchester and Floyd, (1977) (Section 5.2.2).

Unfortunately, this method has proved unsuccessful with island arc rocks because many of the minor minerals, such as the Fe-Ti oxides, crystallise out early, which leads to extensive overlapping of the basaltic, basaltic andesite, andesite and dacite fields (Pearce, 1996; Fig. 7). Therefore, instead of using an incompatible element we have chosen to use a compatible element, which will be gradually removed from the melt throughout the crystallisation sequence, by several minerals, and so will reflect the fractionation from basalt to rhyolite. This non-reliance on a single minor phase makes it less likely that compositional fields will overlap.

Although Sc and Cr are moderately successful at separating the data into compositional fields, Co is the most effective. However, not all of the originally studied 2042 samples reported data for Co; consequently the new discrimination plot was constructed from a reduced data set of 1009 samples that contained data for both Th and Co (Appendix B.2).

During hydrothermal and weathering processes Co is relatively immobile and has an ionic potential similar to Ti, Cr and Ni. A Co-SiO_2 variation diagram is plotted in Figure 5.5b. The data are again taken from the Aleutian and Honshu arcs (Nakano, 1993; Nakano 1994 and Hildreth *et al.*, 2004) and forms a good liquid line of descent. Figure 5.5b demonstrates that the silica and the Co are not mobile in the Aleutian and Honshu rocks and, as such, the K_2O-SiO_2 diagram of Peccerillo and

Taylor (1976) can be used to classify the 1009 samples. Consequently, this data can subsequently be used to construct the compositional fields in the Co-Th diagram.

In addition, the immobility of Co in the Devils Racecourse lavas can be seen in the Co-Zr diagram in Figure 5.5c where a good liquid line of decent is formed. This is in contrast to Figure 5.5d, which displays a SiO_2-Zr variation diagram of the altered Devils Racecourse lavas. A clear liquid line of descent is not observed and the data suggests that the Si has been mobilised and can not be used for classification.

Consequently, Co is used as a proxy for silica to determine the fractionation of altered volcanic island arc lavas. The Co values for the new Co-Th diagram are comparable to the silica values in the K_2O-SiO_2 diagram, however, it is important to note that Co behaves opposite to that of silica, i.e. silica increases but Co decreases with increased fractionation.

5.2.6 Construction of the Co-Th discrimination diagram

The new Co-Th discrimination diagram is designed to act as an immobile element "equivalent" of the K_2O-SiO_2 diagram of Peccerillo and Taylor (1976). The Th and Co will act as proxies for K and Si respectively. The diagram will not discriminate between subalkaline and alkaline compositions, but will classify subalkaline island arc rocks as IAT, CA, HK and SHC.

The data quality from the Earth Reference Data and Models Database is a slight concern for this study. Some of the data is old and it is recognised that analytical precision in earlier studies is not as good as modern high precision ICP analyses. For example, the trace element data from Dietrich *et al.* (1978) were obtained by instrumental neutron activation analysis (INAA), which did not precisely analyse certain trace elements (e.g. Ta, U and Th) in some of the samples because they were below the detection limit of the instrument. Conversely, more recent studies such as Zellmer *et al.* (2003) and Castillo and Newhall (2004) analyse most of their trace elements using high precision ICP-MS. Nevertheless, the data from the older studies were used in the construction of the new diagram because there is a lack of modern studies which present arc Co and Th data.

The arc data classified on the basis of $K_2O + SiO_2$ have been plotted on a Co vs Th plot (Figs. 5.6 and 5.7). It can be seen that the samples fall into quite clearly

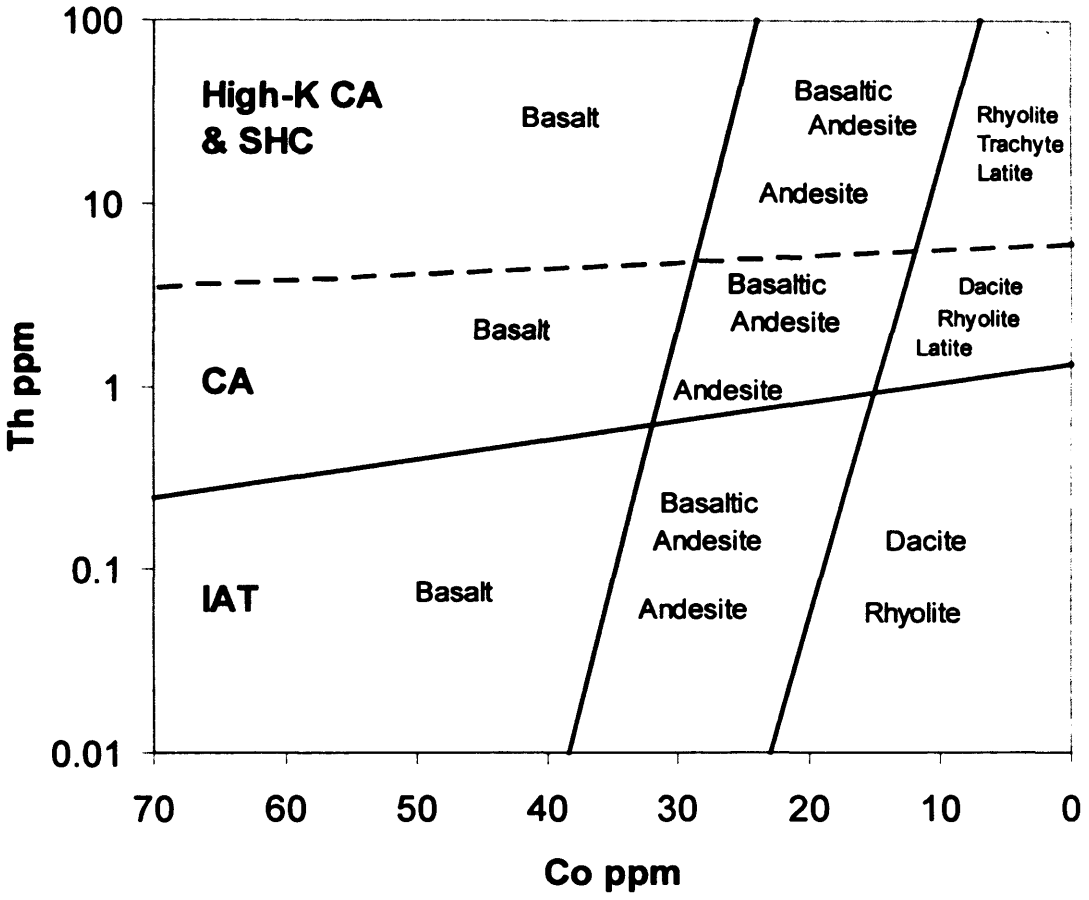

Figure 5.6 – The completed Co-Th discrimination diagram. The field boundaries are: basalt - basaltic andesite and Andesite, X-38.4, 24, Y-0.01, 100; basaltic andesite/andesite – dacite/rhyolite, X-23, 7, Y-0.01, 100; IAT – CA, X-70, 0, Y-0.245, 1.35; CA-high K CA/SHC, X-70, 0, Y-3.5, 6.

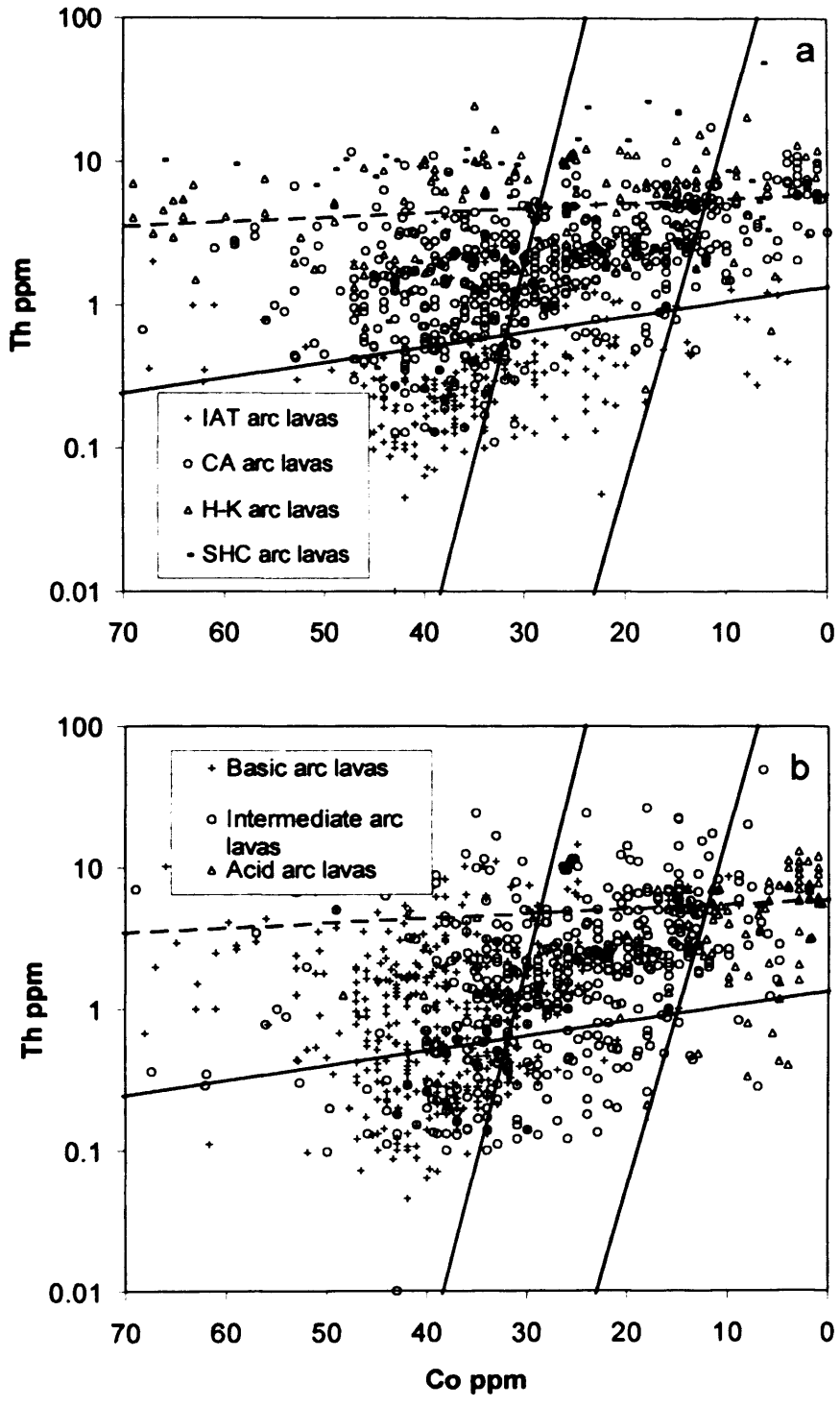

Figure 5.7 – 1009 samples plotted on the Co-Th discrimination diagram. (a) samples plotted as tholeiite, calc-alkaline, high-K calc-alkaline and shoshonitic compositions; (b) samples plotted as basic, intermediate and acid compositions.

defined fields; however, for each rock type percentage contours were used to construct field boundaries. The contours can either be drawn around the mean or the peak position of the distribution of the data (Le Bas *et al.*, 1992; Pearce, 1996). The Co-Th diagram contained some anomalous samples with extremely high Co or Th concentrations, therefore, the mean values gave erroneous results. Thus, percentage contours have been constructed around the peak distribution positions.

Pearce (1996) used the 90% contour (i.e. enclosing 90% of the samples) to revise the Zr/TiO_2-Nb/Y diagram of Winchester and Floyd (1977), whereas Le Bas *et al.* (1992) used the 75% contour to construct the fields on the Total Alkali Silica diagram. The 85% contour was chosen for the Co-Th diagram because (i) it encloses the vast majority of the data and (ii) it enables most of the scatter away from the peak distribution to be eliminated. The 85% contours show little overlap for the 1009 basic, intermediate and acidic lavas as determined by the K_2O-SiO_2 diagram. The basalt, basaltic andesite-andesite and dacite-rhyolite fields are well constrained, although a clear division is not possible between basaltic andesite and andesite.

The IAT and CA lavas show little overlap and form well defined fields; however, the separation between HK and SHC lavas is not as clear (Fig. 5.7). This is due to a lack of samples and hence lack of a reliable distribution peak. A dashed line represents the qualitative boundary between the CA and the HK and SHC lavas. A quantitative boundary could not be accurately constructed between the CA and the HK and SHC lavas again due to the lack of samples and lack of a reliable distribution peak. However most of the HK and SHC data falls to the top of the dashed line on Figure 5.7. It should also be noted that the number of samples for trachyte and latite in the database were extremely small, which may necessitate revision of these fields as more data becomes available.

Following construction of the Co-Th classification diagram, data from the Bismark and Kurile island arcs were used to test its accuracy based on unaltered rocks from modern intra-oceanic island arcs. A total of 121 samples from the Earth Reference Data and Models Database (http://www.earthref.org) (Appendix B.3) have been plotted on Figure 5.8. The diagram accurately classifies the samples, and although there is some scatter, most of the samples fall within the "correct" fields. The SHC samples in the Bismark and Kurile island arc data plot at low Th values below the aforementioned boundary line, however, the IAT and CA samples plot

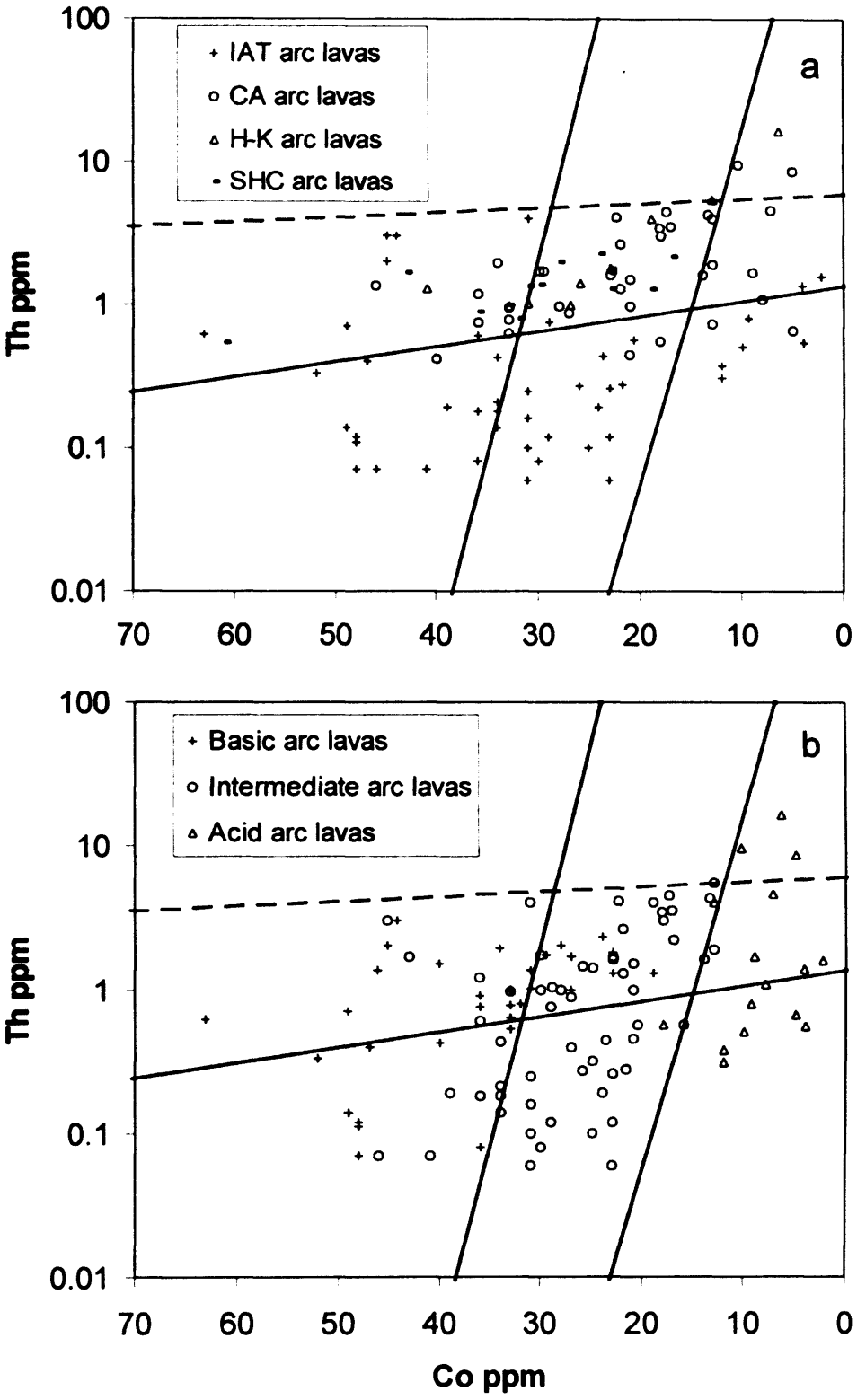

Figure 5.8 – Co vs Th discrimination diagrams (a) tholeiite, calc-alkaline, high-K calc-alkaline and shoshonitic and (b) basic, intermediate and acidic lavas from the Bismark and Kurile island arcs.

mostly within their respective fields. The Co-Th discrimination diagram is therefore presented as a suitable classification diagram for island arc lavas (Fig. 5.6).

5.2.7 Archean and Proterozoic Case Studies

It has been demonstrated that the Co-Th discrimination diagram accurately classifies post-Mesozoic island arc rocks. To further demonstrate the usefulness of the diagram Archean IAT and CA arc lavas from the Superior Province, Canada were plotted (Fig. 5.9). The data were obtained from the Earth Reference Data and models database (http://www.earthref.org) (Appendix B.4). By averaging the data from the post-Mesozoic arcs and the Superior Province it was noted that the Archean lavas have higher Th contents for a given Co content (Appendix B.2 and B.4). This results in the IAT lavas plotting mostly within the CA field and in turn the CA rocks plotting above the dashed line suggesting SHC affinities.

Th abundances within Archean IAT and CA lavas are ~ 90-120% higher than in the recent arc lavas used in this study. Similarly, Co abundances for given Th contents are also slightly higher (~ 20-50%) in the Archean lavas than in the post-Mesozoic arc lavas. It is not obvious how differing amounts of partial melting, related to the higher mantle temperatures in the Archean (Rapp *et al.*, 1991), can be responsible for the Co and Th increases. Larger amounts of partial melting would produce increases in Co abundances but it would also decrease the Th abundance, which is opposite to what is observed. The higher abundance is probably derived from the Archean upper mantle being more enriched than post-Mesozoic upper mantle source regions because less crustal material has been extracted from it (e.g. Workman and Hart, 2005), however, a full explanation to the cause of the element abundance increase is beyond the scope of this study.

A modified Co-Th diagram was constructed, to account for the Archean Th and Co enrichment using the arc lavas from the Superior Province (Figs. 5.9, 5.10 and 5.11). Testing the modified diagram was difficult due to the lack of island arc analyses from Archean greenstone belts. However, a small data set of 62 samples from the Baltic Shield, the Western Australian and Kaapvaal cratons were obtained from the Earth Reference Data and Models Database (http://www.earthref.org) (Fig. 5.12) (Appendix B.5).

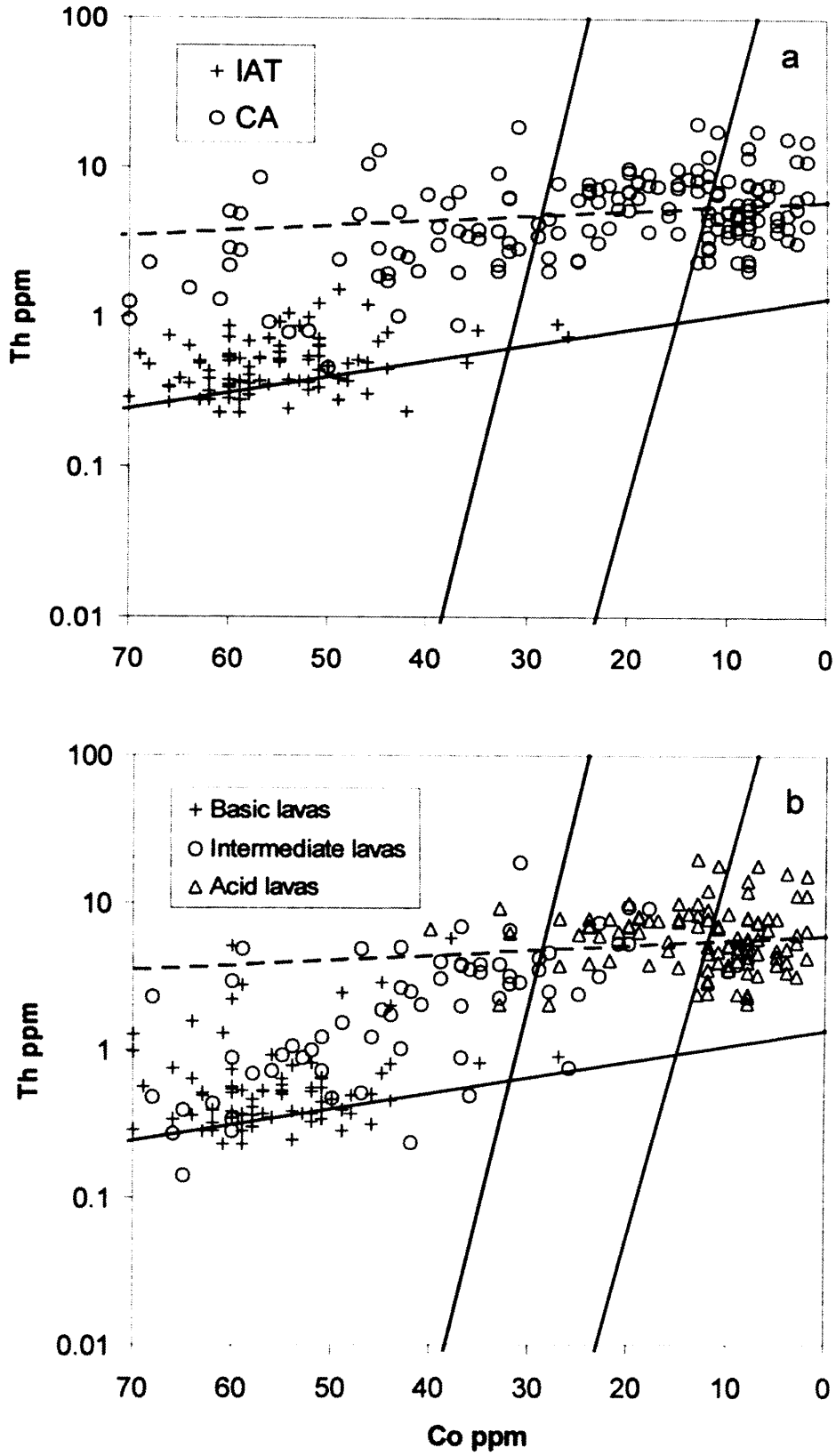

Figure 5.9 – (a) IAT and CA and (b) basic, intermediate and acidic lavas from the Superior Province, Canada. The samples do not plot within the correct fields due to the high Th and Co abundances in Archean arc lavas (Appendix B.4).

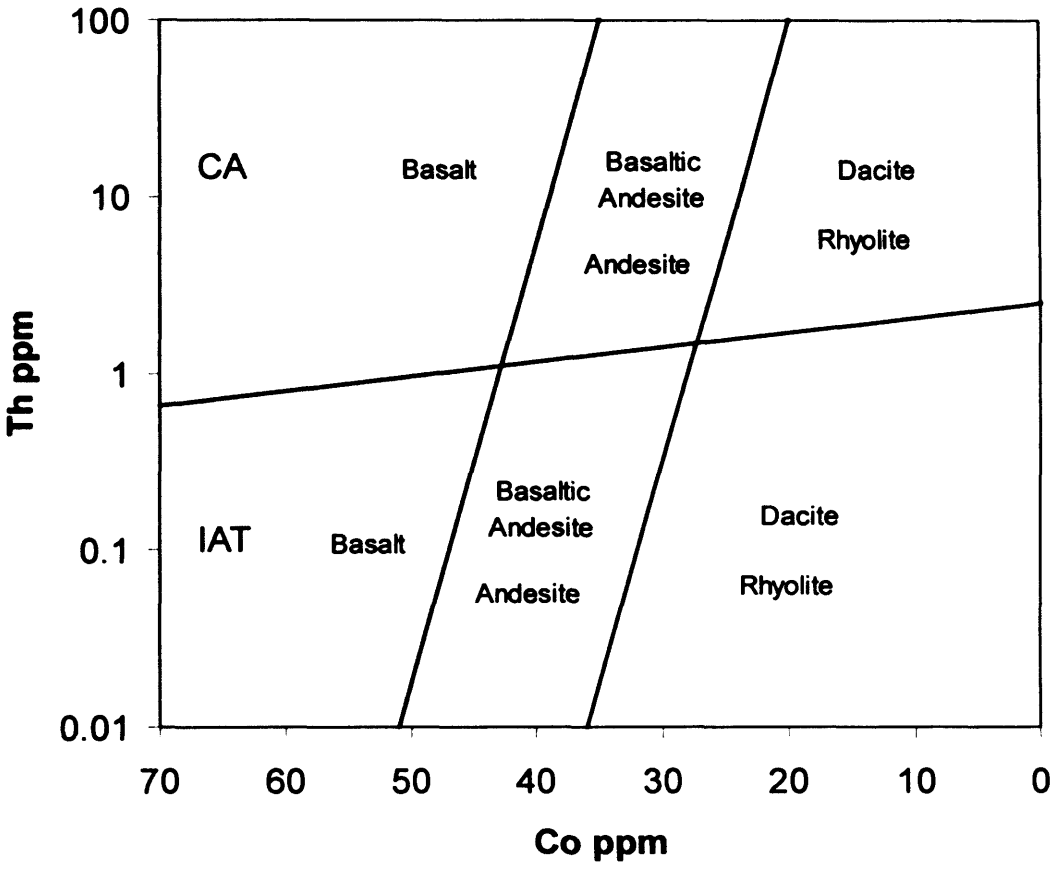

Figure 5.10- Modified Co-Th diagram to be used on Archean island arc lavas. The field boundaries are: basalt - basaltic andesite and andesite, X-51, 35, Y-0.01, 100; basaltic andesite/andesite – dacite/rhyolite, X-36, 20, Y-0.01, 100; IAT – CA, X-70, 0, Y-0.66, 2.5.

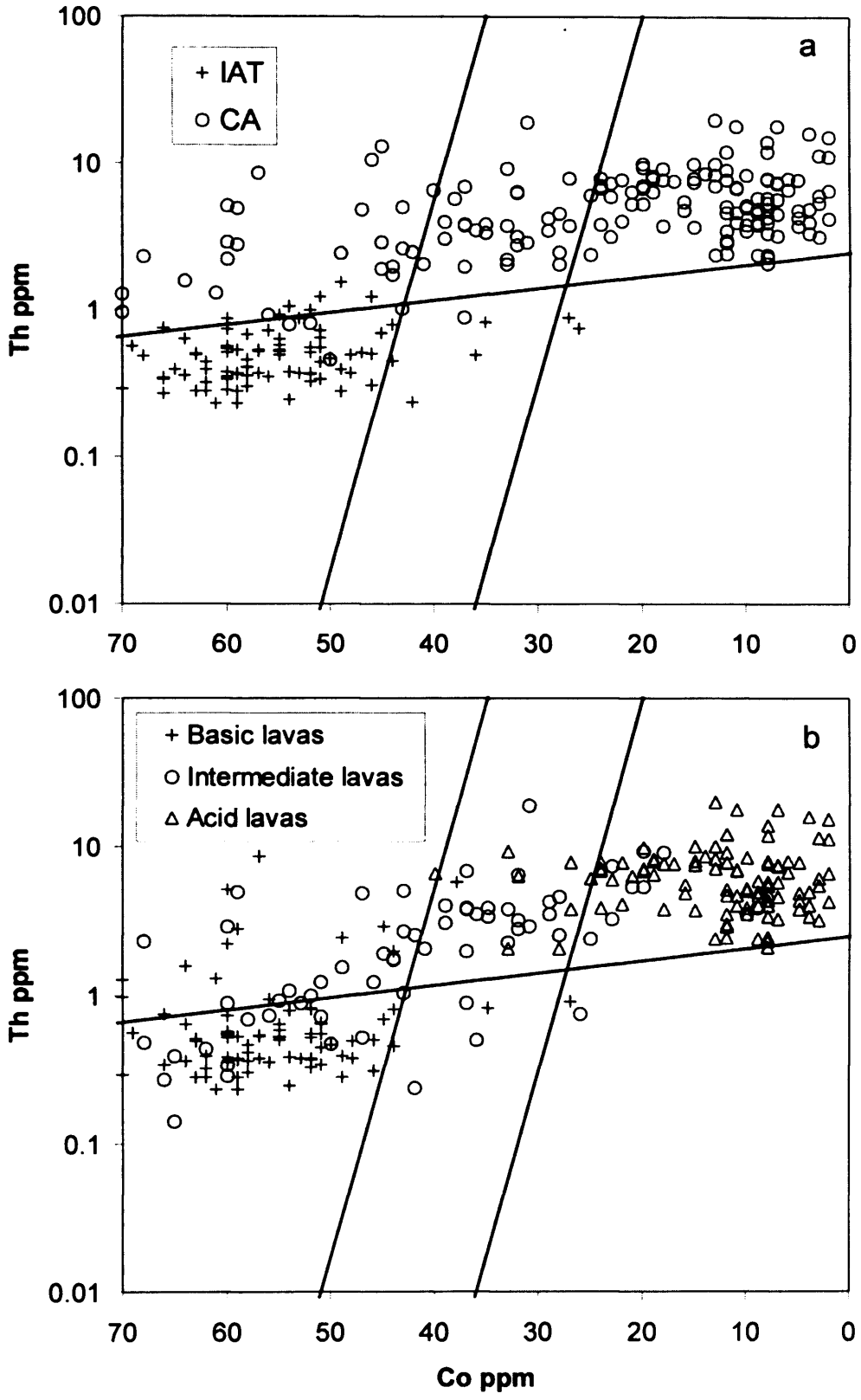

Figure 5.11 – Modified Co-Th diagrams displaying (a) IAT and CA and (b) basic, intermediate and acidic island arc lavas of the Superior Province, Canada.

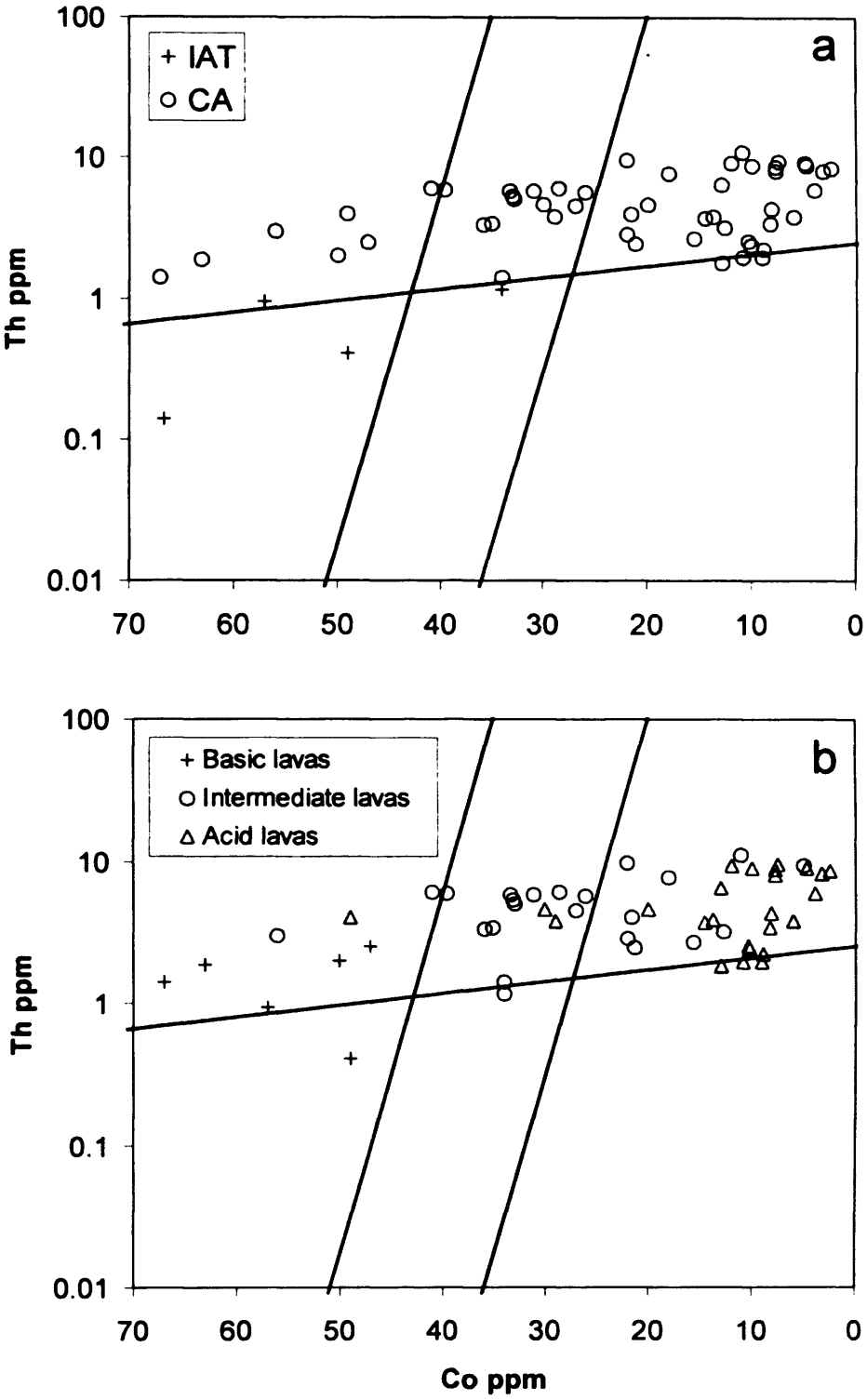

Figure 5.12 – Modified Co-Th diagrams displaying (a) IAT and CA and (b) basic, intermediate and acidic island arc lavas of the Baltic Shield, Western Australian and Kaapvaal cratons.

The Th in the Archean samples is immobile and can be used to classify the LILE, LREE and actinide enrichment in the rocks. Consequently, using the modified Co-Th plot, the Archean data plots within the correct fields with regards to IAT and CA, however, the HK and SHC fields have been removed due to a complete lack of samples.

Classifying the Superior Province Archean rocks on the basis of their fractionation is problematic because SiO_2 values within these samples do not always form coherent trends with immobile elements such as Zr. Therefore, classifying these rocks on the K_2O vs SiO_2 diagram is not always an accurate method of determining the extent of fractionation of the lavas prior to them being plotted on the Co-Th diagram. The silica may have been mobilised by secondary alteration and metamorphism or may have been relatively enriched due to the removal of mobile elements. Conversely, some Archean lavas do display coherent silica trends and so can be used for constructing the new boundaries of the modified Co-Th diagram. Co displays more coherent liquid lines of descent than the silica in the Baltic Shield, Western Australian and Kaapvaal rocks and it is therefore proposed that the Co values should be used to assess the fractionation of Archean island arc lavas (Polat and Kerrich, 2001; Hollings and Kerrich, 2004).

Proterozoic volcanic lavas which have subduction component signatures have been tested on the *original* Co-Th diagram. The data was obtained from the Proterozoic Transvaal and Soutpansberg successions, South Africa (2.1-2.2 Ga) and the Coldbrook Group, Canada (630-600 Ma) (Crow and Condie, 1990; Dostal and McCutheon, 1990). The Proterozoic island arc lavas plot within the correct fields for both fractionation and LILE, LREE and actinide classification on the original Co-Th diagram. Consequently the modified Archean Co-Th diagram is not required for classifying altered Proterozoic island arc lavas.

5.2.8 Summary

The Co-Th discrimination diagram fulfils two requirements, it identifies the extent of enrichment of LILE, LREE and actinides of an altered lava by using Th as a proxy for K and it uses Co as a proxy for silica to identify how fractionated an arc lava is. The use of this diagram is especially valuable for lavas within tropical regions due to the more intense weathering, but, works equally well with rocks that

have undergone hydrothermal alteration. However, it should be stressed that other immobile trace element discrimination diagrams, petrography and field evidence, should be used when studying a suite of lavas because of the fields of any discrimination diagram being based upon probability contours. The latite, trachyte, HK and SHC fields on the diagram have been constructed with small data sets, thus it may be necessary to modify these fields as more data becomes available. However, the Co-Th plot is presented as a discrimination diagram which can accurately classify altered island arc lavas and will be used in Chapter 6 and 7 to classify the Jamaican arc lavas.

5.3 Development of the Th/Zr-La/Yb, Ce/Lu-Sm/Yb, La/Hf-Sm/Y and Th/Hf-Sm/Yb discrimination diagrams

5.3.1 Rationale for development

Determining the LILE, LREE and actinide enrichment of island arc lavas is not only important in classifying arc rocks, but, it also provides important information about the petrogenesis of those lavas. Certain immobile trace element discrimination diagrams have previously been constructed to determine the affinity of arc lavas e.g. the Th/Yb-Ta/Yb diagram of Pearce (1982) (Section 5.2.4). Nevertheless, this study aims to construct several more discrimination diagrams using immobile trace elements. These new diagrams will be used in conjunction with the Th/Yb-Ta/Yb and Co-Th diagrams to assess as fully as possible the LILE, LREE and actinide enrichment of an altered island arc lava.

Chapter 2 has demonstrated the importance to tectonic models of Caribbean evolution of the successful identification and dating of IAT and CA arc lavas. Consequently, these new diagrams should be able to further constrain the IAT, CA and SHC affinity of the Jamaican arc lavas in this study. The temporal identification of IAT and CA arc lavas in the Caribbean, together with a full petrogenetic analysis, will provide information on the possibility that the composition of the arc lavas changed as a result of the collision of the Caribbean oceanic plateau with the Great Arc of the Antilles in the Albian/Aptian or Campanian (Chapter 2).

5.3.2 The formation of IAT, CA and SHC rocks

On the K_2O vs SiO_2 discrimination diagram IAT lavas have lower K_2O concentrations than CA rocks, and in turn CA have lower abundances than HK and SHC rocks (Peccerillo and Taylor, 1976). CA rocks are more enriched, relative to IAT rocks, in LILE, LREE and certain actinides relative to HFSE, HREE, Ti and Y. Furthermore, SHC lavas are more enriched in these elements relative to CA rocks (Saunders *et al.*, 1980; Tatsumi *et al.*, 1986; Bau *et al.*, 1993; Arculus, 2003).

The relative enrichment in arc rocks of the most incompatible elements is produced by a variety of processes such as small degrees of partial melting, large amounts of fractional crystallisation, crustal assimilation and/or input of an LILE, LREE and actinide enriched component into a mantle source region or mantle derived magma (e.g. Saunders *et al.*, 1980; Pearce, 1982; Tatsumi *et al.*, 1986; Stern *et al.*, 1993; Miller *et al.*, 1994; Brenan *et al.*, 1995; Pearce and Peate, 1995; Keppler, 1996; Pearce, 1996). The formation of IAT, CA and SHC rocks in an intra-oceanic island arc could involve all of these processes. The differing chemistry of lavas produced by variable degrees of partial melting and fractionation is also related to the source mineralogy and fractionating mineralogy (Pearce, 1982). Therefore, the formation of IAT, CA and SHC lavas is highly complex and could potentially involve several petrogenetic processes.

5.3.3 The construction of the new discrimination diagrams

In order to construct suitable discrimination diagrams to solely distinguish IAT, CA and SHC rocks using immobile trace elements a number of considerations have to be taken into account: (1) Trace elements have to be chosen that reflect the enrichment of incompatible elements in SHC and CA lavas relative to IAT rocks; (2) For comparisons to be made, any new discrimination diagram has to be comparable to the conventional diagrams e.g. a tholeiitic lava on the K_2O vs SiO_2 diagram would have to be a tholeiitic lava in all the new diagrams; (3) The chemistry and petrogenesis of arc lavas has to be considered in order for the correct elements to be chosen (see Sections 5.2.3 and 5.2.4); (4) The new diagrams will be more valuable if they can also distinguish tholeiitic, calcalkaline and shoshonitic lavas in other tectonic environments.

Previously defined IAT, CA and SHC lavas (Section 5.2.5.1, Fig. 5.3 and Appendix B) were used to construct the new diagrams. The number of subduction components involved in arc genesis and the transport of certain elements by aqueous fluids and silicate melts derived from the slab is complex and controversial (Section 5.2.3). However, as with the Co-Th diagram, for the purpose of the construction of these new diagrams the subduction component(s) are characterised as a single entity that enriches the sub-arc mantle. It is also assumed that elements such as the LREE and Th are mobile in slab-derived aqueous fluids and behave in a similar manner to the LILE (e.g. Tatsumi *et al.*, 1986; Keppler, 1996) (Section 5.2.3).

LILE, LREE, Th, U and Pb have lower partition coefficients than most of the HFSE and HREE (with the exception of Nb and Ta) during "normal" mantle melting (McCulloch and Gamble, 1991). The more incompatible nature of these elements results in them having larger concentrations in a melt formed by small amounts of partial melting or a melt remaining after large scale fractional crystallisation (Pearce, 1996). Rb, Ba, Th, K, U, Pb, Sr and the LREE have similarly low distribution coefficients during partial melting of a mantle source region and during aqueous fluid release from a subducting slab (McCulloch and Gamble, 1991). Conversely, although Nb and Ta have low partition coefficients during "normal" mantle melting, they have high partition coefficients during aqueous fluid/slab interaction (Tatsumi *et al.*, 1989; McCulloch and Gamble, 1991). Th and the LREE are also immobile during subsurface weathering (Pearce, 1982).

Therefore, the relative enrichment of LREE and Th relative to the HFSE and HREE can be used as a proxy for the enrichment of K relative to the HFSE and HREE (Section 5.2.5.1). Thus, the abundances of LREE and/or Th or ratios of the LREE and Th relative to HFSE or HREE can be used to distinguish IAT, CA and SHC lavas.

Arc magmas, unlike magmas produced in other tectonic environments show a relative depletion of Nb and Ta (McCulloch and Gamble, 1991). This occurs due to the higher distribution coefficients (>1) of Nb and Ta between an aqueous fluid-subducted basaltic slab interaction compared to a melt-subducted basaltic slab or mantle interaction (McCulloch and Gamble, 1991; Pearce and Peate, 1995; Pearce, 1996). Therefore, if the new discrimination diagrams are to be used for lavas in other tectonic environments it would be logical not to use Nb and Ta in their construction.

The new diagrams are constructed using unaltered island arc data from the post-Mesozoic Aleutian, Banda, Central American, Honshu, Izu-Bonin, Kamchatka, Kermadec, Lesser Antilles, Luzon, Mariana, New Hebrides, New Zealand, Papua New Guinea, Ryukyu, Sunda and Tonga arcs. The same data was used to construct the Co-Th discrimination diagram and all references to the data used can be found in Appendix B.

The IAT, CA and SHC lavas were plotted on La/Hf, La/Yb, Ce/Lu, Th/Zr, Th/Hf, Sm/Yb and Sm/Y ratio diagrams (Figs. 5.13 and 5.14). The different lava suites exhibited distinct separation i.e. the IAT have lower Th/Zr ratios than the SHC rocks. Once it was shown that the IAT, CA and SHC data separated into different fields in Th-LREE/HFSE-HREE space it was then necessary to statistically construct boundary lines between them.

Mr Martin Wolstencroft helped in the construction of these new diagrams. His expertise in using the computer program *Generic Mapping Tools* (GMT) enabled percentage contours to be constructed around the data. All the data collection, statistical decisions and data interpretation were performed by the author.

It was originally thought that the IAT, CA and SHC lavas could be separated using the mean average values, however, as with data for the Co-Th diagram, this gave poor results due to several samples having anomalously high concentrations of the respective incompatible trace elements. For example, if 90% of a data set contains values which vary between 0.1-0.2, and the remaining 10% have very high values (from 0.3-10) the calculated mean value would give an anomalously high value. As such, it was decided to separate the IAT, CA and SHC data using the median average values, which identifies the centre point of the data. The position of the median value then enabled percentage contours to be accurately constructed around the data.

The proximity of a particular point to the median (n) was then calculated using:

$$n = \sqrt{(X_n - Med_X)^2 + (Y_n - Med_Y)^2}$$

Where X_n is the value of x for the point, Y_n is the value of y for the point, Med_x is the median of the x dataset and Med_y is the median of the y dataset

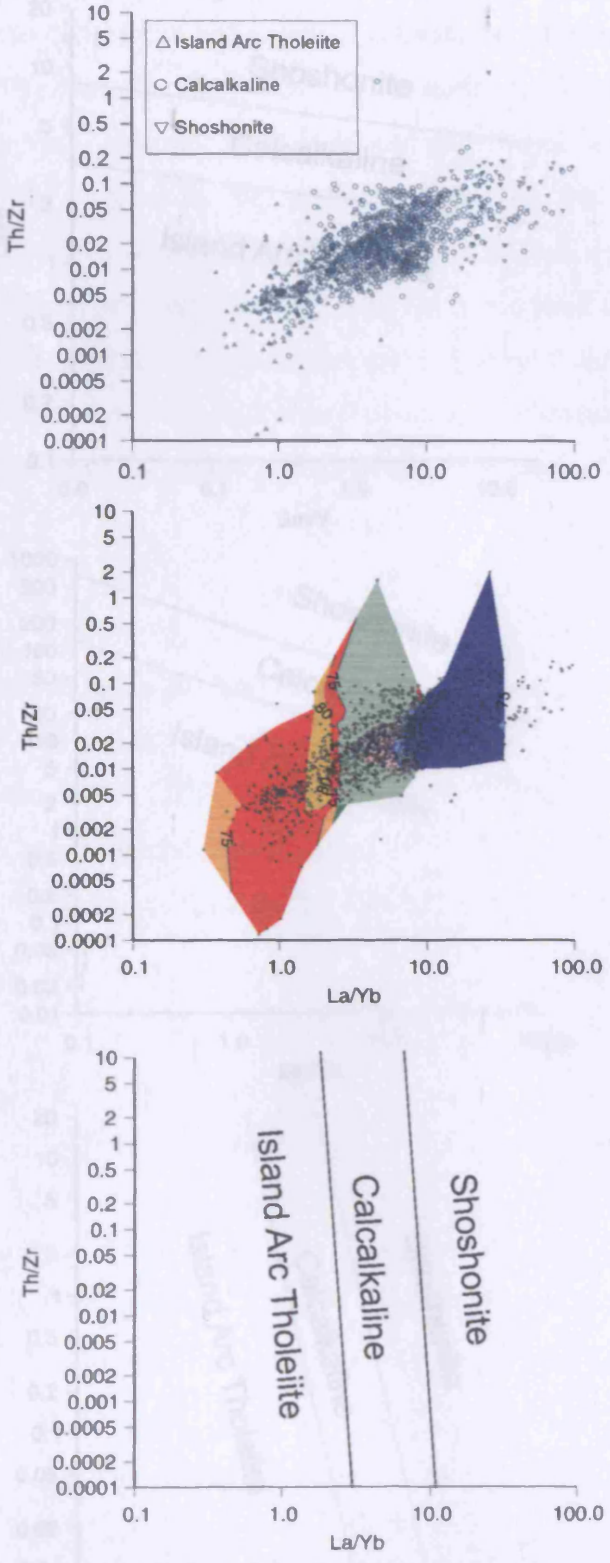

Figure 5.13 – Step by step construction of the IAT, CA and SHC boundary lines in the Th/Zr-La/Yb classification diagram (a) Diagram with IAT, CA and SHC data; (b) Construction of the 75, 80 and 85% contours separating the data into three distinct fields (see text); (c) Boundary lines drawn to separate the three fields.

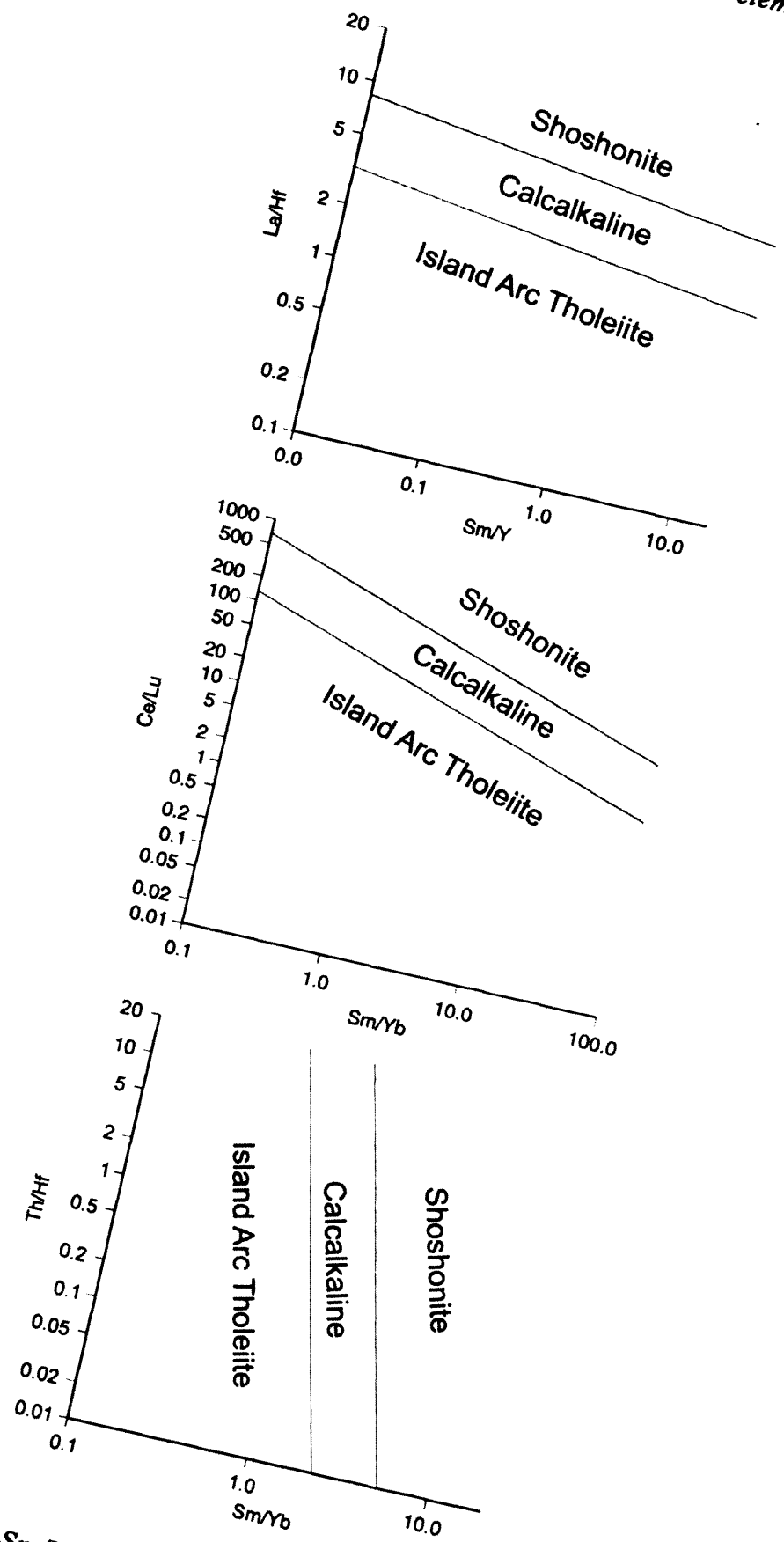

Figure 5.14 – Ce/Lu-Sm/Yb, La/Hf-Sm/Y, Th/Hf-Sm/Yb classification diagrams.

(M. Wolstencroft pers. comm. 2006). This allowed the data to be ranked according to how close they are to the median and enabled percentage contours to be constructed.

Pearce (1996) used the 90% contour (i.e. enclosing 90% of the samples) to revise the Zr/TiO_2-Nb/Y diagram of Winchester and Floyd (1977), Le Bas *et al.* (1992) used the 75% contour to construct the fields on the Total Alkali Silica diagram and 85% contours were used to construct the Co-Th diagram (Section 5.2.6). For the new diagrams in this study the 75% contours were used to form the IAT, CA and SHC fields because (i) they encloses the vast majority of the data, (ii) it enables most of the scatter away from the peak distribution to be eliminated and (iii) there is little overlap between the 75% contour fields (Figs. 5.13 and 5.14).

5.3.4 Summary

The Th/Zr- La/Yb, La/Hf- Sm/Y, Ce/Lu- Sm/Yb and the Th/Hf-Sm/Yb ratio diagrams will now be utilised in conjunction with the Th/Yb-Ta/Yb and Co-Th diagrams to fully assess the LILE, LREE and actinide enrichment of the Jamaican island arc rocks. The successful identification of the IAT and CA rocks and their subsequent dating will help constrain models of Caribbean plate tectonic evolution.

Chapter 6

Major, trace element and Pb-Sr-Hf-Nd isotope geochemistry and ^{40}Ar-^{39}Ar geochronology of Jamaican igneous rocks

6.1 Introduction

This chapter presents geochemical and geochronological data for the igneous rocks sampled in the Cretaceous inliers and in the Tertiary Wagwater belt of Jamaica. The geochemistry and geochronology provides information on both the origin and evolution of the igneous rocks in Jamaica and the evolution of the Caribbean plate from the early Cretaceous to the Tertiary.

Igneous rocks were collected over wide areas in the Central, Above Rocks, Blue Mountain, Benbow and the Sunning Hill Inliers and the Tertiary Wagwater Basin (Chapter 3). The primary objectives were to classify the igneous rocks with respect to fractionation and LILE, LREE and actinide enrichment, and to assess their tectonic affinities i.e. did they originate in a subduction-related setting, a mid-ocean ridge or an oceanic plateau? Once their affinities have been determined, the geochemistry and ^{40}Ar-^{39}Ar dating are used to study the origin and evolution of the rocks (Chapter 7). Additionally, the geochemical sections for the Bath-Dunrobin lavas and tuffs in Chapters 6 and 7 have been formulated as a separate paper, which has been accepted for publication in Lithos.

The temporal and spatial identification of arc, MORB, back arc or plateau rocks in Jamaica is valuable in determining plate tectonic evolution of the region by identifying when, where, and how the different volcanic rocks formed. A full

summary of the analytical techniques used in this thesis can be found in Appendices C and D.

6.2 Degree of alteration

All of the igneous rocks sampled in Jamaica have been subject to varying degrees of alteration due to both tropical weathering and hydrothermal and metamorphic processes (Chapters 4 and 5). This alteration complicates any standard geochemical interpretation by modifying the primary geochemical abundances and ratios of the mobile elements.

Any geochemical approach to determine the primary geochemical features of the Jamaican rocks has to firstly investigate the extent to which certain elements have been mobilised. If there has been significant elemental mobility, the petrogenesis must be studied using immobile elements. A detailed discussion of the mobility and immobility of elements can be found in Chapters 4, 5 and Section 4.1.2. In summary, elements that are readily mobilised include Ca, Mg, Na, K, Rb, Ba, Sr, Pb and U, whereas Zr, Hf, Nb, Ta, Y, Ti, Cr, Co, P, Ni, the REE, Th, Ga and Sc are generally immobile (cf. Floyd and Winchester, 1975, 1978; Winchester and Floyd, 1976, 1977; Pearce, 1982, 1996; Arculus, 1987; Summerfield, 1997; Polat *et al.*, 2002).

6.3 Identification and Interpretation

6.3.1 Classification

The alteration of the Jamaican igneous rocks has changed their primary mineralogy and chemistry. This prevents them from being classified using modal mineral proportions, CIPW norms, mobile elements and oxides and so the rocks can only be classified by using immobile trace elements and their isotopes (Chapter 5). Therefore, the immobile element classification diagrams described in Chapter 5 (e.g. the Zr/Ti vs Nb/Y diagram of Winchester and Floyd (1977) and Floyd and Winchester (1978) and the new Co-Th discrimination diagram) is used to classify the igneous rocks from Jamaica. The immobile trace element ratio discrimination plots

developed with Mr Martin Wolstencroft (PhD student, Cardiff University 2005-2008), which statistically separate lavas into IAT, CA and SHC fields, will also be used to aid in the classification of these altered volcanic arc lavas (Chapter 5).

6.3.2 Tectonic affinity

Previous work on Jamaica and the other islands in the Greater Antilles (Chapters 2 and 3) demonstrates that the igneous rocks in the Cretaceous inliers and in the Tertiary Wagwater Belt may be derived from either an island arc, MORB or oceanic plateau setting (Jackson, 1987; Donnelly *et al.*, 1990; Kerr *et al.*, 2003).

An igneous rock from a particular tectonic setting will often have a unique geochemistry displaying a relative enrichment and/or depletion in certain elements and radiogenic isotopes. These relative enrichments and depletions along with field and petrographic evidence will be used to identify the tectonic affinity of the rock. Some simple field and geochemical characteristics that may be used in a tectonic discrimination can be seen in Table 2.1, Chapter 2.

6.4 The Bath-Dunrobin Formation, Blue Mountain Inlier - Oceanic Plateau Rocks

Nineteen samples from the Bath-Dunrobin Formation in the Blue Mountain Inlier were analysed for major and trace elements (Section E.5 and E.9 Appendix E). These samples are comprised of 17 basalts and 2 tuffs. Of these samples, 6 were analysed for Pb-Sr-Hf-Nd isotopes (Appendix D). In addition, sample AHBD07, which is a felsic dyke that cross-cuts the peridotites at Cedar Valley, is discussed in Section 6.6.

6.4.1 Element mobility

All the Bath-Dunrobin lavas have experienced varying degrees of alteration and element mobility due to tropical weathering, hydrothermal and metamorphic processes. Therefore, it is important to determine to what extent the primary geochemical features of the Bath-Dunrobin lavas have been modified.

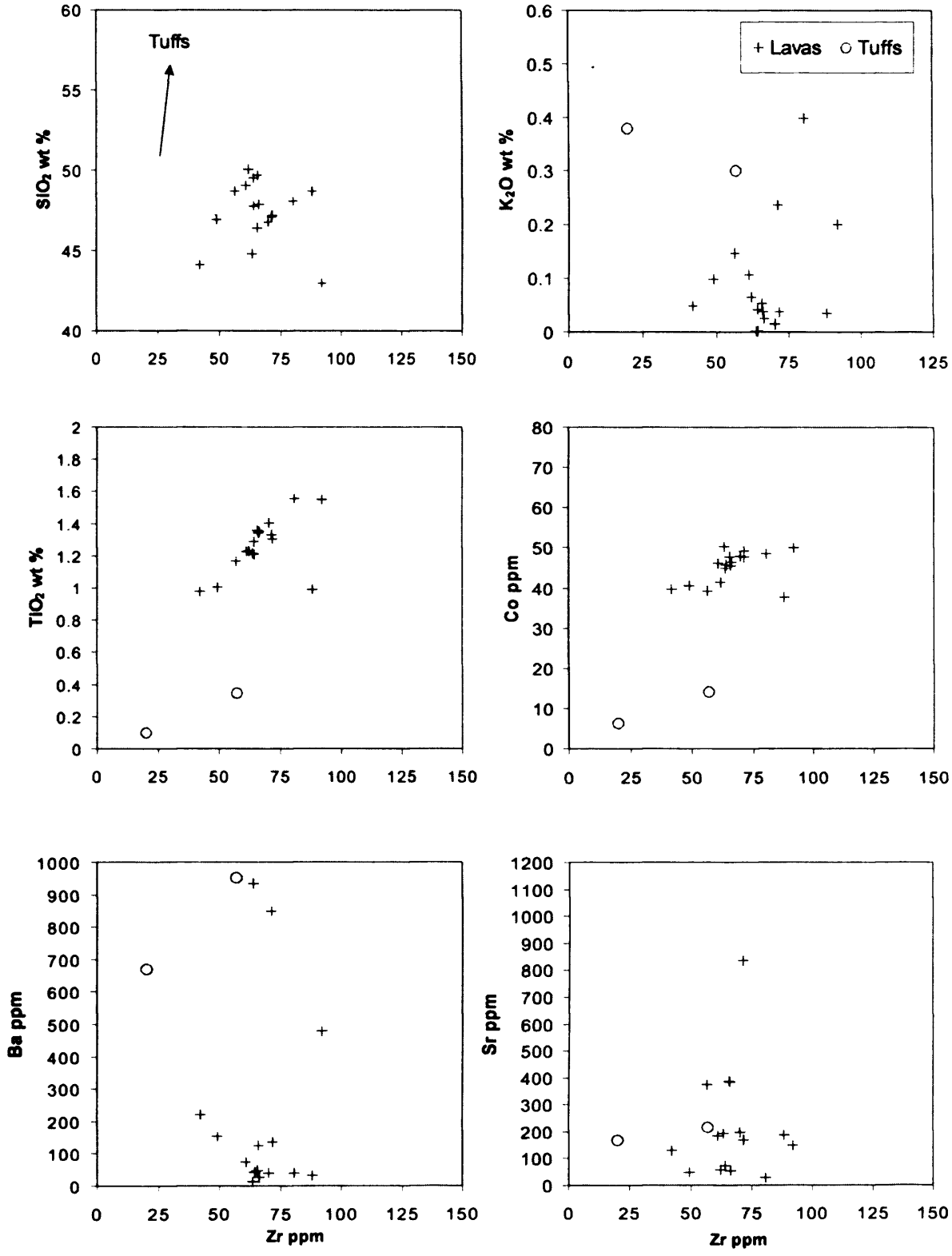

Figure 6.1 – Selected plots of major and trace elements vs. Zr for the Bath-Dunrobin rocks. The degree of mobility of an element is represented by its correlation with Zr. A mobile element shows no correlation, whereas, an immobile element displays a good correlation. A correlation can be a straight or curved line depending on whether the element is incompatible and/or compatible during fractional crystallisation or partial melting. AFC processes can also significantly modify liquid lines of descent.

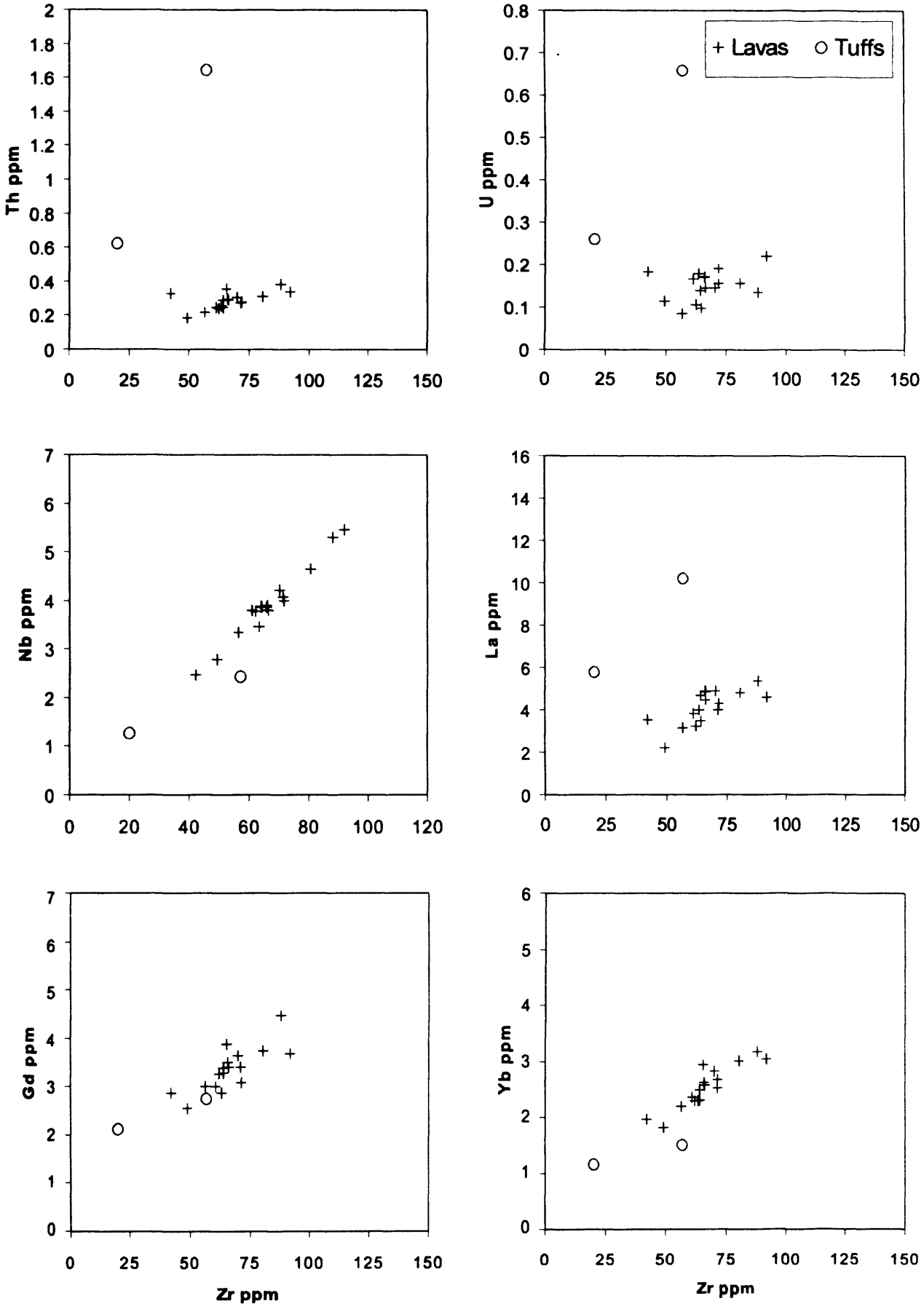

Figure 6.1 – continued.

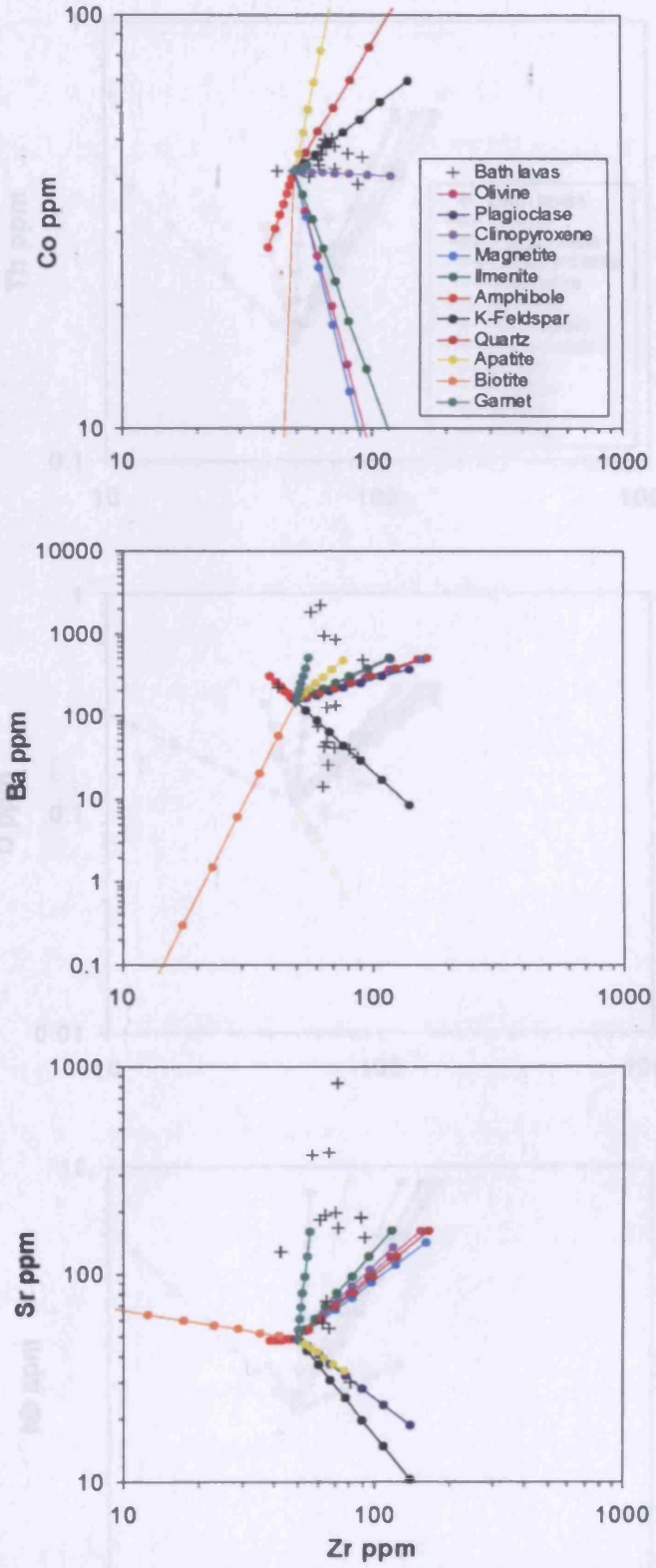

Figure 6.2 – Selected variation diagrams with vectors showing the composition of olivine, plagioclase, clinopyroxene, magnetite, ilmenite, amphibole, K-feldspar, quartz, apatite, biotite, and garnet with up to 70% fractional crystallisation of the AHBD23 starting composition (each tick represents 10% crystallisation) (Appendices E and G).

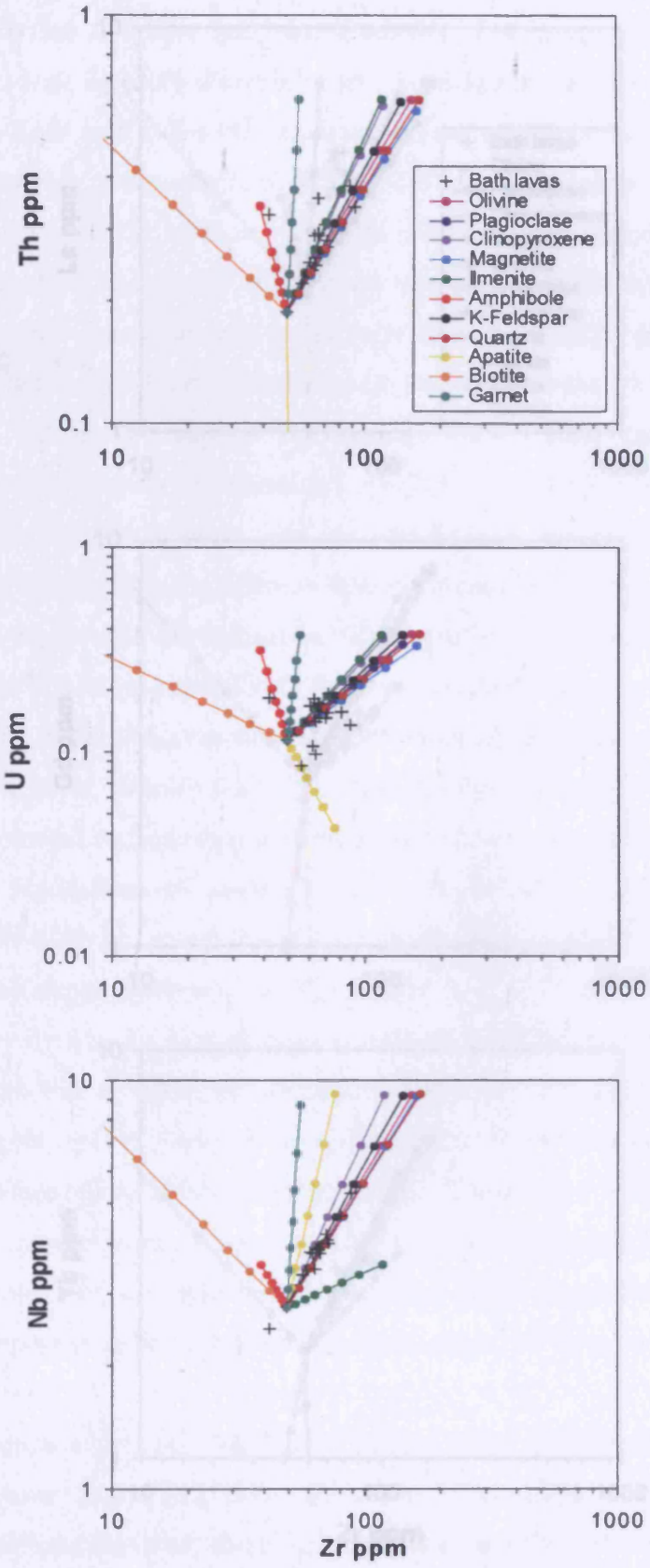

Figure 6.2 – continued

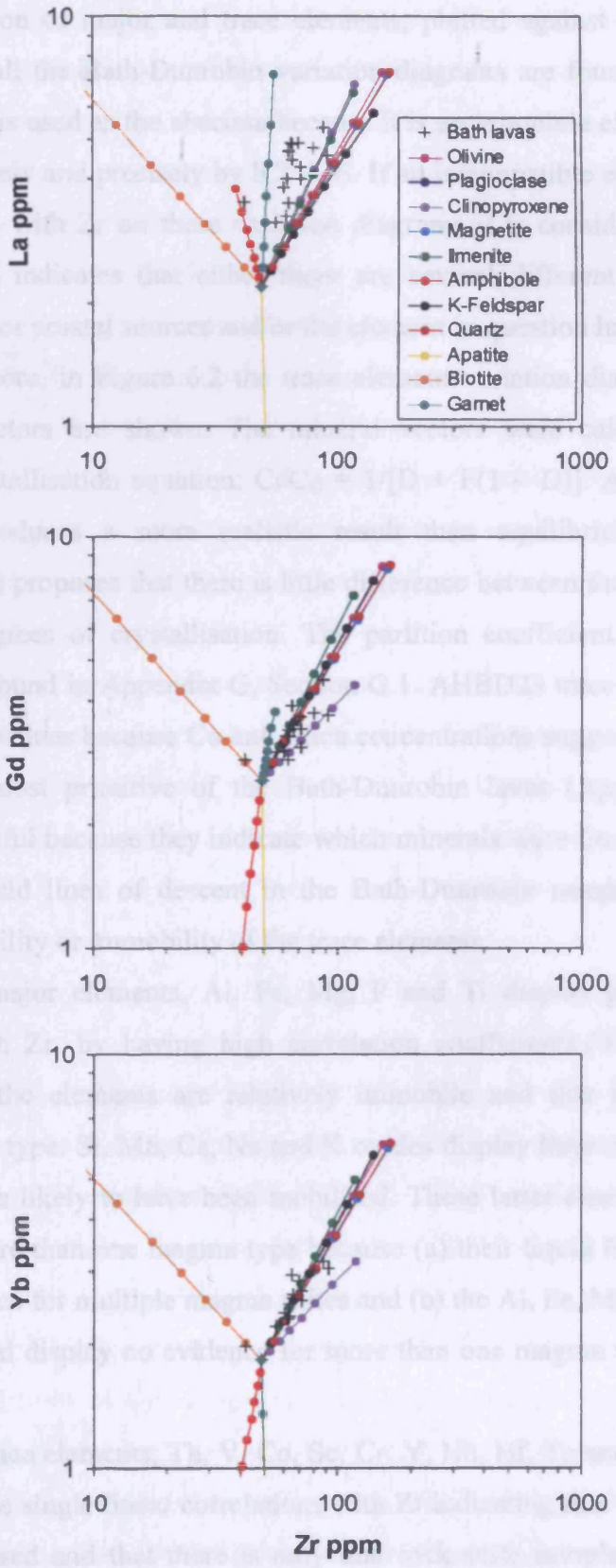

Figure 6.2 – continued

A selection of major and trace elements, plotted against Zr, are shown in Figure 6.1 and all the Bath-Dunrobin variation diagrams are found in Section E.9, Appendix E. Zr is used as the abscissa because it is an immobile element and can be analysed accurately and precisely by ICP-MS. If an incompatible element produces a good correlation with Zr on these variation diagrams it is considered immobile. A poor correlation indicates that either there are several different rock suites with different mantle or crustal sources and/or the element in question has been mobilised.

Furthermore, in Figure 6.2 the trace element variation diagrams are logged and mineral vectors are shown. The mineral vectors were calculated using the equilibrium crystallisation equation: $C_l/C_O = 1/[D + F(1 - D)]$. Although Rayleigh fractionation produces a more realistic result than equilibrium crystallisation, Rollinson (1993) proposes that there is little difference between the two mechanisms at moderate degrees of crystallisation. The partition coefficient data and related sources can be found in Appendix G, Section G.1. AHBD23 trace element data was used for the C_O values because Co and silica concentrations suggest that this sample is one of the most primitive of the Bath-Dunrobin lavas (Appendix E). These diagrams are useful because they indicate which minerals were fractionating in order to form the liquid lines of descent in the Bath-Dunrobin samples and they also confirm the mobility or immobility of the trace elements.

Of the major elements, Al, Fe, Mg, P and Ti display good single linear correlations with Zr, by having high correlation coefficients (Fig. 6.1 and E.9), indicating that the elements are relatively immobile and that there is only one sampled magma type. Si, Mn, Ca, Na and K oxides display little correlation with Zr and are therefore likely to have been mobilised. These latter elements do not show evidence for more than one magma type because (a) their liquid lines of descent do not show evidence for multiple magma suites and (b) the Al, Fe, Mg, P and Ti oxides are immobile and display no evidence for more than one magma type (Fig. 6.1 and E.9).

Of the trace elements, Th, V, Co, Sc, Cr, Y, Nb, Hf, Ta and the REE display good to moderate single linear correlations with Zr indicating that the elements have not been mobilised and that there is only one rock suite sampled from the Bath-Dunrobin area (Figs 6.1 and 6.2). However, the data for Ba, Sr, U and Ga do not form liquid lines of descent and it is likely that these elements have been mobilised (Figs. 6.1, 6.2 and E.9). The mineral vector diagrams in Figure 6.2 also demonstrate

that the Bath-Dunrobin liquid lines of descent are formed by the fractional crystallisation of predominantly olivine, plagioclase feldspar and clinopyroxene.

It is assumed here that similar major and trace elements have been mobilised in the tuff samples, but, unfortunately there are not enough samples to fully assess element mobility on the variation diagrams. Nevertheless, the element data for the tuffs does not fall on the same liquid lines of descent as the Bath-Dunrobin lavas for immobile elements, suggesting that they represent a different magma type. This is understandable considering that pyroclastic deposits can be dispersed over wide areas; hence, they could represent material from distant and chemically different eruptive vents and thus be derived from different magma source regions. The composition of the tuffs is further complicated because they are probably composed of "accidental" igneous material, consequently, their chemistry may not represent their primary magmatic composition.

In conclusion, when interpreting the geochemical data for the Bath-Dunrobin lavas, it is important to exercise caution when using Si, Mn, Ca, Na, K, Ba, Sr, U and Ga (although Ga is not mobilised in other studies, see Section 6.2) because of their mobility (Figs. 6.1, 6.2 and E.9). In particular, the Pb and Sr isotopic ratios may have been modified.

6.4.2 Major elements

A full table of the major element analysis can be found in Section E.5, Appendix E. The SiO_2 and MgO concentrations of the lavas range from 43.0-50.0 wt. % and 5.8-8.4 wt. % respectively. The SiO_2 and MgO values imply that the lavas have basaltic compositions. However, the mobility of SiO_2 in these lavas makes this interpretation potentially unreliable. In addition, K_2O and Na_2O, which are usually important in classifying igneous rocks, are also mobile. Consequently, the total alkali silica (TAS) and SiO_2 vs K_2O diagrams cannot be used for classifying these lavas. Discrimination diagrams such as Zr/Ti-Nb/Y and Co-Th (Winchester and Floyd, 1977; Floyd and Winchester, 1978; Hastie *et al.*, 2007) use immobile trace elements and on these plots the Bath-Dunrobin lavas classify as tholeiitic basalts (Fig. 6.3).

The Co-Th discrimination diagram is specifically designed to assist in the classification of altered arc lavas (Hastie *et al.*, 2007) and, on this diagram, the tuffs

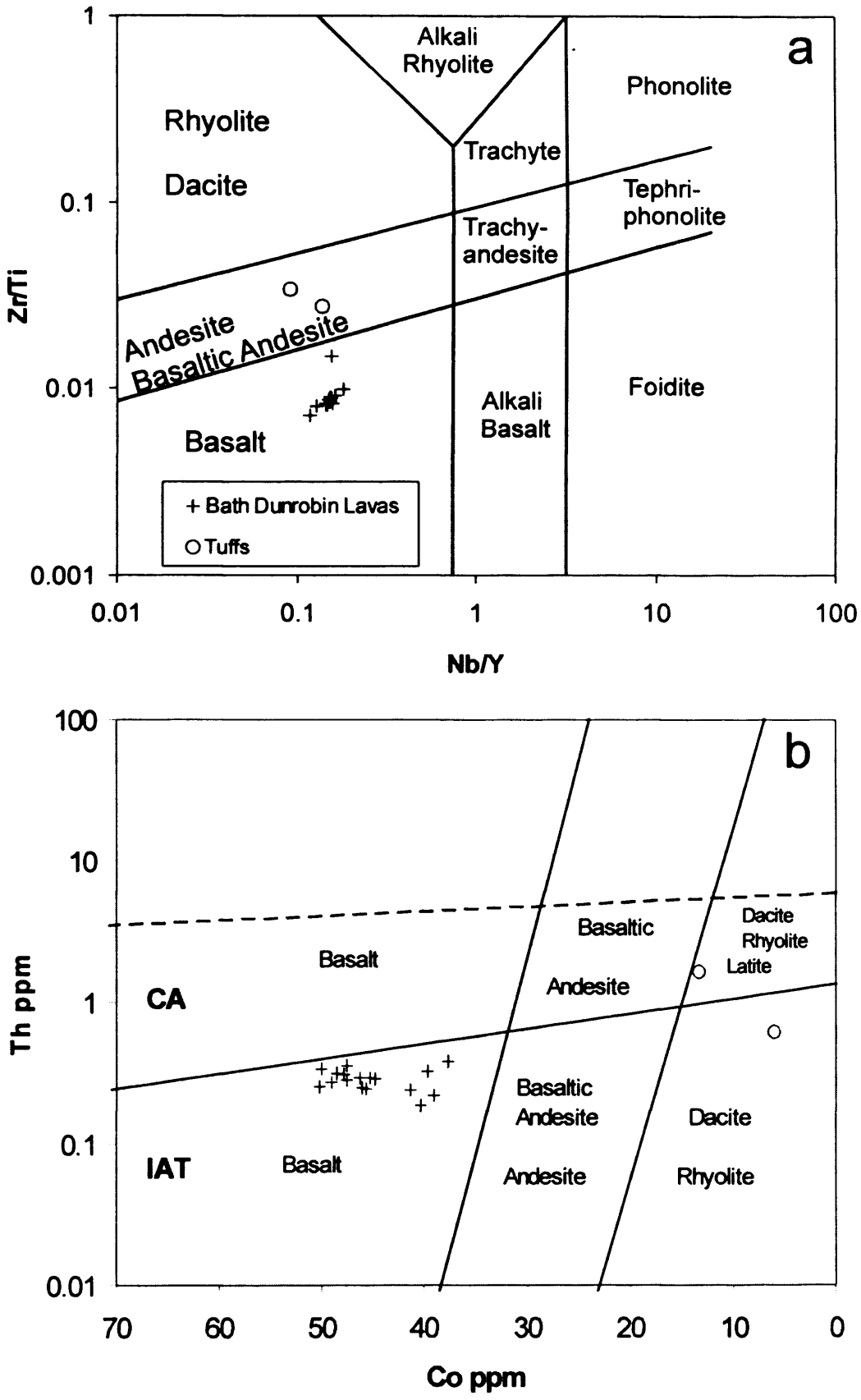

Figure 6.3 – (a) Zr/Ti vs Nb/Y and (b) Co vs Th discrimination diagrams (Pearce, 1996; Hastie *et al.*, 2007).

within the Bath-Dunrobin succession classify as IAT/CA dacites/rhyolites with very low MgO contents ($\leq$ 2 wt. %) (Fig. 6.3).

6.4.3 Trace elements

The trace element variation diagrams display predictable trends for immobile trace elements e.g. Cr decreases with increasing Zr and the REE increase with increasing Zr (Figs. 6.1, 6.2 and E.9). The liquid lines of descent are relatively linear and do not show inflections associated with the crystallisation of new minerals (Figs. 6.1, 6.2 and E.9). Figure 6.4 has chondrite-normalised REE and primitive mantle-normalised multi-element diagrams for the Bath-Dunrobin lavas. The basalts possess flat, near-parallel chondrite-normalised REE and primitive mantle-normalised trace element patterns. Some of the lavas have positive and negative Eu and Ti anomalies indicating the accumulation and/or fractionation of feldspars and Fe-Ti oxides in the magma. On the multi-element diagram, all the elements, with the exception of Th, are ~ 4-8 times that of estimated primitive mantle values. Th is depleted in comparison to the other elements with values only 2-4 times higher than primitive mantle values. Primitive mantle-normalised (pmn) trace element ratios, such as $(La/Yb)_{pmn}$ = 0.82-1.37, $(La/Nd)_{pmn}$ = 0.7-1.18, $(Ce/Lu)_{pmn}$ = 0.93-1.2 and $(Pr/Yb)_{pmn}$ = 0.95-1.28, do however, indicate some degree of heterogeneity with LREE being both enriched and depleted relative to the MREE and HREE.

The absence of negative Nb and Ta anomalies indicates that the Bath-Dunrobin lavas do not have an arc or back-arc affinity (Fig. 6.4). Rather, the basalts are enriched in Nb, Ta and LREE relative to HREE and other high field strength elements (HFSE) when compared to N-MORB. Even the relatively depleted Bath-Dunrobin samples are not as depleted as average N-MORB (Fig. 6.5). Conversely, the Jamaican lavas are more depleted in Nb, Ta and the LREE (relative to the HREE and other HFSE) than typical ocean island basalts (OIB) (Fig. 6.5). In the trace element ratio diagrams of Figure 6.5, the Bath-Dunrobin lavas have a similar composition to lavas from the Ontong Java plateau and other Caribbean plateau lavas, and plot between the compositions of average MORB and OIB.

The Nb/Y - Zr/Y diagram (Fig. 6.6) has proved useful in distinguishing plume derived lavas from MORB (Fitton *et al.*, 1997). On this diagram, plume-related lavas from Iceland plot between two parallel tramlines whereas N-MORB and

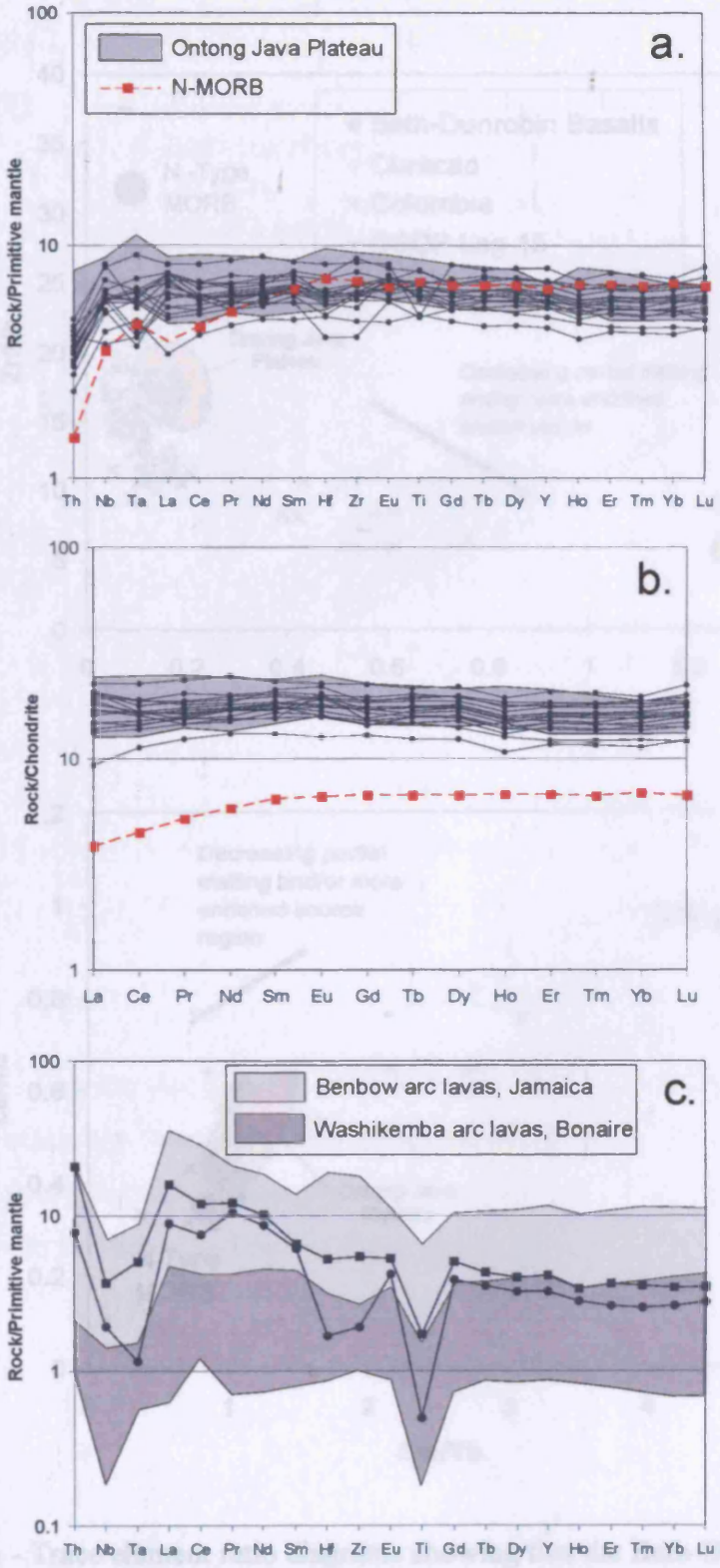

Figure 6.4 – (a) Primitive mantle-normalised multi-element plot and (b) chondrite-normalised REE plot of the Bath-Dunrobin lavas. (c) Primitive mantle-normalised multi-element plot of the tuffs found intercalated with the basaltic lavas. Normalising values from McDonough and Sun, (1995). Data sources for the Ontong Java rocks, the Benbow lavas and the Washikemba lavas can be found in Appendix F.

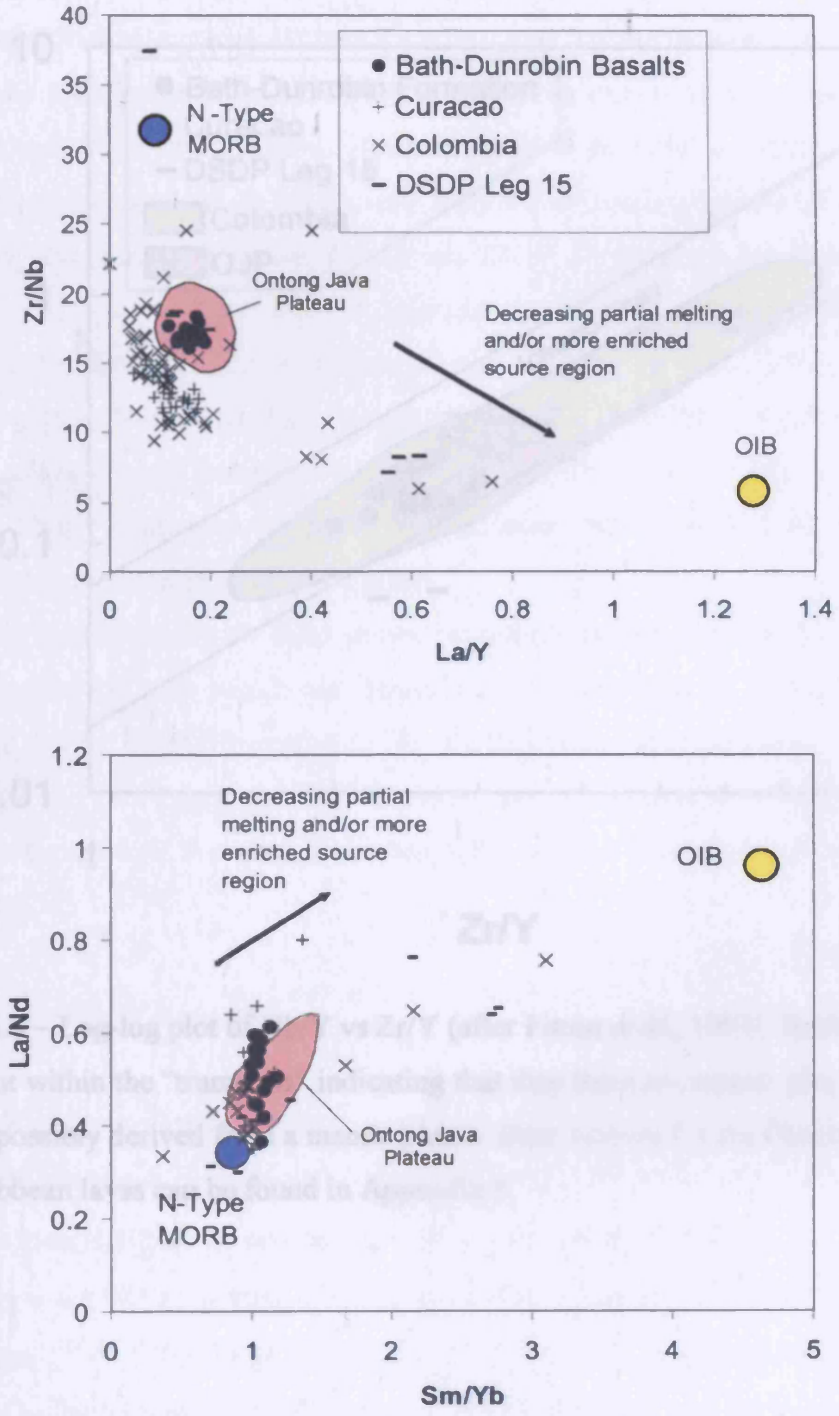

Figure 6.5 - Trace element ratio diagrams showing that the Bath-Dunrobin lavas have similar trace element ratios to the Ontong Java plateau and other plateau lavas from around the Caribbean region. MORB and OIB values from Sun & McDonough (1989). Data sources for the Ontong Java and the Caribbean lavas can be found in Appendix F.

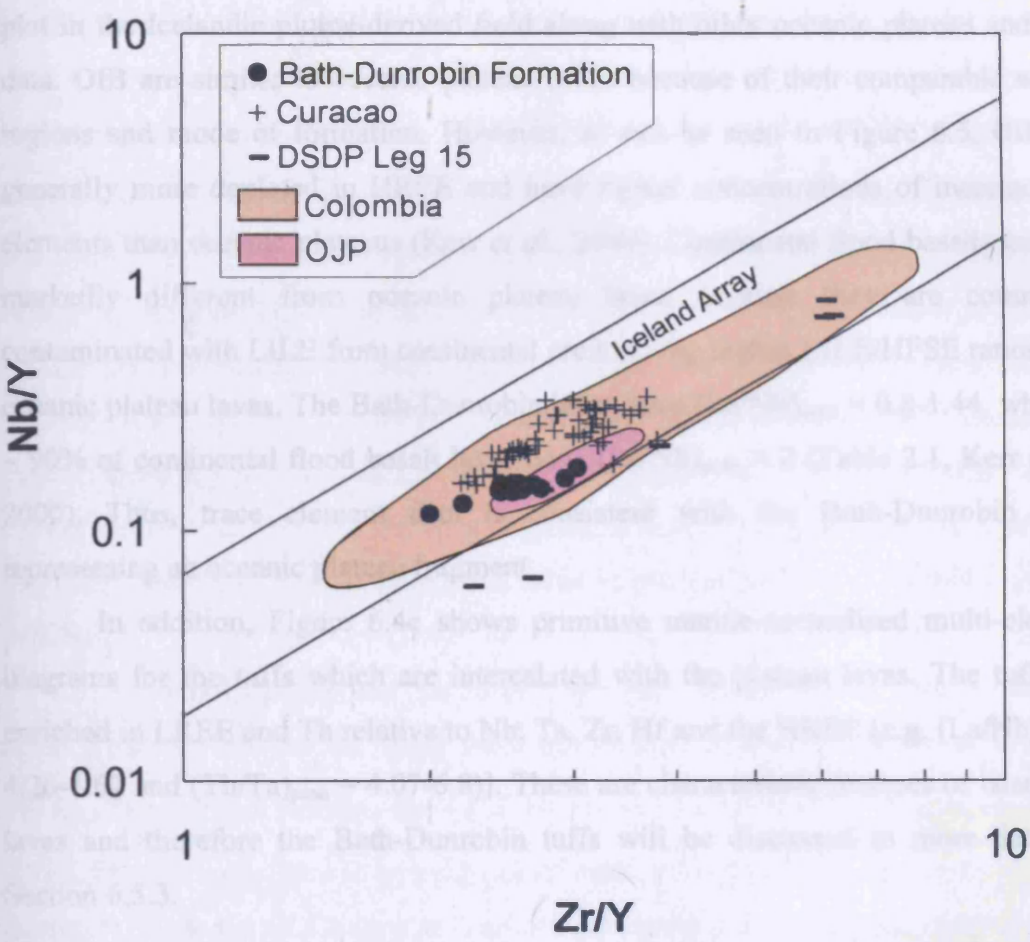

Figure 6.6 – Log-log plot of Nb/Y vs Zr/Y (after Fitton *et al.*, 1997). Bath-Dunrobin lavas plot within the "tramlines" indicating that they have an oceanic plateau origin and are possibly derived from a mantle plume. Data sources for the Ontong Java and the Caribbean lavas can be found in Appendix F.

arc data plot below the lower tramline (Fitton *et al.*, 1997). The Bath-Dunrobin lavas plot in the Icelandic plume-derived field along with other oceanic plateau and OIB data. OIB are similar to oceanic plateau rocks because of their comparable source regions and mode of formation. However, as can be seen in Figure 6.5, OIB are generally more depleted in HREE and have higher concentrations of incompatible elements than oceanic plateaus (Kerr *et al.*, 2000). Continental flood basalts are also markedly different from oceanic plateau lavas because they are commonly contaminated with LILE from continental crust giving higher LILE/HFSE ratios than oceanic plateau lavas. The Bath-Dunrobin lavas have $(La/Nb)_{pmn}$ = 0.8-1.44, whereas ~ 90% of continental flood basalt lavas have $(La/Nb)_{pmn} > 2$ (Table 2.1, Kerr *et al.*, 2000). Thus, trace element data is consistent with the Bath-Dunrobin lavas representing an oceanic plateau fragment.

In addition, Figure 6.4c shows primitive mantle-normalised multi-element diagrams for the tuffs which are intercalated with the plateau lavas. The tuffs are enriched in LREE and Th relative to Nb, Ta, Zr, Hf and the HREE [e.g. $(La/Nb)_{pmn}$ = 4.26-4.62 and $(Th/Ta)_{pmn}$ = 4.07-6.8)]. These are characteristic features of island arc lavas and therefore the Bath-Dunrobin tuffs will be discussed in more detail in Section 6.5.3.

6.4.4 Pb-Sr-Hf-Nd isotopes

Radiogenic isotope data for samples AHBD10, 16, 18, 19, 23 and 28 are shown in Figures 6.7 - 6.10 and Appendix D. The lavas were age-corrected to 88.5 Ma (Section 6.4.5) and possess $\varepsilon_{Nd}(i)$ = +7.6 – +9.0, $\varepsilon_{Hf}(i)$ = +12.0 – +12.8, $(^{87}Sr/^{86}Sr)i$ = 0.7034 – 0.7056, $(^{206}Pb/^{204}Pb)i$ = 19.04 – 19.67, $(^{207}Pb/^{204}Pb)i$ = 15.54 – 15.60 and $(^{208}Pb/^{204}Pb)i$ = 38.64 – 39.03 (Figures 6.7 - 6.10 and Appendix D).

On the basis of $(La/Yb)_{pmn}$ ratios the samples have been split into two groups: AHBD16, 23 and 28 have $(La/Yb)_{pmn}$ = 0.82-0.97 and are relatively depleted in comparison to AHBD10, 18 and 19 which have $(La/Yb)_{pmn}$ = 1.08-1.37 and are more enriched. However, in terms of their radiogenic isotopes the samples do not fall into chemically-distinct groups. This indicates that the range of trace element chemistry observed in the Bath-Dunrobin lavas is not due to the involvement of isotopically

different source regions with different depletion histories, but rather is because of varying degrees of partial melting of the same, or chemically similar, source regions.

As with many volcanic rocks which have undergone tropical weathering and seawater hydrothermal alteration, initial $^{87}Sr/^{86}Sr$ ratios extend to high values at near constant $\varepsilon_{Nd}(i)$ values (Fig. 6.7). The samples were acid-leached during preparation and thus $^{87}Sr/^{86}Sr$ values should represent the primary igneous composition. However, the Bath-Dunrobin lavas have been extensively altered and it is possible that the leaching process has not removed all the secondary alteration products. It can be seen from Figure 6.7 that the elevated $^{87}Sr/^{86}Sr$ ratios (even after intense acid leaching) are a common feature of most Caribbean plateau lavas (cf. Kerr *et al.*, 1996b; Hauff *et al.* 2000b) and so it is possible that this might represent a primary magmatic feature of Caribbean plateau lavas in general and Bath-Dunrobin lavas in particular.

One possibility is that the lavas have been contaminated with continental crust. However this can be firmly ruled out as such contamination would decrease the $\varepsilon_{Nd}(i)$ ratio and increase the LILE/HFSE and LREE/HFSE ratios (Kerr *et al.*, 2000). Furthermore, there is no evidence of continental crust beneath Jamaica, which is largely made up of Cretaceous-Tertiary carbonate and island arc igneous rocks overlying an assumed late Jurassic-Cretaceous altered oceanic basement (Robinson *et al.*, 1971; Draper, 1986). The island arc lavas cannot be responsible for contaminating the Bath-Dunrobin lavas and increasing their $^{87}Sr/^{86}Sr$ ratios because they would give similar geochemical signatures to contamination by continental crust (Kerr *et al.*, 2000).

The $^{87}Sr/^{86}Sr$ ratio in late Cretaceous seawater reached values of 0.7077 (Veizer, 1989). Therefore, it is possible that contamination with seawater-altered Cretaceous oceanic crust or carbonate could explain the elevated $^{87}Sr/^{86}Sr$ values in the Bath-Dunrobin lavas, with only minimal modification of Nd isotope ratios. Kerr *et al* . (1996 b) identified similar $^{87}Sr/^{86}Sr$ signatures in hydrofluoric acid-leached oceanic plateau basalts from Curaçao and suggested that these elevated $^{87}Sr/^{86}Sr$ ratios could be explained by the partial melting of hydrous phases in seawater-altered oceanic crust by hot ascending plume melts. Altered basalts contain increased concentrations of Na_2O. Thus a correlation between Na_2O and $^{87}Sr/^{86}Sr$ could imply

altered oceanic crustal contamination However, the mobilisation of the Na in the Bath-Dunrobin basalts makes such an assessment impossible.

Alternatively, <10% carbonate contamination of an ascending melt could form basalts with $^{87}Sr/^{86}Sr$ ratios of ~0.705 which would not result in a significant rise in the CaO content of the lavas (Kerr *et al.*, 1996b). Over 10% carbonate contamination would still increase the $^{87}Sr/^{86}Sr$ ratio but it would also increase the CaO content of the magmas. Unlike the Curaçao samples, the Ca in the Bath-Dunrobin lavas has been mobilised; therefore, like Na_2O, it is impossible to determine if there is a correlation between CaO and $^{87}Sr/^{86}Sr$ (E.9, Appendix E).

Révillon *et al.* (2002) analysed $^{87}Sr/^{86}Sr$ ratios of fresh clinopyroxenes in Gorgona lavas and found them to be lower than whole rock values, thus demonstrating that the $^{87}Sr/^{86}Sr$ increase in these particular Caribbean plateau lavas is because of secondary alteration and not due to the assimilation of altered oceanic crust or carbonate. Consequently, the elevated $^{87}Sr/^{86}Sr$ ratios in the Bath-Dunrobin lavas *may* be formed by similar secondary alteration processes. However, this could only be conclusively proven with a $(^{87}Sr/^{86}Sr)i$ study on separated Jamaican clinopyroxenes.

On $(^{207}Pb/^{204}Pb)i - (^{206}Pb/^{204}Pb)i$ and $(^{208}Pb/^{204}Pb)i - (^{206}Pb/^{204}Pb)i$ plots (Fig. 6.8), the Bath-Dunrobin lavas lie below the Northern Hemisphere Reference Line (NHRL) of Hart (1984), and could theoretically lie on a mixing line between HIMU and averaged MORB, which represents the depleted MORB mantle (DMM) component. None of the samples lie to the left of the NHRL, so it is unlikely that they contain EM1 or EM2 mantle components. The Bath-Dunrobin basalts generally possess more radiogenic Pb isotope ratios than other plateau basalts from either the Caribbean or the Ontong Java plateaux. Although enriched and depleted mantle components have been described from other plateau lavas in the Caribbean (e.g. Thompson *et al.*, 2003; Geldmacher *et al.*, 2003); the Bath-Dunrobin lavas are derived from a mantle source which is more enriched in $(^{206}Pb/^{204}Pb)i$ and $(^{208}Pb/^{204}Pb)i$. The Bath-Dunrobin lavas also fall on convincing theoretical mixing lines between HIMU and DMM in Pb-Nd isotopic isotope space and are more enriched in $(^{206}Pb/^{204}Pb)i$ and $(^{208}Pb/^{204}Pb)i$ at a given $\varepsilon_{Nd}(i)$ value than most of the other Caribbean oceanic plateau samples and the Ontong Java lavas (Fig. 6.9).

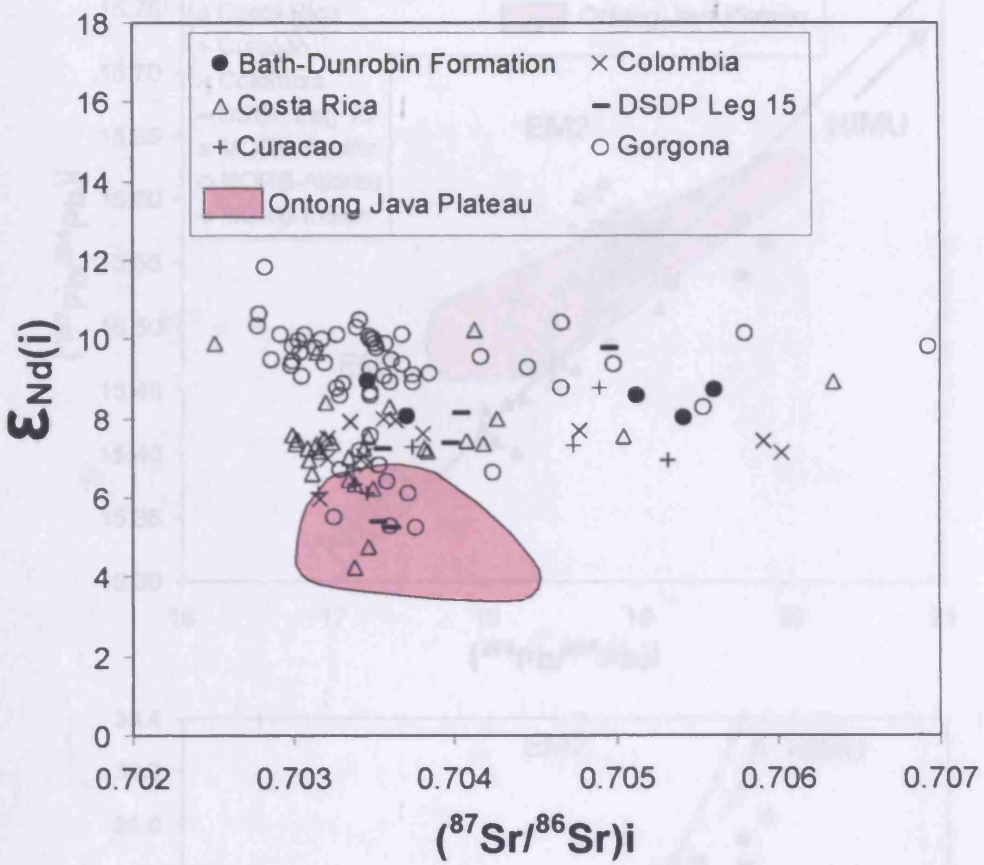

Figure 6.7 – $(^{87}Sr/^{86}Sr)i$ - $\varepsilon_{Nd}(i)$ diagram for the Bath-Dunrobin lavas, samples from other Caribbean oceanic plateau fragments and the Ontong Java Plateau (Appendices D and F).

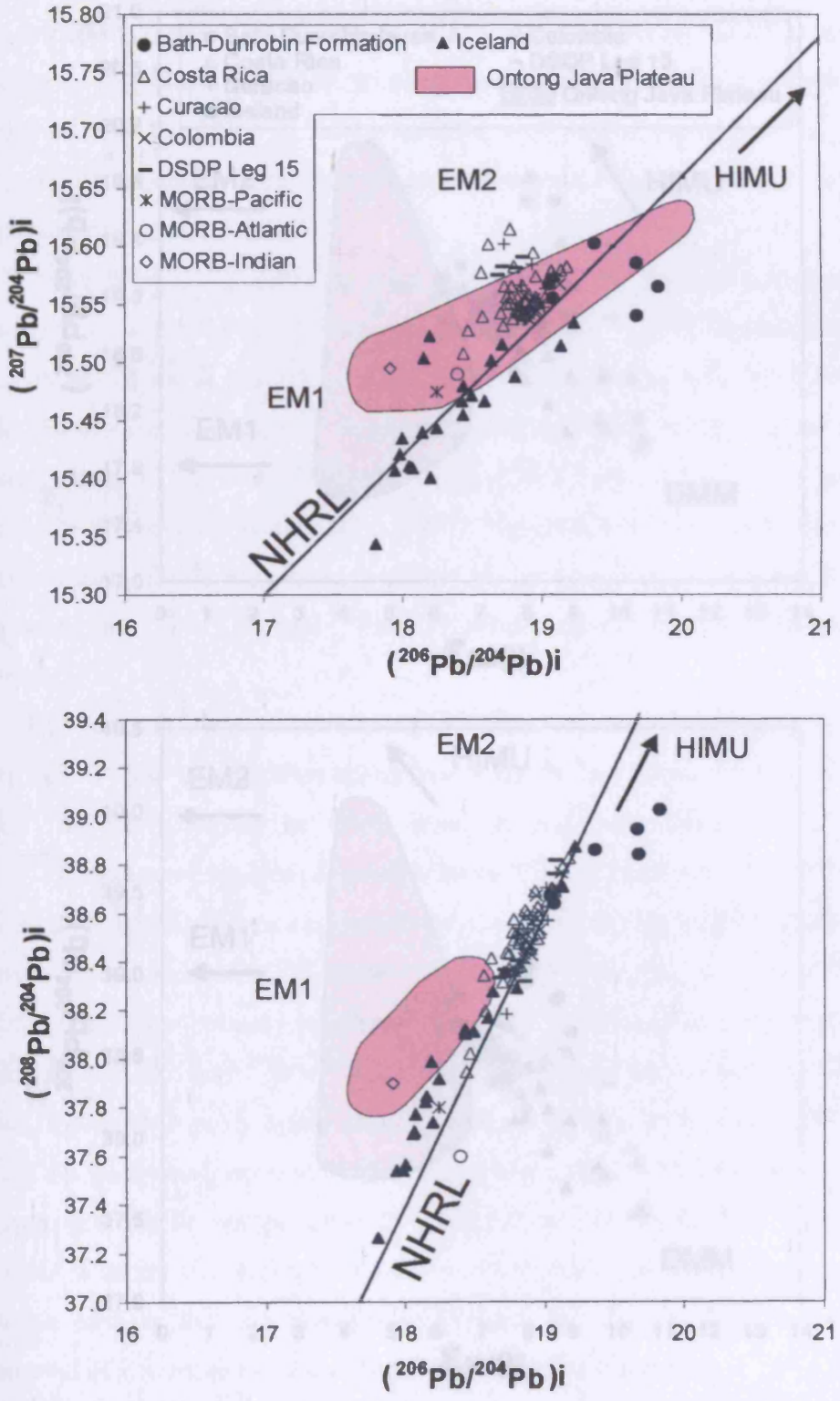

Figure 6.8 – Plots of $(^{207}Pb/^{204}Pb)i$ – $(^{206}Pb/^{204}Pb)i$ and $(^{208}Pb/^{204}Pb)i$ - $(^{206}Pb/^{204}Pb)i$ for the Bath-Dunrobin lavas, samples from other Caribbean oceanic plateau fragments, Iceland, N-MORB and the HIMU, EM1 and EM2 mantle end members. NHRL = Northern Hemisphere Reference Line (Hart, 1982) (Appendices D and F).

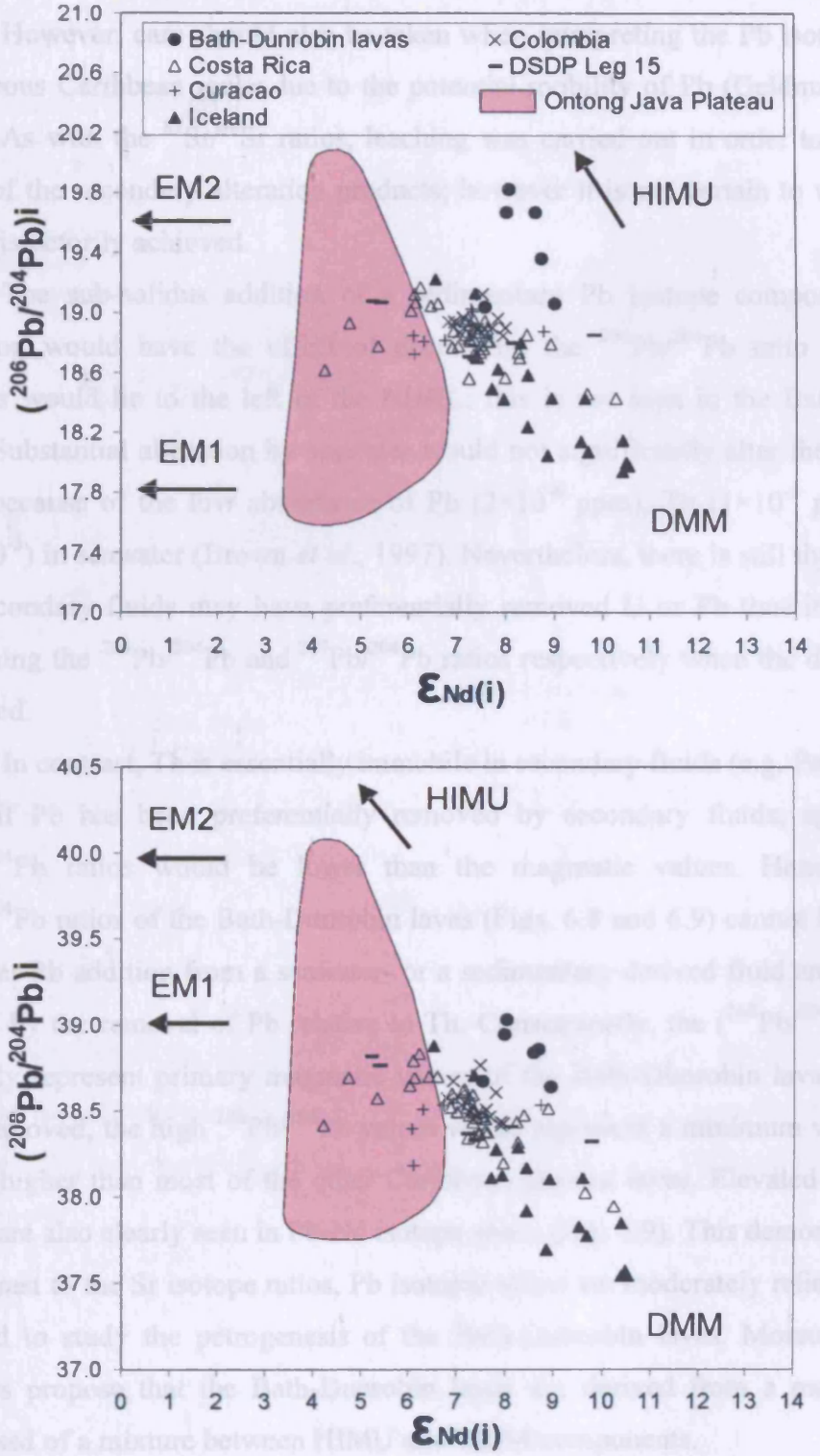

Figure 6.9 – Plots of $(^{206}Pb/^{204}Pb)i$ and $(^{208}Pb/^{204}Pb)i$- $\varepsilon_{Nd}(i)$ for the Bath-Dunrobin lavas, samples from other Caribbean oceanic plateau fragments, Iceland, N-MORB and the HIMU, EM1, EM2 and DMM mantle end members (Appendices D and F).

However, care should also be taken when interpreting the Pb isotope data in Cretaceous Caribbean rocks due to the potential mobility of Pb (Geldmacher *et al.*, 2003). As with the $^{87}Sr/^{86}Sr$ ratios, leaching was carried out in order to reduce the effect of the secondary alteration products; however it is not certain to whether this was satisfactorily achieved.

The sub-solidus addition of a sedimentary Pb isotope component during alteration would have the effect of decreasing the $^{206}Pb/^{204}Pb$ ratio so that the samples would lie to the left of the NHRL; this is not seen in the Bath-Dunrobin lavas. Substantial alteration by seawater would not significantly alter the Pb isotope ratios because of the low abundance of Pb (2×10^{-6} ppm), Th (1×10^{-5} ppm) and U (3.2×10^{-3}) in seawater (Brown *et al.*, 1997). Nevertheless, there is still the possibility that secondary fluids may have preferentially removed U or Pb thus increasing or decreasing the $^{206}Pb/^{204}Pb$ and $^{207}Pb/^{204}Pb$ ratios respectively when the data are age-corrected.

In contrast, Th is essentially immobile in secondary fluids (e.g. Pearce, 1982). Thus, if Pb has been preferentially removed by secondary fluids, age-corrected $^{208}Pb/^{204}Pb$ ratios would be lower than the magmatic values. Hence the high $^{208}Pb/^{204}Pb$ ratios of the Bath-Dunrobin lavas (Figs. 6.8 and 6.9) cannot be produced by either Pb addition from a seawater- or a sedimentary-derived fluid and cannot be formed by the removal of Pb relative to Th. Consequently, the $(^{208}Pb/^{204}Pb)i$ values probably represent primary magmatic values of the Bath-Dunrobin lavas. If Pb has been removed, the high $^{208}Pb/^{204}Pb$ values would represent a minimum value, which is still higher than most of the other Caribbean plateau lavas. Elevated Pb isotopic values are also clearly seen in Pb-Nd isotope space (Fig. 6.9). This demonstrates that, in contrast to the Sr isotope ratios, Pb isotopic ratios are moderately reliable and can be used to study the petrogenesis of the Bath-Dunrobin lavas. Moreover, the Pb isotopes propose that the Bath-Dunrobin lavas are derived from a mantle source composed of a mixture between HIMU and DMM components.

Nd and Hf isotope systems are more resistant to alteration than the Sr and Pb isotopic systems; hence, their ratios should represent the primary composition of the lavas (e.g. White and Patchett, 1984). The positive $\varepsilon_{Nd}(i)$ and $\varepsilon_{Hf}(i)$ values of the Bath-Dunrobin basalts indicate that the source region has a long term history of incompatible element depletion (Fig. 6.10). In Hf-Nd isotopic space, the Bath-

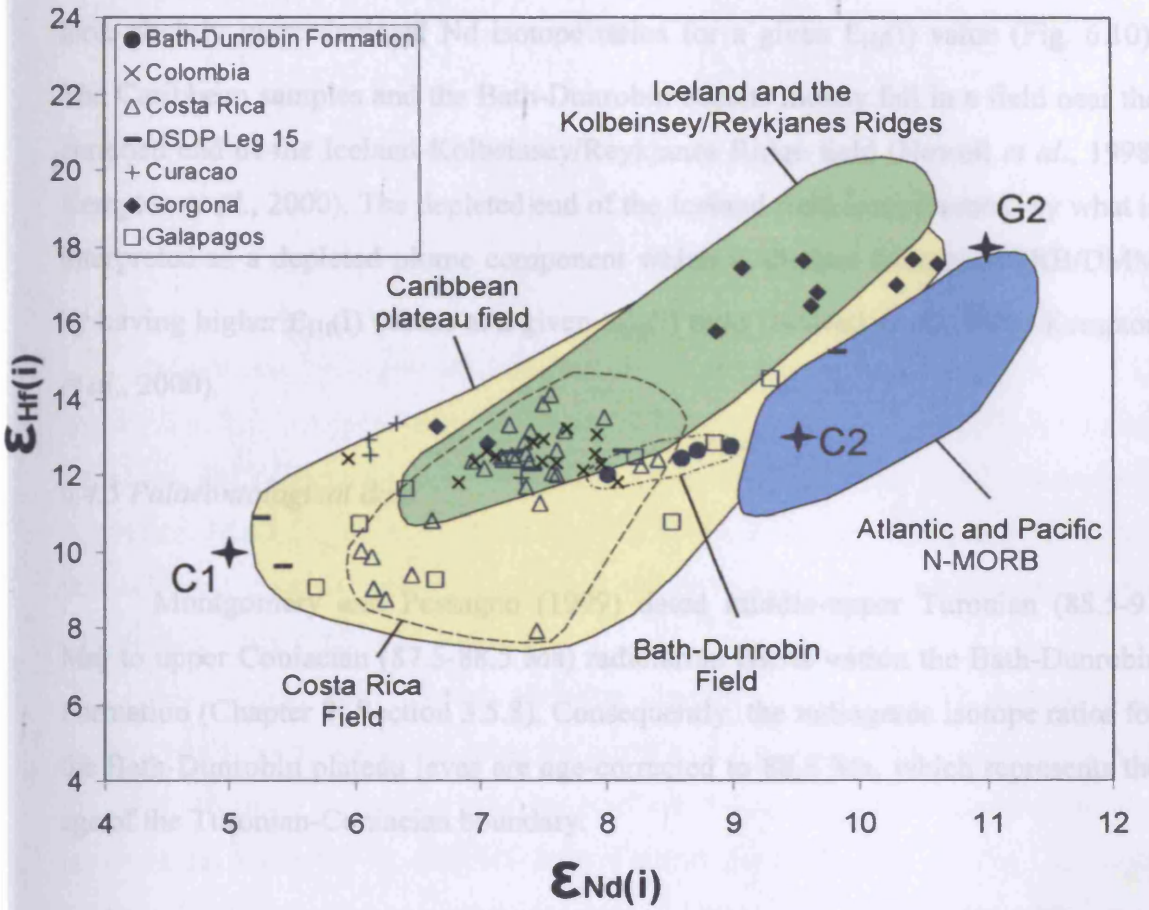

Figure 6.10 – Plot of $\varepsilon_{Nd}(i)$ - $\varepsilon_{Hf}(i)$ for the Bath-Dunrobin lavas, samples from other Caribbean oceanic plateau fragments, Iceland and N-MORB. (Appendices D and F). C1, C2 and G2 end-members are taken from Thompson *et al.* (2003) and are defined in Chapter 7.

Dunrobin lavas plot with the rest of the Caribbean plateau samples, although they do have slightly more depleted Nd isotope ratios for a given $\varepsilon_{Hf}(i)$ value (Fig. 6.10). The Caribbean samples and the Bath-Dunrobin basalts mostly fall in a field near the enriched end of the Iceland-Kolbeinsey/Reykjanes Ridge field (Nowell *et al.*, 1998; Kempton *et al.*, 2000). The depleted end of the Iceland field is represented by what is interpreted as a depleted plume component which is distinct from N-MORB/DMM by having higher $\varepsilon_{Hf}(i)$ values at a given $\varepsilon_{Nd}(i)$ ratio (Nowell *et al.*, 1998; Kempton *et al.*, 2000).

6.4.5 Palaeontological data

Montgomery and Pessagno (1999) dated middle-upper Turonian (88.5-91 Ma) to upper Coniacian (87.5-88.5 Ma) radiolarian cherts within the Bath-Dunrobin Formation (Chapter 3, Section 3.5.8). Consequently, the radiogenic isotope ratios for the Bath-Dunrobin plateau lavas are age-corrected to 88.5 Ma, which represents the age of the Turonian-Coniacian boundary.

6.5 Island Arc Rocks – The Benbow, Above Rocks, Sunning Hill and Central Inliers

6.5.1 The Benbow Inlier - the Devils Racecourse Formation

6.5.1.1 Element mobility

Major and trace element variation diagrams are shown in Figures 6.11, 6.12 and Section E.10, Appendix E. Only the Ca, Ti, P and Mn oxides show convincing liquid lines of descent for both the lower and upper lavas of the Devils Racecourse Formation. MgO, FeO*, Al_2O_3, Na_2O and K_2O have all been variably mobilised such that a liquid line of descent for either the lower or upper successions is not discernable (Figs. 6.11, 6.12 and E.10).

The logged trace element variation diagrams in Figure 6.12 show mineral vectors which were calculated using the equilibrium crystallisation equation, as with the Bath-Dunrobin lavas. The partition coefficient data and related sources can also be found in Appendix G. AHBI16 trace element data was used for the C_O values because its Co and silica concentrations suggest that it is one of the most primitive of the Benbow lavas (Fig. 6.12 and Appendix E).

As expected, Th, Hf, Nb, Ta, Y, Co, V and the REE are immobile, and form two distinct liquid lines of descent for the upper and lower lavas. The upper lavas are generally more enriched in these elements at a given Zr concentration and they commonly form steeper/more enriched trends (Figs. 6.11, 6.12 and E.10). Pb, Ba and Ga have been mobilised as no liquid lines of descent can be seen (Figs. 6.11, 6.12 and E.10). The scatter of the data for MgO, FeO*, Al_2O_3, Na_2O, K_2O, Pb, Ba and Ga is not formed by several magma suites with different mantle or crustal sources because the immobile elements only show two differing magma types (Fig. 6.11, 6.12 and E.10). Thus, these elements have been mobilised and should not be used in studying the petrogenesis of the Devils Racecourse lavas.

Peculiarly, the Sc data for the lower Devils Racecourse lavas forms a good liquid line of descent (E.10), however, Sc in the upper lavas appears to have been mobilised (Section E.10, Appendix E). This relationship is also seen with the U data (Fig. 6.11, 6.12 and E.10). U shows a good liquid line of descent for the lower

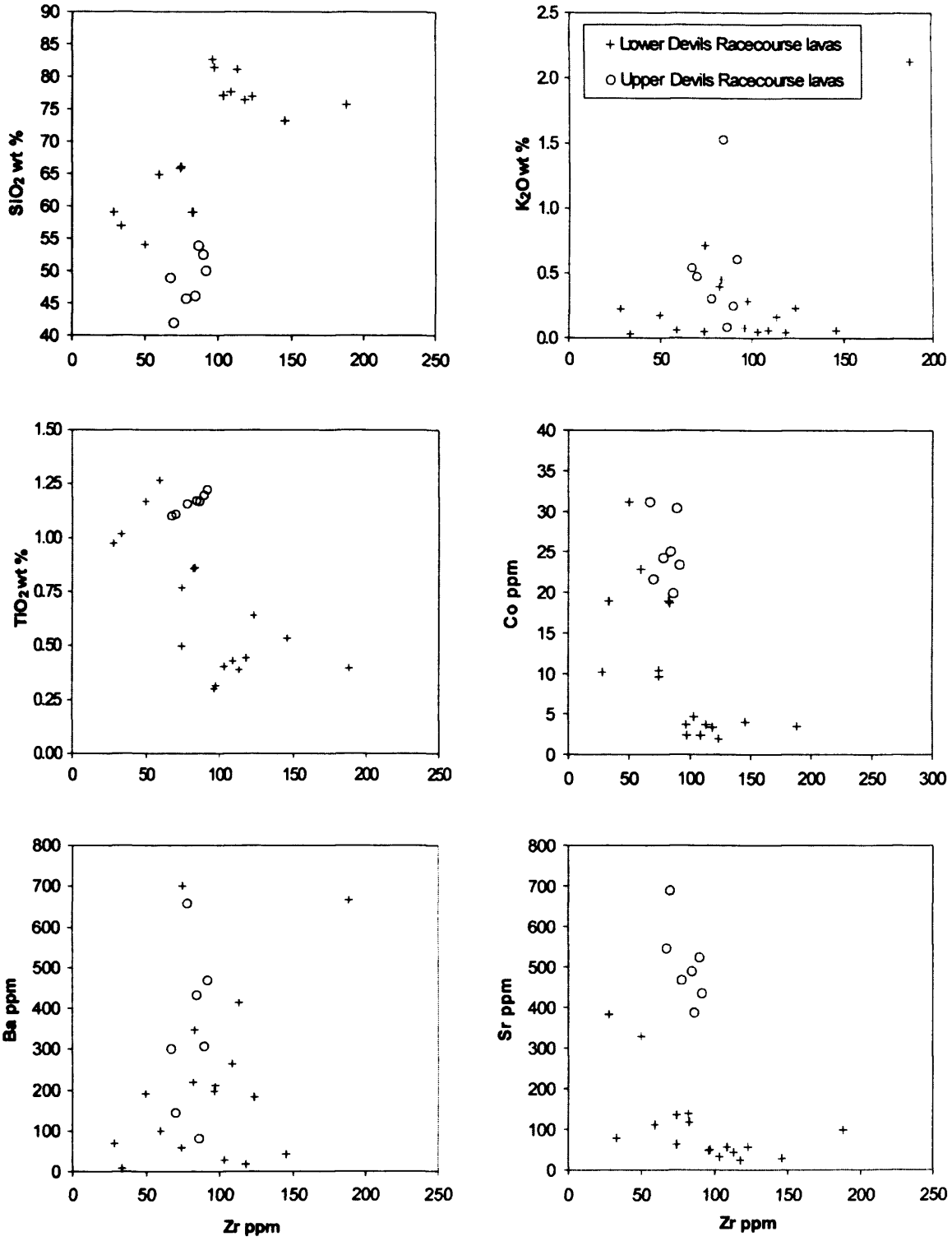

Figure 6.11 – Selected variation diagrams for major and trace elements vs. Zr for the Devils Racecourse lavas. The degree of mobility of an element is represented by its correlation with Zr. A mobile element will show no correlation, whereas, an immobile element displays a good correlation. A correlation can be a straight or curved line depending on whether the element is incompatible and/or compatible during fractional crystallisation.

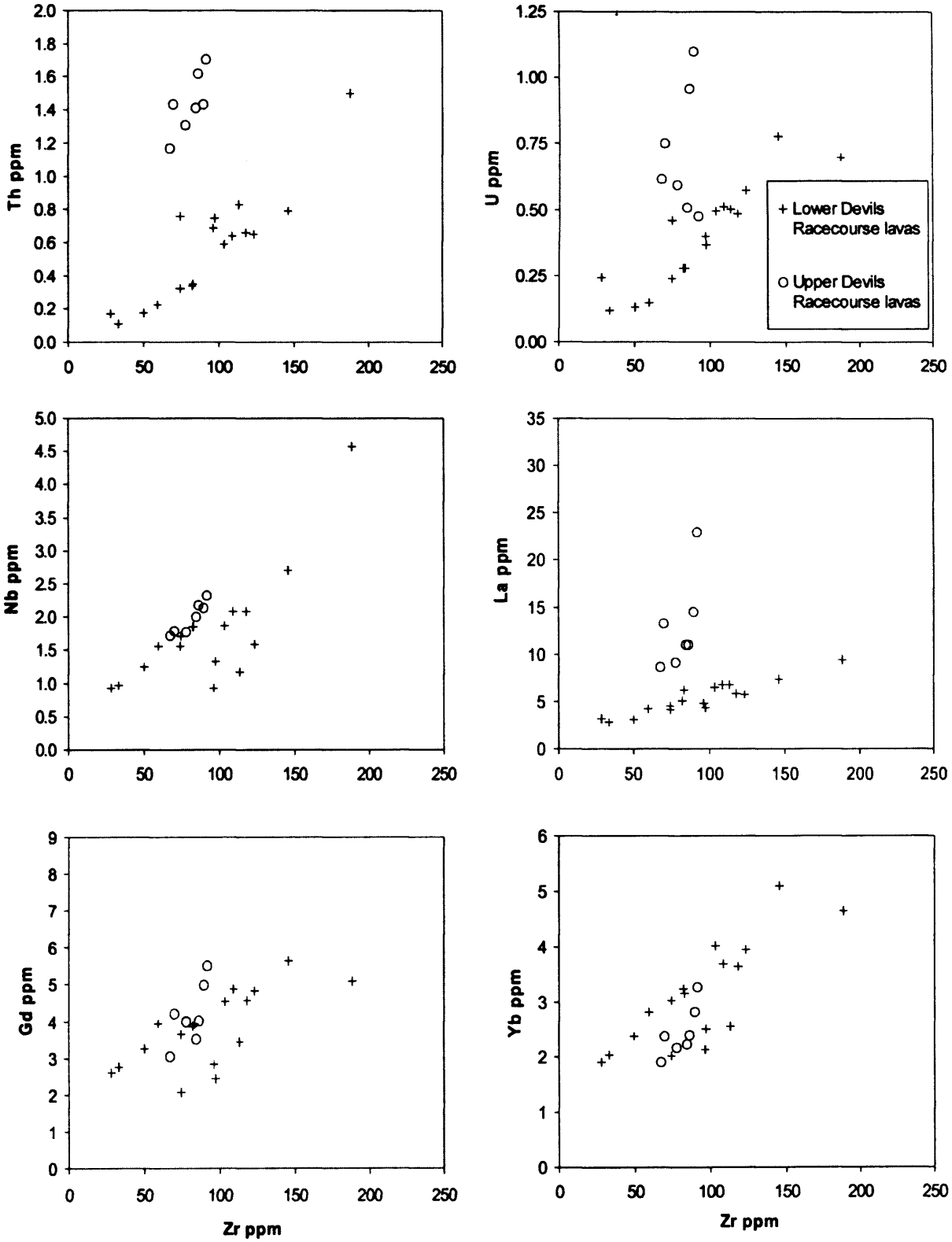

Figure 6.11 – continued.

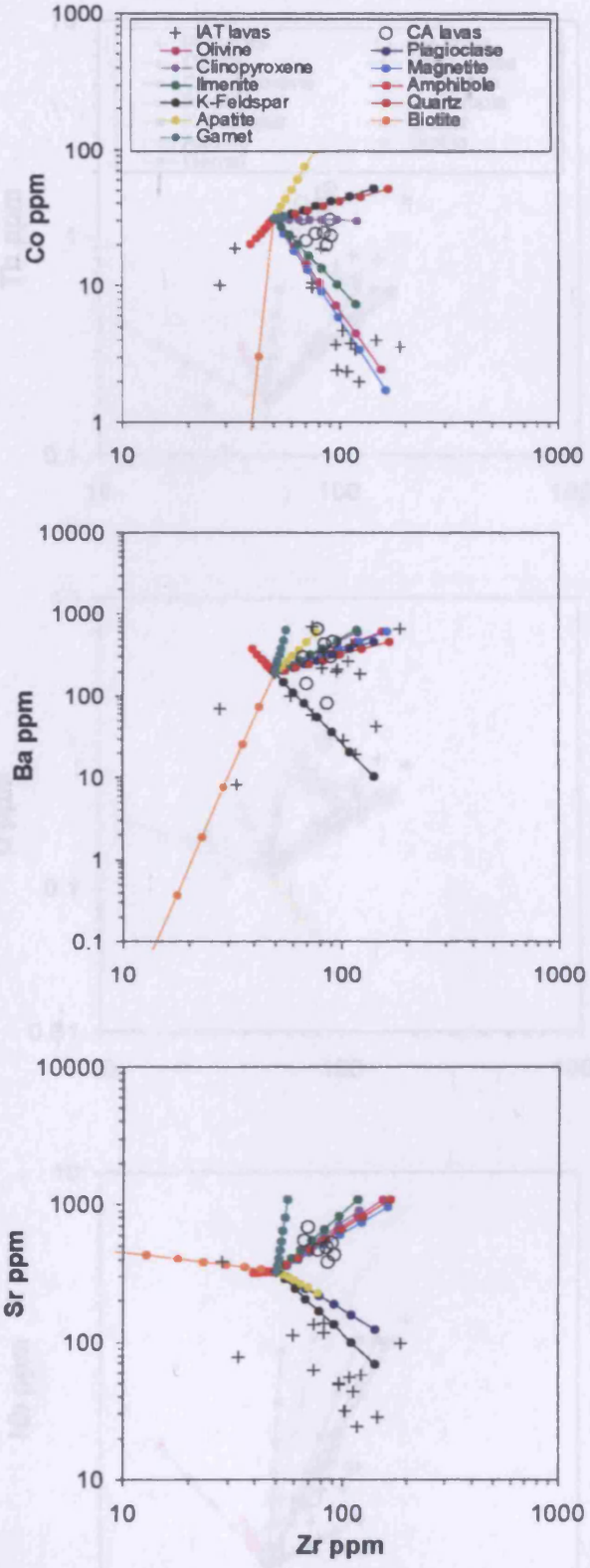

Figure 6.12 – Selected variation diagrams with vectors showing the composition of olivine, plagioclase, clinopyroxene, magnetite, ilmenite, amphibole, K-feldspar, quartz, apatite, biotite, and garnet with up to 70% fractional crystallisation of the AHBI16 starting composition (each tick represents 10% crystallisation) (Appendices E and G).

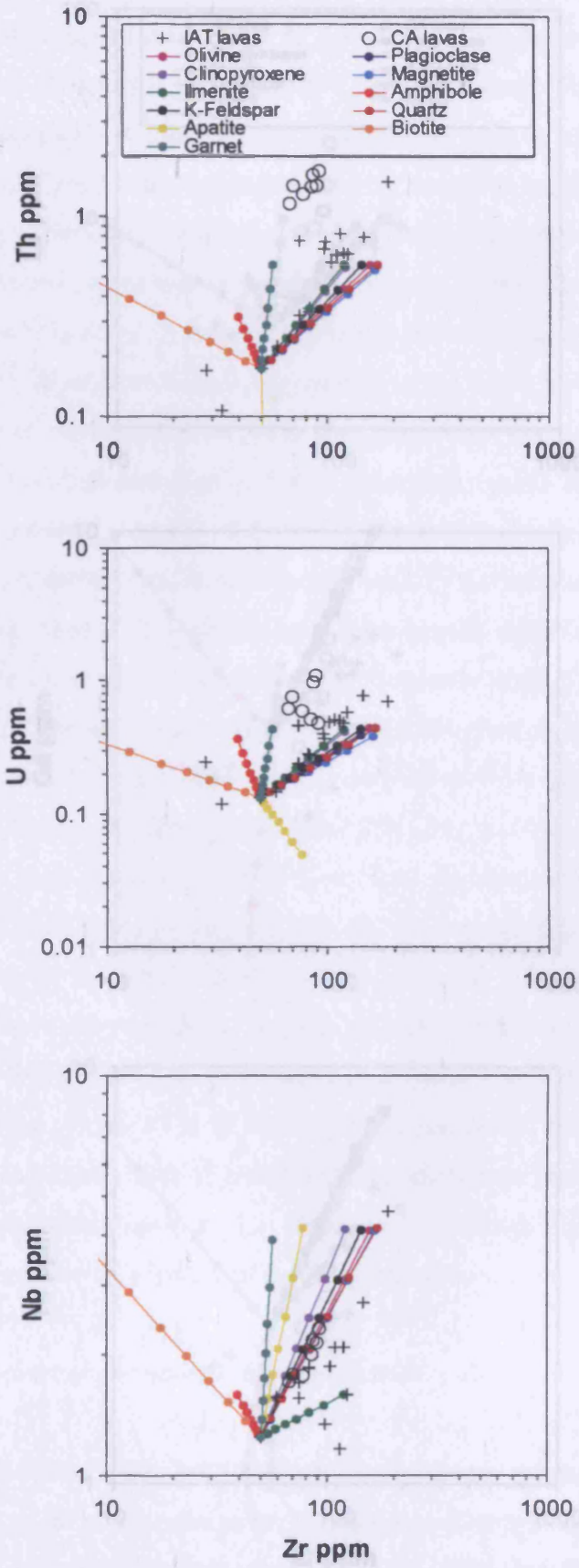

Figure 6.12 – continued

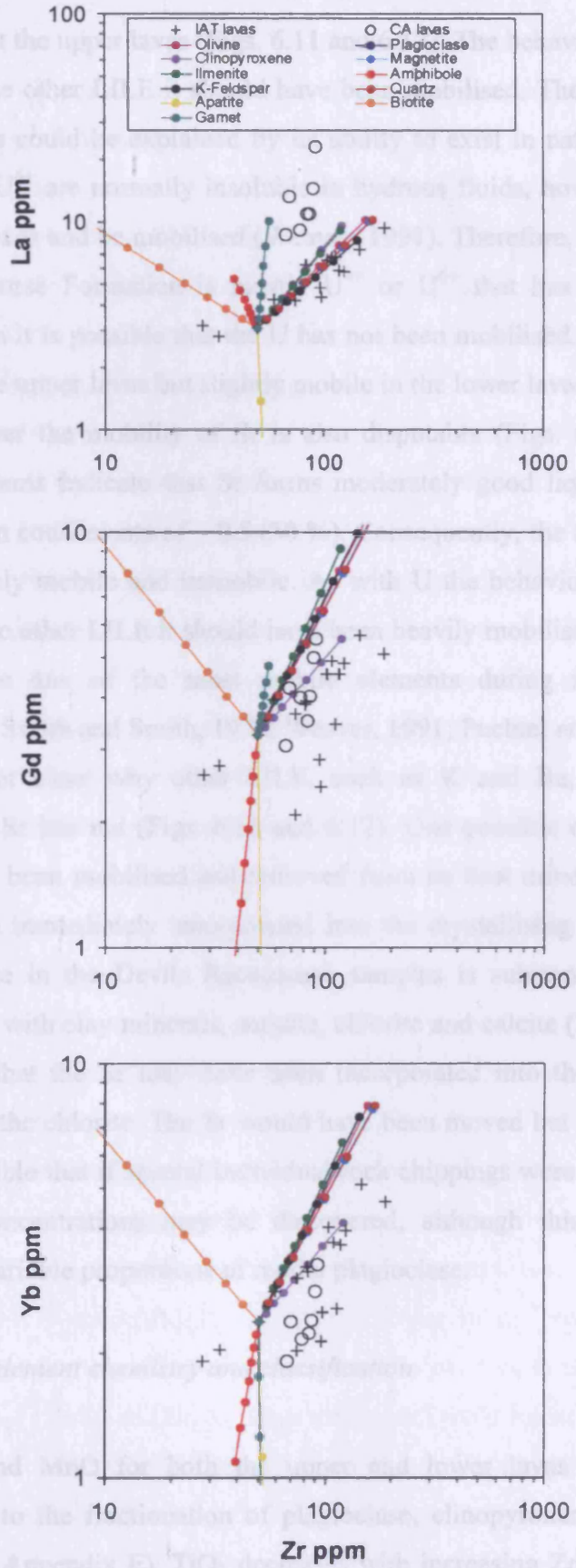

Figure 6.12 – continued

samples but not the upper lavas (Figs. 6.11 and 6.12). The behaviour of U is puzzling because like the other LILE it should have been mobilised. The immobility of U in the lower lavas could be explained by its ability to exist in nature as two different ions. U^{4+} and U^{6+} are normally insoluble in hydrous fluids, however, U^{6+} can form soluble complexes and be mobilised (Weaver, 1991). Therefore, if the U in the lower Devils Racecourse Formation is mostly U^{4+} or U^{6+} that has not formed soluble complexes then it is possible that the U has not been mobilised. Conversely, SiO_2 is immobile in the upper lavas but slightly mobile in the lower lavas (Fig. 6.11).

Moreover the mobility of Sr is also disputable (Figs. 6.11 and 6.12). The variation diagrams indicate that Sr forms moderately good liquid lines of descent with correlation coefficients of ~ 0.5 (50 %). Consequently, the Sr can be considered to be moderately mobile and immobile. As with U the behaviour of Sr is puzzling because like the other LILE it should have been heavily mobilised since Sr is widely regarded to be one of the most mobile elements during secondary alteration processes (e.g. Smith and Smith, 1976; Weaver, 1991; Puchtel *et al.*, 1999).

It is not clear why other LILE, such as K and Ba, have been heavily mobilised and Sr has not (Figs. 6.11 and 6.12). One possible explanation could be that the Sr has been mobilised and removed from its host mineral (plagioclase) but some has been immediately incorporated into the crystallising secondary minerals. The plagioclase in the Devils Racecourse samples is substantially altered and is being replaced with clay minerals, sericite, chlorite and calcite (Table A.1). As such, it is possible that the Sr may have been incorporated into the clay minerals, the sericite and/or the chlorite. The Sr would have been moved but not far, probably << 1cm. It is possible that if several individual rock chippings were analysed a variation in their Sr concentrations may be discovered, although this would equally be explained by variable proportions of modal plagioclase.

6.5.1.2 Major element chemistry and classification

CaO and MnO for both the upper and lower lavas show characteristic decreases due to the fractionation of plagioclase, clinopyroxene and Fe-Ti oxides (Section E.10, Appendix E). TiO_2 decreases with increasing Zr in the lower Devils Racecourse lavas but increases in the upper lavas (Fig. 6.11). The decrease is clearly because of the fractional crystallisation of Fe-Ti oxides in the lower Devils

Racecourse magmas. The increase in the upper magmas is caused by the absence of fractionating Fe-Ti oxides. An increase in SiO_2 with increasing Zr is expected during a normal magma fractionation sequence (Fig. 6.11).

The SiO_2 concentrations (although slightly mobilised in the case of the lower lavas) show that the upper lavas have basaltic/basaltic andesite compositions (SiO_2 = 42.01- 53.85 wt. %) and the lower lavas vary from basal dacites/rhyolites (SiO_2 = 64.8 – 82.63 wt. %) to overlying andesites/basaltic andesites (SiO_2 = 53.98 – 59.44 wt. %) (Appendices A, E and Chapter 4).

The discrimination diagrams, Co-Th (Chapter 5), Th/Yb-Ta/Yb (Pearce, 1982), Th/Zr-La/Yb, Ce/Lu-Sm/Yb, La/Hf-Sm/Y and Th/Hf-Sm/Yb (Chapter 5), have been used to classify the Devils Racecourse lavas (Figs. 6.13 and 6.14). The results from each of these diagrams are summarised on Table 6.1. The diagrams indicate that the lower Devils Racecourse Formation lavas (AHBI01, 03, 05, 06, 07, 16-23 and 26-30) have IAT affinities and range in composition from dacites/rhyolites at the base to basaltic andesites nearer the top. The upper Devils Racecourse Formation lavas (AHBI09-15) have CA affinities and range in composition from basalts to probable basaltic andesites (Figs. 6.13, 6.14 and Table 6.1).

6.5.1.3 Trace elements

Trace element variation diagrams likewise show predictable trends for immobile trace elements e.g. Co decreases with increasing Zr and the REE increase with increasing Zr (Figs. 6.11, 6.12 and E.10). For Hf, Nb, Ta, Tb, Ho, Dy, Er, Yb, Lu and Y, the lower and upper Devils Racecourse lavas have a single linear trend line suggesting that the upper and lower lavas are derived from the same magma source region (Figs. 6.11, 6.12 and E.10). However, variation diagrams for Th, La, Ce, Sm, Nd and U show that the upper and lower lavas form two distinct linear trends with the upper lavas having greater abundances of these elements at a given Zr content (Figs. 6.11, 6.12 and E.10). Thus the upper Devils Racecourse lavas are more enriched in Th, U and the LREE than the lower lavas. This implies that the upper and lower Devils Racecourse lavas are derived from chemically different source regions.

The enrichment is further seen on N-MORB-normalised (n-mn) multi-element, chondrite-normalised REE diagrams and incompatible element ratio

	Sample	Th/Yb-Ta/Yb	Co-Th	Th/Hf-Sm/Yb	Ce/Lu-Sm/Yb	La/Hf-Sm/Y	Th/Zr-La/Yb
Lower Devils Racecourse lavas	AHBI01						
	AHBI03						
	AHBI05						
	AHBI06						
	AHBI07						
Upper Devils Racecourse lavas	AHBI09						
	AHBI10						
	AHBI11						
	AHBI12						
	AHBI13						
	AHBI14						
	AHBI15						
Lower Devils Racecourse lavas	AHBI16						
	AHBI17						
	AHBI18						
	AHBI19						
	AHBI20						
	AHBI21						
	AHBI22						
	AHBI23						
	AHBI26						
	AHBI27						
	AHBI28						
	AHBI30						

Table 6.1 – The alkalinity results from plotting the Benbow inlier samples on the Co-Th, Th/Yb-Ta/Yb, Th/Hf-Sm/Yb, Ce/Lu-Sm/Yb, La/Hf-Sm/Y and Th/Zr-La/Yb diagrams; Pink, IAT; Brown, CA; Green, SHC.

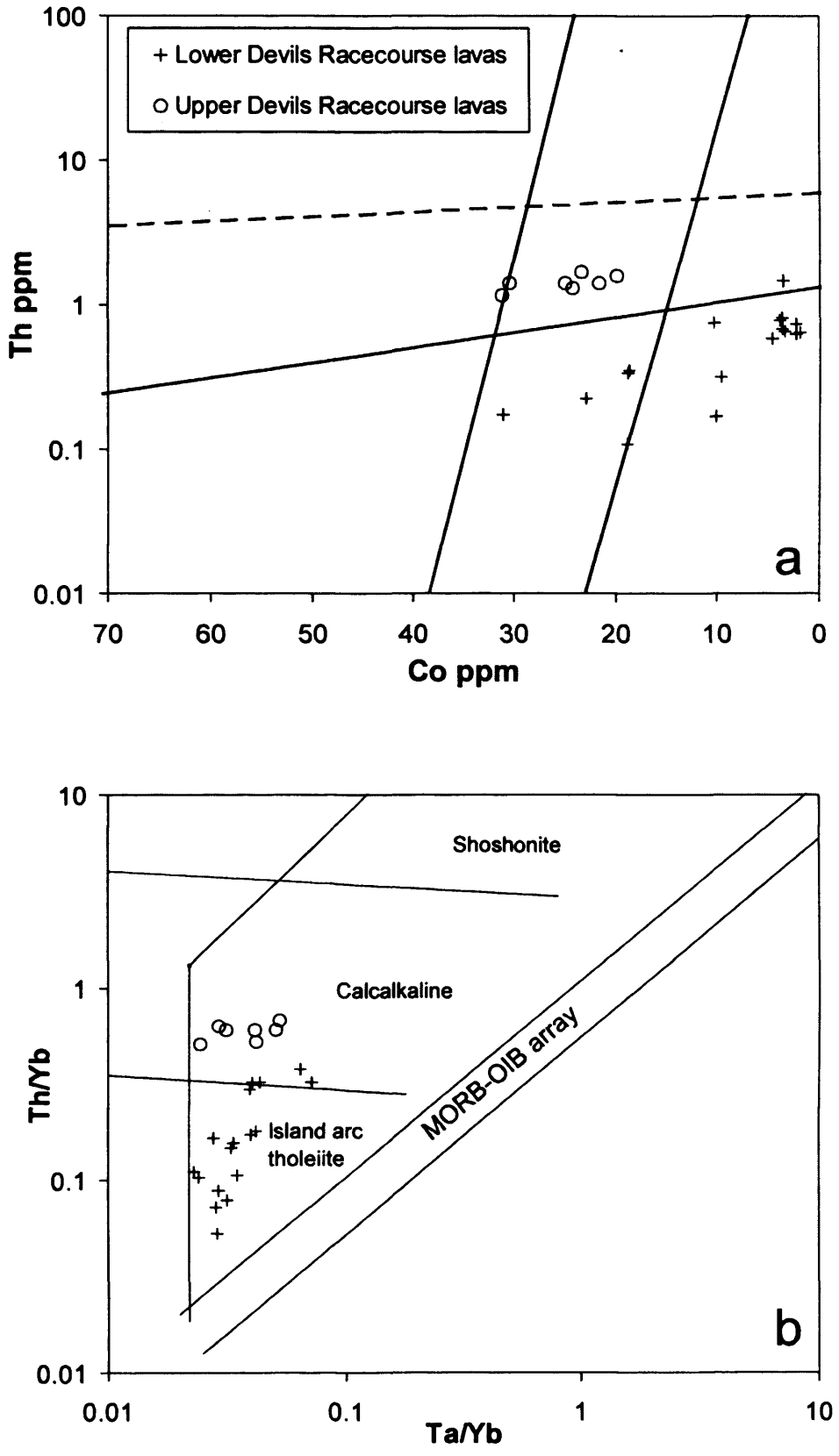

Figure 6.13 – (a) Co - Th and (b) Th/Yb – Ta/Yb discrimination diagrams (Pearce, 1996; Hastie *et al.*, 2007).

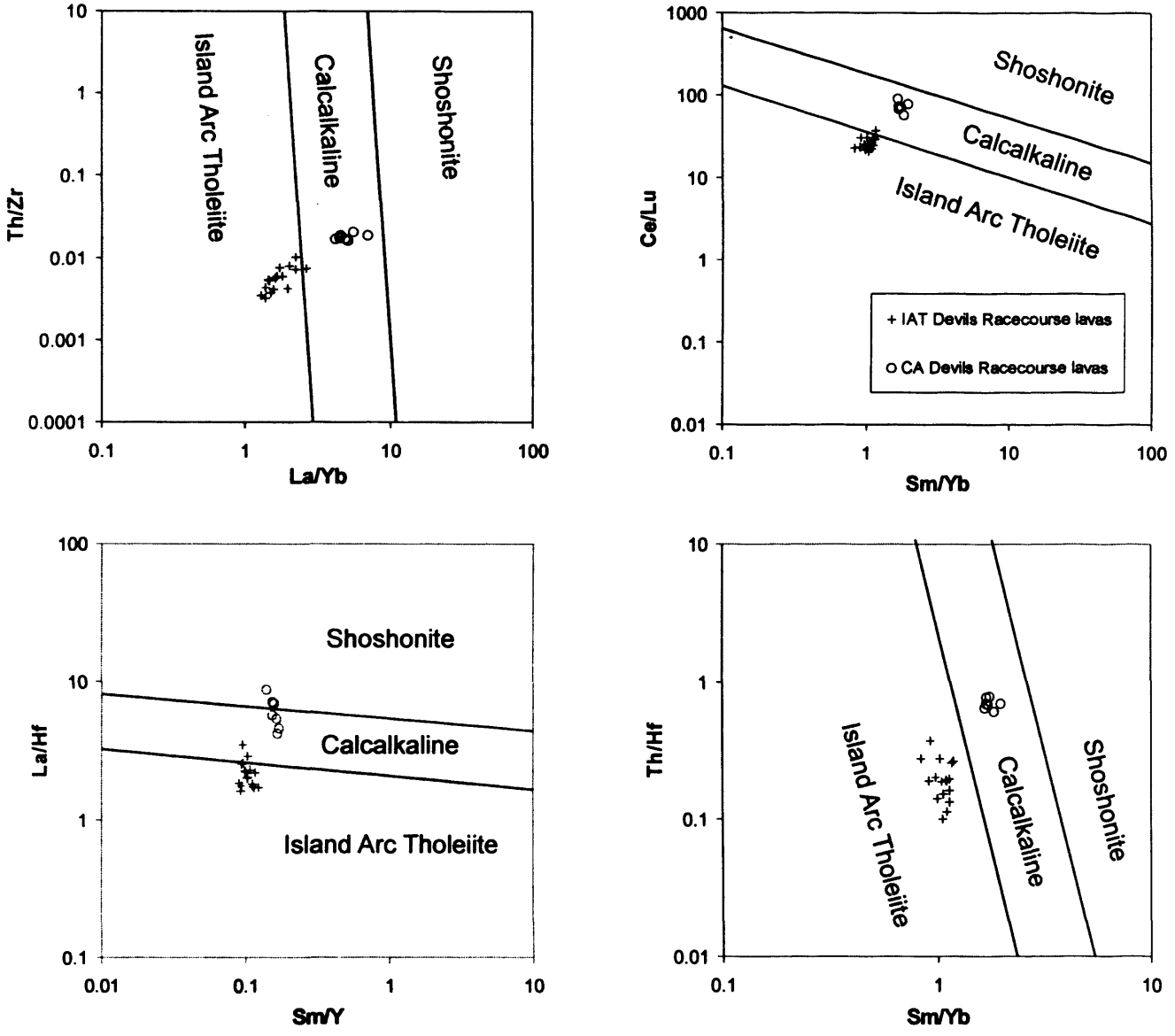

Figure 6.14 - Th/Zr-La/Yb, Ce/Lu-Sm/Yb, La/Hf-Sm/Y and Th/Hf-Sm/Yb discrimination diagrams showing the IAT and CA affinity of the lower and upper Devils Racecourse lavas respectively. The differing trace element ratios in conjunction with the variation diagrams and isotope ratios indicate that the arc rocks are derived from chemically different source regions.

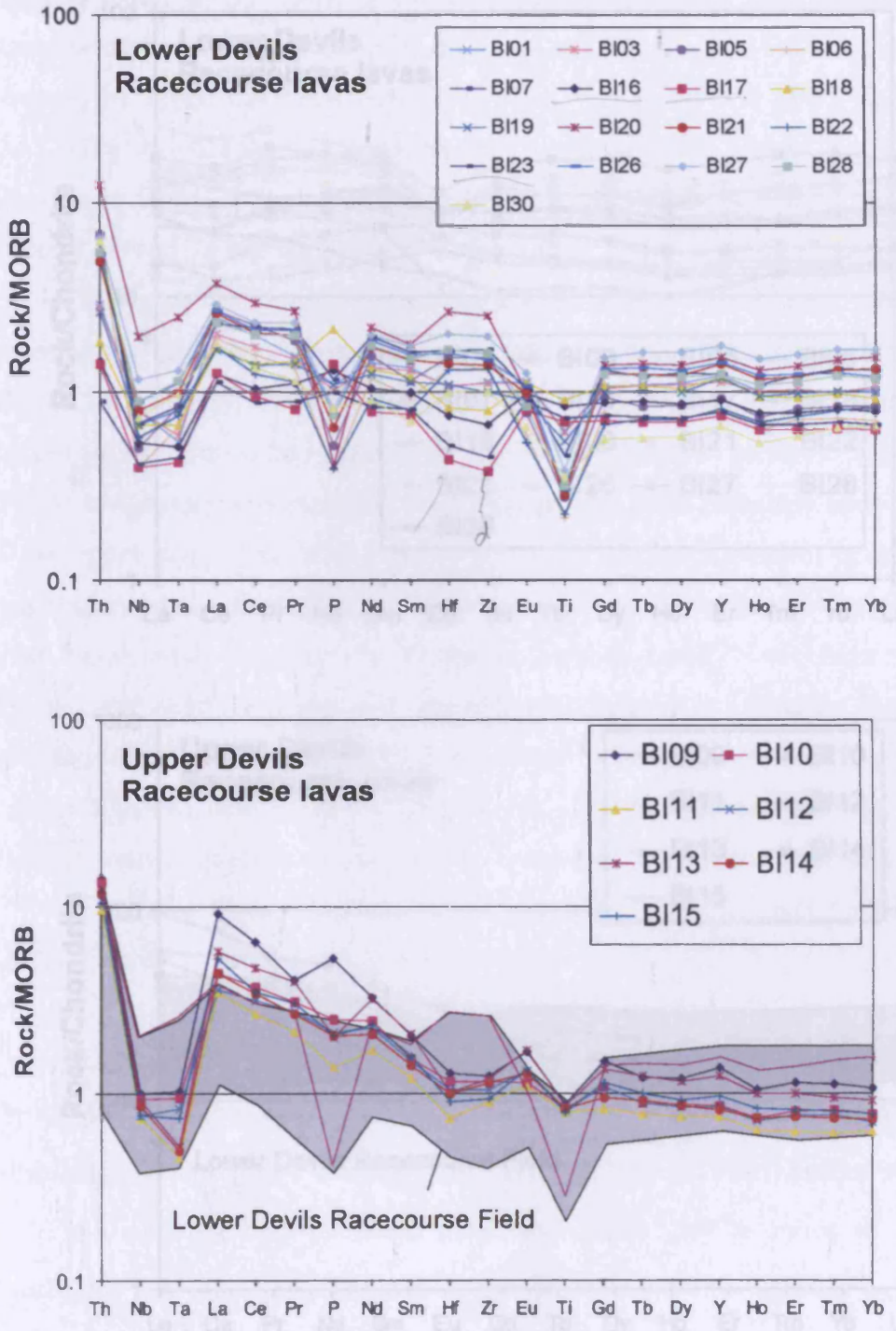

Figure 6.15 – N-MORB-normalised multi-element diagrams of the Devils Racecourse lavas. Normalising values are taken from Sun and McDonough (1989).

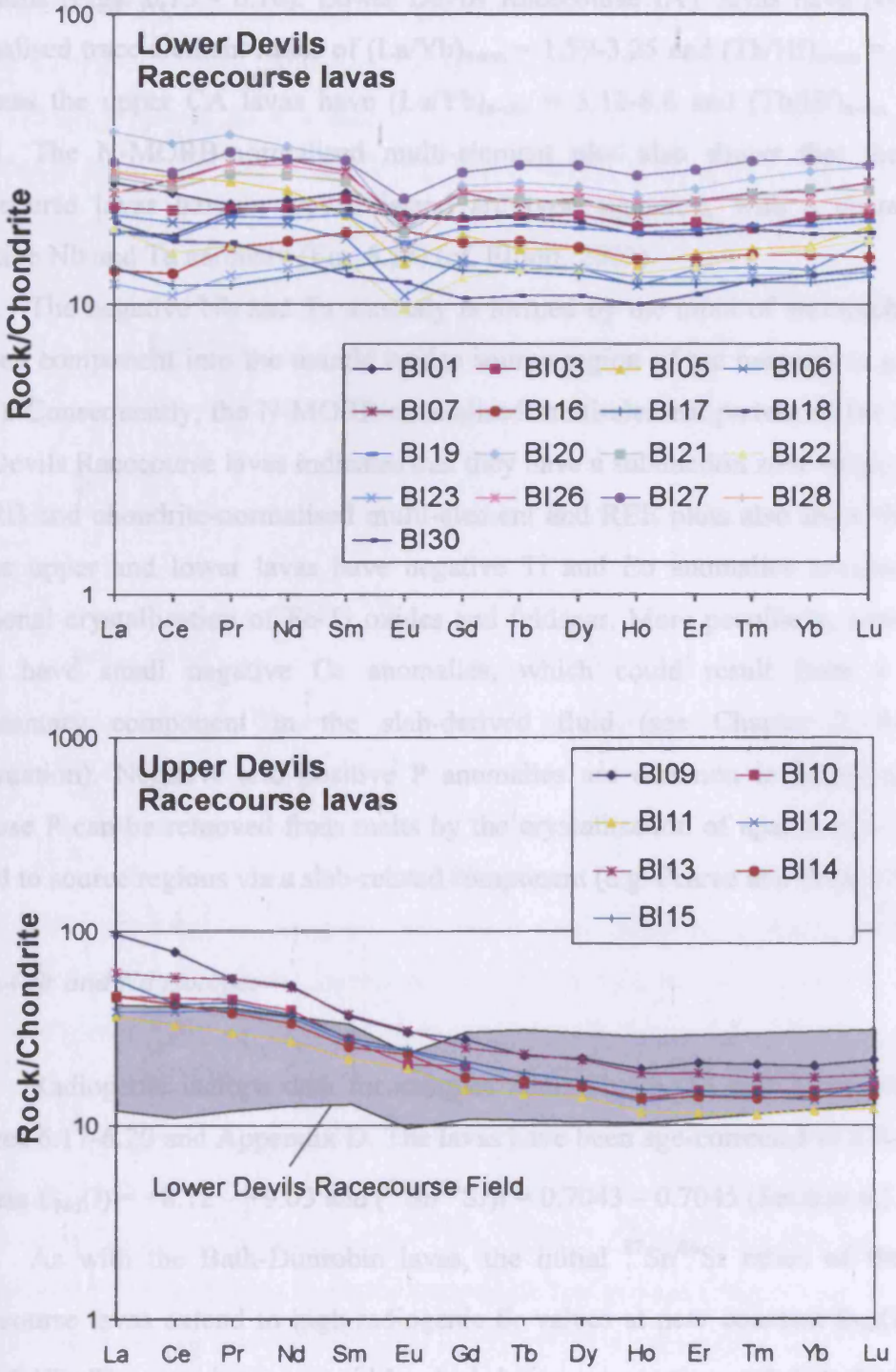

Figure 6.16 – Chondrite-normalised REE diagrams of the Devils Racecourse lavas. Normalising values are taken from McDonough and Sun (1995).

diagrams (Figs. 6.13 - 6.16). Lower Devils Racecourse IAT lavas have N-MORB-normalised trace element ratios of $(La/Yb)_{n\text{-}mn}$ = 1.59-3:25 and $(Th/Hf)_{n\text{-}mn}$ = 1.7-6.38 whereas the upper CA lavas have $(La/Yb)_{n\text{-}mn}$ = 5.12-8.6 and $(Th/Hf)_{n\text{-}mn}$ =10.45-13.31. The N-MORB-normalised multi-element plot also shows that the Devils Racecourse lavas have a typical island arc type signature, with a characteristic negative Nb and Ta anomaly (Fig. 6.15) (cf. Elliott, 2003).

The negative Nb and Ta anomaly is formed by the input of an enriched slab-derived component into the mantle wedge source region of arc magmas (e.g. Elliott, 2003). Consequently, the N-MORB-normalised multi-element pattern of the IAT and CA Devils Racecourse lavas indicates that they have a subduction zone origin. The N-MORB and chondrite-normalised multi-element and REE plots also show that some of the upper and lower lavas have negative Ti and Eu anomalies because of the fractional crystallisation of Fe-Ti oxides and feldspar. More peculiarly, some of the lavas have small negative Ce anomalies, which could result from a pelagic sedimentary component in the slab-derived fluid (see Chapter 7 for more information). Negative and positive P anomalies are common in island arc lavas because P can be removed from melts by the crystallisation of apatite and it can be added to source regions via a slab-related component (e.g. Pearce and Peate, 1995).

6.5.1.4 Sr and Nd isotopes

Radiogenic isotope data for samples AHBI01, 03, 13 and 27 are shown in Figures 6.17-6.20 and Appendix D. The lavas have been age-corrected to 120 Ma and possess $\varepsilon_{Nd}(i)$ = +8.12 – +9.03 and $(^{87}Sr/^{86}Sr)i$ = 0.7043 – 0.7045 (Section 6.5.1.7).

As with the Bath-Dunrobin lavas, the initial $^{87}Sr/^{86}Sr$ ratios of the Devils Racecourse lavas extend to high radiogenic Sr values at near constant $\varepsilon_{Nd}(i)$ values (Fig. 6.17). The samples were acid-leached during preparation and thus the $^{87}Sr/^{86}Sr$ values should be more representative of the primary igneous composition. However, like the Bath-Dunrobin lavas, these arc lavas have been extensively altered and so it is unclear whether the leaching processes removed all the secondary alteration products.

Nevertheless, Nd is considered to be immobile during secondary alteration processes and consequently the $\varepsilon_{Nd}(i)$ values should represent the primary

composition of the arc lavas (White and Patchett, 1984). The $\varepsilon_{Nd}(i)$ values of the Devils Racecourse lavas plot below the Atlantic/Pacific MORB field (Fig. 6.17). Nd is moderately mobile in a slab-derived fluid/melt and, as such, Nd is generally enriched in island arc lavas (Pearce and Peate, 1995). This enriched slab component imparts the lower $\varepsilon_{Nd}(i)$ values on the arc lavas, thus explaining the position of the Devils Racecourse lavas in Figure 6.17. The CA lava (AHBI13) has lower $\varepsilon_{Nd}(i)$ values than the IAT lavas (AHBI01, 03 and 27) suggesting that it was derived from a source region with a greater mass fraction, or more enriched, slab component.

6.5.1.5 Pb isotope systematics – problems with altered igneous rocks

The lavas possess $(^{206}Pb/^{204}Pb)i = 16.51 - 18.75$, $(^{207}Pb/^{204}Pb)i = 15.45 - 15.56$ and $(^{208}Pb/^{204}Pb)i = 37.19 - 38.19$. On a $(^{207}Pb/^{204}Pb)i - (^{206}Pb/^{204}Pb)i$ plot the Devils Racecourse lavas lie above the Northern Hemisphere Reference Line (NHRL) of Hart (1984) (Fig. 6.18). The IAT lavas seem to lie on a theoretical mixing line between pelagic/terrigenous sediments and N-MORB.

The IAT lavas have the same Pb isotope composition (in $(^{207}Pb/^{204}Pb)i$-$(^{206}Pb/^{204}Pb)i$ space) as samples from the Lesser Antilles, Vanuatu, Tonga and Kermadec arcs, although the Lesser Antilles data do extend into the sediment field and the Vanuatu lavas are closer to average N-MORB values. Unusually, the CA lava has very low $(^{206}Pb/^{204}Pb)i$ and $(^{207}Pb/^{204}Pb)i$ values (Fig. 6.18).

On a $(^{208}Pb/^{204}Pb)i - (^{206}Pb/^{204}Pb)i$ diagram, the IAT lavas plot close to the NHRL and with the samples from the Tonga, Kermadec, Vanuatu and Lesser Antilles island arcs (Fig. 6.18). Similar to the $(^{207}Pb/^{204}Pb)i - (^{206}Pb/^{204}Pb)i$ diagram, the IAT rocks could fall on a mixing line between pelagic/terrigenous sediment and N-MORB. The CA lava has very low $(^{208}Pb/^{204}Pb)i - (^{206}Pb/^{204}Pb)i$ values (Fig. 6.18).

Pb isotopes are conventionally used to determine the slab contribution in island arc lavas (e.g. Ewart *et al.*, 1998; Class *et al.*, 2000). However, the use of Pb isotopes in the petrogenesis of the Jamaican igneous rocks may be of limited use due to the potential mobility of Pb (Geldmacher *et al.*, 2003; also see Section 6.4.4). The variation diagrams in Sections E.10-E.14, Appendix E demonstrate that U and Th form good liquid lines of descent for the majority of the Jamaican igneous rocks

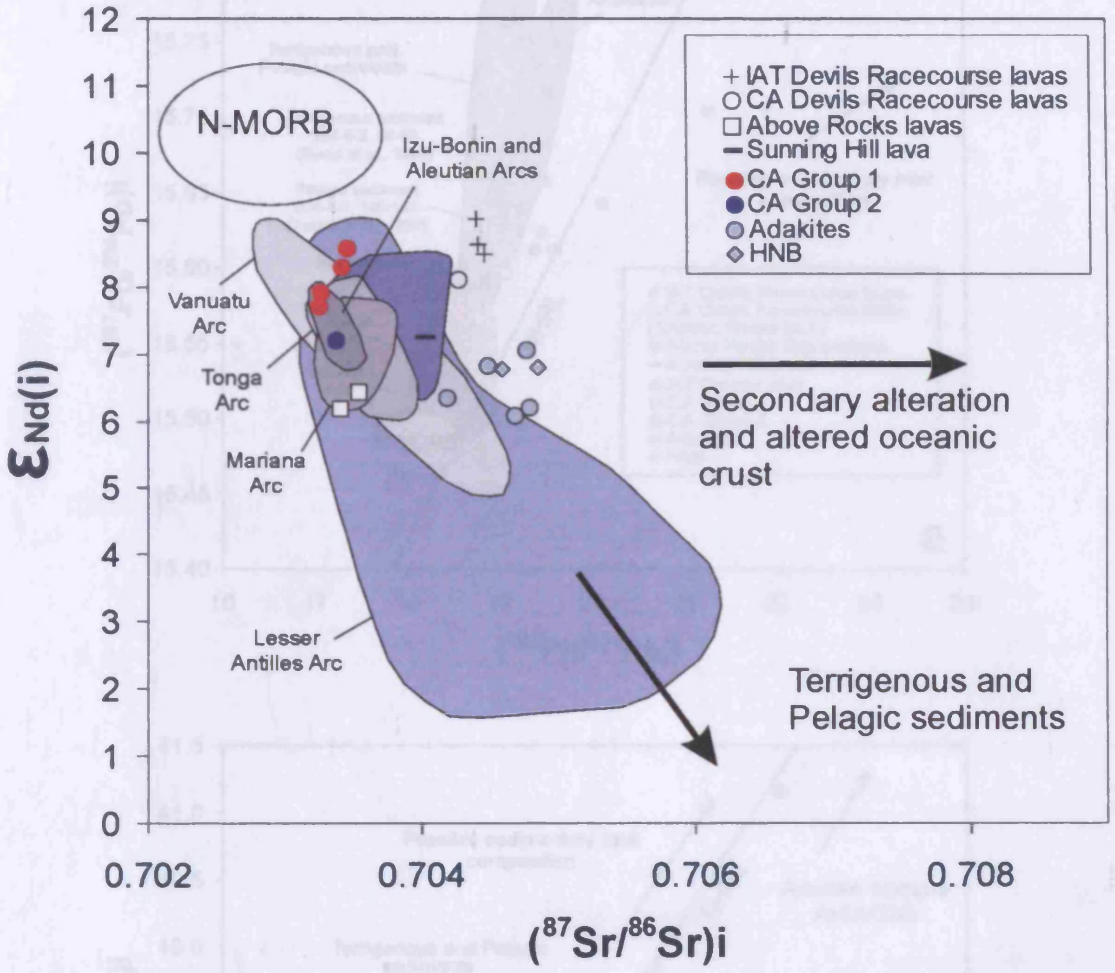

Figure 6.17 - $\varepsilon_{Nd}(i)$ - $(^{87}Sr/^{86}Sr)i$ diagram with Jamaican island arc lavas plotted alongside fields for the Izu-Bonin, Aleutian, Vanuatu, Tonga, Mariana and Lesser Antilles island arcs. Data sources for the Jamaica and the island arcs are listed in Appendices D and F.

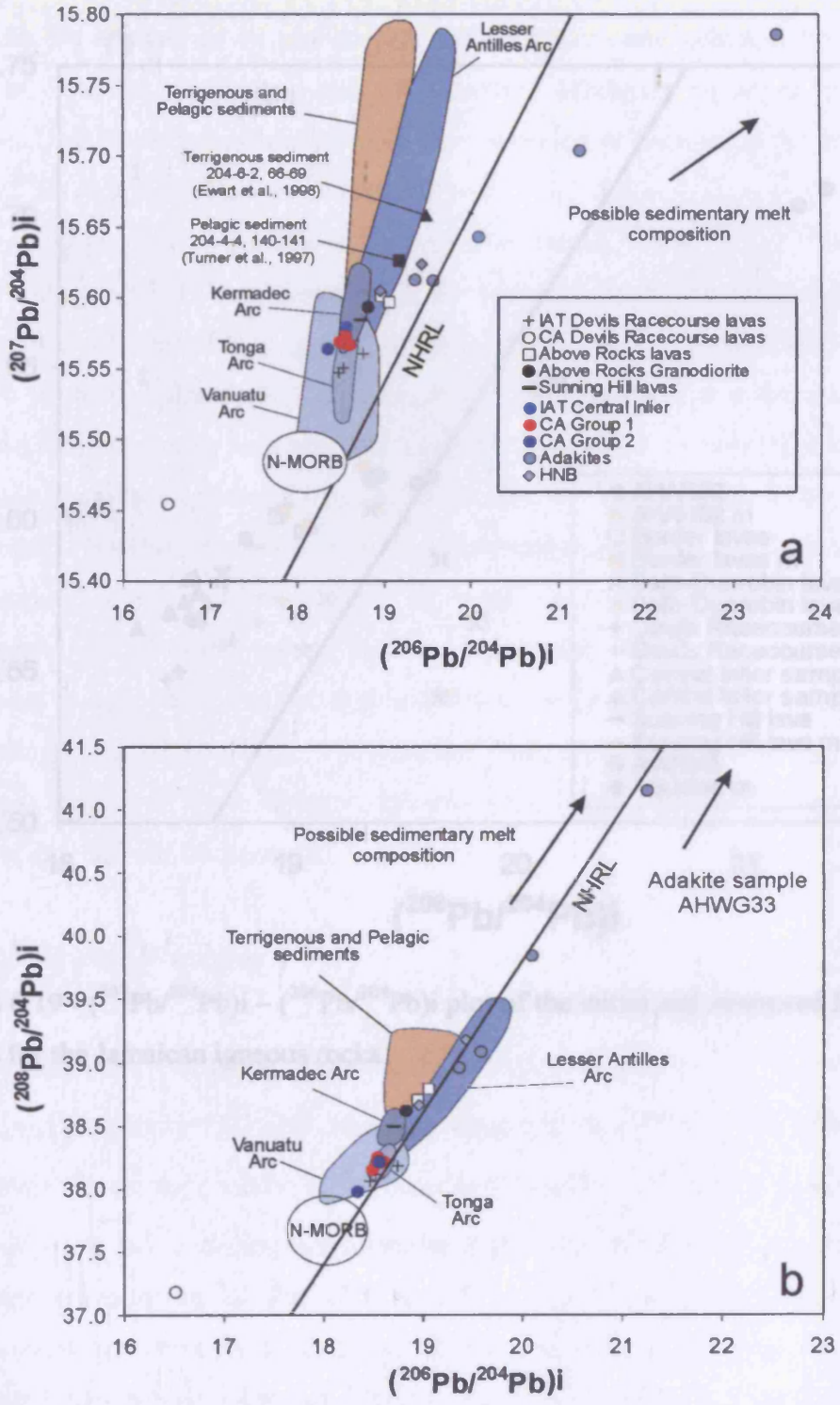

Figure 6.18 – Plots of $(^{207}Pb/^{204}Pb)i$ – $(^{206}Pb/^{204}Pb)i$ and $(^{208}Pb/^{204}Pb)i$ and $(^{206}Pb/^{204}Pb)i$ for the Jamaican island arc rocks which lie alongside fields for the Vanuatu, Tonga and Kermadec island arcs and pelagic and terrigenous sediments. Data sources for the island arcs are listed in Appendices D and F. NHRL = Northern Hemisphere Reference Line (Hart, 1982).

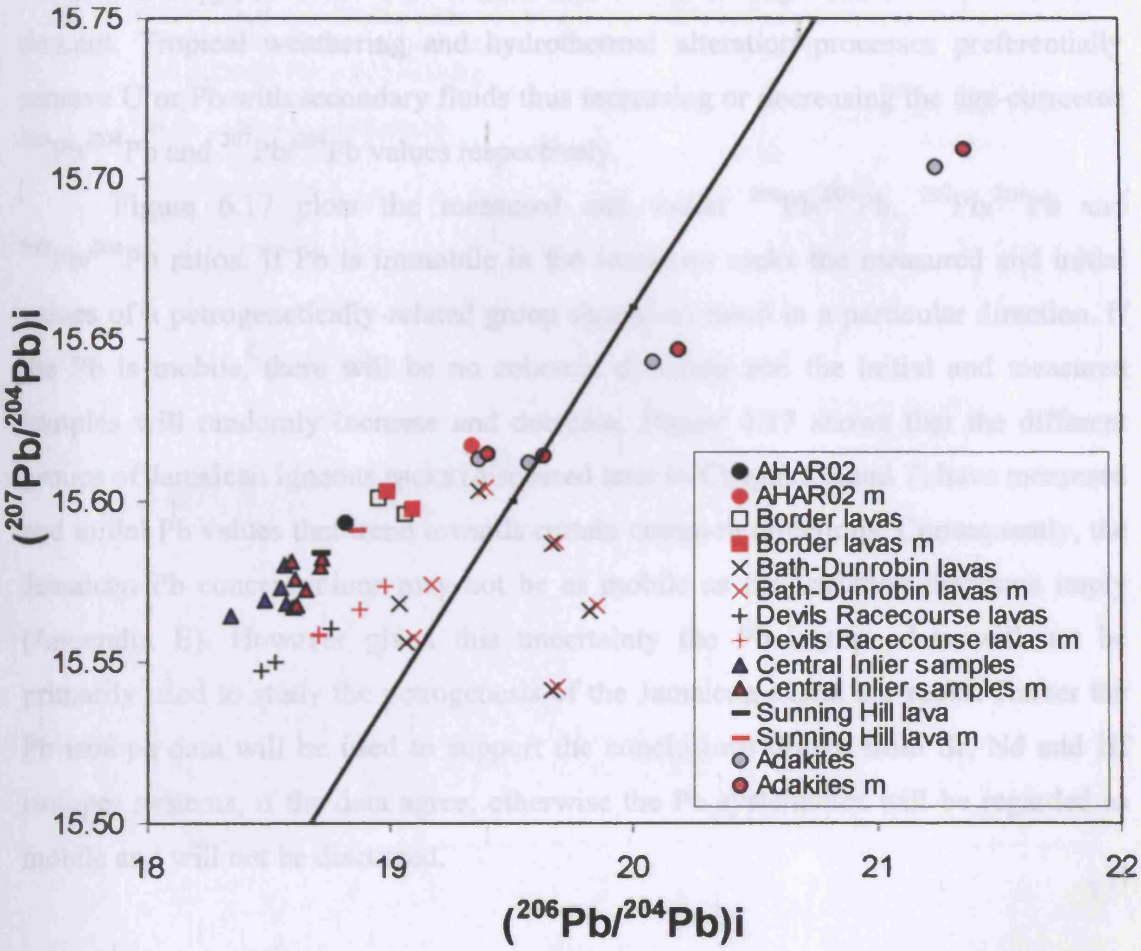

Figure 6.19 - $(^{207}Pb/^{204}Pb)i$ – $(^{206}Pb/^{204}Pb)i$ plot of the initial and measured Pb isotopic values for the Jamaican igneous rocks.

whereas Pb appears to be mobile and does not form any coherent liquid lines of descent. Tropical weathering and hydrothermal alteration processes preferentially remove U or Pb with secondary fluids thus increasing or decreasing the age-corrected $^{206}Pb/^{204}Pb$ and $^{207}Pb/^{204}Pb$ values respectively.

Figure 6.17 plots the measured and initial $^{206}Pb/^{204}Pb$, $^{207}Pb/^{204}Pb$ and $^{208}Pb/^{204}Pb$ ratios. If Pb is immobile in the Jamaican rocks the measured and initial values of a petrogenetically-related group should all trend in a particular direction. If the Pb is mobile, there will be no coherent direction and the initial and measured samples will randomly increase and decrease. Figure 6.17 shows that the different groups of Jamaican igneous rocks (discussed later in Chapters 6 and 7) have measured and initial Pb values that trend towards certain common directions. Consequently, the Jamaican Pb concentrations may not be as mobile as the variation diagrams imply (Appendix E). However given this uncertainty the Pb isotope data will not be primarily used to study the petrogenesis of the Jamaican island arc rocks. Rather the Pb isotope data will be used to support the conclusions drawn from Sr, Nd and Hf isotopes systems, if the data agree; otherwise the Pb systematics will be regarded as mobile and will not be discussed.

6.5.1.6 Nd and Hf isotopes

The lavas possess $\varepsilon_{Nd}(i) = +8.12 - 9.03$ and $\varepsilon_{Hf}(i) = +13.22 - 14.97$ (Fig. 6.20 and Appendix D). The variation diagrams for Nd and Hf (Section E.10, Appendix E) and the position of the lavas in the $\varepsilon_{Nd}(i) - \varepsilon_{Hf}(i)$ plot demonstrates that both elements lack post-eruption alteration signatures, and that the data represents the primary composition of the IAT and CA lavas. For comparison, the Devils Racecourse arc lavas have been plotted with other arc lavas from the Cretaceous Bonaire and the post-Mesozoic Mariana, Izu-Bonin, Aleutian, New Britain, Sunda and Lesser Antilles intra-oceanic island arcs. Fields for Atlantic/Pacific N-MORB, Iceland and pelagic and terrigenous sediments are also shown to constrain the possible source components of the Jamaican lavas.

The IAT and CA lavas have $\varepsilon_{Hf}(i)$ values (+13.22 – +14.97) which are similar to Atlantic/Pacific N-MORB (Nowell *et al.*, 1998; Kempton *et al.*, 2000). However,

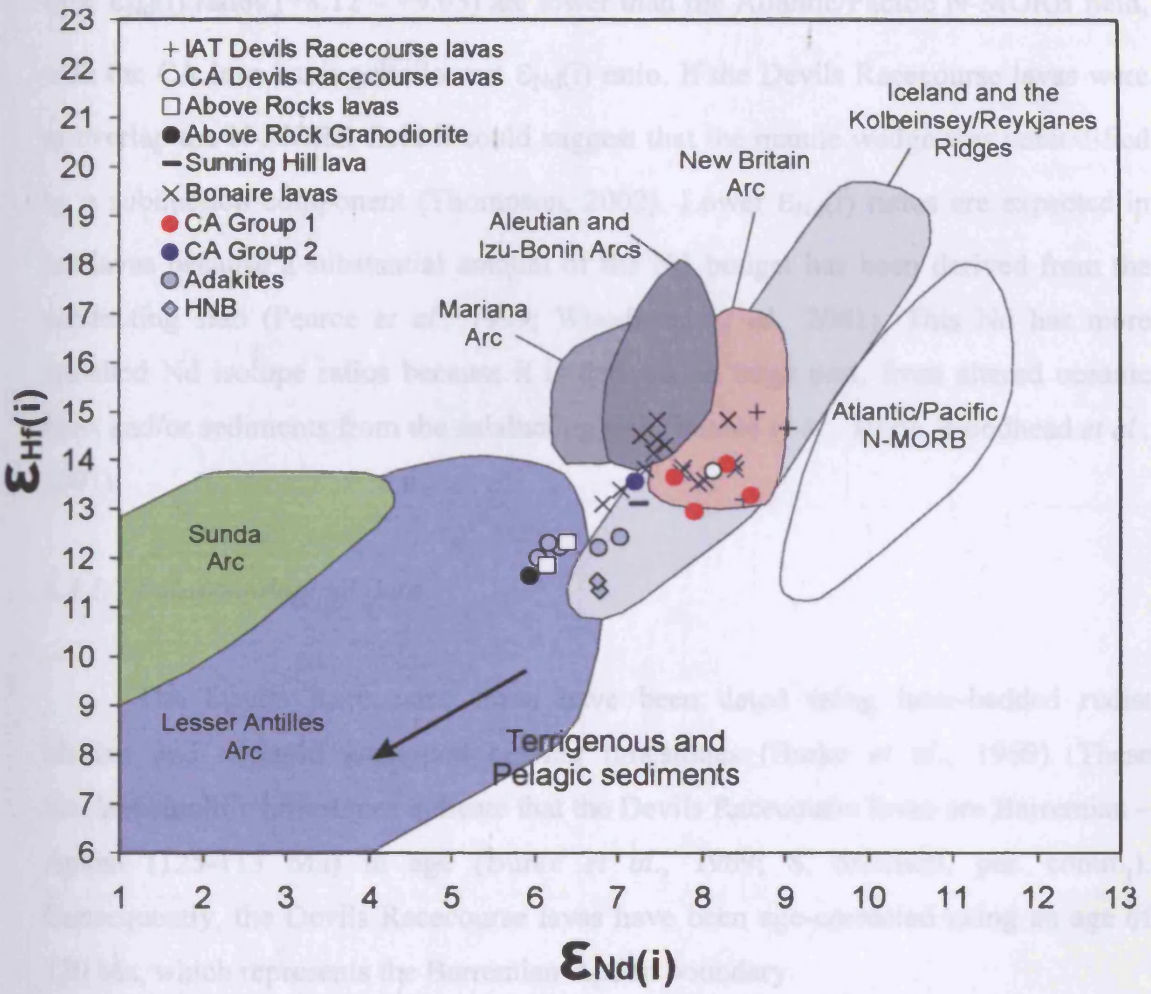

Figure 6.20 – Plot of $\varepsilon_{Nd}(i)$ - $\varepsilon_{Hf}(i)$ for the Jamaican island arc rocks which lie alongside fields for the Mariana, Aleutian, Izu-Bonin, New Britain, Sunda and Lesser Antilles island arcs. Data sources for the island arcs are listed in Appendices D and F.

their $\varepsilon_{Nd}(i)$ ratios (+8.12 – +9.03) are lower than the Atlantic/Pacific N-MORB field, with the CA lava having the lowest $\varepsilon_{Nd}(i)$ ratio. If the Devils Racecourse lavas were to overlap the N-MORB field it could suggest that the mantle wedge was unmodified by a subduction component (Thompson, 2002). Lower $\varepsilon_{Nd}(i)$ ratios are expected in arc lavas because a substantial amount of the Nd budget has been derived from the subducting slab (Pearce *et al.*, 1999; Woodhead *et al.*, 2001). This Nd has more enriched Nd isotope ratios because it is derived, in large part, from altered oceanic crust and/or sediments from the subducting slab (Pearce *et al.*, 1999; Woodhead *et al.*, 2001).

6.5.1.7 Palaeontological data

The Devils Racecourse lavas have been dated using inter-bedded rudist bivalve and nerineid gastropod bearing limestones (Burke *et al.*, 1969). These bioclastic/oolitic limestones indicate that the Devils Racecourse lavas are Barremian – Aptian (125-113 Ma) in age (Burke *et al.*, 1969; S. Mitchell, per. comm.). Consequently, the Devils Racecourse lavas have been age-corrected using an age of 120 Ma, which represents the Barremian-Aptian boundary.

6.5.2 The Above Rocks and Sunning Hill Inliers and the Bath-Dunrobin tuffs

Only a limited number of lavas were collected from the Sunning Hill inlier, but because the rocks are similar to the lavas in the Above Rocks inlier, both sets of data are considered together. Nineteen samples were analysed from the Above Rocks Inlier; 2 from the Mt Charles Formation, 5 from the Border Formation, 10 from the granodiorite and 2 xenoliths from the granodiorite (Chapters 3 and 4). Two samples were collected from the Sunning Hill Inlier and these samples will be compared to the Benbow and Bath-Dunrobin arc (tuff) rocks.

6.5.2.1 Element mobility

Major and trace element variation diagrams are shown in Figures 6.21, 6.22 and Section E.11, Appendix E. There are enough samples from the granodiorite and

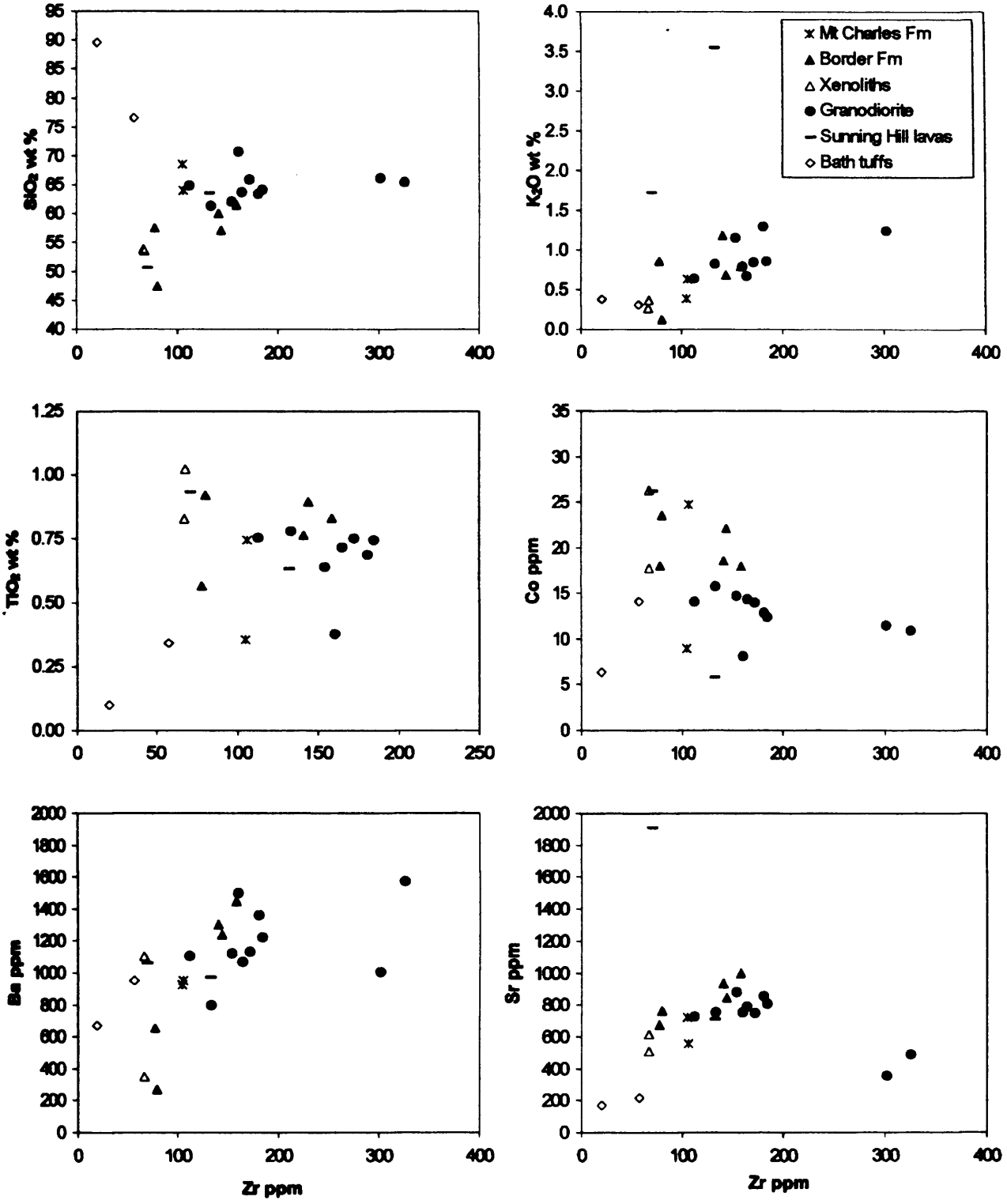

Figure 6.21 – Selected variation diagrams for major and trace elements vs. Zr for the Above Rocks, Sunning Hill and Bath-Dunrobin arc samples (see Appendix E).

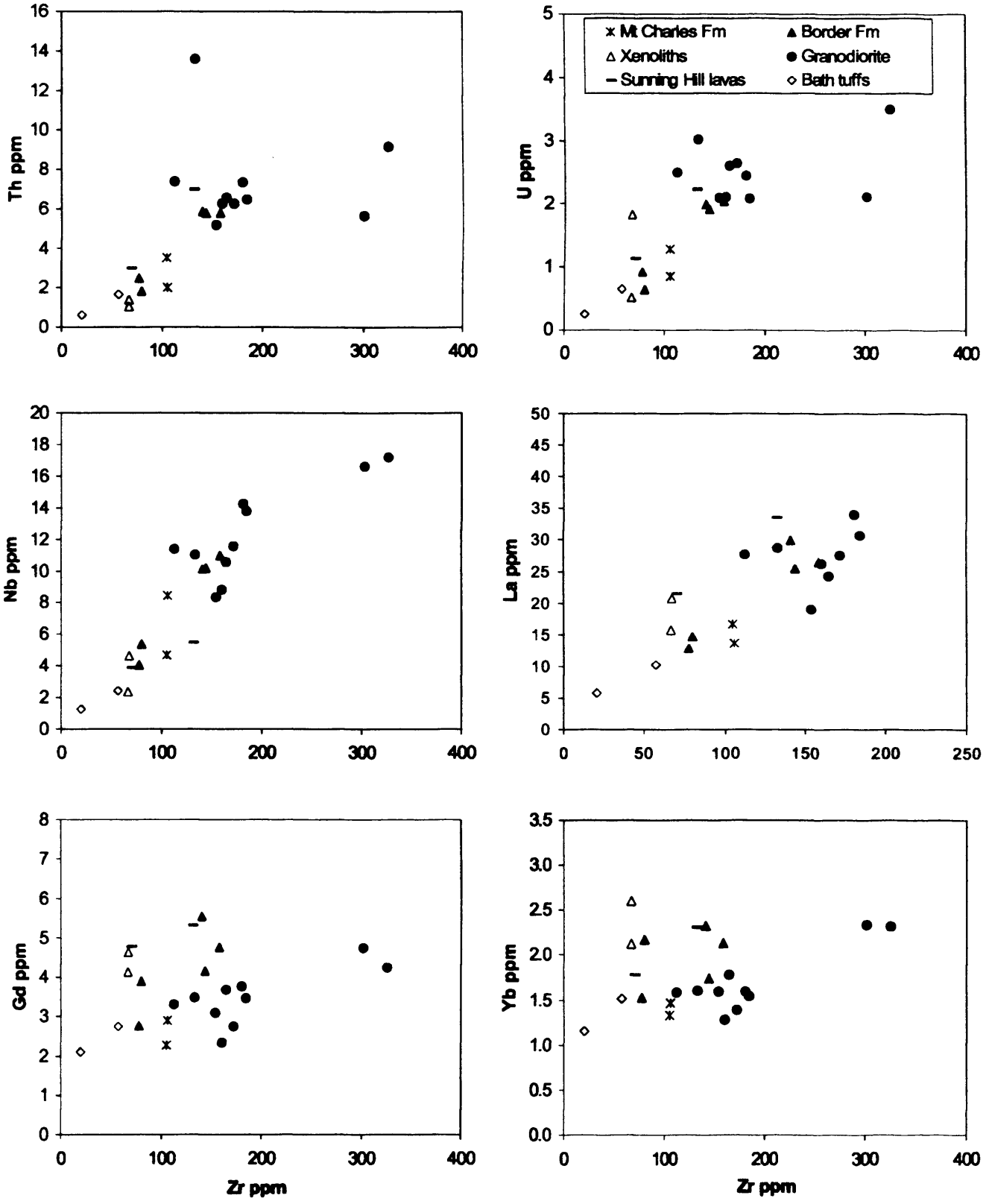

Figure 6.21 – continued.

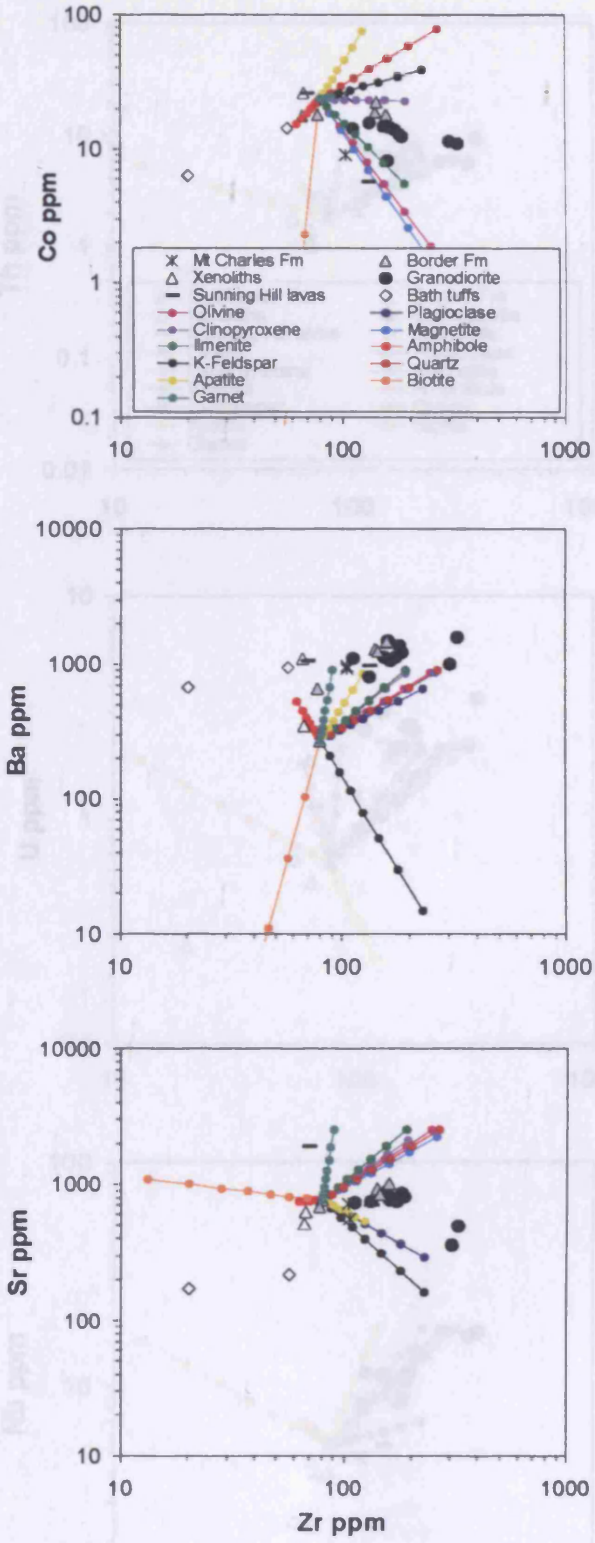

Figure 6.22 – Selected variation diagrams with vectors showing the composition of olivine, plagioclase, clinopyroxene, magnetite, ilmenite, amphibole, K-feldspar, quartz, apatite, biotite, and garnet with up to 70% fractional crystallisation of the AHAR16 starting composition (each tick represents 10% crystallisation) (Appendices E and G).

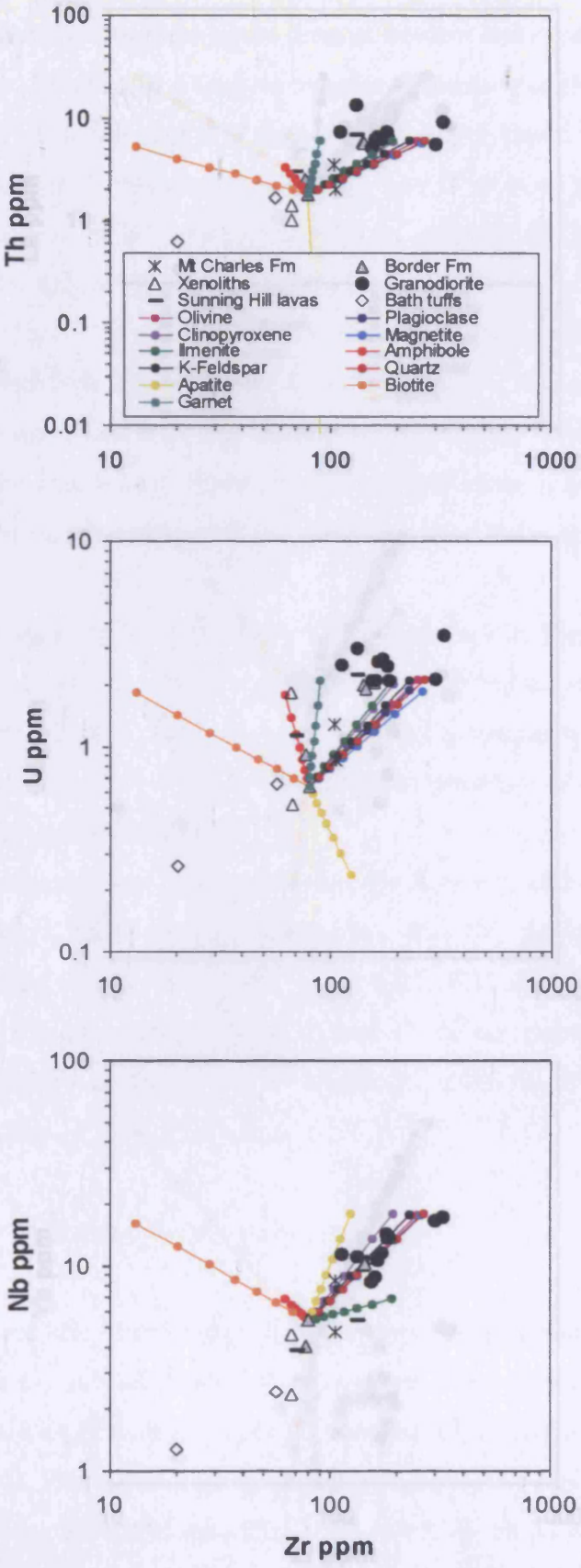

Figure 6.22 – continued

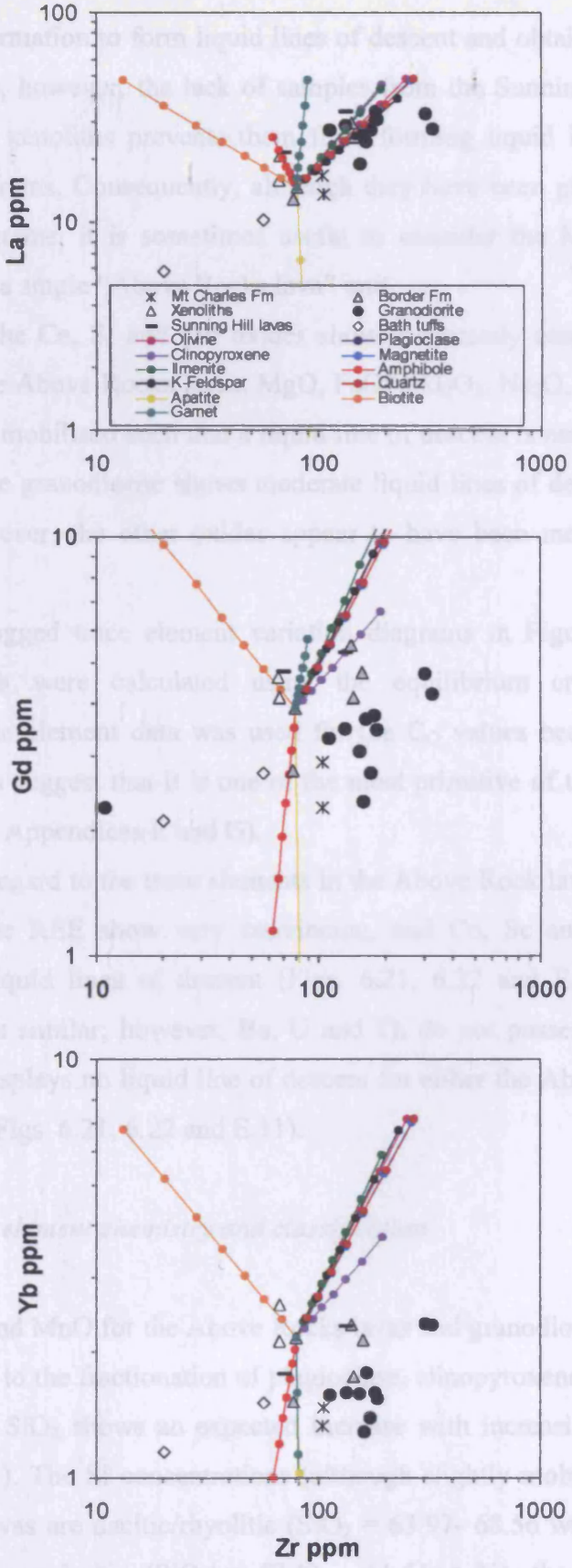

Figure 6.22 – continued

the Border Formation to form liquid lines of descent and obtain source and alteration characteristics, however, the lack of samples from the Sunning Hill and Mt Charles units and the xenoliths prevents them from forming liquid lines of descent in the variation diagrams. Consequently, although they have been plotted separately in the variation diagrams, it is sometimes useful to consider the Mt Charles and Border formations as a single "Above Rocks lava" unit.

Only the Ca, Si and Mn oxides show moderately convincing liquid lines of descent for the Above Rocks lavas. MgO, FeO*, Al_2O_3, Na_2O, TiO_2 and K_2O have all been variably mobilised such that a liquid line of descent is not discernable (Fig. 6.21 and E.11). The granodiorite shows moderate liquid lines of descent for Ca, Si, K, Al and Mn, however, the other oxides appear to have been mobilised (Fig. 6.21 and E.11).

The logged trace element variation diagrams in Figure 6.22 show mineral vectors which were calculated using the equilibrium crystallisation equation. AHAR16 trace element data was used for the C_O values because its Co and silica concentrations suggest that it is one of the most primitive of the lavas in this section (Fig. 6.12 and Appendices E and G).

With regard to the trace elements in the Above Rock lavas, Ba, Sr, Nb, Ta, Hf, Th, U and the REE show very convincing, and Co, Sc and Y show moderately convincing, liquid lines of descent (Figs. 6.21, 6.22 and E.11). The data for the granodiorite is similar; however, Ba, U and Th do not possess good liquid lines of descent. Pb displays no liquid line of descent for either the Above Rocks lavas or the granodiorite (Figs. 6.21, 6.22 and E.11).

6.5.2.2 Major element chemistry and classification

CaO and MnO for the Above Rocks lavas and granodiorite show characteristic decreases due to the fractionation of plagioclase, clinopyroxene, amphibole and Fe-Ti oxides, while SiO_2 shows an expected increase with increasing Zr abundance (Fig. 6.21 and E.11). The Si concentrations (although slightly mobilised) suggest that the Mt Charles lavas are dacitic/rhyolitic (SiO_2 = 63.97- 68.56 wt. %), the Border lavas are basaltic to andesitic (SiO_2 = 47.42 – 61.51wt %), the xenoliths are basaltic andesites (SiO_2 = 53.56 – 53.88 wt. %) and the Sunning Hill lavas consist of a basalt

		Th/Yb-Ta/Yb	Co-Th	Th/Hf-Sm/Yb	Ce/Lu-Sm/Yb	La/Hf-Sm/Y	Th/Zr-La/Yb
Mt Charles Formation	AHAR13						
	AHAR19						
Border Formation	AHAR14						
	AHAR15						
	AHAR16						
	AHAR17						
	AHAR18						
Xenolith	AHAR04						
	AHAR12						
Sunning Hill lavas	AHSUN102						
	AHSUN105						
Bath-Dunrobin Tuff	AHBD12						
	AHBD22						

Table 6.2 – The alkalinity results from plotting the Above Rocks, Sunning Hill and Bath-Dunrobin samples on the Co-Th, Th/Yb-Ta/Yb, Th/Hf-Sm/Yb, Ce/Lu-Sm/Yb, La/Hf-Sm/Y and Th/Zr-La/Yb diagrams; Pink, IAT; Brown, CA; Green, SHC.

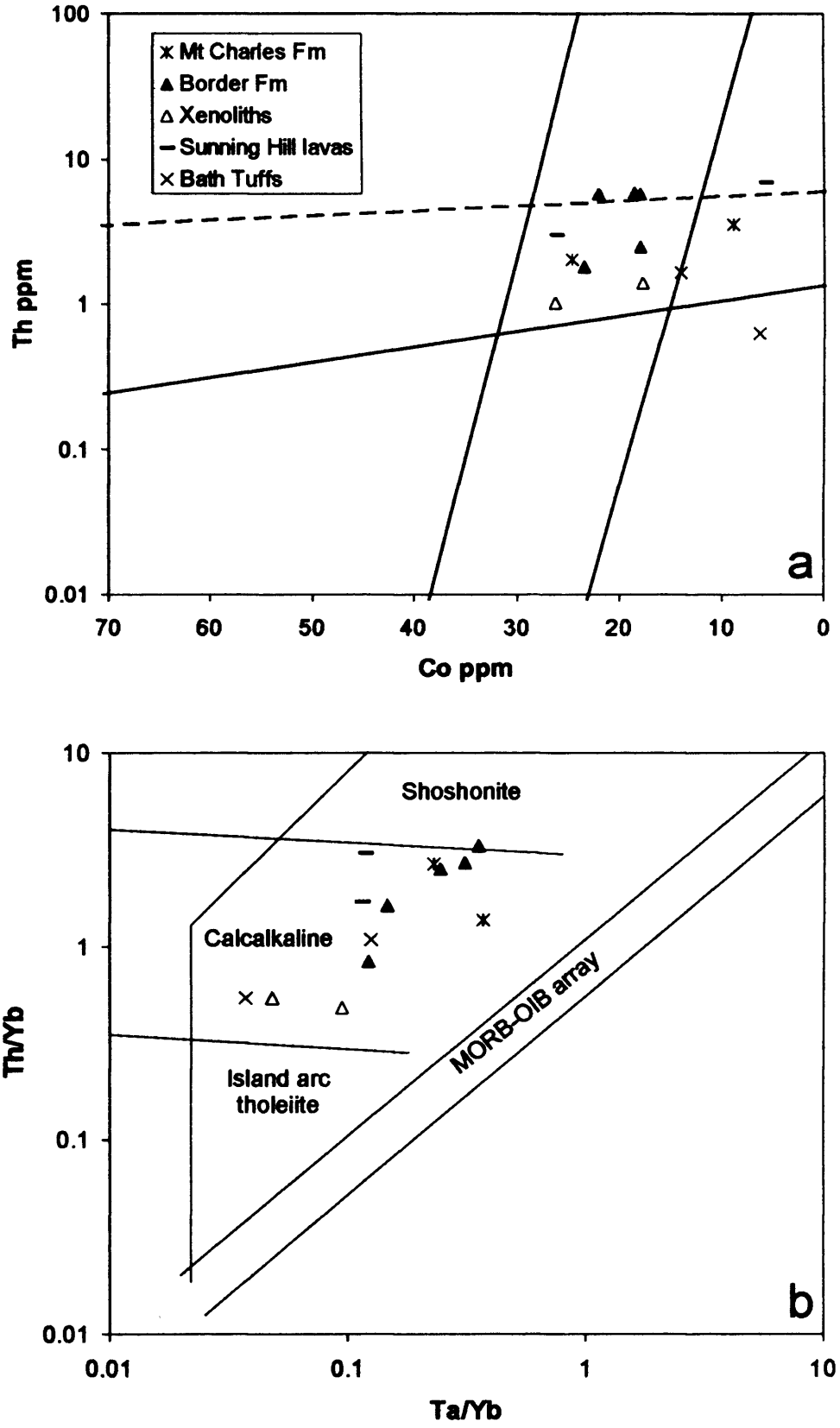

Figure 6.23 – (a) Co vs Th and (b) Zr/Ti vs Nb/Y discrimination diagrams with the Above Rocks, Sunning Hill and Bath-Dunrobin samples plotted (Pearce, 1996; Hastie *et al.*, 2007).

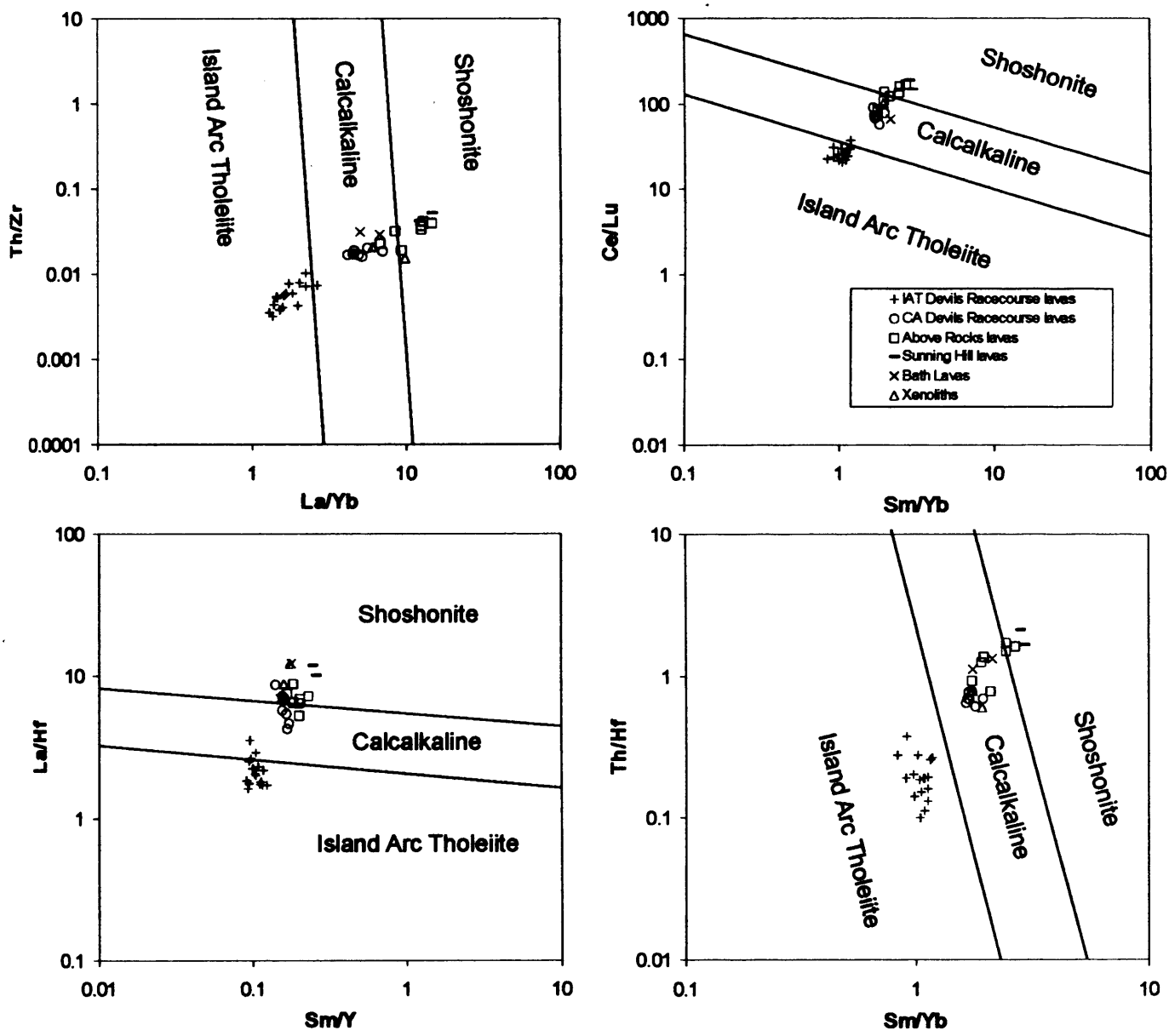

Figure 6.24 - Th/Zr-La/Yb, Ce/Lu-Sm/Yb, La/Hf-Sm/Y and Th/Hf-Sm/Yb discrimination diagrams showing the IAT, CA and SHC affinity of the Above Rocks, Sunning Hill and Bath-Dunrobin rocks. The differing trace element ratios in conjunction with the variation diagrams and isotope ratios indicate that the arc rocks are derived from chemically different source regions.

and a dacite (SiO_2 = 50.73 and 63.56 wt. %). The granodiorite was classified by Reed, (1966) and Issacs and Jackson, (1987) as having granodioritic to granitic compositions; this is supported by the present study which finds that the granodiorite has SiO_2 values of 61.30 – 70.65 wt. %.

The Co-Th (Chapter 5), Th/Yb-Ta/Yb (Pearce, 1982), Th/Zr-La/Yb, Ce/Lu-Sm/Yb, La/Hf-Sm/Y and Th/Hf-Sm/Yb (Chapter 5) discrimination diagrams are used to classify the Above Rocks and Sunning Hill lavas and xenoliths (Figs. 6.23, 6.24 and Table 6.2). The Co-Th and Th/Yb-Ta/Yb diagrams indicate that the Mt Charles lavas are composed of a CA andesite and dacite, the Border lavas are CA and SHC basaltic andesites and andesites, the xenoliths are CA basaltic andesites and the Sunning Hill lavas are composed of a SHC basaltic andesite and dacite/rhyolite Figs. 6.23, 6.24 and Table 6.2).

The variation diagrams suggest that both Si and Co have been variably mobilised by secondary alteration processes (Figs. 6.21 and 6.22). Therefore, neither element gives a wholly reliable measure of the fractionation classification of the lavas. However, Co-Th is the most reliable discrimination diagram because it utilises Th on the Y-axis which is immobile, unlike K and Na. Nevertheless, the Co-Th and SiO_2 fractionation discrimination results do show good agreement with one another (Table 6.2).

The granodiorite samples have not been plotted on the Co-Th (Chapter 5), Th/Yb-Ta/Yb (Pearce, 1982), Th/Zr-La/Yb, Ce/Lu-Sm/Yb, La/Hf-Sm/Y and Th/Hf-Sm/Yb discrimination diagrams because (a) the diagrams were not designed to classify intrusive rocks and (b) Th (which many of the diagrams utilise) has been mobilised or affected by cumulate processes in the granodiorite rocks.

6.5.2.3 Trace element chemistry of the lavas and xenoliths

Trace element variation diagrams show predictable trends for the immobile trace elements, e.g. the REE increase with increasing Zr (Figs. 6.21, 6.22 and E.11). The Sr liquid line of descent for the granodiorite samples is curved (Fig. 6.21). At low Zr the Sr values increase because of the increasing concentration of Sr in the melt due to the removal of crystallising minerals. However, at high Zr values, the Sr content decreases because of the fractionation of plagioclase feldspar within the source magma. Conversely, evidence for plagioclase fractionation is not seen in the Eu

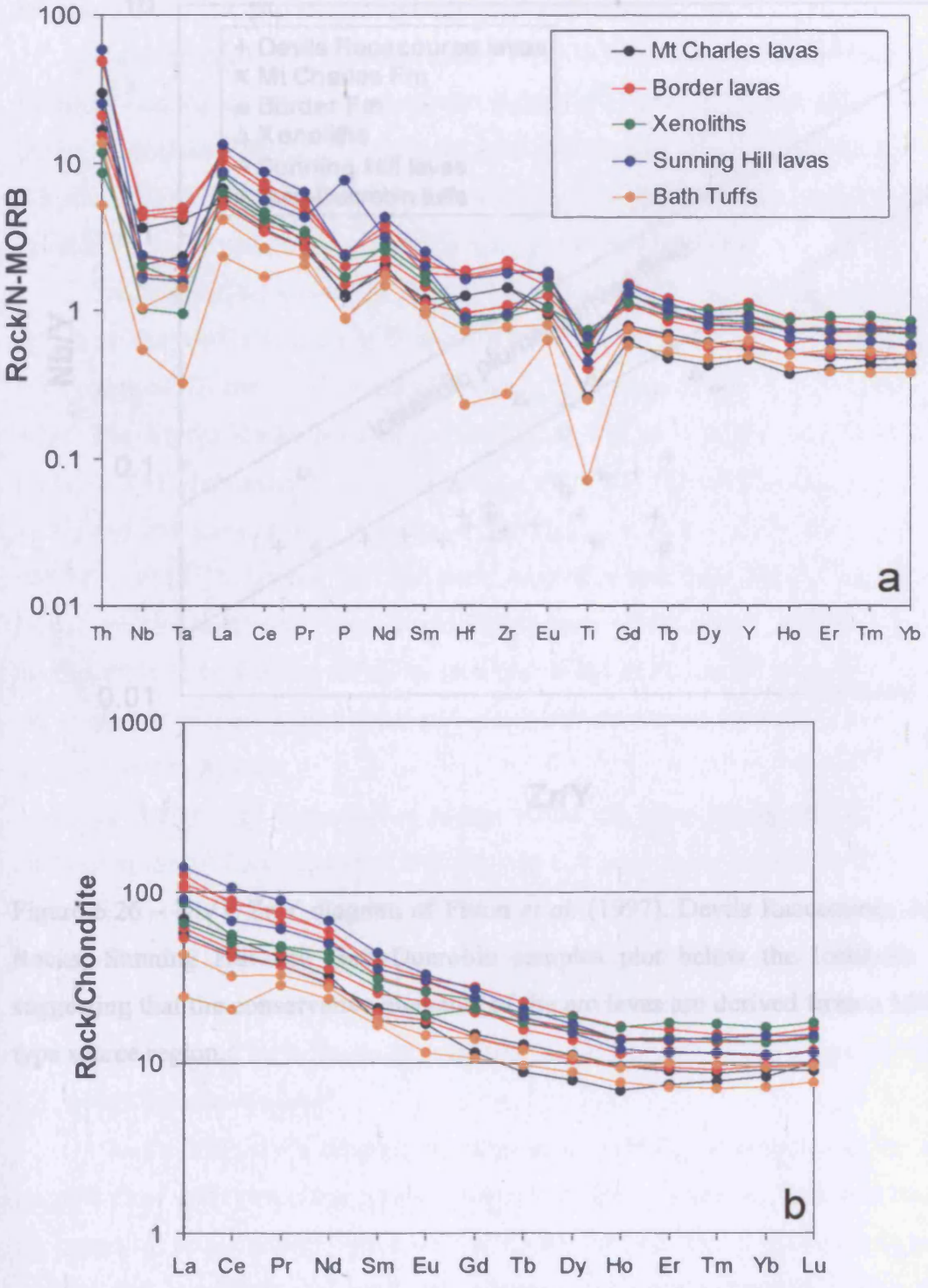

Figure 6.25 – (a) N-MORB-normalised multi-element and (b) chondrite-normalised REE diagrams of the Above Rocks, Sunning Hill and Bath-Dunrobin rocks. Normalising values are taken from Sun and McDonough (1989) and McDonough and Sun (1995).

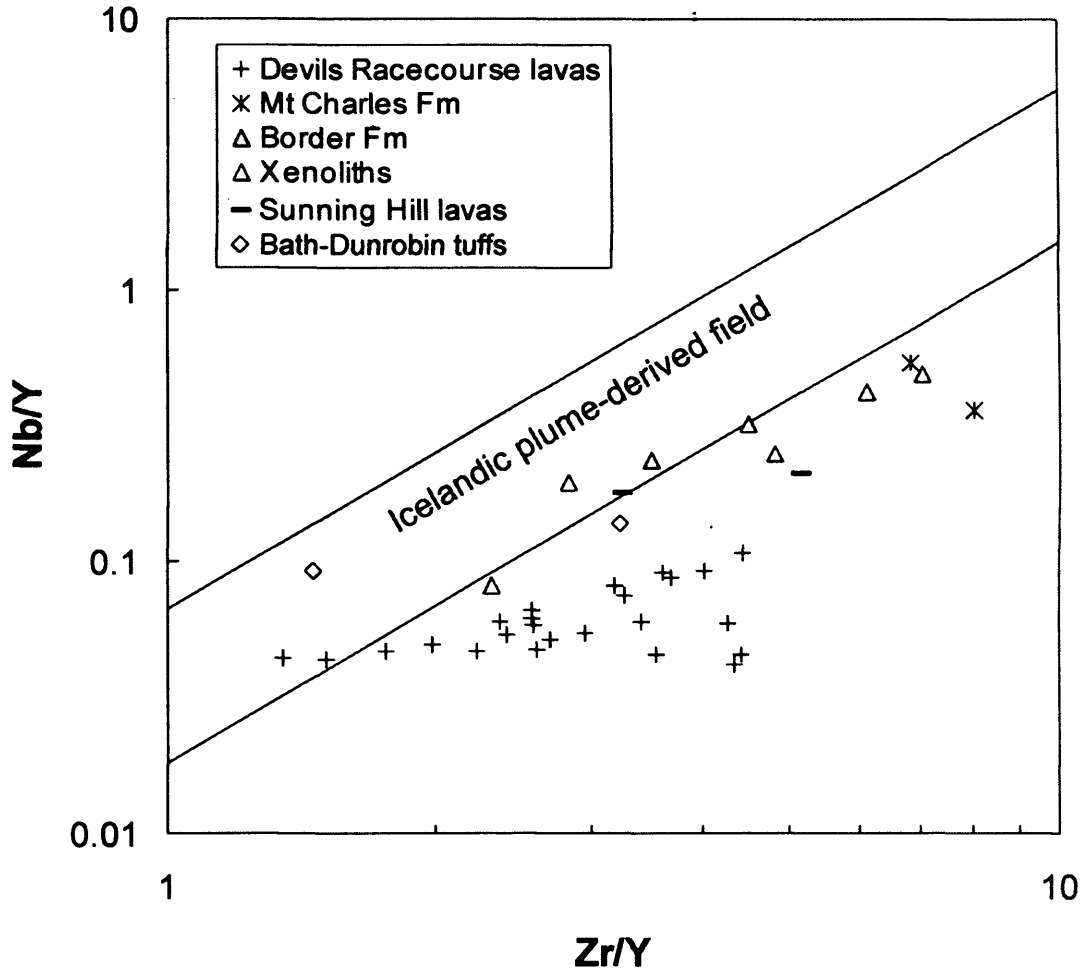

Figure 6.26 – Nb/Y-Zr/Y diagram of Fitton *et al.* (1997). Devils Racecourse, Above Rocks, Sunning Hill and Bath-Dunrobin samples plot below the Icelandic field suggesting that the conservative elements of the arc lavas are derived from a MORB-type source region.

variation diagram, which implies that the Eu in the magma source region is oxidised and exists as Eu^{3+}, a feature unsurprising in island arc rocks.

Incompatible trace element ratio, N-MORB-normalised multi-element and chondrite-normalised REE diagrams are shown in Figures 6.25 and 6.26. Like the Devils Racecourse lavas, the Sunning Hill and Above Rocks samples all have characteristic arc-like negative Nb and Ta anomalies. They also have negative Ti and variable P anomalies due to Fe-Ti oxide and apatite fractionation.

Relative to the upper CA Devils Racecourse rocks, the lavas, xenoliths and tuffs from the Above Rocks and Sunning Hill inliers and Bath-Dunrobin volcanics all have enriched Th and LREE concentrations compared to HFSE, HREE and Y (Fig. 6.24). The Above Rocks lavas have $(La/Yb)_{n\text{-}mn}$ = 8.24 – 17.83 and $(Th/Hf)_{n\text{-}mn}$ = 13.34 – 29.51, the xenoliths have $(La/Yb)_{n\text{-}mn}$ = 7.4 – 11.96 and $(Th/Hf)_{n\text{-}mn}$ = 10.28 – 13.42, and the Sunning Hill lavas have $(La/Yb)_{n\text{-}mn}$ = 14.8 – 17.77 and $(Th/Hf)_{n\text{-}mn}$ =28.37 – 36.14. Assuming that the lavas, xenoliths and tuffs formed by moderate partial melting and underwent moderate degrees of fractional crystallisation the incompatible trace element ratios, as seen above and in Figure 6.24, should represent the primary chemistry of the lavas and indicate if they were derived from similar or different source regions.

In Figure 6.24 the enriched nature of the CA lavas results in them plotting away from the IAT samples. Additionally, the CA lavas from the Devils Racecourse Formation mostly plot at lower Th/Hf, La/Hf, La/Yb, Th/Zr, Sm/Yb, Sm/Y and Ce/Lu ratios than the CA lavas from the Above Rocks and Sunning Hill inliers. The Sunning Hill data mostly have higher ratios than all of the other samples, and the Above Rocks lavas, xenoliths and Bath-Dunrobin tuffs plot in a field between the Sunning Hill and CA Devils Racecourse lavas.

On the Nb/Y-Zr/Y diagram of Fitton *et al.* (1997), the majority of the lavas, xenoliths and tuffs plot either near the lower tramline or below it. This indicates that the conservative elements of these arc rocks were derived from a MORB-type mantle wedge and were not affected by plateau-type mantle material (Fig. 6.26). Nevertheless, the Nb/Y-Zr/Y diagram may be unsuitable for classifying certain evolved igneous rocks because of the potential compatibility of Nb and Zr in fractionating zircon and/or amphibole. However, most of the island arc rocks in Jamaica have basaltic to andesitic compositions and therefore do not represent very "evolved" igneous rocks.

6.5.2.4 Sr, Nd and Pb isotopes

Radiogenic isotope data for samples AHAR02, 16, 18 and AHSUN105 are shown in Figures 6.17-20 and Appendix D. AHAR16 and 18 are from the Border Formation and AHAR02 is from the Above Rocks granodiorite (Appendix A). No samples were analysed for isotopes from the Mt Charles Formation, the xenoliths or the Bath-Dunrobin tuffs.

The Border lavas are age-corrected to 70.5 Ma (Section 6.5.2.6) and possess $\varepsilon_{Nd}(i) = +6.15 - 6.40$, $(^{87}Sr/^{86}Sr)i = 0.7034 - 0.7035$, $(^{206}Pb/^{204}Pb)i = 18.95 - 19.06$, $(^{207}Pb/^{204}Pb)i = 15.59 - 15.6$ and $(^{208}Pb/^{204}Pb)i = 38.69 - 38.79$ (Figs. 6.17-20 and Appendix D). The granodiorite is age-corrected to 64 Ma and has $\varepsilon_{Nd}(i) = +5.92$, $(^{87}Sr/^{86}Sr)i = 0.7076$, $(^{206}Pb/^{204}Pb)i = 18.81$, $(^{207}Pb/^{204}Pb)i = 15.59$ and $(^{208}Pb/^{204}Pb)i = 38.61$. AHSUN105 is age-corrected to 70.5 Ma and has $\varepsilon_{Nd}(i) = +7.24$, $(^{87}Sr/^{86}Sr)i = 0.7040$, $(^{206}Pb/^{204}Pb)i = 18.71$, $(^{207}Pb/^{204}Pb)i = 15.58$ and $(^{208}Pb/^{204}Pb)i = 38.48$ (Figs. 6.17-20 and Appendix D).

Unlike the Bath-Dunrobin plateau and Benbow arc lavas, the initial $^{87}Sr/^{86}Sr$ ratios for the Border, Above Rocks and Sunning Hill rocks do not extend to high radiogenic Sr values at near constant $\varepsilon_{Nd}(i)$ values (Fig. 6.17), implying either that Sr isotopes in these rocks have not been significantly affected by alteration or that, in this instance, the acid leaching during sample preparation was effective. Therefore the Sr isotope systematics are more likely to be a reliable indicator of the source components involved in the genesis of these arc lavas (Fig. 6.17).

The lavas plot with arc data from the Mariana, Kermadec, Lesser Antilles, Tonga, Aleutian, Izu-Bonin and Vanuatu intra-oceanic island arcs. The modern-day arc data fall on numerous mixing lines between an N-MORB end-member and a pelagic/terrigenous end-member. This occurs because the Nd and Sr isotope ratios of the mantle wedge are enriched by a slab-derived component (Section 6.5.1.4) (e.g. Pearce and Peate, 1995). Consequently, the position of the Above Rocks and Sunning Hill samples in Figure 6.17 may be explained by a similar mixing line (s).

On the $(^{207}Pb/^{204}Pb)i - (^{206}Pb/^{204}Pb)i$ plot (Fig. 6.18) the lavas lie above the NHRL and have higher $(^{207}Pb/^{204}Pb)i$ and $(^{206}Pb/^{204}Pb)i$ ratios than the IAT and CA Devils Racecourse lavas (Fig. 6.18). The Border samples have higher $(^{206}Pb/^{204}Pb)i$

ratios (18.95-19.06) than the Sunning Hill lava (18.71), suggesting that they may contain a larger sediment/crustal component (Fig. 6.18).

The $(^{208}Pb/^{204}Pb)i - (^{206}Pb/^{204}Pb)i$ plot (Fig. 6.18) supports the $(^{207}Pb/^{204}Pb)i - (^{206}Pb/^{204}Pb)i$ diagram by indicating that the Border and Sunning Hill lavas also have higher $(^{208}Pb/^{204}Pb)i$ ratios than the IAT Benbow lavas and may thus be composed of a larger sedimentary/crustal component. The Border lavas, in turn, have higher $(^{208}Pb/^{204}Pb)i$ ratios than the Sunning Hill lava, suggesting that they are made up of a more enriched sedimentary/crustal Pb isotopic component (Fig. 6.18).

6.5.2.5 Nd and Hf isotopes

The Border lavas possess $\varepsilon_{Nd}(i) = +6.15 - 6.40$ and $\varepsilon_{Hf}(i) = +11.86 - 12.34$, the granodiorite has $\varepsilon_{Nd}(i) = +5.92$ and $\varepsilon_{Hf}(i) = +11.64$ and SUN105 has $\varepsilon_{Nd}(i) = +7.24$ and $\varepsilon_{Hf}(i) = +13.14$ (Fig. 6.20 and Appendix D). The variation diagrams for Nd and Hf (Section E.11, Appendix E) and the position of the Border and Sunning Hill lavas in the $\varepsilon_{Nd}(i) - \varepsilon_{Hf}(i)$ plot indicates that both elements have not been modified by post-magmatic alteration processes. For comparison the Above Rocks and Sunning Hill samples have been plotted with other arc lavas from the Cretaceous Bonaire and the post-Mesozoic Mariana, Izu-Bonin, Aleutian, New Britain, Sunda and Lesser Antilles intra-oceanic island arcs.

The Border lavas have $\varepsilon_{Hf}(i) = +11.86 - 12.34$ which results in them plotting at the enriched end of the Atlantic/Pacific N-MORB field (Nowell *et al.*, 1998; Kempton *et al.*, 2000). These lavas also possess the most enriched $\varepsilon_{Nd}(i)$ ratios of all of the "normal" Jamaican arc lavas (Fig. 6.20). The Sunning Hill lava has more enriched $\varepsilon_{Nd}(i)$ and $\varepsilon_{Hf}(i)$ values relative to most of the other Jamaican rocks, and the Above Rocks granodiorite has the most enriched $\varepsilon_{Nd}(i)$ and $\varepsilon_{Hf}(i)$ ratios of any other igneous rock in this study (Fig. 6.20).

6.5.2.6 Palaeontological and geochronological data

No absolute stratigraphical or palaeontological ages exist for the Above Rocks or Sunning Hill samples. A fission track age on apatite from the Above Rocks granodiorite gives an age of 60.4 ± 3.4 Ma. Radiometric studies of the granodiorite also give ages of: 64 ± 5 Ma (biotite – method not stated), 67 ± 5 Ma (biotite – K/Ar age) and 64 Ma (sphene – U/Pb) (Ahmad and Sharma, 1987).

However, the Above Rocks granodiorite has been variably altered and because no sedimentological or palaeontological ages can be used to constrain the age of the pluton it was decided to date one of the samples using the argon radiometric technique to support the aforementioned geochronology. Two biotite mineral separates from AHAR02 were analysed to give inverse isochron ages of 66.26 ± 0.65 Ma and 63.65 ± 0.96 Ma and a step heating plateau age of 64.31 ± 0.53 Ma (Appendix D) (Figs. 6.27 and 6.28). All of these dates are similar and, if averaged, the Above Rocks granodiorite would have an age of 64.23 Ma. The argon isochron ages, which are regarded as the most reliable (Dr D. Barfod pers. comm.), also average out as 64.95 Ma. Consequently, the radiogenic isotopes for the Above Rocks granodiorite were age-corrected to 64 Ma.

No age data exists for the Mt Charles or Border Formations; therefore, AHAR14 (Border lava) was also dated using the argon radiometric technique (Fig. 6.29). A plagioclase separate was analysed to give an inverse isochron age of 70.5 ± 2.1 Ma and a step heating plateau age of 68.91 ± 0.42 Ma. The Mt Charles and Border Formation radiogenic data are therefore age corrected to the more reliable isochron age of 70.5 Ma (Appendix D) (Fig. 6.29). This older age for the Above Rocks lavas is supported in the field because they are intruded by the younger granodiorite and they are unconformably overlain by Tertiary limestones, demonstrating that they have a pre-Tertiary age.

The radiogenic isotopes for the Sunning Hill sample AHSUN105 are also age corrected to 70.5 Ma. This is because the Sunning Hill lavas have a similar chemistry to the Above Rocks lavas and they are assumed to have erupted at a similar time. However, no stratigraphical evidence can confirm this and AHSUN105 was not dated because of the sample limit in this study. The Bath-Dunrobin tuffs are intercalated with the Bath-Dunrobin plateau lavas, which indicates that they are ~ 90 Ma.

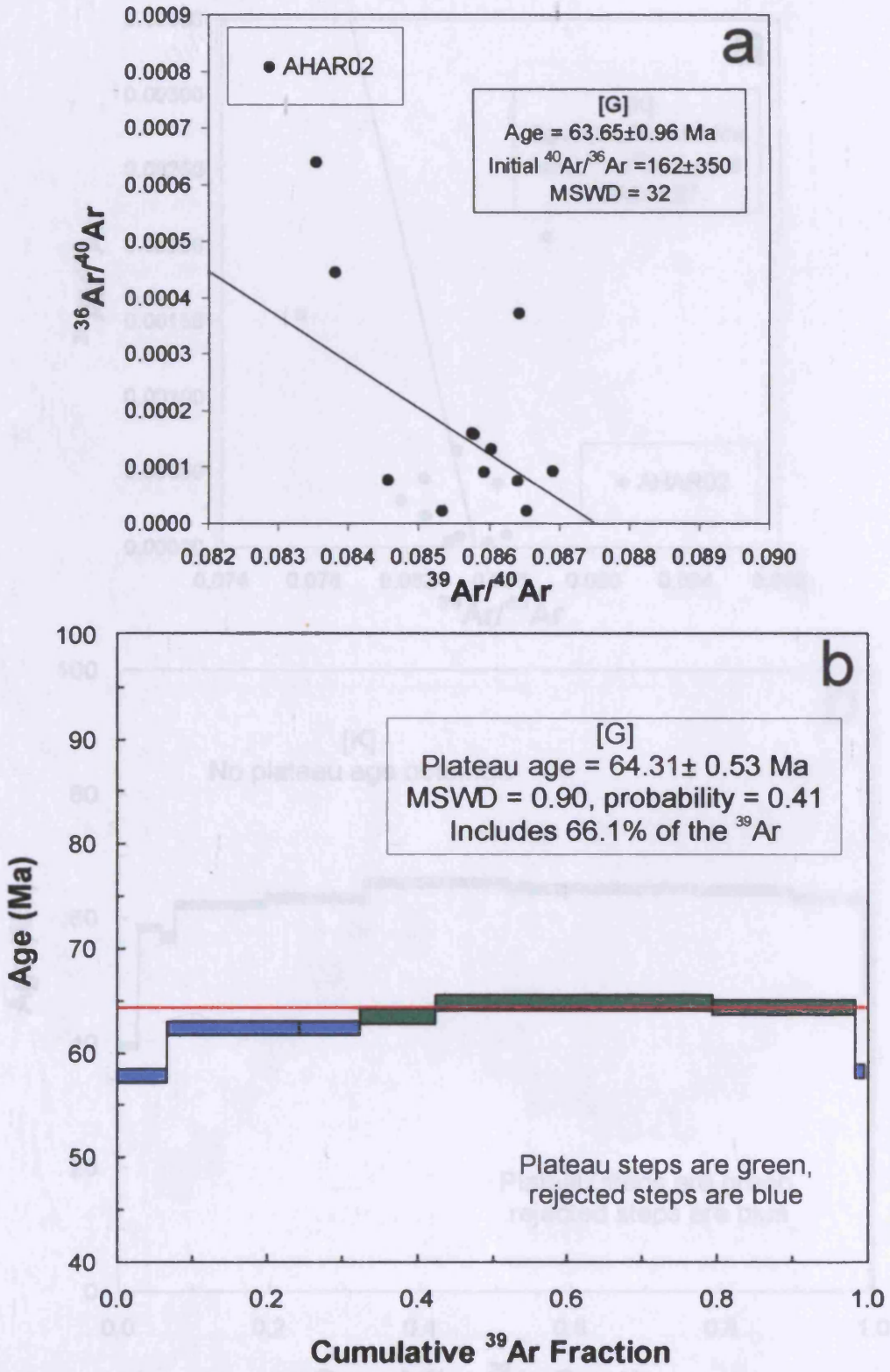

Figure 6.27 – (a and b) Ar-Ar inverse isochron and step heating plateau plots for AHAR02 run [G].

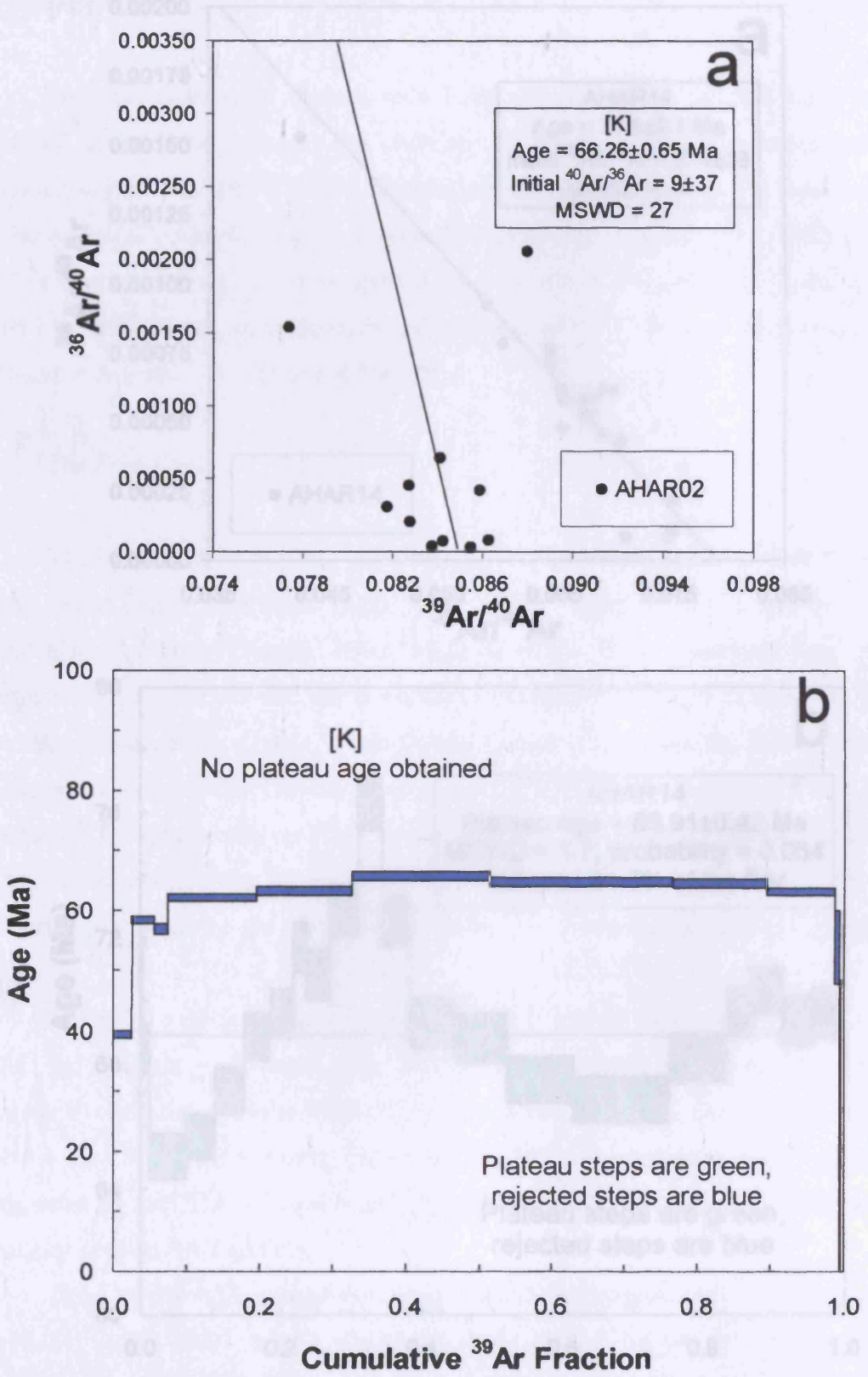

Figure 6.28 – (a and b) Ar-Ar inverse isochron and step heating plateau plots for AHAR02 run [K].

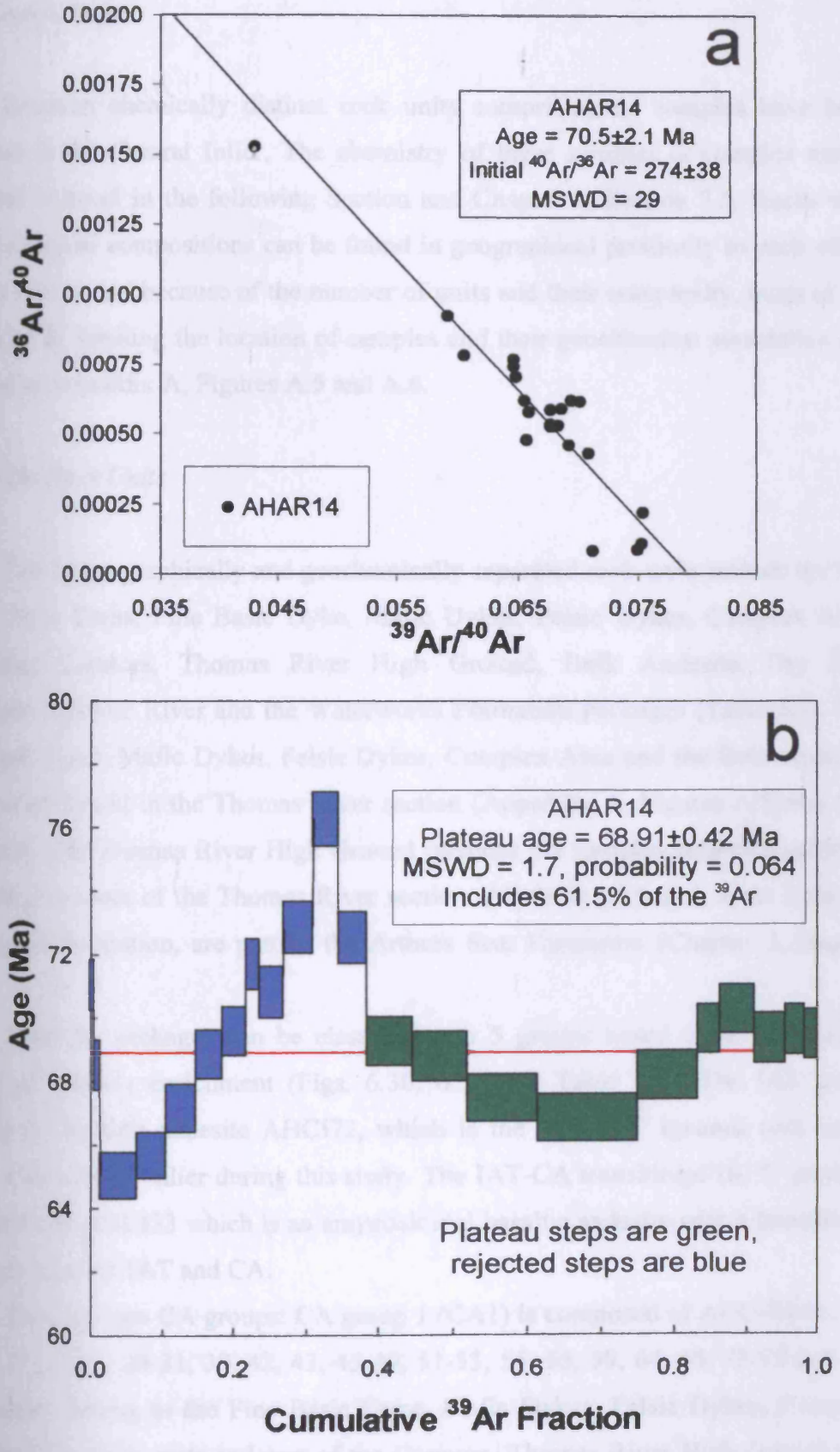

Figure 6.29 – (a and b) Ar-Ar inverse isochron and step heating plateau plots for AHAR14.

6.5.3 Central Inlier

Fourteen chemically distinct rock units comprising 61 samples have been identified in the Central Inlier. The chemistry of these samples is complex and is described in detail in the following Section and Chapter 7, Section 7.5. Rocks with similar chemical compositions can be found in geographical proximity to each other. For this reason, and because of the number of units and their complexity, maps of the Central inlier detailing the location of samples and their geochemical association can be found in Appendix A, Figures A.5 and A.6.

6.5.3.1 The Rock Units

The 14 geographically and geochemically separated rock units include the Old Works, Nine Turns, Fine Basic Dyke, Mafic Dykes, Felsic Dykes, Complex Area, Friendship, Connors, Thomas River High Ground, Bulk Andesite, Dry Hill, Grantham, Crooked River and the Waterworks Formation packages (Table 6.3). The Fine Basic Dyke, Mafic Dykes, Felsic Dykes, Complex Area and the Bulk Andesite packages are found in the Thomas River section (Appendix A, Figures A.5 and A.6, Table 6.3). The Thomas River High Ground includes the samples collected uphill to the north and south of the Thomas River section. All these packages, apart from the Waterworks Formation, are part of the Arthurs Seat Formation (Chapter 3, Section 3.5).

These 14 packages can be classified into 5 groups based upon their LILE, LREE and actinide enrichment (Figs. 6.30, 6.31 and Table 6.3). The IAT group contains the basaltic andesite AHCI72, which is the only IAT igneous rock to be found in the Central inlier during this study. The IAT-CA transitional (ICT) group is represented by AHCI33 which is an amygdaloidal basaltic andesite with a transitional chemistry between IAT and CA.

There are two CA groups: CA group 1 (CA1) is composed of AHCI03-06, 14, 16, 18, 21, 23-27, 29-31, 39, 42, 43, 45-49, 51-53, 55, 56, 59, 64, 65, 73-75 and 79. The samples belong to the Fine Basic Dyke, Mafic Dykes, Felsic Dykes, Complex Area and Friendship units and part of the Connors, Thomas River High Ground and Bulk Andesite units; CA group 2 (CA2) is composed of AHCI07, 08, 15, 19, 20, 22, 28, 35-37, 40, 62, 63, 76-78 which belong to the Dry Hill and Grantham units and

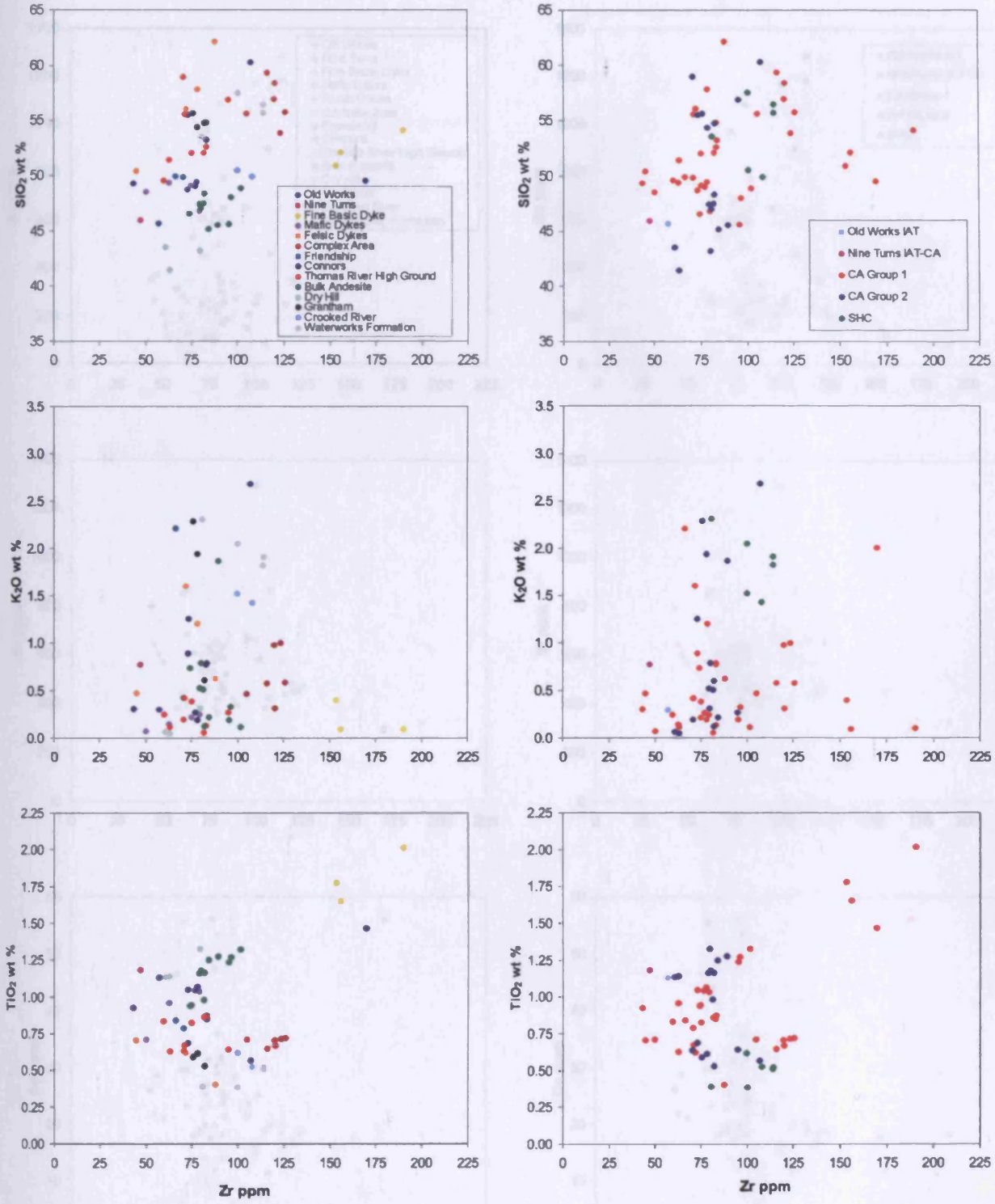

Figure 6.30 – Selected variation diagrams for major and trace elements vs. Zr for the Central Inlier samples. The degree of mobility of an element is represented by its correlation with Zr. A mobile element will show no correlation, whereas, an immobile element displays a good correlation. A correlation can be a straight or curved line depending on whether the element is incompatible and/or compatible during fractional crystallisation.

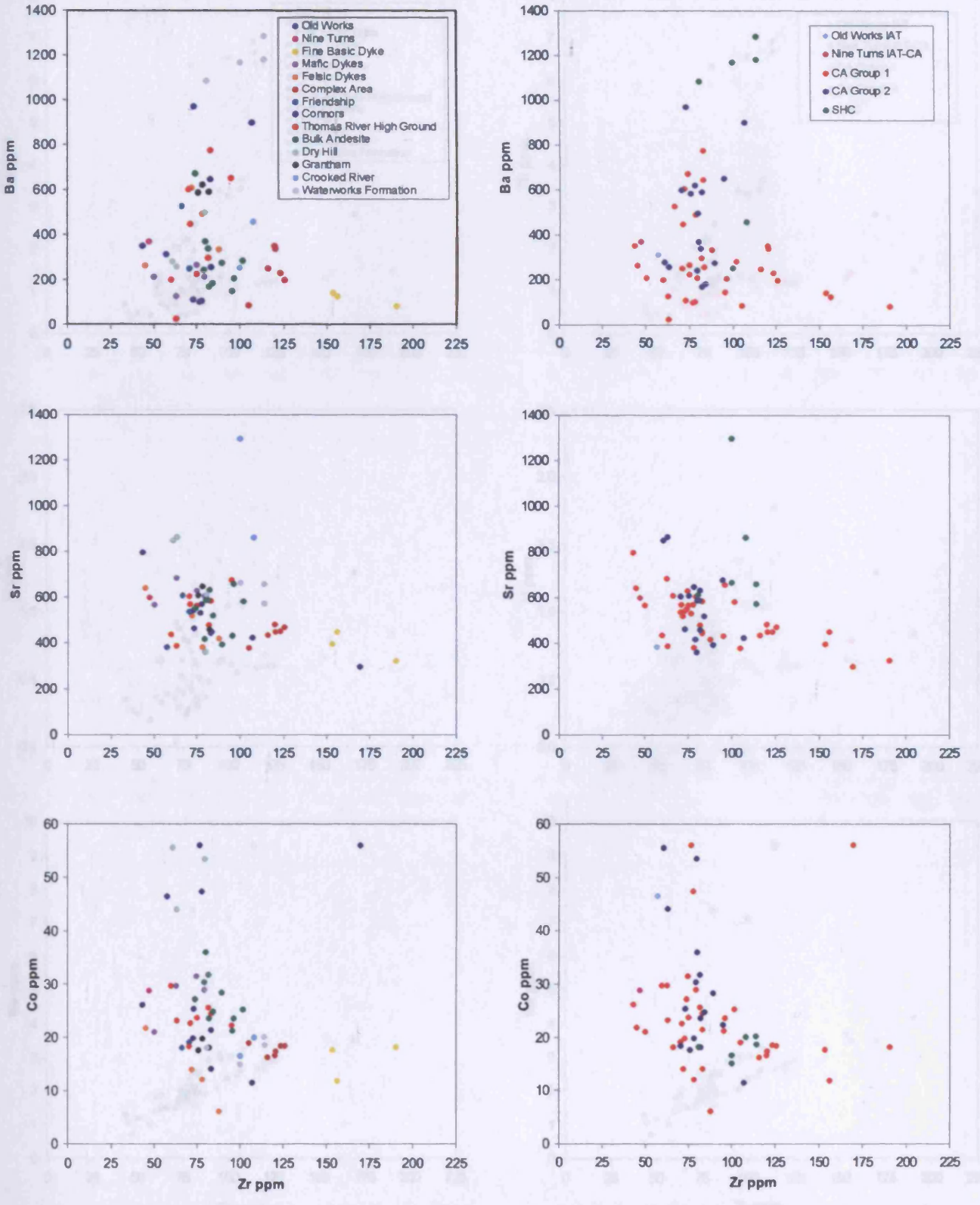

Figure 6.30 – continued.

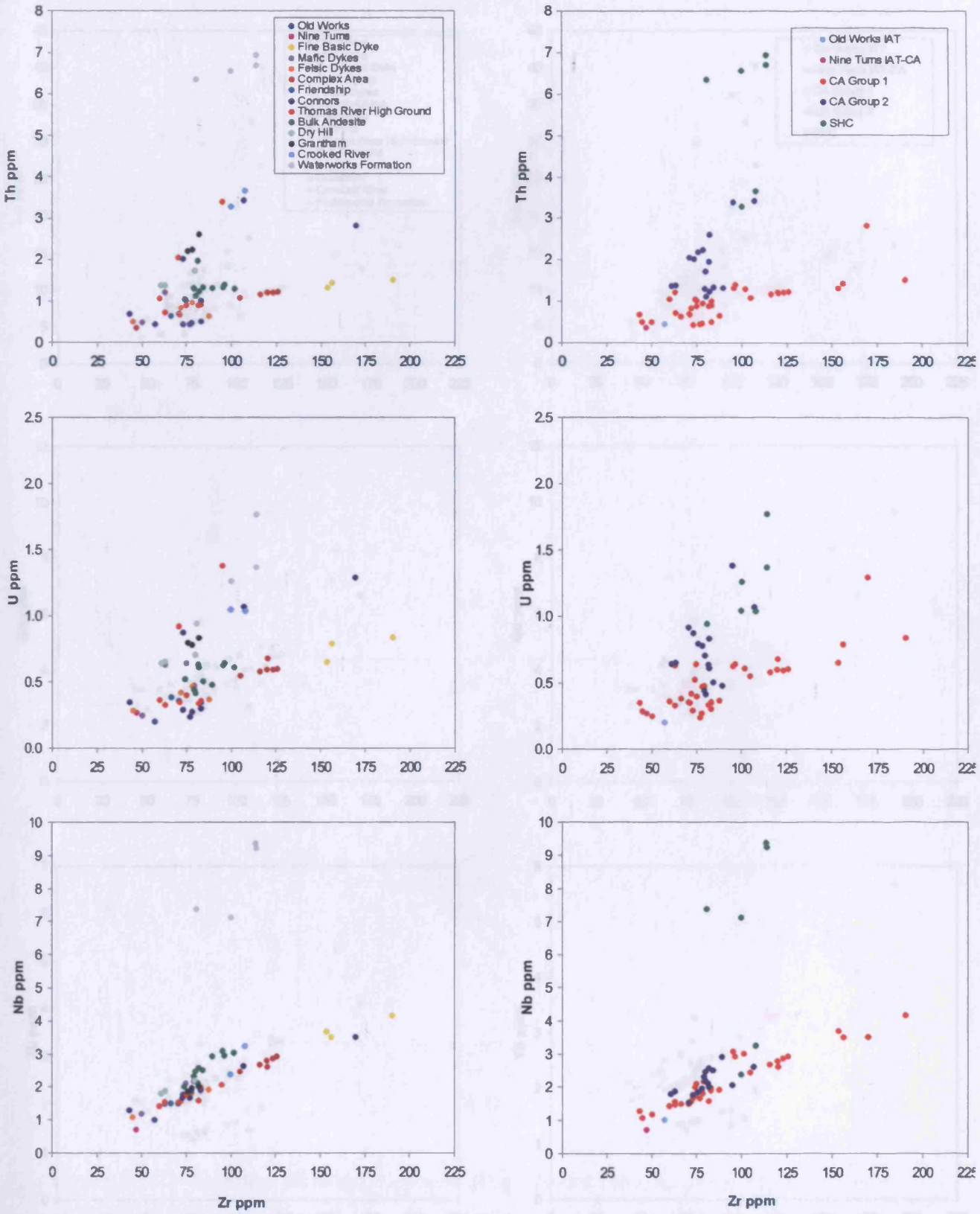

Figure 6.30 – continued.

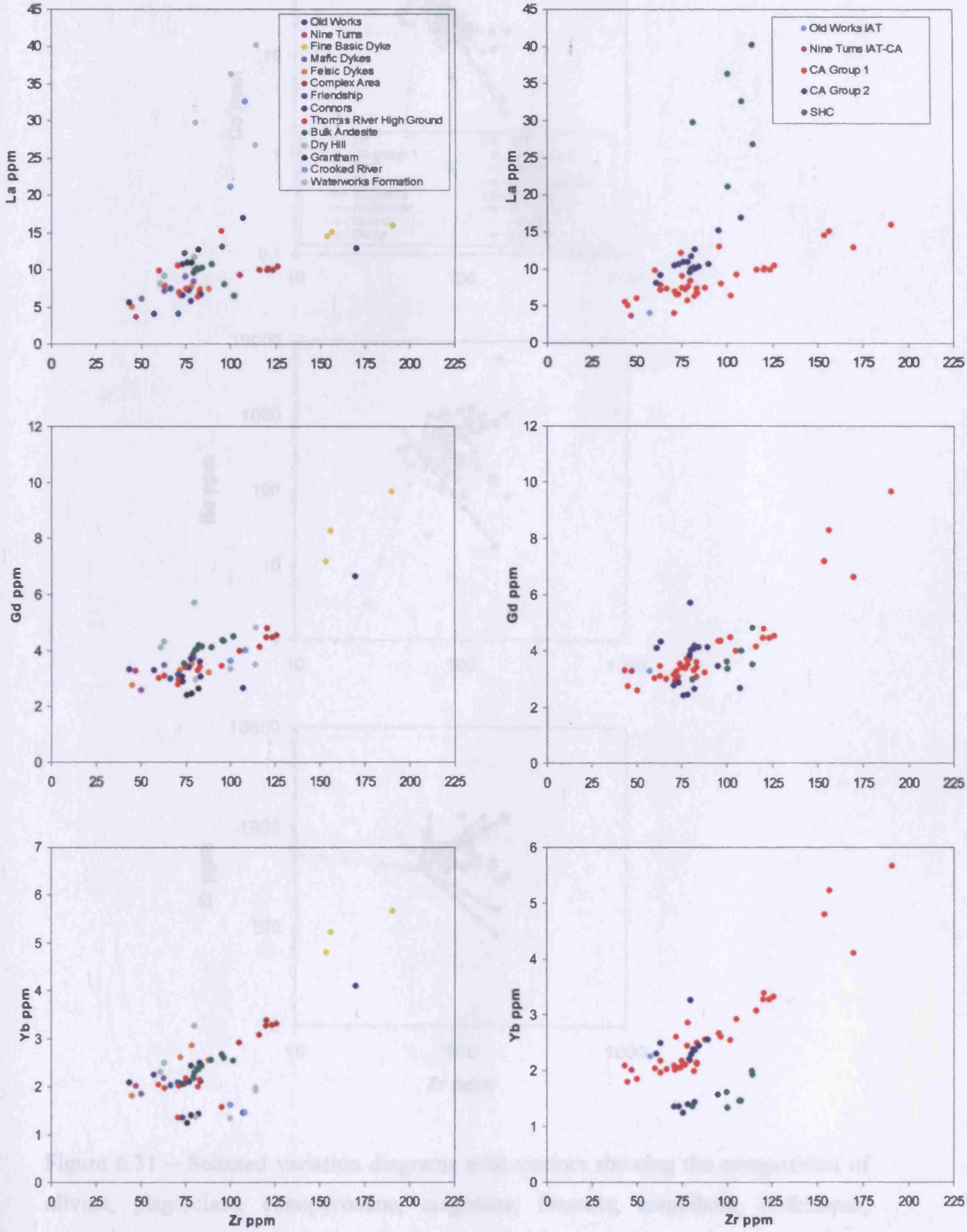

Figure 6.30 – continued.

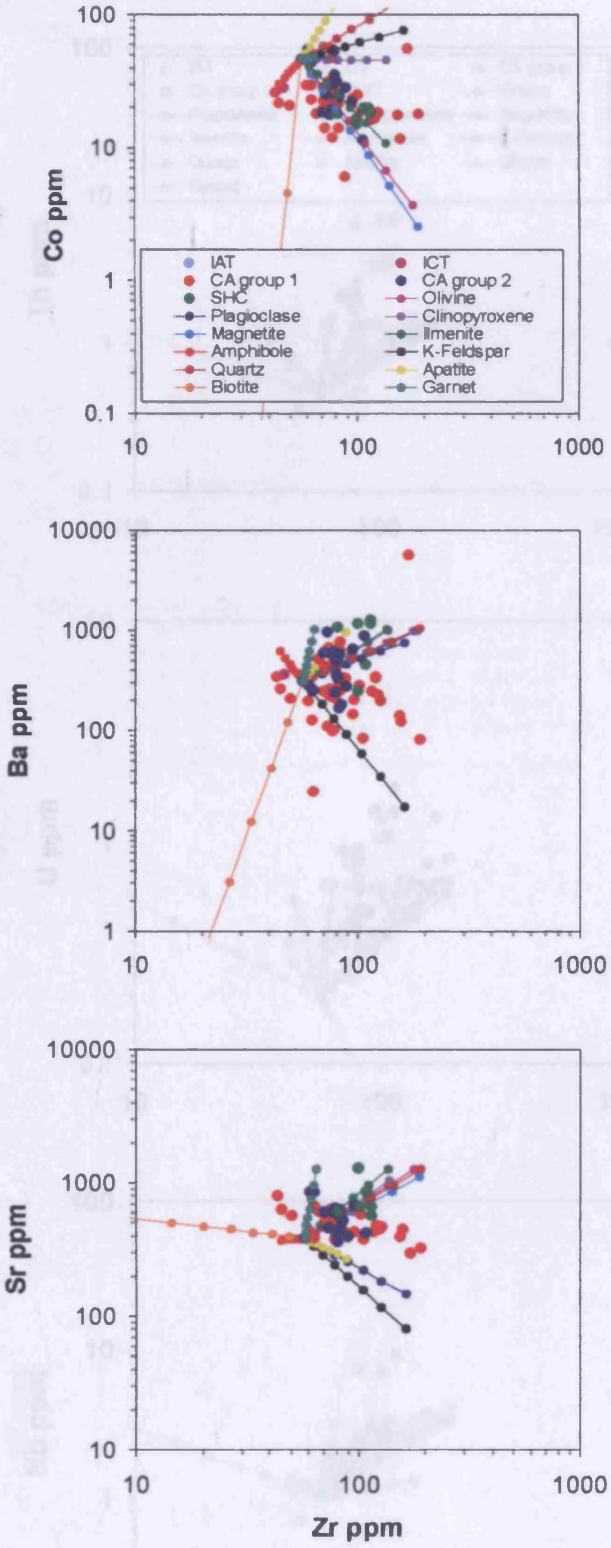

Figure 6.31 – Selected variation diagrams with vectors showing the composition of olivine, plagioclase, clinopyroxene, magnetite, ilmenite, amphibole, K-feldspar, quartz, apatite, biotite, and garnet with up to 70% fractional crystallisation of the AHCI72 starting composition (each tick represents 10% crystallisation) (Appendices E and G).

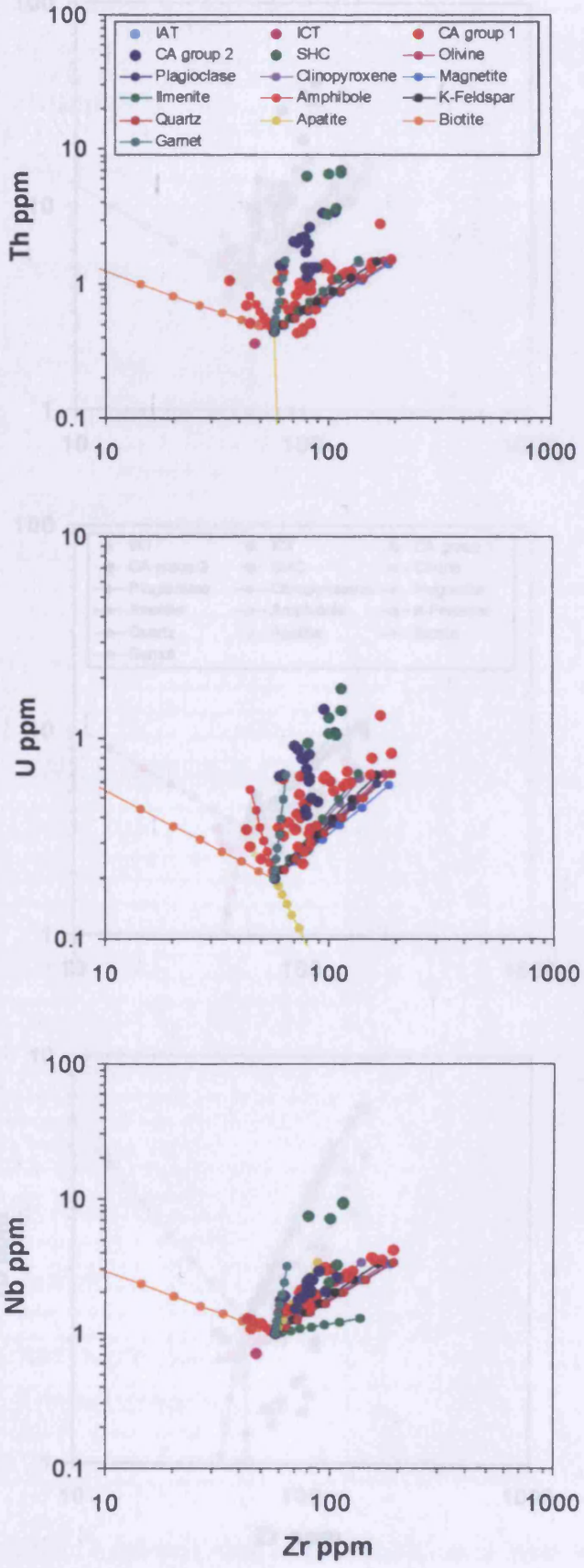

Figure 6.31 – continued

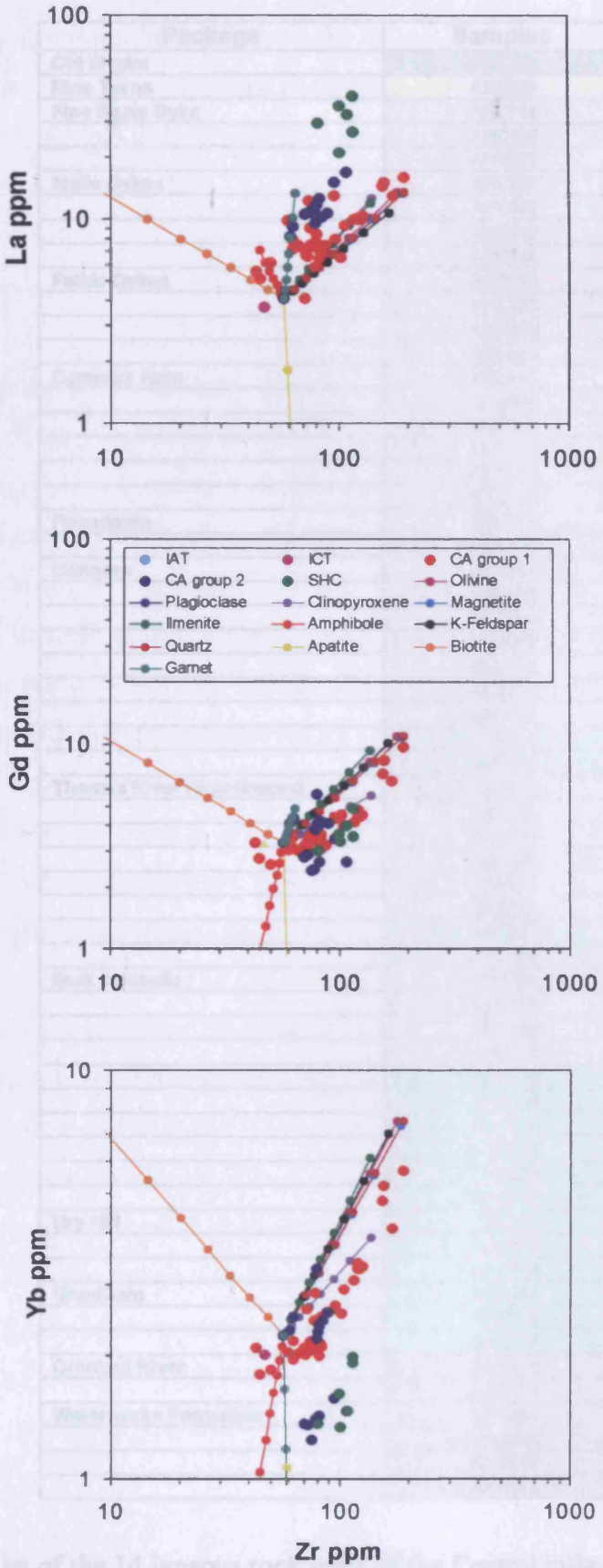

Figure 6.31 – continued

Package	Samples
Old Works	AHCI72
Nine Turns	AHCI33
Fine Basic Dyke	AHCI14
	AHCI16
	AHCI21
Mafic Dykes	AHCI27
	AHCI42
	AHCI43
	AHCI46
Felsic Dykes	AHCI18
	AHCI23
	AHCI25
	AHCI29
Complex Area	AHCI45
	AHCI47
	AHCI48
	AHCI51
	AHCI52
	AHCI53
Friendship	AHCI55
	AHCI56
Connors	AHCI59
	AHCI64
	AHCI65
	AHCI73
	AHCI74
	AHCI75
	AHCI79
	AHCI62
	AHCI63
Thomas River High Ground	AHCI03
	AHCI04
	AHCI05
	AHCI06
	AHCI30
	AHCI31
	AHCI07
	AHCI08
Bulk Andesite	AHCI24
	AHCI26
	AHCI39
	AHCI49
	AHCI15
	AHCI19
	AHCI20
	AHCI22
	AHCI28
	AHCI40
Dry Hill	AHCI76
	AHCI77
	AHCI78
Grantham	AHCI35
	AHCI36
	AHCI37
Crooked River	AHCI10
	AHCI11
Waterworks Formation	AHCI09
	AHCI09A
	AHCI12
	AHCI13

Table 6.3 – List of the 14 igneous rock units of the Central inlier and the samples that comprise them. Colour coding indicates the classification of the samples; Blue, IAT; Yellow, IAT-CA transition; Brown, CA group 1; Green, CA group 2; Pink, SHC.

comprise the remaining samples from the Connors, Thomas River High Ground and Bulk Andesite packages. The final group is the SHÇ group that is composed of the samples AHCI09, 09a, 10-13 which represent the Crooked River and Waterworks Formation units.

6.5.3.2 Element mobility

Major and trace element variation diagrams are shown in Figures 6.30, 6.31 and Section E.12, Appendix E. For each element the variation diagrams show the geochemistry of the 14 packages and the 5 groups (Fig. 6.30). The Ca, Si, P, Ti and Fe oxides show good to moderate liquid lines of descent in all the packages and groups, whereas the MgO, Al_2O_3, Na_2O, MnO and K_2O have largely all been mobilised such that a liquid line of descent is not discernable (Figs. 6.27, 6.28 and E.12). However, MgO, Al_2O_3, Na_2O, MnO and K_2O do show some good liquid lines of descent for a small number of rock packages e.g. K, Mn, Mg and Al, are immobile in the Waterworks Formation, Complex Area, Felsic Dykes and Bulk Andesite packages respectively (Figs. 6.30 and 6.31).

The logged trace element variation diagrams in Figure 6.31 use AHCI72 trace element data for the C_O values because its Co and silica concentrations suggest that it is one of the most primitive of the Central Inlier rocks (Appendices E and G). With regard to the trace elements Th, the REE, Y, Ta, Nb, U, Sr, Sc and Co show good to moderate liquid lines of descent whereas Pb and Ba are largely mobile in many of the units (Figs. 6.30, 6.31and E.12).

In addition, although, Pb, Ba, MgO, Al_2O_3, Na_2O, MnO and K_2O are immobile in a small number of instances (Fig. 6.30 and E.12) it was decided not to use them in the petrogenesis of the Central inlier. This is because these elements and oxides are mobile in many of the Central inlier packages and other igneous rocks in Jamaica. Therefore, in order for the Jamaican arc rocks to be geochemically compared to one other, both in the Central inlier and the other Cretaceous inliers, these elements are not used.

6.5.3.3 Major element chemistry and classification

The liquid lines of descent for the 14 rock units show both increases and decreases on Ca, P, Ti and Fe oxide variation diagrams (Fig. 6.27 and E.12). This suggests that Fe-Ti oxides, apatite and plagioclase have fractionated from the magmas in some of these units, but not from others. The only oxide which increases with increasing Zr in all units is SiO_2.

The SiO_2 concentrations (although slightly mobilised) suggest that the Old Works IAT, and the Nine Turns ICT are basalts (SiO_2 = 45.69-45.95 wt. %) and that the Fine Basic Dyke and Mafic Dykes packages in the Thomas River locality are basalts and basaltic andesites (SiO_2 = 46.79-54.13 wt. %) (Table 6.4). Conversely, the Felsic Dykes package contains four samples with silica values suggesting that they are basaltic to dacitic (SiO_2 = 50.41-62.18 wt. %). The rocks of the Complex Area are basaltic andesites and andesites (SiO_2 = 53.90-59.37 wt. %) and paradoxically, the Bulk Andesite rocks are basalts (SiO_2 = 45.14-48.88 wt. %) (Table 6.4). The rocks which make up the Thomas River High Ground unit are basaltic to andesitic with SiO_2 = 49.56-59.00 wt. %. The Friendship rocks are basaltic (SiO_2 = 49.85-49.94 wt. %) and the large outcrops of lavas around Connors are basaltic to andesitic with SiO_2 = 48.72- 55.55 wt. %. The rocks of the more Th and LREE-enriched CA2 and SHC groups also have silica values which suggest that they are basic to intermediate in composition. The Dry Hill and Grantham igneous rocks have SiO_2 = 41.44-55.66 wt. % and the Crooked River and Waterworks Formation have SiO_2 = 49.91-57.52 wt. %.

However, like the other Jamaican samples, the silica values only give an estimate of the extent of evolution of the Central inlier samples. The silica appears to be slightly mobilised and the mobility of K and Na prevents the rocks from being classified on the TAS diagram. Co has also been slightly mobilised, but no more so than SiO_2 and the Co-Th diagram utilises Th which is immobile. As such, the Co-Th (Chapter 5) and Th/Yb-Ta/Yb (Pearce, 1982) plots have been used in conjunction with the Th/Hf-Sm/Yb, Ce/Lu-Sm/Yb, La/Hf-Sm/Y and Th/Zr-La/Yb diagrams to determine the LILE, LREE and actinide enrichment of the Central inlier rocks (Table 6.4).

Because of the number of samples in the inlier, the fractionation and LILE, LREE and actinide enrichment results of the six discrimination diagrams are shown in Table 6.4. Where the Co-Th and silica (TAS) results differ, the Co interpretation is

		Fractionation Determination		Alkalinity Determination					
		Silica values	Co-Th	Th/Yb-Ta/Yb	Co-Th	Th/Hf-Sm/Yb	Ce/Lu-Sm/Yb	La/Hf-Sm/Y	Th/Zr-La/Yb
Old Works	AHCI72								
Nine Turns	AHCI33								
Fine Basic Dyke	AHCI14								
	AHCI16								
	AHCI21								
Mafic Dykes	AHCI27								
	AHCI42								
	AHCI43								
	AHCI46								
Felsic Dykes	AHCI18								
	AHCI23								
	AHCI25								
	AHCI29								
Complex Area	AHCI45								
	AHCI47								
	AHCI48								
	AHCI51								
	AHCI52								
	AHCI53								
Friendship	AHCI55								
	AHCI56								
Connors	AHCI59								
	AHCI64								
	AHCI65								
	AHCI73								
	AHCI74								
	AHCI75								
	AHCI79								
	AHCI62								
	AHCI63								
Thomas River High Ground	AHCI03								

	AHCI04								
	AHCI05								
	AHCI06								
	AHCI30								
	AHCI31								
	AHCI07								
	AHCI08								
Bulk Andesite	AHCI24								
	AHCI26								
	AHCI39								
	AHCI49								
	AHCI15								
	AHCI19								
	AHCI20								
	AHCI22								
	AHCI28								
	AHCI40								
Dry Hill	AHCI76								
	AHCI77								
	AHCI78								
Grantham	AHCI35								
	AHCI36								
	AHCI37								
Crooked River	AHCI10								
	AHCI11								
Waterworks Fm	AHCI09								
	AHCI09A								
	AHCI12								
	AHCI13								

Table 6.4 – The fractionation and alkalinity results from plotting the Central inlier samples on the Co-Th, Th/Yb-Ta/Yb, Th/Hf-Sm/Yb, Ce/Lu-Sm/Yb, La/Hf-Sm/Y and Th/Zr-La/Yb diagrams; Blue - Basalt; Yellow - Basaltic andesite-andesite; Purple - Dacite; Pink - IAT; Brown - CA; Green - SHC.

preferred because (a) Co has liquid lines of descent with higher correlation coefficients and is thus slightly less mobile on the variation diagrams (e.g. the R^2 values for the Bulk Andesite package in the SiO_2 and Co variation diagrams are 0.04 and 0.3 respectively) and (b) the Co results confirm petrographic observations e.g. the Co-Th data correctly identifies the dacites whereas the silica data does not (Table A.1, Appendix A).

The Old Works sample produces a clear IAT chemistry whereas the Nine Turns lava has a chemistry which is transitional between both IAT and CA. The majority of the CA lavas plot as such on most of the discrimination diagrams. Occasionally; a CA lava will plot as an IAT or SHC on one or two of the diagrams. However, as explained in Chapter 5, the discrimination diagrams are all based on 75 to 85% probability contours. Therefore, it is statistically possible for a CA lava to be misinterpreted on a single diagram. This is why six discrimination diagrams were utilised in this study. However, it is interesting to note that the less enriched CA1 rocks are interpreted as IAT on some of the discrimination plots whereas the more enriched CA2 samples sometimes plot as SHC. The SHC samples also plot as SHC on the majority of the plots.

AHCI56 and AHCI63 have a transitional chemistry between IAT-CA and CA-SHC respectively (Table 6.4). Nevertheless, these samples have not been split into separate groups but have instead been incorporated into the CA1 and CA2 groups. This is because of geographic considerations: AHCI72 (IAT) and AHCI33 (ICT) are geographically distinct in the field and their chemistry is clearly IAT and transitional respectively (Table 6.4). Conversely, AHCI56 and AHCI63 are inter-layered with a substantial number of other flows/intrusives which all give clear CA1 and CA2 type compositions. AHCI56 and AHCI63 also plot close to or on the boundary lines in three of the discrimination plots. Therefore, these samples are placed in the same groups as the igneous rocks with which they are associated with in the field.

6.5.3.4 Trace element chemistry

The trace element variation diagrams show predictable trends for the immobile trace elements e.g. Th increases with increasing Zr concentration (Figs. 6.30 and 6.31). Sr increases and decreases with higher Zr values, which is a reflection of whether plagioclase is fractionating in the magma source region(s). There is no

evidence for plagioclase fractionation in the Eu variation diagram which implies that the Eu in the magma source region(s) is oxidised and exists as Eu^{3+}. As discussed above, the 14 packages can be split into 5 groups. The IAT and ICT groups; however, have no liquid lines of descent as they both consist of only one sample.

In terms of Th, U and the LREE, the SHC and CA2 groups have steeper/more enriched liquid lines of decent than the CA1 group. SHC has a higher concentration of Th and LREE at a given Zr than CA2, which in turn has a higher concentration of these elements than CA1 (Figs. 6.30, 6.31 and E.12). However, this situation changes when the MREE are examined, as the SHC and part of the CA2 data fall on a similar trend to the CA1 samples (Figs. 6.30, 6.31 and E.12). With the HREE and Y, the SHC form a liquid line of descent below the CA1 trend and the CA2 group splits into three liquid lines of decent (Figs. 6.30, 6.31 and E.12). The first CA2 liquid line of descent has a similar trend to that seen for the Th, U, LREE and the MREE; the second trend is parallel to the CA1 trend, and the third trend runs parallel to the liquid line of descent for the SHC group. The SHC and the third CA2 trend have lower HREE and Y at a given Zr concentration than the CA1 samples (Figs. 6.30, 6.31 and E.12).

This decrease and division of the liquid lines of descent in the CA2 and SHC groups is also seen in the oxides. TiO_2, FeO* and P_2O_5 have similar liquid lines of descent for the CA and SHC groups as the HREE and Y variation diagrams. However, these oxide diagrams show that the CA1 group also splits into two with some CA1 samples forming a trend similar to the SHC data (Fig. 6.30 and E.12).

Conversely, although there is some scatter, the Ta and Nb variation diagrams show that all packages, except the Waterworks Formation, lie on a single liquid line of descent (Figs. 6.30, 6.31 and E.12). This suggests that the source region(s) for the IAT, ICT, CA1 and CA2 groups and the Crooked River package had similar Nb and Ta concentrations at a given Zr value. The Waterworks Formation forms a separate liquid line of descent which indicates that it has higher Nb and Ta values at a given Zr concentration than the other 13 units.

The petrogenesis of the igneous rocks in the Central inlier can be further analysed using immobile incompatible trace element ratios and N-MORB-normalised multi-element diagrams (Figs. 6.32 and 6.33). As with other Jamaican arc lavas from the Benbow, Above Rocks and Blue Mountains inliers, the Central inlier rocks have characteristic arc-like negative Nb and Ta anomalies. They also have negative Ti

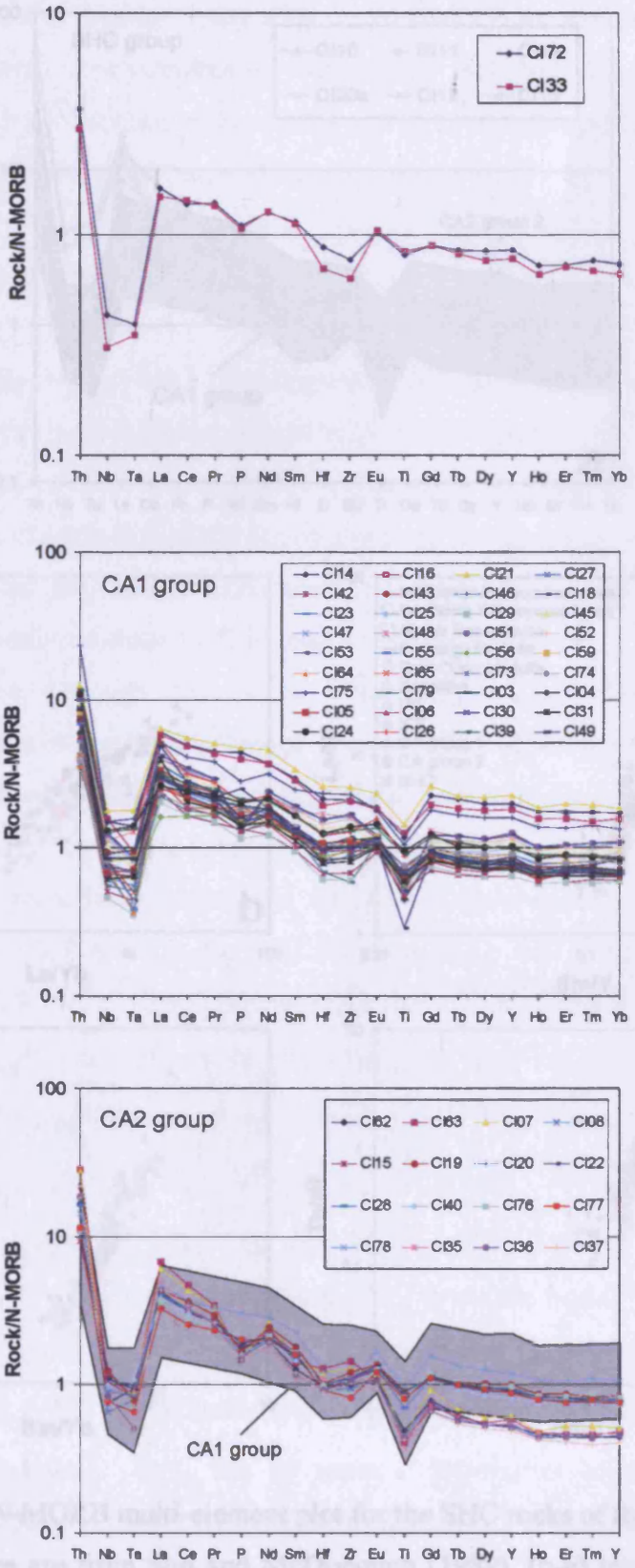

Figure 6.32 – N-MORB multi-element plots for the IAT, ICT, CA1 and CA2 rocks of the Central Inlier. Normalising values from Sun and McDonough (1989).

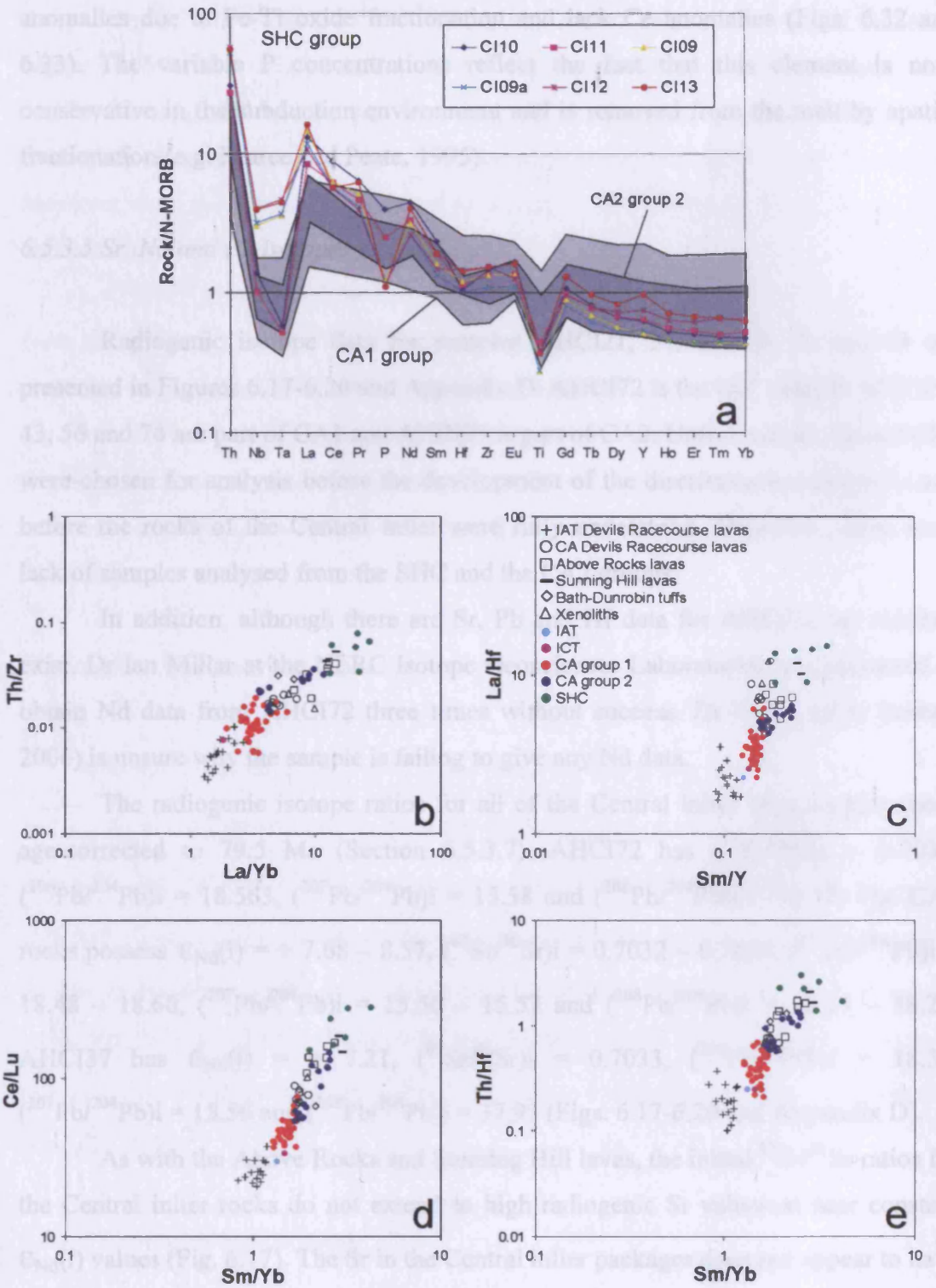

Figure 6.33 – (a) N-MORB multi-element plot for the SHC rocks of the Central Inlier. Normalising values are from Sun and McDonough (1989). (b-e) incompatible trace element ratio diagrams. The differing trace element ratios in conjunction with the variation diagrams and isotope ratios suggest that the arc rocks are derived from chemically different source regions.

anomalies due to Fe-Ti oxide fractionation and lack Ce anomalies (Figs. 6.32 and 6.33). The variable P concentrations reflect the fact that this element is non-conservative in the subduction environment and is removed from the melt by apatite fractionation (e.g. Pearce and Peate, 1995).

6.5.3.5 Sr, Nd and Pb isotopes

Radiogenic isotope data for samples AHCI21, 37, 43, 56, 72 and 74 are presented in Figures 6.17-6.20 and Appendix D. AHCI72 is the IAT sample, AHCI21, 43, 56 and 74 are part of CA1 and AHCI37 is part of CA2. Unfortunately, the samples were chosen for analysis before the development of the discrimination diagrams and before the rocks of the Central Inlier were fully understood. Therefore, there are a lack of samples analysed from the SHC and the CA2 groups.

In addition, although there are Sr, Pb and Hf data for AHCI72, no Nd data exist. Dr Ian Millar at the NERC Isotope Geosciences Laboratories has attempted to obtain Nd data from AHCI72 three times without success. Dr Millar (pers. comm. 2006) is unsure why the sample is failing to give any Nd data.

The radiogenic isotope ratios for all of the Central inlier samples have been age-corrected to 79.5 Ma (Section 6.5.3.7). AHCI72 has $(^{87}Sr/^{86}Sr)i = 0.7035$, $(^{206}Pb/^{204}Pb)i = 18.563$, $(^{207}Pb/^{204}Pb)i = 15.58$ and $(^{208}Pb/^{204}Pb)i = 38.22$. The CA1 rocks possess $\varepsilon_{Nd}(i) = +7.68 - 8.57$, $(^{87}Sr/^{86}Sr)i = 0.7032 - 0.7034$, $(^{206}Pb/^{204}Pb)i = 18.48 - 18.60$, $(^{207}Pb/^{204}Pb)i = 15.56 - 15.57$ and $(^{208}Pb/^{204}Pb)i = 38.15 - 38.24$. AHCI37 has $\varepsilon_{Nd}(i) = +7.21$, $(^{87}Sr/^{86}Sr)i = 0.7033$, $(^{206}Pb/^{204}Pb)i = 18.34$, $(^{207}Pb/^{204}Pb)i = 15.56$ and $(^{208}Pb/^{204}Pb)i = 37.97$ (Figs. 6.17-6.20 and Appendix D).

As with the Above Rocks and Sunning Hill lavas, the initial $^{87}Sr/^{86}Sr$ ratios for the Central inlier rocks do not extend to high radiogenic Sr values at near constant $\varepsilon_{Nd}(i)$ values (Fig. 6.17). The Sr in the Central inlier packages does not appear to have been heavily mobilised; thus, the Sr isotope systematics may be reliable in determining the source components involved in the genesis of these lavas. The Central Inlier samples plot with the Mariana, Kermadec, Lesser Antilles, Tonga, Aleutian, Izu-Bonin and Vanuatu intra-oceanic island arcs, and could theoretically lie on a mixing line between an N-MORB end-member and a pelagic/terrigenous sediment end-member (Fig. 6.17).

On a ($^{207}Pb/^{204}Pb$)i – ($^{206}Pb/^{204}Pb$)i plot the lavas lie above the NHRL and have higher ($^{207}Pb/^{204}Pb$)i ratios than the IAT Devils Racecourse lavas but lower ratios than the CA Sunning Hill and Border lavas (Fig. 6.18). The IAT and CA1 rocks lie on a theoretical mixing line between pelagic/terrigenous sediments and N-MORB. However, the CA2 sample is displaced to lower ($^{206}Pb/^{204}Pb$)i ratios, towards the EM1 end-member (Fig. 6.18).

($^{208}Pb/^{204}Pb$)i – ($^{206}Pb/^{204}Pb$)i systematics (Fig. 6.18) support the evidence from the ($^{207}Pb/^{204}Pb$)i – ($^{206}Pb/^{204}Pb$)i diagram by indicating that the IAT and CA1 rocks are more enriched in ($^{208}Pb/^{204}Pb$)i than the IAT Devils Racecourse lavas, but are more depleted than the Sunning Hill and Border lavas. Conversely, CA2 is not displaced to EM1 compositions. It has less ($^{208}Pb/^{204}Pb$)i than the other Jamaican arc rocks and hypothetically lies on a mixing line from pelagic/terrigenous sediments to N-MORB.

6.5.3.6 Nd and Hf isotopes

AHCI72 has $\varepsilon_{Hf}(i) = + 14.27$, the CA1 lavas possess $\varepsilon_{Nd}(i) = + 7.68 - 8.57$ and $\varepsilon_{Hf}(i) = + 12.97 - 13.92$ and AHCI37 has $\varepsilon_{Nd}(i) = +7.21$ and $\varepsilon_{Hf}(i) = + 13.60$ (Fig.6.20 and Appendix D). Relative to N-MORB the Central inlier samples have enriched (low) $\varepsilon_{Nd}(i)$ values at constant $\varepsilon_{Hf}(i)$ values, demonstrating that a slab-related component was likely involved in their genesis. The CA1 field overlaps the fields for IAT/CA Devils Racecourse and Bonaire lavas. The CA2 sample plots at lower $\varepsilon_{Nd}(i)$ values and is slightly more enriched in Nd isotopes than the Sunning Hill lava (Fig. 6.20).

6.5.3.7 Geochronological data

Like the Above Rocks lavas, no absolute stratigraphical or palaeontological ages exist for the Central inlier igneous rocks. Consequently, two samples, one from CA group 1 (AHCI39) and the other from CA group 2 (AHCI37), were prepared for argon dating analysis (Fig. 6.34). Unfortunately a mistake at the Scottish Universities Environmental Research Centre (SUERC) meant that sample AHCI37 was lost (see

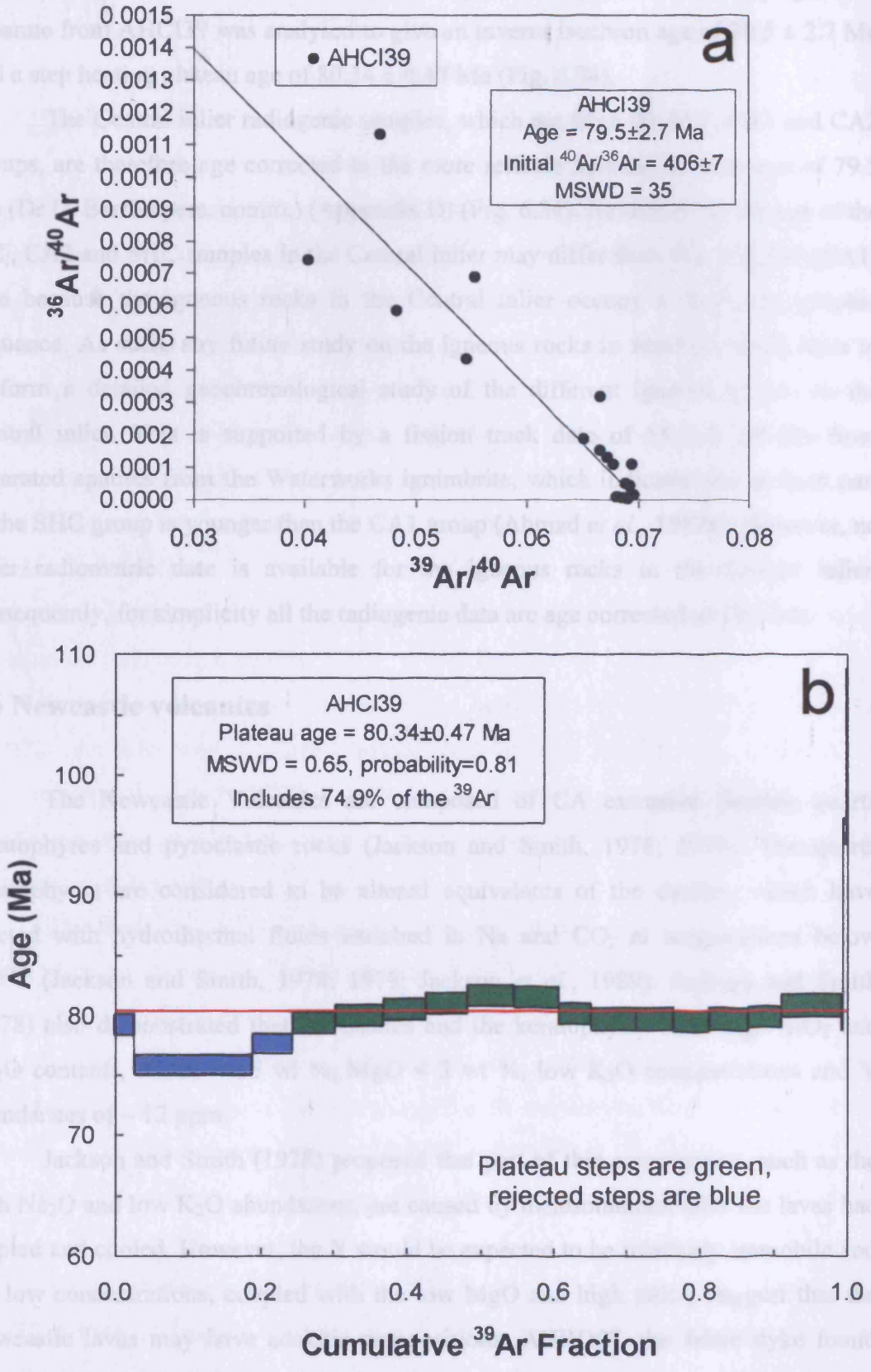

Figure 6.34 – (a and b) Ar-Ar inverse isochron and step heating plateau plots for AHCI39.

Appendix D) and thus no date was obtained for this sample. However, a plagioclase separate from AHCI39 was analysed to give an inverse isochron age of 79.5 ± 2.7 Ma and a step heating plateau age of 80.34 ± 0.47 Ma (Fig. 6.34).

The Central inlier radiogenic samples, which are from the IAT, CA1 and CA2 groups, are therefore age corrected to the more reliable inverse isochron age of 79.5 Ma (Dr D. Barfod pers. comm.) (Appendix D) (Fig. 6.34). Nevertheless, the age of the IAT, CA2 and SHC samples in the Central inlier may differ from the AHCI39 (CA1) date because the igneous rocks in the Central inlier occupy a thick stratigraphic sequence. As such, any future study on the igneous rocks in Jamaica would have to perform a detailed geochronological study of the different igneous groups in the Central inlier. This is supported by a fission track date of 55.3 ± 2.8 Ma from separated apatites from the Waterworks ignimbrite, which indicates that at least part of the SHC group is younger than the CA1 group (Ahmad *et al.*, 1987a). However, no other radiometric date is available for the igneous rocks in the Central inlier, consequently, for simplicity all the radiogenic data are age corrected to 79.5 Ma.

6.6 Newcastle volcanics

The Newcastle Volcanics are composed of CA extrusive dacites, quartz keratophyres and pyroclastic rocks (Jackson and Smith, 1978; 1979). The quartz keratophyres are considered to be altered equivalents of the dacites, which have reacted with hydrothermal fluids enriched in Na and CO_2 at temperatures below 400°C (Jackson and Smith, 1978; 1979; Jackson *et al.*, 1989). Jackson and Smith (1978) also demonstrated that the dacites and the keratophyres have high SiO_2 and Na_2O contents, Al_2O_3 > 15 wt %, MgO < 3 wt %, low K_2O concentrations and Y abundances of ~ 12 ppm.

Jackson and Smith (1978) proposed that part of this composition, such as the high Na_2O and low K_2O abundances, are caused by metasomatism after the lavas had erupted and cooled. However, the Y would be expected to be relatively immobile and the low concentrations, coupled with the low MgO and high silica, suggest that the Newcastle lavas may have adakitic compositions. AHBD07, the felsic dyke found intruding the Cedar Valley peridotite, has a similar chemistry to the Newcastle

Volcanics. This sample is discussed and compared with the Newcastle lavas in this section.

6.6.1 What is an adakite?

Adakites are part of the sodium rich trondhjemite-tonalite-dacite (TTD) suite of igneous rocks which make up a significant proportion of Precambrian gneiss terranes and a small proportion of Phanerozoic orogenic suites (Drummond and Defant, 1990; Rapp *et al.*, 1991; Drummond *et al.*, 1996). At 70 wt. % SiO_2, the TTDs can be split into two geochemical types: a low-Al type - < 15 wt. % Al_2O_3 and a high-Al type - > 15 wt. % Al_2O_3. This Al_2O_3 variability is formed because of the presence or absence of hornblende in TTD petrogenesis (Defant and Drummond, 1990; Defant and Drummond, 1993; Drummond and Defant, 1990): i.e. the removal of sub-aluminous hornblende by fractional crystallisation or as a refractory source component would cause the melt to evolve to relatively high Al_2O_3 contents (Drummond and Defant, 1990).

There are three main models for the formation of TTDs. In the first, the magmas are generated by direct partial melting of a mantle source. However, Drummond and Defant (1990) suggest that low degrees of partial melting of the mantle are unfeasible and would only produce melts as felsic as basaltic andesite, alkali basalt or boninite.

The second model proposes that fractional crystallisation of a basaltic magma can produce basalt-andesite-dacite-rhyolite (BADR) suites in ancient to recent arcs, gabbro-diorite-tonalite-trondhjemite suites in the Precambrian and plagiogranites in ophiolites (Drummond and Defant, 1990; Rapp *et al.*, 1991; Drummond *et al.*, 1996). Nevertheless, this process is also not thought to be responsible for forming the large volumes of TTDs because of the lack of intermediate igneous rocks in TTD successions (Drummond and Defant, 1990; Rapp *et al.*, 1991; Drummond *et al.*, 1996).

The third model, and the one which is most widely accepted, involves the partial melting of basaltic source material which has been transformed into either amphibolite, eclogite, or some transitional state in which garnet/amphibole are stable (Defant and Drummond, 1990; 1993; Drummond and Defant, 1990; 1996; Rapp *et al.*,

1991; Defant *et al.*, 1992). The low-Al TTDs represent low pressure partial melts of a basaltic source with subsequent plagioclase removal (Drummond *et al.*, 1996).

Drummond and Defant (1990) and Drummond *et al.* (1996) defined adakites as a sub-type of Cenozoic TTDs that had similar chemistry to the high-Al TTD gneisses. Defant *et al.* (1992) defined the 'type adakite' major and trace element and isotopic chemistry as:

- $SiO_2 > 56\%$
- $Al_2O_3 > 15\%$ (rarely lower)
- MgO usually <3% (rarely above 6%)
- Low Y and HREE (Y and Yb < 18 and 1.9 ppm respectively)
- High Sr (rarely < 400 ppm)
- Low HFSE
- $^{87}Sr/^{86}Sr < 0.7040$

Relative to the low-Al samples, adakites and high-Al TTDs have high Sr concentrations and higher La/Sm, Sr/Y and Zr/Y ratios. They also have lower Y, Sc and Yb concentrations (Rapp *et al.*, 1991; Drummond *et al.*, 1996; Polat and Kerrich, 2001). The presence of hornblende and garnet in the residue is essential in explaining the high Al_2O_3 and low K/Rb, Sc, Nb, HREE and Y (Defant and Drummond, 1993; Drummond *et al.*, 1996).

Defant and Drummond (1990) defined the term adakite using samples from 13 localities which are all associated with the subduction of young (< 25 Ma), hot and buoyant oceanic lithosphere and proposed that these subducting young oceanic slabs partially melt to form adakitic magma (Drummond and Defant, 1990; Defant *et al.*, 1992; 1996; Defant and Drummond, 1993). Drummond *et al.* (1996) and Yogodzinski *et al.* (1995) argued that slab melting is feasible if either the subducting slab is hot and young, or at the initiation of subduction where there is a new hot mantle wedge, or due to the presence of high shear stresses during oblique or slow subduction. Experimental evidence has demonstrated that, in order to produce the major and trace element chemistry of adakite and high-Al TTDs, hydrous partial melting of a basaltic source occurs at P-T conditions of > 15 kbar and >750°C to leave a garnet amphibolite to eclogite residue (Drummond and Defant, 1990; Drummond *et al.*, 1996).

An alternative theory to slab melting for the genesis of adakites is the partial melting of over thickened continental arc crust (Drummond and Defant, 1990;

Drummond *et al.*, 1996). However, adakites have very low Sr isotope ratios whereas continental arc melts have high ratios (Defant *et al.*, 1992; Drummond *et al.*, 1996). In addition, melts derived from continental arc crust usually have high Y, Cs, U and HREE contents due to a lack of garnet in their petrogenesis. Conversely, some continental melts do have adakite signatures; this is because of: (1) partial melting of a garnet-bearing crustal source; (2) AFC assimilation of a garnet-bearing crustal source by a mantle-derived melt or, (3) mixing of crustal and arc melts (Drummond *et al.*, 1996). Castillo *et al.* (2007) have also suggested that adakites from the Sulu arc are not derived from slab melts but could be formed by either complex magmatic differentiation processes or by re-melting lower island arc crust.

Drummond and Defant, 1990 proposed that producing adakites by partial melting of under-plated basaltic material of "normal" thickness is not a feasible petrogenetic model for their formation. Usually an under-plated source is not deep enough to have an amphibolite-eclogite chemistry. Therefore, any melt derived from this basaltic material would not have Al_2O_3 >15% or low Y and Yb concentrations (Drummond and Defant, 1990). However, a thick keel below an oceanic plateau may be deep enough to have an amphibolite-eclogite mineralogy (e.g. Kerr *et al.*, 2003) and with subsequent partial melting may produce an adakitic melt.

As a subducting slab partially melts and the adakitic magmas ascend, they will naturally react with the overlying mantle wedge. The degree of interaction is dependant on many factors, such as the ascent rate of the magma, the subduction angle, the slab geotherm and depth of melting, thickness of the overriding lithosphere and the amount of prior adakite-mantle reaction within the melt ascent conduit. Experimental studies of TTD melt-peridotite reactions at elevated pressures (15-30 kbar) have shown that the melt will react with peridotite producing orthopyroxene, ± garnet, ± hornblende, ± clinopyroxene, ± plagioclase, ± phlogopite and ± spinel in the metasomatised peridotite (Johnston and Wyllie, 1989; Drummond *et al.*, 1996; Kepezhinskas *et al.*, 1996). The mantle metasomatism would initially produce hornblende-bearing harzburgite followed by hornblende-bearing orthopyroxenite. The TTD melt would become more CaO and MgO enriched (Drummond *et al.*, 1996; Polat and Kerrich, 2001).

Yogodzinski *et al.* (1994) and Yogodzinski *et al.* (1995) in the western Aleutians have studied the effects of slab melt-mantle interaction. They define two high-Mg andesite (HMA) types: a Piip-type and an Adak-type. They interpret the

Piip-type HMA as volcanic rocks derived from an enriched peridotite source that was generated by mixing depleted MORB mantle with minor (~ 4 %) adakite melts. Adak-type HMA (termed transitional adakites by Drummond *et al.*, (1996)) represent CaO and MgO-rich adakites that are produced as slab melts that incompletely interacted with the mantle wedge during ascent. Keleman (1990) also proposed that a reaction between a felsic slab melt and mantle peridotite will cause a sharp increase in the MgO and Ni content of the melt due to olivine dissolution. Therefore, adakitic melts may not sufficiently mix with the mantle wedge peridotites; if they do they will produce a HMA (Chapter 7) (e.g. Polat and Kerrich, 2001).

6.6.2 Are the Newcastle lavas adakites?

Using the geochemical constraints of Defant *et al.* (1992), it can be seen that the Newcastle lavas are predominantly adakitic in composition. They all possess > 56% SiO_2 and < 3% MgO. Their Al_2O_3 contents are mostly over 15% and they have very low Y (<< 18 ppm), HFSE and HREE (Yb = << 1.9 ppm) abundances (Appendix E, Section E6). Nevertheless, they do not have the high Sr contents that have been discovered in other adakites. The average Sr abundance of the Newcastle lavas is 130 ppm, which is much lower than the > 400 ppm values in the majority of other adakites. However, their initial $^{87}Sr/^{86}Sr$ ratios are ~ 0.7040, which is similar to other adakites. On the Yb-Al_2O_3 diagram of Drummond *et al.* (1996), which separates low-Al TTDs and high-Al TTDs, the Newcastle lavas plot in the adakite/high-Al TTD field (Fig. 6.35).

On the Ni-Cr diagram of Drummond *et al.* (1996), most of the Newcastle lavas plot in the adakite field and do not have the transitional chemistry of the Piip- and Adak-type HMAs (Fig. 6.35). AHBD07 is also a dacite which has a characteristic adakite composition with 73.13 wt. % SiO_2, 15.15 wt. % Al_2O_3, 3.4 ppm Y and 0.22 ppm Yb (Fig. 6.35 and Appendix E).

6.6.3 Element mobility and differentiation classification

Unfortunately, unlike the rocks discussed earlier in this chapter, Zr variation diagrams cannot be used to study the petrogenesis of the Jamaican adakites because

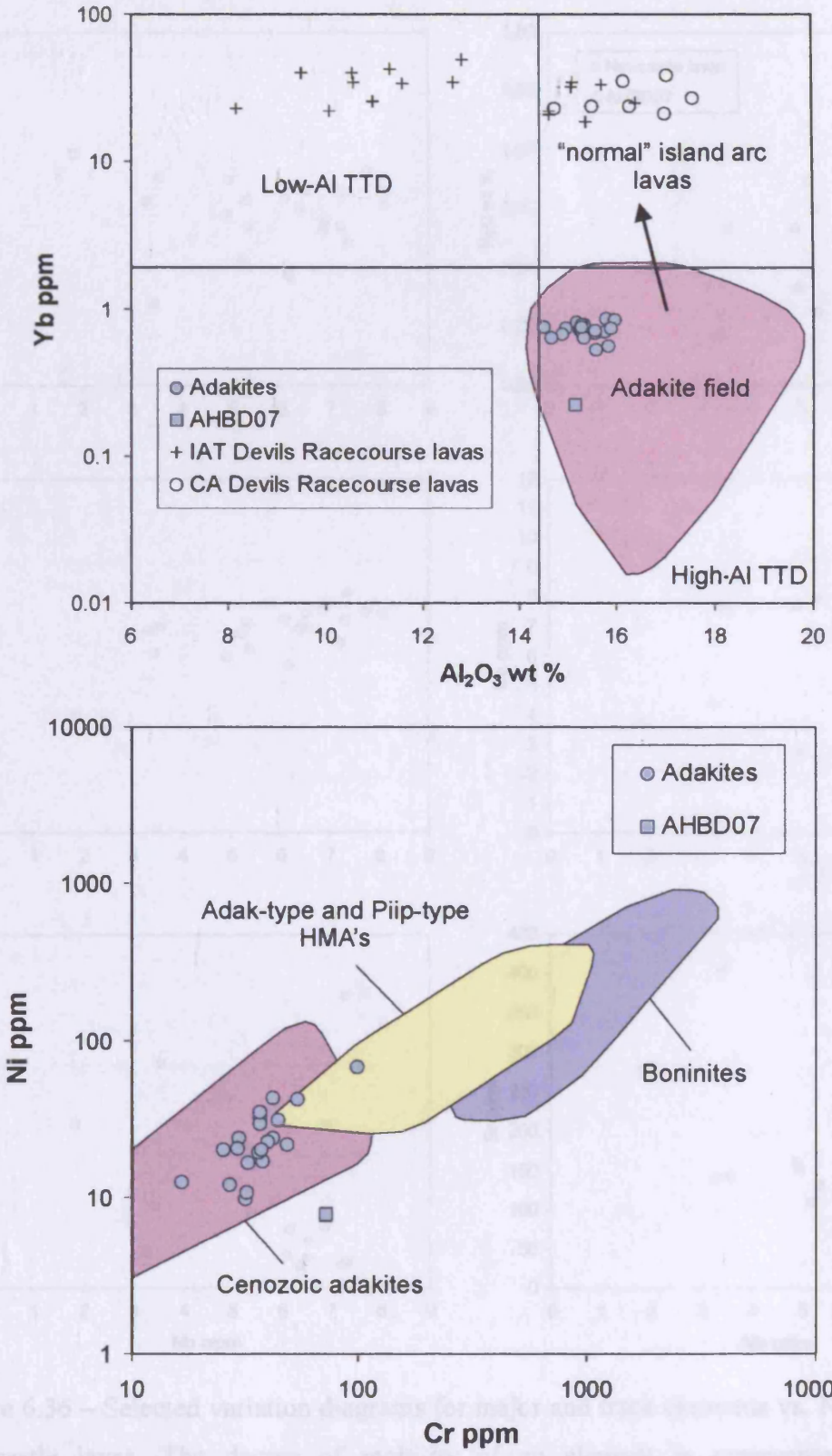

Figure 6.35 – (a) Yb-Al_2O_3 and (b) Ni-Cr discrimination diagrams of Drummond *et al.* (1996). The Devils Racecourse lavas are shown in (a) for a comparison with a "normal" arc lava suite.

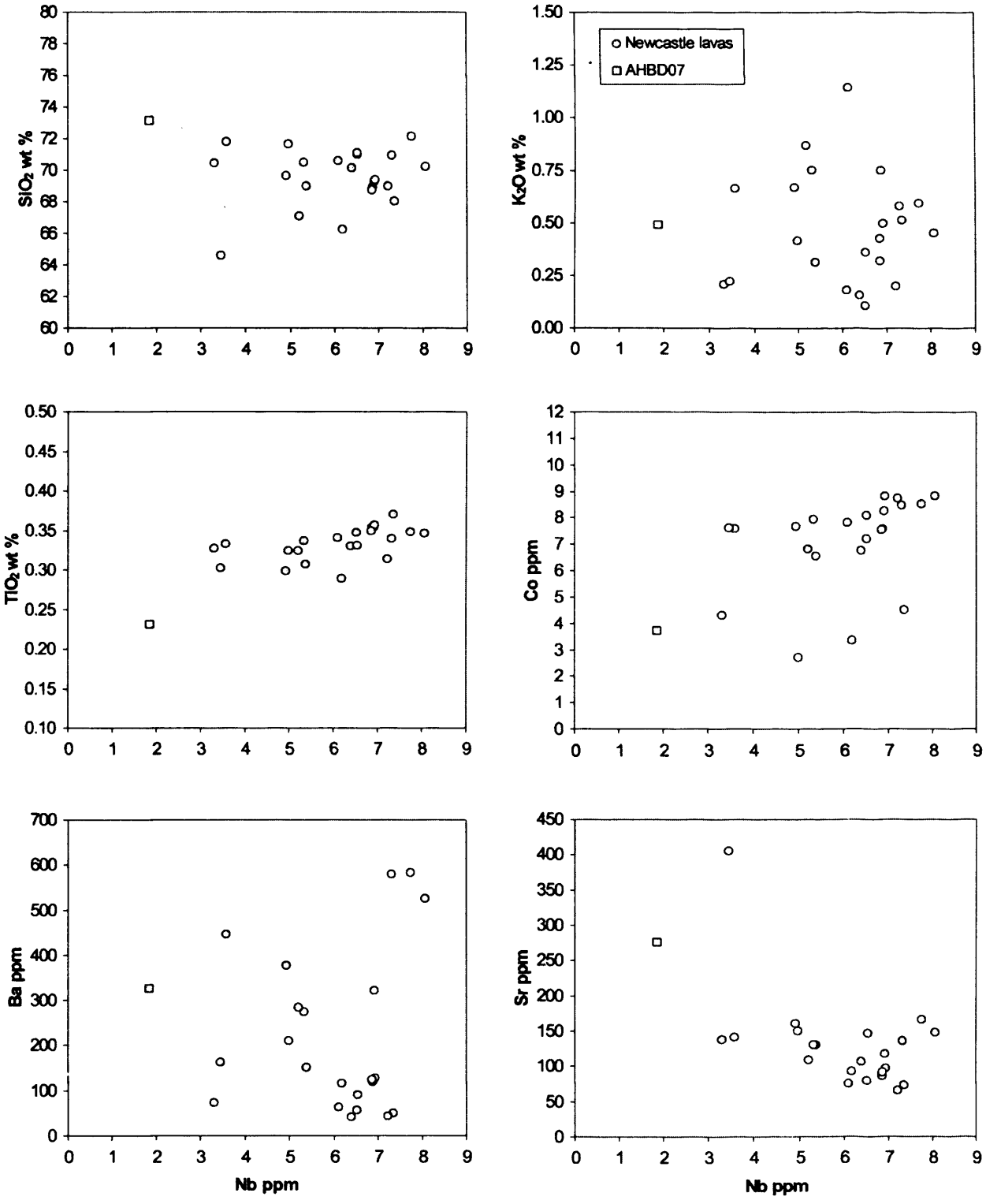

Figure 6.36 – Selected variation diagrams for major and trace elements vs. Nb for the Newcastle lavas. The degree of mobility of an element is represented by its correlation with Nb. A mobile element will show no correlation, whereas, an immobile element displays a good correlation. A correlation can be a straight or curved line depending on whether the element is incompatible and/or compatible during fractional crystallisation.

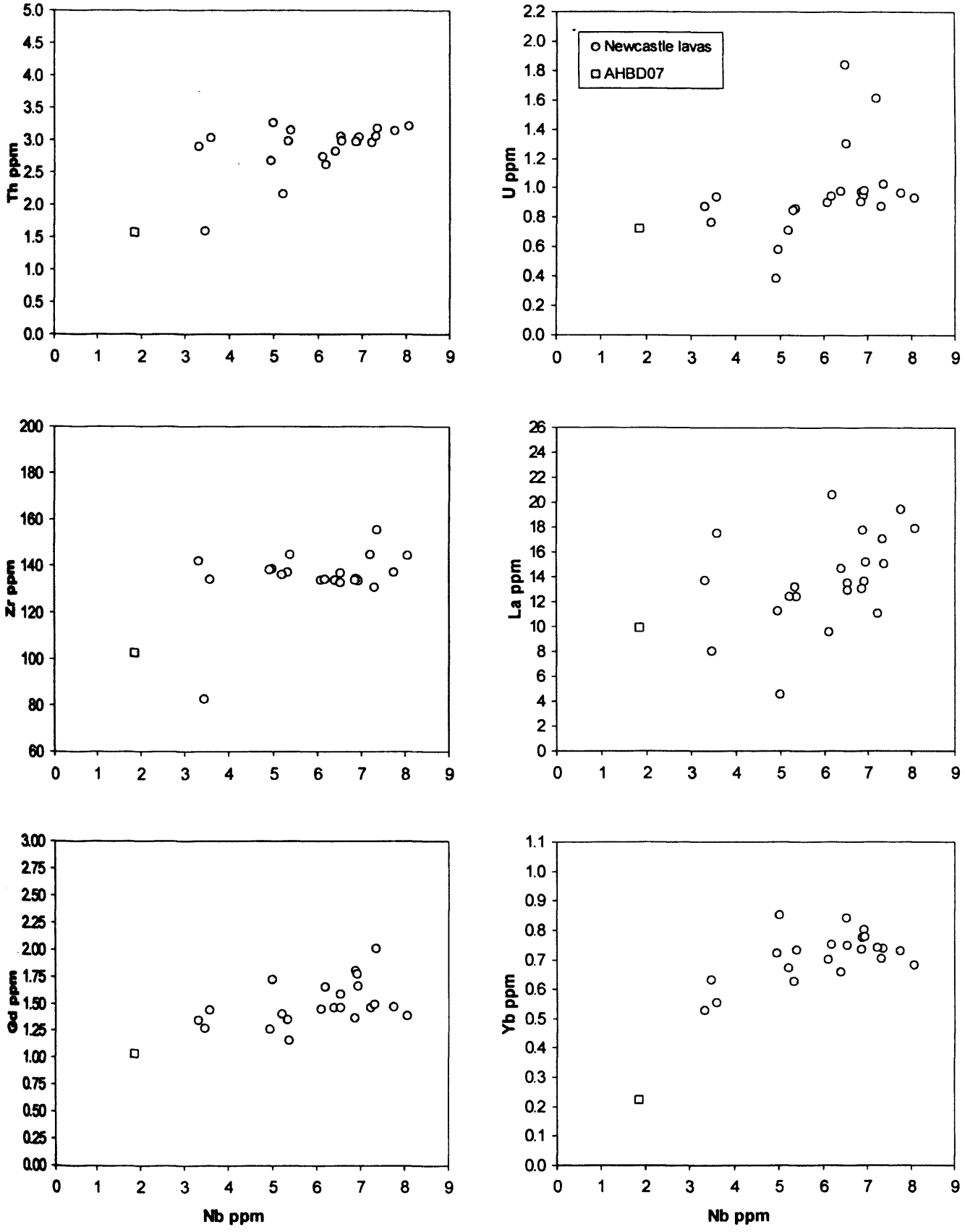

Figure 6.36 – continued.

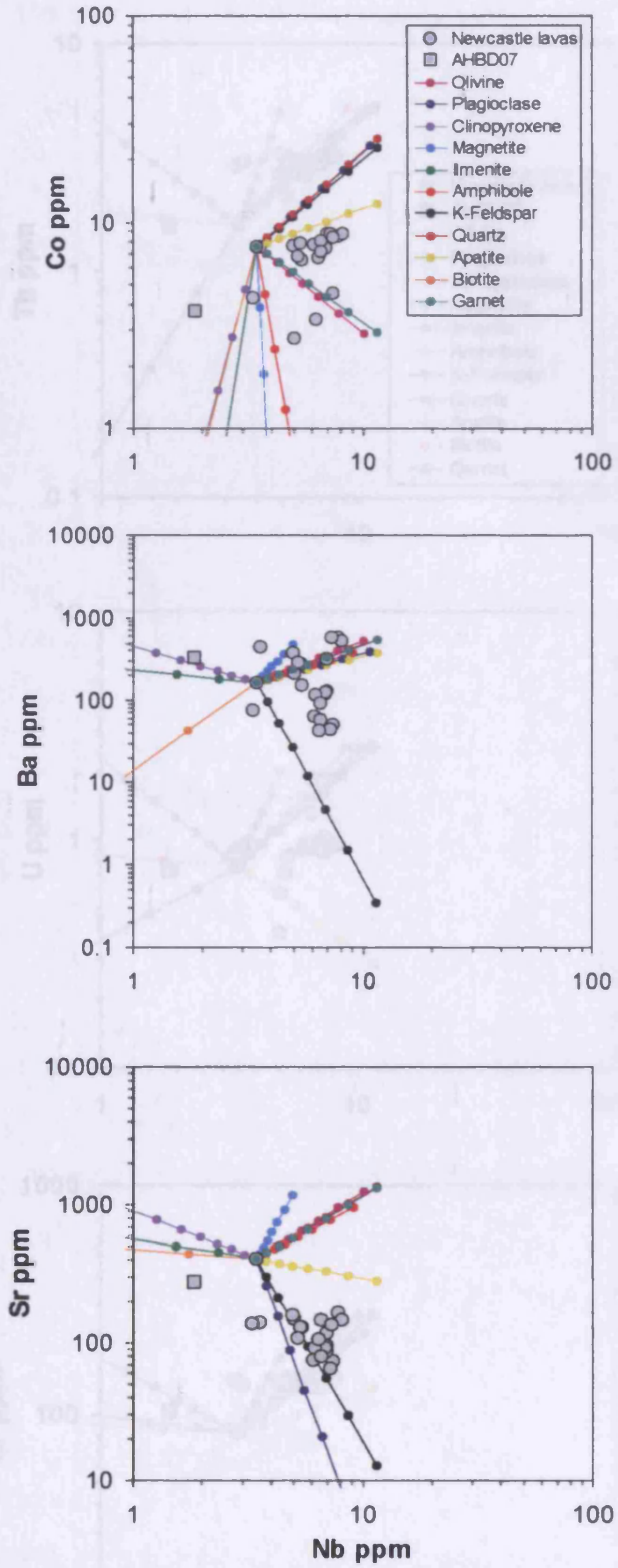

Figure 6.37 – Selected variation diagrams with vectors showing the composition of olivine, plagioclase, clinopyroxene, magnetite, ilmenite, amphibole, K-feldspar, quartz, apatite, biotite, and garnet with up to 70% fractional crystallisation of the AHWG34 starting composition (each tick represents 10% crystallisation) (Appendices E and G).

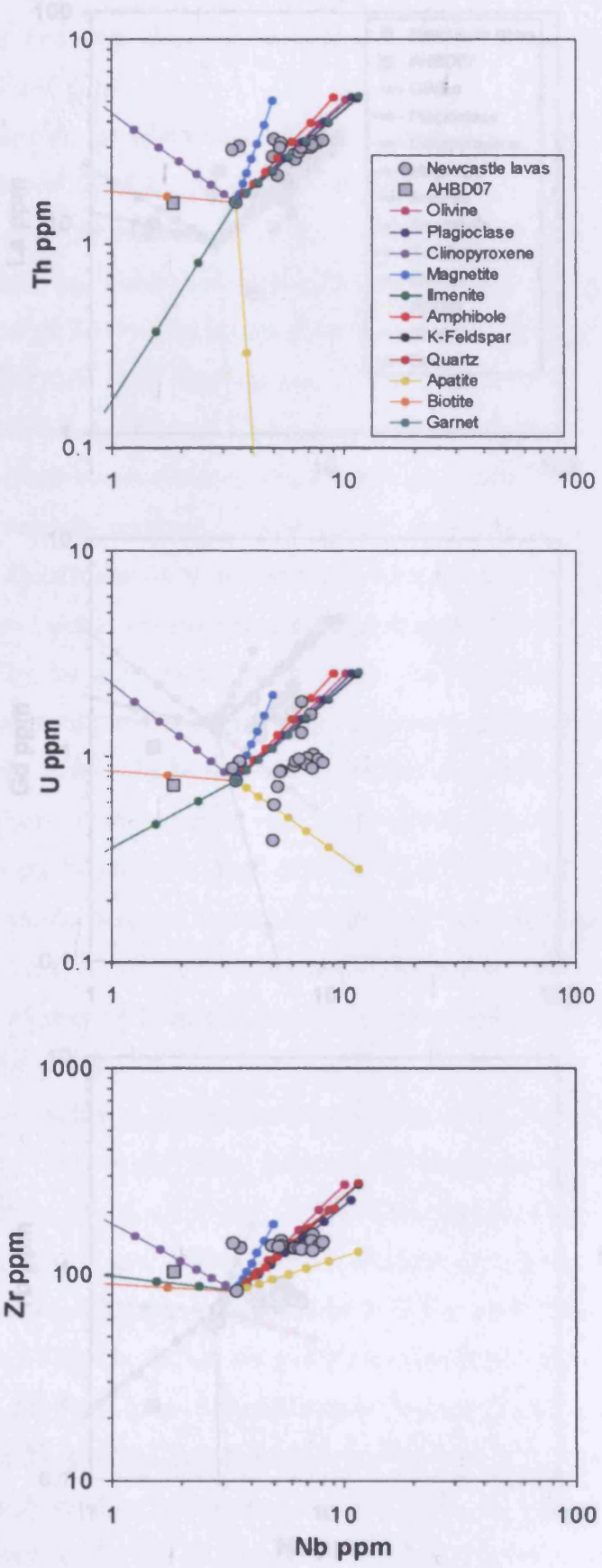

Figure 6.37 – continued

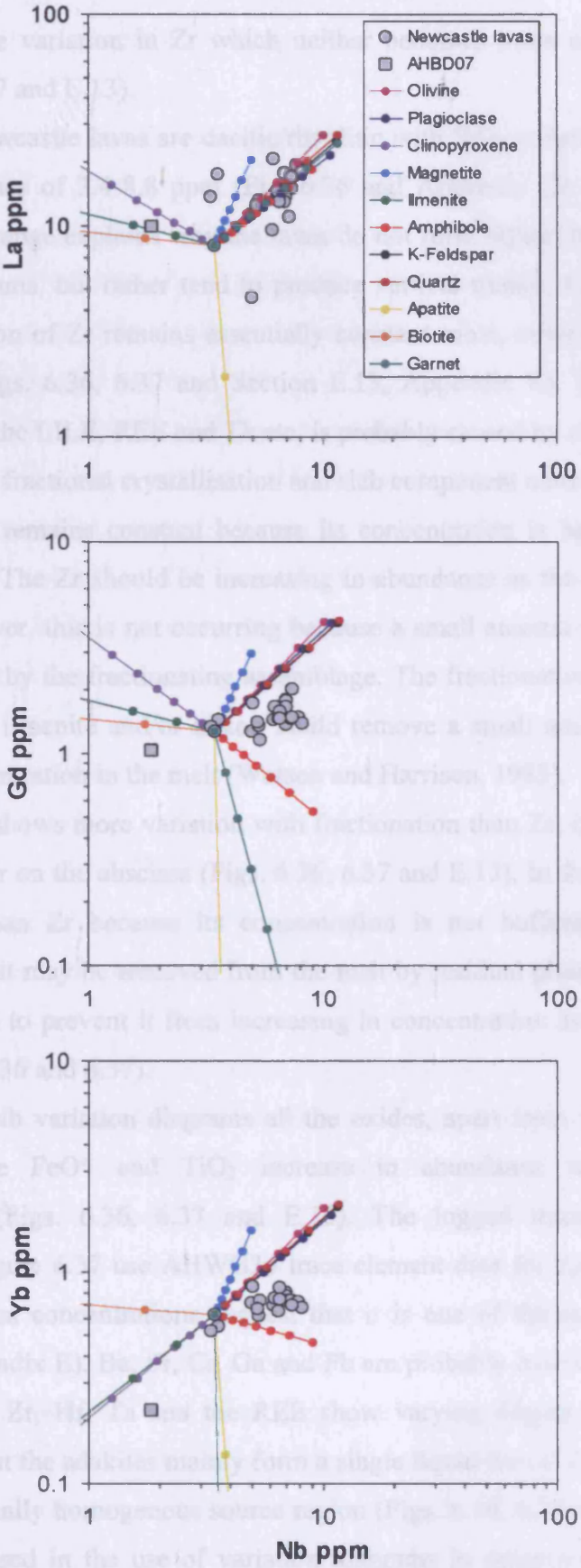

Figure 6.37 – continued

they show little variation in Zr which neither becomes more enriched or depleted (Figs. 6.36, 6.37 and E.13).

The Newcastle lavas are dacitic/rhyolitic with SiO_2 values of 66.24-72.16 wt. % and Co values of 3.4-8.8 ppm (Fig. 6.36 and Appendix D). This narrow acidic compositional range explains why the lavas do not form liquid lines of descent on Zr variation diagrams, but rather tend to produce vertical trends. Additionally, whereas the concentration of Zr remains essentially constant most, other elements vary more widely (e.g. Figs. 6.36, 6.37 and Section E.13, Appendix E). The variation in the abundances of the LILE, REE and Th etc, is probably caused by a complex mixture of partial melting, fractional crystallisation and slab component addition processes.

The Zr remains constant because its concentration is being buffered in the adakitic melts. The Zr should be increasing in abundance as the melt becomes more evolved; however, this is not occurring because a small amount of Zr is being taken out of the melt by the fractionating assemblage. The fractionation of a small amount of hornblende, ilmenite and/or zircon could remove a small amount of Zr and thus buffer its concentration in the melt (Watson and Harrison, 1983).

As Nb shows more variation with fractionation than Zr, it has been used as a substitute for Zr on the abscissa (Figs. 6.36, 6.37 and E.13). In the adakitic melts, Nb varies more than Zr because its concentration is not buffered during fractional crystallisation; it may be removed from the melt by residual phases (e.g. amphibole), but not enough to prevent it from increasing in concentration as the adakitic liquids evolve (Figs. 6.36 and 6.37).

In the Nb variation diagrams all the oxides, apart from FeO* and TiO_2, are mobilised. The FeO* and TiO_2 increase in abundance with increasing Nb concentration (Figs. 6.36, 6.37 and E.13). The logged trace element variation diagrams in Figure 6.37 use AHWG34 trace element data for the C_O values because its Co and silica concentrations suggest that it is one of the most primitive of the adakites (Appendix E). Ba, Sr, Cr, Ga and Pb are probably mobilised whereas Th, U, V, Co, Sc, Y, Zr, Hf, Ta and the REE show varying degrees of immobility and demonstrate that the adakites mainly form a single liquid line of descent suggestive of a single chemically homogenous source region (Figs. 6.36, 6.37 and E.13). However, caution is advised in the use of variation diagrams in determining the mobility of elements in such evolved rocks because of the increasing compatibility of certain trace elements (e.g. the REE) in acidic magmas (Fig. 6.37 and Chapter 7).

6.6.4 CA vs SHC classification

The distinctive chemistry of adakites makes them difficult to classify on the basis of their LILE, LREE and actinide enrichment. With "normal" altered arc rocks, the Co-Th (Chapter 5), Th/Yb-Ta/Yb (Pearce, 1982), Th/Hf-Sm/Yb, Ce/Lu-Sm/Yb, La/Hf-Sm/Y and Th/Zr-La/Yb discrimination diagrams are used for classification. However, the complex "decoupling" of the LILE, HFSE, REE and the transition elements during partial melting, slab flux, peridotite hybridisation and fractional crystallisation of the acidic adakites makes the use of the above discrimination diagrams unfeasible. The Co-Th, La/Hf-Sm/Y and Th/Hf-Sm/Yb diagrams classify most of the rocks as CA, whereas the Th/Yb-Ta/Yb, Th/Zr-La/Yb and Ce/Lu-Sm/Yb plots classify the majority of the lavas as SHC (Figs. 6.38 and 6.39). Consequently, it is concluded that it is not practical to define adakites in terms of IAT, CA or SHC because of their unique mode of formation*.

6.6.5 Trace element chemistry

Trace element ratio, N-MORB-normalised multi-element and chondrite-normalised REE diagrams are shown in Figures 6.39 and 6.40. As with the other Jamaican arc rocks, the adakite samples all have characteristic arc-like negative Nb and Ta anomalies.

Negative Ti, Sr and P anomalies are the result of Fe-Ti oxide, plagioclase and apatite fractionation respectively and/or differing degrees of partial melting. Petrography on the Newcastle lavas shows that they contain abundant plagioclase phenocrysts (Table A.1 and Chapter 4). Significant plagioclase fractionation in the magma or the retention of plagioclase in the adakite magma source region during peridotite hybridisation could remove Sr from the melt, thus generating the low Sr values in these adakites (Section 7.6.4) (Condie, 2005).

The multi-element plot also highlights the extremely low HREE and Y abundances and the lower MREE concentrations relative to Th, the LREE, Zr and Hf in the Newcastle rocks (Fig. 6.40). The chondrite-normalised diagram displays the Th

** - The data for a further 69 adakite samples, from the Earth Reference Data and models database (http://www.earthref.org) (Appendix F), were plotted on the discrimination diagrams (data not shown for clarity). These samples also demonstrated the ineffectiveness of these diagrams in classifying adakites.*

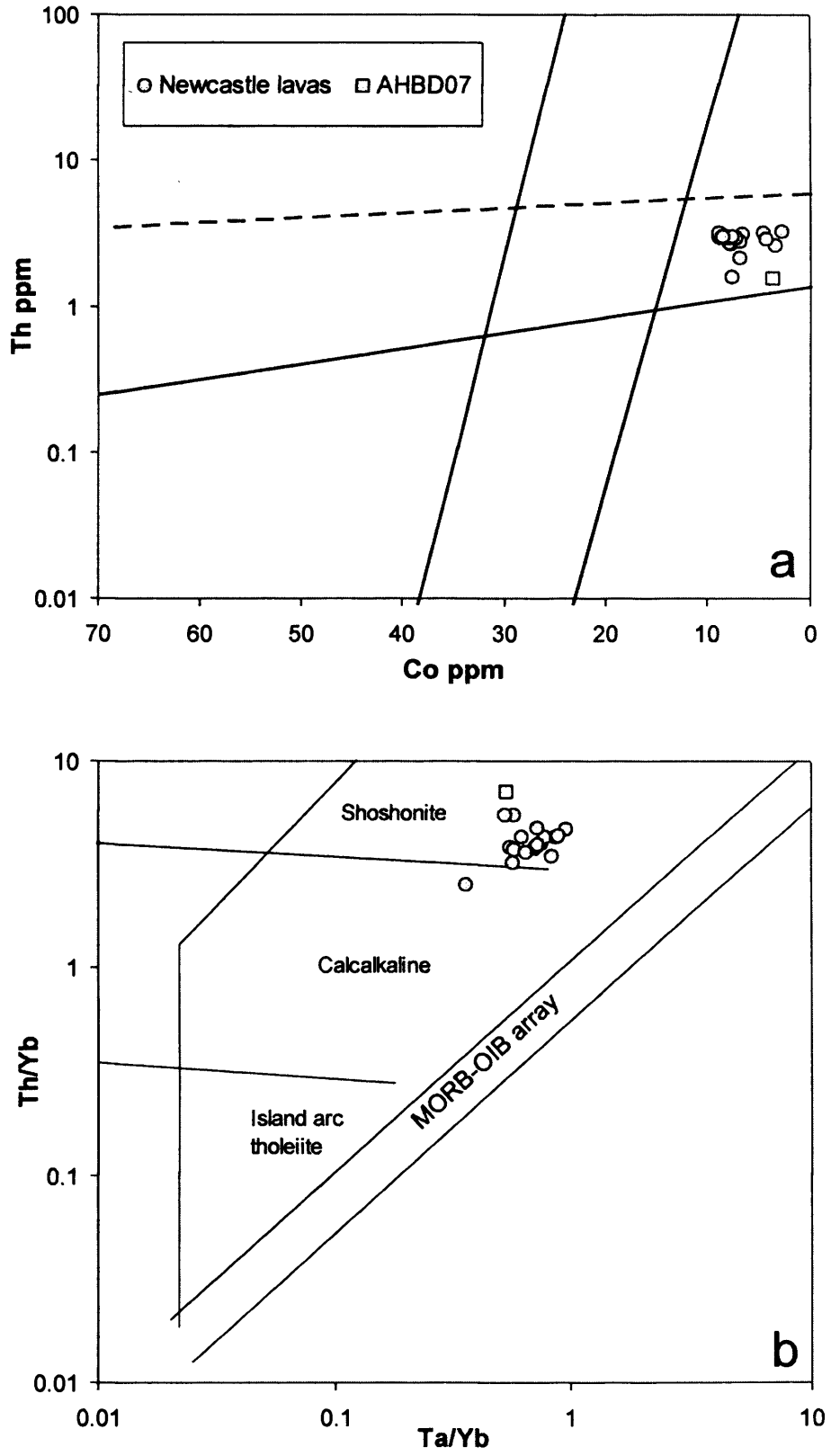

Figure 6.38 – (a) Co-Th and (b) Th/Yb-Ta/Yb discrimination diagrams showing the dacitic/rhyolitic nature of the adakites. They also show, in conjunction with Figure 6.30, the disparity when classifying the adakites on the basis of their LILE, LREE and actinide enrichment (Pearce, 1982; Hastie *et al.*, 2007).

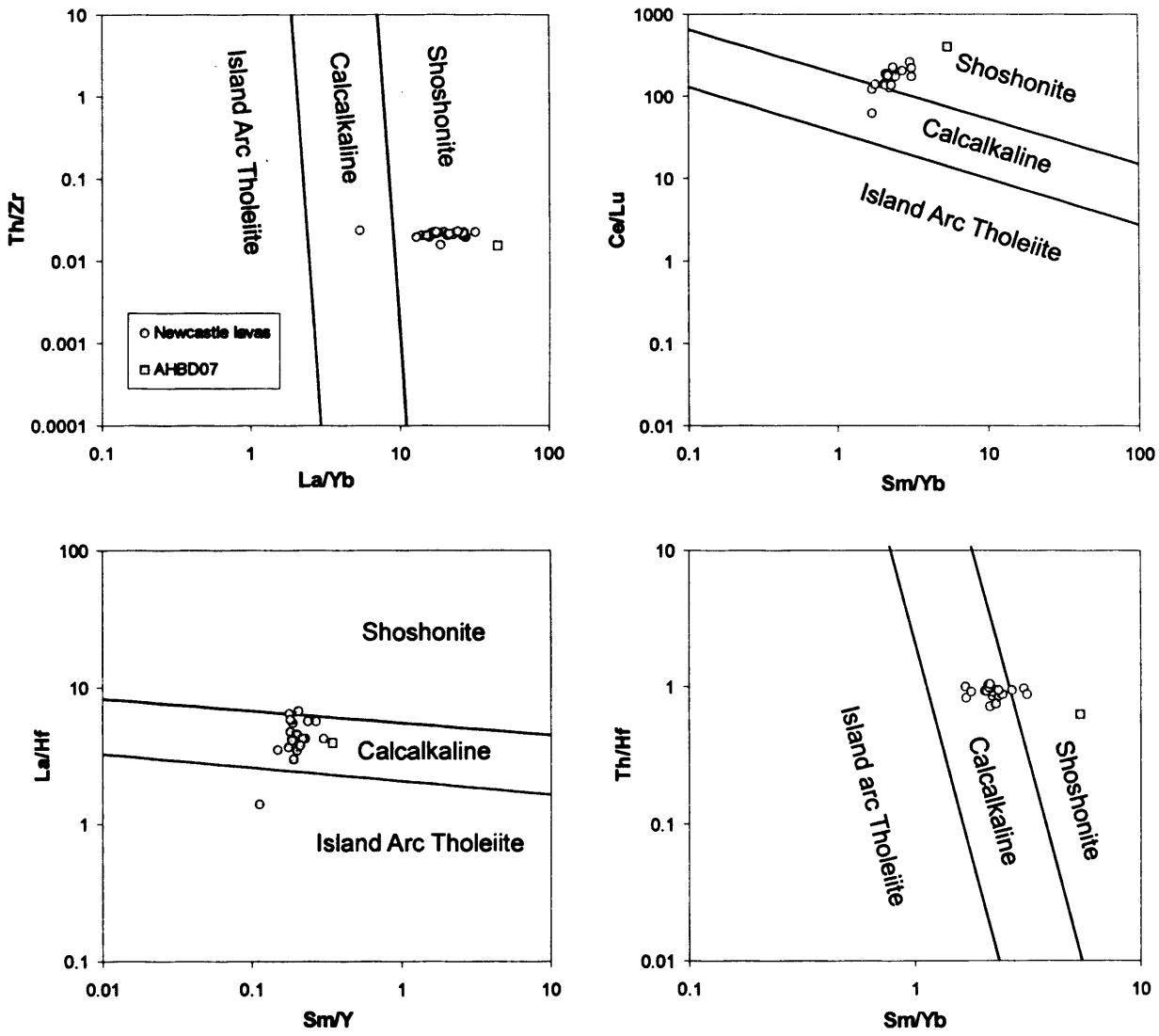

Figure 6.39 - Th/Zr-La/Yb, Ce/Lu-Sm/Yb, La/Hf-Sm/Y and Th/Hf-Sm/Yb discrimination diagrams showing the disparity of classifying the adakites with regards to their LILE, LREE and actinide enrichment. The La/Hf-Sm/Y and Th/Hf-Sm/Yb diagrams classify most of the rocks as CA, whereas the Th/Zr-La/Yb and Ce/Lu-Sm/Yb plots classify the majority of the lavas as SHC.

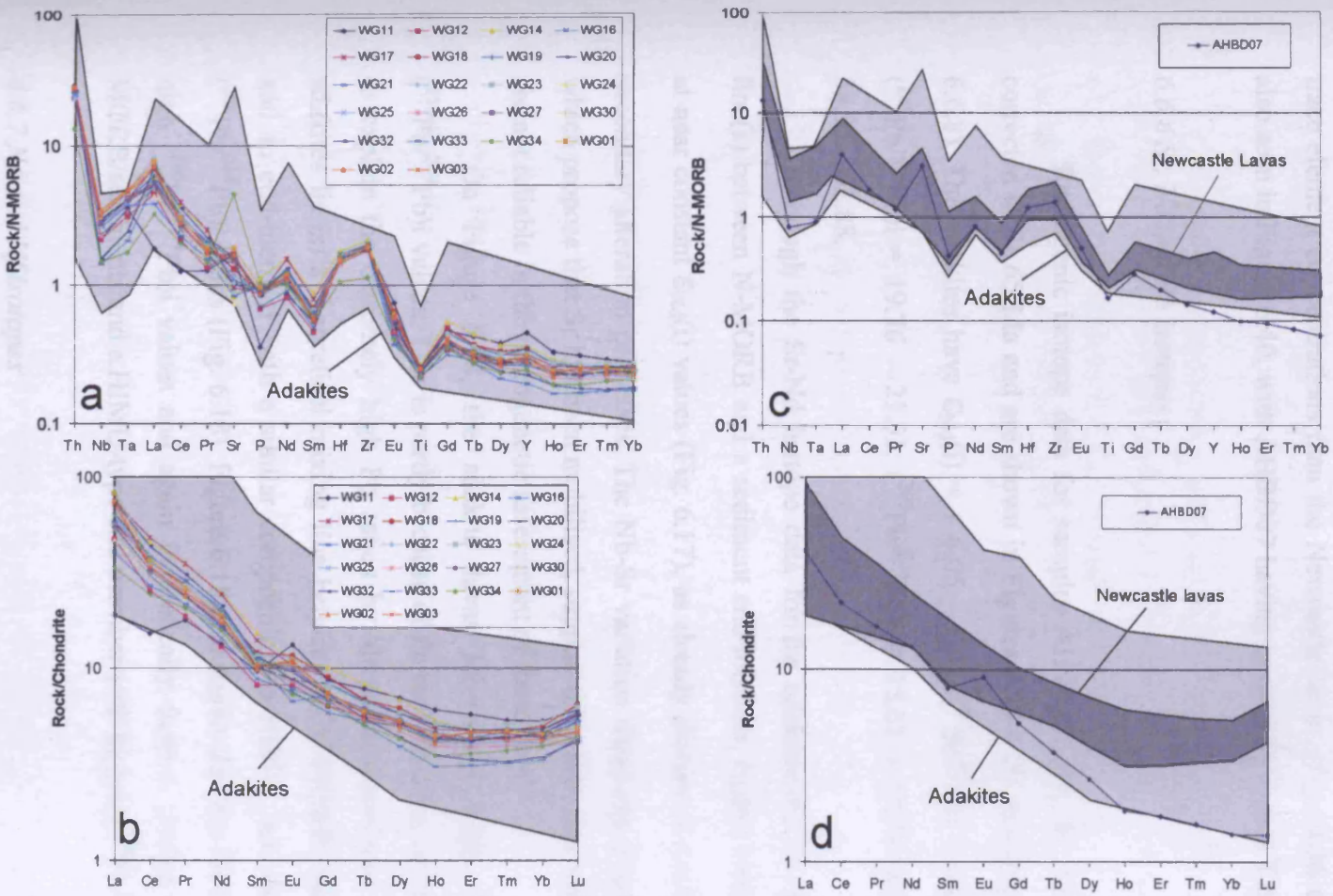

Figure 6.40 – (a-b) N-MORB-normalised multi-element and chondrite-normalised REE plots for the Newcastle adakites. (c-d) N-MORB-normalised multi-element and chondrite-normalised REE diagrams for AHBD07. Normalising values from Sun and McDonough (1989), McDonough and Sun (1995) and references for adakite data are in Appendix F.

and LREE enrichment in the Newcastle adakites. It also demonstrates that the adakites possess an "off-centred U-shaped" pattern (Fig. 6.40b). AHBD07 plots as a high-Al TTD in Figure 6.35, has similar multi-element patterns in Figure 6.40 and has lower trace element concentrations than the Newcastle lavas (Figs. 6.36 and 6.37). This is also seen in Figure 6.40, with AHBD07 having lower HREE and Y concentrations.

6.6.6 Sr, Nd and Pb isotopes

Radiogenic isotope data for samples AHWG12, 19, 21, 32 and 33 are age-corrected to 51.65 Ma and are shown in Figures 6.17-6.20 and Appendix D (Section 6.6.8). The adakites have $\varepsilon_{Nd}(i) = + 6.05 - 7.02$, $(^{87}Sr/^{86}Sr)i = 0.70418 - 0.70479$, $(^{206}Pb/^{204}Pb)i = 19.36 - 23.51$, $(^{207}Pb/^{204}Pb)i = 15.61 - 15.78$ and $(^{208}Pb/^{204}Pb)i = 38.95 - 42.88$.

Although the Sr-Nd isotope data for the adakites lie on theoretical mixing line(s) between N-MORB and a sediment end-member, higher initial $^{87}Sr/^{86}Sr$ ratios at near constant $\varepsilon_{Nd}(i)$ values (Fig. 6.17), as already discussed, could be the result of secondary alteration processes. The Nb-Sr variation diagrams (Figs. 6.36 and 6.37), which propose that Sr has been mobilised, support this view. Accordingly, Sr isotopes are not reliable in the petrogenetic assessment of these lavas.

On Figure 6.18, the adakite lavas have very high $(^{207}Pb/^{204}Pb)i$ and $(^{206}Pb/^{204}Pb)i$ values. This is partly because of Pb mobilisation; however, it is difficult to explain the extremely high Pb ratios by alteration alone (see Chapter 7). The adakites lie on a theoretical mixing line between an N-MORB/sediment component and an end-member with a similar composition to HIMU, but with slightly higher $(^{206}Pb/^{204}Pb)i$ ratios (Fig. 6.18). Figure 6.18 also shows that the Newcastle lavas have high $(^{208}Pb/^{204}Pb)i$ values and again theoretically form a mixing line between N-MORB/sediments and a HIMU-type end member with higher $(^{206}Pb/^{204}Pb)i$ ratios.

6.6.7 Nd and Hf isotopes

The adakite lavas have $\varepsilon_{Nd}(i) = + 6.05 - 7.02$ and $\varepsilon_{Hf}(i) = + 12.03 - 12.48$ (Fig. 6.20 and Appendix D). The samples plot with, or around, the Above Rocks lavas

and are more enriched than most of the modern arc lavas shown, except for the Lesser Antilles and Sunda island arc rocks. Relative to N-MORB, the adakites have lower $\varepsilon_{Nd}(i)$ values and enriched $\varepsilon_{Hf}(i)$ ratios (Nowell *et al.*, 1998; Kempton *et al.*, 2000).

6.6.8 Stratigraphical and geochronological data

The Newcastle volcanics are found in the middle subgroup of the Paleocene to lower Eocene Wagwater group (Chapter 7). This implies that they have an age of ~ 50 Ma; however, to confirm this date, sample AHWG03 was analysed using the Ar-Ar radiometric dating technique (Appendix D) (Figs. 6.41 and 6.42). Two groundmass separates, 8A and 8B, were run to obtain inverse isochron ages of 51.7 ± 1 Ma and 51.6 ± 1.1 Ma and step heating plateau ages of 52.98 ± 0.35 Ma and 52.56 ± 0.32 Ma (Figs. 6.41 and 6.42). As with the other samples in this study the inverse isochron ages will be used for age-correcting the adakite radiogenic data. The average of the two inverse isochron plots is 51.65 Ma and this is the age which is used to age-correct the isotopes.

6.7 Halberstadt Volcanics

The Halberstadt volcanics are found with the Newcastle adakites and are composed of extrusive basalts and spilites (Jackson and Smith, 1978; 1979; Jackson *et al.*, 1989; Jackson and Scott, 1997). Jackson and Smith, (1978; 1979) propose that the geochemistry of the Halberstadt basalts is similar to that of the tholeiitic rocks from the Colombia River Basalts and the Deccan Traps with LREE enrichment and similar Ti-Zr-Y concentrations (Chapter 3). Rocks with OIB or plateau-type geochemistry are commonly found with adakite successions and are termed High-Nb basalts.

6.7.1 What are High-Nb Basalts (HNB)?

HNBs are generally associated with adakite successions and when found at subduction zones they are always associated with the subduction of young oceanic crust (Defant *et al.*, 1992; Castillo *et al.*, 2007). These rocks are rare, their

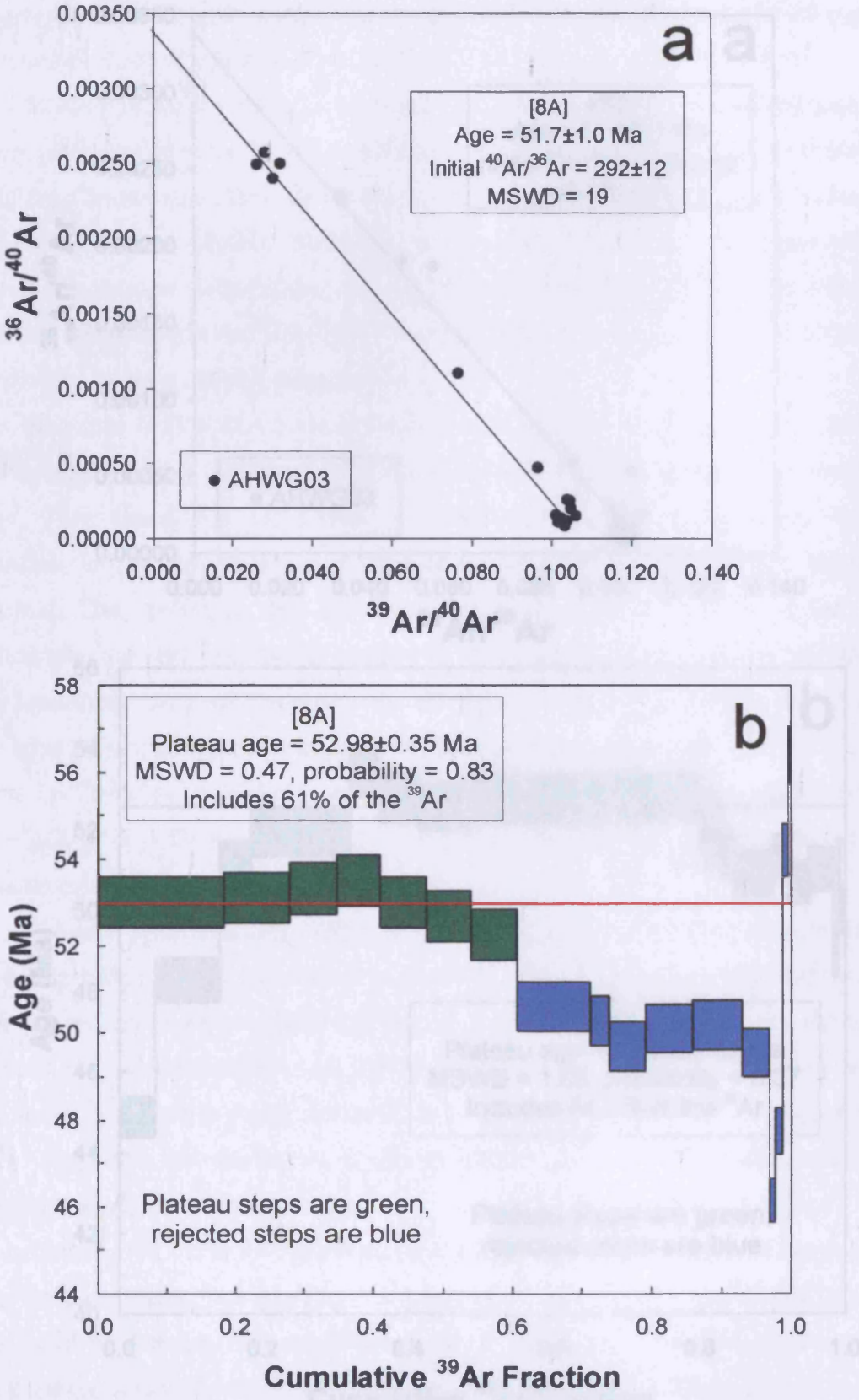

Figure 6.41 - (a and b) Ar-Ar inverse isochron and step heating plateau plots for AHWG03 run [8A].

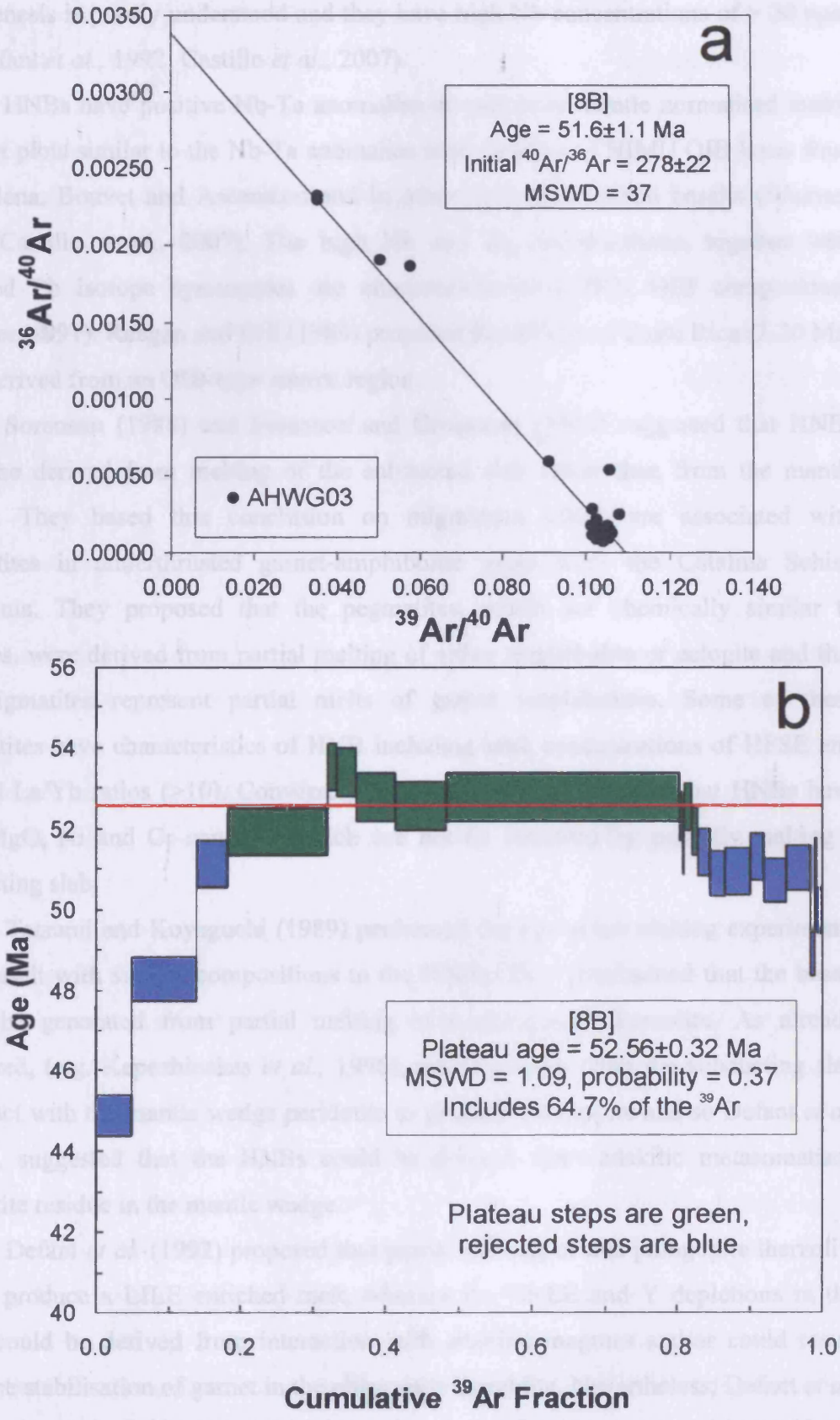

Figure 6.42 - (a and b) Ar-Ar step heating plateau and inverse isochron plots for AHWG03 run [8B].

petrogenesis is poorly understood and they have high Nb concentrations of > 20 ppm (cf. Defant *et al.*, 1992; Castillo *et al.*, 2007).

HNBs have positive Nb-Ta anomalies on primitive mantle normalised multi-element plots similar to the Nb-Ta anomalies seen on plots of HIMU OIB lavas from St. Helena, Bouvet and Ascension and in other continental alkali basalts (Weaver, 1991; Castillo *et al.*, 2007). The high Nb and Ta concentrations, together with enriched Pb isotope systematics are characteristic of HIMU OIB compositions (Weaver, 1991). Reagan and Gill (1989) proposed that HNBs in Costa Rica (2-20 Ma) were derived from an OIB-type source region.

Sorenson (1988) and Sorenson and Grossman (1989) suggested that HNBs could be derived from melting of the subducted slab rather than from the mantle wedge. They based this conclusion on migmatites which are associated with pegmatites in underthrusted garnet-amphibolite rocks from the Catalina Schist, California. They proposed that the pegmatites, which are chemically similar to adakites, were derived from partial melting of either amphibolite or eclogite and that the migmatites represent partial melts of garnet amphibolites. Some of these migmatites have characteristics of HNB including high concentrations of HFSE and Sr, and La/Yb ratios (>10). Conversely, Defant *et al.* (1992) noted that HNBs have high MgO, Ni and Cr contents, which can not be achieved by partially melting a subducting slab.

Tatsumi and Koyaguchi (1989) performed high pressure melting experiments on a basalt with similar compositions to the HNBs. They determined that the basalt could be generated from partial melting of a phlogopite lherzolite. As already discussed, (e.g. Kepezhinskas *et al.*, 1996), adakitic melts from the subducting slab can react with the mantle wedge peridotite to produce phlogopite and so Defant *et al.* (1992), suggested that the HNBs could be derived from adakitic metasomatised peridotite residue in the mantle wedge.

Defant *et al.* (1992) proposed that partial melting of this phlogopite lherzolite would produce a LILE enriched melt, whereas the HREE and Y depletions in the HNB could be derived from interaction with adakitic magmas and/or could result from the stabilisation of garnet in the phlogopite lherzolite. Nevertheless, Defant *et al.* (1992) also argued that the phlogopite and/or garnet in the source region could not explain the high HFSE composition of the HNBs. Phlogopite alone would also produce high-Al melts; whereas the HNBs have low-Al compositions (Fig. 6.58).

However, large scale partial melting of amphibolite would produce low-Al melts and high HFSE contents (Defant *et al.*, 1992). Consequently, an adakite-hybridised amphibole/phlogopite garnet peridotite residue could melt to form HNB compositions.

Conversely, Castillo *et al.* (2007) argued that the HNBs in the Sulu arc did not require adakitic melts for their formation. They propose that the HNBs are derived from the mixing of enriched OIB-type and depleted N-MORB-type mantle components. They demonstrated that the N-MORB mantle wedge of the Sulu arc is contaminated with OIB-type material from the source of the South China Sea intraplate lavas. The melting of this "marble cake" formed the Sulu HNB compositions.

6.7.2 Element mobility

Major and trace element variation diagrams are shown in Figures 6.43, 6.44 and Section E.14, Appendix E. The Si, Al, Ti and P oxides show convincing liquid lines of descent, which suggests that the HNBs are derived from a single chemically homogenous source region. MgO, FeO*, MnO, Na_2O, CaO and K_2O have been variably mobilised such that a liquid line of decent is not discernable (Fig. 6.43 and E.14).

The logged trace element variation diagrams in Figure 6.44 use AHHB02 trace element data for the C_O values because its Co and silica concentrations suggest that it is one of the most primitive of the HNBs (Appendix E). Co, Th, U, Ga, Y, Nb, Hf, Ta and the REE show convincing liquid lines of descent whereas no trend is observed for Ba, Sr, V, Sc, Cr and Pb (Figs. 6.43, 6.44 and E.14).

TiO_2 and P_2O_5 show characteristic increases due to the lack of Fe-Ti oxide and apatite fractionation, whereas SiO_2 shows an unexpected increase with decreasing Zr abundance (Fig. 6.43 and E.14). This suggests that the Zr is being removed by a fractionating phase in a mafic melt. The Zr may be removed from the melt by fractionating amphibole and/or biotite, however, the rocks do not contain amphibole or biotite phenocrysts. In addition, the trend of the SiO_2 liquid line of descent is not mirrored by Th or U. These elements would behave incompatibly with amphibole and biotite in a mafic melt, and when plotted against Zr, the Zr would be expected to

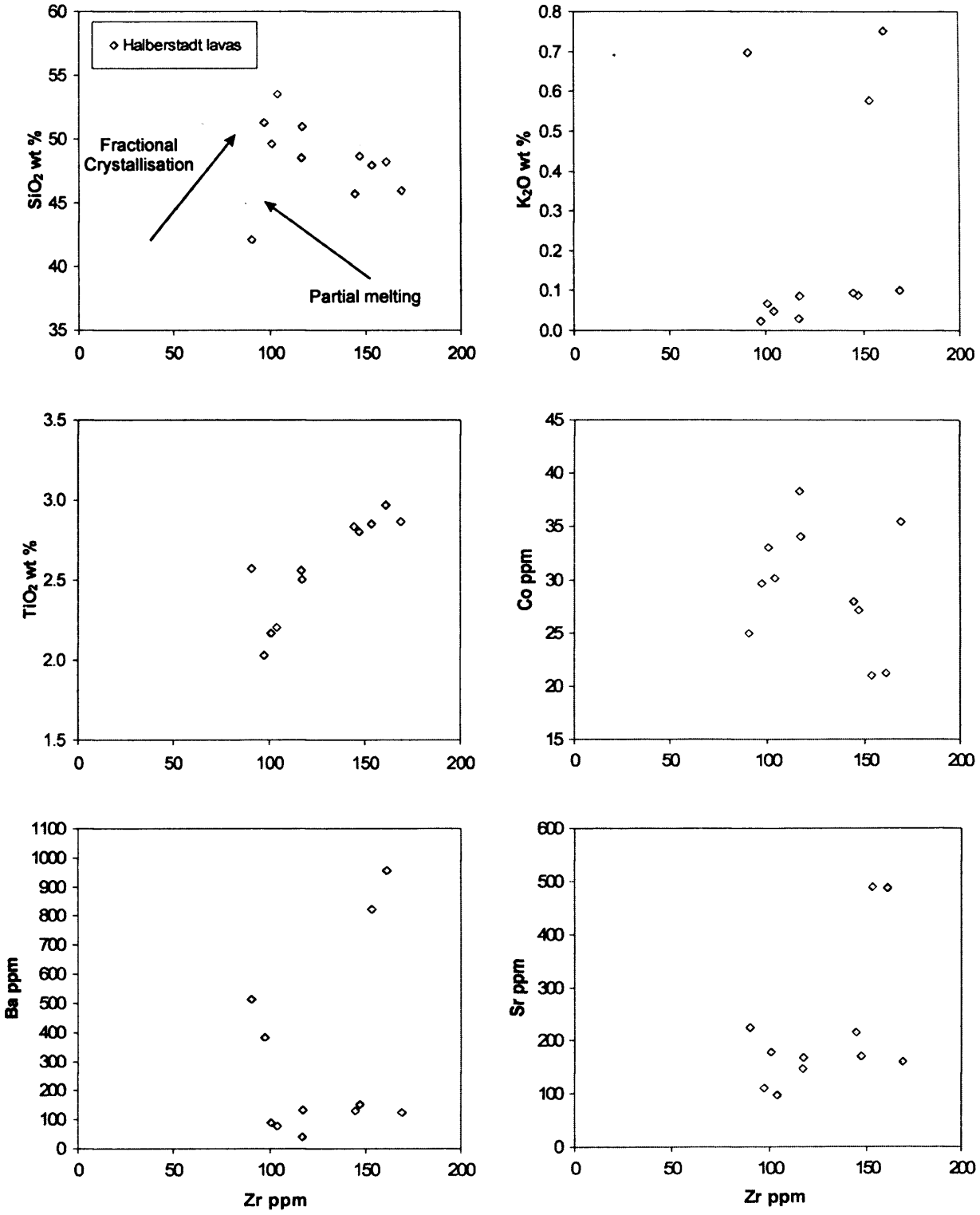

Figure 6.43 – Selected variation diagrams for major and trace elements vs. Zr for the Halberstadt lavas. The degree of mobility of an element is represented by its correlation with Zr. A mobile element will show no correlation, whereas, an immobile element displays a good correlation. A correlation can be a straight or curved line depending on whether the element is incompatible and/or compatible during fractional crystallisation and/or partial melting.

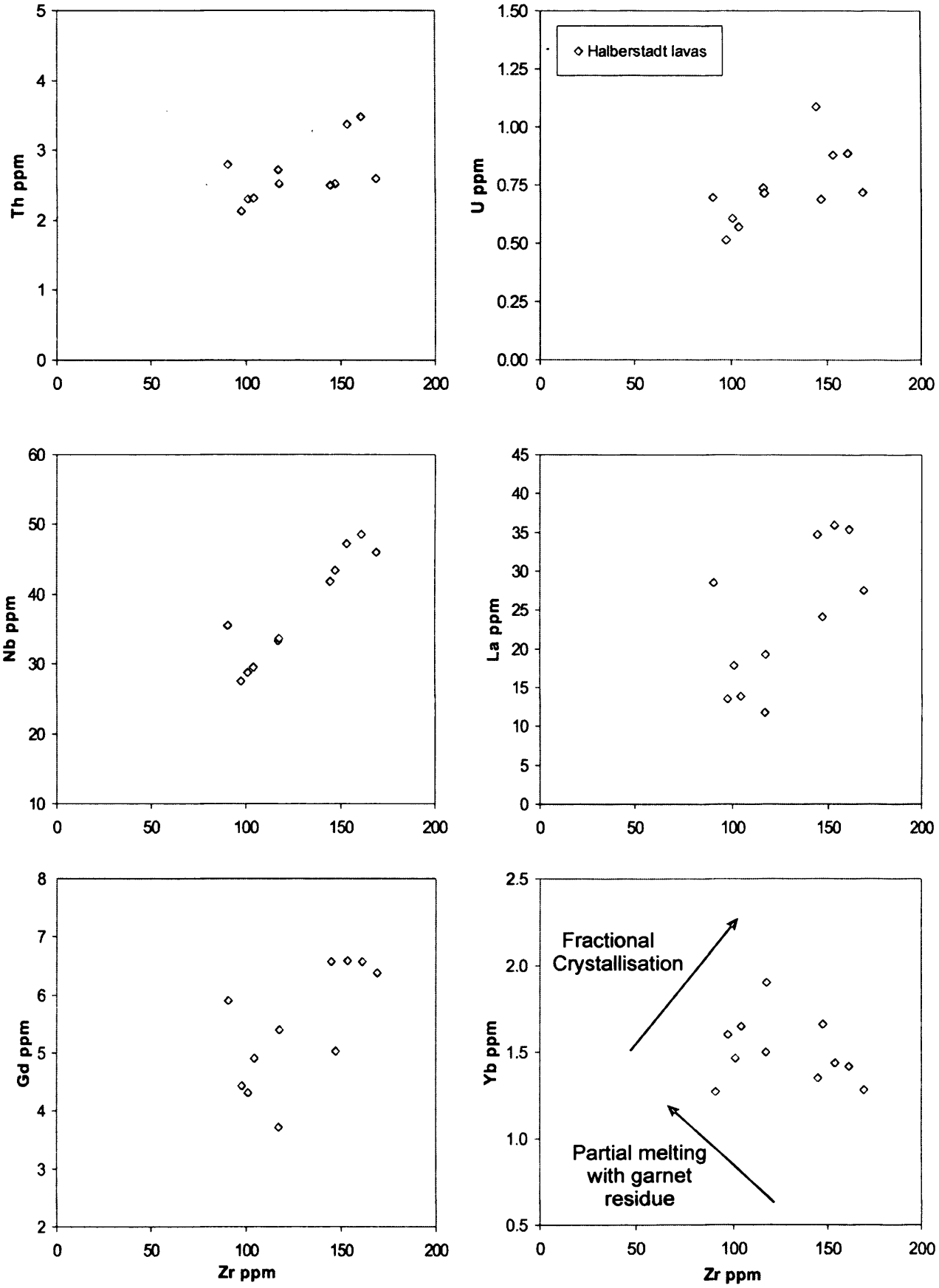

Figure 6.43 – continued.

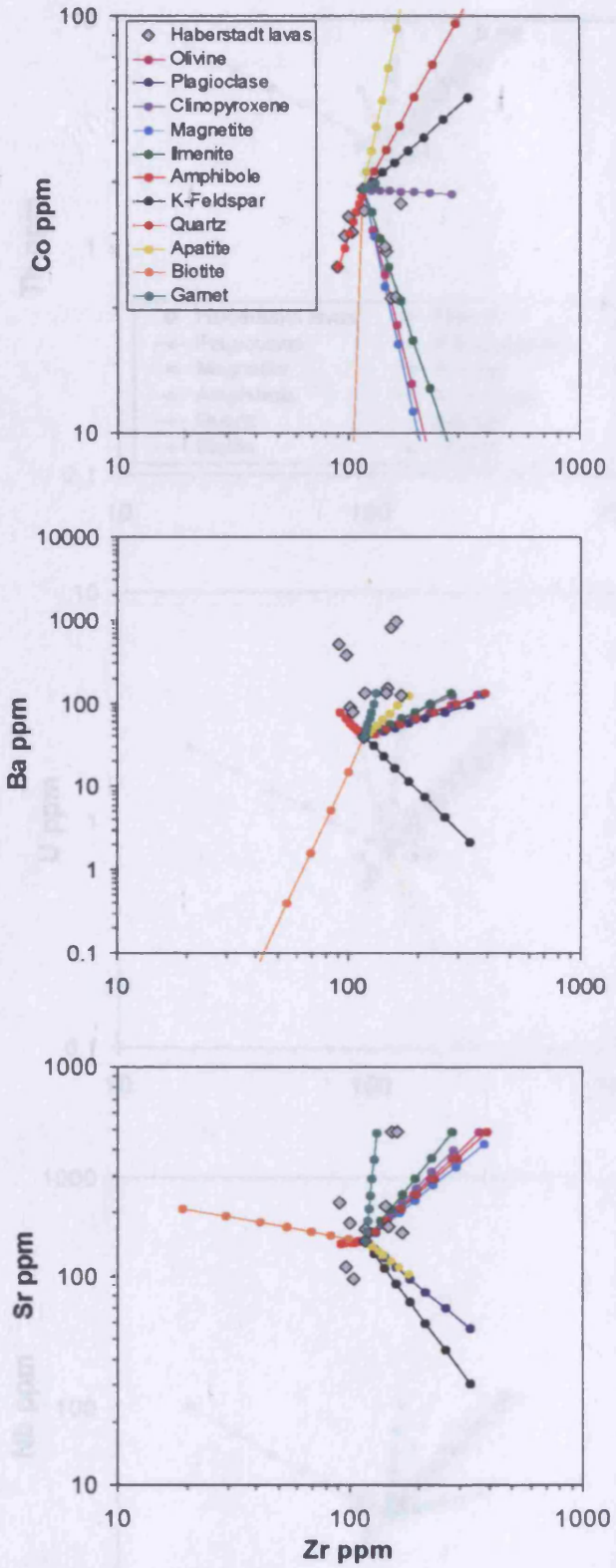

Figure 6.44 – Selected variation diagrams with vectors showing the composition of olivine, plagioclase, clinopyroxene, magnetite, ilmenite, amphibole, K-feldspar, quartz, apatite, biotite, and garnet with up to 70% fractional crystallisation of the AHHB02 starting composition (each tick represents 10% crystallisation) (Appendices E and G).

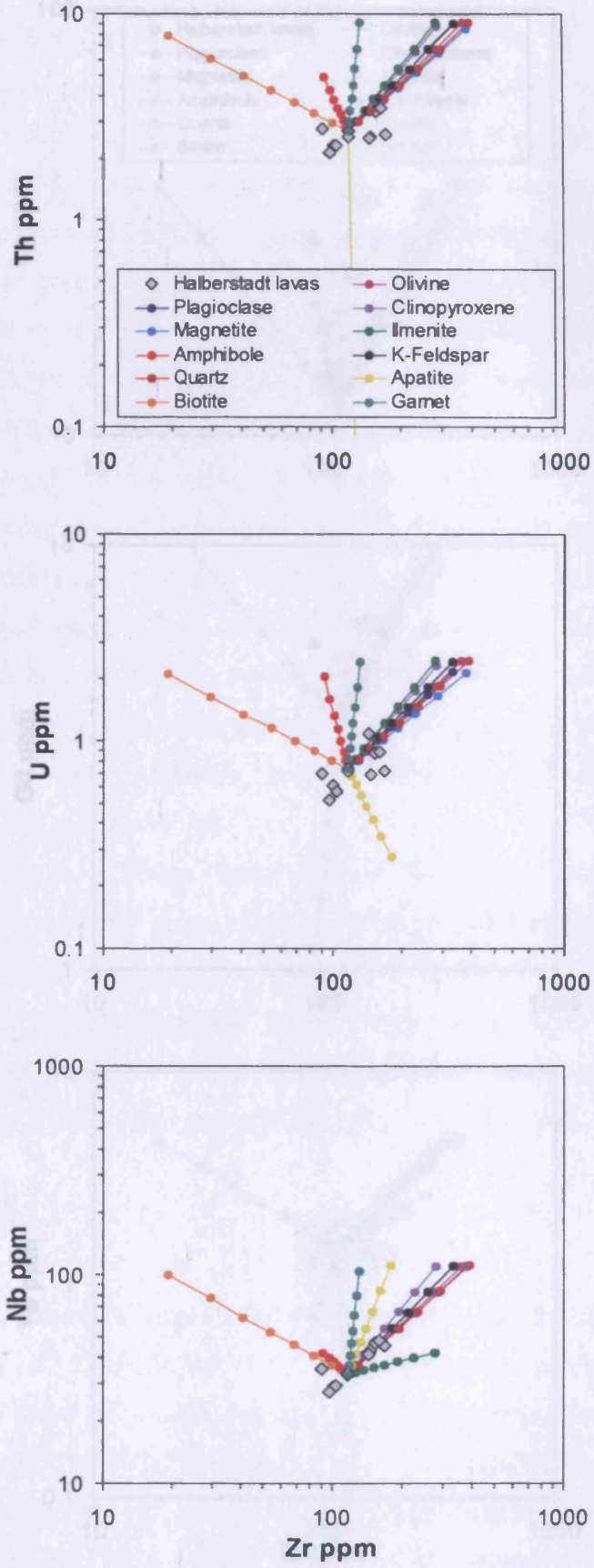

Figure 6.44 – continued

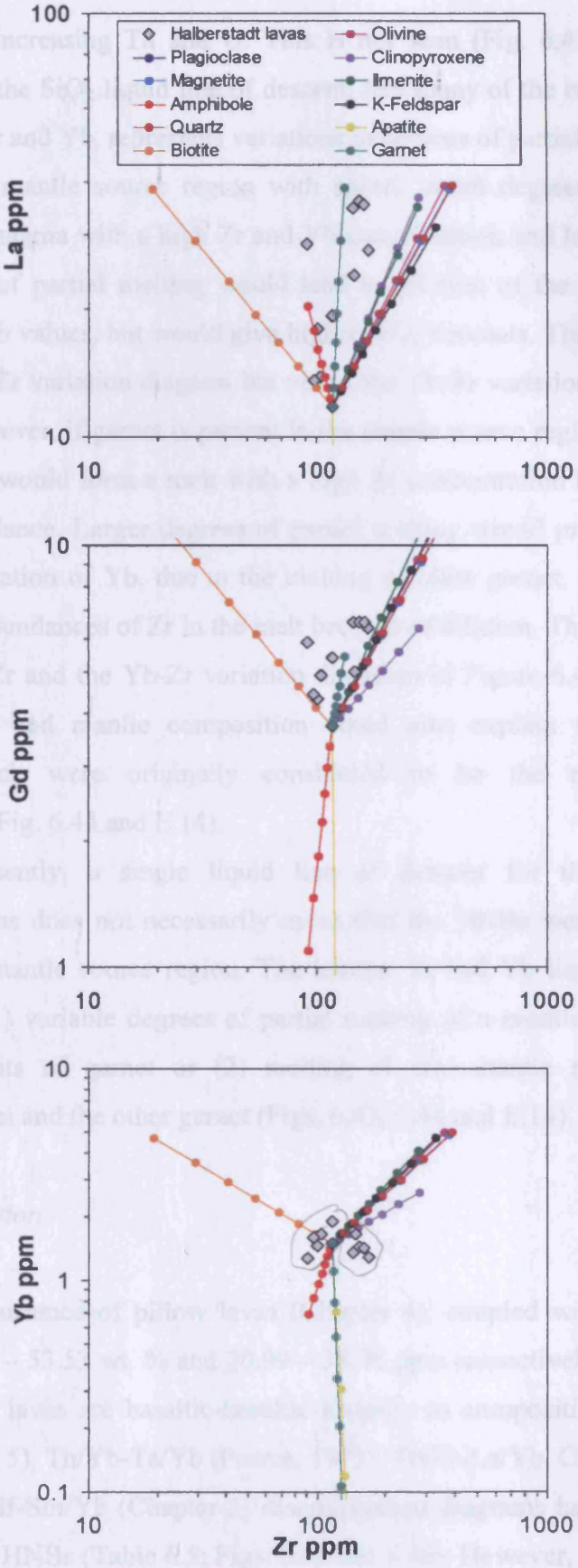

Figure 6.44 – continued

decrease with increasing Th and U. This is not seen (Fig. 6.43); conversely, it is concluded that the SiO_2 liquid line of descent, like many of the other major and trace elements e.g. Zr and Yb, represents variations in degrees of partial melting.

With a mantle source region with spinel, small degrees of partial melting would form a magma with a high Zr and Yb concentration and lower SiO_2; however, larger degrees of partial melting would lead to dilution of the trace elements with lower Zr and Yb values, but would give higher SiO_2 contents. This scenario is seen in the HNB SiO_2-Zr variation diagram but not in the Yb-Zr variation diagram (Fig. 6.43 and E.14). However, if garnet is present in the mantle source region small amounts of partial melting would form a melt with a high Zr concentration but with a lower Yb and SiO_2 abundance. Larger degrees of partial melting would produce a melt with a higher concentration of Yb, due to the melting of more garnet, and SiO_2 but would lead to lower abundances of Zr in the melt because of dilution. This scenario is seen in both the SiO_2-Zr and the Yb-Zr variation diagrams in Figure 6.43. This variation in partial melting and mantle composition could also explain the TiO_2 and P_2O_5 increases, which were originally considered to be the result of fractional crystallisation (Fig. 6.43 and E.14).

Consequently, a single liquid line of descent for the elements of the Halberstadt lavas does not necessarily mean that the HNBs were derived from one homogeneous mantle source region. The inverse Si and Yb liquid lines of descent may indicate (1) variable degrees of partial melting of a mantle source region with variable amounts of garnet or (2) melting of two mantle source regions, one containing spinel and the other garnet (Figs. 6.43, 6.44 and E.14).

6.7.3 Classification

The occurrence of pillow lavas (Chapter 4), coupled with the SiO_2 and Co values of 42.13 – 53.53 wt. % and 20.99 – 38.36 ppm respectively, demonstrates that the Halberstadt lavas are basaltic-basaltic andesite in composition (Table 6.5). The Co-Th (Chapter 5), Th/Yb-Ta/Yb (Pearce, 1982), Th/Zr-La/Yb, Ce/Lu-Sm/Yb, La/Hf-Sm/Y and Th/Hf-Sm/Yb (Chapter 5) discrimination diagrams have been used to try and classify the HNBs (Table 6.5; Figs. 6.45 and 6.46). However, as with the adakites, the HNBs have a distinctive chemistry that is not thought to have been formed from "normal" island arc magmatic processes. Therefore, the diagrams developed in this

	Fractionation Determination		Alkalinity Determination					
	Silica values	Co-Th	Th/Yb-Ta/Yb	Co-Th	Th/Hf-Sm/Yb	Ce/Lu-Sm/Yb	La/Hf-Sm/Y	Th/Zr-La/Yb
AHHB01								
AHHB02								
AHHB03								
AHHB04								
AHHB05								
AHHB07								
AHHB08								
AHHB09								
AHWG08								
AHWG09								
AHWG10								

Table 6.5 – The fractionation and alkalinity results from plotting the Halberstadt samples on the Co-Th, Th/Yb-Ta/Yb, Th/Hf-Sm/Yb, Ce/Lu-Sm/Yb, La/Hf-Sm/Y and Th/Zr-La/Yb diagrams; Blue - Basalt; Yellow - Basaltic Andesite; Brown - CA; Green - SHC.

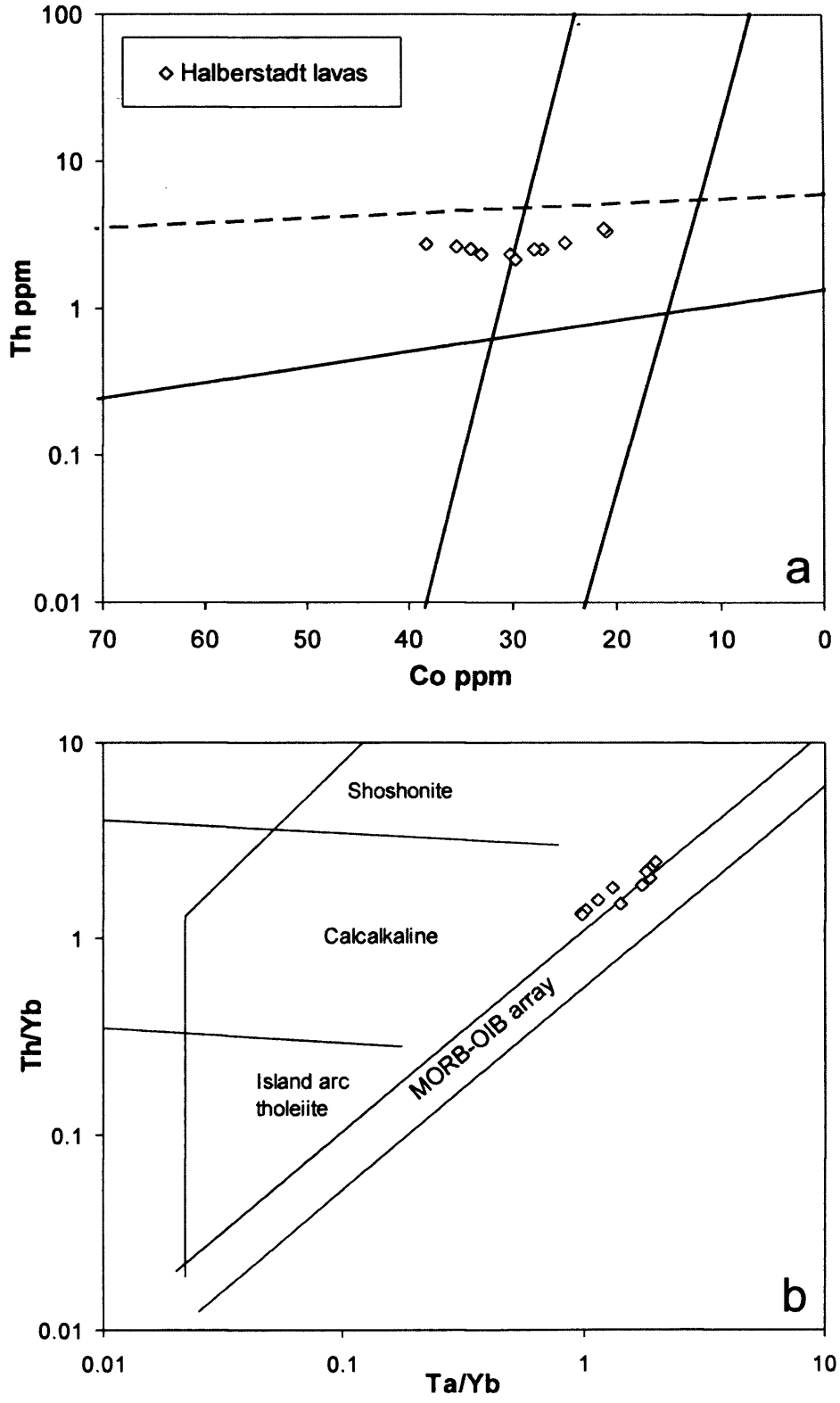

Figure 6.45 – (a) Co-Th and (b) Th/Yb-Ta/Yb discrimination diagrams showing the Halberstadt lavas (Pearce, 1982; Hastie *et al.*, 2007).

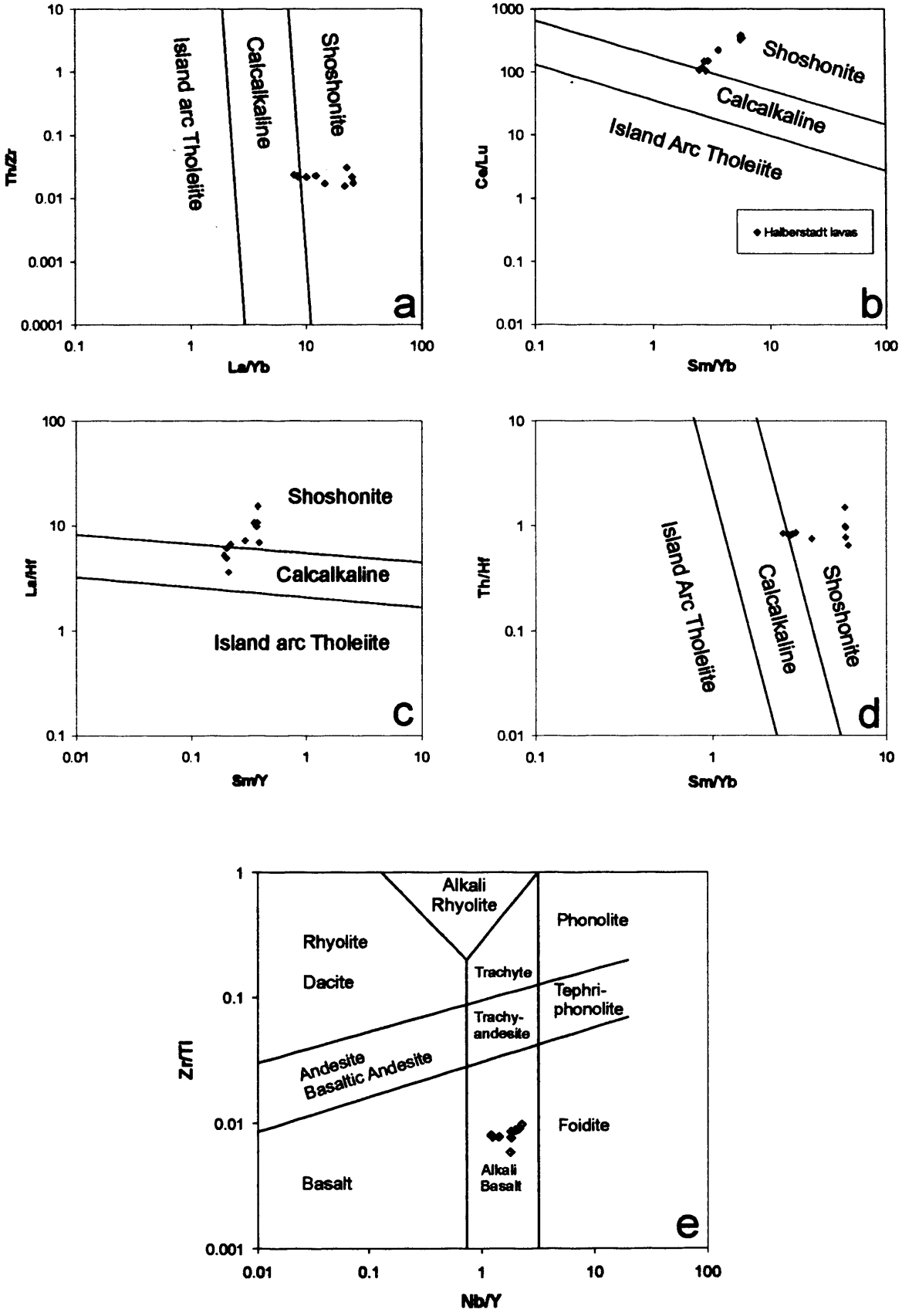

Figure 6.46 – (a-d) Th/Zr-La/Yb, Ce/Lu-Sm/Yb, La/Hf-Sm/Y and Th/Hf-Sm/Yb discrimination diagrams; (e) OIB-derived HNBs classified as alkali basalts on the updated Zr/Ti-Nb/Y diagram (Pearce, 1996).

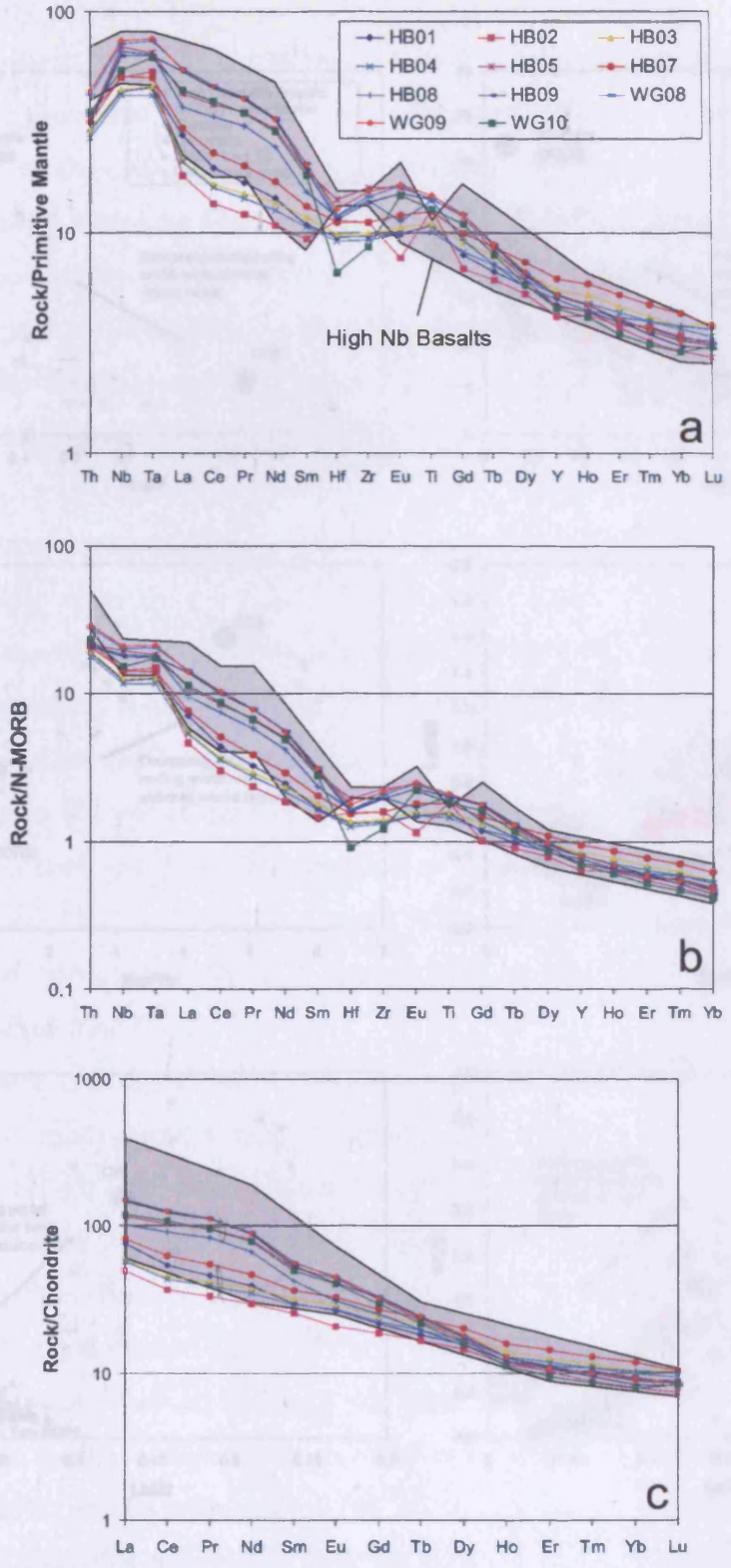

Figure 6.47 – (a and b) Primitive mantle and N-MORB-normalised multi-element patterns and (c) Chondrite-normalised REE diagram for the Halberstadt HNBs, with fields for HNBs from the Cenozoic Sulu island arc and the Costa Rica/Panama subduction zone. Normalising data from McDonough and Sun (1995) and references for the HNB data can be found in Appendix F.

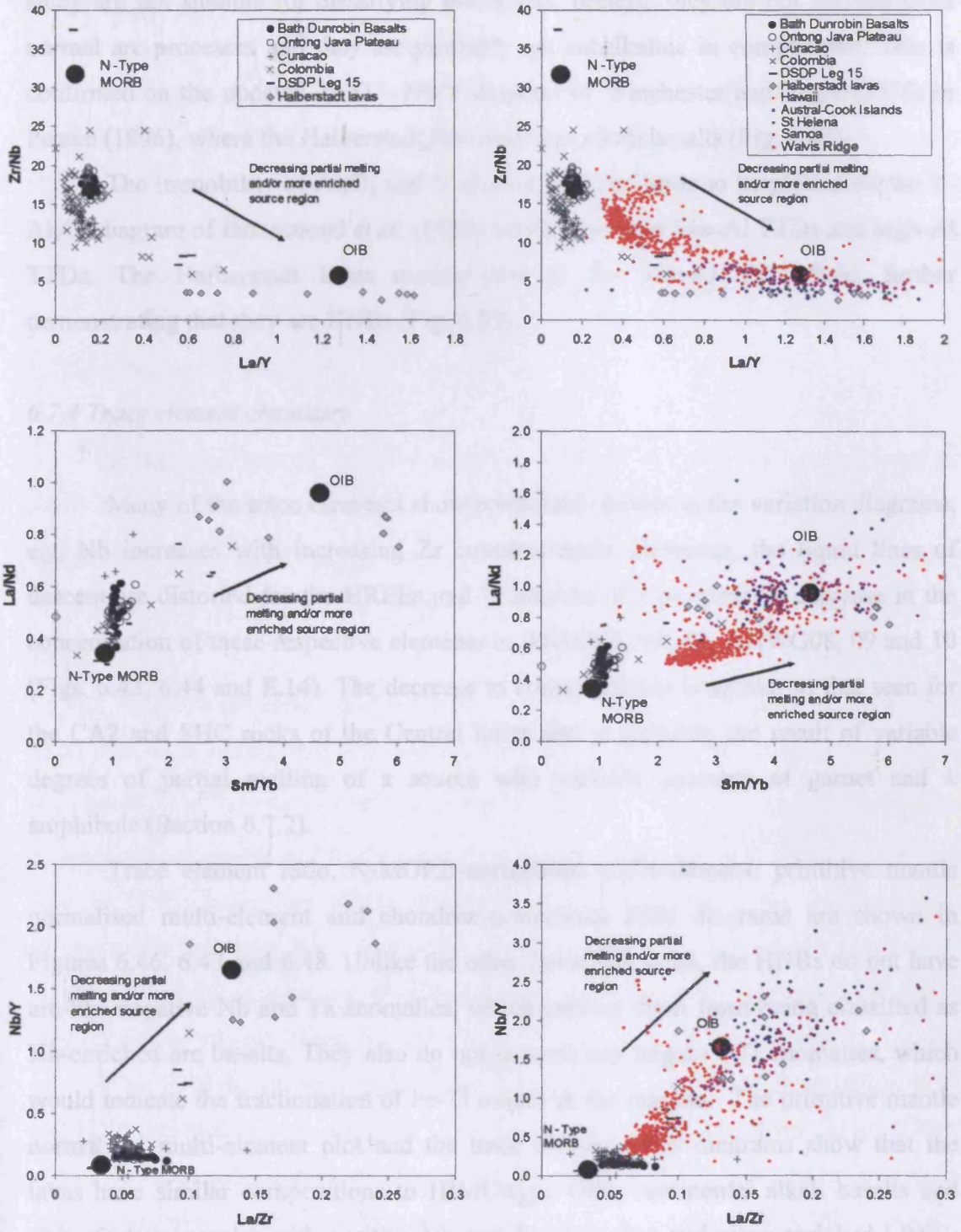

Figure 6.48 – Trace element ratio diagrams demonstrating that the Halberstadt lavas have an OIB-type chemistry rather than an N-MORB or plateau composition. References for OIB data can be found in Appendix F.

study are not suitable for classifying the HNBs, because they are not derived from normal arc processes and they are probably not subalkaline in composition. This is confirmed on the updated Zr/Ti – Nb/Y diagram of Winchester and Floyd (1976) in Pearce (1996), where the Halberstadt HNBs plot as alkali basalts (Fig. 6.46).

The immobility of Al_2O_3 and Y also enables the lavas to be plotted on the Y-Al_2O_3 diagram of Drummond *et al.* (1996) which separates low-Al TTDs and high-Al TTDs. The Halberstadt lavas mostly plot in the low-Al TTD field, further demonstrating that they are HNBs (Fig. 6.35).

6.7.4 Trace element chemistry

Many of the trace elements show predictable trends in the variation diagrams, e.g. Nb increases with increasing Zr concentrations. However, the liquid lines of descent are distorted for the HREEs and Y because of a progressive decrease in the concentration of these respective elements in AHHB05, 08, 09, AHWG08, 09 and 10 (Figs. 6.43, 6.44 and E.14). The decrease in concentrations is similar to that seen for the CA2 and SHC rocks of the Central inlier and is probably the result of variable degrees of partial melting of a source with variable amounts of garnet and ± amphibole (Section 6.7.2).

Trace element ratio, N-MORB-normalised multi-element, primitive mantle normalised multi-element and chondrite-normalised REE diagrams are shown in Figures 6.46, 6.47 and 6.48. Unlike the other Jamaican rocks, the HNBs do not have arc-like negative Nb and Ta anomalies, which prevent them from being classified as Nb-enriched arc basalts. They also do not possess any negative Ti anomalies, which would indicate the fractionation of Fe-Ti oxides in the magma. The primitive mantle normalised multi-element plot and the trace element ratio diagrams show that the lavas have similar compositions to HIMU-type OIB, continental alkali basalts and slab window samples with positive Nb and Ta anomalies and more enriched LREE-Th/MREE-HREE-Y ratios (Figs. 6.47 and 6.48).

The HREE and Y concentrations are low relative to Th, the LREE, the MREE, Zr and Hf, thus, demonstrating that garnet and ± amphibole are involved in the petrogenesis of the lavas. When compared to the LREE, the MREE are not as depleted as the HREE (Fig. 6.47). The normalised multi-element and REE diagrams also lack a "U" shaped pattern. These features imply that garnet is the dominant

mineral responsible for the depletion of the HREE, and if amphibole was in the source region, it was present in very small quantities. Consequently, if garnet was present in the source region of all of the HNB samples, as proposed in the N-MORB-normalised multi-element, primitive mantle normalised multi-element and chondrite-normalised REE diagrams, the "inverse" liquid lines of descent for Yb (and other HREEs and Y) are formed by variable degrees of partial melting of a mantle source region with variable amounts of garnet.

6.7.5 Sr, Nd and Pb isotopes

Radiogenic isotope data for samples AHHB03 and 07 are age-corrected to 51.65 Ma and are shown in Figures 6.17-6.20 and Appendix D (Section 6.7.7). The Halberstadt lavas have $\varepsilon_{Nd}(i)$ = + 6.77 – 6.80, ($^{87}Sr/^{86}Sr$)i = 0.7046 – 0.7048, ($^{206}Pb/^{204}Pb$)i = 18.95 - 19.44, ($^{207}Pb/^{204}Pb$)i = 15.60 – 15.62 and ($^{208}Pb/^{204}Pb$)i = 38.65 – 39.18.

The Sr in the HNBs may have been mobilised. Thus although the Halberstadt lavas plot on a mixing curve(s) between an N-MORB and a sediment end-member, high initial $^{87}Sr/^{86}Sr$ ratios at near constant $\varepsilon_{Nd}(i)$ values (Fig. 6.17) are probably due to secondary alteration and hydrothermal processes. However, it is important to note that the HNBs have very similar Nd-Sr isotope systematics to the adakites. This suggests that they may have had similar primary isotope compositions which were subsequently subject to similar alteration processes. Conversely, the radiogenic ratios may reflect the primary chemistry of both the adakites and HNBs (Chapter 7).

The HNB lavas have high ($^{207}Pb/^{204}Pb$)i and ($^{206}Pb/^{204}Pb$)i ratios (Figs. 6.18 and 6.49) and plot close to a sample of terrigenous sediment from Ewart *et al.* (1999) and a pelagic sediment from Turner *et al.* (1997). They also have a similar composition to the more-depleted adakites and the Border lavas (Fig. 6.18). However, it may not be realistic to compare the Halberstadt lavas to arc rocks considering that the former are derived from an OIB-type source region. On Figure 6.49 the HNBs have similar compositions to OIB lavas from Samoa, Society and the Austral Cook islands. Nevertheless, the Pb has been mobilised. Therefore, although the HNBs plot with OIB rocks, the Pb isotopes can not be used to further study their petrogenesis.

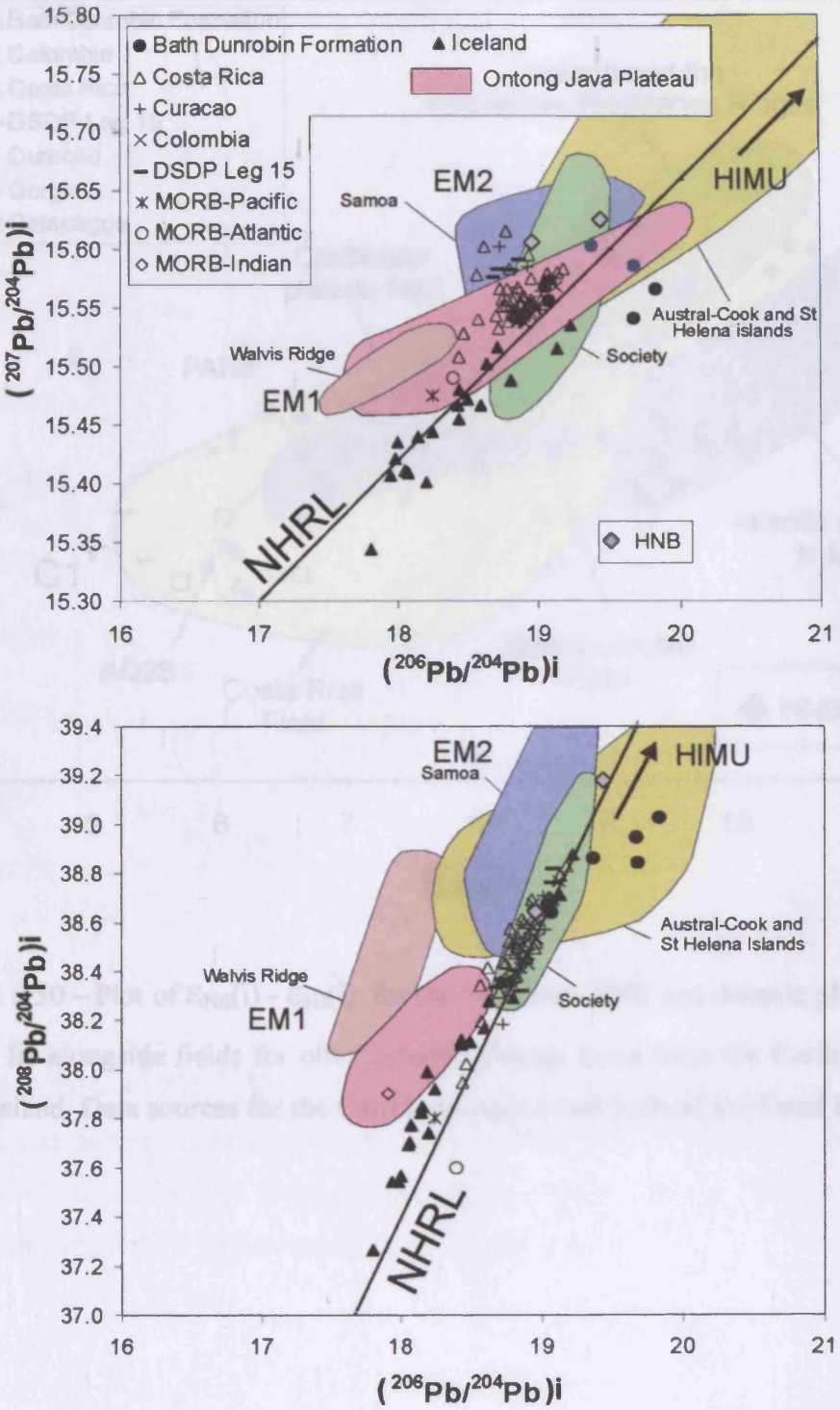

Figure 6.49 – Plots of $(^{207}Pb/^{204}Pb)i$ – $(^{206}Pb/^{204}Pb)i$ and $(^{208}Pb/^{204}Pb)i$ and $(^{206}Pb/^{204}Pb)i$ for the Halberstadt HNBs compared to the Jamaican and Caribbean plateau lavas and OIB lavas from the Walvis Ridge, Samoa, Society and the Austral-Cook and St Helena islands. Data sources for the island arcs are listed in Appendix F.

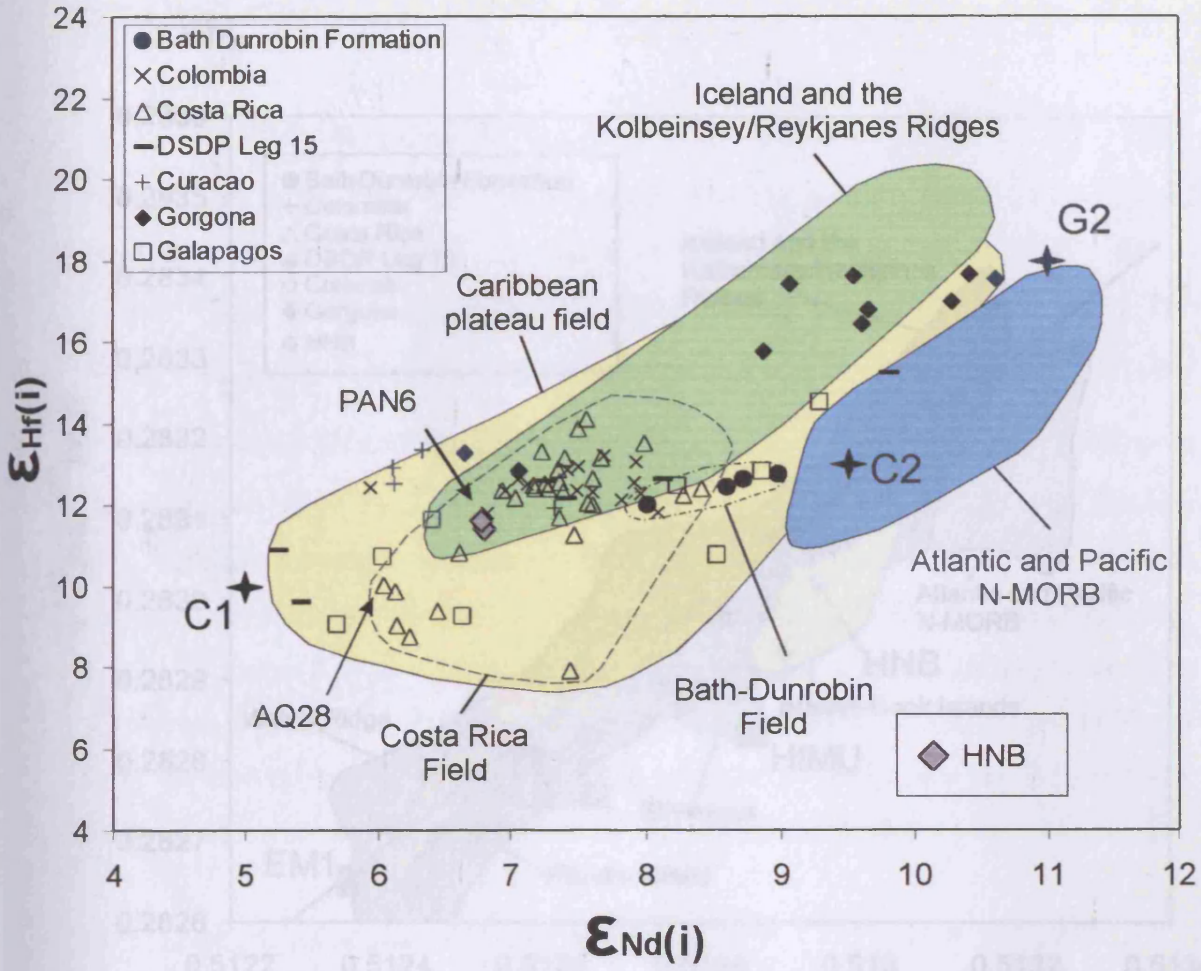

Figure 6.50 – Plot of $\varepsilon_{Nd}(i)$ - $\varepsilon_{Hf}(i)$ for the Jamaican HNB and oceanic plateau rocks, which lie alongside fields for other oceanic plateau lavas from the Caribbean region and Iceland. Data sources for the Caribbean region and Iceland are listed in Appendix F.

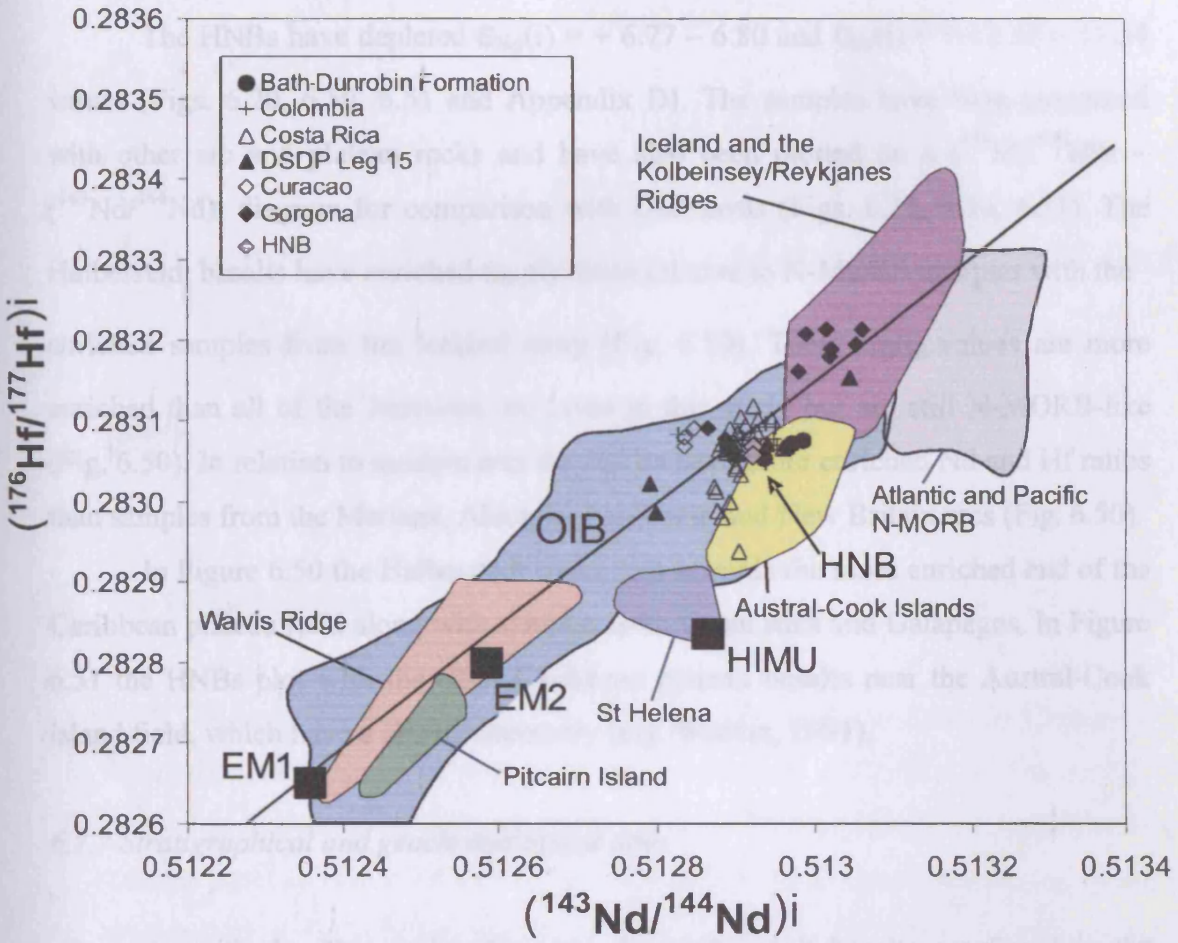

Figure 6.51 – $(^{176}Hf/^{177}Hf)i$ – $(^{143}Nd/^{144}Nd)i$ diagram comparing the Halberstadt HNBs with plateau lavas from around the Caribbean and modern OIB lavas from the Austral-Cook, Pitcairn, St Helena islands and the Walvis Ridge. Data sources for the Caribbean region and Iceland are listed in Appendix F.

6.7.6 Nd and Hf isotopes

The HNBs have depleted $\varepsilon_{Nd}(i) = +6.77 - 6.80$ and $\varepsilon_{Hf}(i) = +11.35 - 11.54$ values (Figs. 6.20, 6.50, 6.51 and Appendix D). The samples have been compared with other arc and plateau rocks and have also been plotted on a ($^{176}Hf/^{177}Hf$)i – ($^{143}Nd/^{144}Nd$)i diagram for comparison with OIB lavas (Figs. 6.20, 6.50, 6.51). The Halberstadt basalts have enriched $\varepsilon_{Nd}(i)$ ratios relative to N-MORB and plot with the enriched samples from the Iceland array (Fig. 6.50). Their $\varepsilon_{Hf}(i)$ values are more enriched than all of the Jamaican arc lavas in this study but are still N-MORB-like (Fig. 6.50). In relation to modern arcs the HNBs have more enriched Nd and Hf ratios than samples from the Mariana, Aleutian, Izu-Bonin and New Britain arcs (Fig. 6.50).

In Figure 6.50 the Halberstadt rocks plot towards the more enriched end of the Caribbean plateau field along with samples from Costa Rica and Galapagos. In Figure 6.51 the HNBs plot with the other Caribbean plateau basalts near the Austral-Cook island field, which have a HIMU chemistry (e.g. Weaver, 1991).

6.7.7 Stratigraphical and geochronological data

As with the Newcastle volcanics, the Halberstadt basalts are found in the middle subgroup of the Paleocene to lower Eocene Wagwater group (Chapter 7). It is therefore assumed that the HNBs are a similar age to the Newcastle Volcanics. Consequently the Halberstadt radiogenic data is age-corrected to 51.65 Ma (Appendix D).

Chapter 7

Petrogenesis of the Jamaican igneous rocks, and their relationship to the tectonic evolution of the Caribbean plate

7.1 Introduction

In this chapter, the geochemical and geochronological data in Chapter 6 are interpreted, and integrated with the field information in Chapter 4. The aim of the chapter is to determine the petrogenesis of the oceanic plateau, OIB and island arc derived igneous rocks. This involves studying the geochemical nature and potential source regions of the different rock types. In particular, the relative importance of the mantle plume, the mantle wedge and the slab-related components will be ascertained. This information will then be used, in conjunction with other tectonic, sedimentary and palaeontological evidence, to model the evolution of Jamaica from the early Cretaceous to the lower Tertiary. This model of Jamaican evolution will then be used to place Jamaica within the current tectonic models of Caribbean plate evolution.

7.2 Petrogenesis of the Bath-Dunrobin plateau basalts and island arc tuffs

7.2.1 The degree of fractional crystallisation in the Bath-Dunrobin lavas

It is difficult to determine the amount of fractional crystallisation required to form the Bath-Dunrobin plateau lavas because, with MgO contents of 5.81-8.41 wt. %, no sample has been found which could feasibly represent a parental magma composition. Kerr *et al.* (1996b) reported picritic and basaltic oceanic plateau lavas from the island of Curaçao in the southern Caribbean with similar isotopes and trace element ratios to the Bath-Dunrobin lavas. These authors determined that the primary magmas of these lavas crystallised olivines with at least Fo_{90} and that the primary liquids contained ~ 15 wt % MgO. Petrological modelling by Kerr *et al.* (1996b) also showed that only olivine and Cr-spinel crystallise until the MgO concentration in the magma falls to ~ 8 %.

Therefore, if we assume that the parental magmas for the Bath-Dunrobin lavas had similar MgO contents to those of the Curaçao lavas, we can calculate, using olivine (Fo_{90}) and sample CUR92-3 from Kerr *et al.* (1996b) as a parental magma, that the Bath-Dunrobin lavas are likely to have undergone 25-30% fractional crystallisation. However, this calculation can only estimate the amount of fractional crystallisation because of the uncertainty with regard to the composition of the Bath-Dunrobin parental liquid and of the extracted olivine.

It is also assumed that only olivine and small amounts of Cr-spinel were fractionating. However, some of the more evolved Bath-Dunrobin samples contain plagioclase phenocrysts, indicating that plagioclase had started to fractionate out of the melt (Table A.1, Appendix A). Figure 6.2 also shows that the liquid lines of descent for the Bath-Dunrobin lavas are formed by predominantly olivine, plagioclase and clinopyroxene fractional crystallisation. Nevertheless, as most of the lavas are aphyric and possess MgO values ~ 8 wt %, the amount of plagioclase and clinopyroxene fractionation is likely to have been small. The most evolved basalts also possess negative Ti anomalies indicating that they have also begun to crystallise Fe-Ti oxides (Fig. 6.4).

7.2.2 Mantle source region(s) of the Bath-Dunrobin plateau lavas

On ($^{207}Pb/^{204}Pb$)i – ($^{206}Pb/^{204}Pb$)i and ($^{208}Pb/^{204}Pb$)i – ($^{206}Pb/^{204}Pb$)i plots (Fig. 6.8) the Bath-Dunrobin lavas lie on a line between HIMU and averaged MORB, which represents the DMM component. None of the samples lie to the left of the NHRL suggesting that they contain little EM1 or EM2 mantle components. The Bath-Dunrobin basalts generally possess more radiogenic Pb isotope ratios than other plateau basalts from the Caribbean region and the Ontong Java Plateaux (Chapter 6).

Although enriched and depleted mantle components have been described from other plateau lavas in the Caribbean (e.g. Thompson *et al.*, 2004; Geldmacher *et al.*, 2003); the Bath-Dunrobin lavas are derived from a mantle source which is more enriched in ($^{206}Pb/^{204}Pb$)i and ($^{208}Pb/^{204}Pb$)i. The Bath-Dunrobin lavas also plot on mixing lines between HIMU and DMM in Pb-Nd isotopic isotope space and are more enriched in ($^{206}Pb/^{204}Pb$)i and ($^{208}Pb/^{204}Pb$)i at a given $\varepsilon_{Nd}(i)$ value than most of the other Caribbean oceanic plateau samples and the Ontong Java lavas (Figs. 6.8 and 6.9).

Hf and Nd isotopic data further constrain the petrogenesis of the Bath-Dunrobin lavas. From Figure 6.10, it is possible to argue that the Caribbean plateau lavas (including the Bath-Dunrobin samples) could have been derived from a source composed of a mixture of an enriched component and the depleted plume component similar to that observed on Iceland (Nowell *et al.*, 1998; Kempton *et al.*, 2000).

However, when considered on their own, the Bath-Dunrobin lavas form a short linear trend from an enriched component towards the Atlantic/Pacific N-MORB field. Using Hf and Nd isotopic data from DSDP Leg 15 and Aruba, Thompson *et al.* (2004) constructed a Caribbean plateau field in Hf-Nd isotope space and proposed a mixing line between an enriched (C1) and a depleted (C2) end member to explain the composition of Caribbean plateau lavas (Fig. 6.10). The Bath-Dunrobin lavas also lie on this mixing line and it could be argued that they too are derived from the same source region as the DSDP Leg 15 and Aruba lavas.

Nevertheless, Figure 6.10 shows significantly greater Nd and Hf isotopic variability within the Caribbean plateau when data from Curaçao, Colombia and Costa Rica are also included (Kerr *et al.*, 1996b; Hauff *et al.*, 2000ab; Geldmacher *et al.*, 2003). Indeed, the Caribbean plateau lavas from Costa Rica form a linear trend

between HIMU and the G2 end member of Thompson *et al.* (2004), which is similar to the depleted plume component of Nowell *et al.* (1998) and Kempton *et al.* (2000).

Therefore, taking all the Caribbean oceanic plateau data as a single group (including Gorgona and Galapagos), the data form a mixing line between HIMU and a depleted mantle plume component. However, individual trends can be observed for several of the different lava successions of the Caribbean plateau, thus further demonstrating the significant local heterogeneity of the mantle plume that formed the Caribbean plateau (c.f. Kerr *et al.* 2002). Although it has been proposed that the Cretaceous rocks on Gorgona, and the more recent Galapagos volcanism, are not related to the same mantle plume as that which formed the Caribbean oceanic plateau (Pindell and Kennan, 2001; Kerr and Tarney, 2005), even if these rocks are excluded, the Caribbean field still trends towards the depleted plume end member of Nowell *et al.* (1998) and Kempton *et al.* (2000). The Caribbean plateau field does not include samples from DSDP Leg 15 site 152 because these are younger lavas (~80 Ma) with an N-MORB-like geochemistry (Chapter 2) (Sinton *et al.*, 1998).

A depleted mantle plume component distinct from MORB is also confirmed by positive ΔNb values on the Nb/Y-Zr/Y plot (Fig. 6.5). Indeed Thompson *et al.* (2004) calculated that it would require mixing of ~ 90 % of a DMM component with an enriched plateau component (C1 of Thompson *et al.*, 2004) for a positive ΔNb value to become negative. These conclusions are consistent with those of Hauff *et al.* (2000a), who proposed that the Caribbean plateau rocks were derived from a mixed HIMU and DMM-type source which was not the same as that of MORB.

It is important to note that, unlike the isotopic Pb data, the Bath-Dunrobin lavas do not plot closer to the HIMU end-member on Figure 6.10, principally because the OIB field in Hf-Nd isotope space is a reflection of the greater compatibility of Lu and Sm over Hf and Nd during normal mantle partial melting and differentiation over geological time. A depletion event in the past would preferentially remove Hf and Nd relative to Lu and Sm resulting in higher Sm/Nd and Lu/Hf ratios. Over time, these ratios would lead to depleted Hf and Nd isotope ratios. Therefore, the source region for the Jamaican plateau lavas underwent a substantial incompatible element depletion event which over time formed the depleted Nd and Hf isotope systematics seen in the lavas (Fig. 6.9). Thus, although the Bath-Dunrobin source region had a larger HIMU component, it was also subject

to larger degrees of partial melting during a period in the past which resulted in more-depleted Nd and Hf isotope signatures than other Caribbean plateau lavas.

The relative enrichment and depletion of incompatible trace element ratios, together with constant Nd, Pb and Hf isotopic values demonstrates that the Bath-Dunrobin plateau lavas are formed by differing degrees of partial melting, with the $(La/Yb)_{pmn}$ enriched samples requiring lower degrees of partial melting. The flat REE patterns and $(Gd/Yb)_{pmn}$ values of ~ 1 also show that there was either a lack of garnet in the source region thus suggesting spinel peridotite as a source material or that the extent of partial melting was high enough to melt the garnet in a garnet peridotite source region.

In summary, it is proposed that the Jamaican Bath-Dunrobin plateau basalts are formed by variable degrees of partial melting of a spinel or garnet peridotite source region composed of a HIMU and depleted plume component. This source region for the Jamaican lavas had a higher HIMU component than the rest of the Caribbean plateau lavas.

7.2.3 The Bath-Dunrobin tuffs

The 90 Ma tuffs represent CA, dacitic/rhyolitic pyroclastic deposits which must have originated from a nearby active convergent margin. They have characteristic arc-like chemistry with enrichments in Th and LREE relative to the HFSE and HREE (Figs. 6.4 and 6.25) and a significant negative Nb-Ta anomaly e.g. (La/Nb)pmn = 4.26-4.62 and (Ce/Ta)pmn = 0.83-1.45). Figure 6.4 also shows that the tuffs have primitive mantle-normalised multi-element patterns similar to Cretaceous island arc lavas from the Benbow Inlier, Jamaica and the Washikemba Formation, Bonaire. This comparison shows that the Bath-Dunrobin tuffs have similar arc chemistry to other arc rocks in the Caribbean, although the lower Cretaceous age of the Benbow and Washikemba lavas (Smit, 1977; Thompson *et al.*, 2004; Hastie *et al.*, 2007) precludes the tuffs from being petrogenetically related to these arc lavas.

Although pyroclastic rocks can be deposited > 1000 km from their source (Francis and Oppenheimer, 2004 and references therein), their presence within the Bath-Dunrobin lava succession suggests that ~ 90 Ma the Caribbean oceanic plateau

was located close to an active arc. To the author's knowledge, these are the first intercalated, arc-derived, tuff layers to be reported from Caribbean oceanic plateau successions (cf. Kerr *et al.*, 2003). Thus, this unique occurrence within the Bath-Dunrobin Formation is significant with regard to the evolution of the Caribbean plate. This is because the tuff layers provide evidence that the Caribbean oceanic plateau ~ 90 Ma may have been close to the subduction zone on the western side of South America and the Great Arc of the Antilles.

Consequently, the presence of these tuffs may indicate that the Caribbean oceanic plateau was too far to the east relative to North America at 90 Ma to encounter the Galapagos hotspot. This supports the conclusions of Pindell and Kennan (2001) and proposes that the Caribbean oceanic plateau was derived from another active hotspot in the Turonian-Coniacian that was further to the east relative to North America.

7.2.4 Summary

1. The Bath-Dunrobin Formation is composed of a thick sequence of late Cretaceous extrusive, tholeiitic, massive/pillow basalts, with intercalated tuffs which erupted in the Turonian-Coniacian (~ 90 Ma).
2. Immobile trace elements of the Jamaican rocks demonstrate that the Bath-Dunrobin lavas have a tholeiitic basaltic chemistry and that the tuffs are CA dacites/rhyolites.
3. The Bath-Dunrobin lavas are derived from the same heterogeneous mantle plume which formed the Caribbean oceanic plateau. Isotope data suggest that the mantle source region of the basalts was composed of a mixture between HIMU and a depleted component.
4. The Bath-Dunrobin source region is distinct from the source regions for other Caribbean oceanic plateau lavas because it has a larger HIMU component giving it more radiogenic Pb isotope ratios. When the constituent parts of the Caribbean plateau are considered as a single entity it is clear that the depleted end member is composed of a source region similar to the depleted plume component proposed for Iceland (Kempton *et al.*, 2000).

5. The island arc tuffs indicate that the Caribbean plateau was close to the volcanic arc along western South America and the Great Arc of the Antilles at ~ 90 Ma. Their presence also suggests that the Caribbean oceanic plateau may not have been derived from the Galapagos hotspot.

7.3 Petrogenesis of the Benbow island arc lavas

7.3.1 Fractional crystallisation in the Benbow lavas

Unlike the Bath-Dunrobin lavas, the degree of fractionation in the Benbow arc rocks cannot be modelled because no primitive Devils Racecourse lava has been discovered. However, decreasing concentrations of CaO, MnO and Sr with increasing Zr in both the upper and lower lavas indicates that plagioclase, clinopyroxene and Fe-Ti oxides are fractionating (Section E.10, Appendix E). TiO_2 decreases with increasing Zr in the lower Devils Racecourse lavas and increases in the upper lavas (Fig. 6.11), which is clearly due to the fractional crystallisation of Fe-Ti oxides in the lower Devils Racecourse magmas. This interpretation is supported by Figure 6.12 which indicates that the IAT lavas are formed by predominantly olivine, K-feldspar, plagioclase and Fe-Ti oxide fractionation. Additionally, the CA lavas are formed by fractional crystallisation of olivine, plagioclase, clinopyroxene and Fe-Ti oxides (Fig. 6.12). There is also evidence for minor amphibole fractional crystallisation because of the slightly lower Gd and Yb values in some of the IAT lavas (Fig. 6.12).

N-MORB-normalised multi-element plots and chondrite-normalised REE diagrams also show negative P and Eu anomalies. Eu in its reduced Eu^{2+} form is removed by plagioclase and alkali feldspars. Positive and negative P anomalies are respectively formed with a slab input and by P being removed from magmas because of the crystallisation of apatite.

7.3.2 The mantle wedge component

The upper Devils Racecourse lavas are more enriched than the lower Devils Racecourse lavas in LREE and Th relative to Y, the HFSE (including Nb and Ta)

and HREE. This enrichment could be due to smaller degrees of partial melting/larger degrees of fractional crystallisation and the input of a more enriched slab-derived component into the mantle source region of the upper Devils Racecourse lavas. Variable degrees of partial melting or fractional crystallisation alone cannot form the enrichment in the upper lavas because on an N-MORB-normalised multi-element plot (Figs. 6.15 and 6.16) the lavas have a characteristic arc-like negative Nb and Ta anomaly, which demonstrates that the upper and lower lavas have been enriched by a high LREE and Th component.

The negative Nb and Ta anomaly is produced by the input of an enriched slab-derived component into the source region of arc magmas (e.g. Elliott, 2003). The low concentration of Nb and Ta in the slab component is the result of the high $D_{slab/fluid}$ coefficient between Nb and Ta and the subducting slab and an aqueous fluid (e.g. McCulloch and Gamble, 1991; Pearce and Peate, 1995). This is in marked contrast to elements such as Ba, Rb, K, Sr, Th, LREE, U and Pb which have extremely low $D_{slab/fluid}$ values (e.g. McCulloch and Gamble, 1991; Pearce and Peate, 1995). Partial melting and/or fractional crystallisation alone would not produce a Nb or Ta anomaly because of the low K_D values of these elements during "normal" mantle melting well away from a subduction zone (e.g. McCulloch and Gamble, 1991).

Consequently, the enrichment in LREE, Th and U in the CA lavas relative to the IAT rocks is mostly due to either (i) the input of a more-enriched slab-derived component into the arc source region or (ii) the input of a larger volume of the same slab component into the source region of the upper Devils Racecourse lavas. Nevertheless, it is possible that variable partial melting and fractional crystallisation enhanced the enriched signature of the upper Devils Racecourse lavas.

Additionally, if the lavas formed by extremely low degrees of partial melting, ratios such as Nb/Zr, Ta/Hf and Ta/Yb would be affected because of the lower partition coefficients of Nb and Ta compared to Zr, Hf or Yb during normal mantle melting (see references in Appendix G). Small amounts of partial melting or large degrees of fractional crystallisation would increase the Nb/Zr, Ta/Hf and Ta/Yb ratios. Conversely, the input of a slab-derived component would not alter these ratios because the elements have $D_{slab/fluid}$ values >1 (Tatsumi *et al*, 1986; McCulloch and Gamble, 1991; Pearce and Parkinson, 1993; Keppler, 1996).

As can be seen in Figure 7.1, the lower IAT and upper CA Devils Racecourse lavas have similar Nb/Zr and Ta/Hf ratios. Thus it is not thought that partial melting or fractional crystallisation enhanced the enrichment of the CA lavas. These conservative element ratios also demonstrate that the mantle source component in the IAT and CA Benbow lavas had an N-type MORB composition. This N-MORB type input from the mantle wedge is confirmed by the Nb/Y-Zr/Y diagram on which both lava suites plot below the lower tramline of the plume-derived field of Fitton *et al* (1997) (Fig. 7.1).

Sr, Pb and Nd isotopes cannot be used for studying the chemistry of the mantle wedge component of an island arc lava because they are modified by the slab component (Section 7.3.3). However, it has been proposed that Hf is an ideal tracer for studying the chemistry of the mantle wedge because it is immobile during weathering and hydrothermal processes and is behaves conservatively in slab-derived aqueous fluids (White and Patchett, 1984; Pearce *et al.*, 1999). Conversely, Hf is non-conservative, much like Zr and Nb, in a siliceous melt derived from the subducting slab (Pearce and Peate, 1995). Nevertheless, Hf can be used in conjunction with other conservative elements (e.g. the Nb/Y-Zr/Y diagram of Fitton *et al.*, (1997) and the Th/Yb-Ta/Yb plot of Pearce (1982)) to determine the geochemistry of the mantle wedge because conservative elements should not be effected by aqueous slab-related components.

However, a recent study by Woodhead *et al.* (2001) has presented Nd and Hf isotopic evidence to indicate that conservative elements, including Hf, may be mobile in both aqueous fluids and siliceous melts from the subducting slab. If they are correct, it may not be appropriate to assume that the Hf isotopic systematics represent the mantle wedge composition when they could have been enriched by components from the descending slab. Nevertheless, if Hf is considered to be conservative, the $\varepsilon_{Hf}(i)$ values in Figure 6.20 demonstrate that the IAT and CA Devils Racecourse lavas have Atlantic/Pacific N-MORB ratios. This supports the Nb, Ta, Hf and Zr trace element data in Figure 7.1.

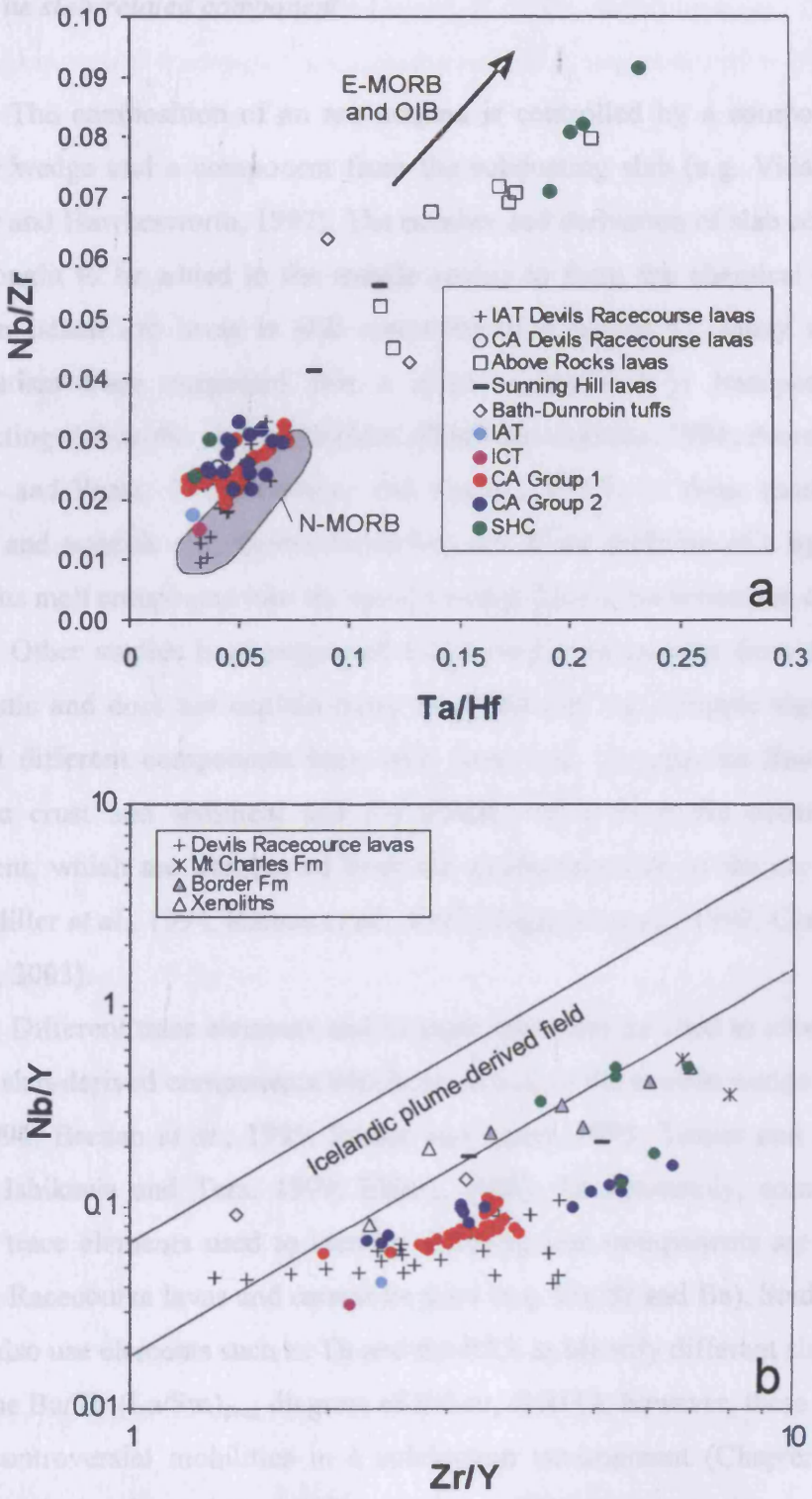

Figure 7.1 – (a) Nb/Zr-Ta/Hf ratio diagram and (b) the Nb/Y-Zr/Y diagram of Fitton *et al* (1997). The conservative elements show the N-MORB and ME-MORB composition of the mantle wedge of the various Jamaican arc lavas (see text).

7.3.3 The slab-related component

The composition of an arc magma is controlled by a component from the mantle wedge and a component from the subducting slab (e.g. Vidal *et al.,* 1989; Turner and Hawkesworth, 1997). The number and derivation of slab components that are thought to be added to the mantle wedge to form the chemical characteristics seen in island arc lavas is still controversial (Chapter 5). Many models of arc magmatism have suggested that a single component is transported from the subducting slab to the arc source (McCulloch and Gamble, 1991; Pearce, 1982, 1996; Pearce and Peate, 1995; Tatsumi and Kogiso, 1997). In these models the LILE, LREE and actinide enrichment forms because of the addition of a hydrous fluid or siliceous melt component into the mantle wedge during the formation of arc magmas.

Other studies have suggested that a single component from the slab is too simplistic and does not explain many trace element and isotopic signatures and so several different components have been proposed: (a) aqueous fluid from altered oceanic crust and sediment and (b) silicate melts from the oceanic basalt and sediment, which are transported from the subducting slab to the arc source region (e.g. Miller *et al.,* 1994; Brenan *et al.,* 1995; Regelous *et al.,* 1997; Class *et al.,* 2000; Elliott, 2003).

Different trace elements and isotopic ratios can be used to identify the nature of the slab-derived components which are added to the mantle wedge (e.g. Miller *et al.,* 1994; Brenan *et al.*, 1995; Pearce and Peate, 1995; Turner and Hawkesworth, 1997; Ishikawa and Tera, 1999; Elliott, 2003). Unfortunately, some of the most useful trace elements used to identify differing slab components are mobile in the Devils Racecourse lavas and cannot be used (e.g. Pb, Sr and Ba). Studies on modern lavas also use elements such as Th and the REE to identify different slab components (e.g. the Ba/Th-$(La/Sm)_{pmn}$ diagram of Elliott, (2003)), however, these elements have very controversial mobilities in a subduction environment (Chapter 5). It is still unclear whether Th and the LREE's can be mobilised in supercritical aqueous fluids, or if a slab-derived sedimentary melt is required (Chapter 5).

If, on a multi-element plot, a baseline is drawn connecting the conservative elements a qualitative measure of the whole subduction component can be determined. The abundance of elements up to the baseline represents the elemental

contribution given from the partial melting of the mantle wedge. The subduction component would represent the percentage of the non-conservative elements that lie above the baseline (Pearce, 1983; Pearce and Peate, 1995). An absolute percentage is difficult to determine unless the nature and degree of partial melting and fractional crystallisation can be calculated. Nevertheless, if the degree of partial melting and fractional crystallisation is moderate and the nature of the source area is constant, there should be little effect on the percentage abundances of the subduction contribution compared to the mantle wedge contribution.

However, Hawkesworth *et al.* (1991) suggested that it is unfeasible to consider the entire enrichment above the baseline as slab-derived. They used isotopes to determine that a large proportion of the elements above the baseline are derived from the mantle and not the slab. They proposed that slab-derived aqueous fluids are able to selectively leach the non-conservative elements from the mantle wedge en route to the zone of partial melting. To resolve this issue Pearce and Peate (1995) have re-defined the enrichment above the baseline to represent a slab-related, rather than a slab-derived, component.

Th, La, Ce, Pr and Nd are enriched above the baseline in N-MORB-normalised multi-element plots of averaged Jamaican lavas (Table 7.1). Sm is enriched in some of the Jamaican arc lavas but appears to be conservative in others. This is not surprising given that Sm is considered to be only slightly non-conservative (e.g. Tatsumi *et al.*, 1986; Pearce and Peate, 1995). Although P is also mobile in the subduction environment, P added via a slab component has not been assessed because of possible crystallisation of apatite during magma evolution.

The CA lavas of the upper Devils Racecourse Formation have higher absolute abundances of Nd than the IAT lavas, and they have higher average Nd/Yb ratios of 7.33 and 3.34 respectively. The higher Nd/Yb ratios in the CA lavas accompanied by the more enriched $\varepsilon_{Nd}(i)$ values can not be formed by moderate partial melting or fractional crystallisation processes. The differing $\varepsilon_{Nd}(i)$ value indicates that the CA lavas are derived from a different source region to the IAT lavas. This source region was more enriched in Nd (and presumably other incompatible trace elements) and had more enriched Nd isotope systematics. However, was the slab component composed of altered oceanic material, sedimentary material or both?

	Th	La	Ce	Pr	Nd	Sm
IAT, Devils Racecourse Formation	85	58	44	38	26	-
CA, Devils Racecourse Formation	94	84	78	71	63	39
Above Rocks lavas	90	64	54	46	36	-
Sunning Hill lavas	95	85	78	74	64	42
Bath-Dunrobin Tuffs	93	76	68	71	65	48
IAT, Central Inlier	88	73	64	61	46	33
ICT, Central Inlier	91	74	70	65	54	44
CA Group 1, Central Inlier	87	75	67	61	46	26
CA Group 2, Central Inlier	93	81	73	67	56	34
SHC, Central Inlier	94	80	64	61	55	21

Table 7.1 – The estimated percentage contribution of Th, LREE and Sm from the slab-related component for averaged Jamaican arc lavas. Pink, > 90%; Purple, 80-90%; Blue 70-80%; Green, 60-70%; Yellow, < 60%.

Although the different slab components cannot be quantified by immobile trace elements, the presence of a negative Ce anomaly (Figs. 6.15 and 6.16) in some of the Devils Racecourse lavas suggests that the slab-derived component contained a significant proportion of pelagic sedimentary material. Negative Ce anomalies are associated with phosphate-rich phases in pelagic sediments and red clay sediments in oxidising environments where Ce^{3+} is oxidised to Ce^{4+}. The Ce^{4+} in the sediments is more insoluble than La^{3+} and thus the slab-derived component has a negative Ce anomaly which subsequently forms a negative Ce anomaly in the arc lavas (Ben Othman *et al.*, 1989; McCulloch and Gamble, 1991; Plank and Langmuir, 1998; Elliott, 2003). Thus, the Ce anomalies in the Devils Racecourse lavas suggest that at least part of their slab-related component has a pelagic sedimentary affinity.

The IAT data on $(^{207}Pb/^{204}Pb)i$ – $(^{206}Pb/^{204}Pb)i$ and $(^{208}Pb/^{204}Pb)i$ – $(^{206}Pb/^{204}Pb)i$ plots forms mixing lines between ocean floor sediments and N-MORB. This supports the negative Ce anomalies and proposes that a sedimentary component is involved in the petrogenesis of the Benbow lavas.

Conversely, the origin of the elevated Devils Racecourse $(^{87}Sr/^{86}Sr)i$ ratios remains uncertain. Although a secondary alteration process could be responsible for the high ratios in the Bath-Dunrobin lavas, the Sr in the Devils Racecourse lavas does not appear to have been heavily mobilised (Fig. 6.11). O'Nions *et al.* (1978) demonstrated that the $^{87}Sr/^{86}Sr$ ratio of ocean floor basalts increases with secondary alteration processes without affecting the Nd isotope systematics. Therefore, if an oceanic crust-derived fluid entered the mantle wedge, any subsequent melting within the wedge would form an arc magma with a higher $^{87}Sr/^{86}Sr$ ratio than N-MORB (Hawkesworth *et al.*, 1979). Thus, the higher initial $^{87}Sr/^{86}Sr$ ratios in the Devils Racecourse lavas may be derived from a large aqueous fluid component from the altered crust of the subducting oceanic slab. Nevertheless, no unaltered minerals in the Devils Racecourse Formation were analysed for $^{87}Sr/^{86}Sr$ ratios, hence, the origin of the high values remains uncertain.

75% of the Sr and Pb budget of a typical arc basalt is derived from the slab-derived component (Pearce *et al.*, 1999). This is why the Sr and Pb isotope systems are commonly used for studying the source components of an arc magma. However, these isotopes are unreliable in the Devils Racecourse lavas. The Nd and Hf isotope systems are more resistant to alteration than the Sr and Pb isotopic systems.

Therefore, these ratios should represent the primary composition of the arc lavas (e.g. White and Patchett, 1984; Pearce *et al.*, 1999).

Nd is ideal for studying the subduction component because it is estimated that ~ 25% of the Nd budget of an average arc basalt is derived from the subducting slab (Pearce *et al.*, 1999). However, like Th, the mobility of Nd in subduction environments is controversial. While some argue that Th and the LREE (including Nd) are mobile in aqueous fluids derived from a subducting slab (e.g. Tatsumi *et al.*, 1986; Brenan and Watson, 1991; McCulloch and Gamble, 1991; Pearce and Peate, 1995, Keppler, 1996; Woodhead *et al.*, 2001), others contend that Th and the LREE are not mobile in a slab-derived aqueous fluid, and propose that the entire slab-derived Th and LREE budget in an arc magma is derived from a sediment melt (e.g. McDermott and Hawkesworth, 1991; Turner and Hawkesworth, 1997; Turner *et al.*, 1996 and Elliott, 2003). However, as has been noted in this Chapter and Chapter 5, this study considers the slab flux to represent a single component and that Th and the LREEs are mobile in aqueous fluids.

In the Benbow arc lavas, it is difficult to determine whether the $\varepsilon_{Nd}(i)$ enriched component is derived from a basaltic/sediment aqueous fluid and/or a sedimentary/basaltic melt. However, the Devils Racecourse lavas plot at the high $\varepsilon_{Nd}(i)$ end of the Bonaire samples and the Mariana, Izu-Bonin, Aleutian and New Britain arcs. These are termed the "fluid dominated arcs" by Woodhead *et al*, (2001) because, on component discrimination diagrams, their enrichment is considered to be formed by the metasomatism of their respective mantle wedges by basaltic/sediment aqueous fluids.

The Devils Racecourse data do not plot near the Sunda or Lesser Antilles data, which both have enriched (low) $\varepsilon_{Nd}(i)$ and $\varepsilon_{Hf}(i)$ values. It has been interpreted that the Lesser Antilles and Sunda arcs have been enriched by either a sedimentary melt from the descending slab or by assimilation of crustal material as the arc magmas ascend through the island arc crust (White and Dupre, 1986; Davidson, 1987; Thirlwall *et al*, 1996). It could therefore be argued that the addition of a sedimentary/crustal component/melt is of relatively minor importance in the petrogenesis of the Benbow lavas.

However, although the Devils Racecourse lavas plot with the "fluid dominated" arcs, the data could equally be explained by mixing between an N-MORB and a sedimentary source component. Woodhead *et al.* (2001) also assume that Th and LREE can only be transported in sedimentary melts, which is contrary to many other studies. Thus, the "fluid dominated" versus "sediment dominated" arc division of Woodhead *et al.* (2001) may not stand up to scrutiny.

In conclusion, the slab-derived component involved in the petrogenesis of the Devils Racecourse lavas was composed of material from both the subducting altered oceanic crust and of a possible sediment veneer on the subducting slab. Section 7.8 outlines the final conclusions on the potential source components of the island arc rocks.

7.3.4 Summary

1. The lower and upper Devils Racecourse lavas represent a Barremian – Aptian island arc succession.
2. The lower lavas are basaltic andesites to dacites/rhyolites and have a clear IAT chemistry. The upper lavas are CA basalts and basaltic andesites which frequently form pillow lavas.
3. Assessing the petrogenesis of the Benbow island arc lavas is difficult due to the mobility of many of the elements which are normally used in the study of modern intra-oceanic island arcs.
4. The Hf, Nb, Ta, Tb, Ho, Dy, Er, Yb, Lu and Y variation diagrams coupled with Nb/Zr, Ta/Hf and Ta/Yb ratios and the Hf isotopic evidence demonstrates that the IAT and CA Devils Racecourse arc lavas are derived from a chemically-similar mantle wedge of N-MORB composition.
5. The distinct Th and LREE/HFSE and HREE ratios and Sr-Pb-Nd-Hf isotope systematics indicate that the IAT and CA lavas were enriched by chemically distinct slab fluxes. These fluxes contained altered oceanic and sedimentary components.

7.4 The petrogenesis of the Above Rocks, Sunning Hill and the Bath-Dunrobin island arc rocks

7.4.1 Liquid lines of descent and fractional crystallisation

In addition to the CaO and MnO liquid lines of descent in Figure 6.21 (Section 6.5.2.2), the immobile elements in Figure 6.22 demonstrate that the Above Rocks lavas are predominantly formed by the fractional crystallisation of olivine, K-feldspar, plagioclase, Fe-Ti oxides, ± quartz and ± amphibole.

The liquid lines of descent for the incompatible immobile trace elements of the Above Rocks lavas and granodiorite suggest that they were derived from chemically different source regions (e.g. the lavas have a steeper trend in the Nb variation diagram) (Figs. 6.21, 6.22 and Section E.11, Appendix E). However, the lack of data from the Mt Charles and Sunning Hill lavas makes further comparisons impossible. Care should also be taken when studying the granodiorite liquid lines of descent because the pluton represents an evolved cumulate intrusion (Section E.11, Appendix E).

Nevertheless, the trace elements which form good liquid lines of descent imply a single chemically distinct source region for the Above Rocks lavas and indicate that the elements which do not form liquid lines of descent have been mobilised by sub-solidus alteration processes. The single source region also demonstrates that the slightly scattered trends of Co, Sc and Y are not the result of multiple source regions, but are formed because of the slight mobilisation of these respective elements (Section E.11, Appendix E). Many of the mobile elements (e.g. Na and Pb) may have also been mobilised in the granodiorite. However, the seemingly mobile behaviour of other elements such as Th in the granodiorite together with the less apparent trends in the immobile REE may be related to cumulate processes (Section E.11, Appendix E).

In Figure 7.2, the Above Rocks, Sunning Hill and Bath-Dunrobin lavas and tuffs are compared with the IAT and CA lavas from the Devils Racecourse Formation. The La-Zr diagram clearly shows that the Above Rocks, Sunning Hill and Bath-Dunrobin volcanics are more enriched in La at a given Zr content than the Devils Racecourse IAT. They also seem to be as enriched in La, and follow a similarly steep

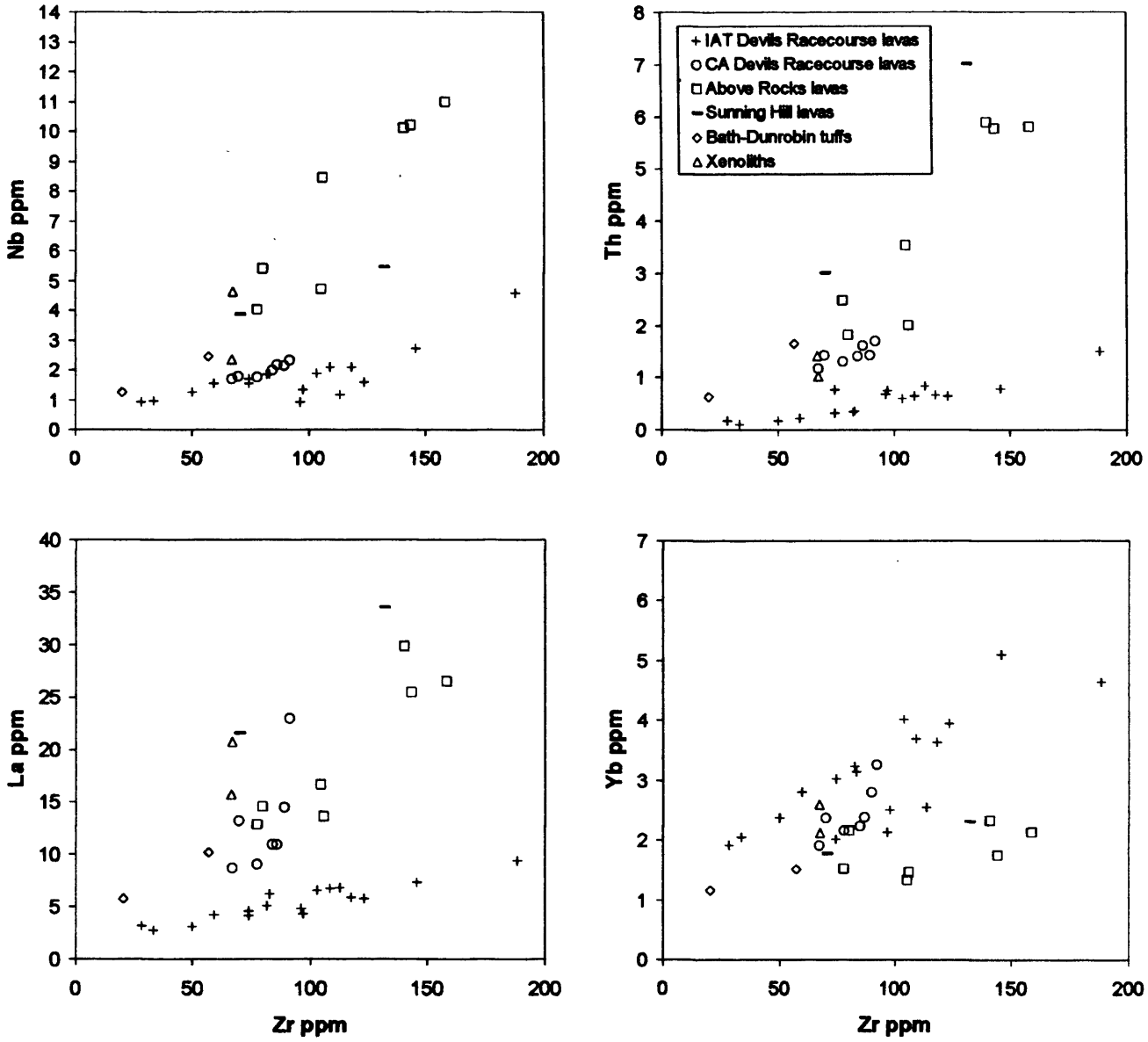

Figure 7.2 – Nb, Th, La and Yb-Zr variation diagrams showing the differing liquids lines of descent for the Benbow, Above Rocks, Sunning Hill and Bath-Dunrobin arc samples.

trend to the Devils Racecourse CA lavas. This is not that surprising considering that the Above Rocks, Sunning Hill and Bath-Dunrobin rocks are also CA in nature. The similar liquid lines of descent in La-Zr space implies that all the CA lavas (including the Devils Racecourse lavas) could be from the same source region.

However, a closer study of the La-Zr data demonstrates that the Devils Racecourse CA data form a steeper trend than the Above Rocks lavas (Fig. 7.2). Th, Nb and Yb-Zr variation diagrams also show that the Above Rocks data forms distinctly different liquid lines of descent than the Devils Racecourse CA lavas. Therefore, this implies that the Above Rocks and Benbow lavas are from chemically distinct source regions.

The Sunning Hill, Bath-Dunrobin and xenolith data cannot be interpreted as liquid lines of descent because of the lack of samples. Nevertheless, it can be seen in Figure 7.2 that these units may or may not be linked to the trends of the Above Rocks or Devils Racecourse lavas. The Sunning Hill lavas are more enriched in La and Th at a given Zr value than the Above Rocks and Devils Racecourse lavas. They are also more enriched and depleted in Nb than the Benbow and Above Rocks samples respectively. This implies that the Sunning Hill lavas could be derived from a chemically-different source region to the other lavas.

The data for the Bath-Dunrobin tuffs and xenoliths can be easily incorporated into the liquid lines of descent of the Above Rocks lavas in all of the diagrams in Figure 7.2. This suggests that the Bath-Dunrobin tuffs and xenoliths may have been derived from a source region chemically-similar to that of the Above Rocks lava source region.

7.4.2 Mantle wedge component

The Nb/Y-Zr/Y and Th/Yb-Ta/Yb diagrams show that the N-MORB involved in the petrogenesis of the Above Rocks, Sunning Hill and Bath-Dunrobin arc samples was either more enriched than the Devils Racecourse N-MORB end-member and/or had garnet in its source region. Figure 7.1 (a Nb/Zr-Ta/Hf diagram) shows that the Above Rocks, Sunning Hill and Bath-Dunrobin samples do not plot with the Benbow lavas and N-MORB, but, have more enriched Nb/Zr and Ta/Hf ratios towards E-MORB/OIB. Although the Nb/Y and Zr/Y ratios could be affected by garnet in the

source region the Nb/Zr and Ta/Hf ratios would not be affected. Additionally, the samples mostly plot below the lower tramline in the Nb/Y- Zr/Y diagram suggesting that the Nb and Ta enrichment is because of a more enriched MORB source. This "MORB-enrichment" also explains the high absolute abundances of Nb and Ta in the N-MORB-normalised multi-element diagram (Fig 6.25a), although these could also be enhanced by small degrees of partial melting or by high levels of fractional crystallisation (Fig. 6.22).

The classification of MORB as N or E-type MORB has been defined on the basis of trace elements such as La and Ce and Sr and Pb isotope ratios (Saunders *et al.*, 1988; Debaille *et al.*, 2006). Unfortunately these elements are either affected by alteration or enhanced by subduction components in the Jamaican arc lavas; thus the author is reluctant to define the enriched MORB end-member for the Above Rocks, Sunning Hill and Bath-Dunrobin arc samples as E-MORB. Instead the MORB end-member will be referred to as the 'more-enriched' MORB end-member (ME-MORB).

The Above Rocks and Sunning Hill lavas have $\varepsilon_{Hf}(i)$ values of + 11.86 -13.14, which are similar to the enriched Atlantic/Pacific N-MORB values (Nowell *et al.*, 1998; Kempton *et al.*, 2000) (Fig. 7.3). The more enriched nature of the MORB-type end-member for these arc rocks is demonstrated because they have lower $\varepsilon_{Hf}(i)$ values than the other arc rocks from Jamaica, Bonaire and from the Mariana, Aleutian, Izu-Bonin and New Britain arcs. The Border lavas, with regard to their $\varepsilon_{Hf}(i)$ values, plot towards the enriched end of the N-MORB field (Fig. 7.3). Consequently, assuming that Hf is conservative in the subduction environment, the enriched nature of the Above Rocks and Sunning Hill samples is due to a more chemically-enriched mantle wedge and not a result of a slab component or variable degrees of partial melting or fractionation.

7.4.3 Slab-related component

Unfortunately, the immobile trace elements of the Above Rocks and Sunning Hill samples do not hint at the nature of the slab-related component, although the element budget supplied to the mantle wedge via this slab component can still be qualitatively assessed (Table 7.1). The lack of a Ce anomaly does not necessarily

indicate that a sediment component was not involved. Sedimentary slab-derived fluids and melts can enrich the mantle wedge in non-conservative elements without producing a Ce anomaly (McCulloch and Gamble, 1991).

In Figure 7.3 the Border and Sunning Hill rocks have relatively enriched $\varepsilon_{Nd}(i)$ values, which plot below the N-MORB field indicating that an enriched Nd slab component was fluxed into the mantle wedge. The enriched $\varepsilon_{Nd}(i)$ values could also be partly derived from the more enriched MORB component. Both the Border and Sunning Hill samples have more enriched $\varepsilon_{Nd}(i)$ values than the CA Devils Racecourse lava ($\varepsilon_{Nd}(i)$ = + 8.12) and they have higher Nd/Yb ratios of 10.98 and 13.21 respectively. Moreover, the Border lavas have more enriched $\varepsilon_{Nd}(i)$ values (+ 6.15 - 6.40) than the Sunning Hill lava (+ 7.24). Consequently, the IAT and CA Devils Racecourse, the CA Border and CA Sunning Hill lavas represent at least four chemically different slab fluxes as indicated by the incompatible trace element ratios (Fig. 6.24 and Section 7.4.1).

The Sunning Hill lava has a higher initial $^{87}Sr/^{86}Sr$ ratio than the Border samples. Like the Benbow lavas, the origin of this higher initial $^{87}Sr/^{86}Sr$ ratio is uncertain and could be because of post-eruptive alteration processes. However, the lack of analysed Sunning Hill samples prevents the construction of a liquid line of descent which could demonstrate the potential mobility of the Sunning Hill lavas. Conversely, although the petrography of the lavas indicates that the rocks have been heavily altered (Chapter 4 and Table A.1, Appendix A) the initial $^{87}Sr/^{86}Sr$ ratios of the Border and Sunning Hill rocks may represent their primary geochemical compositions; the immobile character of the Sr in the Border lavas suggests that this may be the case.

Thus, the higher Sr ratios in the Sunning Hill lava (relative to the Border lavas) could be due to the assimilation of altered hydrous basalts or Cretaceous carbonates during magma ascent (Kerr *et al.*, 1996b). Moreover, the high values could also be because of the source region for the Sunning Hill lava having a larger altered oceanic crust-derived fluid or melt component (O'Nions *et al.*, 1978; Hawkesworth *et al.*, 1979). These considerations also apply to the high initial $^{87}Sr/^{86}Sr$ ratio in the granodiorite; however in this case the high ratio could also be explained by cumulate plagioclase phases introducing an "anomalous" chemistry to the granite. Nevertheless,

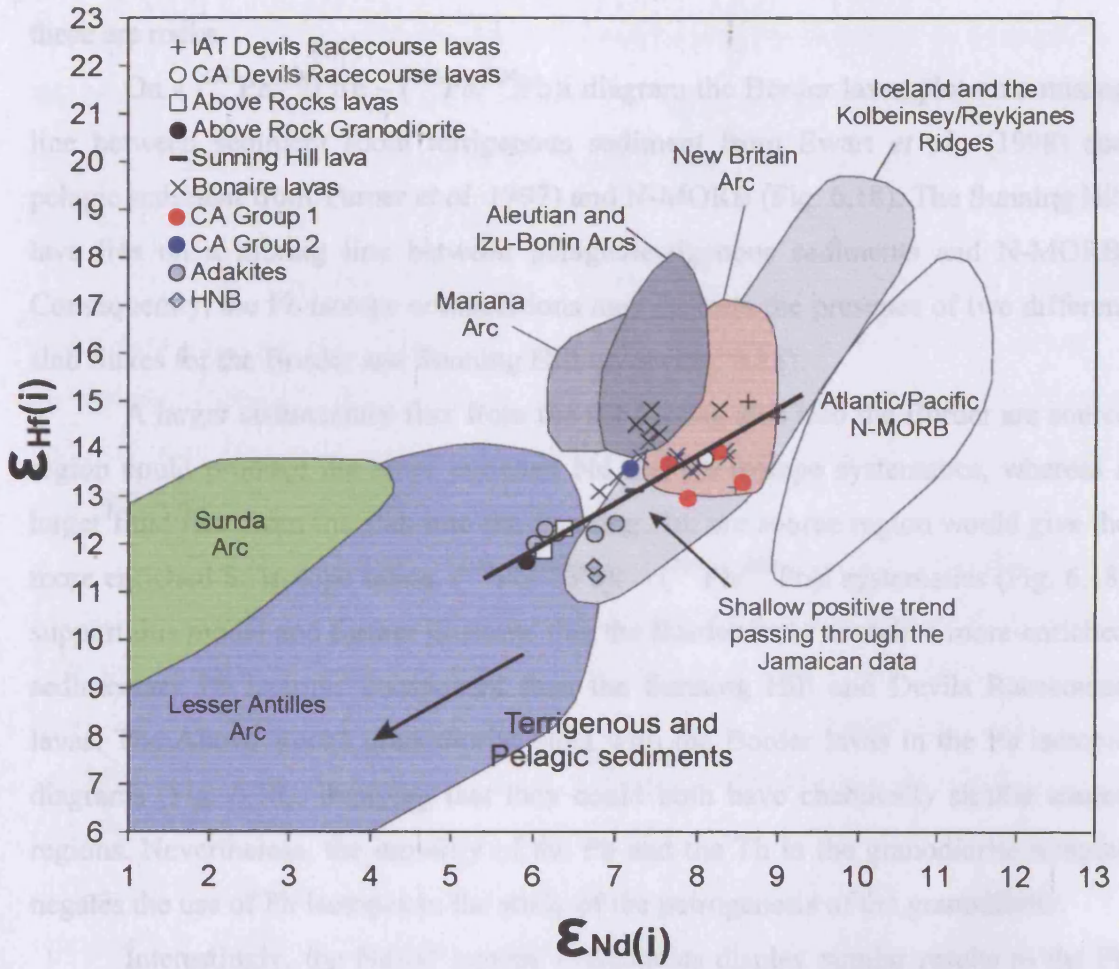

Figure 7.3 – Plot of $\varepsilon_{Nd}(i)$ - $\varepsilon_{Hf}(i)$ for the Jamaican island arc rocks which lie alongside fields for the Mariana, Aleutian, Izu-Bonin, New Britain, Sunda and Lesser Antilles island arcs. The shallow positive slope shows that as the Jamaican arc lavas become more enriched in $\varepsilon_{Nd}(i)$ they also become more enriched in $\varepsilon_{Hf}(i)$. Data sources for the island arcs are listed in Appendix F.

this uncertainty limits the use of Sr isotopes in assessing the petrogenesis of these arc rocks.

On a ($^{207}Pb/^{204}Pb$)i – ($^{206}Pb/^{204}Pb$)i diagram the Border lavas plot on a mixing line between sediment (both terrigenous sediment from Ewart *et al.*, (1998) and pelagic sediment from Turner *et al.* 1997) and N-MORB (Fig. 6.18). The Sunning Hill lava lies on a mixing line between pelagic/terrigenous sediments and N-MORB. Consequently, the Pb isotope compositions may indicate the presence of two different slab fluxes for the Border and Sunning Hill lavas (Fig. 6.18).

A larger sedimentary flux from the subducting slab into the Border arc source region could produce the more enriched Nd and Pb isotope systematics, whereas a larger fluid flux from the slab into the Sunning Hill arc source region would give the more enriched Sr isotope ratios. ($^{208}Pb/^{204}Pb$)i – ($^{206}Pb/^{204}Pb$)i systematics (Fig. 6.18) support this model and further illustrate that the Border lavas contain a more-enriched sedimentary Pb isotopic component than the Sunning Hill and Devils Racecourse lavas. The Above Rocks granodiorite plots with the Border lavas in the Pb isotopic diagrams (Fig. 6.18), implying that they could both have chemically similar source regions. Nevertheless, the mobility of the Pb and the Th in the granodiorite samples negates the use of Pb isotopes in the study of the petrogenesis of the granodiorite.

Interestingly, the Nd-Hf isotope systematics display similar results to the Pb isotopic data (Fig. 7.3). Both the Sunning Hill and Border lavas have lower $\varepsilon_{Nd}(i)$ and $\varepsilon_{Hf}(i)$ than the IAT and CA Devils Racecourse samples. Moreover, the Border lavas and the Above Rocks granodiorite are more enriched than the Sunning Hill lava. The Above Rocks and Sunning Hill lavas have $\varepsilon_{Nd}(i)$ ratios (+ 6.15 – 7.24) that are distinctly lower than the Atlantic and Pacific N-MORB field. This suggests that a slab-derived enriched Nd component has been introduced into the ME-MORB mantle wedge prior to partial melting and magma formation (Pearce *et al.*, 1999; Woodhead *et al.*, 2001).

A shallow trend can be drawn through the Jamaican data, on the $\varepsilon_{Nd}(i) - \varepsilon_{Hf}(i)$ plot from the Border lavas to the IAT Devils Racecourse samples (Fig. 7.3). The slope indicates that as the lavas become more enriched in $\varepsilon_{Nd}(i)$, they also acquire slightly more enriched $\varepsilon_{Hf}(i)$ values. The lower $\varepsilon_{Nd}(i)$ values in the arc lavas are derived from

the addition of an enriched slab-related component into their source regions. Therefore, if Hf is not conservative in the subduction environment, as proposed by Woodhead *et al.* (2001), the slight decrease in $\varepsilon_{Hf}(i)$ values with decreasing $\varepsilon_{Nd}(i)$ could be explained by a Hf-bearing component transferred from the subducting slab into the source region of the arc magmas.

As with the Benbow lavas, determining whether the $\varepsilon_{Nd}(i)$ enriched component is derived from a basaltic/sediment aqueous fluid and/or a sedimentary/basaltic melt is difficult. The Sunning Hill lava plots with the Bonaire data and with the "fluid dominated" Mariana, Izu-Bonin, Aleutian and New Britain arcs of Woodhead *et al.* (2001) (Fig. 7.3).

The Border lavas (and the granodiorite) plot with the "sediment dominated" Lesser Antilles arc; away from the "fluid dominated arcs" of Woodhead *et al.* (2001). Like the present-day Lesser Antilles arc, the source of the Border lavas may have been enriched by either a sedimentary melt from the descending slab or by assimilation of crustal material as the arc magmas ascend through the island arc crust (White and Dupre, 1986; Davidson, 1987; Thirlwall *et al.*, 1996; Woodhead *et al.*, 2001). HFSE are not thought to be mobile in slab-derived aqueous fluids, but are mobilised in sedimentary/basaltic melts (Tatsumi *et al.*, 1986; McCulloch and Gamble, 1991; Pearce and Peate, 1995). Therefore, the lower $\varepsilon_{Hf}(i)$ values in the Border lavas (and the Above Rocks granodiorite) could be derived from a slab-related component that was dominated by a sedimentary/basaltic melt. Equally, the more enriched nature could also be derived from a ME-MORB source region (Section 7.4.2).

However, like the Benbow lavas, it is unrealistic to conclude that the enrichment in Nd isotopes in the Sunning Hill lava was derived from a slab-related aqueous fluid (c.f. the fluid dominated arcs of Woodhead *et al.*, 2001), as the composition of the lava could equally be explained by mixing between N-MORB and a sedimentary source component. Section 7.8 will discuss the origin of the $\varepsilon_{Nd}(i)$, Th, U and LREE enriched slab-derived component in more detail.

7.4.4 Xenoliths

Of the two xenoliths analysed from the Above Rocks granodiorite, one has a composition (AHAR04), which demonstrates that it was derived from an ME-MORB source region (Fig. 7.1). The second xenolith (AHAR12) has conservative trace element systematics indicating that it was derived from an N-MORB source region, similar to the Devils Racecourse lavas (Fig. 7.1).

The xenoliths also have characteristic arc compositions with well-developed negative Nb and Ta anomalies in an N-MORB-normalised multi-element plot (Fig. 6.25). Neither of these samples were analysed for isotopes, however, their incompatible trace element ratios plot with samples from the CA Devils Racecourse and Above Rocks lavas and the Bath-Dunrobin tuffs (Fig. 6.21). Consequently, the xenoliths may be arc lavas from the Devils Racecourse, Mt Charles and/or Border Formations that were incorporated into the granodiorite as it intruded into the surrounding country rock.

7.4.5 Summary

1. The Above Rocks and Sunning Hill lavas are ~ 70.5 Ma old.
2. The Mt Charles lavas are composed of a CA andesite and dacite, the Border lavas are CA and SHC basaltic andesites and andesites, the xenoliths are CA basaltic andesites and the Sunning Hill lavas are composed of SHC basaltic andesite and dacite.
3. The Above Rocks, Sunning Hill and Bath-Dunrobin samples have been variably subjected to post-eruption alteration processes, which have mobilised many of their LILE.
4. All the samples have characteristic island arc chemistry. They are enriched in Th and LREE relative to the HFSE and HREE. They also have negative Nb and Ta anomalies on the N-MORB-normalised multi-element diagram.
5. The Nb, Ta, Tb, Ho, Dy, Er, Yb, Lu and Y variation diagrams coupled with Nb/Zr, Ta/Hf and Ta/Yb ratios demonstrate that the Above Rocks and Sunning Hill lavas, the Bath-Dunrobin tuffs and one of the xenoliths (AHAR04) are derived from a ME-MORB source region. The second

xenolith (AHAR12) has conservative trace element systematics indicating that it was derived from an N-MORB source region, similar to the Devils Racecourse lavas.

6. The Th and LREE/HFSE and HREE ratios and Nd and Hf isotope systematics indicate that these rocks have been contaminated by a more enriched slab-related component than the Devils Racecourse and Bonaire arc lavas. The Sunning Hill lavas have more enriched Th and LREE/HFSE and HREE ratios but the Border lavas have more enriched $\varepsilon_{Nd}(i)$ and $\varepsilon_{Hf}(i)$ values. The enriched Hf isotope ratios of the Border and Sunning Hill lavas could be explained by a slab-related melt or the ME-MORB source (see Section 7.8).
7. To conclude, the Above Rocks, Sunning Hill and Bath-Dunrobin samples were derived from different source regions that also differed from the source of the Benbow lavas. The Devils Racecourse lavas and AHAR12 were derived from an N-MORB source whereas AHAR04, the Above Rocks, Sunning Hill and Bath-Dunrobin rocks were derived from a ME-MORB source. Different slab components also enriched the Above Rocks, Sunning Hill and Bath-Dunrobin samples to form their differing trace element and $\varepsilon_{Nd}(i)$ and $\varepsilon_{Hf}(i)$ ratios.

7.5 The petrogenesis of the Central Inlier arc rocks

7.5.1 Liquid lines of descent and fractional crystallisation

A decrease in the liquid lines of descent for CaO, P_2O_5, TiO_2, FeO* and Sr in some of the Central inlier packages suggests plagioclase, Fe-Ti oxides and apatite fractional crystallisation (Sections 6.5.3.3 and 6.5.3.4). Additionally, Figure 6.31 indicates that the CA1 and CA2 igneous rocks are predominantly formed by the fractional crystallisation of olivine, plagioclase, Fe-Ti oxides, clinopyroxene and amphibole. Similarly, the SHC group formed by fractional crystallisation of olivine, plagioclase, amphibole and Fe-Ti oxides (Fig. 6.31).

In order to assess the petrogenesis of the Central inlier arc rocks, they are compared to the island arc samples from the Benbow, Above Rocks and Blue Mountains inliers. The La-Zr diagram in Figure 7.4 shows that the IAT and ICT samples plot with the IAT data from the Devils Racecourse Formation. The CA1 rocks have an intermediate trend between the IATs of the Devils Racecourse Formation and the CA lavas of the Above Rocks samples. The liquid line of descent for the CA2 lavas is parallel to the trend of the CA Above Rocks lavas, whereas the CA Benbow lavas have a steeper trend. The SHC lavas are the most enriched with higher La concentrations for a given Zr value. This could suggest that the CA1 lavas are from a chemically distinct source, whereas the CA2 and SHC samples may be related to some of the other Jamaican CA lavas.

However, the Th and Nb vs Zr variation diagrams demonstrate that the CA2 and SHC rocks have differing liquid lines of descent to the other Jamaican CA lavas, and thus, they are unlikely to be from a related source region (Fig. 7.4). In the Th diagram CA2 again shows a similar trend to the CA Above Rocks data, but, this trend is not observed in the Nb plot. The SHC has similar trends to the CA Benbow and Above Rocks samples in the La and Nb plots respectively, but has a different trend on the Th plot. The Th plot also suggests that the Waterworks and Crooked River samples have two differing trends.

La, Nb and Th should not be removed from a melt during moderate fractional crystallisation because they have very low partition coefficients in basaltic-andesitic melts for all fractionating minerals (see references in Appendix G); therefore, the increase of these elements reflects their increased concentration in the melt with increasing fractional crystallisation. The fact that the Central inlier rocks display liquid lines of descent with different trends to that of the other Jamaican samples indicates that they are not from a related source region.

On the Yb-Zr variation diagram, all of the CA1 samples and some of the CA2 rocks have trends which parallel those of the Benbow lavas (Fig. 7.4). The remaining CA2 data and all of the SHC samples lie on a trend line with the CA Above Rocks lavas below the other Jamaican data; they have low Yb concentrations at a given Zr abundance. Thus, the CA1, CA2 and SHC rocks were derived from chemically different source regions from both each another and the rest of the igneous rocks in Jamaica. Moreover, unlike Th, La and Nb, Yb in basaltic-andesitic melts is

compatible with amphibole and garnet. However, the low Yb values in the SHC, Above Rocks and some of the CA2 samples are not due to fractionating garnet and amphibole because the Yb trends are not decreasing. Additionally, although amphibole is a common fractionating mineral in CA and SHC magmas, garnet is not usually a fractionating phase in basaltic-rhyolitic melts (Pearce, 1982; Rollinson, 1993 and references in Appendix G).

Nevertheless, garnet may still be responsible for the low Yb abundances if these aforementioned lavas were derived from a source region in the garnet stability field of the mantle wedge (below 60 km depth). Garnet ± amphibole in the source region during partial melting followed by amphibole fractionation would produce lower Yb values while still forming a "normal" fractionating trend (Fig 7.4). In addition, the MREE, the other HREE and Y are also compatible with amphibole and garnet in basaltic-andesitic magmas; with compatibility in the order of HREE>Y>MREE (references in Appendix G). This increasing compatibility can be seen in the Central inlier variation diagrams (Figs. 6.30, 6.31 and E.12). There is a gradual decrease in the concentration of incompatible elements relative to Zr in, part of, and all of, the CA2 and SHC groups respectively from Th and the LREEs to the HREEs and Y.

All of the SHC samples have these lower Yb values and, thus, it is probable that garnet ± amphibole in the source region, produced their liquid lines of descent in Figure 6.30 and E.12. CA2 is more complex due to the group splitting into three trends. The samples from the Dry Hill unit maintain their more enriched liquid line of descent from Th and the LREEs to the HREEs. As such, these lavas probably originated from a source in the spinel stability field. In the second group the HREE and Y values decrease slightly so that CA2 samples from the Bulk Andesite unit have a similar liquid line of descent as the CA1 samples. These samples may represent a melt derived from a source with a small amount of garnet ± amphibole. The third group behaves comparable to the SHC samples and therefore they could be formed from a similar source region.

CA2 are composed of rocks which have HFSE, HREE and Y N-MORB-normalised concentrations of ~ 1. They are distinct from the CA1 samples because they have higher concentrations of Th and the LREE relative to their HFSE, HREE and Y contents (Figure 6.32). However, the CA2 group is also composed of samples

that have the same N-MORB-normalised Th and LREE enrichment but have much lower HREE and Y values (Fig. 6.32). These are the same samples that belong to the aforementioned third group, and which plot with the SHC group on the HREE and Y variation diagrams. The HREE and Y-depletion in these samples is probably because of garnet ± amphibole in their source region.

The SHC N-MORB-normalised multi-element plot also indicates the presence of two subgroups (Fig. 6.33). The Crooked River samples have a similar chemistry to the Th and LREE enriched, HREE and Y-depleted CA2 samples, although they have higher Th and LREE concentrations compared to their HREE and Y abundances. Thus, although they have a SHC chemistry, the Crooked River samples have N-MORB-normalised Nb and Ta values of ~ 1, but also have the depleted HREE and Y systematics indicating the presence of garnet ± amphibole in their petrogenesis.

The Waterworks ignimbrites have comparable chemistry to the Crooked River samples except that they have high N-MORB-normalised abundances of Nb and Ta, similar to the Above Rocks lavas, but still with depleted HREE and Y abundances. If the Waterworks and Crooked River units are derived from the same source region, the higher Nb and Ta values could be due to lower or higher degrees of partial melting or fractional crystallisation. Conversely, the high values may because of the Waterworks samples being derived from a different source region e.g. one with a higher Nb and Ta concentration.

The CA1 data splits into two liquid lines of descent in the TiO_2, FeO* and P_2O_5 variation diagrams. The decrease in concentrations does not provide any information on potential source regions, but merely represents the crystallisation of Fe-Ti oxides and apatite in the island arc magmas.

7.5.2 Mantle wedge component

The extremely low Nb and Ta values for the IAT and ICT samples demonstrates that their mantle source region could be more depleted in incompatible elements than N-MORB (Fig. 6.32). Some of the CA1 rocks also have slightly lower and higher normalised Nb and Ta abundances. However, these Nb and Ta values are accompanied by equally low and high HFSE, HREE and Y contents. This variation in

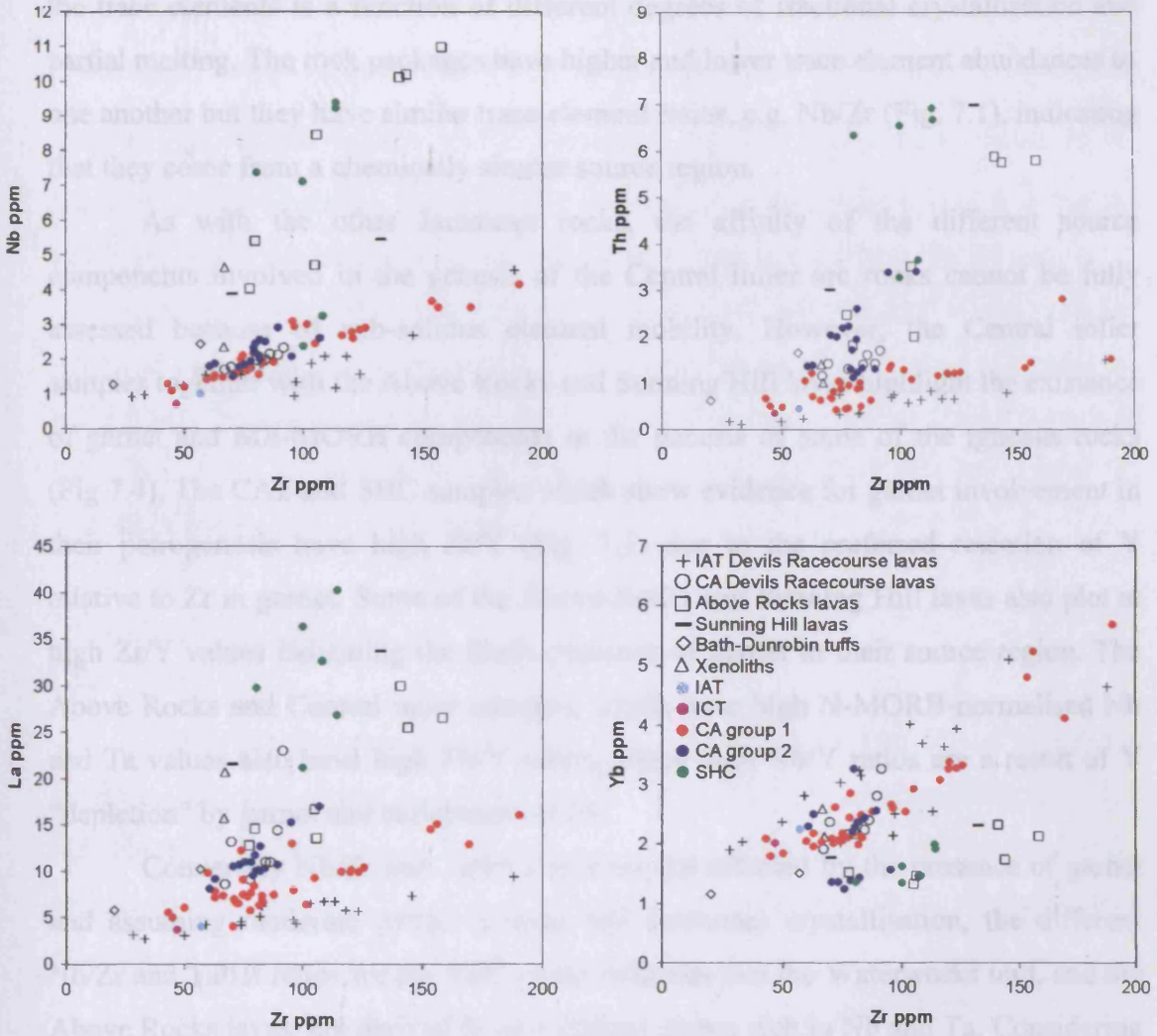

Figure 7.4 – Nb, Th, La and Yb-Zr variation diagrams showing the differing liquid lines of descent for the Central, Benbow, Above Rocks, Sunning Hill and Bath-Dunrobin arc samples.

the trace elements is a function of different degrees of fractional crystallisation and partial melting. The rock packages have higher and lower trace element abundances to one another but they have similar trace element ratios, e.g. Nb/Zr (Fig. 7.1), indicating that they come from a chemically similar source region.

As with the other Jamaican rocks, the affinity of the different source components involved in the genesis of the Central inlier arc rocks cannot be fully assessed because of sub-solidus element mobility. However, the Central inlier samples together with the Above Rocks and Sunning Hill lavas highlight the existence of garnet and ME-MORB components in the genesis of some of the igneous rocks (Fig 7.4). The CA2 and SHC samples which show evidence for garnet involvement in their petrogenesis have high Zr/Y (Fig. 7.1) due to the preferred retention of Y relative to Zr in garnet. Some of the Above Rocks and Sunning Hill lavas also plot at high Zr/Y values indicating the likely presence of garnet in their source region. The Above Rocks and Central inlier samples, which have high N-MORB-normalised Nb and Ta values also have high Nb/Y ratios. These high Nb/Y ratios are a result of Y "depletion" by garnet and enrichment of Nb.

Conversely Nb/Zr and Ta/Hf ratios are not affected by the presence of garnet and assuming moderate partial melting and fractional crystallisation, the different Nb/Zr and Ta/Hf ratios for the SHC group indicates that the Waterworks unit, and the Above Rocks lavas, are derived from a distinct source rich in Nb and Ta. Considering that Nb and Ta are usually conservative elements in the subduction environment, the enriched Nb and Ta component has to be related to the mantle wedge or to the assimilation of some Nb- and Ta-enriched material during magma ascent. Additionally, small amounts of partial melting of the same source region may also produce the high Nb and Ta characteristics in the Waterworks Formation.

The Nb/Zr-Ta/Hf and Nb/Y-Zr/Y diagrams show that the IAT and CA Devils Racecourse lavas, CA1, CA2 and Crooked River samples came from a chemically similar mantle wedge composed of N-MORB (Fig. 7.1). The Waterworks ignimbrites, Sunning Hill lavas, Bath-Dunrobin tuffs and Above Rocks lavas are enriched in Nb and Ta relative to Zr and Hf because they are derived from a mantle wedge composed of ME-MORB material. The Above Rocks, Sunning Hill, CA2 samples AHCI07, 08, 35-37, 62, and 63 and the Waterworks ignimbrites have a depletion of HREE and Y, indicating the likely importance of garnet ± amphibole in their petrogenesis (Fig. 7.4).

The Border lavas, and to a much lesser extent, the Sunning Hill lavas have lower $\varepsilon_{Hf}(i)$ values than the other Jamaican lavas, which are thought to be derived from an ME-MORB mantle wedge source region. The higher $\varepsilon_{Hf}(i)$ value in the Sunning Hill lava relative to the Border lavas, may be explained by the fact that the lava plots at the depleted end of the ME-MORB field in the Nb/Zr-Ta/Hf and Nb/Y-Zr/Y diagrams (Fig. 7.1). It is therefore the least ME-MORB-like of the enriched Jamaican arc samples. Consequently, the Waterworks ignimbrites may represent the ME-MORB-type end-member and the Sunning Hill lavas, Above Rocks lavas and Bath-Dunrobin tuffs may represent mixtures between the N-MORB source and the Waterworks-ME-MORB end-member.

7.5.3 Slab-related component

The immobile trace elements of the Central inlier samples do not hint at the nature of the slab-related component. Again, the lack of Ce anomalies does not indicate that a sediment component was not involved. Sedimentary slab-derived fluids and melts can enrich the mantle wedge in non-conservative elements without producing a Ce anomaly (McCulloch and Gamble, 1991).

The same trace element ratio plots used to determine the Th and LREE enrichment of the previous Jamaican arc rocks are used here to study the potential slab source components of the Central inlier samples (Fig. 6.33). The IAT sample plots at the enriched end of the IAT Devils Racecourse lavas, whereas the ICT lava mostly plots between the IAT and CA lavas of the Devils Racecourse and CA1 respectively (Fig. 6.33). The three other groups form distinct fields in all four of the trace element ratio diagrams, the CA2 and SHC groups being more enriched in Th, and the LREE relative to the HFSE, HREE and Y. CA1 is also clearly more enriched in these LILE and LREE than the IAT lavas of the Devils Racecourse Formation. Assuming that the rocks are formed by moderate degrees of partial melting and fractional crystallisation, the incompatible trace element ratios indicate that they were derived from chemically-different source regions.

If the Sr isotope systematics for all of the Jamaican arc rocks represent their primary compositions, the $(^{87}Sr/^{86}Sr)i$ - $\varepsilon_{Nd}(i)$ data suggests that the CA1 and CA2

samples are derived from different source regions to one another and the other Jamaican arc lavas. Conversely, if the high ($^{87}Sr/^{86}Sr$)i ratios at near constant ε_{Nd}(i) values in the Devils Racecourse and Sunning Hill lavas are an alteration feature, the primary ($^{87}Sr/^{86}Sr$)i ratios of these samples may be similar to the CA1 and CA2 compositions respectively (Fig. 6.17).

The immobility of Sr in some of the Jamaican arc lavas suggests that the ($^{87}Sr/^{86}Sr$)i ratios could represent the primary igneous values of the arc rocks, and so the ($^{87}Sr/^{86}Sr$)i increase in the Devils Racecourse and Sunning Hill lavas may be due to a slab flux dominated by aqueous fluids from altered oceanic crust or the assimilation of altered hydrous basalts or Cretaceous carbonates during magma ascent (O'Nions *et al.*, 1978; Hawkesworth *et al.*, 1979; Kerr *et al.*, 1996). Nevertheless, like the other Jamaican samples, this uncertainty limits the use of Sr isotopes in assessing the petrogenesis of these arc lavas.

In Figures 6.17, 6.20 and 7.3, the CA1 rocks have similar ε_{Nd}(i) values to the CA Devils Racecourse and the Sunning Hill lavas. The CA2 sample has a slightly more enriched (lower) ε_{Nd}(i) ratio than the Sunning Hill lava. All of the Central igneous rocks plot below the N-MORB field in Figures 6.17 and 6.20, indicating that a slab-derived Nd-enriched component was added to the mantle wedge. The CA2 lava plots below the CA1 rocks, demonstrating that a more Nd-enriched slab-related component was added to its source region (Fig. 7.1).

Ascertaining whether the ε_{Nd}(i) enriched component is derived from a basaltic/sediment aqueous fluid and/or a basaltic/sediment melt is very difficult. The Central samples plot with the Bonaire data and with the "fluid dominated" Mariana, Izu-Bonin, Aleutian and New Britain arcs (Fig. 7.3). However, even if the Jamaican rocks are related to a fluid-dominated arc, the distinction between a fluid from the altered crust and/or fluid from a sedimentary cover is not possible. This is because the discrimination diagrams developed to distinguish between different slab components utilise mobile elements (e.g. Elliott, 2003).

Nevertheless, the combined Sr-Pb-Nd isotope and incompatible trace element ratio data demonstrates that the CA1 and CA2 arc rocks are derived from at least 2 distinct slab-related components, which are compositionally unique in relation to the

Benbow, Above Rocks, Sunning Hill and the Blue Mountain arc rocks (Figs 7.3 and 7.4).

7.5.4 Summary

1. The CA1 sample AHCI39 has an age of 79.5 Ma and the Waterworks ignimbrites were deposited ~ 55.3 Ma.
2. The Central inlier rocks all have characteristic island arc affinities and can be sub-divided geographically and chemically into 14 sample packages or 5 rock groups. These 5 divisions are mainly based on the Th and LREE enrichment of the rocks and include the IAT, ICT, CA1, CA2 and SHC groups.
3. Conservative element abundances and ratios and isotopic values indicate that the Crooked River package, together with the IAT, ICT, CA1 and CA2 groups, are derived from similar N-MORB source regions to those of the IAT and CA Devils Racecourse Formation. The Waterworks Formation package is derived from a ME-MORB source, as are the Above Rocks, Sunning Hill and Bath-Dunrobin samples.
4. The Th and LREE/HFSE and HREE ratios and Nd and Hf isotope systematics indicate that the Central inlier igneous rocks have been contaminated by at least four enriched slab-related components (Figs. 6.27, 6.31, 6.33, 7.3 and 7.4).
5. The SHC group and part of the CA2 group are also derived from a source region containing garnet ± amphibole to form their depleted HREE and Y geochemistry.

7.6 The petrogenesis of the Newcastle adakites

7.6.1 Previous studies

As reviewed in Section 6.6, high-Al TTGs are rare and have mostly been found in Archean sequences principally because of the higher mantle temperatures at

that time, which meant that slab melting was more likely (e.g. Richter, 1985; Drummond and Defant, 1990). Conversely, lower mantle temperatures in the Phanerozoic prevent most subducting slabs from melting. However, some slabs do melt (Section 6.6.1) to form adakites (Drummond and Defant, 1990; Rapp *et al.*, 1991; Yogodzinski *et al.*, 1995).

Many adakite researchers have studied the petrogenesis of the TTGs and adakites on the basis of CIPW normative Ab-An-Or proportions and Sr/Y-Y contents (Section 6.6.1). However, as already discussed in Section 6.3.1, the alteration of the Jamaican samples precludes the use of normative values and Sr in assessing the petrogenesis of the adakites. Therefore, a full comparative study of Jamaican adakites with adakites in the literature is not possible.

7.6.2 Composition of a possible mantle wedge protolith

Jamaican adakites have low MREE, HREE and Y concentrations relative to Th, LREE, Zr and Hf. The scale of the depletion can be quantified by comparing the adakite trace element ratios with the ratios from the enriched Above Rocks lavas. The average $(La/Yb)_{n\text{-}mn}$ ratio and $(La)_{n\text{-}mn}$ value for the adakites is 24.11 and 5.55 respectively, whereas the Above Rocks lavas have an averaged $(La/Yb)_{n\text{-}mn}$ ratio of 13.41 and an averaged $(La)_{n\text{-}mn}$ value of 7.98. Thus, even though the Above Rocks lavas have higher La abundances (Appendix E), their $(La/Yb)_{n\text{-}mn}$ ratio is still significantly lower than the ratio in the adakites. This is because of the extremely depleted HREE and Y abundances relative to Th and the LREE values in the adakites.

Conversely, the average $(Th/Hf)_{n\text{-}mn}$ ratio for the adakites is 15.64 whereas the Above Rocks have an average ratio of 22.49. As with the $(La)_{n\text{-}mn}$ concentrations the Above Rocks lavas are more enriched in Th and the LREEs relative to the HFSE than the adakites.

Partition coefficients for the MREE, HREE and Y are >1 for clinopyroxene, hornblende, biotite, garnet, ilmenite, apatite and zircon in a dacitic/rhyolitic melt (see references in Appendix G). The partition coefficients for Nb and Ta are > 1 for hornblende, biotite, ilmenite and zircon in a dacitic/rhyolitic melt (Appendix G). The LREE are compatible in clinopyroxene, hornblende, biotite, ilmenite, apatite and zircon in a dacitic melt, while Th, Zr and Hf are compatible in amphibole, zircon and

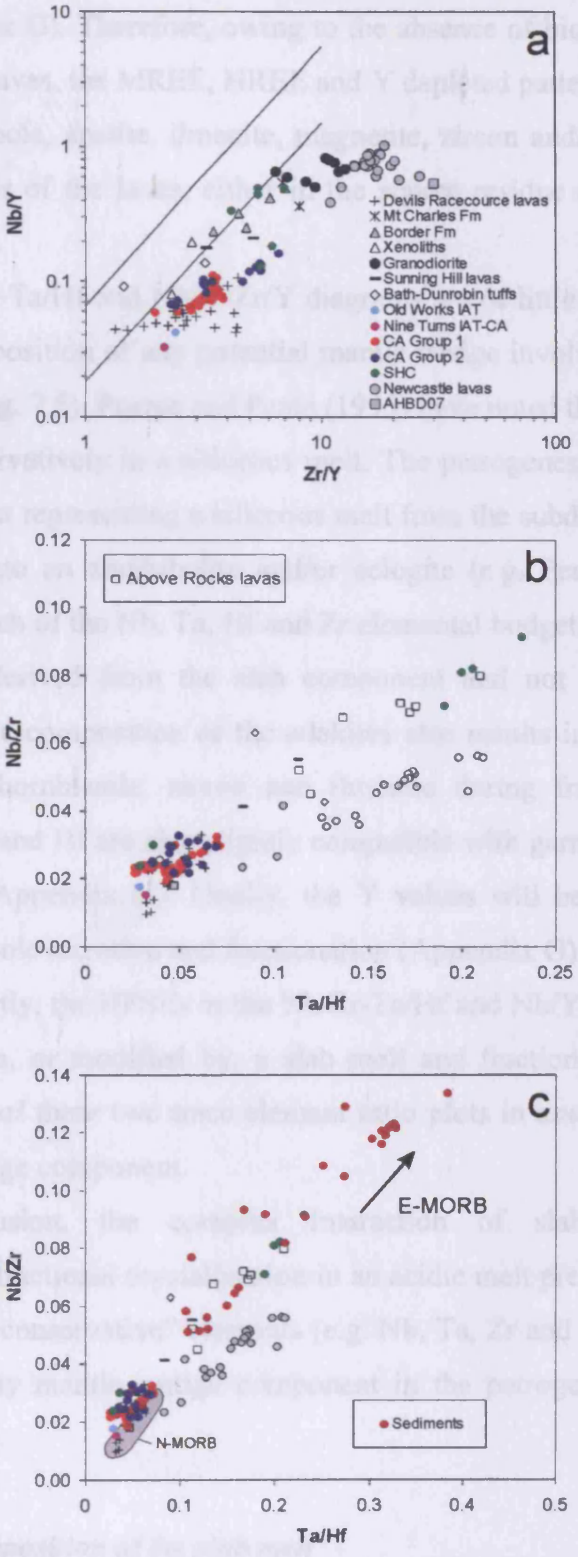

Figure 7.5 – (a) Nb/Y – Zr/Y diagram (Fitton *et al.*, 1997) and (b and c) Nb/Zr – Ta/Hf plots of the "normal" Jamaican arc and adakitic rocks. The "normal" Jamaican arc rocks include the Devils Racecourse, Mt Charles, Border, Sunning Hill, Bath-Dunrobin and Central inlier samples.

ilmenite (Appendix G). Therefore, owing to the absence of biotite and clinopyroxene in the Newcastle lavas, the MREE, HREE and Y depleted patterns could be formed as a result of amphibole, apatite, ilmenite, magnetite, zircon and/or garnet involvement in the petrogenesis of the lavas, either in the source residue and/or as fractionating phases in the melt.

The Nb/Zr-Ta/Hf and Nb/Y-Zr/Y diagrams are of little use in determining the geochemical composition of any potential mantle wedge involved in the petrogenesis of the adakites (Fig. 7.5). Pearce and Peate (1995) have noted that many of the HFSEs behave non-conservatively in a siliceous melt. The petrogenesis of adakites relies on the slab component representing a siliceous melt from the subducting slab when it has been converted into an amphibolite and/or eclogite (e.g. Pearce and Peate, 1995). Consequently, much of the Nb, Ta, Hf and Zr elemental budget of the Newcastle lavas may have been derived from the slab component and not the mantle wedge. In addition, the acidic composition of the adakites also results in the Nb and Ta being compatible with hornblende, zircon and ilmenite during fractional crystallisation (Appendix G). Zr and Hf are also slightly compatible with garnet, zircon and ilmenite and hornblende (Appendix G). Finally, the Y values will be affected by probable garnet and amphibole retention and fractionation (Appendix G) (Fig. 7.5).

Consequently, the HFSEs in the Nb/Zr-Ta/Hf and Nb/Y-Zr/Y plots could have been derived from, or modified by, a slab melt and fractional crystallisation. This precludes the use of these two trace element ratio plots in assessing the composition of any mantle wedge component.

In conclusion, the complex interaction of slab melting, peridotite hybridisation and fractional crystallisation in an acidic melt prevents the use of any of the "incompatible conservative" elements (e.g. Nb, Ta, Zr and Hf) in determining the composition of any mantle wedge component in the petrogenesis of the Jamaican adakites.

7.6.3 Possible composition of the slab melt

Additional trace element ratio data are presented in Figure 7.6. For the other Jamaican arc rocks, the elements in these diagrams are essentially incompatible. The exceptions to this would include some small possible garnet and/or amphibole and

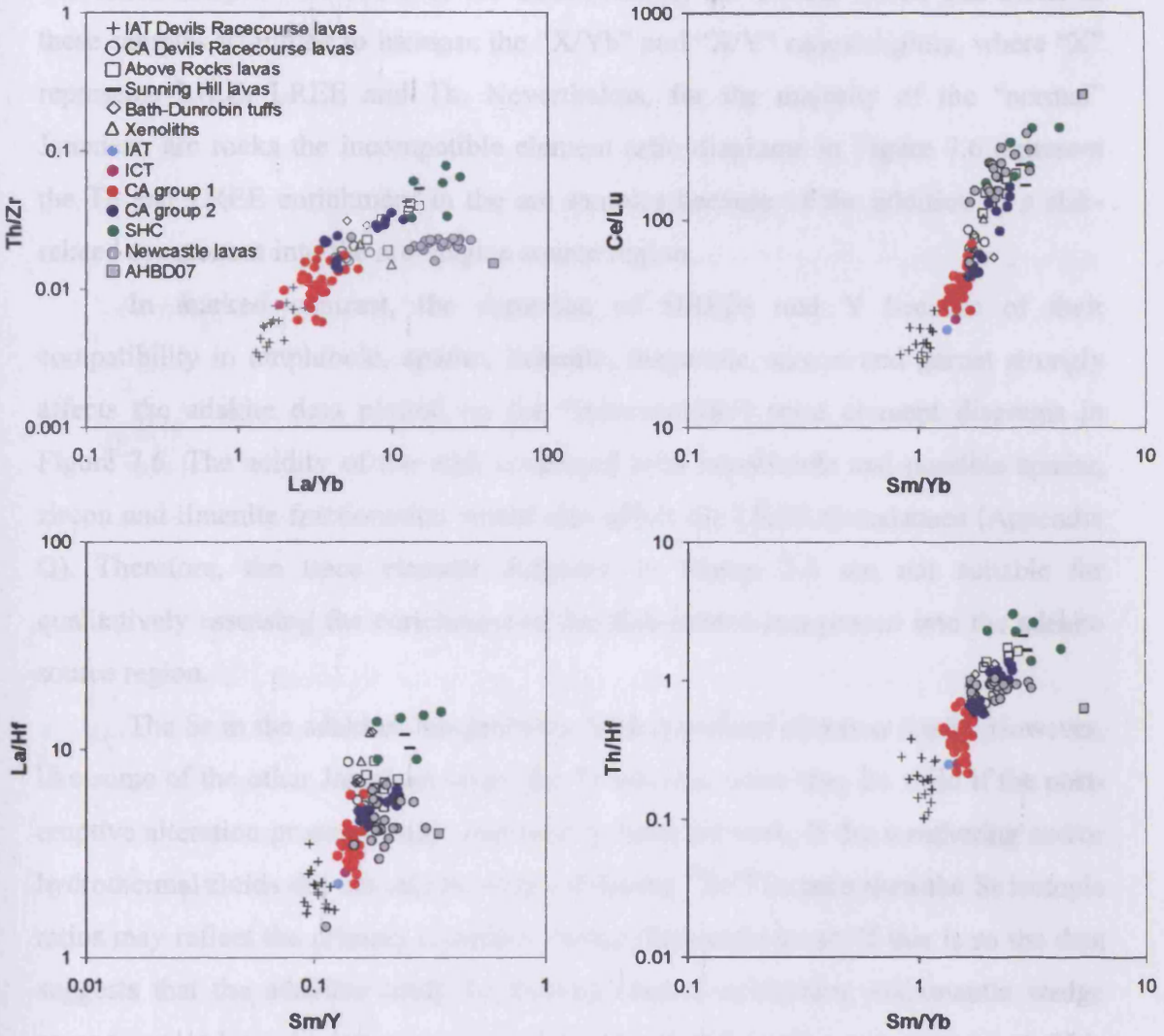

Figure 7.6 - Th/Zr-La/Yb, Ce/Lu-Sm/Yb, La/Hf-Sm/Y and Th/Hf-Sm/Yb discrimination diagrams showing the LILE, LREE and actinide enrichment of the Newcastle adakites relative to the other Jamaican arc rocks.

apatite involvement in the petrogenesis of the Above Rocks lavas, Waterworks Formation samples and some of the CA2 rocks in the Central inlier. The effect in these samples would be to increase the "X/Yb" and "X/Y" ratios slightly, where "X" represents LILE, LREE and Th. Nevertheless, for the majority of the "normal" Jamaican arc rocks the incompatible element ratio diagrams in Figure 7.6 represent the Th and LREE enrichment in the arc samples because of the addition of a slab-related component into the arc magma source region.

In marked contrast, the depletion of HREEs and Y because of their compatibility in amphibole, apatite, ilmenite, magnetite, zircon and garnet strongly affects the adakite data plotted on the "incompatible" trace element diagrams in Figure 7.6. The acidity of the melt combined with hornblende and possible apatite, zircon and ilmenite fractionation would also affect the LREE abundances (Appendix G). Therefore, the trace element diagrams in Figure 7.6 are not suitable for qualitatively assessing the enrichment of the slab-related component into the adakite source region.

The Sr in the adakites has probably been mobilised (Section 6.6.3). However, like some of the other Jamaican lavas, the Sr isotopic ratios may be valid if the post-eruptive alteration processes only *removed* Sr from the rock. If the weathering and/or hydrothermal fluids did not add Sr with a different $^{87}Sr/^{86}Sr$ ratio then the Sr isotopic ratios may reflect the primary chemistry of the Newcastle lavas. If this is so the data suggests that the adakites could be derived from a subducting slab/mantle wedge component and a pelagic/terrigenous sedimentary/continental crust component. This hypothesis is supported by the Nd-Hf isotope systematics in Figure 6.20 where the adakites plot on a theoretical mixing line between Atlantic/Pacific N-MORB and Pelagic/Terrigenous sediment.

The Sr and Nd isotope ratios of the adakites are more enriched (lower $\varepsilon_{Nd}(i)$ and higher $(^{87}Sr/^{86}Sr)i$) than most of the other intra-oceanic island arc samples (Fig. 6.17). If these adakites are partly composed of a siliceous slab melt component, this may increase the initial $^{87}Sr/^{86}Sr$ ratio of the mantle source be cause of the high $^{87}Sr/^{86}Sr$ ratio of altered, subducted ocean floor basalts (O'Nions *et al.*, 1978; Hawkesworth *et al.*, 1979). The enriched Sr and Nd ratios could also be derived from a sedimentary veneer on the slab. This sediment would also partially melt with the basaltic slab and could transport a more-enriched Nd and Sr component into the

mantle source that would subsequently form the adakite magmas. Conversely, the more enriched isotope ratios may be formed by the assimilation of crustal island arc rocks, hydrous MORB and plateau basalts and/or Cretaceous carbonates into "normal" adakitic magmas to form their enriched Nd and Sr isotope ratios.

Although the Pb isotope results cannot be used to quantifiably model the petrogenesis of the adakites, the extremely enriched (high) Pb ratios (Fig. 6.18) can not be explained by secondary alteration processes alone. The Pb isotopes suggest that the Newcastle arc magmas were contaminated with a U-Th enriched component during formation. This excess Th and U would, over time, produce the enriched radiogenic Pb isotope systematics (Fig. 6.18). HIMU components have high U/Pb and Th/Pb ratios (e.g. Hart, 1988; Hart *el al.*, 1992) and it is interesting to note that the plateau lavas in Jamaica have a larger HIMU-type isotopic signature than other plateau rocks in the Caribbean (Section 7.2). Therefore, could a HIMU-type component be involved in the petrogenesis of the adakite magmas?

Sediments can also contain large concentrations of Th and U. Th is found in significant quantities in continental detritus and can be scavenged by Fe-Mn oxyhydroxides and clays (Ben Othman *et al.*, 1989; Plank and Langmuir, 1998). U is abundant in detrital phases and in reducing pelagic sediments (Ben Othman *et al.*, 1989; Plank and Langmuir, 1998). The Th and U concentrations in these sediments are then either enriched or depleted depending on the volume of biogenic oozes which they are associated with; biogenic oozes are very affective at diluting Th, REE, Pb and U concentrations in sediments (Plank and Langmuir, 1998).

Therefore, although sediments do not have the high Pb ratios seen in the adakites, a small partial melt of a sediment veneer which is composed of terrigenous and detrital pelagic clays and turbidites with little or no biogenic oozes may produce a U-Th rich melt. This melt could mix with further magmas from the subducting slab to produce a magma with very high Th/Pb and U/Pb ratios which will subsequently react with the overlying peridotite to form the adakitic melts. Ben Othman *et al* (1989) have also argued that hydrothermally-altered ocean crust is enriched in U, while the Pb is mobilised and removed.

Consequently, the high Pb isotopic ratios could be derived from several sources. The ratios have been increased by time-integrated decay of a Th- and U-enriched component, which was added to the adakite source region ~ 52 Ma. This

enriched Th and U component could be derived from (a) a small-degree sedimentary melt from a subducting slab and/or (b) from the melting/assimilation of a HIMU-type oceanic plateau component, and/or (c) melting of hydrothermally-altered subducted oceanic crust.

Additionally, the relatively enriched $\varepsilon_{Nd}(i)$ and $\varepsilon_{Hf}(i)$ values demonstrate that the adakites cannot be derived from either a DMM-derived melt which has subsequently fractionated or from a solely basaltic slab melt. Sm, Nd, Hf and Lu are immobile during the alteration of oceanic crust. Consequently, if these elements had been derived from either of the two aforementioned sources alone, the samples would be expected to plot in or near to the N-MORB field in Nd and Hf isotopic space. The relatively low Nd and Hf isotopic ratios support the Pb isotopic data and suggest that a U/Pb, Th/Pb, $\varepsilon_{Nd}(i)$ and $\varepsilon_{Hf}(i)$ enriched component was present during the genesis of the adakite magmas. Unfortunately the $\varepsilon_{Nd}(i)$ and $\varepsilon_{Hf}(i)$ values do not indicate whether this was a sedimentary melt or a HIMU-type oceanic plateau melt.

7.6.4 Modelling adakite fractional crystallisation

The chemistry of the adakites is partly formed by fractional crystallisation processes. It has already been shown that the fractionation of K-feldspar, plagioclase feldspar, quartz, magnetite, clinopyroxene, hornblende, biotite, ilmenite, apatite and zircon can modify an andesitic/dacitic adakite melt. To determine which minerals were fractionating to alter the chemistry of the Newcastle adakites the lavas have been plotted on logged variation diagrams in Figure 6.37. Logged Ce-Nb, Dy-Nb and Y-Nb variation diagrams have also been presented in Figure 7.7 to support the findings of the diagrams in Figure 6.37 and to develop a theoretical crystallising assemblage that would explain the adakite liquid line of descent. The range of elements plotted will demonstrate how Th, U, LREE, MREE, HREE and Y behave during the fractional crystallisation of these adakites.

The mineral vectors were calculated using the equilibrium crystallisation equation: $C_l/C_O = 1/[D + F(1 - D)]$, as in Chapter 6. Partition coefficient data and sources can be found in Appendix G. AHWG34 trace element data were again used

for the C_O values because high Cr, Ni, Co and low silica concentrations demonstrate that this sample is one of the most primitive of the adakites (Appendix E).

Figures 6.37 and 7.7 demonstrate that with regards to Y and the HREE the Newcastle adakites require fractional crystallisation of predominantly K-Feldspar, quartz and plagioclase feldspar. Small amounts of apatite and/or amphibole are also needed due to the majority of the data falling below the K-Feldspar, quartz and plagioclase feldspar trend lines (Figs. 6.37 and 7.7). AHBD07 has much lower trace element abundances than the other adakites. If the sample is petrogenetically related to the other adakites, it could be formed by predominantly ilmenite, ± apatite fractionation (Figs. 6.37 and 7.7).

With regard to the Th, U and the LREE, most of the lavas can be formed by predominantly K-feldspar, quartz and plagioclase fractionation. The majority of the samples also require amphibole and/or apatite and/or magnetite fractionation (Figs. 6.37 and 7.7). AHBD07 also require ilmenite and/or biotite fractionation. The variation diagrams for Dy and Gd (the MREE) mirror these results, and additionally indicate that ilmenite fractionation may be required to form AHBD07 (Figs. 6.37 and 7.7).

Modelling demonstrates that the fractionation trend for the majority of the Newcastle adakites can be explained by up to 60 % fractional crystallisation from a starting composition represented by AHWG34. The alteration of the major elements and the lack of micro-probe analyses on the phenocryst assemblages prevent the fractioning assemblage from being modelled using least squared analysis. However, the mineral vectors in Figures 6.37 and 7.7, the presence of plagioclase feldspar, K-feldspar, amphibole and quartz phenocrysts in the adakites in combination with the modelling suggest that the fractionating assemblage would include predominantly plagioclase feldspar, K-Feldspar, amphibole, quartz, ilmenite and apatite crystallising in the ratio 50:16:5:6:2:1 respectively (Fig. 7.7 and Appendix G). Clinopyroxene and biotite are not considered to be part of the fractionating assemblage because of their absence in the adakites.

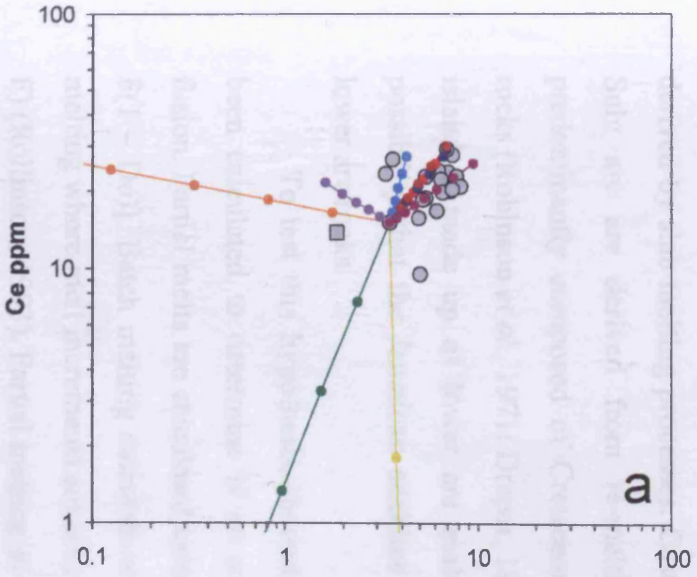

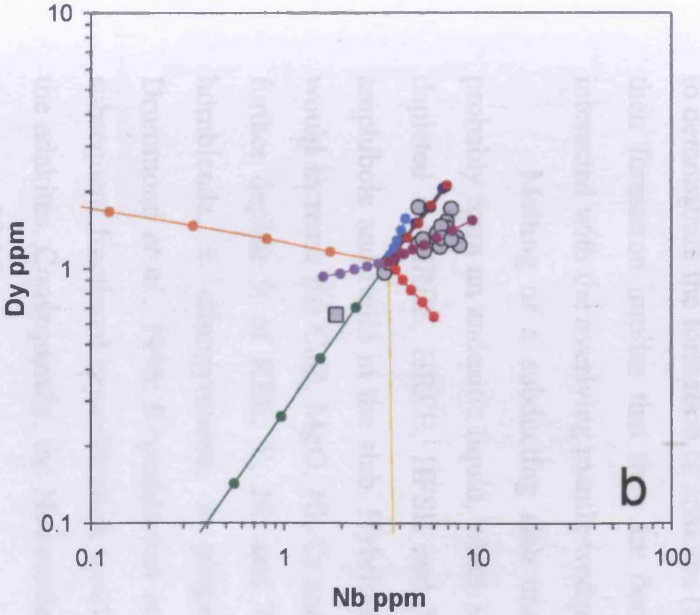

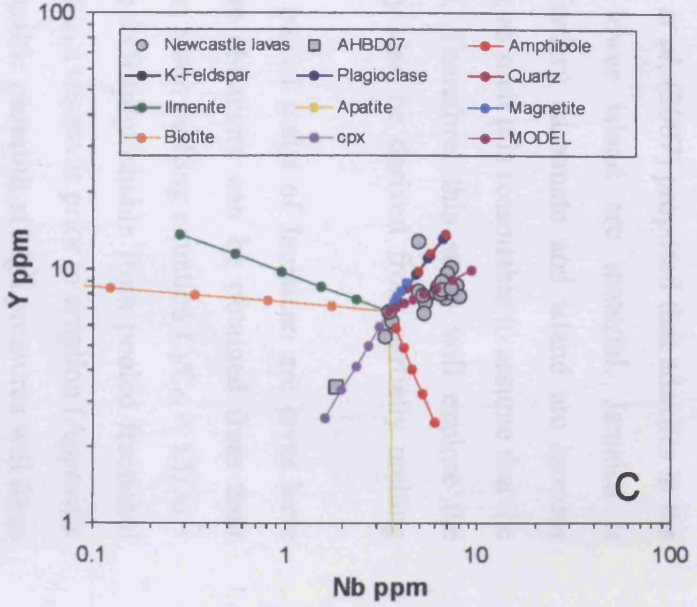

Figure 7.7 – Ce-Nb, Dy-Nb and Y-Nb variation diagrams with vectors showing the composition of plagioclase, K-feldspar, quartz, amphibole, clinopyroxene, biotite, magnetite, ilmenite and apatite with up to 50% fractional crystallisation of the AHWG34 starting composition (each tick represents 10% crystallisation) (Appendix E). The MODEL composition represents the liquid line of descent of a modelled acidic melt with up to 70% fractional crystallisation of 61.25% plagioclase, 20% K-feldspar, 7.5% amphibole, 7.5% quartz, 2.5% Ilmenite and 1.25% apatite (each tick represents 10% crystallisation).

7.6.5 Modelling the formation of the adakites

There are several models in the literature which have been proposed in order to demonstrate the formation of adakites (Section 6.6.1). The most common model for their formation implies that they are derived from a slab melt which has variably interacted with the overlying mantle wedge (e.g. Drummond and Defant, 1990).

Melting of a subducting slab under amphibolite-eclogite conditions would probably form an andesitic liquid, which was enriched in LILE, LREE, Th and U but depleted in MREE, HREE, HFSE and Y due to the retention of residual garnet, amphibole and rutile in the slab. Hybridisation of the adakite liquids with peridotite would increase the CaO, MgO, Ni, Cr and Co concentrations in the melt and in turn further deplete it of REE, Y, Nb and Ta because of orthopyroxene, ± garnet, ± hornblende, ± clinopyroxene, ± plagioclase, and ± spinel fractionation (e.g. Drummond *et al.,* 1996; Kepezhinskas *et al.,* 1996). As the modified melt ascends, subsequent fractional crystallisation would further alter the trace element budget of the adakites. Consequently, the Newcastle lavas may have been derived by a similar process ~ 52 Ma.

Conversely, other researchers have shown that some adakitic melts may not be derived by slab melting processes. Castillo *et al,* (2007) proposed that adakites in the Sulu arc are derived from re-melting lower island arc material. Jamaica is predominantly composed of Cretaceous-Tertiary carbonate and island arc igneous rocks (Robinson *et al.*, 1971; Draper, 1986); as such it is reasonable to assume that the island is made up of lower arc material. Therefore, this study will explore the possibility that the Jamaican adakites may also be derived from partially melting lower arc rocks.

To test this hypothesis, theoretical partial melts of Jamaican arc lavas have been calculated to determine if an adakite chemistry can be obtained from their fusion. Partial melts are calculated using the batch melting equation $C_l/C_O = 1/[Do + F(1 - Do)]$. Batch melting calculations are indistinguishable from pooled fractional melting where melt increments are collected in a reservoir prior to eruption (Appendix F) (Rollinson, 1993). Partial melting of a basaltic protolith at high pressures will form intermediate magmas, and as such, partition coefficients for andesitic liquids are used in the modelling calculations (e.g. Drummond and Defant, 1990) (Figs 7.8 and 7.9).

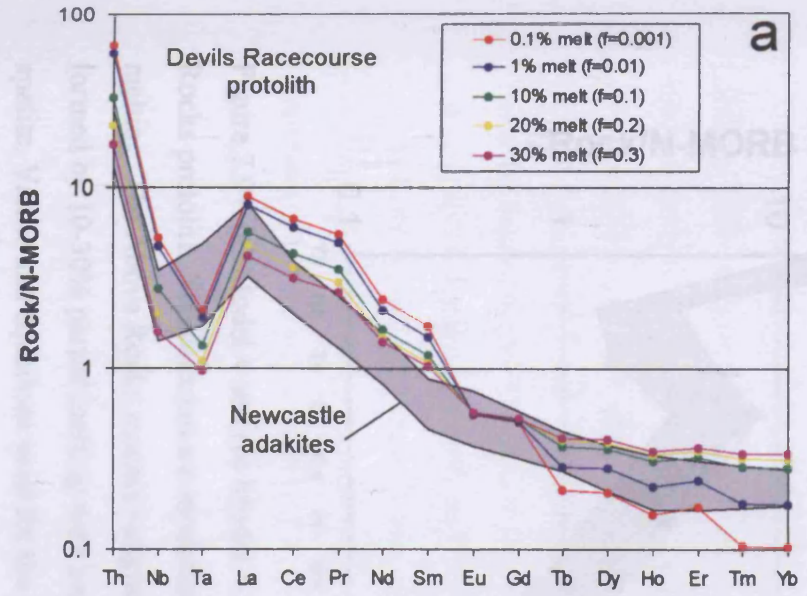

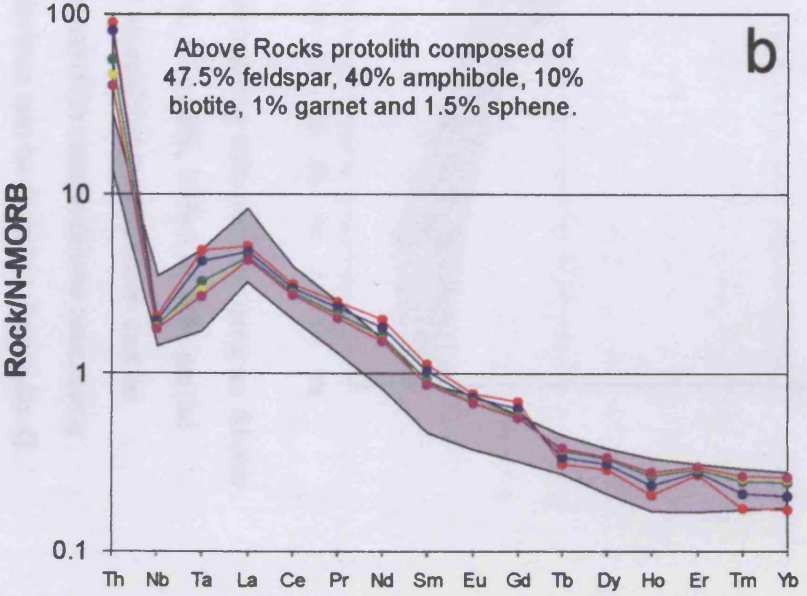

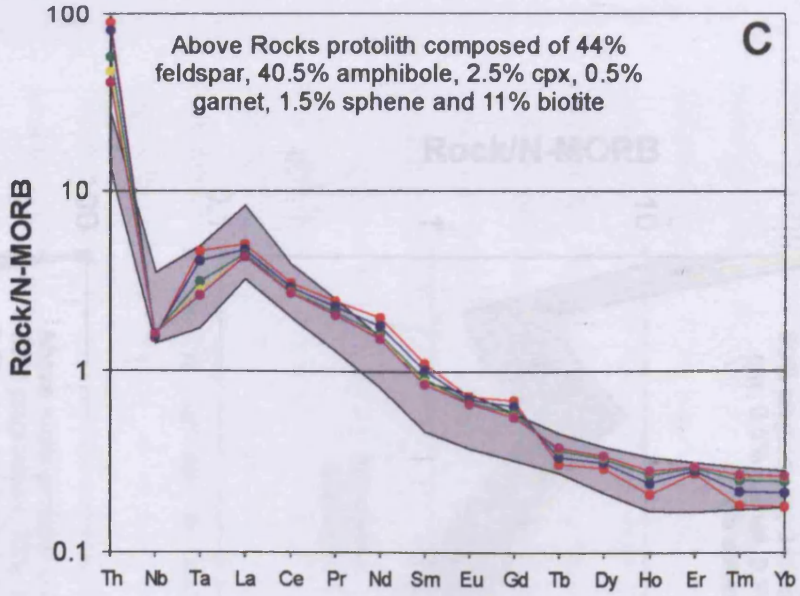

Figure 7.8 – Modelled partial melting calculations using (a) a Devils Racecourse protolith (Model 1) and (b and c) an Above Rocks protolith (Models 2 and 3). The calculations modelled 0.1%, 1%, 10%, 20% and 30% partial melting of the protoliths. The Above Rocks models indicate that an adakitic composition can be formed by various degrees of partial melting with variable protolith compositions (see text). Values and equations used for the calculations can be found in Appendix G.

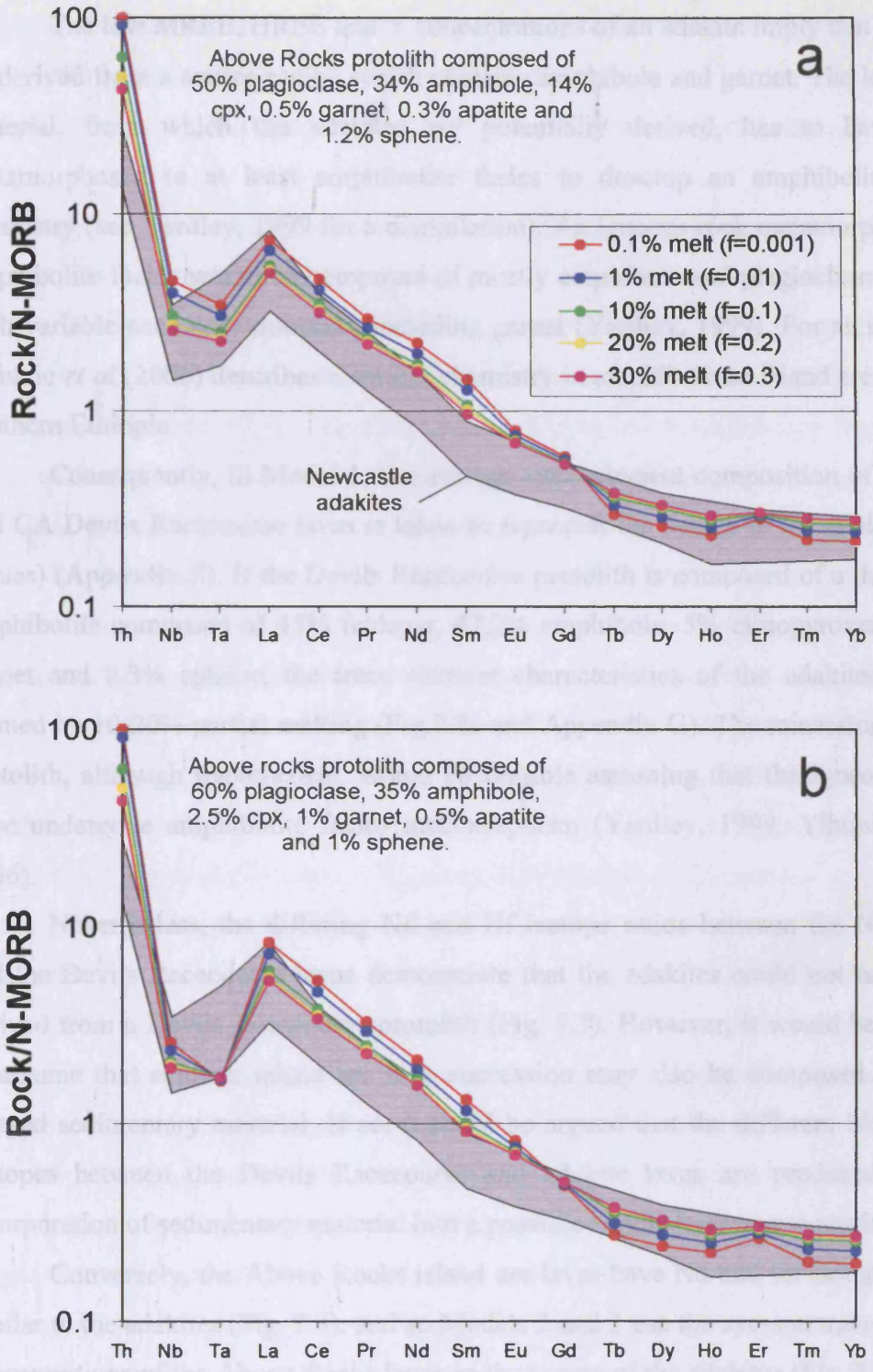

Figure 7.9 – (a) Model 4 and (b) Model 5. Partial melting calculations using an Above Rocks protolith. The calculations modelled 0.1%, 1%, 10%, 20% and 30% partial melting. The Above Rocks models indicate that an adakitic composition can be formed by 10-30% partial melting with variable protolith compositions containing apatite. Values and equations used for the calculations can be found in Appendix G.

The low MREE, HREE and Y concentrations of an adakite imply that it has to be derived from a source region which contains amphibole and garnet. The lower arc material, from which the adakites are potentially derived, has to have been metamorphosed to at least amphibolite facies to develop an amphibolite-garnet chemistry (see Yardley, 1999 for a compilation). An igneous rock metamorphosed to amphibolite facies would be composed of mostly amphibole and plagioclase feldspar with variable accessory minerals, including garnet (Yardley, 1999). For an example, Yihunie *et al* (2006) describes a similar chemistry in amphibolized island arc rocks in southern Ethiopia.

Consequently, in Model 1, the average trace element composition of the IAT and CA Devils Racecourse lavas is taken to represent the source of the adakites (Co values) (Appendix E). If the Devils Racecourse protolith is composed of a theoretical amphibolite composed of 45% feldspar, 47.2% amphibole, 5% clinopyroxene, 2.5% garnet and 0.3% sphene, the trace element characteristics of the adakites can be formed by 10-20% partial melting (Fig.7.8a and Appendix G). The mineralogy of the protolith, although hypothetical, would be feasible assuming that the igneous rocks have undergone amphibolite facies metamorphism (Yardley, 1999; Yihunie *et al.*, 2006).

Nevertheless, the differing Nd and Hf isotope ratios between the Newcastle and the Devils Racecourse lavas demonstrate that the adakites could not have been derived from a Devils Racecourse protolith (Fig. 7.3). However, it would be feasible to assume that a lower island arc lava succession may also be composed of inter-layered sedimentary material. If so, it could be argued that the different Nd and Hf isotopes between the Devils Racecourse and adakite lavas are produced by the incorporation of sedimentary material into a possible Devils Racecourse partial melt.

Conversely, the Above Rocks island arc lavas have Nd and Hf isotopic ratios similar to the adakites (Fig. 7.3), and so Models 2 and 3 use the average trace element concentrations of the Above Rocks lavas as the source of the adakites (Fig. 7.8b,c and Appendix G).

To fully explore the potential grade of metamorphism that the Above Rocks lavas may have been subjected to at depth, Model 2 is composed of a theoretical amphibolite protolith that implies that all the clinopyroxene is converted into secondary minerals. In Model 2, the Above Rocks protolith is composed of 47.5%

feldspar, 40% amphibole, 10% biotite, 1% garnet and 1.5% sphene (sphene is found in the Above Rocks lavas, Chapter 4). The results of this model show that 10-30% partial melting of this protolith can produce melts with adakitic compositions (Fig. 7.8b).

Model 3 uses a second theoretical Above Rocks protolith composed of 44% feldspar, 40.5% amphibole, 2.5% clinopyroxene, 11% biotite, 0.5% garnet and 1.5% sphene. This second protolith is modelled because it is common for amphibolites to contain relict pyroxenes (e.g. Yihunie *et al.*, 2006). As such Model 3 assumes that not all of the clinopyroxene is converted into amphibole and biotite during amphibolite facies metamorphism. The results of Model 3 imply that an adakite chemistry can also be produced by 10-30% partial melting of the island arc protolith (Fig. 7.8c).

In addition, it is also possible that apatite may be present in the Above Rocks protolith. Consequently, the formation of an adakite melt can be further modelled with differing mineral proportions and with apatite as a residual phase (e.g. Fig. 7.9). Models 4 and 5 demonstrate the formation of an adakitic liquid with theoretical Above Rocks protoliths being composed of 50% plagioclase, 34% amphibole, 14% clinopyroxene, 0.5% garnet, 0.3% apatite, 1.2% sphene and 60% plagioclase, 35% amphibole, 2.5% clinopyroxene, 1% garnet, 0.5% apatite, 1.2% sphene respectively. Both of the apatite models demonstrate that the adakite melts can be formed by 10-30% partial melting (Fig 7.9).

Although hypothetical, an important outcome of this modelling is that partial melting of a metamorphosed Jamaican island arc protolith can produce adakitic partial melts with similar isotope and trace element ratios to the Newcastle lavas. Th is the only element for which the modelling does not consistently produce the concentrations observed in the adakites. This is because the partition coefficients for certain minerals with andesitic liquids are not available for Th. The Th partition coefficient for sphene and apatite is derived from a trachytic composition. In addition, the partition coefficients for all the elements with garnet are dacitic values because of the lack of values for andesitic compositions.

Moreover, if the Newcastle adakitic lavas are formed by partial melting of the lower arc crust, there would still need to be an end-member involved in the petrogenesis that was enriched in U/Pb and Th/Pb ratios to explain the high $(^{207}Pb/^{204}Pb)i$, $(^{208}Pb/^{204}Pb)i$ and $(^{206}Pb/^{204}Pb)i$ values in the adakites. This component

could be derived from inter-bedded sedimentary material in a lower island arc amphibolite protolith.

7.6.6 Summary

The major and trace element concentrations of the adakites have been derived from the combination of complex post-eruptive alteration, partial melting, fractional crystallisation, slab component? and hybridisation processes. Consequently, although trace elements are useful in determining the involvement of minerals such as garnet and amphibole in the petrogenesis of the adakites their use is limited in resolving the source components that formed the adakitic magmas.

The Nb and Ta anomaly in the N-MORB-normalised multi-element diagrams demonstrates that the adakites are composed of an island-arc-like Th and LREE enriched component (Fig. 6.40). Nevertheless, it is unclear whether this component is derived from a lower island arc protolith or is from a subducted slab melt which has subsequently hybridised with a mantle wedge component.

These potential end-members cannot be identified on the basis of trace elements; however, Sr-Nd-Pb-Hf isotopes propose that the adakites could be derived from a subducting slab/mantle wedge component and a pelagic/terrigenous sedimentary/continental crust component. The enriched Pb, Nd and Hf isotope systematics additionally suggest that at least one of the components was enriched in U/Pb, Th/Pb, $\varepsilon_{Nd}(i)$ and $\varepsilon_{Hf}(i)$ and could be derived from a sedimentary or a HIMU-type oceanic plateau melt.

Furthermore, modelling has demonstrated that the adakite magmas could also be derived from 10-30% partial melting of an amphibolized lower island arc crust with a similar trace element and isotopic composition to the Above Rocks lavas. Consequently, the process which was responsible for the formation of the Newcastle lavas remains unclear because both the "slab melting" and "lower arc melting" models explain the derivation of the adakites.

However, the lower Sr concentrations in the Newcastle adakites suggest that plagioclase may have been left as a residual phase during adakite formation. A plagioclase residue would not be formed by partially melting a subducting slab because it would not be stable at such high pressures; therefore, implying that the

adakites were derived from the partial melting of lower island arc material (Section 6.6.5). Conversely, the low Sr abundances could equally be formed through plagioclase feldspar fractional crystallisation.

7.7 The petrogenesis of the Halberstadt high-Nb basalts

7.7.1 Potential source component(s)

Assuming moderate levels of partial melting and fractional crystallisation, the more enriched nature of the OIB-type source region of the Halberstadt lavas is compared with the source region of the Bath-Dunrobin plateau lavas (Figs. 7.10 and 7.11).

The average La/Yb and Nb/Zr ratios for the HNBs are 16.48 and 0.3 respectively. The same ratios for the Bath-Dunrobin plateau lavas are 1.62 and 0.059 respectively. The high La/Yb ratio in the HNBs stems from (1) the Halberstadt source region containing higher La concentrations and (2) lower Yb abundances in the HNB melt because of the presence of garnet in the HNB source region (Chapter 6). The La values for the HNB and the plateau lavas are 23.89 and 4.14 respectively and the Yb values are 1.5 and 2.54 respectively. In addition, the higher Nb/Zr ratios in the Halberstadt lavas are due to the HNB source region being more enriched in Nb than the plateau source region (Chapter 6 and Appendix E). The Nb concentrations in the HNB and plateau lavas are 37.77 and 3.92 respectively (Chapter 6 and Appendix E).

As such, unlike the Bath-Dunrobin plateau lavas, the Halberstadt rocks have higher LILE-LREE/HFSE (except Nb and Ta)-HREE ratios which results in them plotting close to average OIB in Figures 6.48 and 7.11. Therefore, these ratio diagrams provide evidence to support an OIB-type source region for these alkali basalts. On the Nb/Y-Zr/Y diagram of Fitton *et al.* 1997 (Fig. 7.10) the Halberstadt lavas plot in the enriched portion of the Iceland array and, on the Nb/Zr – Ta/Hf diagram, they plot close to average HIMU-OIB suggesting an enriched HIMU-OIB-type source region for the HNBs (Figs. 7.10 and 7.11). In Figure 6.50, the HNBs plot with the enriched oceanic plateau samples from Costa Rica, Colombia, Galapagos and

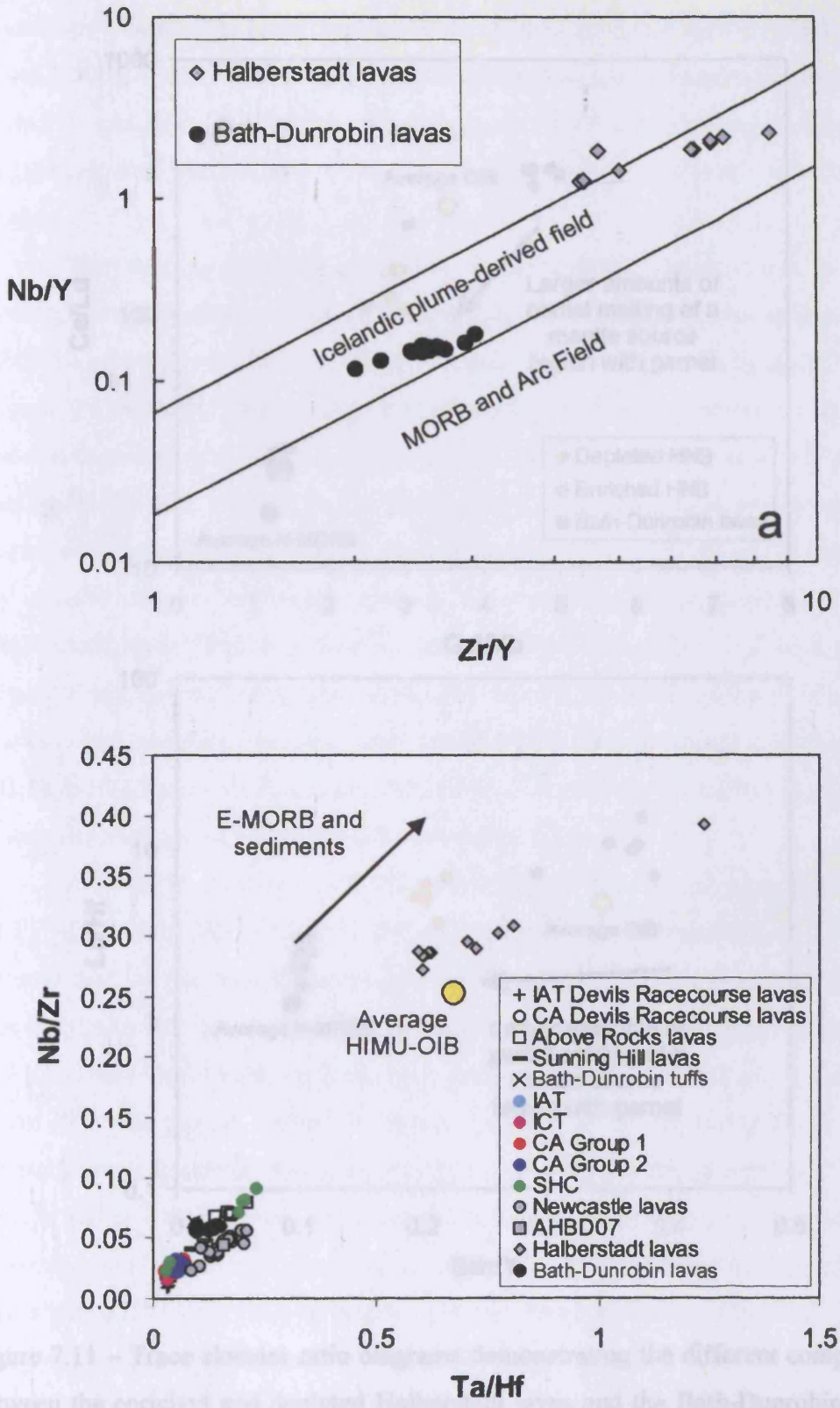

Figure 7.10 – (a) Nb/Y-Zr/Y diagram of Fitton *et al* (1997) and (b) Nb/Zr-Ta/Hf diagram comparing the Halberstadt HNBs with the Jamaican arc and plateau rocks.

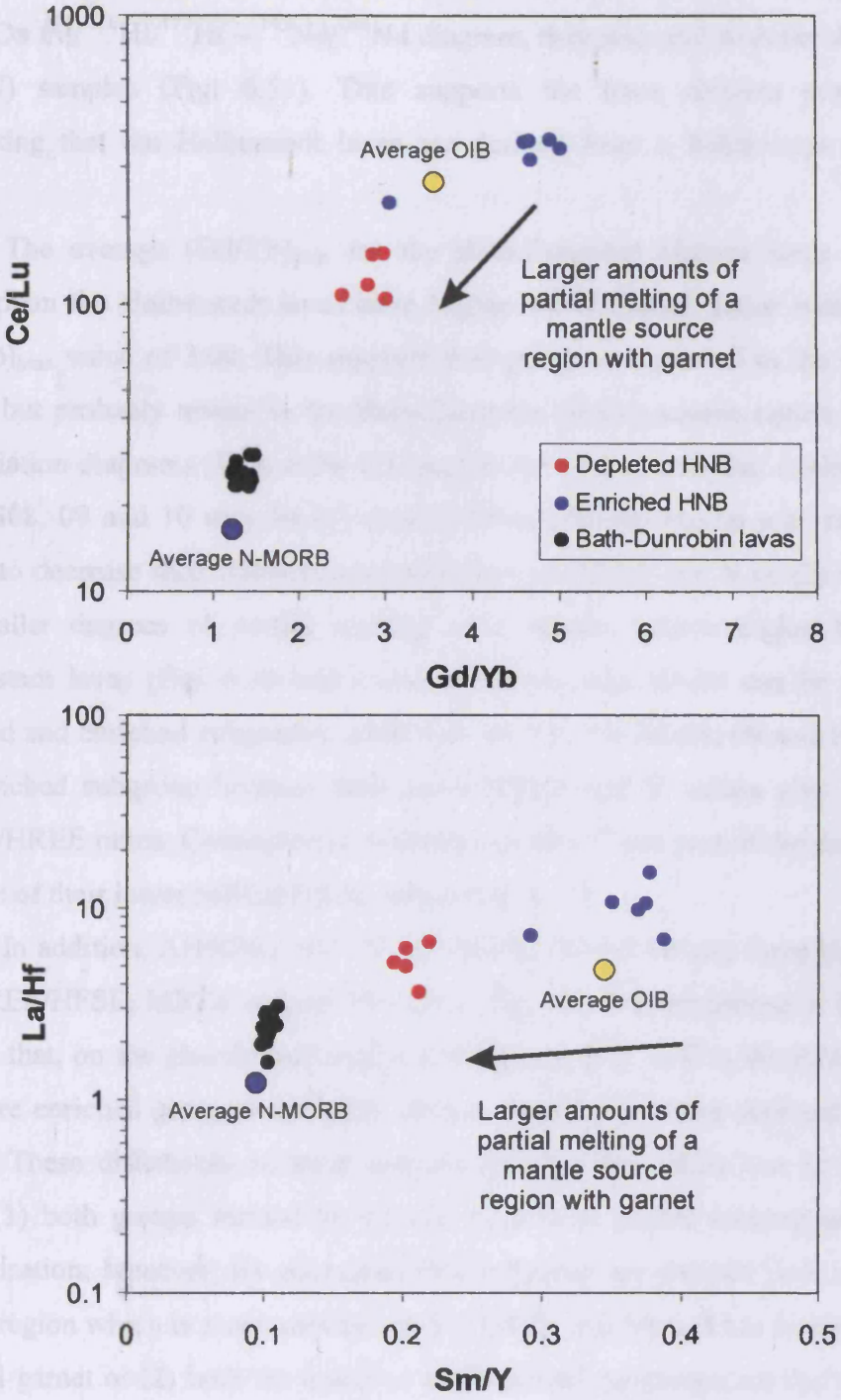

Figure 7.11 – Trace element ratio diagrams demonstrating the different compositions between the enriched and depleted Halberstadt lavas and the Bath-Dunrobin plateau rocks.

data from Iceland, and have more enriched Nd and Hf ratios than the Bath-Dunrobin lavas. On the $^{176}Hf/^{177}Hf - ^{143}Nd/^{144}Nd$ diagram, they also plot with the Austral-Cook (HIMU) samples (Fig. 6.51). This supports the trace element systematics by suggesting that the Halberstadt lavas are derived from a HIMU-type OIB source region.

The average $(Gd/Yb)_{pmn}$ for the Bath-Dunrobin plateau lavas is 1.08. By comparison the Halberstadt lavas have higher MREE/HREE ratios with an average $(Gd/Yb)_{pmn}$ value of 3.00. This suggests that garnet was present in the HNB source region but probably absent in the Bath-Dunrobin plateau source region. In addition, the variation diagrams (Figs. 6.36, 6.37 and E.14) demonstrate that AHHB05, 08, 09, AHWG08, 09 and 10 may be (1) derived from a source region with more residual garnet to decrease their absolute concentrations of HREE and Y or (2) were formed by smaller degrees of partial melting of a similar source region to the other Halberstadt lavas (Fig. 6.36 and E.14). Therefore, the HNBs can be divided into depleted and enriched subgroups. AHHB05, 08, 09, AHWG08, 09 and 10 are part of the enriched subgroup because their lower HREE and Y values give them higher MREE/HREE ratios. Consequently AHHB01-04 and 07 are part of the depleted group because of their lower MREE/HREE ratios (Fig. 7.11).

In addition, AHHB05, 08, 09, AHWG08, 09 and 10 also have higher Th, Nb and LREE/HFSE, MREE and HREE ratios (Fig. 7.11). Furthermore, it is interesting to note that, on the chondrite-normalised REE plot (Fig. 6.47c) the REE patterns of the more enriched group are slightly steeper than those of the depleted group (Fig. 6.47c). These differences in trace element patterns and ratios can be explained if either (1) both groups formed by similar degrees of partial melting and fractional crystallisation; however, the more enriched subgroup are derived from an OIB-type source region which is more enriched in Th, LREE and Nb and has larger amounts of residual garnet or (2) both the enriched and depleted subgroups are derived from the same garnet-OIB-type source region and the more enriched nature of the former subgroup is derived from smaller degrees of partial melting.

Unfortunately, the Nd and Hf isotope analyses cannot resolve the petrogenesis of the enriched and depleted subgroups. Owing to time constraints, the samples were analysed for isotopes before all of the ICP-MS trace element data had been obtained for the Halberstadt lavas. Therefore, there is no isotope analysis for a HNB from the

enriched subgroup. Accordingly, the process which formed the two differing subgroups is unclear until a sample from the enriched group is analysed for radiogenic isotopes.

However, the "inverse" SiO_2 and Yb vs. Zr variation diagrams, as described in Sections 6.7.2 and 6.7.4, Chapter 6, demonstrate that the liquid lines of descent in these aforementioned plots can only be formed using variable degrees of partial melting, although the abundances of source garnet could also vary. Consequently, it is concluded that the enriched and depleted HNBs are formed from predominantly varying degrees of partial melting of the same garnet-OIB-type source region and not from two geochemically different source regions.

7.7.2 Adakite and HNB relationship

Interestingly, the HNBs have very similar Nd and Hf isotope ratios to the adakites and the Border lavas. The close association of adakites and HNBs has led some (e.g. Defant *et al.,* 1992) to propose that these two magma types are petrogenetically related. Therefore, in Jamaica, their comparable Nd and Hf isotopes and similar ages (~ 52 Ma) implies that they may have been derived from an isotopically similar source region (Fig. 6.20). However, no source component can be related to both the Halberstadt and Newcastle lavas. The adakites are derived from a slab melt or lower arc material and the HNBs have an affinity with a HIMU-OIB source. Consequently, it is very difficult to model how the Jamaican adakites and HNBs could be petrogenetically related.

7.7.3 Formation of the Jamaican HNBs – theories from the literature

If the adakitic magmas of the Newcastle lavas are formed from partial melting of a young subducting slab at ~ 52 Ma the magmas may have variably hybridised with the mantle wedge, converting it into a phlogopite, garnet and amphibolite lherzolite (e.g. Kepezhinskas *et al.,* 1996). The adakitic magmas would subsequently ascend through the arc crust to be erupted as thick lava flows in the Wagwater fallen basin. The altered lherzolite residue may then partially melt to produce HNBs which would ascend and erupt as the Halberstadt lavas. This process would explain the similar Nd

and Hf isotopes between the adakites and the HNBs. However, it has been demonstrated by a number of authors (e.g. Sajona *et al.* 1993) that this process would form Nb enriched arc basalts and not HNBs.

Conversely, HNB compositions are very similar to alkalic basalts erupted on the Antarctic Peninsula, Northern Baja Range, California and British Colombia (Hole, 1990; Hole *et al.*, 1991). These basalts have similar compositions to OIB and continental alkalic basalts and are supposedly derived by a "slab window" process (Hole, 1990; Hole *et al.*, 1991).

Slab windows are areas along subduction zones that are not underlain by a subducting slab (Dickson and Snyder, 1979; Thorkelson and Taylor, 1989; Hole *et al.*, 1991). The underlying asthenosphere will ascend to fill the void left behind by the absence of the subducting plate. This asthenosphere will undergo decompression melting to form the alkalic basalts (Dickson and Snyder, 1979; Thorkelson and Taylor, 1989; Hole *et al.*, 1991). Alternatively, similar alkali basalts can also be generated by decompression melting in response to the extension of thickened lithosphere (e.g. continental rifting).

The slab window derived basalts have low LILE/Nb-Ta ratios (e.g. Th/Ta ~ 1.2) and high absolute HFSE abundances (e.g. up to 80 ppm Nb at ~ 9 wt. % MgO). The Halberstadt lavas have an averaged Th/Ta ratio of ~ 1.25, and >> 25 ppm Nb with MgO values of 3-10 wt. %. None of the slab window derived alkali basalts mentioned above have been formed by lithospheric attenuation. However, rift-associated passive asthenospheric upwelling can also form alkali basalts with similar compositions (Hole, 1990; Hole *et al.*, 1991).

Consequently, it is possible that the Halberstadt lavas were derived from a slab window during the subduction of the Proto Caribbean crust beneath Jamaica at ~ 52 Ma. It is also possible that lithospheric attenuation of the Great Arc of the Antilles at ~ 52 Ma, not only formed the Wagwater and Montpelier-Newmarket fallen basins on Jamaica, but may have allowed enriched asthenosphere to ascend such that subsequent decompression melting of this material generated the alkali basalts of the Halberstadt Formation.

7.7.4 – Forming the HNBs by melting N-MORB, DMM and oceanic plateau material

In addition to the petrogenetic models in Section 7.7.3, HNB formation could involve a similar process as described by Castillo *et al.* (2007). These authors argue that HNBs may be formed from the partial melting of a heterogeneous "marble cake" mantle source region composed of an enriched OIB-type and a depleted MORB-type source.

The Pacific model of Caribbean plate evolution demonstrates that the Caribbean plate is largely composed of an oceanic plateau that was tectonically emplaced between the North and South American continents after ~ 80 Ma (Chapter 2). It is thus possible that the Halberstadt HNBs are derived from partially melting a mixture of enriched oceanic plateau peridotite and depleted MORB that may lie under Jamaica and the Caribbean region. The basaltic Halberstadt lavas have to be derived from the melting of an ultramafic source because partially melting a basaltic protolith at high pressures will form intermediate magmas (e.g. Drummond and Defant, 1990).

$\varepsilon_{Nd}(i)$ and $\varepsilon_{Hf}(i)$ mixing diagrams are shown in Figure 7.12 and demonstrate that the HNBs can be formed by mixing of N-MORB and primitive mantle end-members and of depleted MORB mantle (DMM) and primitive mantle. The primitive mantle composition represents a theoretical ultramafic oceanic plateau source component. Primitive mantle trace element concentrations are taken from McDonough and Sun, (1995) and the isotope ratios are obtained from the plateau sample AQ28, which represents an ideal mixing end-member for the HNB compositions because of its low Nd and Hf isotope systematics (Fig. 6.50) (Hauff *et al.* 2000b). AQ28 is a sample from the Quepos Complex on Costa Rica, which is interpreted as obducted material from the Galapagos hotspot (Section 2.6.8, Chapter 2) (Hauff *et al.* 2000b). The DMM trace element and isotope values are from Workman and Hart, (2005). N-MORB data was averaged from Sun and McDonough, (1989); Rollinson, (1993); Nowell *et al.* (1998) and Kempton *et al.* (2000) (Appendix F).

If an N-MORB melt is formed by decompression melting due to lithospheric extension below Jamaica at ~ 52 Ma, the MORB melt may mix and initiate partial melting of the Caribbean oceanic plateau keel, which is best represented by primitive mantle values. Figure 7.12a shows that the HNB composition can be formed by

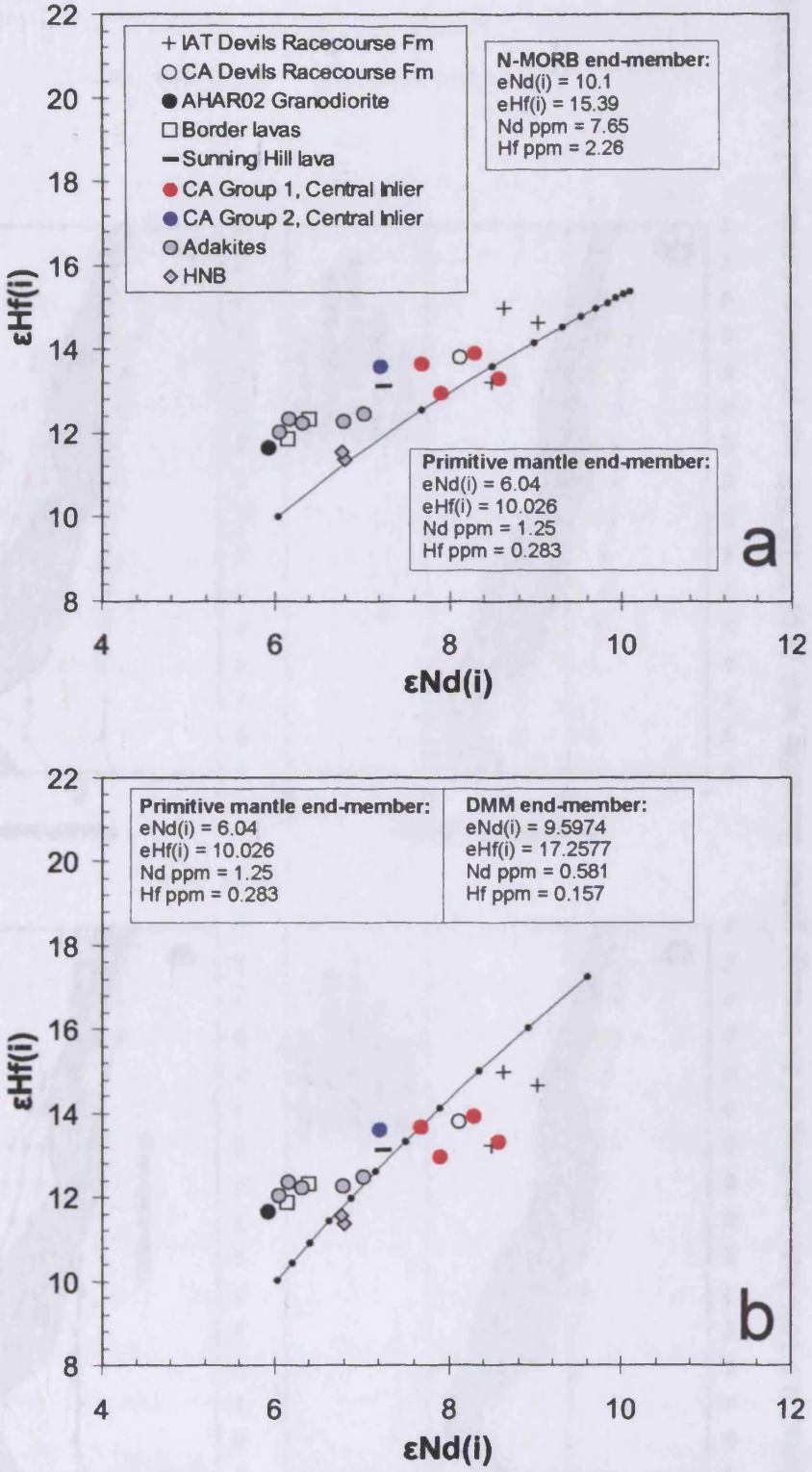

Figure 7.12 - Modelling the formation of the Halberstadt HNBs with (a) N-MORB and primitive mantle end-members and (b) DMM and primitive mantle end-members. Each tick on the mixing line represents 10% intervals (Appendix G).

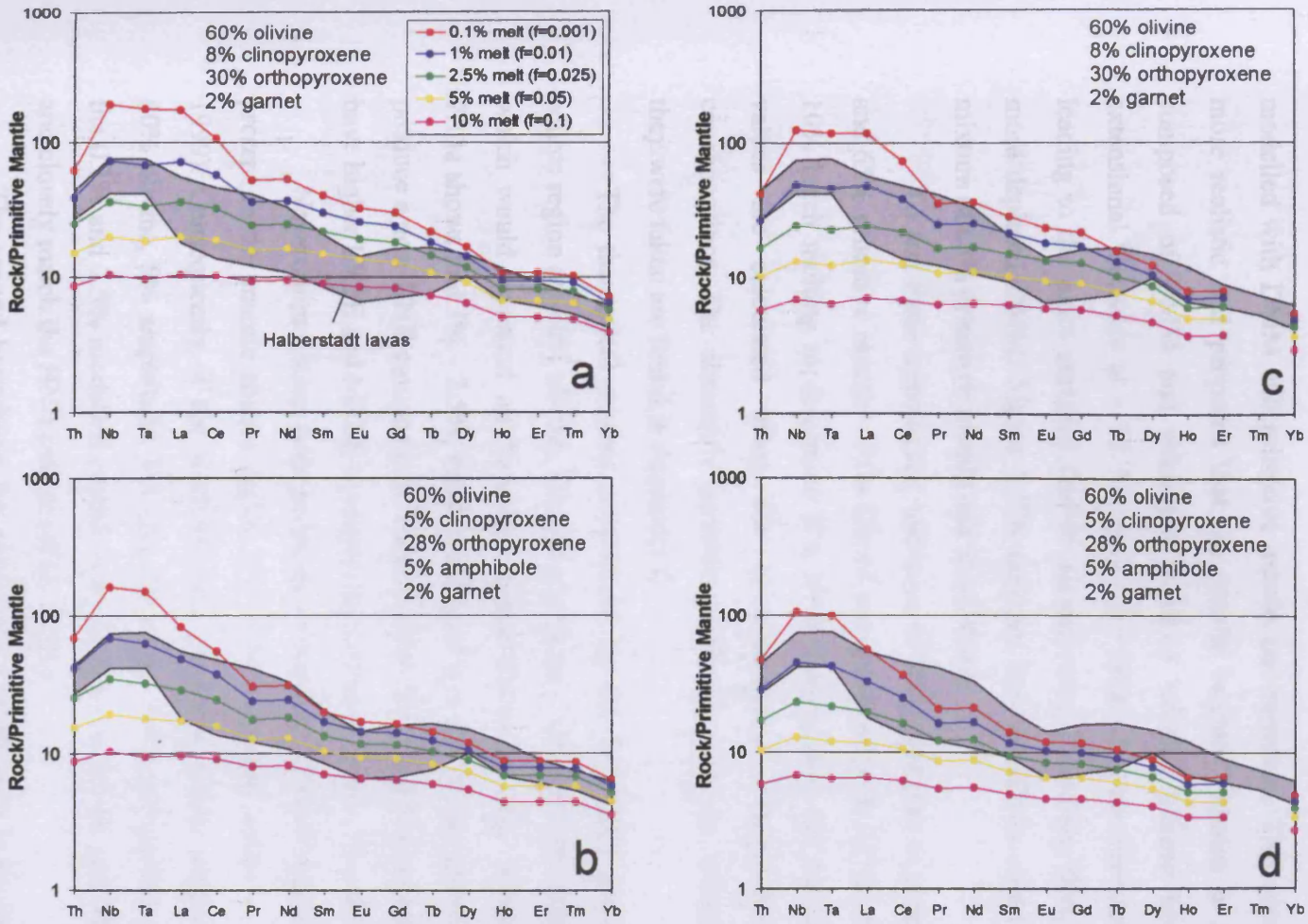

Figure 7.13 - Modelled 0.1-10% batch melting of an average garnet lherzolite with (a-b) N-MORB and primitive mantle and (c-d) DMM and primitive mantle end-members. (a and c) represent source regions with no amphibole, whereas, (b and d) have source regions with 5% amphibole. C_O and partition coefficient data can be found in Appendix G.

mixing of 4% N-MORB with 96% primitive mantle. It should be noted, however, that the MORB and primitive mantle end-members within these models are purely theoretical and may not represent the true composition of the components which mix to form the HNBs.

Figure 7.12b also demonstrates that the HNB $\varepsilon_{Nd}(i)$ and $\varepsilon_{Hf}(i)$ values can be modelled with DMM and primitive mantle end-members. This scenario is probably more realistic and proposes that the mantle beneath Jamaica is a "marble cake" composed of DMM and relatively enriched residual plateau keel material. The extensional tectonics at ~ 52 Ma may have induced decompression partial melting leading to the more enriched fusible plateau material melting first, followed by the more depleted DMM. Figure 7.12b suggests that the HNBs could be formed by a mixture of 65% primitive mantle and 35% DMM.

To test these hypotheses, mixtures of 96% primitive mantle - 4% N-MORB and 65% primitive mantle - 35% DMM are modelled with 0.1%, 1%, 2.5%, 5% and 10% batch melting to determine if a HNB composition can be produced. The C_O values are calculated using the aforementioned end-member mixtures and concentrations. The ultramafic partition coefficients and the references from which they were taken are found in Appendix G.

The theoretical mineral proportions for the N-MORB and primitive mantle source region are 60% olivine, 8% clinopyroxene, 30% orthopyroxene and 2% garnet, which would represent an "average" garnet lherzolite (e.g. Wilson, 1997). Figure 7.13a shows that 1% - 2.5%, batch melting of this theoretical garnet lherzolite would produce a near HNB composition. However, the 1% and 2.5% modelled compositions have higher LREE and MREE concentrations relative to Nb, Ta and Th (Fig. 7.13a).

Nevertheless, it has been proposed in Section 6.7.3 that amphibole may also be present in the mantle source region if it is hydrous and below ~ 10 km (Yardley, 1999). Consequently, if the N-MORB and primitive mantle source is composed of 60% olivine, 5% amphibole, 5% clinopyroxene, 28% orthopyroxene and 2% garnet the 0.1% and 2.5% modelled partial melts have lower LREE and MREE abundances and closely match the HNB patterns (Fig. 7.13b).

The second hypothesis for generating a HNB melt is by partially melting a mantle source region composed of DMM and primitive mantle components. By using the 60% olivine, 8% clinopyroxene, 30% orthopyroxene and 2% garnet, "average"

garnet lherzolite it is demonstrated that a near-HNB composition can be formed with a 1% partial melt (Fig. 7.13c). Nonetheless, the LREE and MREE concentrations are also relatively high compared to the Nb, Ta and Th abundances (Fig. 7.13c). However, if 5% amphibole is again added to the source region the HNB compositions can be affectively modelled with 0.1-1% partial melting (Fig. 7.13d).

Consequently, although the N-MORB, DMM and primitive mantle end-members are theoretical they do suggest that a HNB melt could be derived from a DMM/N-MORB-primitive mantle mixture by 0.1-2.5% partial melting. The modelling also implies that amphibole and garnet are required in the Halberstadt source region to form the relative depletions in the REEs compared to Nb, Ta and Th.

7.7.5 – Forming the HNBs by melting oceanic plateau material alone: would a subsequent HNB liquid melt the adakitic source region?

Although a mixture of N-MORB/DMM and primitive mantle can partially melt to form melts with compositions similar to the Halberstadt lavas it is possible that partially melting an oceanic plateau keel alone may also form HNBs. The Halberstadt lavas have $\varepsilon_{Nd}(i) = +6.77 - 6.80$ and $\varepsilon_{Hf}(i) = +11.35 - 11.54$, which are very similar to the Colombian plateau sample PAN6 from Kerr *et al.* (1997), which has $\varepsilon_{Nd}(i)$ 6.83 and $\varepsilon_{Hf}(i)$ + 11.76. Therefore, it is isotopically possible to derive the Halberstadt samples from part of the Caribbean oceanic plateau alone (Fig. 6.50).

Primitive mantle trace element concentrations are used for the C_O values because they are considered to represent an ultramafic oceanic plateau keel composition. If the "average" garnet lherzolite composed of 60% olivine, 8% clinopyroxene, 30% orthopyroxene and 2% garnet is again used it can be seen in Figure 7.14a that 1-2.5% partial melting can form HNB-like liquids. However, similar to the DMM/N-MORB-primitive mantle mixtures the liquids have higher LREE and MREE concentrations relative to Nb, Ta and Th. Nevertheless, the addition of 5% amphibole into the ultramafic plateau keel produces HNB compositions with 1-2.5% partial melts (Fig. 7.14b).

In conclusion, the Halberstadt basalts can be derived from a mantle source region composed of N-MORB-primitive mantle, DMM-primitive mantle or primitive mantle alone. It is unclear which of these source regions is responsible; however, a

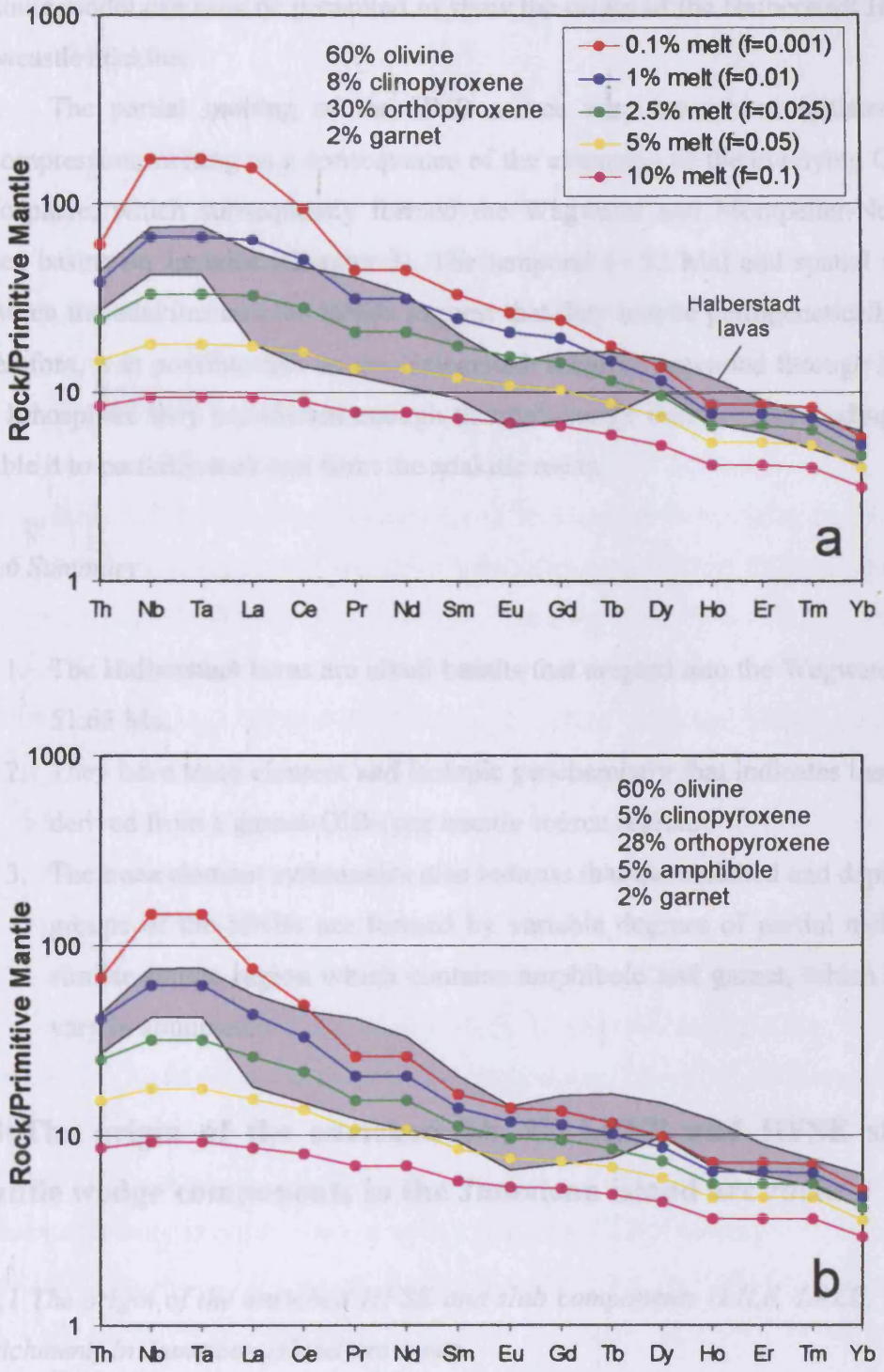

Figure 7.14 – (a and b) Modelled 0.1-10% batch melting of an average garnet lherzolite ± amphibole with primitive mantle compositions alone (see text). C_O and partition coefficient data can be found in Appendix G.

tectonic model can now be presented to show the origin of the Halberstadt HNBs and Newcastle adakites.

The partial melting of the HNB source may have been initiated due to decompression melting as a consequence of the extension of the overlying Caribbean lithosphere, which subsequently formed the Wagwater and Montpelier-Newmarket fallen basins on Jamaica (Chapter 3). The temporal (~ 52 Ma) and spatial similarity between the adakites and the HNBs suggest that they maybe petrogenetically related. Therefore, it is possible that as the Halberstadt magmas ascended through the island arc lithosphere they transferred enough thermal energy into the surrounding crust to enable it to partially melt and form the adakitic melts.

7.7.6 Summary

1. The Halberstadt lavas are alkali basalts that erupted into the Wagwater basin ~ 51.65 Ma.
2. They have trace element and isotopic geochemistry that indicates that they are derived from a garnet-OIB-type mantle source region.
3. The trace element systematics also indicate that the enriched and depleted sub-groups of the HNBs are formed by variable degrees of partial melting of a similar source region which contains amphibole and garnet, which may also vary in abundance.

7.8 The origin of the enriched Th, U, LREE and HFSE slab and mantle wedge components in the Jamaican island arc rocks

7.8.1 The origin of the enriched HFSE and slab components (LILE, LREE, U and Th enrichment) in Jamaican island arc lavas

The similar Nd and Hf isotope ratios of the adakites and the Border lavas together with a slight garnet signature in some of the Above Rocks lavas suggests that they may be related. The Above Rocks and Sunning Hill lavas and the Bath-Dunrobin tuffs are not adakitic because they lack the low MgO, Yb and Y contents (Appendix E). Moreover, even though the SiO_2 has been mobilised in the Above Rocks lavas, the

Co-Th diagram indicates that they are not acidic and probably do not represent melts with > 56 wt % SiO_2.

The Above Rocks, Sunning Hill and Bath-Dunrobin rocks are also not high-Mg andesites (HMA), as they do not have high MgO, Cr and Ni values. They also lack high La/Yb ratios and low FeO* concentrations (Appendix E), unlike typical HMA's from the Aleutian island arc and the Superior Province (Yogodzinski *et al.*, 1995; Polat and Kerrich, 2001). This indicates that these lavas have a "normal" island arc affinity and do not have a HMA composition.

The adakites, Above Rocks, Sunning Hill and Bath-Dunrobin samples also plot in separate fields on the trace element ratio diagrams in Figures 7.5 and 7.6. This further demonstrates that the aforementioned rock units are petrogenetically-unrelated (also see Section 7.6.2). However, it has been discussed that it is difficult to determine whether the high Nb/Zr and Ta/Hf ratios in the Bath-Dunrobin tuffs and the Sunning Hill and Above Rocks lavas are derived from a more enriched MORB source (ME-MORB) or a slab melt component. The samples are not from an OIB or plateau source because they mostly plot below the lower tramline on the Nb/Y-Zr/Y diagram (Fig. 7.1). Although, it is interesting to note that a few samples do plot within the Iceland array, which does suggest that an OIB or Plateau component maybe present in the ME-MORB source region.

Slab melt components, when entering the mantle wedge, will hybridise with the peridotite and subsequently form HMAs. The Bath-Dunrobin, Above Rocks and Sunning Hill rocks do not have a HMA composition. Thus, the involvement of a slab melt component in their petrogenesis is unlikely. Consequently the enriched HFSE nature of the Above Rocks, Sunning Hill and Bath-Dunrobin samples is probably because of a more enriched mantle wedge (the ME-MORB source).

This reasoning also precludes the other Jamaican arc rocks (including the SHC and CA2 rocks in the Central Inlier) from having a slab melt involved in their petrogenesis. They do not have adakitic or HMA compositions (Appendix E) and any enrichment of the HFSEs is a result of variably enriched N-MORB and ME-MORB mantle wedges. In that case, the enrichment in Th, U and the LREE in the Jamaican arc rocks is due to supercritical aqueous fluids which are derived from the altered basaltic crust and/or sedimentary veneer on the subducting lithospheric slab.

Consequently, a tectonic model can be presented which can detail the origin of the Jamaican arc rocks. In this model, the island arc source region below Jamaica was composed of two geochemically-distinct mantle wedge compositions. The first of these was composed of N-MORB and the second was more enriched in Nb and Ta and is the ME-MORB component. The IAT and CA Devils Racecourse lavas, IAT, ICT, CA1, CA2 and Crooked River samples were derived from the N-MORB component whereas the Waterworks ignimbrites, Sunning Hill lavas, Bath-Dunrobin tuffs and Above Rocks lavas are related to the ME-MORB component. Both the N-MORB and ME-MORB source regions existed above and below the garnet stability field. This enabled AHCI07, 08, 35-37, 62, and 63 and the ignimbrites to be formed in the garnet field whereas the remaining samples were derived from spinel peridotite. Conversely, it could also be argued that the Jamaican arc rocks that lack garnet signatures were also derived from garnet peridotite, and the degree of partial melting was large enough to melt out all of the garnet.

The enriched Nb/Zr and Ta/Hf ratios (Fig 7.1) coupled with more enriched Nd and Hf isotope systematics of the Waterworks ignimbrites, Sunning Hill lavas, Bath-Dunrobin tuffs and Above Rocks lavas relative to the other arc lavas precludes the former rocks from being derived from a similar N-MORB source by differing degrees of partial melting or fractional crystallisation, although these processes could enhance the signature.

In this model, the N-type and ME-type MORB mantle source regions were contaminated to varying degrees by chemically different slab-related components to produce the wide range in slab flux trace element and isotopic compositions in the Jamaican arc rocks (Figs. 7.3 and 7.6). The slab flux was composed of an altered oceanic crust/sediment-derived aqueous fluid and not a slab melt be cause of the Jamaican island arc rocks lacking HMA and adakite compositions.

7.8.2 Modelling the slab-derived component in the Jamaican island arc rocks

From the evidence discussed in Section 7.8.1, it is clear that most Jamaican island arc rocks formed by aqueous slab fluids mixing with spinel and/or garnet peridotite in the overlying heterogeneous mantle wedge. Modelling the concentration and volume of this mixture is difficult. Previous studies (e.g. Class *et al.*, 2000) have

utilised Sr and Pb isotope systems to model the amount and composition of the various island arc components. Unfortunately, as previously discussed, these isotope systems are not as reliable with altered rocks because of their potential mobility during tropical weathering and hydrothermal processes. However, the Nd and Hf isotope systems are more resistant to alteration (White and Patchett, 1984) and can be used to model the formation of altered island arc lavas (e.g. Thompson, 2002; Thompson *et al.*, 2004).

Figures 7.15 and 7.16 show the Jamaican arc lavas plotted in Nd-Hf isotope space along with several calculated mixing curves between Atlantic/Pacific-type N-MORB (i.e. the assumed mantle wedge) and a sedimentary component. Thompson (2002) and Thompson *et al.* (2004) made similar assumptions when they calculated mixing curves for the Cretaceous Washikemba Lava Formation, Bonaire. They chose an average Pacific pelagic sediment end-member and two Pacific MORB-end-members to construct their mixing lines (Curves 1 and 2, Fig. 7.15).

These two mixing curves of Thompson, (2002) and Thompson *et al.* (2004) do not successfully model the Jamaican arc data, as the Hf isotope ratios for both the modelled curves are too depleted (high) (Fig. 7.15). Consequently, it may be unrealistic to use Pacific MORB and pelagic sediments as end-members for the Jamaican and Bonaire arc lavas. Much of the mantle wedge feeding the arc magmas of the Great Arc of the Antilles was probably from Atlantic-type mantle (Chapter 2) and the proximity of the Great arc to the North American and South American continents (e.g. Burke, 1988) suggests that terrigenous sediments should be included into the sedimentary end-member.

A Pacific terrigenous/pelagic sedimentary end-member was calculated by averaging Pacific sedimentary data from Pearce and Peate (1995) and Woodhead *et al.* (2001). The composition of average Atlantic and Pacific N-MORB was calculated using data from Sun and McDonough, (1989); Rollinson, (1993); Nowell *et al.* (1998) and Kempton *et al.* (2000). These N-MORB and sedimentary end-members form Curve 3 (Fig. 7.15). Unfortunately, this curve also has excessively depleted Hf ratios, which means the curve does not successfully model the Jamaican arc data.

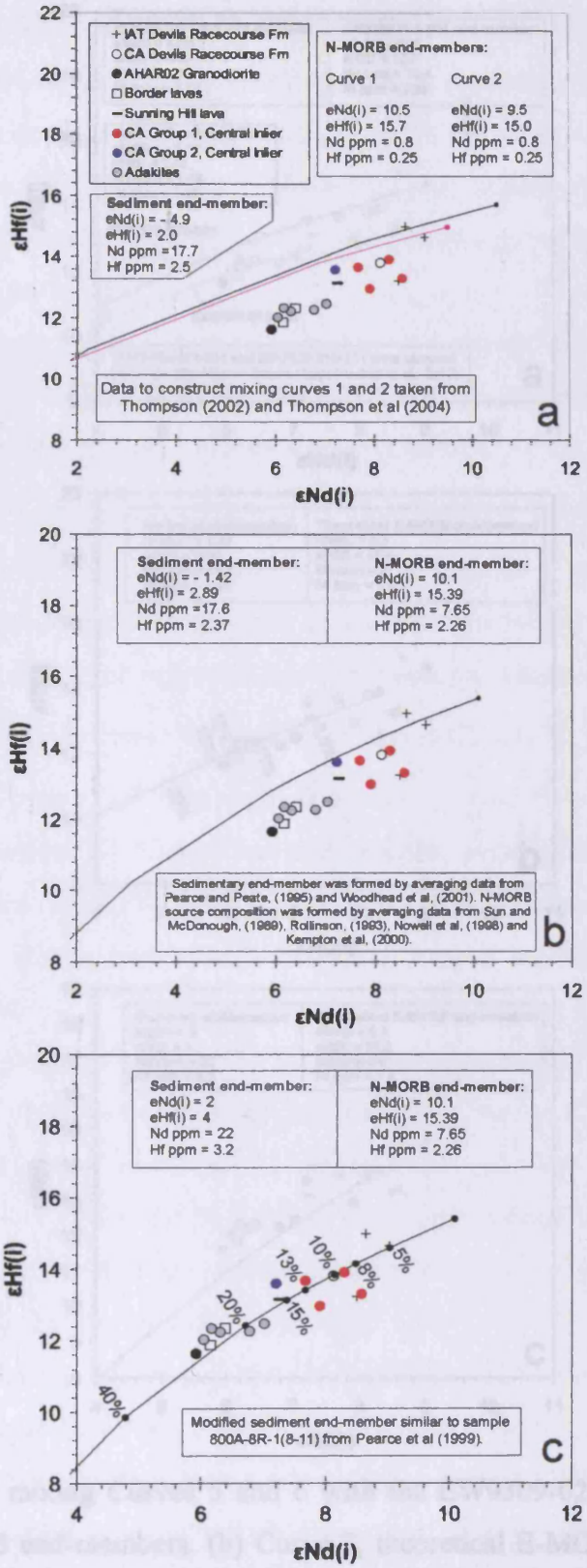

Figure 7.15 – (a) mixing Curves 1 and 2 from Thompson (2002) and Thompson *et al* (2004). (b and c) mixing Curves 3 and 4 respectively. Values along Curve 4 represent the percentage of bulk sediment added to the N-MORB end-member.

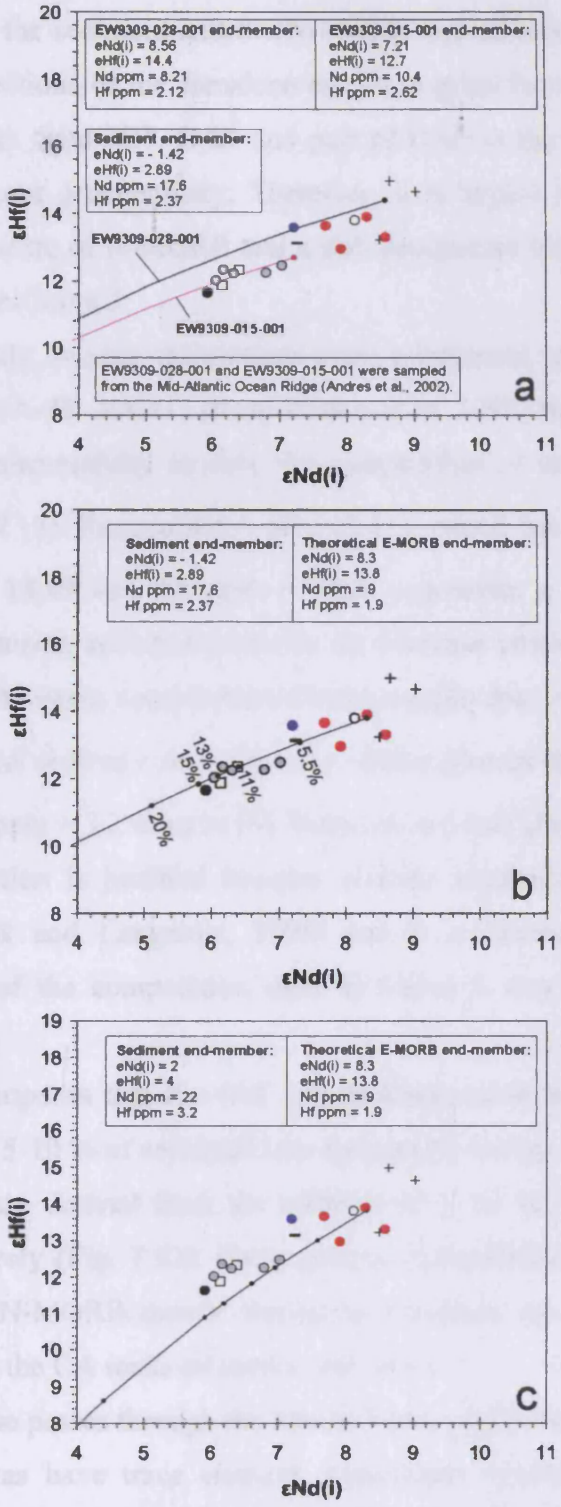

Figure 7.16 – (a) mixing Curves 5 and 6 with the EW9309-028-001 and EW9309-015-001 E-MORB end-members. (b) Curve 7, theoretical E-MORB end-member for the Above Rocks and Sunning Hill rocks. Values along the curve represent the percentage of bulk sediment added to the E-MORB end-member. (c) Curve 8, which combines data from Curves 4 and 7.

Modifying the sediment and the N-MORB end-members to take into account the unique compositions of the Jamaican arc lavas gives better results. The Benbow lavas and the rocks from ICT, CA1 and part of CA2 in the Central Inlier have N-MORB trace element geochemistry. Therefore, it is logical to assume that they are composed of a mixture of N-MORB and a slab component with a differing chemistry to that calculated in Curve 3.

Consequently, mixing calculations using a sediment of similar composition to Pacific sample 800A-8R-1(8-11) (from Pearce *et al.* 1999) produces a mixing curve (Curve 4) which successfully models the composition of the Benbow and Central inlier rocks (Fig. 7.15). Sample 800A-8R-1(8-11), which has $\varepsilon_{Nd}(i) = 1.01$, $\varepsilon_{Hf}(i) = 5.41$, Nd ppm = 18.49 and Hf ppm = 2.64, represents a mixture of cherts and volcanogenic sediments collected close to the Mariana island arc (see Pearce *et al.* 1999). Although the exact composition of this sample does not model the Jamaican rocks, a hypothetical sediment with a similar composition of $\varepsilon_{Nd}(i) = 2$, $\varepsilon_{Hf}(i) = 4$, Nd ppm = 22 and Hf ppm = 3.2 does fit the Jamaican arc data (Fig. 7.15). The use of this modified composition is justified because oceanic sedimentary compositions vary widely (e.g. Plank and Langmuir, 1998) and it is theoretically possible that a sedimentary pile of the composition used in Curve 4 was subducted to form the Jamaican arc lavas.

Curve 4 proposes that the IAT Devils Racecourse lavas were derived from bulk addition of ~ 5-10 % of sediment into the mantle wedge. CA Devils Racecourse, CA1 and CA2 were derived from the addition of ~ 10 %, ~ 8-13 % and ~ 15 % sediment respectively (Fig. 7.12). Consequently, the addition of a larger volume of sediment into an N-MORB mantle wedge may explain the more enriched Th and LILE chemistry in the CA rocks relative to the IATs.

Curve 4 also passes through the Above Rocks and Sunning Hill data; however, because these lavas have trace element systematics which suggest that they are derived from a mantle wedge that is more enriched than N-MORB it is not realistic to use this mixing curve to quantify their source components. Thus, mixing Curve 3 is modified to include an E-MORB-like component instead of an N-MORB composition (Fig. 7.16).

E-MORB trace element and Nd and Hf isotope data have been obtained from Sun and McDonough (1989), Andres *et al.* (2002), Andres *et al.* (2004) and Debaille

et al. (2006) and references therein (Appendix F). The data in these references demonstrate that E-MORB has a very wide range of isotopic ratios and trace element concentrations with $\varepsilon_{Nd}(i)$ -5.33 - + 9.95, $\varepsilon_{Hf}(i)$ + 1.0 - + 20.97, Nd ppm 4.94 - 51.9 and Hf ppm 1.22 - 6.79 (Fig. 7.16). No E-MORB sample from the aforementioned references formed a mixing curve that passed through the Above Rocks and Sunning Hill data; however, samples EW9309-028-001 and EW9309-015-001 from the Mid-Atlantic Ridge (Andres *et al.* 2002) are used as end-members in mixing Curves 5 and 6 (Fig. 7.16).

Curve 5 (EW9309-028-001) passes close to the Sunning Hill lava and Curve 6 (EW9309-015-001) passes through the Above Rocks lavas and granodiorite (Fig. 13), Unfortunately neither of these mixing curves can account for both the Above Rocks and Sunning Hill samples. Nevertheless, with the wide range of E-MORB compositions in the published literature, it is feasible to hypothesise that an E-MORB-like mantle component was involved in the genesis of both the Above Rocks and Sunning Hill rocks. If the E-MORB composition was similar to both EW9309-028-001 and EW9309-015-001 and had $\varepsilon_{Nd}(i)$ + 8.3, $\varepsilon_{Hf}(i)$ + 13.8, Nd ppm 9 and Hf ppm 1.9 it would produce mixing Curve 7, which would pass through both the Above Rocks and Sunning Hill data (Fig. 7.16).

Consequently, Curve 7 successfully models the composition of the Above Rocks and Sunning Hill lavas and suggests that they are derived from the bulk addition of ~ 11-13 % and ~ 5.5 % sediment respectively (Fig. 7.16). The Above Rocks granodiorite seems to be derived from the addition of ~ 15 % sediment, although the cumulate nature of the granodiorite makes this result tenuous. The sediment end-member in Curve 7 is the same as Curve 3. If the modified sediment composition in Curve 4 is used then mixing Curve 8 is produced (Fig. 7.16). Curve 8 does not pass through the arc data as it has Hf isotope ratios which are too enriched (Fig. 7.16).

Although these modelled mixing curves are theoretically possible, there are a number of factors that should be taken into consideration (a) The mantle wedge component in the Above Rocks and Sunning Hill samples is not represented by a true E-MORB composition, but is instead an ME-MORB component. Consequently the results of the mixing models for the Above Rocks and Sunning Hill data represents minimum values because the ME-MORB end-member may not be as enriched as the

E-MORB component. There is also the possibility that a plateau-type component may be present in the ME-MORB source; (b) An aqueous fluid from the subducting altered basaltic crust would also have contributed to the Nd (and possibly the Hf) budget of the arc lavas. Therefore, the estimated percentage of sediment transported into the mantle wedge to form the Jamaican arc magmas is probably too high and so represents a maximum value; and (c) The addition of a slab-derived sedimentary component into the mantle wedge would be via an aqueous fluid, not by bulk assimilation of part of the subducted sedimentary pile. A sedimentary fluid would be more enriched in incompatible trace elements (e.g. McCulloch and Gamble, 1991) than the bulk sediment from which it was derived. Therefore, this also suggests that the estimated sediment addition is a maximum value.

Chapter 8

Conclusions

8.1 Introduction

This Chapter pulls together the main conclusions of the thesis. The source regions of all of the Jamaican igneous rocks are presented and used to model Jamaica's role in Caribbean plate evolution. The aims of the study, outlined in Chapter 1, are answered and discussed with an emphasis on recommended future work in Jamaica.

8.2 Source regions for the Jamaican island arc, oceanic plateau and HNB samples: A summary

If the liquid lines of descent on the variation diagrams, and the data in the trace element ratio (e.g. Nb/Zr, Zr/Y, Th/Zr and La/Yb) and the $\varepsilon_{Nd}(i)$ - $\varepsilon_{Hf}(i)$ diagrams are considered then it is possible to identify at least 5 mantle wedge components and 8 slab components in the Jamaican island arc rocks.

The first of the 5 mantle wedge source regions is represented by an N-MORB-type composition which is found in the Benbow lavas and the Crooked River package and IAT, ICT, CA1 and CA2 groups in the Central inlier. The 2nd source is composed of the ME-MORB end-member and is represented by the SHC Waterworks Formation in the Central inlier. The remaining 3 source regions correspond to the Above Rocks, Sunning Hill and Bath-Dunrobin samples which are mixtures between N-MORB and the ME-MORB end-member.

Incompatible trace element variation and ratio diagrams together with the $\varepsilon_{Nd}(i)$ and $\varepsilon_{Hf}(i)$ isotope data imply that there are at least 8 chemically different slab-source components. These components are represented by the (1) IAT Devils Racecourse lavas, (2) CA Devils Racecourse lavas, (3) Above Rocks lavas, (4) Sunning Hill lavas, (5) ICT, (6) CA1, (7) CA2 and (8) the Bath-Dunrobin tuffs which are each chemically distinctive in terms of their trace elements and/or isotopes (e.g. Figs. 6.33, 7.3 and 7.4). The IAT and SHC groups from the Central Inlier may represent different slab fluxes or they may be part of the IAT Devils Racecourse and Sunning Hill fluxes respectively. Unfortunately, their slab component affinity can not be resolved because of the lack of radiogenic isotope and radiometric age data.

The majority of the island arc rocks are mafic/intermediate and lack garnet signatures suggesting they were either derived from a spinel peridotite mantle wedge source or that they are the product of large degree partial melting of a garnet peridotite source, from which all the garnet has been melted out. The Above Rocks, Sunning Hill and CA2 samples AHCI07, 08, 35-37, 62, and 63 and the Waterworks ignimbrites show a depletion in HREE and Y, indicating the likely importance of garnet ± amphibole in their petrogenesis (Fig. 7.4).

Additionally, on the basis of trace element and isotope systematics, the Bath-Dunrobin plateau lavas, the adakites and the HNBs represent at least three other chemically distinct source regions (e.g. Figs. 7.3 and 7.5). In summary, the Bath-Dunrobin plateau lavas are derived from a ~ 90 Ma heterogeneous mantle plume source. The Bath-Dunrobin source region is distinct from the source regions for other Caribbean oceanic plateau lavas because it has a larger HIMU component giving it more radiogenic Pb isotope ratios.

The major and trace element concentrations of the adakites have been derived from the combination of complex post-eruptive alteration, partial melting, fractional crystallisation, slab component(?) and hybridisation processes. The geochemistry supports the theory that instead of being related to a melt from a subducting slab, the Jamaican adakites are derived from a lower crustal garnet amphibolite with inter-bedded sedimentary material. The lower arc material has a similar trace element and isotope geochemistry to the Above Rocks lavas and the sedimentary component would impart high U/Pb and Th/Pb ratios into the resultant adakite liquids in order to produce their time-integrated high Pb isotope signatures.

The HNBs are derived from a HIMU-type OIB source, which contained garnet and amphibole and so is distinct from the source region of the oceanic plateau. The number of source regions for the Jamaican rocks may increase if (a) future data on the IAT and SHC groups in the Central Inlier demonstrate that they are comprised of compositionally distinct slab components and (b) the HNBs can be split into enriched and depleted subgroups on the basis of a heterogeneous source region. However, the trace element systematics in Sections 6.7 and 7.7 strongly suggest that the enriched and depleted HNB subgroups are formed by differing degrees of partial melting, which therefore implies that they are derived from the same source region.

8.3 The evolution of Jamaica and the Caribbean plate: insights from the igneous rocks

Using the geochemical interpretations in Chapters 6 and 7 it is possible to place Jamaica in the Pacific model of Caribbean plate evolution. The evolutionary model shown in Figure 2.4, Chapter 2 is modified and shown in Figure 8.1.

8.3.1 Barremian (~120 Ma) – Albian (~110 Ma)

Jamaica formed the northernmost part of the Great Arc of the Antilles and was located north of the section of the arc which will eventually form modern Cuba (Fig. 8.1a). During this time the IAT and CA Devils Racecourse lavas erupted along with the IAT and ICT rocks of the Central Inlier. Additionally, tholeiitic and calcalkaline rocks of a similar Barremian-Albian age have been discovered in other Caribbean islands: Albian IAT, CA and boninitic rocks in Cuba; Barremian-Albian IAT, CA and boninites of the Maimaon Formation, Amina Schists, Los Ranchos Formation and Loma La Vega and Las Guajabas volcanics of Hispaniola; early Albian IAT Pre-Robles Formation in Puerto Rico; upper Aptian-upper Albian IAT Water Island and Lousenhoj Formations in the Virgin Islands; and upper Albian IAT rocks in Bonaire and Tobago (see review in Donnelly *et al.*, 1990 and Kerr *et al.*, 2003).

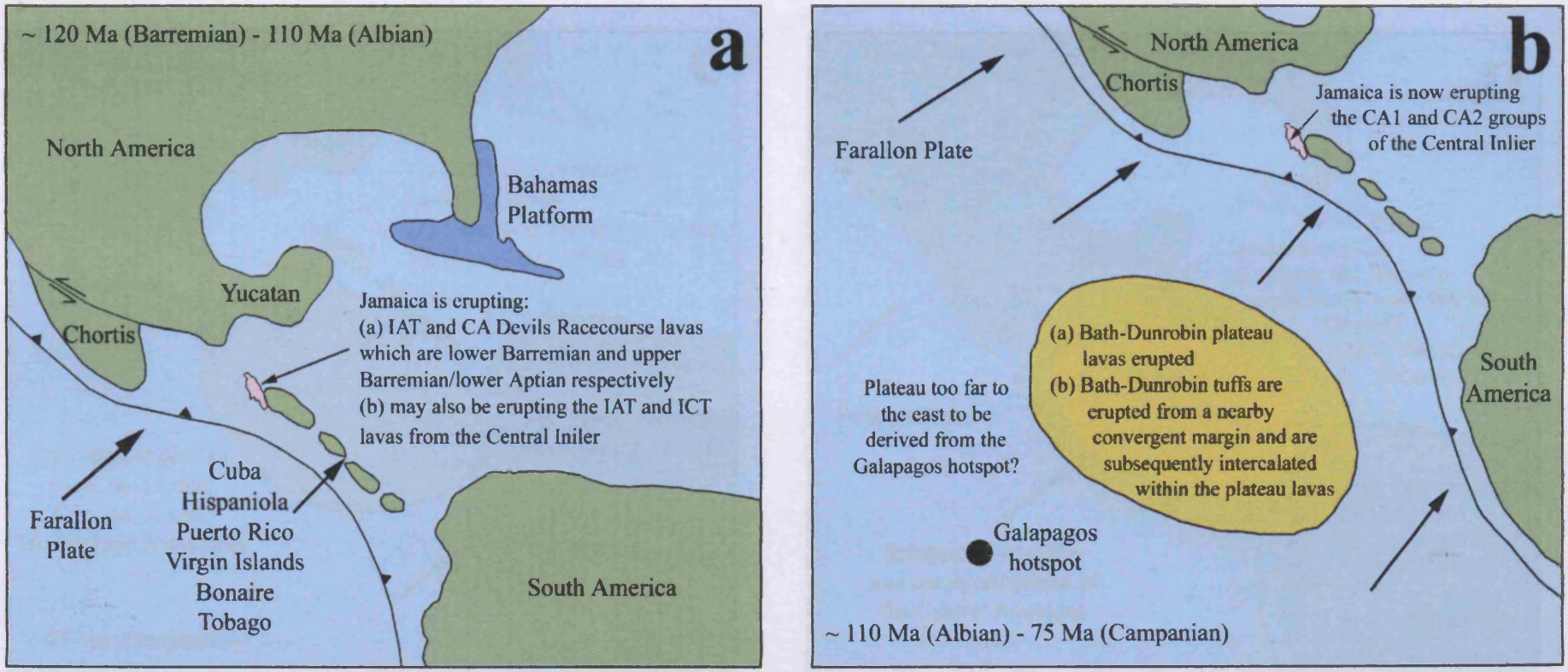

Figure 8.1 – Modified schematic diagrams reconstructing the evolution of Jamaica and the Caribbean plate from the early Cretaceous to the late Tertiary.

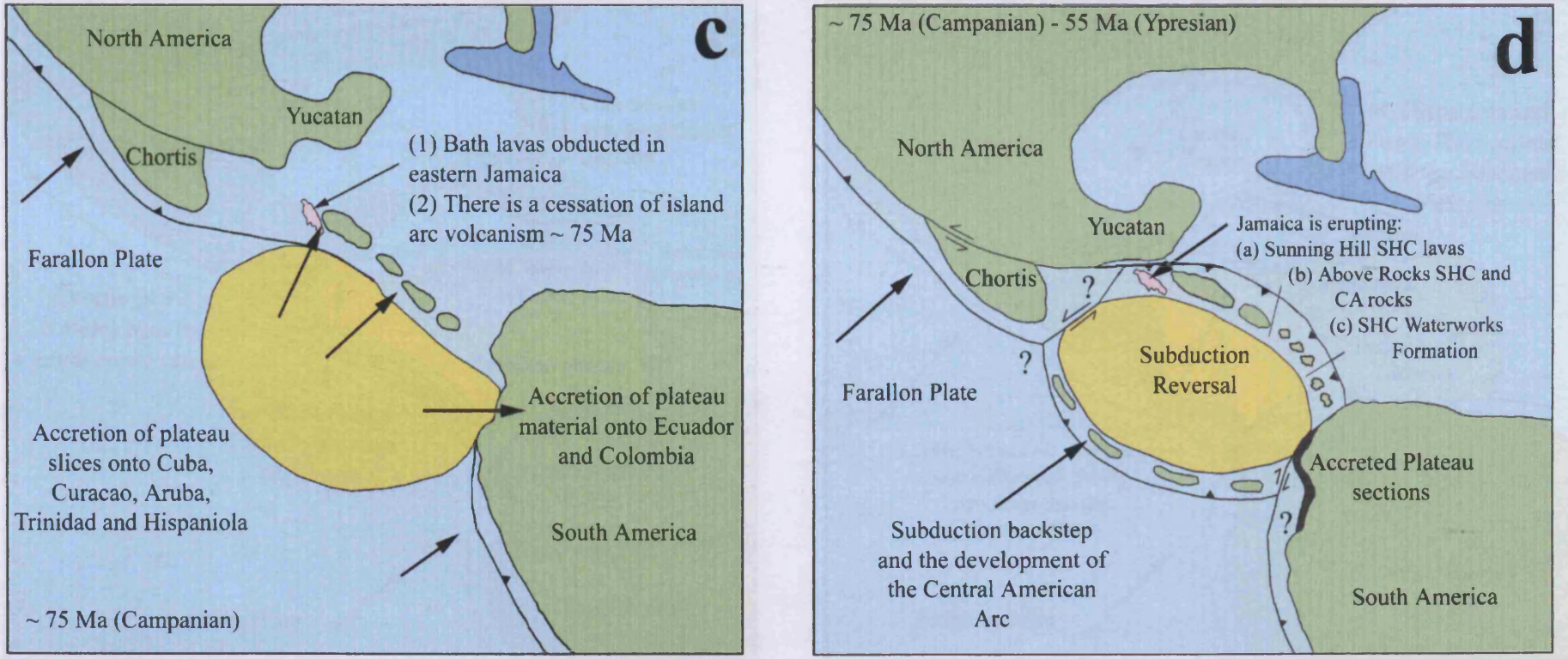

Figure 8.1 – continued.

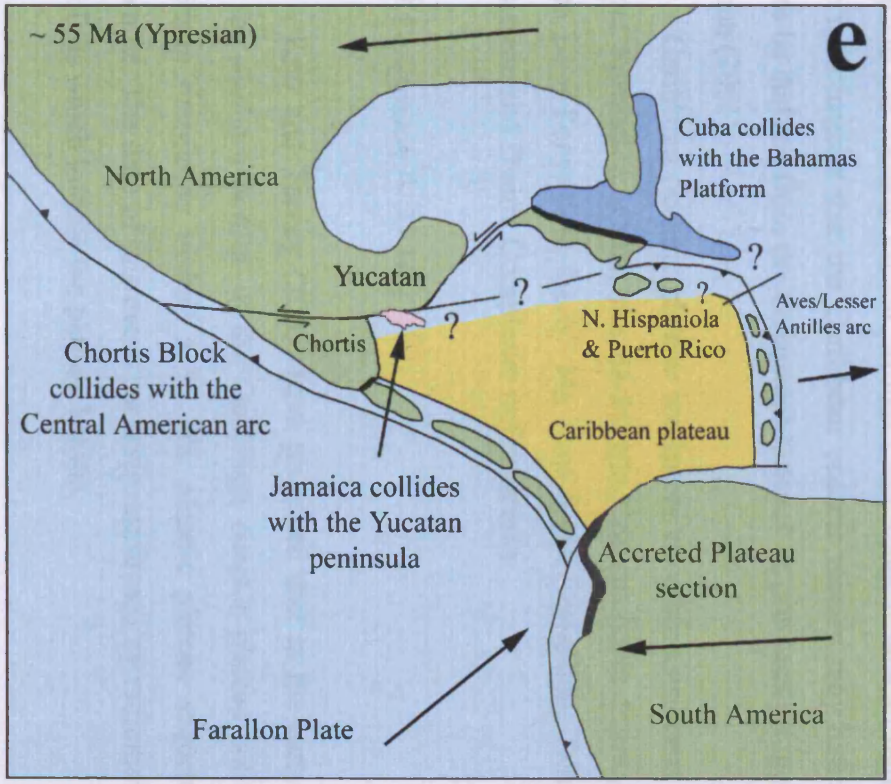

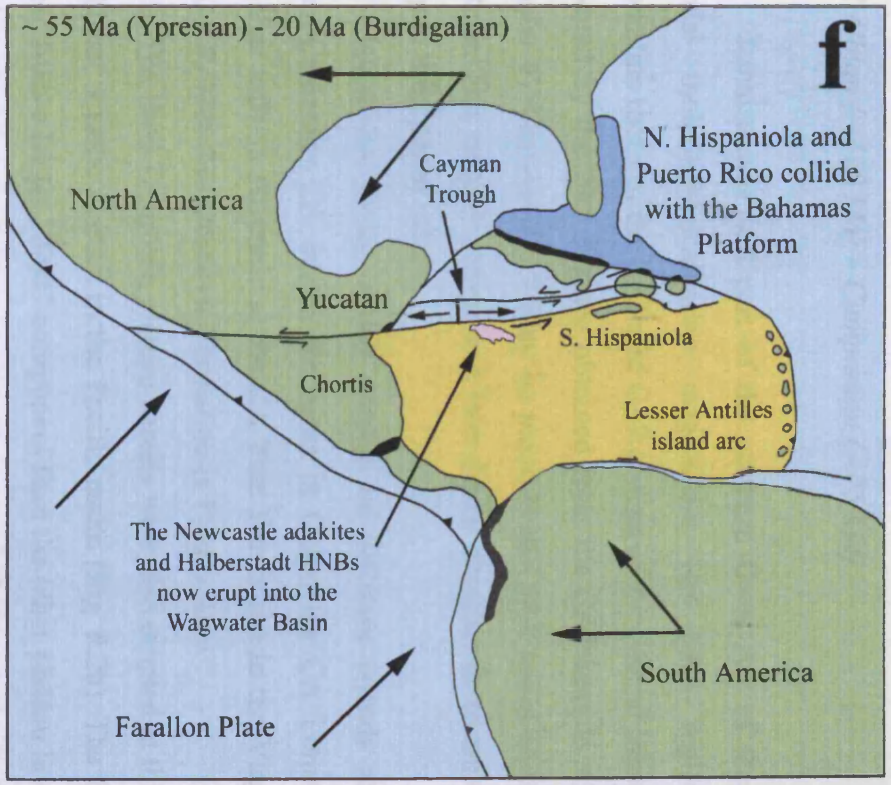

Figure 8.1 – continued.

8.3.2 Albian (~ 110 Ma) – Campanian (~ 75 Ma)

Jamaica was still part of the northern Great Arc of the Antilles; however, bimodal tholeiitic-calcalkaline magmatism has been replaced by unimodal calcalkaline rocks of the CA1 and CA2 groups of the Central Inlier (Fig. 8.2b). This is supported by the 79.5 Ma age obtained from the CA1 sample AHCI39 in this study (Chapter 6). Conversely, it may be possible that IAT rocks erupt in Jamaica during this time. This may be proven at a later date if accurate dates are obtained on the IAT group in the Central Inlier.

Island arc rocks, which erupted on different islands at this time include: Albian-Coniacian CA island arc rocks in Cuba; the CA Loma La Vega and Las Guajabas tuffs in Hispaniola; the CA Tutu Formation in the Virgin Islands; the IAT and CA Robles-Rio Orocovis Formation in Puerto Rico.

The Bath-Dunrobin plateau basalts were also erupted at this time as part of the Caribbean oceanic plateau in the Pacific realm (Fig. 8.2b). The Bath-Dunrobin lavas formed from a larger HIMU component than the other plateau lavas in the Caribbean. The inter-bedded Bath-Dunrobin tuffs were probably derived from the convergent margin in the western Proto-Caribbean and South American region. The presence of these tuffs implies that the Caribbean oceanic plateau may have been too far to the east to be derived from the Galapagos hotspot, as previously suggested by Pindell and Kennan (2001).

Caribbean oceanic plateau sequences on other Caribbean islands include: the Margot Formation, Cuba; the 88-90 Ma Curaçao Lava Formation; the 88-90 Ma Aruba Lava Formation; the 87 Ma Sans Souci Formation, Trinidad; the 86-92 Ma Dumisseau and Duarte Complexes in Hispaniola.

8.3.3 Campanian (~ 75 Ma)

Kerr and Tarney (2005) have proposed that in the early Campanian (83-80 Ma) the southern portion of the Caribbean oceanic plateau collided with the South American margin to obduct a 90 Ma oceanic plateau sequence in Ecuador and Colombia. The date of this event has been confirmed by radiometric ages on tonalitic batholiths which intrude the plateau basalts.

Conversely, the continued eruption of island arc lavas to at least 79.5 Ma in Jamaica indicates that the northern portion of the Caribbean oceanic plateau collided with the Great Arc of the Antilles some time after the South American collision. Unfortunately, because of the lack of Ar-Ar radiometric ages on Jamaican igneous rocks the timing of the northern collision can not be further constrained. However, this study tentatively dates the plateau collision with the northern portion of the Great Arc of the Antilles at ~ 75 Ma (Fig 8.1c). During this period volcanism in the Great Arc of the Antilles appears to have ceased for at least ~ 5 Ma.

8.3.4 Campanian (~75 Ma) – Ypresian (~55 Ma)

Collision of the plateau resulted in subduction back step and polarity reversal, which led to the subduction of proto-Caribbean crust beneath the Great Arc of the Antilles. The Great Arc began to fragment into northern, central and southern segments (Fig. 8.1d). Jamaica along with Cuba, Hispaniola and Puerto Rico is part of the northern segment of the arc (Fig. 8.1d).

Island arc volcanism commenced again along the entire length of the arc and in Jamaica the CA and SHC Above Rocks and Sunning Hill lavas and the SHC Waterworks ignimbrites were erupted (Fig. 8.1d). This is supported by the 70.5 Ma age obtained from the Above Rocks sample AHAR14 and the ~55 Ma fission track age from the Waterworks ignimbrite (Ahmad *et al.*, 1987a). These lavas and tuffs have high absolute abundances of the HFSE (e.g. Nb and Zr) and have more enriched Nb/Zr, Ta/Hf and $\varepsilon_{Hf}(i)$ ratios indicating that they are derived from a more enriched mantle wedge (the ME-MORB source). Their incompatible trace element ratios and $\varepsilon_{Nd}(i)$ are also more enriched suggesting that these arc rocks are derived from a source region with a greater mass fraction of, or more enriched, slab component.

This enriched island arc geochemistry relative to the older island arc lavas can be explained by the tectonic evolution of the Caribbean plate (Fig. 8.1d). The island arc magmas along the Great Arc of the Antilles at this time are derived from a different (more enriched) mantle wedge than before and a different subducting slab, which will flux more enriched slab components into the mantle wedge. This explains the distinct change in arc chemistry from the CA1 and CA2 lavas of the Central inlier

to the CA-SHC rocks of the Waterworks Formation, Above Rocks lavas and the Sunning Hill lavas.

These more enriched SHC and CA island arc rocks are also found on other Caribbean islands: 86-74 Ma SHC island arc rocks in Cuba and SHC and CA lavas in Puerto Rico (see review in Donnelly *et al.* 1990) and Kerr *et al.* 2003).

8.3.5 Ypresian (~55 Ma)

Following eruption of the Waterworks ignimbrites at ~55 Ma, igneous activity on Jamaica ceased for a second time (Fig. 8.1e). This is because the northern segment of the Great Arc of the Antilles broke into three. Jamaica, in the west, collided with the Yucatan peninsula; Cuba, in the centre, continued to move to the northeast and collided with the Bahamas Platform; Hispaniola and Puerto Rico, to the east, also move to the northeast to eventually collide with the Bahamas Platform.

8.3.6 Ypresian (~55 Ma) – Burdigalian (~20 Ma)

By the Oligocene all of the Greater Antilles islands, apart from Jamaica, had collided with the Bahamas Platform. The opening of the Cayman Trough in the Eocene/Oligocene (Rosencrantz and Sclater, 1986) not only transferred Cuba onto the North American plate but also tectonically transported Jamaica to the east (Fig. 8.1f). This movement of Jamaica was probably accommodated on the Swan Island – Plantain Garden – Enriquillo transform fault system (Figure 2.2, Chapter 2).

The Cayman Trough and its associated sinistral transform fault zones are considered to be an extended pull apart basin that records ~1100 km of sinistral offset between the North American and Caribbean plates (Rosencrantz and Sclater, 1986; Burke, 1988; Pindell and Barrett, 1990). Consequently, Jamaica, which is located on the transform fault system, has undergone extensional tectonics which subsequently formed the Montpelier-Newmarket and Wagwater fallen basins (Chapter 3). These basins are filled with Paleocene/Eocene sediments and the 51.65 Ma Newcastle adakites and Halberstadt HNBs.

It has already been proposed that the formation of both the Newcastle and Halberstadt lavas could be petrogenetically linked; indeed they were both erupted at the same time within the Wagwater basin (Chapter 3). It is possible that the

extensional tectonics which formed the Wagwater basin initiated decompression melting in up w elling oceanic plateau sourc e mantle /DMM to form the HNBs. Extension of the Jamaican crust may have also allowed the hot HNB melts to ascend and promote partial melting of lower island arc (Above Rocks) material to form the adakitic melts, thus explaining the pene-contemporaneous eruption of adakites and HNBs in the Wagwater basin.

8.4 Have all issues been addressed?

This study set out to principally address four main objectives in order to understand how Jamaica and the Caribbean plate have evolved from the early Cretaceous to the Tertiary. These objectives were to:

1. *Construct a detailed geochemical and temporal study of post-Jurassic igneous rocks on Jamaica.*

A large number of igneous rocks have now been discovered and identified on Jamaica. The rocks have been analysed for major and trace elements, Sr-Nd-Pb-Hf radiogenic isotopes and argon geochronology. This geochemistry has been used to study the petrogenesis of the rocks, which has enabled Jamaica to be placed within the tectonic framework of the evolution of the Caribbean plate (Section 8.2).

2. *Determine if the Galapagos hotspot is a viable source for the Caribbean oceanic plateau.*

Although not conclusively proven, the identification of the island arc derived tuff layers within the Bath-Dunrobin plateau lavas does suggest that the Caribbean oceanic plateau may have been located too far to the east at ~ 90 Ma to be derived from the Galapagos hotspot.

3. *Further constrain the timing of the subduction polarity reversal.*

Unfortunately the lack of Ar-Ar dates prevented the timing of the subduction polarity reversal being determined. However, the cessation of igneous activity on Jamaica (and other islands in the Caribbean) from ~80 – 70 Ma suggests that the reversal occurred during this period.

4. *Determine the timing and cause of the IAT to CA change in the island arc chemistry. Was it due to a subduction polarity reversal or due to a changing source composition over time?*

Bimodal Barremian and Albian IAT and CA lavas have been identified in Jamaica. Early CA lavas are found on Cuba and Hispaniola and post Aptian IAT rocks have been discovered on Puerto Rico. Consequently, IAT and CA lavas co-exist at the same time in the Great Arc of the Antilles, although, in the late Cretaceous the eruption of IAT lavas cease. This study does not support an abrupt IAT to CA change (e.g. Donnelly *et al.*, 1990) but indicates that the Great Arc of the Antilles evolved from a bimodal IAT-CA composition to a unimodal CA chemistry that finally evolved into a bimodal CA-SHC arc. The more enriched CA chemistry, relative to an IAT composition, is a result of differing slab components being fluxed into the mantle wedge and is <u>not</u> due to subduction polarity reversal.

The more important question for future studies would be to determine the timing and cause of the unimodal CA to bimodal CA-SHC change in arc chemistry. Based on the revised model presented herein, this change in chemistry seems to be connected to the subduction polarity reversal because of the changing mantle source region from N-MORB to ME-MORB and the different slab fluxes from the subducting Proto-Caribbean lithosphere.

8.5 Future Work

This study has identified numerous plateau, island arc and HNB igneous successions in Jamaica. The rocks have been analysed for major and trace elements, Sr-Nd-Pb-Hf radiogenic isotopes and argon geochronology. This geochemistry has

been used to study the petrogenesis of the rocks, which has enabled Jamaica to be placed within the tectonic framework of the evolution of the Caribbean plate. However, not all of the Jamaican successions have been studied and those that were still need further isotope and geochronolgical studies to constrain the different source regions of the various igneous rocks. As such, future work should include:

1) More immobile trace element and radiogenic isotope analyses on the existing igneous rocks. This will constrain the evolution and origin of (a) the N-MORB and ME-MORB mantle wedge components; (b) the different slab components in the island arc lavas, especially for the IAT and SHC groups in the Central inlier; (c) the source region of the Newcastle adakites; (d) the source region(s) of the Halberstadt HNBs. Particular emphasis should be placed upon the ME-MORB to determine if it represents a oceanic plateau-DMM-type mixture.
2) More geochronological data to constrain the ages of all of the igneous successions, especially for the Central Inlier groups, so that the timing of the subduction polarity reversal can be determined. This will also resolve the timing of the CA to CA-SHC change in island arc chemistry, which is possibly linked to the subduction polarity reversal.
3) Collection of more samples from the Jamaican Cretaceous inliers. Particular focus should be placed on the Lucea, Giblatore and St Peter's Inliers which contain igneous rocks that have not been studied in this thesis. The petrogenesis of Miocene alkali igneous rocks around Low Layton and volcanic successions in the Blue Mountain interior also need to be assessed. The Westphalia and Hibernian amphibolite and blueschist, in the Plantain-Garden fault zone, should also be analysed. These schists may represent exhumed lower crustal material; therefore, they may be able to constrain the possible source regions of the Newcastle adakites and Halberstadt HNBs.

References

Ahmad, R., Lal, N., Sharma, P.K., 1987a. Fission-track age of ignimbrite from Summerfield Formation, Jamaica. Caribbean Journal of Science. 23, 444-448.

Ahmad, R., Lal, N., Sharma, P.K., 1987b. A Fission-track age for The Above Rocks granodiorite, Jamaica. Caribbean Journal of Science. 23, 450-452.

Alvarado, G.E., Deyner, P., Sinton, C.W., 1997. The 89Ma Tortugal komatiitic suite, Costa Rica: Implications for a common geological origin of the Caribbean and eastern Pacific region from a mantle plume. Geology 25, 439-442.

Andres, M., Blichert-Toft, J., Schilling., 2002. Hafnium isotopes in basalts from the southern Mid-Atlantic Ridge from 40°S to 55°S: Discovery and Shona plume-ridge interactions and the role of recycled sediments. Geochemistry Geophysics Geosystems. 3.

Andres, M., Blichert-Toft, J., Schilling., 2004. Nature of depleted upper mantle beneath the Atlantic: evidence from Hf isotopes in normal mid-ocean ridge basalts from 79°N to 55°S. Earth and Planetary Science Letters. 225, 89-103.

Arculus, R.J., 1987. The significance of source versus process in the tectonic controls of magma genesis. Journal of Volcanology and Geothermal Research. 32, 1-12.

Arculus, R.J., 2003. Use and Abuse of the Terms Calcalkaline and Calcalkalic. Journal of Petrology. 44, 929-935.

Arndt, N.T., Kerr, A.C., Tarney, J., 1997. Dynamic melting in plume heads: the formation of Gorgona komatiites and basalts. Earth and Planetary Science Letters. 146, 289-301.

Arndt, N.T., Weis, D., 2002. Oceanic plateaus as windows to the Earth's Interior: an ODP success story, Joides Journal, Special Issue, 28: 79-84,

Ave Lallemant, H.G., 1997. Transpression, displacement partitioning, and exhumation in the eastern Caribbean/South American plate boundary zone. Tectonics. 16, 272-289.

Bateson, J.H., 1974. Notes on the geology of the Bath area and their relationship to the Cretaceous rocks of the Blue Mountains. Journal of the Geological Society of Jamaica. 14, 22-30.

References

Bau, M., Knittel, U., 1993. Significance of slab-derived partial melts and aqueous fluids for the genesis of tholeiitic and calk-alkaline island arc basalts: evidence from Mt. Arayat, Philippines. Chemical Geology. 105, 233-251

Beccaluva, L., Coltorti, M., Giunta, G., Iturralde Vinent, M., Navarro, E., Siena, F., Urbani, F., 1996. Cross sections through the ophiolitic units of the Southern and Northern Margins of the Caribbean Plate, in Venezuela (Northern Cordilleras) and Central Cuba. Ofioliti. 21(2). 85-103.

Beets, D.J., Maresch, W.V., Klaver, G.T., Mottana, A., Bocchio, R., Beunk, F.F., Monen, H.P., 1984. Magmatic rock series and high-pressure metamorphism as constraints on the tectonic history of the southern Caribbean. In: The Caribbean-South American plate boundary and regional tectonics. The Geological Society of America. Vol. Memoir 162.

Ben Othman, D., White, W.M., Patchett, J., The geochemistry of marine sediments, island arc magma genesis, and crust-mantle recycling. Earth and Planetary Science Letters. 94, 1-21.

Blichert-Toft, J., 2001. On the Lu-Hf isotope geochemistry of silicate rocks. Geostandards Newsletter - the Journal of Geostandards and Geoanalysis 25, 41-56.

Bowland, C.L., Rosencrantz, E., 1988. Upper crustal structure of the western Colombian Basin, Caribbean Sea. Geological Society of America Bulletin. 100, 534-546.

Brenan, J.M., Watson, E.B., 1991. Partitioning of trace elements between olivine and aqueous fluids at high P-T conditions: implications for the effect of fluid composition on trace element transport. Earth and Planetary Science Letters. 107, 672-688.

Brenan, J.M., Shaw, H.F., Ryerson, F.J., 1995. Experimental-Evidence for the Origin of Lead Enrichment in Convergent-Margin Magmas. Nature. 378, 54-56.

Brown, E., Colling, A., Park, D., Phillips, J., Rothery, D., Wright, J., 1997. Seawater: its composition, properties and behaviour, Open University, 86-87.

Burke, K., Coates, A.G., Robinson, E., 1969. Geology of the Benbow Inlier and Surrounding Areas, Jamaica. Transactions of the Fourth Caribbean Geological Conference, Port of Spain, Trinidad, 229 – 307. (Dated 1968).

Burke, K., 1988. Tectonic evolution of the Caribbean. Annual Review of Earth and Planetary Science 16, 201-230.

Byrne, D.B., Suarez, G., and McCann, W.R., 1985. Muertos Trough subduction - microplate tectonics in the northern Caribbean? Nature. 317, 420-421.

References

Calais, E., Mercier de Lépinay, B., 1991. From transtension to transpression along the northern Caribbean plate boundary off Cuba: implications for the Recent motion of the Caribbean plate. Tectonophysics. 186, 329-350.

Calais, E., Béthoux, N., Mercier de Lépinay, B., 1992. From transcurrent faulting to frontal subduction: A seismotectonic study of the northern Caribbean plate boundary from Cuba to Puerto Rico. Tectonics. 11, 114-123.

Campbell, I.H., Griffiths, R.W. and Hill, R.I., 1989. Melting in an Archaean mantle plume: heads it's basalts, tails its komatiites. Nature. 339, 697-699.

Campbell, I.H., Griffiths, R.W., 1990. Implications of mantle plume structure for the evolution of flood basalts. Earth and Planetary Science Letters 99, 79-93.

Campbell, I.H., 2007. Testing the plume theory. Chemical Geology, In press.

Castillo, P.R., Newhall, C.G., 2004. Geochemical constraints on possible subduction components in lavas of Mayon and Taal volcanoes, southern Luzon, Philippines. Journal of Petrology. 45, 1089-1108.

Castillo, P.R., Rigby, S.J., Solidum, R.U., 2007. Origin of high field strength element enrichment in volcanic arcs: Geochemical evidence from the Sulu Arc, southern Philippines. Lithos. doi:10.1016/j.lithos.2006.12.012.

Class, C., Miller, D.M., Goldstein, S., Langmuir, C., 2000. Distinguishing melt and fluid subduction components in Umnak Volcanics, Aleutian Arc. Geochemistry Geophysics Geosystems 1, paper 1999GC000010.

Condie, K.C., 2005. TTGs and adakites: are they both slab melts? Lithos. 80, 33-44.

Courtillot, V., Danaille, A., Besse, J., Stock, J., 2003. Three distinct of hotspots in the Earth's mantle. Earth and Planetary Science Letters. 205, 295-308.

Chubb, L.J., Burke, K., 1963. Age of the Jamaican Granodiorite. Geological Magazine. 100, 524-532.

Crow, C., Condie, K.C., 1990. Geochemistry and Origin of early Proterozoic volcanic rocks from the Transvaal and Soutpansberg successions, South Africa. Precambrian Research. 47, 17-26.

Davidson, J.P., 1987. Crustal contamination versus subduction zone enrichment: examples from the Lesser Antilles and implications for the mantle source composition of island arc lavas. Geochimica et Cosmochimica Acta. 51, 2185-2198.

Debaille, V., Blichert-Toft, J., Agranier, A., Doucelance, R., Schiano, P., Albarede., 2006. Geochemical component relationships in MORB from the Mid-Atlantic Ridge, 22-35°N. Earth and Planetary Science Letters. 241, 844-862.

References

Defant, M.J., Drummond, M.S., 1990. Derivation of some modern arc magmas by melting of young subducted lithosphere. Nature. 347, 662-665.

Defant, M.J., Jackson, T.E., Drummond, M.S., De-Boer, J.Z., Bellon, H., Feigenson, M.D., Maury, R.C., Stewart, R.H., 1992. The geochemistry of young volcanism throughout western Panama and southeastern Costa Rica: an overview. Journal of the Geological Society, London. 149, 569-579.

Defant, M.J., Drummond, M.S., 1993. Mount St. Helens: Potential example of the partial melting of the subducted lithosphere in a volcanic arc. Geology. 21, 547-550.

DeLong, S.E., Grippi, J., Burke, K., 1983. Geochemistry of some igneous rocks from the Lucea Inlier, Western Jamaica: A preliminary report. Journal of the Geological Society of Jamaica. 22, 10-15.

Dickinson, W.R., Snyder, W.S., 1979. Geometry of subducted slabs related to San Andreas transform. Journal of Geology. 87, 609-627.

Diebold, J.B., Stofta, P.L., Buhl, P., Truchan, M., 1981. Venezuela basin crustal structure. Journal of Geophysical Research. 86, 7901-7923.

Dietrich, V.J., Emmerman, R., Oberhansli, R., Puchelt, H., 1978. Geochemistry of basaltic and gabbroic rocks from the west Mariana basin and the Marian trench. Earth and Planetary Science Letters. 39, 127-144.

Donnelly, T., Rogers, J., Pushkar, P., Armstrong, R., 1971. Chemical evolution of the igneous rocks of the eastern West Indies: An investigation of thorium, uranium, and potassium distributions and lead and strontium isotopic ratios. In: T. Donnelly (Editor), Caribbean Geophysical, Tectonic, and Petrologic Studies. Geological Society of America Memoir. Geological Society of America, Boulder, CO, pp. 181-224.

Donnelly, T.W., 1972. Deep-water shallow-water, and sub-areal island arc volcanism: Example from the Virgin Islands. In: R. Shagam (Editor), Studies in Earth and Space Sciences. 401-414.

Donnelly, T.W., 1973. Late Cretaceous basalts from the Caribbean, a possible flood basalt province of vast size. EOS 54, 1004.

Donnelly, T.W., Rogers, J.J.W., 1978. The distribution of Igneous rocks throughout the Caribbean. Geologie en Mijnbouw. 57, 151-162.

Donnelly, T.W., Rogers, J.J.W., 1980. Igneous series in Island Arcs: The Northeastern Caribbean compared with Worldwide Island Arc assemblages. Bulletin of Volcanology. 43, 347-382.

Donnelly, T.W., Beets, D., Carr, M.J., Jackson, T., Klaver, G., Lewis, J., Maury, R., Schellenkens, H., Smith, A.L., Wadge, G., Westercamp, D., 1990. History and tectonic setting of Caribbean magmatism. In: Dengo, G., Case, J.E.

(Eds.), The Geology of North America, Volume H, The Caribbean Region. Geological Society of America, Boulder, Colorado, pp. 339-374.

Dostal, J., McCutcheon, S.R., 1990. Geochemistry of Late Proterozoic basaltic rocks from southeastern New Brunswick, Canada. Precambrian Research. 47, 83-98.

Draper, G., 1986. Blueschists and associated rocks in eastern Jamaica and their significance for Cretaceous plate-margin development in the northern Caribbean. Geological Society of America Bulletin 97, 48-60.

Draper, G., 1987. A revised tectonic model for the evolution of Jamaica. In: Ahmad, R. (Editor). Proceedings of a workshop on the status of Jamaican geology. Geological Society of Jamaica, Special Issue. 151-169.

Draper, G., Gutierrez, G., Lewis, J.F., 1996. Thrust emplacement of the Hispaniola peridotite belt: Orogenic expression of the mid-Cretaceous Caribbean arc polarity reversal? Geology. 24, 1143-1146.

Drummond, M.S., Defant, M.J., 1990. A model for trondhjemite-tonalite-dacite genesis and crustal growth via slab melting: Archean to modern comparisons. Journal of Geophysical Research. 95, 21,503-21,521.

Drummond, M.S., Defant, M.J., Kepezhinskas, P.K., 1996. Petrogenesis of slab-derived trondjemite-tonalite-dacite/adakite magmas. Transactions of the Royal Society of Edinburgh: Earth Sciences. 87, 205-215.

Duncan, R.A., Hargraves, R.B., 1984. Plate tectonic evolution of the Caribbean region in the mantle reference frame. In: Bonini, W.E., Hargraves, R.B., Shagam R. (Eds.), The Caribbean-South America Plate Boundary and Regional Tectonics. Geological Society of America Memoir 162, 81-93.

Dunham, A., 1996. Jamaican Jaunts – and Geology. Petros, Journal of the Sylvester-Bradley Geological Society. University of Leicester. 34, 22-23.

Edgar, N.T., Ewing, J.I., Hennion, J., 1971. Seismic refraction and reflection in the Caribbean Sea. American Association of Petroleum Geology 55, 833-870.

Eldholm, O., Coffin, M., 2000. Large igneous provinces and plate tectonics. AGU Monograph, 121, 309-326.

Elliott, T., 2003. Tracers of the Slab. Inside the subduction Factory. Geophysical Monograph. 138, 23-45.

Eva, A.N., McFarlane, N., 1985. Tertiary to early Quaternary carbonate facies relationships in Jamaica, Fourth Latin American Geological Conference Port-of-Spain, Trinidad, 210-219.

References

Ewart, A., 1982. The mineralogy and petrology of Tertiary-Recent orogenic volcanic rocks: with special reference to the andesitic-basaltic compositional range. In: Thorpe, R.S., (Ed.) Andesites, J. Wiley and Sons, Chichester, pp. 25-83.

Ewart, A., Collerson, K.D., Regelous, M., Wendt, J.I., Niu, Y., 1998. Geochemical Evolution within the Tonga-Kermadec-Lau Arc-Back-arc Systems: the Role of Varying Mantle Wedge Composition in Space and Time. Journal of Petrology. 39, 331-368.

Ewing, J., Talwani, M., Ewing, M., Edgar, T., 1967. Sediments of the Caribbean. International Conference on Tropical Oceanography Proceedings University of Miami. 5, 88-102.

Fitton, J.G., Saunders, A.D., Norry, M.J., Hardarson, B.S., Taylor, R.N., 1997. Thermal and chemical structure of the Iceland plume. Earth and Planetary Science Letters 153, 197-208.

Floyd, P.A. and Winchester, J.A., 1975. Magma type and tectonic setting discrimination using immobile elements. Earth and Planetary Science Letters. 27, 211-218.

Floyd, P.A., Winchester, J.A., 1978. Identification and discrimination of altered and metamorphosed volcanic rocks using immobile elements Chemical Geology. 21, 291-306.

Francis, P., Oppenheimer, C., 2004. Volcanoes. Oxford University Press.

Geldmacher, J., Hanan, B.B., Blichert-Toft, J., Harpp, K., Hoernle, K., Hauff, F., Werner, R., Kerr, A.C., 2003. Hafnium isotopic variations in volcanic rocks from the Caribbean Large Igneous Province and Galapagos hot spot tracks. Geochemistry Geophysics Geosystems 4, paper number 2002GC000477.

Giunta, G., 2002. The peri-Caribbean ophiolites: structure, tectono-magmatic significance and geodynamic implications. Caribbean Journal of Earth Science. 36, 1-20.

Harlow, G.E., 2004. Two high-pressure – low-temperature serpentinite matrix melange belts, Motagua fault zone, Guatemala: A record of Aptian and Maastrichtian collisions. Geological Society of America. 32, 17-20.

Hart, S.R., 1984. A large-scale isotope anomaly in the Southern Hemisphere mantle. Nature 309, 753-757.

Hart, S.R., 1988. Heterogeneous mantle domains: signatures, genesis and mixing chronologies. Earth and Planetary Science Letters. 90, 273-296.

Hart, S.R., Hauri, E.H., Oschmann, L.A., Whitehead, J.A., 1992. Mantle plumes and entrainment: isotopic evidence. Science. 256, 517-520.

References

Hastie, A.R. Kerr, A.C., Pearce, J.A., Mitchell, S.F., 2007. Classification of altered volcanic island arc rocks using immobile trace elements: Development of the Co-Th discrimination diagram. Journal of Petrology, In press.

Hauff, F., Hoernle, K., Tilton, G., Graham, D.W., Kerr, A.C., 2000a. Large volume recycling of oceanic lithosphere over short time scales: Geochemical constraints from the Caribbean Large Igneous Province. Earth and Planetary Science Letters 174, 247-263.

Hauff, F., Hoernle, K., van den Bogaard, P., Alvarado, G.E., Garbe-Schonberg, C.D., 2000b. Age and geochemistry of basaltic complexes in western Costa Rica: Contributions to the geotectonic evolution of Central America. Geochemistry Geophysics Geosystems 1, paper number 1999GC000020.

Hawkesworth, C.J., O'Nions, R.K., Arculus, R.J., 1979. Nd and Sr isotope geochemistry of island arc volcanics, Grenada, Lesser Antilles. Earth and Planetary Science Letters. 45, 237-248.

Hawkesworth, C.J., Hergt, J.M., Ellam, R.M., McDermott, F., 1991. Element fluxes associated with subduction related magmatism. Philosophical Transactions of the Royal Society of London Series A. 335, 393-405.

Herzburg, C. and O'Hara, M. J., 2002. Plume-associated ultramafic magmas of Phanerozoic age. Journal of Petrology. 43, 1857-1883.

Hildreth, W., Fierstein, J., Siems, D.F., Budahn, J.R., Ruiz, J., 2004. Rear-arc vs. arc-front volcanoes in the Katmai reach of the Alaska Peninsula: a critical appraisal of across-arc compositional variation. Contributions to Mineralogy and Petrology. 147, 243-275.

Hoernle, K., Bogaard, P.vd., Werner, R., Lissinna, B., Hauff, F., Alvarado, G., Garbe-Schönberg, D., 2002. Missing history (16-71 Ma) of the Galapagos hotspot: Implications for the tectonic and biological evolution of the Americas. Geology. 30, 795-798.

Hoernle, K., Hauff, F., Bogaard, P.vd., 2004. 70 m.y. history (139-69 Ma) for the Caribbean large igneous province. Geology. 32, 697-700.

Hofmann, A.W., 1997. Mantle geochemistry: The message from oceanic volcanism. Nature. 385, 219-229.

Hole, M.J., 1990. Geochemical evolution of Pliocene-Recent post-subduction alkalic basalts from Seal Nunataks, Antarctic Peninsula. Journal of Volcanology and Geothermal Research. 40, 149-167.

Hole, M.J., Rogers, G., Saunders, A.D., Storey, M., 1991. Relation between alkalic volcanism and slab-window formation. Geology. 19, 657-660.

Hollings, P., Kerrich, R., 2004. Geochemical systematics of tholeiites from the 2.86 Ga Pickle Crow Assemblage, northwestern Ontario: arc basalts with positive and negative Nb-Hf anomalies. Precambrian Research. 134, 1-20.

Horsfield, W.T., 1974. Major faults in Jamaica. Journal of the Geological Society of Jamaica. 14, 1-4.

Horsfield, W.T., Roobol, M.J., 1974. A tectonic model for the evolution of Jamaica. Journal of the Geological Society of Jamaica. 14, 31-38.

Iddings, J.P., 1892. The origin of igneous rocks. Bulletin of the Philosophical Society Washington. 12, 89-213.

Isaacs, M.C., Jackson, T.A., 1987. The mineralogy and geochemistry of plutonic rocks from Jamaica. In: R. Ahmad (Editor), Proceedings of a Workshop on the Status of Jamaican Geology. Geological Society of Jamaica, 95-106.

Ishikawa, T., Tera, F., 1999. Two isotopically distinct fluid components involved in the Mariana arc: Evidence from Nb/B ratios and B, Sr, Nd and Pb isotope systematics. Geology. 27, 83-86.

Jackson, T.A. and Smith, T.E., 1978. Metasomatism in the Tertiary volcanics of the Wagwater Belt, Jamaica, Geologie en Mijnbouw. 57, 213-220.

Jackson, T.A., Smith, T.E., 1979. The petrochemistry of some mafic volcanics, Jamaica, West Indies. Transactions of the 4th Latin American Geological Conference, Port-of-Spain, Trinidad 387-396.

Jackson, T.A., Rodrigues, K., Smith, T.E., 1980. The composition and tectonic importance of Cretaceous pillow lavas from Whitehall, St. Thomas, Jamaica. Journal of the Geological Society of Jamaica 19, 40-45.

Jackson, T.A., 1985. St Peter's Inlier -- Fact or Fiction? Journal of the Geological Society of Jamaica. 23, 44-49.

Jackson, T.A., 1987. The petrology of Jamaican Cretaceous and Tertiary volcanic rocks and their tectonic significance. In: Ahmad R. (Ed.), Proceedings of a Workshop on the Status of Jamaican Geology. Geological Society of Jamaica, Kingston. pp. 107-119.

Jackson, T.A., Smith, T.E., Isaacs, M.C., 1989. The significance of geochemical variations in Cretaceous volcanic and plutonic rocks of intermediate and felsic composition from Jamaica. Journal of the Geological Society of Jamaica. 26, 33-42.

Jackson, T.A., Scott, P.W., 1997. A welded tuff boulder from within the Wagwater Belt, Jamaica. Journal of the Geological Society of Jamaica. 32, 25-28.

Jackson, T.A., Lewis, J.F., Scott, P.W., Manning, P.A.S., 1998. The petrology of lamprophyre dikes in the Above Rocks granitoid, Jamaica: Evidence of

rifting above a subduction zone during the early Tertiary. Caribbean Journal of Science. 34, 1-11.

Johnston, A.D., Wyllie, P.J., 1989. The system tonalite-peridotite-H_2O at 30 kbar with applications to hybridization in subduction zone magmatism. Contributions to Mineralogy and Petrology. 102, 257-264.

Kelemen, P.B., 1990. Reaction between ultramafic rock and fractionating basaltic magmas I. Phase relations, the origin of calc-alkaline magma series, and the formation of discordant dunite. Journal of Petrology. 31, 51-98.

Kempton, P.D., 1995. Common Pb chemical procedures for silicate rocks and minerals, methods of data correction and an assessment of data quality at the NERC Isotope Geosciences Laboratory, NIGL Report Series, No. 78.

Kempton, P.D., Fitton, J.G., Saunders, A.D., Nowell, G.M., Taylor, R.N., Hardarson, B.S., Pearson, G., 2000. The Iceland plume in space and time: a Sr-Nd-Pb-Hf study of the North Atlantic rifted margin. Earth and Planetary Science Lettters 177, 255-271.

Kempton, P.D., Pearce, J.A., Barry, T.L., Fitton, J.G., Langmuir, C., Christie, D.M., 2002. Sr-Nd-Pb-Hf isotope results from ODP Leg 187: evidence for mantle dynamics of the Australian-Antarctic discordance and origin of the Indian MORB source. Geochemistry Geophysics Geosystems 3, paper number 2002GC00320.

Kepezhinskas, P., Defant, M.J., Drummond, M.S., 1996. Progressive enrichment of island arc mantle by melt-peridotite interaction inferred from Kamchatka xenoliths. Geochimica et Cosmochimica Acta. 60, 1217-1229.

Keppler, H., 1996. Constraints from partitioning experiments on the composition of subduction-zone fluids. Nature 380, 237-240.

Kerr, A.C., Tarney, J., Marriner, G.F., Nivia, A., Saunders, A.D., Klaver, G.T., 1996a. The geochemistry and tectonic setting of late Cretaceous Caribbean and Colombian volcanism. Journal of South American Earth Sciences 9, 111-120.

Kerr, A.C., Tarney, J., Marriner, G.F., Klaver, G.T., Saunders, A.D., Thirlwall, M.F., 1996b. The geochemistry and petrogenesis of the late-Cretaceous picrites and basalts of Curacao, Netherlands Antilles: A remnant of an oceanic plateau. Contributions to Mineralogy and Petrology 124, 29-43.

Kerr, A.C., Marriner, G.F., Arndt, N.T., Tarney, J., Nivia, A., Saunders, A.D., Duncan, R.A., 1996c. The petrogenesis of Gorgona komatiites, picrites and basalts: new field, petrographic and geochemical constraints. Lithos. 37, 245-260.

Kerr, A.C., Marriner, G.F., Tarney, J., Nivia, A., Saunders, A.D., Thirlwall, M.F., Sinton, C.W., 1997. Cretaceous basaltic terranes in western Colombia:

Elemental, Chronological and Sr-Nd isotopic constraints on petrogenesis. Journal of Petrology. 38, 677-702.

Kerr, A.C., 1998a. Oceanic plateau formation: A cause of mass extinction and black shale deposition around the Cenomanian-Turonian boundary. Journal of the Geological Society of London 155, 619-626.

Kerr, A.C., Tarney, J., Nivia, A., Marriner, G.F. and Saunders, A.D., 1998b. The internal structure of oceanic plateaus: Inferences from obducted Cretaceous terranes in western Colombia and the Caribbean. Tectonophysics. 292, 173-188.

Kerr, A.C., Iturralde-Vinent, M.A., Saunders, A.D., Babbs, T.L., Tarney, J., 1999. A new plate tectonic model of the Caribbean: Implications from a geochemical reconnaissance of Cuban Mesozoic volcanic rocks. Geological Society of America Bulletin 111, 1581-1599.

Kerr, A.C., White, R.V., Saunders, A.D., 2000. LIP reading: Recognizing oceanic plateaux in the geological record. Journal of Petrology 41, 1041-1056.

Kerr, A.C., Aspden, J.A., Tarney, J., Pilatasig, L.F., 2002a. The nature and provenance of accreted oceanic terranes in western Ecuador: geochemical and tectonic constraints. Journal of the Geological Society, London 159, 577-594.

Kerr, A.C., Tarney, J., Kempton, P.D., Spadea, P., Nivia, A., Marriner, G.F., Duncan, R.A., 2002b. Pervasive mantle plume head heterogeneity: Evidence from the late Cretaceous Caribbean-Colombian oceanic plateau. Journal of Geophysical Research-Solid Earth 107(B7), paper 2001JB000790.

Kerr, A.C., White, R.V., Thompson, P.M.E., Tarney, J., Saunders, A.D., 2003. No Oceanic Plateau - No Caribbean Plate? The Seminal Role of an Oceanic Plateau in Caribbean Plate Evolution. In: Bartolini, C., Buffler, R.T., Blickwede, J. (Editors.), The Circum Gulf of Mexico and Caribbean: Hydrocarbon Habitats Basin Formation and Plate Tectonics. American Association of Petroleum Geology Memoir, 79, 126-268.

Kerr, A.C., Tarney, J., 2005. Tectonic evolution of the Caribbean and northwestern South America: The case for accretion of two Late Cretaceous oceanic plateaus. Geology 33, 269-272.

Kimura, G., Ludden, J., 1995. Peeling oceanic crust in subduction zones. Geology. 23, 217-220.

Krijnen, J.P., Lee Chin, A.C., 1978. Geology of the northern, central and southeastern Blue Mountains, Jamaica, with a provisional compilation map of the entire inlier. Geologie en Mijnbouw 57, 243-250.

Krijnen, J.P., MacGillavry, H.J., van Dommelen, H., 1993. Review of Upper Cretaceous orbitoidal larger foraminifera from Jamaica, West Indies, and their connection with rudist assemblages. In: Wright, R.M., Robinson, E.

(Eds.) Biostratigraphy of Jamaica, Geological Society of Jamaica Memoir 182, 29-63.

Kuno, H., 1968. Differentiation of basalt magmas. In Hess, H.H., Poldervaart, A.A., (editors.) Basalts: The Poldervaart Treatise on Rocks of Basaltic Composition, 2. New York: Interscience, 623-688.

Land, L.S., 1979. The fate of reef-derived sediment on the north Jamaican island slope. Marine Geology. 29, 55-71.

Lapierre, H., Dupuis, V., Mercier de Lépinay, B., Tardy, M., Ruiz, J., Maury, R.C., Hernandez, J., Loubet, M., 1997. Is the Lower Duarte Igneous Complex (Hispaniola) a Remnant of the Caribbean Plume-Generated Oceanic Plateau? Journal of Geology. 105, 111-120.

Le Bas, M.J., Le Maitre, R.W., Steckeisen, A., Zanettin, B., 1986. A chemical classification of volcanic rocks based on the total alkali-silica diagram. Journal of Petrology 27, 745-750.

Le Bas, M.J., Le Maitre, R.W., Woolley, A.R., 1992. The constuction of the total alkali-silica chemical classification of volcanic rocks. Mineralogy and Petrology 46, 1-22.

Lebron, M.C. and Perfit, M.R., 1993. Stratigraphic and petrochemical support subduction polarity reversal of the Cretaceous Caribbean Island arc. Journal of Geology. 101, 389-396.

Leroy, S., Mauffret, A., 1996. Intraplate deformation in the Caribbean region. Journal of Geodynamics 21, 113-122.

Lewis, J.F., Harper, C.T., Kemp, A.W., Stipp, J.J., 1972. Potassium-argon retention ages of some Cretaceous rocks from Jamaica. Geological Society of America Bulletin. 84, 335-340.

Lewis, J.F., Draper, G., 1990. Geological and tectonic evolution of the northern Caribbean Margin. In: G. Dengo and J.E. Case (Editors), The Caribbean Region. The Geology and North America. The Geological Society of America, Boulder, Co, pp. 77-140.

Ludwig, W.J., Houtz, R.E., Ewing, J.I., 1975. Profiler-sonobuoy measurements in the Colombia and Venezuela Basins, Caribbean Sea. American Association of Petroleum Geology 59, 115-123.

Mann, P., Hempton, M.R., Bradley, D.C., Burke, K., 1983. Development of pull-apart basins. Journal of Geology. 91, 529-554.

Mann, P., Burke, K., 1984. Cenozoic rift formation in the northern Caribbean. Geology. 12, 732-736.

References

Manning, P.A.S., McCain, T.W., 1989. Report of a field meeting to the Above Rocks Inlier, north St Catherine and south St Mary, 3 December 1988. The Journal of the Geological Society of Jamaica. 26, 43-50.

Mauffret, A., Leroy, S., 1997. Seismic stratigraphy and structure of the Caribbean igneous province. Tectonophysics 283, 61-104.

McCulloch, M.T., Gamble, J.A., 1991. Geochemical and Geodynamical constraints on subduction zone magmatism. Earth and Planetary Science Letters. 102, 358-374.

McDermott, F., Hawkesworth, C., 1991. Th, Pb and Sr isotope variations in young island arc volcanics and oceanic sediments. Earth and Planetary Science Letters. 104, 1-15.

McDonald, I., Viljoen, K.S., 2006. Platinum-group element geochemistry of mantle eclogites: a reconnaissance study of xenoliths from the Orapa kimberlite, Botswana. Applied Earth Science (Trans. Inst. Min. Metall. B). 115. 81-93.

McDonough, W.F., Sun, S.-s., 1995. The composition of the Earth Chemical Geology. 120, 223-253.

Meschede, M., Frisch, W., 1998. A plate-tectonic model for the Mesozoic and Early Cenozoic history of the Caribbean plate. Tectonophysics 296, 269-291.

Miller, D.M., Goldstein, S., Langmuir, C., 1994. Cerium/lead and lead isotope ratios in arc magmas and the enrichment of lead in the continents. Nature. 368, 514-519.

Mitchell, S.F., Blissett, D., 1999. The Cretaceous-Paleocene Summerfield Formation, Jamaica: One or Two Ignimbrites? Caribbean Journal of Science. 35, 304-309.

Mitchell, S.F., 2000. Facies analysis of a Cretaceous-Paleocene volcaniclastic braid-delta. Geological Society of Trinidad and Tobago. Presented 10-13th July.

Mitchell, S.F., Blissett, D., 2001. Lithostratigraphy of the Late Cretaceous to ?Paleocene succession in the western part of the Central Inlier of Jamaica. Caribbean Journal of Science. 35, 19-31.

Mitchell, S. F., 2002. Field guide to the geological evolution of the Maastrictian rocks of the Central Inlier, Jamaica. Caribbean Journal of Science. 36, 27-38.

Mitchell, S.F., 2003. Sedimentary and tectonic evolution of central Jamaica. In: Bartolini, C., Buffler, R.T., Blickwede J.F., (Editors.), The Circum-Gulf of Mexico and the Caribbean: hydrocarbon habitats, basin formation, and plate tectonics. American Association of Petroleum Geologists Memoir 79, 605-623.

Mitchell, S.F., 2004. Lithostratigraphy and palaeogeography of the White Limestone Group In: Donovan, S. K. (Ed.), The mid-Cainozoic White Limestone Group of Jamaica. Cainozoic Research. 3, 5-29.

Mitchell, S.F., 2006. Timing and implications of Late Cretaceous tectonic and sedimentary events in Jamaica. Geologica Acta, 4, 171-178.

Montgomery, H., Pessagno, E.A., Jr., Lewis, J.F., Schellekens, J., 1994. Paleogeography of Jurassic fragments in the Caribbean. Tectonics. 13, 725-732.

Montgomery, H., Pessagno, E.A., Jr., 1999. Cretaceous microfaunas of the Blue Mountains, Jamaica, and of the northern and central basement complexes of Hispaniola. In: Mann, P. (Ed.), Caribbean Basins. Sedimentary Basins of the World. Elsevier Science B.V., Amsterdam, The Netherlands, pp. 237-246.

Miyashiro, A., 1974. Volcanic rock series in island arcs and active continental margins. American Journal of Science. 274, 321-355.

Műller, R.D., Royer, J.Y., Lawver, L.A., 1993. Revised Plate Motions Relative to the Hotspots from Combined Atlantic and Indian-Ocean Hotspot Tracks. Geology. 21(3), 275-278.

Müller, R.D, Royer, J.-Y, Cande, S.C., Roest, W.R., Maschenkov, S., 1999. New constraints on the Late Cretaceous/Tertiary plate tectonic evolution of the Caribbean. In: P. Mann (Editor), Caribbean Basins. Sedimentary Basins of the World. Elsevier Science B.V., Amsterdam, The Netherlands, 33-59.

Münker, C., Weyer, S., Scherer, E., Mezger, K., 2001. Separation of high field strength elements (Nb, Ta, Zr, Hf) and Lu from rock samples for MC-ICPMS measurements. Geochemmistry Geophysics Geosystems 2, paper number 2001GC000183.

Nakano, S., 1993. Ueno basaltic rocks I: Heterogeneous magmas at two monogenetic volcanoes. Journal of Japanese Association of Mineralogy Petrology and Economic Geology. (Ganseki Kobutsu Kosho Gakkai-Shi). 88, 272-288.

Nakano, S., 1994. Ueno basaltic rocks II: Chemical variation in the Kiso Province, to the south of the Ontake volcano. Journal of Japanese Association of Mineralogy Petrology and Economic Geology. (Ganseki Kobutsu Kosho Gakkai-Shi). 89, 115-130.

Nowell, G.M., Kempton, P.D., Noble, S.R., 1998. High precision Hf isotope measurements of MORB and OIB by thermal ionisation mass spectrometry: insights into the depleted mantle. Chemical Geology 149, 211-233.

Nowell, G.M., Parrish, R.R., 2001. Simultaneous acquisition of isotope compositions and parent/daughter ratios by non-isotope dilution solution-mode Plasma Ionisation Multi-collector Mass Spectrometry (PIMMS). In: Holland G.,

Tanner S.D. (Ed.s), Plasma source mass spectrometry - The new millennium. Royal Society of Chemistry, Cambridge, pp. 298-310.

O'Nions, R.K., Carter, S.R., Cohen, R.S., Evensen, N.M., Hamilton, P.J., 1978. Pb Nd and Sr isotopes in oceanic ferromanganese deposits and ocean floor basalts. Nature. 273, 435 – 438.

Patchett, P.J., 1983. Hafnium isotope results from mid-ocean ridges and Kerguelen. Lithos. 16, 47-51.

Peacock, M.A., 1931. Classification of igneous rock series. Journal of Geology. 39, 54-67.

Pearce, J.A., Cann, J.R., 1973. Tectonic setting of basic volcanic rocks determined using trace element analyses. Earth and Planetary Science Letters. 19, 290-300.

Pearce, J.A., 1982. Trace element characteristics of lavas from destructive plate boundaries. In: Thorpe, R.S., (Ed.) Andesites, J. Wiley and Sons, Chichester, pp. 525-547.

Pearce, J.A., 1983. Role of the sub-continental lithosphere in magma genesis at active continental margins. In Continental Basalts and Mantle Xenoliths. Hawkesworth, C.J., Norry, M.J., (editors). Nantwich, U.K. Shiva, 230-249.

Pearce, J.A., Parkinson, I.J., 1993. Trace element models for mantle melting: application to volcanic arc petrogenesis. Geological Society of London Special Publication. 76, 373-403.

Pearce, J.A., Peate, D.W., 1995. Tectonic implications of the composition of volcanic arc magmas. Annual Reviews Earth and Planetary Science Letters. 23, 251-285.

Pearce, J.A., 1996. A User's Guide to Basalt Discrimination Diagrams. In: Wyman, D.A. (ed.), Trace Element Geochemistry of Volcanic Rocks: Applications for Massive Sulphide Exploration. Geological Association of Canada, Short Course Notes 12, 79-113.

Pearce, J.A., Kempton, P.D., Nowell, G.M., Noble, S.R., 1999. Hf-Nd Element and Isotope Perspective on the Nature and Provenance of Mantle and Subduction Components in Western Pacific Arc-Basin Systems. Journal of Petrology. 40, 1579-1611.

Peccerillo, R., Taylor, S.R., 1976. Geochemistry of Eocene calc-alkaline volcanic rocks from the Kastamonu area, northern Turkey. Contributions to Mineralogy and Petrology. 58, 63-81.

Perfit, M.R., Heezen, B.C., 1978. The geology and evolution of the Cayman Trench. Geological Society of America Bulletin. 89, 1155-1174.

Pindell, J.L., Barrett, S.F., 1990. Geological evolution of the Caribbean region: a plate tectonic perspective. In: Dengo, G., Case J.E. (Eds.), The Geology of North America. Geological Society of America, Boulder, Colorado, The Caribbean Region, Volume H, pp. 405-432.

Pindell, J., Kennan, L., 2001. Kinematic Evolution of the Gulf of Mexico and Caribbean. 21st Annual GCSSEPM Foundation Bob F. Perkins Research Conference.

Plank, T., Langmuir, C., 1998. The chemical composition of subducting sediment and its consequences for the crust and mantle. Chemical Geology. 145, 325-394.

Polat, A., Kerrich, R., 2001. Magnesian andesites, Nb-enriched basalt-andesites, and adakites from late-Archean 2.7 Ga Wawa greenstone belts, Superior Province, Canada: implications for late Archean subduction zone petrogenetic processes. Contributions to Mineralogy and petrology. 141, 36-52.

Polat, A., Hofmann, A.W., Rosing, M.T., 2002. Boninite-like volcanic rocks in the 3.7-3.8 Ga Isua greenstone belt, West Greenland: geochemical evidence for intra-oceanic subduction zone processes in the early Earth. Chemical Geology. 184(3-4), 231-254.

Puchtel, I.S., Hofmann, A.W., Amelin, Yu.V., Garbe-Schönberg, C.D., Samsonov, A.V., Shchipansky, A.A., 1999. Combined mantle plume-island arc model for the formation of the 2.9 Ga Sumozero-Kenozero greenstone belt, SE Baltic Shield: Isotope and trace element constraints. Geochimica et Cosmochimica Acta. 63, 3579-3595.

Rapp, R.P., Watson, E.B., Miller, C.F., 1991. Partial melting of amphibolite/eclogite and the origin of Archean trondhjemites and tonalites. Precambrian Research. 51, 1-25.

Reagan, M.K., Gill, J.B., 1989. Coexisting calcalkaline and high-niobium basalts from Turrialba volcano, Costa Rica: Implications for residual titanites in arc magma sources. Journal of Geophysical Research. 94, 4619-4633.

Reed, A.J., 1966. Geology of the Bog Walk quadrangle, Jamaica. Geological Survey Department, Jamaica, Bulletin. 6, 54.

Regelous, M., Collerson, K.D., Ewart, A., Wendt, J.I., 1997. Trace element transport rates in subduction zones: evidence from Th, Sr and Pb isotope data for Tonga-Kermadec arc lavas. Earth and Planetary Science Letters. 150, 291-302.

Révillon, S., Arndt, N.T., Hallot, E., Kerr, A.C., Tarney, J., 1999. Petrogenesis of picrites from the Caribbean Plateau and the North Atlantic magmatic province. Lithos 494), 1-21.

References

Révillon, S., Hallot, E., Arndt, N.T., Chauvel, C., Duncan, R.A., 2000. A complex history for the Caribbean plateau: Petrology, geochemistry, and geochronology of the Beata Ridge, south Hispaniola. Journal of Geology 108, 641-661.

Révillon, S., Chauvel, C., Arndt, N.T., Pik, R., Martineau, F., Fourcade, S., Marty, B., 2002. Heterogeneity of the Caribbean plateau mantle source: Heterogeneity of the Caribbean plateau mantle source: Sr, O and He isotopic compositions of olivine and clinopyroxene from Gorgona Island. Earth and Planetary Science Letters 205, 91-106.

Reymer, A., Schubert, G., 1986. Rapid growth of some major segments of continental crust. Geology. 14, 299-302.

Richards, M.A., Duncan, R.A., Courtillot, V.E., 1989. Flood basalts and hot spot tracks. plume heads and tails. Science. 246, 103-107.

Richter, F.M., Models for the Archean thermal regime. Earth and Planetary Science Letters. 73, 350-360.

Rickwood, P.C., 1989. Boundary lines within petrologic diagrams which use oxides of major and minor elements. Lithos. 22, 247-263.

Robinson, E., Lewis, J.F., Cant, R.V., 1971. Field guide to aspects of the geology of Jamaica, IFI Guidebook to the Caribbean Island Arc System. American Geological Institute Special Publication, pp. 49.

Robinson, E., 1988. Late Cretaceous and early Tertiary sedimentary rocks of the Central Inlier, Jamaica. Journal of the Geological Society of Jamaica. 24, 49-67.

Robinson, E., 1994. Jamaica. In: Donovan, S.K., Jackson, T.A. (Eds.), Caribbean Geology: An Introduction. University of the West Indies Publisher's Association, Kingston, Jamaica, pp. 111-127.

Rollinson, H., 1993. Using geochemical data: evaluation, presentation, interpretation. Pearson education limited 102-170.

Roobol, M.J., 1972. The volcanic geology of Jamaica. Transactions of the 6th Caribbean Geological Conference. 100-107.

Roobol, M.J., Horsfield, W.T., 1976. Seafloor outcrop in the Jamaica Passage. Journal of the Geological Society of Jamaica. 15, 7-10.

Rosencrantz, E., Sclater, J.G., 1986. Depth and age in the Cayman Trough. Earth and Planetary Science Letters. 79, 133-144.

Rosencrantz, E., Ross, M.I., Sclater, J.G., 1988. Age and Spreading History of The Cayman Trough as Determined From Depth, Heat Flow, and Magnetic Anomalies. Journal of Geophysical Research. 93, 2141-2157.

Royse, K.R., Kempton, P.D., Darbyshire, F.D., 1998. Procedure for the analysis of rubidium-strontium and samarium-neodymium isotopes at the NERC Isotope Geosciences Laboratory, NIGL Report Series, No. 121.

Sajona, F.G., Maury, R.C., Bellon, H., Cotton, J., Defant, M.J., Pubellier, M., 1993. Initiation of subduction and the generation of slab melts in western and eastern Mindanao, Philippines. Geology. 21, 1007-1010.

Salters, V.J.M. and Hart, S.R., 1991. The mantle sources of ocean ridges, islands and arcs: the Hf-isotope connection. Earth and Planetary Science Letters. 104, 364-380.

Salters, V.J.M. and White, W.M., 1998. Hf isotope constraints on mantle evolution. Chemical Geology. 145(3-4), 447-460.

Saunders, A.D., Tarney, J., Weaver, S.D., 1980. Transverse geochemical variations across the Antarctic Peninsula: implications for the genesis of calc-alkaline magmas. Earth and Planetary Science Letters. 46, 344-360.

Saunders, A.D., Tarney, J., Kerr, A.C. and Kent, R.W., 1996. The formation and fate of large igneous provinces. Lithos. 37, 81-95.

Schmidt, W., 1988. Stratigraphy and depositional environment of the Lucea Inlier, Western Jamaica. Journal of the Geological Society of Jamaica. 24, 15-36.

Sinton, C.W., Duncan, R.A., Denyer, P., 1997. Nicoya Peninsula, Costa Rica: A single suite of Caribbean oceanic plateau magmas. Journal of Geophysical Research. B102, 15,507-15,520.

Sinton, C.W., Duncan, R.A., Storey, M., Lewis, J., Estrada, J.J., 1998. An oceanic flood basalt province within the Caribbean plate. Earth and Planetary Science Letters 155, 221-235.

Smit, J., 1977. Planktonic formaniferal faunas from the upper part of the Washikemba Formation, Bonaire, 8th Caribbean Geological Conference, Curaçao, pp. 192-193.

Smith, R.E., Smith, S.E., 1976. Comments on the use of Ti, Zr, Y, Sr, K, P and Nb in classification of basaltic magmas. Earth and Planetary Science Letters. 32, 114-120.

Sorenson, S.S., 1988. Petrology of amphibolitic-facies mafic and ultramafic rocks from the Catalina Schist, southern California: metasomatism and migmatization in a subduction zone metamorphic setting. Metamorphic Geology. 6, 405-435.

Sorenson, S.S., Grossman, J.N., 1989. Enrichment of trace elements in garnet amphibolites from paleo-subduction zone: Catalina Schist, southern California. Geochimica et Cosmochimica Acta. 53, 3155-3177.

References

Spadea, P., Espinosa, A., 1996. Petrology and chemistry of late Cretaceous volcanic rocks from the southernmost segment of the Western Cordillera of Colombia (South America). Journal of South American Earth Sciences. 9, 79-90.

Stern, R.J., Jackson, M.C., Fryer, P., Ito, E., 1993. O, Sr, Nd and Pb isotopic composition of the Kasuga cross-chain in the Mariana arc: a new perspective of the K-h relationship. Earth and Planetary Science Letters. 119, 459-475.

Stőckhert, B., Maresch, W.V., Brix, M., Kaiser, C., Toetz, A., Kluge, R., Krűckhans-Lueder, G., 1995. Crustal history of Margarita Island (Venezuela) in detail: Constraint on the Caribbean plate-tectonic scenario. Geology. 23, 787-790.

Summerfield, M.A., 1997. Global Geomorphology. Longman Singapore Publishers (Pte) Ltd: 129-144.

Sun, S.-s., McDonough, W.F., 1989. Chemical and isotope systematics of oceanic basalts: implications for mantle composition and processes. Magmatism in the Ocean Basins Geological Society of London, Special Publication. 42, 313-345.

Tatsumi, Y., Hamilton, D.L., Nesbitt, R.W., 1986. Chemical characteristics of fluid phase released from a subducted lithosphere and origin of arc magmas: evidence from high-pressure experiments and natural rocks. Journal of Volcanology and Geothermal Research 29, 293-309.

Tatsumi, Y., Koyaguchi, T., 1989. An absarokite from a phlogopite lherzolite source. Contributions to Mineralogy and Petrology. 102, 34-40.

Tatsumi, Y., Murasaki, M., Nohda, S., 1992. Across arc variation of lava chemistry in the Izu-Bonin arc: identification of subduction components. Journal of Volcanology and Geothermal Research 49, 179-190.

Tatsumi, Y., Kogiso, T., 1997. Trace element transport during dehydration processes in the subducted oceanic crust: 2. Origin of chemical and physical characteristics in arc magmatism. Earth and Planetary Science Letters. 148, 207-221.

Tatsumi, Y., 2003. Some Constraints on Arc Magma Genesis. Inside the subduction Factory, Geophysical Monograph 138, 277-292.

Thirlwall, M.F., Graham, A.M., Arculus, R.J., Harmon, C.G., Macpherson, C.G., 1996. Resolution of the effects of crustal assimilation, sediment subduction and fluid transport in island arc magmas: Pb-Sr-Nd-O isotope geochemistry of Grenada, Lesser Antilles. Geochimica et Cosmochimica Acta. 60, 4785-4810.

Thirlwall, M.F., 2002. Multicollector ICP-MS analysis of Pb isotopes using a ^{207}Pb-^{204}Pb double spike demonstrates up to 400pm/amu systematic errors in Tl-normalization. Chemical Geology 184, 255-279.

Thompson, P.M.E., 2002. Petrology and geochronology of an arc sequence, Bonaire, Dutch Antilles, and its relationship to the Caribbean Plateau. University of Leicester. PhD Thesis.

Thompson, P.M.E., Kempton, P.D., White, R.V., Kerr, A.C., Tarney, J., Saunders, A.D., Fitton, J.G., 2003. Hf-Nd isotope constraints on the origin of the Cretaceous Caribbean plateau and its relationship to the Galapagos plume. Earth and Planetary Science Letters 217, 59-75.

Thompson, P.M.E., Kempton, P.D., White, R.V., Saunders, A.D., Kerr, A.C., Tarney, J., Pringle, M.S., 2004. Elemental, Hf-Nd isotopic and geochronological constraints on an island arc sequence associated with the Cretaceous Caribbean plateau: Bonaire, Dutch Antilles. Lithos 74, 91-116.

Thorkelson, D.J., Taylor, R.P., 1989. Cordilleran slab windows. Geology. 17, 833-836.

Turner, S., Hawkesworth, C., Calsteren, P.V., Heath, E., Macdonald, R., Black, S., U-series isotopes and destructive plate margin magma genesis in the Lesser Antilles. Earth and Planetary Science Letters. 142, 191-207.

Turner, S., Hawkesworth, C., 1997. Constraints on flux rates and mantle dynamics beneath island arcs from Tonga-Kermadec lava geochemistry. Nature. 389, 568-573.

Underwood, C.J., Mitchell, S.F., 2000. *Serratolamna serrata* (Agassiz) (Pisces, Neoselachii) from the Maastrichtian (Late Cretaceous) of Jamaica. Caribbean Journal of Earth Science. 34, 25-30.

Van der Hilst, R., Mann, P., 1994. Tectonic implications of tomographic images of subducted lithosphere beneath northwestern South America. Geology. 22, 451-454.

Veizer, J., 1989. Sr isotopes in seawater through time. Annual Review Earth Planetary Science 17, 141-167.

Vidal, Ph., Dupuy, C., Maury, R., Richard, M., 1989. Mantle metasomatism above subduction zones: Trace-element and radiogenic isotope characteristics of peridotite xenoliths from Batan Island (Philippines). Geology. 17, 1115-1118.

Wadge, G., Draper, G., 1978. Structural geology of the southeastern Blue Mountains, Jamaica. Geologie en Mijnbouw. Special Issue, 8th Caribbean Geological Conference (Willemstad, 1977). 57, 347-352.

Wadge, G., Eva, A.N., 1978. Structural geology and tectonic significance of the Sunning Hill Inlier. Journal of the Geological Society of Jamaica. 17, 1-15.

Wadge, G., Jackson, T.A., Isaacs, M.C., Smith, T.E., 1982. The ophiolitic Bath-Dunrobin Formation, Jamaica: Significance for Cretaceous plate margin

evolution in the northwestern Caribbean. Journal of the Geological Society, London 139, 321-333.

Wadge, G., Wooden, J.L., 1982. Late Cenozoic alkaline volcanism in the northwestern Caribbean: tectonic setting and Sr isotope characteristics. Earth and Planetary Science Letters. 57, 35-46.

Wadge, G. and Burke, K., 1983. Neogene Caribbean plate rotation and associated Central American tectonic evolution. Tectonics. 2, 633-643.

Wadge, G., MacDonald, R., 1985. Cretaceous tholeiites of the northern continental margin of south America: the Sans Souci Formation of Trinadad. Journal of the Geological Society of London. 142, 297-308.

Walker, R.J., Storey, M., Kerr, A.C., Tarney, J., Arndt, N.T., 1999. Implications of ^{187}Os heterogeneities in a mantle plume: Evidence from Gorgona Island and Curaçao. Geochimica et Cosmochimica Acta. 63, 713-728.

Watson, E.B., Harrison, T.M., 1983. Zircon saturation revisited: temperature and composition effects in a variety of crustal magma types. Earth and Planetary Science Letters. 64, 295-304.

Weaver, B.L., 1991. Trace element evidence for the origin of ocean-island basalts. Geology. 19, 123-126.

White, W.M., Patchett, P.J., 1984. Hf-Nd-Sr isotopes and incompatible element abundances in island arcs: Implications for magma origins and crust-mantle evolution. Earth and Planetary Science Letters 67, 167-185.

White, W.M., Dupre, B., Sediment subduction and magma genesis in the Lesser Antilles. Journal of Geophysical Research. 91B, 5927-5941

White, R.V., Tarney, J., Kerr, A.C., Saunders, A.D., Kempton, P.D., Pringle, M.S. and Klaver, G.T., 1999. Modification of an oceanic plateau, Aruba, Dutch Caribbean: Implications for the generation of continental crust. Lithos. 46(1), 43-68.

Wilson, M., 1989. Igneous Petrogenesis: A Global Tectonic Approach. Chapman & Hall 150-190.

Winchester, J.A. and Floyd, P.A., 1976. Geochemical magma type discrimination: application to altered and metamorphosed basic igneous rocks. Earth and Planetary Science Letters. 28, 459-469.

Winchester, J.A. and Floyd, P.A., 1977. Geochemical discrimination of different magma series and their differentiation products using immobile elements Chemical Geology. 20, 325-343.

Woodhead, J.D., Hergt, J.M., Davidson, J.P., Eggins, S.M., 2001. Hafnium isotope evidence for "conservative" element mobility during subduction zone processes. Earth and Planetary Science Letters. 192, 331-346.

Workman, R.K., Hart, S.R., 2005. Major and trace element composition of the depleted MORB mantle (DMM). Earth and Planetary Science Letters. 231, 53-72.

Yardley, B.W.D., 1999. An introduction to Metamorphic Petrology. Pearson Education Limited, 91-125.

Yihunie, T., Adachi, M., Yamamoto, K., 2006. Geochemistry of the Neoproterozoic metabasic rocks from the Negele area, southern Ethiopia: Tectonomagmatic implications. Journal of African Earth Sciences. 44, 255-269.

Yogodzinski, G.M., Volynets, O.N., Koloskov, A.V., Seliverstov, N.I., 1994. Magnesian andesites and the subduction component in a strongly calcalkaline series at Piip volcano, far western Aleutians. Journal of Petrology. 34, 163-204.

Yogodzinski, G.M., Kay, R.W., Volynets, O.N., Koloskov, A.V., Kay, S.M., 1995. Magnesian andesite in the western Aleutian Komandorsky region: Implications for slab melting and processes in the mantle wedge. Geological Society of America Bulletin. 107, 505-519.

Zellmer, G.F., Hawkesworth, C.J., Sparks, R.S.J., Thomas, L.E., Harford, C.L., Brewer, T.S., Loughlin, S.C., 2003. Geochemical Evolution of the Soufrière Hills Volcano, Montserrat, Lesser Antilles Volcanic Arc Journal of Petrology. 44, 1349-1374.

Appendix A

Sample description and locality

A.1 Sample information and description

Table A.1 of this appendix contains petrographic and field information on each of the samples collected in the two field seasons in Jamaica. The table gives a petrographic description and a grid reference and/or locality description for each sample. It also lists the rock type of each sample and indicates if it was analysed for major and trace elements and/or isotopes.

A.2 Sample locality

The grid reference for each sample is given in Table A.1; however, to compliment this information 8 detailed road maps are shown in Figures A1-A7. These maps illustrate the locality of the samples in the Above Rocks Inlier, Central Inlier, Benbow Inlier, Blue Mountains Inlier and the Wagwater Belt.

Location	Sample Number	Grid Reference and/or Locality	Rock Type	Field Information	Thin Section Analysis	ICP analysis	Isotope and/or ^{40}Ar-^{39}Ar analyses
Bath-Dunrobin Formation	AHBD01	Cedar Valley	Serpentinite	Peridotite intrusion completely serpentinised	The peridotite has been completely serpentinised. > 95% of the rock is composed of serpentine. Only a small amount of cpx and spinel remains.	N	
	AHBD02	Cedar Valley	Peridotite	Slightly serpentinised intrusion	Coarse grained rock composed of olivine, opx, minor cpx and spinel. The olivine and pyroxene are moderately replaced with serpentine. The pyroxene crystals enclose olivine crystals giving poikilitic texture. The rock is mostly composed of olivine with ~ 5-10% *orthopyroxene and up to ~ 5% clinopyroxene* and opaques. Therefore the peridotite is a harzburgite.	N	
	AHBD03	Cedar Valley	Peridotite	Slightly serpentinised intrusion	Coarse grained rock composed of olivine, opx, minor cpx and spinel. The olivine and pyroxene are moderately replaced with serpentine. The pyroxene crystals enclose olivine crystals giving poikilitic texture. The rock is mostly composed of olivine with ~ 5-10% orthopyroxene and up to ~ 5% clinopyroxene and opaques. Therefore the peridotite is a harzburgite.	N	
	AHBD04	Cedar Valley	Peridotite	Slightly serpentinised intrusion	Coarse grained rock composed of olivine, opx, minor cpx and spinel. The olivine and pyroxene are moderately replaced with serpentine. The	N	

Table A.1 – Essential information about the samples collected in this study.

					pyroxene crystals enclose olivine crystals giving poikilitic texture. The rock is mostly composed of olivine with ~ 5-10% orthopyroxene and up to ~ 5% clinopyroxene and opaques. Therefore the peridotite is a harzburgite.		
	AHBD05	Cedar Valley	Peridotite	Slightly serpentinised intrusion	Coarse grained rock composed of olivine, opx, minor cpx and spinel. The olivine and pyroxene are moderately replaced with serpentine. The pyroxene crystals enclose olivine crystals giving poikilitic texture. The rock is mostly composed of olivine with ~ 5-10% orthopyroxene and up to ~ 5% clinopyroxene and opaques. Therefore the peridotite is a harzburgite.	N	
	AHBD06	Cedar Valley	Peridotite	Slightly serpentinised intrusion	Coarse grained rock composed of olivine, opx, minor cpx and spinel. The olivine and pyroxene are moderately replaced with serpentine. The pyroxene crystals enclose olivine crystals giving poikilitic texture. The rock is mostly composed of olivine with ~ 5-10% orthopyroxene and up to ~ 5% clinopyroxene and opaques. Therefore the peridotite is a harzburgite.	N	
	AHBD07	Cedar Valley	Micro-granodiorite	Fresh dyke	Porphyritic rock with plagioclase feldspar, K-feldspar, hornblende and quartz phenocrysts. The groundmass is composed of feldspar, amphibole, quartz and opaques.	Y	
	AHBD08	Cedar Valley	Peridotite	Serpentinised	Coarse grained rock composed of olivine, opx,	N	

				peridotite intrusion	minor cpx and spinel. The olivine and pyroxene are moderately replaced with serpentine. The pyroxene crystals enclose olivine crystals giving poikilitic texture. The rock is mostly composed of olivine with ~ 5-10% orthopyroxene and up to ~ 5% clinopyroxene and opaques. Therefore the peridotite is a harzburgite.		
	AHBD09	Island River	Basalt	Highly altered lava flow	The rock has undergone extreme alteration with primary minerals being very rare. Most of the rock is composed of serpentine, clay minerals, calcite and sericite. < 5 % of the rock is composed of primary feldspar, cpx fragments and opaques. Relic feldspar can also be identified.	Y	
	AHBD10	Island River	Basalt	Highly altered lava flow	The rock is aphyric and is composed of plagioclase feldspar, cpx and opaques. The rock is altered and substantial serpentine and clay minerals are present.	Y	Sr, Nd, Pb and Hf.
	AHBD11	Island River	Basalt	Altered lava flow	The rock is possibly aphyric; however, it is difficult to know due to the extent of alteration. Much of the rock is composed of serpentine, calcite and clay minerals. ~ 5-10 % of the rock is composed of cpx and opaques. Relic feldspars are visible in ppl; nevertheless, they are all (except for a few examples) replaced with secondary minerals.	Y	
	AHBD12	Island River	Rhyolite	Highly altered Tuff	Rock is composed of a glassy fragmented matrix with larger quartz and zeolite crystals.	Y	

	AHBD13	Island River	Basalt	Highly altered lava flow	The rock appears aphyric, however, it is highly altered and as such it is hard to tell. Much of the rock is composed of serpentine, clay minerals and sericite. Quartz veins can be seen in the rock. The rock is composed of a substantial amount of identifiable plagioclase feldspar, cpx, possible olivine and opaques.	Y	
	AHBD14	Island River	Basalt	Highly altered lava flow	The rock is aphyric and is composed of plagioclase feldspar, cpx fragments and opaques. The minerals have been heavily altered into clay minerals, serpentine and sericite. Relic feldspars are also present. Quartz veins can be seen.	Y	
	AHBD15	Island River	Rhyolite	Highly altered Tuff	The rock is heavily altered, fragmented and composed of quartz and zeolites.	N	
	AHBD16	Island River	Basalt	Highly altered lava flow	The rock appears aphyric, however, it is highly altered and as such it is hard to tell. Much of the rock is composed of serpentine, clay minerals and sericite. The rock is composed of a substantial amount of identifiable plagioclase feldspar, cpx, possible olivine and opaques.	Y	Sr, Nd, Pb and Hf.
	AHBD17	Island River	Basalt	Highly altered lava flow	The rock is possibly aphyric; however, it is difficult to know due to the extent of alteration. Much of the rock is composed of serpentine, calcite and clay minerals. ~ 5 % of the rock is composed of cpx and opaques. Relic feldspars are visible in ppl; however, they are all (except for a few examples) replaced with secondary minerals. Calcite veins are present.	N	

	AHBD18	Island River	Basalt	Highly altered lava flow	The rock appears aphyric, however, it is highly altered and as such it is hard to tell. Much of the rock is composed of serpentine, clay minerals and calcite. The rock contains ~ 5-10 % cpx and opaques. Relic feldspars are identified but have been completely replaced with secondary minerals. It is possible that the rock once contained olivine.	Y	Sr, Nd, Pb and Hf.
	AHBD19	Island River	Basalt	Highly altered lava flow	The rock appears aphyric, however, it is highly altered and as such it is hard to tell. Much of the rock has been altered to serpentine, clay minerals and sericite. Patches of chlorite are also present. The rock contains plagioclase feldspar, cpx and opaques. Many of the feldspars have been completely replaced.	Y	Sr, Nd, Pb and Hf.
	AHBD20	Island River	Basalt	Highly altered lava flow		Y	
	AHBD21	Island River	Basalt	Highly altered lava flow		N	
	AHBD22	Island River	Dacite	Highly altered Tuff	Rock is composed of a glassy fragmented matrix with larger quartz and zeolite crystals.	Y	
	AHBD23	Island River	Basalt	Highly altered lava flow	The rock is possibly phyric, due to relic feldspar phenocrysts. However the majority of the rock has been altered to serpentine, calcite, clay minerals and sericite. The groundmass is composed of relic feldspar, cpx fragments and opaques.	Y	Sr, Nd, Pb and Hf.
	AHBD24	Island River	Basalt	Highly altered lava flow	The rock is aphyric and is composed of ~ 90 % plagioclase feldspar, cpx fragments and	Y	

					opaques. The minerals have been heavily altered into clay minerals, serpentine and sericite.		
	AHBD25	Island River	Basalt	Highly altered lava flow		Y	
	AHBD26	Island River	Basalt	Highly altered lava flow		Y	
	AHBD27	N18°14.281 W076°57.982	Basalt	Highly altered lava flow		Y	
	AHBD28	N17°57.153 W076°20.199	Basalt	Highly altered lava flow		Y	Sr, Nd, Pb and Hf.
	AHBD29	N17°57.153 W076°20.199	Basalt	Highly altered lava flow		Y	
	AHBD30	N17°57.153 W076°20.199	Basalt	Highly altered lava flow		Y	
Benbow Inlier	AHBI01	Devils Racecourse Road	Andesite	Altered massive lava flow	The rock is phyric with phenocrysts of plagioclase feldspar and cpx. The feldspar and cpx phenocrysts are being heavily replaced with sericite and chlorite. The groundmass is composed of feldspar, cpx and opaques which have also been heavily altered with sericite and chlorite.	Y	Sr, Nd, Pb and Hf.
	AHBI02	Devils Racecourse Road	Limestone	Altered interbedded unit	The rock is mostly composed of calcite with crystals of quartz, chalcedony, feldspar and myrmekite.	N	
	AHBI03	Devils Racecourse Road	Andesite	Altered massive lava flow	The rock is phyric with phenocrysts of plagioclase feldspar and cpx. The feldspar and cpx phenocrysts are being replaced with sericite	Y	Sr, Nd, Pb and Hf.

					and chlorite. The groundmass is composed of feldspar, cpx and opaques which have also been heavily altered with sericite and chlorite.		
	AHBI04	Devils Racecourse Road	Dacite	Altered massive lava flow	The rock is porphyritic with plagioclase feldspar, K-feldspar and opaque phenocrysts. The feldspars have been slightly replaced by sericite and chlorite. The groundmass is composed of feldspars, quartz and opaques that are being replaced with chlorite and sericite.	N	
	AHBI05	Devils Racecourse Road	Rhyolite	Massive slightly altered lava flow	The rock is porphyritic with phenocrysts of plagioclase feldspar, K-feldspar and opaques. Some of the feldspar phenocrysts have developed sub-grains. Chlorite and sericite are also replacing the feldspar phenocrysts. The groundmass is composed of feldspars, quartz and opaques that are being replaced with clay *minerals, chlorite and sericite. The rock* contains veins of quartz, chlorite and a high interference colour/relief mineral that maybe epidote.	Y	
	AHBI06	Devils Racecourse Road	Rhyolite	Altered massive lava flow	The rock is phyric with phenocrysts of plagioclase feldspar and K-feldspar. The phenocrysts are being replaced with chlorite and sericite. The groundmass is composed of feldspars, quartz and opaques that are being replaced with clay minerals, chlorite and sericite. The rock contains veins of quartz, chlorite and a high interference colour/relief mineral that maybe epidote.	Y	

	AHBI07	Devils Racecourse Road	Dacite	Highly altered massive lava flow	The rock is aphyric and is composed of plagioclase feldspar, K-feldspar, quartz and opaques. The rock has substantial sericite replacement.	Y	
	AHBI08	N18°12.612 W077°00.075	Basaltic Andesite	Altered lava flow	SAMPLE LOST IN POST	N	
	AHBI09	N18°12.612 W077°00.075	Basaltic Andesite	Altered lava flow	The rock is heavily altered. It is porphyritic with plagioclase feldspar phenocrysts. The feldspars are partially replaced with sericite and chlorite. The groundmass is made up of feldspar and opaques (many with needle shapes). The vast majority of the groundmass has been altered to clay minerals, sericite and chlorite.	Y	
	AHBI10	N18°12.612 W077°00.075	Basaltic Andesite	Altered lava flow	The rock is highly altered and is phyric. The phenocrysts are composed of plagioclase feldspar that are heavily replaced with chlorite, sericite and calcite. The groundmass is composed of feldspar and opaques. The vast majority of the groundmass has been altered to clay minerals, sericite, chlorite and calcite.	Y	
	AHBI11	N18°12.612 W077°00.075	Basaltic Andesite	Altered pillow lava	Altered phyric rock with plagioclase feldspar and cpx phenocrysts. The feldspar phenocrysts are partially replaced with chlorite and sericite. The cpx phenocrysts are relatively fresh but have still been altered to chlorite and clay minerals. The groundmass is made up of feldspars, cpx and opaques; however, the vast majority has been altered to clay minerals, sericite and chlorite.	Y	Sr, Nd, Pb and Hf.

	AHBI12	N18°14.137 W076°57.801	Basaltic Andesite	Altered pillow lava with vesicles	The rock is highly altered and is phyric. The phenocrysts are composed of plagioclase feldspar and cpx. The feldspar and cpx phenocrysts are heavily replaced with chlorite, sericite and calcite. The groundmass is composed of feldspar, cpx and needle shaped opaques. The vast majority of the groundmass has been altered to clay minerals, sericite and chlorite.	Y	
	AHBI13	N18°14.137 W076°57.801	Basaltic Andesite	Altered pillow lava with vesicles	The rock is heavily altered. It is porphyritic with plagioclase feldspar phenocrysts that have been partially replaced with sericite and chlorite. The groundmass contains feldspars, cpx fragments? and opaques (some of them needle shaped). The vast majority of the groundmass is composed of clay minerals, sericite and chlorite.	Y	Sr, Nd, Pb and Hf.
	AHBI14	N18°14.137 W076°57.801	Basaltic Andesite	Altered pillow lava with vesicles	Heavily altered phyric rock. Phenocrysts composed of plagioclase feldspar that are fully or partially replaced with clay minerals, sericite and calcite. The groundmass contains feldspars, cpx fragments? and needle shaped opaques. The vast majority of the groundmass is composed of clay minerals, sericite, chlorite and calcite. Relic feldspars are also common.	Y	
	AHBI15	N18°14.281 W076°57.981	Basaltic Andesite	Altered pillow lava with vesicles	Heavily altered phyric rock. Phenocrysts composed of plagioclase feldspar that are fully or partially replaced with clay minerals, sericite and calcite. The groundmass contains feldspars, cpx fragments? and opaques (some of them	Y	

					needle shaped). The vast majority of the groundmass is composed of clay minerals, sericite, chlorite and calcite. Relic feldspars are also common. Calcite veins are seen.		
	AHBI16	N18°12.826 W077°01.733	Basaltic Andesite	Altered lava flow	The altered rock is phyric with plagioclase feldspar and maybe some K-feldspar phenocrysts. The phenocrysts are being replaced with sericite and chlorite. The groundmass is composed of feldspars and opaques that are substantially altered to sericite, clay minerals and chlorite.	Y	
	AHBI17	N18°12.826 W077°01.733	Dacite	Altered lava flow		Y	
	AHBI18	N18°12.826 W077°01.733	Andesite	Highly altered lava flow	The rock has undergone intense weathering. It is not certain to whether the rock is phyric or aphyric. Plagioclase feldspar crystals can be identified and make up ~ 2 % of the rock. The rest of the rock is composed of nodular chlorite, sericite and clay minerals which could represent relic crystals; these are surrounded by more clay minerals, sericite, chlorite, opaques and epidote. The rock contains veins of quartz, chlorite and a high interference colour/relief mineral that is maybe epidote.	Y	
	AHBI19	N18°12.826 W077°01.733	Dacite	Altered lava flow	The rock is porphyritic with phenocryts of plagioclase feldspar and K-feldspar. The feldspars are partially replaced by chlorite, calcite and sericite. The groundmass is composed of feldspars, quartz and opaques that	Y	

					are being replaced with chlorite and sericite.		
	AHBI20	N18°12.550 W077°01.534	Dacite	Altered lava flow		Y	
	AHBI21	N18°12.550 W077°01.534	Dacite	Altered lava flow	The rock appears to be aphyric; however, the heavy alteration makes this interpretation uncertain. Plagioclase feldspar, K-feldspar, quartz and opaques can be identified. Most of the rock has been replaced with clay minerals, minor chlorite and sericite.	Y	
	AHBI22	N18°12.550 W077°01.534	Dacite	Altered lava flow	The rock is porphyritic with phenocryts of plagioclase feldspar and K-feldspar. The phenocryts are slightly altered to sericite. The groundmass is composed of altered feldspar, opaques, clay minerals and sericite.	Y	
	AHBI23	N18°12.826 W077°01.278	Andesite	Altered lava flow		Y	
	AHBI24	N18°12.826 W077°01.278	Dacite	Altered lava flow		N	
	AHBI25	N18°12.826 W077°01.278	Dacite	Altered lava flow	SAMPLE LOST IN POST	N	
	AHBI26	N18°12.550 W077°00.994	Dacite	Altered lava flow	The rock appears to be porphyritic; however, it is difficult to be certain due to the heavy alteration. Plagioclase feldspar and K-feldspar phenocrysts can be identified. These phenocrysts are being slightly replaced with sericite and chlorite. The groundmass is made up of feldspar, quartz and opaques that are heavily replaced with sericite, clay minerals and chlorite. The rock contains veins of quartz,	Y	

					chlorite and a high interference colour/relief mineral that maybe epidote.		
	AHBI27	N18°12.550 W077°00.994	Dacite	Altered lava flow	The rock appears to be phyric; however, it is difficult to be certain due to the heavy alteration. K-feldspar, plagioclase feldspar and quartz phenocrysts can be identified in an altered groundmass of feldspars, quartz and opaques. The feldspar phenocrysts are being replaced with sericite and chlorite. Similarly most of the groundmass is composed of clay minerals, sericite and chlorite.	Y	Sr, Nd, Pb and Hf.
	AHBI28	N18°12.550 W077°00.994	Dacite	Altered lava flow	The rock appears to be porphyritic; however, it is difficult to be certain due to the heavy alteration. Plagioclase feldspar, K-feldspar and quartz phenocrysts can be identified in an altered groundmass of feldspars, quartz and opaques. The feldspar phenocrysts are being replaced with sericite and clay minerals. Similarly most of the groundmass is composed of clay minerals, sericite and chlorite.	Y	
	AHBI29	N18°12.550 W077°00.994	Dacite	Altered lava flow	SAMPLE LOST IN POST	N	
	AHBI30	Mullock N18°12.147 W077°03.267	Dacite	Altered lava flow	The rock appears to be phyric; however, the degree of alteration makes this interpretation uncertain. The phenocrysts include plagioclase feldspar, possibly K-feldspar and quartz. The feldspar phenocrysts have been partially replaced by sericite and chlorite. The rock contains veins of quartz, chlorite and a high	Y	

					interference colour/relief mineral that maybe epidote. The groundmass is made up of feldspar, quartz and opaques that have been heavily replaced with clay minerals, chlorite and sericite.		
Above Rocks Inlier	AHAR01	N18°05.000 W076°52.599	Granodiorite	Intrusion	Altered coarse grained rock composed of plagioclase feldspar, biotite mica, hornblende, quartz and opaques. The alteration has broken down many of the minerals into clay minerals.	Y	
	AHAR02	River section at Zion N18°06.820 W076°53.778	Granodiorite	Fresh intrusion with abundant xenoliths	Coarse grained rock composed of plagioclase feldspar, K-feldspar, biotite mica, hornblende, quartz and opaques. The feldspars have been slightly altered to sericite.	Y	Sr, Nd, Pb and Hf. ^{40}Ar-^{39}Ar
	AHAR03	River section at Zion N18°06.820 W076°53.778	Granodiorite	Fresh intrusion with abundant xenoliths	Coarse grained rock composed of plagioclase feldspar, K-feldspar, biotite mica, hornblende, quartz and opaques. The feldspars have been slightly altered to sericite.	Y	
	AHAR04	River section at Zion N18°06.820 W076°53.778	Basaltic Andesite	Xenolith in the intrusion		Y	
	AHAR05	River section at Zion N18°06.820 W076°53.778	Granodiorite	Fresh intrusion with abundant xenoliths	Coarse grained rock composed of plagioclase feldspar, microcline feldspar, biotite mica, hornblende, quartz and opaques. The feldspars have been slightly altered to sericite.	Y	
	AHAR06	River section at Zion N18°06.820	Granodiorite	Fresh intrusion with abundant xenoliths	Coarse grained rock composed of plagioclase feldspar, biotite mica, hornblende, quartz and opaques. The feldspars have been slightly	Y	

		W076°53.778			altered to sericite.		
	AHAR07	River section at Zion N18°06.820 W076°53.778	Granodiorite	Intrusion with abundant xenoliths	Altered phyric coarse grained rock. The phenocrysts are composed of plagioclase feldspar, possible K-feldspar and hornblende. The groundmass is composed of plagioclase, biotite mica, hornblende, possibly quartz and opaques	Y	
	AHAR08	River section at Zion N18°06.820 W076°53.778	Granodiorite	Intrusion with abundant xenoliths	Altered phyric coarse grained rock. The phenocrysts are composed of plagioclase feldspar, and biotite mica. The finer groundmass is composed of plagioclase feldspar, K-feldspar, biotite mica, minor hornblende, quartz and opaques.	Y	
	AHAR09	River section at Zion N18°06.820 W076°53.778	Granodiorite	Fresh apophysis vein		Y	
	AHAR10	River section at Zion N18°06.820 W076°53.778	Granodiorite	Intrusion with abundant xenoliths	Altered phyric coarse grained rock. The phenocrysts are composed of plagioclase feldspar, K-feldspar (including 1 grain of microcline) and hornblende. The finer groundmass is composed of plagioclase feldspar, K-feldspar, hornblende, quartz and opaques.	Y	
	AHAR11	River section at Zion N18°06.820 W076°53.778	Granodiorite	Fresh intrusion with abundant xenoliths	Coarse grained rock composed of plagioclase feldspar, biotite mica, hornblende, quartz and opaques. The feldspars have been slightly altered to sericite. Possible zircons seen in the biotites.	Y	

	AHAR12	River section at Zion N18°06.820 W076°53.778	Basaltic Andesite	Xenolith in the intrusion	The rock is aphyric and is made up of quartz, an unidentified high interference/ relief mineral and opaques.	Y	
	AHAR13	N18°09.592 W076°53.153	Dacite	Altered massive lava flow	The rock is phyric with phenocrysts of plagioclase feldspar, microcline and quartz. The feldspars are slightly altered to sericite and chlorite. The groundmass is composed of feldspar, quartz, biotite mica and opaques. It is uncertain to whether the biotite is primary or secondary. The groundmass is also being partially replaced with chlorite and clay minerals.	Y	
	AHAR14	N18°09.592 W076°53.153	Andesite	Altered massive lava flow	The rock is porphyritic with phenocrysts of plagioclase feldspar and amphibole. The groundmass is composed of plagioclase, amphibole and opaques. Rock is moderately altered with clay minerals, sericite and Fe-oxyhydroxide staining.	Y	
	AHAR15	N18°09.592 W076°53.153	Andesite	Altered massive lava flow	The rock is porphyritic with phenocrysts of plagioclase feldspar. The groundmass is composed of plagioclase and opaques. Much of the rock has been altered to clay minerals and sericite. Some of the plagioclase phenocrysts have been completely replaced with sericite and epidote. Fe-oxyhydroxide staining is also seen.	Y	
	AHAR16	~ 800 m right of Brainard Square.	Andesite	Altered massive lava flow		Y	Sr, Nd, Pb and Hf. ^{40}Ar-^{39}Ar

	AHAR17	~2 km right of Brainard Square in Sue River Section	Andesite	Altered massive lava flow	The rock is porphyritic with phenocrysts of plagioclase feldspar and amphibole. The feldspar and amphibole phenocrysts are being replaced with sericite and clay minerals. The groundmass is composed of feldspar, amphibole and opaques. Much of the groundmass has been altered to clay minerals and sericite.	Y	
	AHAR18	Brainard Square N18°11.578 W076°53.825	Andesite	Altered massive lava flow	The rock is porphyritic with phenocrysts of plagioclase feldspar. The groundmass is made up of plagioclase feldspar and opaque (some of them sphene) crystals. The rock is highly altered with calcite, clay minerals and sericite replacing most of the mineralogy. Fe-oxyhydroxide staining is common.	Y	Sr, Nd, Pb and Hf.
	AHAR19	Near Cavaliers N18°11.580 W076°53.824	Andesite	Altered massive lava flow	The rock is phyric with plagioclase feldspar phenocrysts that are being heavily replaced with clay minerals, sericite, chlorite and epidote. The groundmass is composed of feldspar and opaques that are also being replaced with clay minerals, sericite and chlorite.	Y	
Sunning Hill Inlier	SUN101	Collected by Dr S. Mitchell	Mafic	Altered pillow lava	NO THIN SECTION	N	
	SUN102	Collected by Dr S. Mitchell	Dacite	Altered pillow lava	The rock is porphyritic with phenocrysts of plagioclase feldspar and opaques. The plagioclase phenocrysts are variably replaced with sericite and calcite. The groundmass is composed of feldspar and opaque needles which are being replaced with clay minerals,	Y	

					sericite and chlorite. Quartz and calcite veins can be identified.		
	SUN103	Collected by Dr S. Mitchell	Mafic	Altered pillow lava	NO THIN SECTION	N	
	SUN104	Collected by Dr S. Mitchell	Mafic	Altered pillow lava	NO THIN SECTION	N	
	SUN105	Collected by Dr S. Mitchell	Basalt	Altered pillow lava	The rock is porphyritic with phenocrysts of plagioclase feldspar and amphibole. The plagioclase phenocrysts are being replaced with sericite and chlorite. The groundmass is composed of needle like feldspar and opaque crystals that show heavy clay mineral, chlorite and calcite alteration.	Y	Sr, Nd, Pb and Hf.
Central Inlier	AHCI01	N18°07.010 W077°22.840	Mafic	Altered dyke?	The rock is altered to such a degree that it is not possible to determine whether or not it was phyric or aphyric. Plagioclase feldspar and opaques can be identified. Most of the rock has been replaced with clay minerals and sericite.	N	
	AHCI02	N18°07.010 W077°22.840	Mafic	Altered lava flow?	The rock is phyric with plagioclase feldspar phenocrysts that are being replaced with sericite, chlorite and epidote. The groundmass is composed of feldspars and opaques, which are also being replaced by sericite, clay minerals and chlorite.	N	
	AHCI03	N18°07.010 W077°22.840	Basaltic Andesite	Altered lava flow?	The rock is substantially altered and is phyric. The phenocrysts are composed of plagioclase feldspars. The groundmass is made up of feldspars and opaques. Both the phenocrysts	Y	

					and the groundmass have been heavily replaced with clay minerals, sericite, chlorite and epidote.		
	AHCI04	N18°07.010 W077°22.840	Basaltic Andesite	Altered dyke?		Y	
	AHCI05	N18°07.336 W077°22.982	Basaltic Andesite	Altered lava flow?	The rock appears to be phyric; however, the degree of alteration makes this interpretation uncertain. The phenocrysts are composed of plagioclase feldspar and an unidentified mineral with up to 2nd order interference colours. The groundmass is made up of feldspar, the unidentified mineral and opaques. Most of the rock is substantially altered to sericite and clay minerals.	Y	
	AHCI06	N18°07.336 W077°22.982	Andesite	Altered dyke?	The rock appears to be medium grained and aphyric. It is composed of plagioclase feldspar, possibly K-feldspar, cpx and opaques. Alteration has occurred due to the presence of clay minerals, sericite and chlorite.	Y	
	AHCI07	N18°07.336 W077°22.982	Andesite	Altered lava flow?	The rock is porphyritic with phenocrysts of plagioclase feldspar and amphibole. Some of the feldspars have concentric compositional zoning. The feldspar phenocrysts are being replaced with sericite. The amphiboles are also being altered to clay minerals. The groundmass is made up of feldspars, amphibole and opaques that are being replaced by sericite and clay minerals.	Y	
	AHCI08	N18°07.336	Andesite	Altered dyke?	The rock has a seriate texture. Plagioclase	Y	

					groundmass is made up of feldspar and opaques. The phenocrysts and groundmass are being replaced with sericite, clay minerals, calcite, chlorite and maybe pumpellyite.		
	AHCI11	N18°08.183 W077°19.619	Andesite	Altered dyke	The rock is highly altered and may have been phyric. Phenocrysts of plagioclase feldspar and cpx are seen. The feldspars have been partly altered to sericite and clay minerals. The groundmass is composed of feldspars, cpx and opaques that are also being replaced by clay minerals, chlorite, calcite, quartz and sericite.	Y	
	AHCI12	N18°05.298 W077°21.824	Andesite	Fresh massive ignimbrite	The rock is composed of pumice fragments and plagioclase feldspar, quartz, hornblende and opaque accidentals/juveniles. Some of the feldspars have concentric compositional zoning. Unlike other ignimbrites that have an isotropic glassy matrix this ignimbrite is altered and the glassy matrix has broken down into clay minerals. The pumice clasts have also been replaced by large amounts of chlorite, sericite and clay minerals such that they can be distinguished from the matrix. Lithic fragments from the older central inlier lavas can be seen.	Y	
	AHCI13	N18°05.298 W077°21.824	Andesite	Fresh massive ignimbrite	The rock is composed of pumice fragments and plagioclase feldspar, quartz, hornblende and opaque accidentals/juveniles. Some of the feldspars have concentric compositional zoning. Unlike other ignimbrites that have an isotropic glassy matrix this ignimbrite is altered and the glassy matrix has broken down into clay	Y	

					minerals. The pumice clasts have also been replaced by large amounts of chlorite, sericite and clay minerals such that they can be distinguished from the matrix. Lithic fragments from the older central inlier lavas can be seen.		
	AHCI14	Thomas River N18°07.581 W077°23.210	Basaltic Andesite	Altered, ~ 60 cm wide, NW-SE trending dyke	The rock appears to be aphyric; however, the degree of alteration makes this interpretation uncertain. The rock is made up of feldspar and opaque crystals that are being replaced with clay minerals, sericite, calcite and chlorite.	Y	
	AHCI15	Thomas River N18°07.581 W077°23.210	Basalt	Heavily altered massive lava flow	The rock is heavily altered and as such it is uncertain to whether it was phyric or aphyric. The rock is made up of feldspar (plagioclase can be identified) and opaque crystals that are being replaced with clay minerals, sericite, calcite and chlorite.	Y	
	AHCI16	Thomas River N18°07.581 W077°23.210	Basaltic Andesite	Altered, ~ 60 cm wide, NW-SE trending dyke	The rock is altered and is aphyric. It is made up of feldspar and opaque crystals that are being replaced with clay minerals, sericite, calcite and chlorite. Quartz has in filled the vesicles in the rock.	Y	
	AHCI17	Thomas River N18°07.581 W077°23.210	Mafic	Altered massive lava flow	The rock is very heavily altered and as such it is uncertain to whether it was phyric or aphyric. The vast majority of the original mineralogy has been replaced by sericite, clay minerals and chlorite. Rare plagioclase feldspar fragments and numerous opaques can be identified.	N	
	AHCI18	Thomas River N18°07.581	Dacite	Altered, ~ 90 cm wide, NE-SW	The rock is altered and is porphyritic. The phenocrysts are composed of feldspar crystals	Y	

		W077°23.210		trending dyke	that have been replaced with sericite, chlorite and epidote. The groundmass is composed of feldspars and opaques that are also altered to sericite, clay minerals, chlorite and epidote.		
	AHCI19	Thomas River N18°07.581 W077°23.210	Basaltic Andesite	Altered massive lava flow	The rock is highly altered and is porphyritic. Plagioclase feldspar and cpx phenocrysts have been identified. Both sets of phenocrysts are heavily replaced with sericite, clay minerals and chlorite. The groundmass is composed of feldspar, cpx and opaques, which have also been replaced with sericite, clay minerals, epidote and chlorite.	Y	
	AHCI20	Thomas River N18°07.581 W077°23.210	Basaltic Andesite	Altered massive lava flow	The rock is highly altered and is porphyritic. Plagioclase feldspar phenocrysts have been identified. The groundmass is made up of feldspar and opaques. The groundmass is being replaced with chlorite, pumpellyite, epidote, clay minerals, calcite, amphibole? and sericite.	Y	
	AHCI21	Thomas River N18°07.581 W077°23.210	Andesite	Altered, ~ 60 cm wide, NW-SE trending dyke	The rock appears to be aphyric, however, the degree of alteration makes this interpretation uncertain. The rock is made up of feldspar, possible cpx fragments? and opaque crystals that are being replaced with clay minerals, sericite, calcite and chlorite.	Y	Sr, Nd, Pb and Hf.
	AHCI22	Thomas River N18°07.581 W077°23.210	Basaltic Andesite	Altered massive lava flow	The rock is altered and is porphyritic. The phenocrysts are composed of plagioclase feldspar and cpx. The phenocrysts are being replaced with sericite, clay minerals, chlorite and epidote. The groundmass is composed of	Y	

					feldspar, cpx and opaques, which have also been replaced with sericite, clay minerals, epidote and chlorite.		
	AHCI23	Thomas River N18°07.581 W077°23.210	Dacite	Altered, ~ 60 cm wide, NE-SW trending dyke	The rock appears to be phyric; however, the degree of alteration makes this interpretation uncertain. The phenocrysts are made up of relic feldspars which are being/been replaced by sericite, chlorite and epidote. Amphibole is also identified and is more resistant to alteration. The groundmass is composed of feldspar and opaques that are being replaced with clay minerals, sericite, calcite, chlorite and epidote.	Y	
	AHCI24	Thomas River N18°07.581 W077°23.210	Basaltic Andesite	Altered massive lava flow		Y	
	AHCI25	Thomas River N18°07.581 W077°23.210	Dacite	Altered, ~ 60 cm wide, NE-SW trending dyke	Altered porphyritic rock with phenocrysts of plagioclase feldspar, quartz and amphibole. The feldspars are being replaced with clay minerals, sericite, epidote and chlorite. The groundmass is made up of feldspar, quartz and opaques which are also altered to clay minerals, sericite and chlorite.	Y	
	AHCI26	Thomas River N18°07.581 W077°23.210	Basaltic Andesite	Altered massive lava flow		Y	
	AHCI27	Thomas River N18°07.581 W077°23.210	Basaltic Andesite	Altered, ~ 1m wide, NW-SE trending dyke		Y	
	AHCI28	Thomas River	Basalt	Altered massive lava		Y	

		N18°07.581 W077°23.210		flow			
	AHCI29	Thomas River N18°07.581 W077°23.210	Dacite	Altered, ~ 2 m wide, N-S trending dyke		Y	
	AHCI30	Road north of Thomas River N18°07.690 W077°23.096	Basaltic Andesite	Altered lava flow		Y	
	AHCI31	Road north of Thomas River N18°07.690 W077°23.096	Basaltic Andesite	Altered lava flow		Y	
	AHCI32	Road north of Thomas River N18°07.690 W077°23.096	Mafic	Altered lava flow		N	
	AHCI33	Road north of Thomas River N18°07.690 W077°23.096	Mafic	Altered amygdale basaltic lava flow		N	
	AHCI34	Grantham N18°08.940 W077°23.864	Mafic	Highly altered lava flow		N	
	AHCI35	Grantham N18°08.940 W077°23.864	Andesite	Highly altered lava flow		Y	
	AHCI35a	Grantham N18°08.940	Mafic	Highly altered lava flow	The rock is heavily altered and thus it is uncertain to whether it was originally phyric or	N	

		W077°23.864			aphyric. Plagioclase feldspar and opaque crystals can be identified. The feldspars, like most of the rock, have been replaced with sericite and clay minerals. Relic cpx possibly exists but has now been replaced with secondary minerals. Fe-oxyhydroxide staining can also be seen.		
	AHCI36	Grantham N18°08.940 W077°23.864	Andesite	Highly altered lava flow	The rock is altered and appears to be porphyritic. The phenocrysts are composed of plagioclase feldspar, K-feldspar, amphibole, biotite and cpx. Some of the feldspars have concentric compositional zoning. The feldspars are being replaced by sericite and clay minerals. The cpx has been altered with clay minerals but is generally more resistant. The groundmass is composed of feldspar, biotite, amphibole, cpx and opaques. The groundmass is also altered with clay minerals and sericite.	Y	Sr, Nd, Pb and Hf.
	AHCI37	Grantham N18°08.940 W077°23.864	Andesite	Highly altered lava flow	Although the rock is altered it appears to be porphyritic. The phenocrysts are composed of plagioclase feldspar, K-feldspar, biotite and cpx. Some of the feldspars have concentric compositional zoning. The feldspars are being replaced by sericite and clay minerals. The cpx has been altered with clay minerals but is generally more resistant. The groundmass is composed of feldspar, cpx, biotite and opaques. The groundmass is also altered with clay minerals and sericite. Fe-oxyhydroxide staining is common.	Y	Sr, Nd, Pb and Hf.

	AHCI38	N18°05.298 W077°21.824	Andesite	Fresh massive ignimbrite	The rock is composed of pumice fragments and plagioclase feldspar, quartz, hornblende and opaque accidentals/juveniles. Some of the feldspars have concentric compositional zoning. Unlike other ignimbrites that have an isotropic glassy matrix this ignimbrite is altered and the glassy matrix has broken down into clay minerals. The pumice clasts have also been replaced by large amounts of chlorite, sericite and clay minerals such that they can be distinguished from the matrix. Lithic fragments from the older central inlier lavas can be seen.	N	
	AHCI39	Thomas River N18°07.581 W077°23.210	Basaltic Andesite	Altered massive lava flow	Although the rock is altered it appears to be porphyritic. The phenocrysts are composed of plagioclase feldspar which are partially altered to chlorite, clay minerals and sericite. The groundmass is made up of feldspar and opaques also replaced with clay minerals, chlorite and sericite. A quartz and chlorite vein is seen.	Y	Sr, Nd, Pb and Hf ^{40}Ar-^{39}Ar.
	AHCI40	Thomas River N18°07.581 W077°23.210	Basaltic Andesite	Altered massive lava flow	The rock is porphyritic with plagioclase feldspar and cpx phenocrysts. The groundmass is made up of feldspars, cpx and opaques. Both the phenocrysts and groundmass have been partially replaced with sericite, clay minerals, chlorite and epidote.	Y	
	AHCI41	Thomas River N18°07.581 W077°23.210	Mafic	Altered massive lava flow	The rock is porphyritic with plagioclase feldspar and cpx phenocrysts. The groundmass is made up of feldspars, cpx and opaques. Both the phenocrysts and groundmass have been partially replaced with sericite, clay minerals,	N	

					chlorite and epidote.		
	AHCI42	Thomas River N18°07.581 W077°23.210	Basaltic Andesite	Altered massive lava flow	Altered porphyritic rock. The phenocryts are composed of plagioclase feldspar which have been partially altered to chlorite, clay minerals and sericite. The groundmass is made up of feldspars and opaques that have subsequently been replaced by chlorite, epidote, clay minerals and sericite.	Y	
	AHCI43	Thomas River N18°07.581 W077°23.210	Basaltic Andesite	Altered, ~ 1m wide, NW-SE trending dyke	The rock is heavily altered and as such it is uncertain to whether it was phyric or aphyric. Plagioclase feldspar and opaques can be identified. Much of the mineralogy has been replaced with clay minerals, sericite, chlorite and epidote.	Y	Sr, Nd, Pb and Hf.
	AHCI44	Thomas River N18°07.581 W077°23.210	Mafic	Altered massive lava flow	SAMPLE LOST IN POST	N	
	AHCI45	Thomas River N18°07.581 W077°23.210	Andesite	Altered massive lava flow	Although the rock is altered it appears to be porphyritic. The phenocrysts are composed of plagioclase feldspar, which are being replaced with sericite, clay minerals, chlorite and epidote. The groundmass is made up of similarly altered feldspars and opaques. Nodules of chlorite, epidote and quartz are seen.	Y	
	AHCI46	Thomas River N18°07.581 W077°23.210	Basalt	Altered massive lava flow	Although the rock is heavily altered it appears to have a seriate texture. Plagioclase feldspars and opaques are identified. The rock is being replaced with clay minerals, chlorite, epidote	Y	

					and sericite.		
	AHCI47	Thomas River N18°07.581 W077°23.210	Andesite	SEE TEXT	The rock appears to be phyric; however the heavy alteration makes this interpretation uncertain. Plagioclase feldspar phenocrysts, partially replaced by sericite, chlorite and epidote, have been identified. The groundmass is composed of feldspar and opaques, which have been replaced with clay minerals, chlorite, epidote and sericite. Chlorite, epidote and quartz veins have been identified.	Y	
	AHCI48	Thomas River N18°07.581 W077°23.210	Andesite	SEE TEXT	The rock appears to be phyric; however, the degree of alteration makes this interpretation uncertain. The phenocrysts are made up of plagioclase feldspar which are being replaced by sericite, chlorite and epidote. The groundmass is composed of feldspar and opaques that are altering to chlorite, sericite, clay minerals and epidote.	Y	
	AHCI49	Thomas River N18°07.581 W077°23.210	Basaltic Andesite	SEE TEXT	The rock is heavily altered and as such it is difficult to determine if it was phyric or aphyric. Plagioclase feldspar and opaques can be identified. The rock has mostly been replaced with clay minerals, chlorite, epidote and sericite. The chlorite can be seen breaking down into epidote.	Y	
	AHCI50	Thomas River N18°07.581 W077°23.210	Dacite	SEE TEXT	The rock is heavily altered and as such it is difficult to determine if it was phyric or aphyric. Feldspar, quartz and opaques can be identified. Much of the rock has been replaced	Y	

					with clay minerals, sericite, chlorite and epidote. Chlorite, epidote and quartz veins are seen.		
	AHCI51	Thomas River N18°07.581 W077°23.210	Basaltic Andesite	SEE TEXT	Altered porphyritic rock. The phenocrysts are composed of plagioclase feldspar and cpx which are partially replaced with sericite, clay minerals, chlorite and epidote. The groundmass is made up of feldspar and opaques, which are also replaced with clay minerals, sericite, chlorite and epidote.	Y	
	AHCI52	Thomas River N18°07.581 W077°23.210	Andesite	SEE TEXT	The rock appears to be phyric with phenocrysts of plagioclase feldspar, which are being replaced with sericite, chlorite and epidote. The feldspars also appear to be forming subgrains of quartz. The groundmass is made up of feldspar and opaques, which are also replaced with clay minerals, sericite, chlorite and epidote. Quartz nodules are also seen, are they broken down feldspars?	Y	
	AHCI53	Thomas River N18°07.581 W077°23.210	Andesite	SEE TEXT	The rock appears to be phyric; however the heavy alteration makes this interpretation uncertain. Plagioclase feldspar phenocrysts, partially replaced by sericite, chlorite and epidote, have been identified. The groundmass is composed of feldspar and opaques, which have been replaced with clay minerals, chlorite, epidote and sericite.	Y	
	AHCI54	Thomas River N18°07.581	Mafic	SEE TEXT	The rock appears to be phyric; however, the degree of alteration makes this interpretation	N	

		W077°23.210			uncertain. The phenocrysts are composed of plagioclase feldspar. The groundmass is made up of feldspars and opaques. The majority of the phenocrysts and groundmass has been heavily replaced with sericite, calcite, clay minerals, chlorite and epidote.		
	AHCI55	North of Friendship N18°07.663 W077°16.335	Andesite	Altered massive lava flow		Y	
	AHCI56	North of Friendship N18°07.663 W077°16.335	Andesite	Altered massive lava flow	The rock appears to be phyric with phenocrysts of plagioclase feldspar. The phenocrysts have been slightly replaced with sericite. The groundmass is made up of feldspar, cpx and opaques. The groundmass is being replaced with sericite and clay minerals.	Y	Sr, Nd, Pb and Hf.
	AHCI57	North of Friendship N18°07.663 W077°16.335	Mafic	Altered massive lava flow	SAMPLE LOST IN POST	N	
	AHCI58	North of Friendship N18°07.663 W077°16.335	Mafic	Altered massive lava flow		N	
	AHCI59	Ginger Ridge N18°04.483 W077°10.454	Andesite	Altered porphyry	The rock is altered to such a degree that it is not possible to determine whether or not it was phyric or aphyric. Plagioclase feldspar and opaques can be identified. Most of the rock has been replaced with clay minerals, sericite,	Y	

					chlorite and epidote.		
	AHCI60	Ginger Ridge N18°04.483 W077°10.454	Mafic	Altered porphyry	The rock is possibly phyric; however, the intense alteration makes the interpretation uncertain. Plagioclase feldspar phenocrysts can be seen and have been partially replaced with sericite, chlorite and epidote. The groundmass is made up of feldspar and opaques that have been heavily replaced with clay minerals, sericite and chlorite.	N	
	AHCI61	Ginger Ridge N18°04.439 W077°10.077	Granodiorite	Altered massive intrusion	Coarse grained rock composed of plagioclase feldspar, hornblende, quartz and opaques. The rock is slightly altered with chlorite, pumpellyite and sericite. The amphiboles are the most altered with chlorite and pumpellyite replacement. The feldspar is being replaced with sericite.	Y	
	AHCI62	Near Conners N18°03.963 W077°09.209	Basaltic Andesite	Altered massive lava flow	The rock appears to be porphyritic; however, the heavy alteration makes a determination difficult. The phenocrysts are composed of plagioclase feldspar, some of which show concentric zonation and an unidentified mineral with high interference colours. The groundmass is composed of feldspar, the unidentified mineral, quartz and opaques. The phenocrysts and much of the groundmass have been altered to clay minerals, sericite, epidote and chlorite.	Y	
	AHCI63	Near Conners N18°03.963 W077°09.209	Dacite	Altered massive lava flow	The rock appears to be porphyritic; however, the heavy alteration makes a determination difficult. The phenocrysts are composed of	Y	

					plagioclase feldspar, some of which show concentric zonation. The groundmass is composed of feldspar, an unidentified mineral with high interference colours, quartz and opaques. The phenocrysts and much of the groundmass have been altered to clay minerals, sericite and chlorite.		
	AHCI64	Near Conners N18°03.963 W077°09.209	Andesite	Altered massive lava flow	The rock appears to be phyric with phenocrysts of plagioclase feldspar. The feldspars are being replaced with sericite, chlorite and epidote. The groundmass is composed of feldspar and opaques which are heavily altered to sericite, chlorite and epidote.	Y	
	AHCI65	Near Conners N18°03.963 W077°09.209	Andesite	Altered massive lava flow	The rock is possibly phyric; however, the alteration makes the interpretation uncertain. Plagioclase feldspar phenocrysts can be seen. The groundmass is made up of feldspar and opaques. The vast majority of the rock has been altered and is composed of clay minerals and sericite.	Y	
	AHCI66	Near Junction N18°04.782 W077°06.648	Mafic	Altered massive lava flow		N	
	AHCI67	Near Junction N18°04.782 W077°06.648	Mafic	Altered massive lava flow		N	
	AHCI68	Near Junction N18°04.782 W077°06.648	Mafic	Altered massive lava flow		N	

	AHCI69	Near Junction N18°04.782 W077°06.648	Mafic	Altered massive lava flow		N	
	AHCI70	Near Junction N18°04.782 W077°06.648	Mafic	Altered massive lava flow		N	
	AHCI71	Near Kentish N18°05.475 W077°09.418	Mafic	Altered massive lava flow		N	
	AHCI72	Near Old Works N18°04.429 W077°06.847	Basaltic Andesite	Altered massive lava flow	The rock is porphyritic with phenocrysts of plagioclase feldspar. The groundmass is composed of feldspar and opaques. The phenocrysts and much of the groundmass have been heavily altered to clay minerals, sericite and chlorite. Calcite alteration is also pervasive throughout the rock.	Y	Sr, Nd, Pb and Hf.
	AHCI73	Near Conners N18°03.963 W077°09.209	Basaltic Andesite	Altered massive lava flow	The rock is porphyritic with phenocrysts of plagioclase feldspar. The groundmass is composed of feldspar and opaques and an un-identified high relief mineral (possibly cpx). The phenocrysts and much of the groundmass have been heavily altered to clay minerals, sericite and chlorite.	Y	
	AHCI74	Near Conners N18°03.963 W077°09.209	Basaltic Andesite	Altered massive lava flow	The rock is phyric with phenocrysts of plagioclase feldspar. The groundmass is composed of feldspar and opaques and an un-identified high relief mineral (possibly cpx). The phenocrysts and much of the groundmass have been heavily altered to clay minerals,	Y	Sr, Nd, Pb and Hf.

					sericite and chlorite.		
	AHCI75	Near Blue Hole N18°03.342 W077°09.731	Basalt	Altered massive lava flow	The rock is porphyritic with phenocrysts of plagioclase feldspar. The groundmass is composed of feldspar and opaques and an un-identified high relief mineral (possibly cpx). The phenocrysts and much of the groundmass have been heavily altered to clay minerals, sericite, epidote and chlorite.	Y	
	AHCI76	Dry Hill N18°02.880 W077°10.795	Basalt	Altered massive lava flow	The rock is porphyritic with phenocrysts of plagioclase feldspar. The groundmass is composed of feldspar and opaques. The phenocrysts and much of the groundmass have been heavily altered to clay minerals, sericite and chlorite. Calcite alteration is also pervasive throughout the rock.	Y	
	AHCI77	Dry Hill N18°02.880 W077°10.795	Basalt	Altered massive lava flow		Y	
	AHCI78	Dry Hill N18°02.880 W077°10.795	Basaltic Andesite	Altered massive lava flow	The rock is phyric with phenocrysts of plagioclase feldspar. The groundmass is composed of feldspar and opaques. The phenocrysts and much of the groundmass have been heavily altered to clay minerals, sericite and chlorite. The minerals have Fe-oxyhydroxide staining. Calcite alteration is also pervasive throughout the rock.	Y	
	AHCI79	N18°03.831 W077°11.960	Basaltic Andesite	Altered massive lava flow	The rock is porphyritic with phenocrysts of plagioclase feldspar. The groundmass is composed of feldspar and opaques. The	Y	

					phenocrysts and much of the groundmass have been heavily altered to clay minerals, sericite and chlorite.		
	AHCI80	Near Rock River N18°03.994 W077°13.139	Mafic	Slightly altered volcaniclastric clast		N	
Newcastle Volcanics	AHWG01	Bito Quarry	Adakite	Altered massive lava flow	The rock is phyric with phenocrysts of plagioclase feldspar and K-feldspar, which are partially altered to sericite. The groundmass is composed of feldspars, quartz? and opaques, which have also been substantially replaced with sericite and clay minerals.	Y	
	AHWG02	Bito Quarry	Adakite	Altered massive lava flow	The rock is porphyritic with phenocrysts of plagioclase feldspar and K-feldspar, which are partially altered to sericite. The groundmass is composed of feldspars, quartz? and opaques. The groundmass has been substantially replaced with sericite and clay minerals.	Y	
	AHWG03	Bito Quarry	Adakite	Altered massive lava flow	The rock is porphyritic with phenocrysts of plagioclase feldspar and K-feldspar, which are partially altered to sericite. The groundmass is composed of feldspars, quartz? and opaques. The groundmass has been substantially replaced with sericite and clay minerals.	Y	^{40}Ar-^{39}Ar
	AHWG04	Bito Quarry	Adakite	Altered massive lava flow	The rock is phyric with phenocrysts of plagioclase feldspar and K-feldspar, which are partially altered to sericite. The groundmass is	N	

					composed of feldspars, quartz? and opaques, which have also been substantially replaced with sericite and clay minerals. Amphibole may also be present.		
	AHWG05	Bito Quarry	Adakite	Altered massive lava flow	The rock is porphyritic with phenocrysts of plagioclase feldspar and K-feldspar, which are partially altered to sericite. The groundmass is composed of feldspars, quartz? and opaques. The groundmass has been substantially replaced with sericite and clay minerals.	N	
	AHWG11	Irish Town N18°02.745 W076°43.665	Adakite	Altered massive lava flow		Y	
	AHWG12	Irish Town to Hopewell N18°03.030 W076°43.480	Adakite	Altered massive lava flow		Y	Sr, Nd, Pb and Hf.
	AHWG13	Irish Town to Hopewell N18°03.030 W076°43.480	Adakite	Altered massive lava flow	The rock has a seriate texture and is composed of plagioclase feldspar, K-feldspar, amphibole, quartz and opaques. The feldspars and amphiboles are being replaced with sericite and chlorite.	N	
	AHWG14	Irish Town to Hopewell N18°03.180 W076°43.409	Adakite	Altered massive lava flow	The rock is substantially altered but appears to be phyric with phenocrysts of plagioclase feldspar and amphibole that are being replaced with sericite and chlorite. The groundmass is composed of feldspars, amphibole, quartz and opaques. This groundmass has also been partially altered to sericite, clay minerals and	Y	

					chlorite.		
	AHWG15	Irish Town to Hopewell N18°03.180 W076°43.409	Adakite	Altered massive lava flow		N	
	AHWG16	Irish Town to Hopewell N18°03.180 W076°43.409	Adakite	Altered massive lava flow		Y	
	AHWG17	North of Redlight N18°03.587 W076°43.352	Adakite	Altered massive lava flow	The rock is porphyritic with plagioclase feldspar, K-feldspar, amphibole and quartz phenocrysts. The feldspars are being replaced with sericite and chlorite. The groundmass is composed of feldspars, amphiboles, quartz and opaques that have also suffered sericite and chlorite alteration.	Y	
	AHWG18	North of Redlight N18°03.587 W076°43.352	Adakite	Altered massive lava flow		Y	
	AHWG19	North of Redlight N18°03.587 W076°43.352	Adakite	Altered massive lava flow		Y	Sr, Nd, Pb and Hf.
	AHWG20	North of Redlight N18°03.587 W076°43.352	Adakite	Altered massive lava flow		Y	
	AHWG21	South of	Adakite	Altered massive lava	The rock is porphyritic with plagioclase	Y	Sr, Nd, Pb

		Newcastle N18°03.981 W076°42.528		flow	feldspar, K-feldspar, amphibole and quartz phenocrysts. The feldspars and amphiboles are being replaced with sericite and chlorite. The groundmass is composed of feldspars, quartz, amphiboles and opaques that have also suffered sericite and chlorite alteration.		and Hf.
	AHWG22	South of Newcastle N18°03.981 W076°42.528	Adakite	Altered massive lava flow		N	
	AHWG23	North of Newcastle N18°04.321 W076°42.670	Adakite	Altered massive lava flow		Y	
	AHWG24	North of Newcastle N18°04.321 W076°42.670	Adakite	Altered massive lava flow		N	
	AHWG25	North of Newcastle N18°04.321 W076°42.670	Adakite	Altered massive lava flow		Y	
	AHWG26	N18°04.566 W076°42.926	Adakite	Altered massive lava flow		Y	
	AHWG27	N18°04.566 W076°43.267	Adakite	Altered massive lava flow	The rock is porphyritic with plagioclase feldspar phenocrysts. The feldspars are being replaced with clay minerals, sericite and chlorite. The groundmass is composed of feldspars, quartz and opaques that have also	Y	

					suffered clay mineral, sericite and chlorite alteration.		
	AHWG28	N18°03.397 W076°44.232	Adakite	Altered massive lava flow	The rock is porphyritic with plagioclase feldspar, K-feldspar, amphibole and quartz phenocrysts. The feldspars and amphiboles are being replaced with clay minerals, sericite and chlorite. The groundmass is composed of feldspars, quartz, amphiboles and opaques that have also suffered clay mineral, sericite and chlorite alteration.	N	
	AHWG29	N18°03.397 W076°44.232	Adakite	Altered massive lava flow		N	
	AHWG30	N18°03.397 W076°44.232	Adakite	Altered massive lava flow		N	
	AHWG31	N18°03.397 W076°44.232	Adakite	Altered massive lava flow		N	
	AHWG32	N18°03.737 W076°44.659	Adakite	Altered massive lava flow		Y	Sr, Nd, Pb and Hf.
	AHWG33	N18°03.927 W076°44.786	Adakite	Altered massive lava flow	The rock is porphyritic with plagioclase feldspar, K-feldspar, amphibole and quartz phenocrysts. The feldspars and amphiboles are being replaced with sericite. The groundmass is composed of feldspars, amphiboles, quartz and opaques, again altered to sericite and chlorite.	Y	Sr, Nd, Pb and Hf.
	AHWG34	N18°03.927 W076°44.786	Adakite	Altered massive lava flow	The rock is porphyritic with plagioclase feldspar, K-feldspar and quartz phenocrysts. The feldspars are being replaced with sericite and chlorite. The groundmass is composed of feldspars, quartz and opaques, again altered to	Y	

					sericite and chlorite.		
Halberstadt Volcanics	AHWG06	Bito Quarry	Continental Alkali Basalt	Highly altered lava flow	Massive alteration has destroyed all the original mineralogy. The rock is now made up of quartz, chlorite, clay minerals and opaques.	N	
	AHWG07	Bito Quarry	Continental Alkali Basalt	Highly altered lava flow	Massive alteration has destroyed all the original mineralogy. The rock is now made up of quartz, chlorite, clay minerals and opaques.	N	
	AHWG08	Bito Quarry	Continental Alkali Basalt	Altered massive lava flow	The rock is phyric? and has amygdales composed of calcite, quartz and chlorite. The phenocrysts are composed of plagioclase feldspar, which are altered to sericite and chlorite. The groundmass is made up of feldspar and opaques that are also being replaced by sericite, clay minerals and chlorite.	Y	
	AHWG09	Bito Quarry	Continental Alkali Basalt	Altered massive lava flow	The rock is porphyritic? and has calcite, quartz and chlorite filled amygdales. The phenocrysts are composed of plagioclase feldspar, which are altered to sericite and chlorite. The groundmass is made up of feldspar and opaques that are also being replaced by sericite, clay minerals and chlorite.	Y	
	AHWG10	Bito Quarry	Continental Alkali Basalt	Altered massive lava flow	The rock is aphyric? and has amygdales composed of calcite, quartz and chlorite. The rock is made up of feldspars and opaques that are being heavily replaced by sericite, clay minerals and chlorite.	Y	
	AHHB01	Newstead to Bito	Continental Alkali Basalt	Altered pillow lava	Altered porphyritic rock with calcite, quartz and chlorite filled amygdales. The phenocrysts are	Y	

		N17°57.622 W076°40.625			composed of plagioclase feldspar, which are altered to sericite and chlorite. The groundmass is made up of feldspar and opaques that are also being replaced by sericite, clay minerals and chlorite.		
	AHHB02	Newstead to Bito N17°57.622 W076°40.625	Continental Alkali Basalt	Altered pillow lava	The rock is porphyritic and has calcite, quartz and chlorite filled amygdales. The phenocrysts are composed of plagioclase feldspar, which are altered to sericite and chlorite. The groundmass is made up of feldspar and opaques that are also being replaced by sericite, clay minerals and chlorite.	Y	
	AHHB03	Newstead to Bito N17°57.622 W076°40.625	Continental Alkali Basalt	Altered pillow lava	Altered phyric rock with calcite, quartz and chlorite filled amygdales. The phenocrysts are composed of plagioclase feldspar, which are altered to sericite and chlorite. The groundmass is made up of feldspar and opaques that are also being replaced by sericite, clay minerals and chlorite.	Y	Sr, Nd, Pb and Hf.
	AHHB04	Newstead to Bito N17°57.622 W076°40.625	Continental Alkali Basalt	Altered pillow lava	Altered phyric rock with calcite, quartz and chlorite filled amygdales. The phenocrysts are composed of plagioclase feldspar, which are altered to sericite and chlorite. The groundmass is made up of feldspar and opaques that are also being replaced by sericite, clay minerals and chlorite.	Y	
	AHHB05	Newstead to Bito N17°57.622	Continental Alkali Basalt	Altered pillow lava	Altered porphyritic? rock with calcite, quartz and chlorite filled amygdales. The phenocrysts are composed of plagioclase feldspar, which are	Y	

		W076°40.625			altered to sericite and chlorite. The groundmass is made up of feldspar and opaques that are also being replaced by sericite, clay minerals and chlorite.		
	AHHB06	Newstead to Bito N17°57.622 W076°40.625	Continental Alkali Basalt	Altered pillow lava		N	
	AHHB07	Newstead to Bito N17°57.622 W076°40.625	Continental Alkali Basalt	Altered pillow lava	Altered phyric rock with calcite, quartz and chlorite filled amygdales. The phenocrysts are composed of plagioclase feldspar, which are altered to sericite and chlorite. The groundmass is made up of feldspar and opaques that are also being replaced by sericite, clay minerals and chlorite.	Y	Sr, Nd, Pb and Hf.
	AHHB08	Newstead to Bito N17°57.622 W076°40.625	Continental Alkali Basalt	Altered pillow lava		Y	
	AHHB09	Newstead to Bito N17°57.622 W076°40.625	Continental Alkali Basalt	Altered pillow lava	Altered phyric? rock with calcite, quartz and chlorite filled amygdales. The phenocrysts are composed of plagioclase feldspar, which are altered to sericite and chlorite. The groundmass is made up of feldspar and opaques that are also being replaced by sericite, clay minerals and chlorite.	Y	

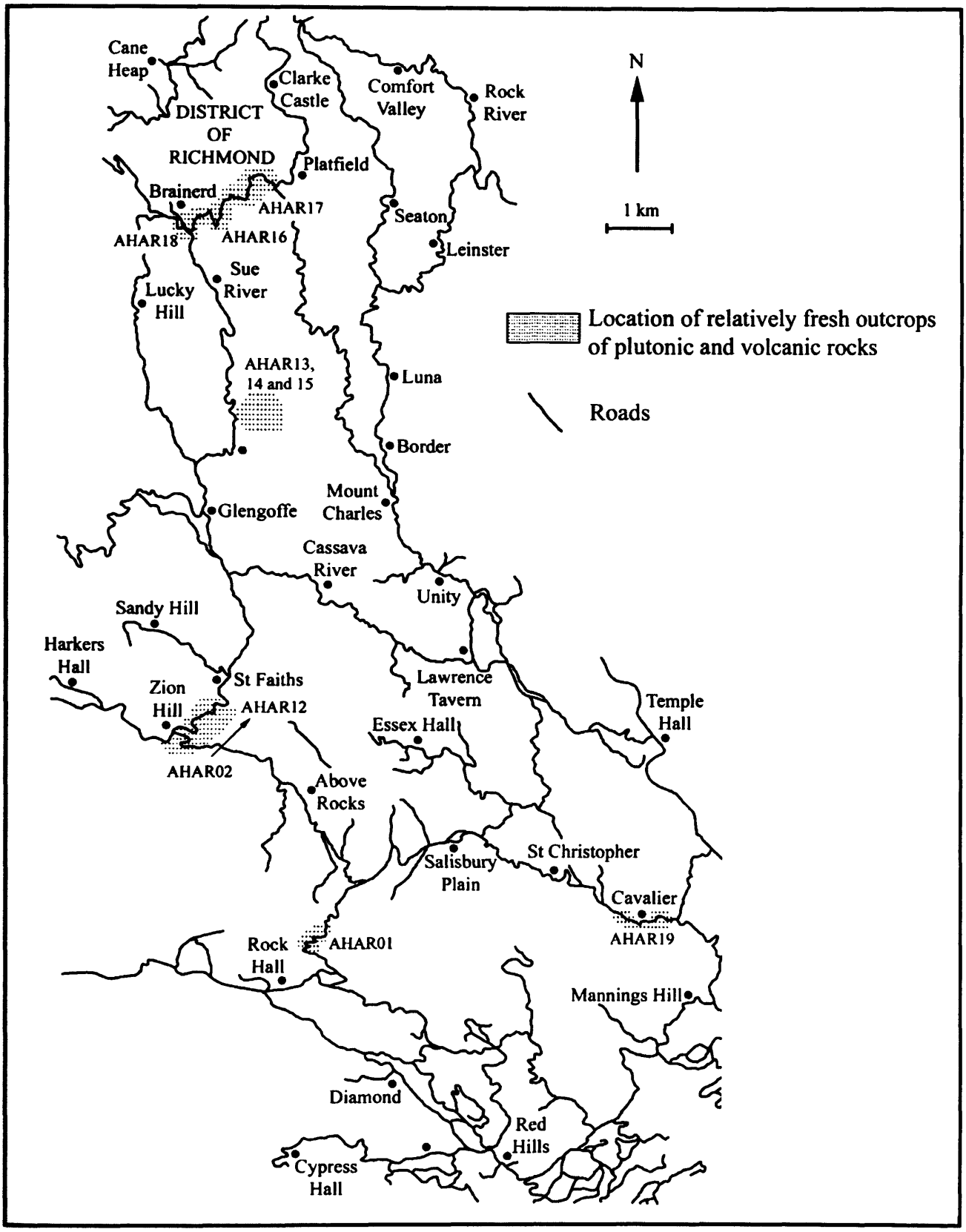

Figure A.1 – Location map for the Above Rocks Inlier samples.

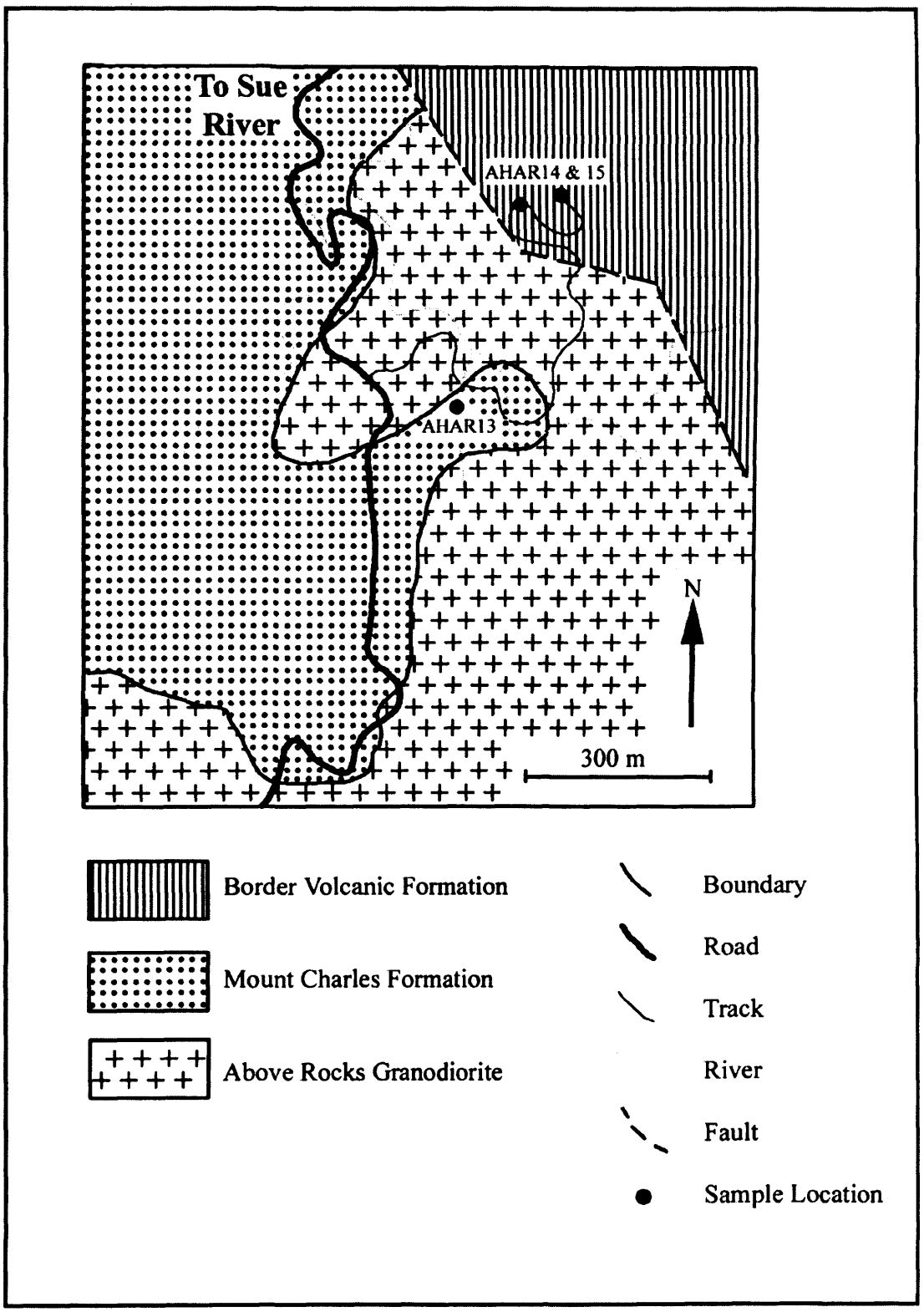

Figure A.2 – Small scale location map for samples AHAR13-15, Above Rocks Inlier (Modified from Manning and McCain, 1989).

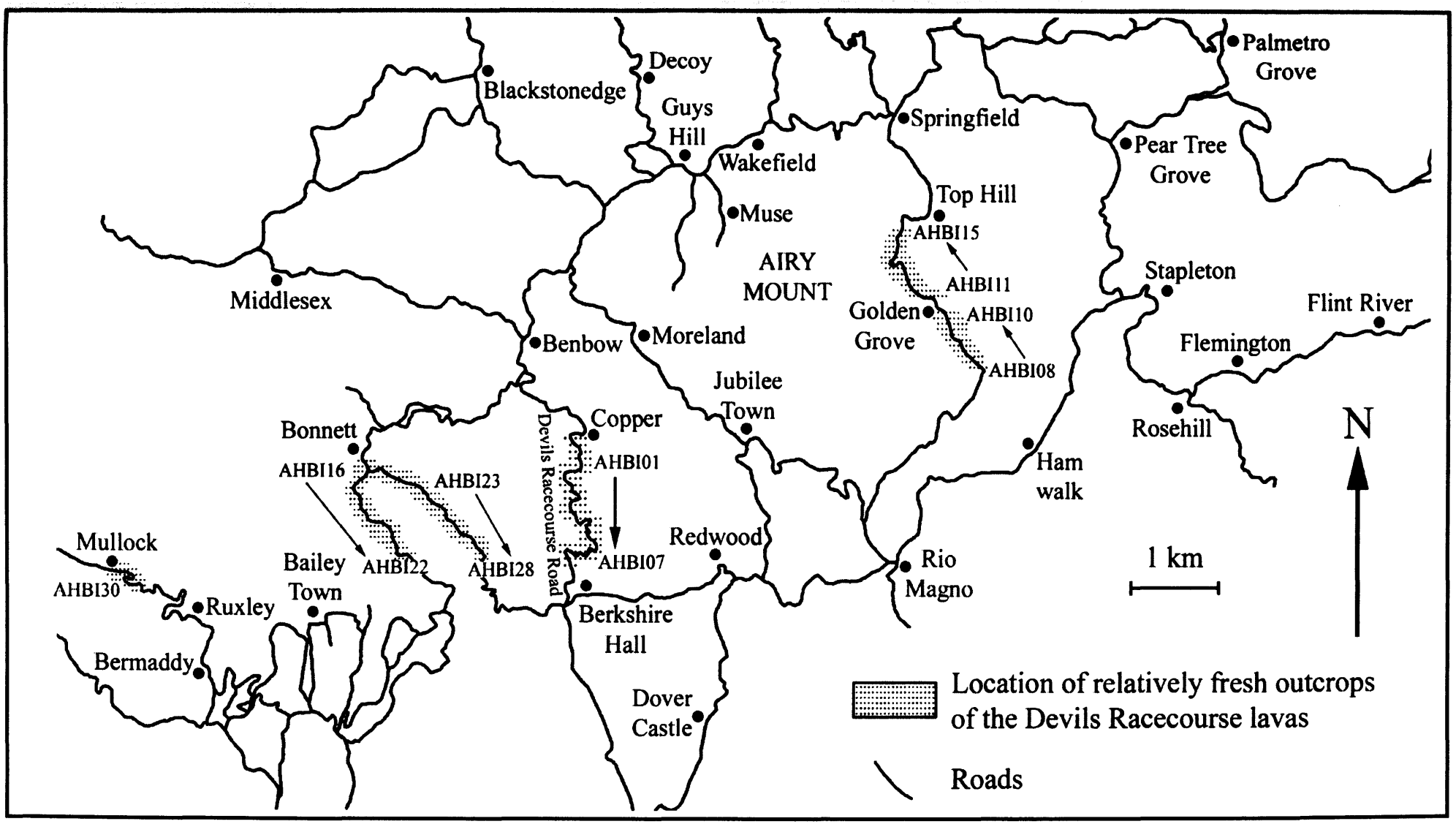

Figure A.3 – Location map for the Benbow Inlier samples.

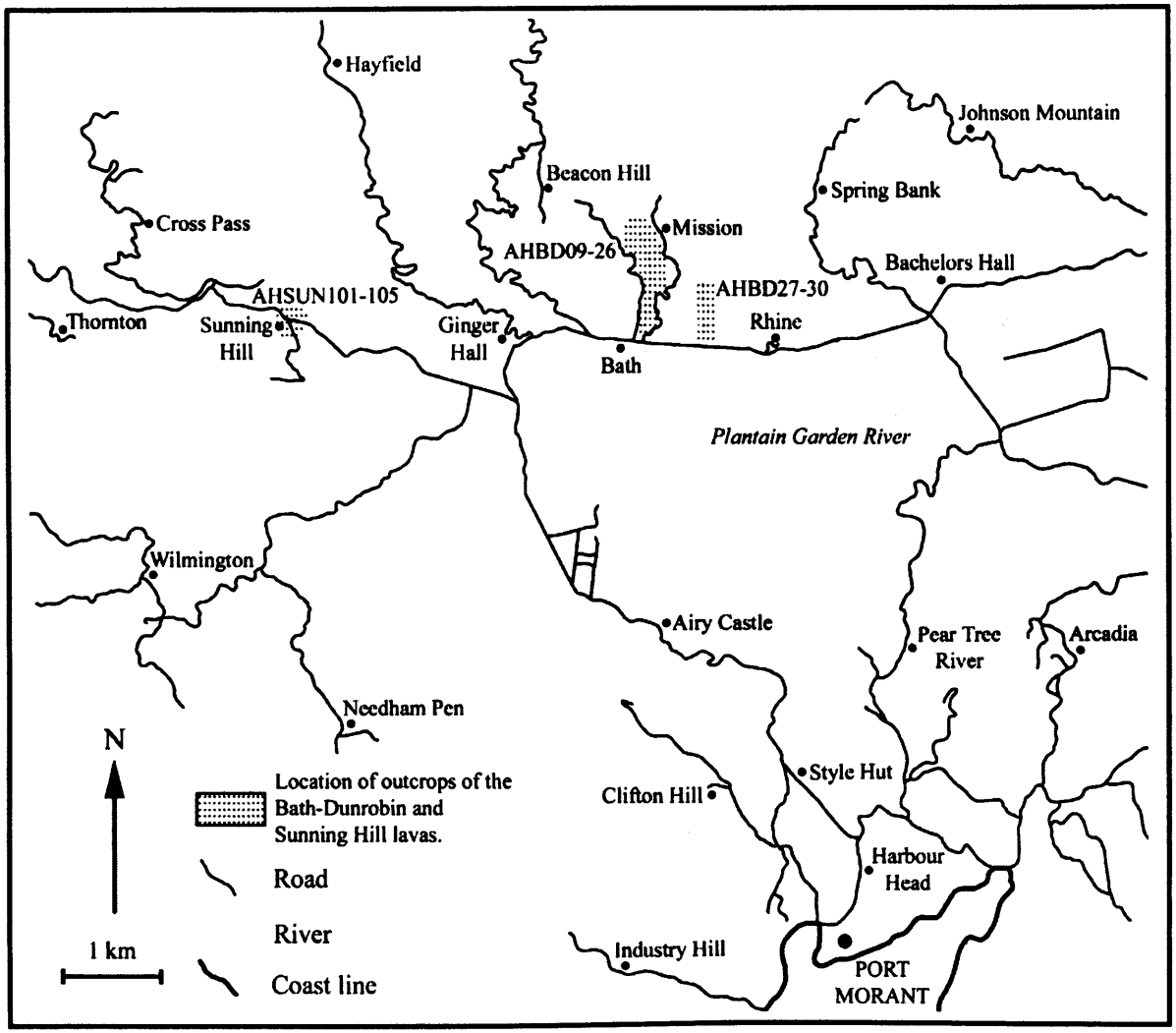

Figure A.4 – Location of the Bath-Dunrobin and Sunning Hill samples, SE Blue Mountains Inlier.

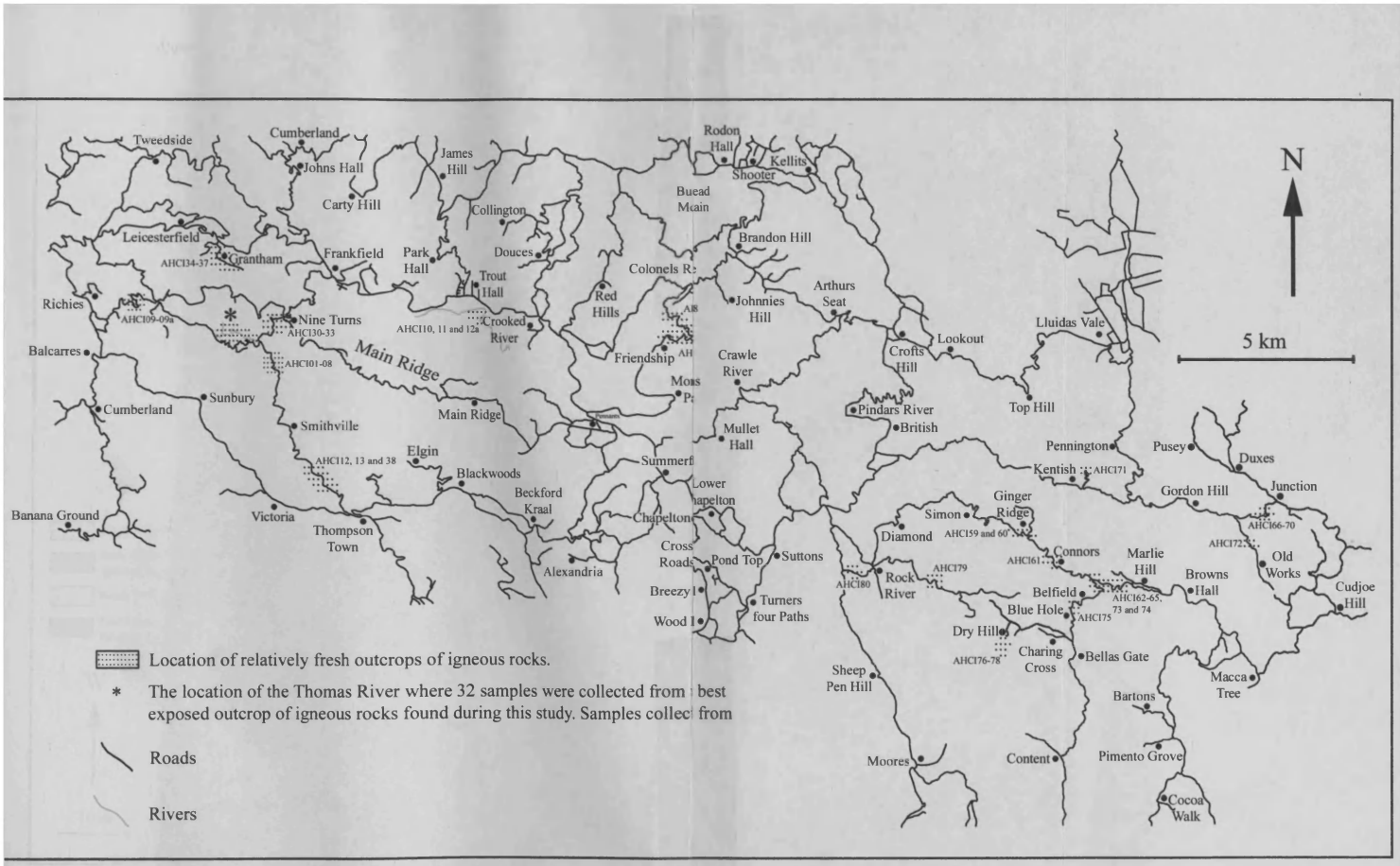

Figure A.5 – Location map for the Central Inlier samples.

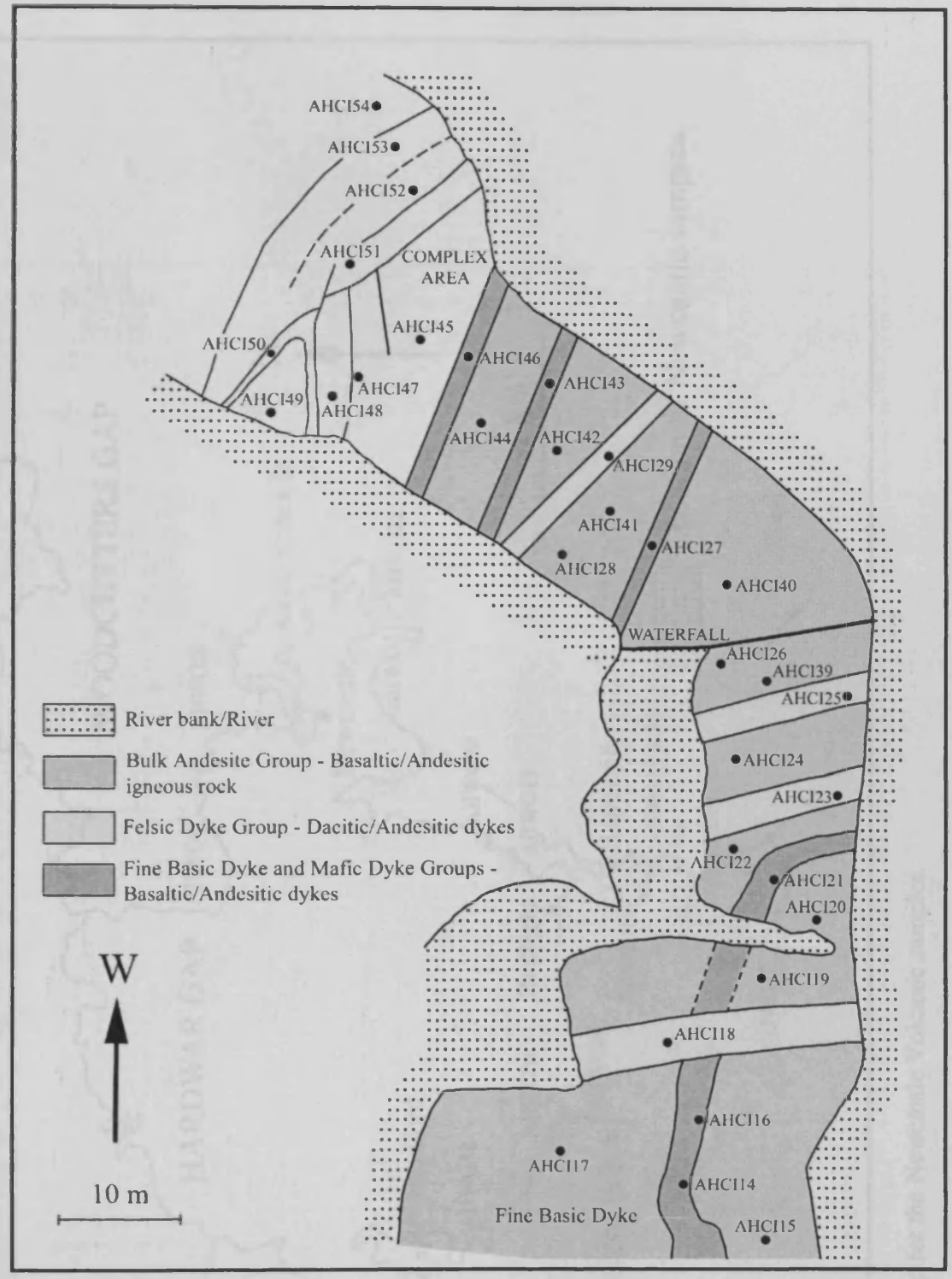

Figure A.6 – Sketch showing the locations of the various samples collected in the Thomas River, Central Inlier.

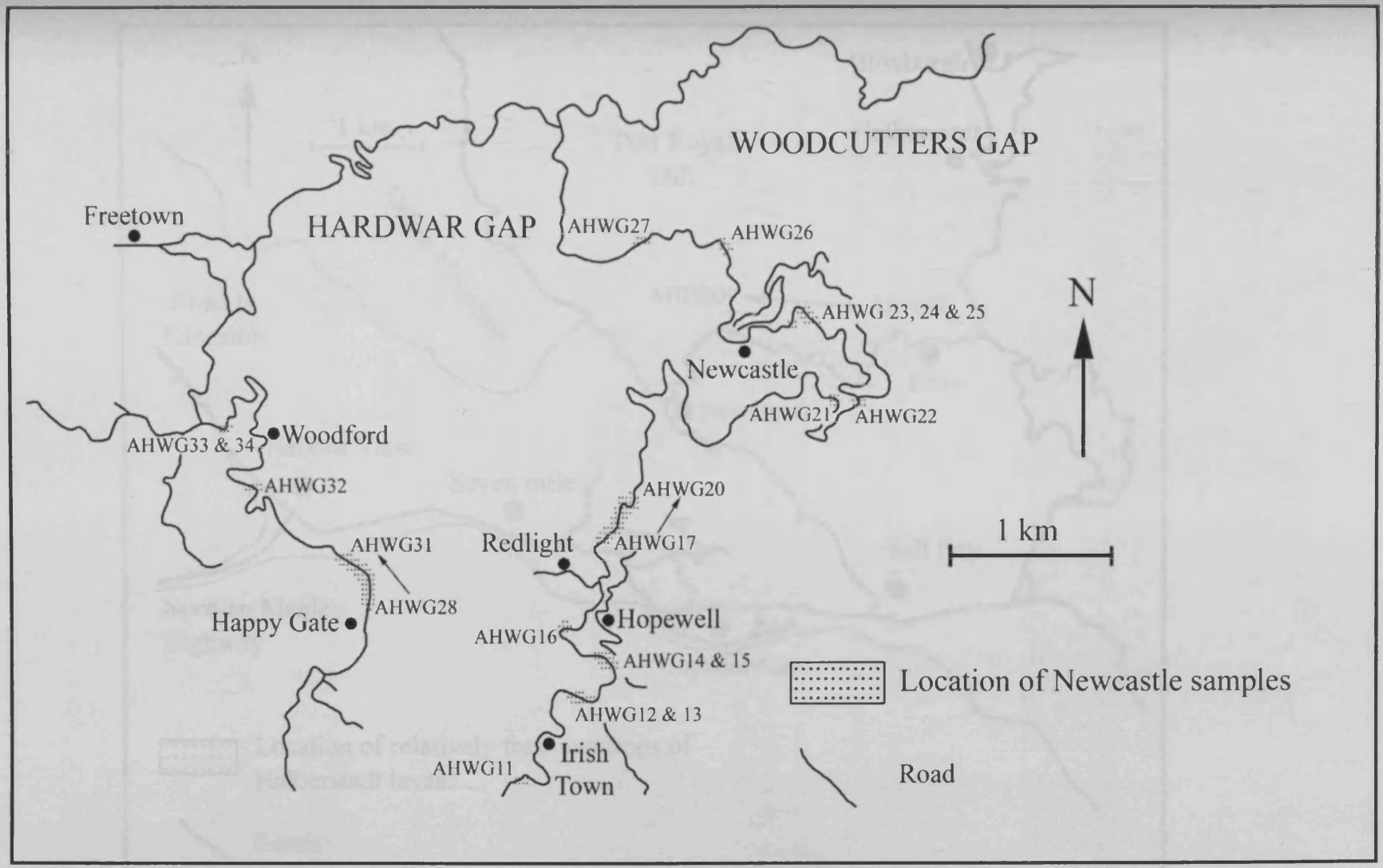

Figure A.7 – Location map for the Newcastle Volcanic samples.

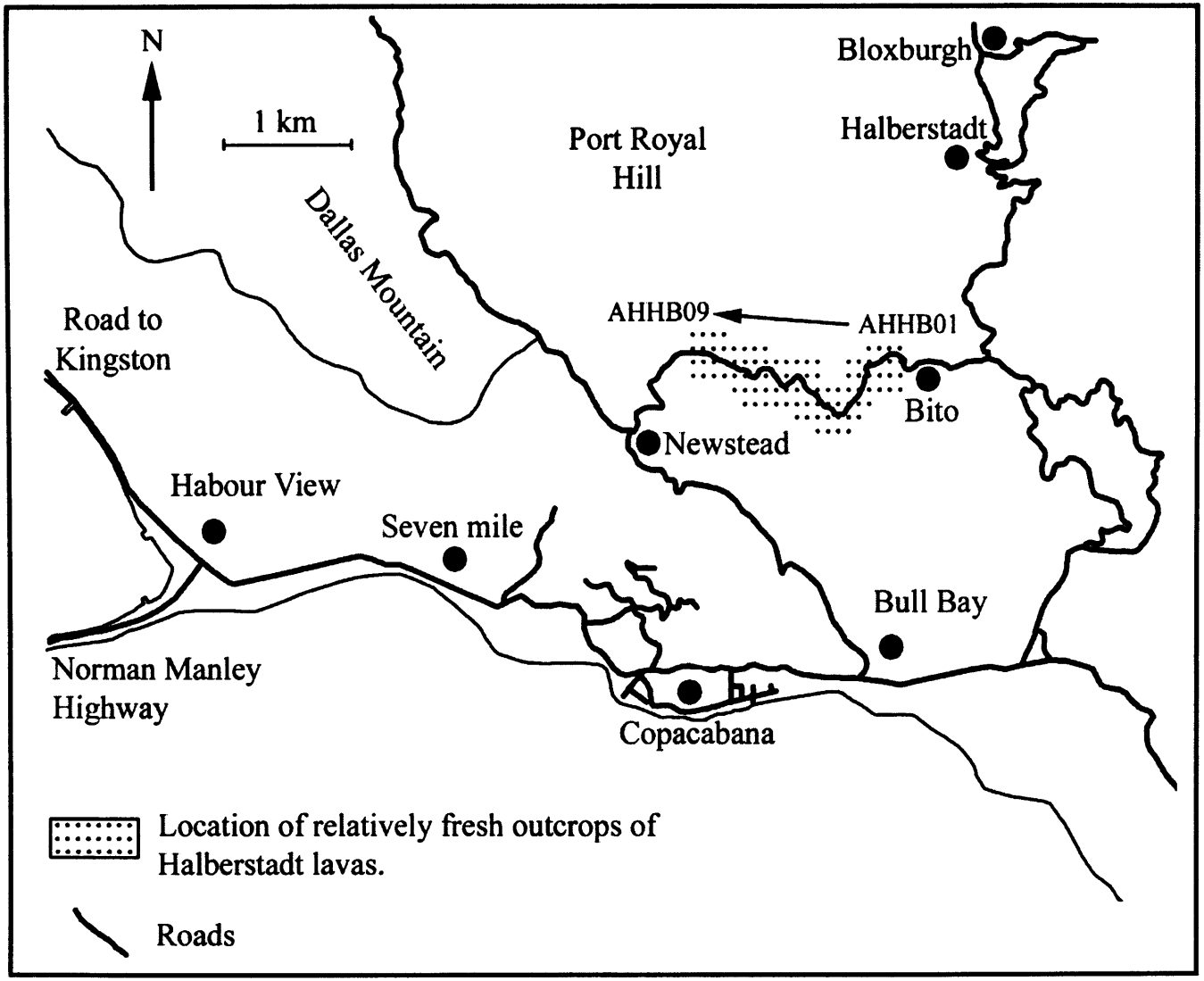

Figure A.8 – Location map for the Halberstadt Volcanic samples.

Appendix B

References used to construct the discrimination diagrams in Chapter 5

B.1 The 2492 samples originally used to develop a new discrimination diagram were taken from the following references:

Arakawa, Y., Kurosawa, M., Takahashi, K., Kobayashi, Y., Tsukui, M., Amakawa, H., 1998. Sr-Nd isotopic and chemical characteristics of the silicic magma reservoir of the Aira pyroclastic eruption, southern Kyushu, Japan. Journal of Volcanology and Geothermal Research. 80, 179-194.

Arculus, R. J., Pearce, J. A., Murton, B. J., Van Der Laan, S. R., 1992. Igneous stratigraphy and major-element geochemistry of holes 786A and 786B. Proceeding of the Ocean Drilling Program Scientific Results. 125, 143-169.

Baker, P. E., 1984. Geochemical evolution of St. Kitts and Montserrat, Lesser Antilles. Journal of the Geological Society of London. 141, 401-411.

Barsdell, M., Smith, I. E. M., Spörli, K. B., 1982. The origin of reversed geochemical zoning in the northern New Hebrides volcanic zone. Contributions to Mineralogy and Petrology. 81, 148-155.

Barsdell, M., 1988. Petrology and petrogenesis of clinopyroxene-rich tholeiitic lavas, Merelava volcano, Vanuatu. Journal of Petrology. 29, 927-964.

Bau, M., Knittel, U., 1993. Significance of slab-derived partial melts and aqueous fluids for the genesis of tholeiitic and calc-alkaline island-arc basalts: Evidence from Mt. Arayat, Philippines. Chemical Geology. 105, 233-251.

Beresford, S. W., Cole, J. W., 2000. Kawerau ignimbrite: A 0.24 Ma ignimbrite erupted from the Okataina caldera complex, Taupo Volcanic Zone, New Zealand. New Zealand Journal of Geology and Geophysics. 43, 109-115.

Bindeman, I. N., Bailey, J. C., 1994. A model of reverse differentiation at Dikii Greben` Volcano, Kamchatka: Progressive basic magma vesiculation in a

silicic magma chamber. Contributions to Mineralogy and Petrology. 117, 263-278.

Black, P. M., Briggs, R. M., Itaya, T., Dewes, E. R., Dunbar, N. W., Kawasaki, K., Kuschel, E., Smith, I. E. M., 1992. K-Ar age data and geochemistry of the Kiwitahi volcanics, western Hauraki Rift, North Island, New Zealand. New Zealand Journal of Geology and Geophysics. 35, 403-413.

Bloomer, S. H., Ewart, A., Hergt, J. M., Bryan, W. B., 1996. Geochemistry and origin of igneous rocks from the outer Tonga forearc (Site 841). Proceeding of the Ocean Drilling Program Scientific Results. 135, 625-646.

Boespflug, X., Dosso, L., Bougault, H., Joron, J. L., 1990. Trace element and isotopic (Sr, Nd) geochemistry of volcanic rocks from the Lau Basin. Geologisches Jahrbuch. 92, 503-516.

Bougault, H., Maury, R. C., El Azzouzi, M., Joron, J. L., Cotten, J., Treuil, M., 1982. Tholeiites, basaltic andesites, and andesites from Leg 60 Sites: Geochemistry, mineralogy and low partition coefficient elements. Initial Report Deep Sea Drilling Program 60, 657-677.

Briggs, R. M., Goles, G. G., 1984. Petrological and trace element geochemical features of the Okete Volcanics, western North Island, New Zealand. Contributions to Mineralogy and Petrology. 86, 77-88.

Briggs, R. M., 1986. Petrology and geochemistry of Maungatautari, a medium-K andesite-dacite volcano. New Zealand Journal of Geology and Geophysics. 29, 273-289.

Briggs, R. M., Fulton, B. W. J., 1990. Volcanism, structure and petrology of the Whiritoa-Whangamata coastal section, Coromandel Volcanic Zone, New Zealand: Facies model evidence for the Tunaiti caldera. New Zealand Journal of Geology and Geophysics. 33, 623-633.

Briggs, R. M., Gifford, M. G., Moyle, A. R., Taylor, S. R., Norman, M. D., Houghton, B. F., Wilson, C. J. N., 1993. Geochemical zoning and eruptive mixing in ignimbrites from Mangakino Volcano, Taupo Volcanic Zone, New Zealand. Journal of Volcanology and Geothermal Research. 56, 175-203.

Brown, S. J. A., Wilson, C. J. N., Cole, J. W., Wooden, J. L., 1998. The Whakamaru group ignimbrites, Taupo Volcanic Zone, New Zealand: Evidence for reverse tapping of a zoned silicic magmatic system. Journal of Volcanology and Geothermal Research. 84, 1-37.

Castillo, P. R., Newhall, C. G., 2004. Geochemical constraints on possible subduction components in lavas of Mayon and Taal volcanoes, southern Luzon, Philippines. Journal of Petrology. 45, 1089-1108.

Churikova, T., Dorendorf, F., Barman, T. R., 2001. Sources and fluids in the mantle wedge below Kamchatka, evidence from across-arc geochemical variation. Journal of Petrology. 42, 1567-1593.

Clark, S. K., Reagan, M. K., Plank, T., 1998. Trace element and U-series systematics for 1963-1965 tephras from Irazu volcano, Costa Rica: Implications for magma generation processes and transit times. Geochimica et Cosmochimica Acta. 62, 2689-2699.

Cole, J. W., Graham, I. J., Gibson, I. L., 1990. Magmatic evolution of the Late Cenozoic volcanic rocks of the Lau Ridge, Fiji. Contributions to Mineralogy and Petrology. 104, 540-554.

Cole, J. W., Brown, S. J. A., Burt, R. M., Beresford, S. W., Wilson, C. J. N., 1998. Lithic types in ignimbrites as a guide to the evolution of a caldera complex, Taupo Volcanic Center, New Zealand. Journal of Volcanology and Geothermal Research. 80, 217-237.

Cole, J. W., Thordarson, T., Burt, R. M., 2000. Magma origin and evolution of White Island (Whakaari) Volcano, Bay of Plenty, New Zealand. Journal of Petrology. 41, 867-895.

Cole, J. W., Gamble, J. A., Burt, D. M., Carroll, L. D., Shelley, D., 2001. Mixing and mingling in the evolution of andesite-dacite magmas: Evidence from co-magmatic plutonic enclaves, Taupo Volcanic Zone, New Zealand. Lithos. 59, 25-46.

Crawford, A. J., Beccaluva, L., Serri, G., Dostal, J., 1986. Petrology, geochemistry and tectonic implications of volcanics dredged from the intersection of the Yap and Mariana trenches. Earth Planetary Science Letters. 80, 265-280.

Defant, M. J., Richerson, P. M., De Boer, J. Z., Stewart, R. H., Maury, R. C., Bellon, H., Drummond, M. S., Fergenson, M. D., Jackson, T. E., 1991. Dacite genesis via both differention and slab melting: Petrogenesis of La Yeguada volcanic complex. Journal of Petrology. 32, 1101-1142.

Defant, M. J., Sherman, S. B., Maury, R. C., Bellon, H., De Boer, J. Z., Davidson, J. P., Kepezhinskas, P. K., 2001. The geology, petrology and petrogenesis of Saba island, Lesser Antilles. Journal of Volcanology and Geothermal Research. 107, 87-111.

Dietrich, V. J., Emmerman, R., Oberhansli, R., Puchelt, H., 1978. Geochemistry of basaltic and gabbroic rocks from the west Mariana basin and the Marian trench. Earth Planetary Science Letters. 39, 127-144.

Dorendorf, F., Wiechert, U., Worner, G., 2000. Hydrated sub-arc mantle: A source for the Kluchevskoy Volcano, Kamchatka/Russia. Earth Planetary Science Letters. 175, 69-86.

Edwards, C. M. H., Menzies, M. A., Thirlwall, M. F., Morris, J. D., Leeman, W. P., Harmon, R. S., 1994. The transition to potassic alkaline volcanism in island arcs: The Ringgit-Beser complex, east Java, Indonesia. Journal of Petrology. 35, 1557-1595.

Eggins, S. M., 1993. Origin and differentiation of picritic arc magmas, Ambae (Aoba), Vanuatu. Contributions to Mineralogy and Petrology. 114, 79-100.

Elliott, T., Plank, T., Zindler, A., White, W., Bourdon, B., 1997. Element transport from slab to volcanic front at the Mariana arc. Journal of Geophysical Research.-Solid Earth. 102, 14991-15019.

Ewart, A., Bryan, W. B., Chappell, B. W., Rudnick, R. L., 1994. Regional geochemistry of the Lau-Tonga arc and back-arc systems. Proceeding of the Ocean Drilling Program Scientific Results. 135, 385-425.

Falloon, T., Crawford, A. J., 1991. The petrogenesis of high-calcium boninite lavas dredged from the northern Tongan ridge. Earth Planetary Science Letters. 102, 375-394.

Fedorov, P. I., Shapiro, M. N., 1998. Neogene volcanics of the Kamchatka isthmus and geodynamics of the Aleutian-Kamchatka junction. Geotectonics. 32, 122-137.

Gamble, J. A., Smith, I. E. M., Mcculloch, M. T., Graham, I. J., Kokelaar, B. P., 1993. The geochemistry and petrogenesis of basalts from the Taupo Volcanic Zone and Kermadec island arc, S. W. Pacific. Journal of Volcanology and Geothermal Research. 54, 265-290.

Gamble, J. A., Wright, I. C., Woodhead, J. D., McCulloch, M. T., 1994. Arc and back-arc geochemistry in the southern Kermadec arc - Ngatoro basin and offshore Taupo Volcanic Zone, SW Pacific: Volcanism associated with extension at consuming plate margins (Smellie, J. L.). Geological Society London, 193-212.

George, R. M., Turner, S. P., Hawkesworth, C. J., Morris, J., Nye, C. J., Ryan, J. G., Zheng, S. H., 2003. Melting processes and fluid and sediment transport rates along the Alaska-Aleutian arc from an integrated U-Th-Ra-Ba isotope study. Journal of Geophysical Research. B108, ECV 6-1-ECV 6-25.

George, R. M., Turner, S. P., Hawkesworth, C. J., Bacon, C. R., Nye, C. J., Stelling, P., Dreher, S. T., 2004. Chemical versus temporal controls on the evolution of tholeiitic and calc-alkaline magmas at two volcanoes in the Alaska-Aleutian arc. Journal of Petrology. 45, 203-219.

Gertisser, R., Keller, J., 2003. Trace element and Sr, Nd, Pb and O isotope variations in medium-K and high-K volcanic rocks from Merapi Volcano, Central Java, Indonesia: Evidence for the involvement of subducted sediments in Sunda arc magma genesis. Journal of Petrology. 44, 457-489.

Gill, J. B., 1976. Composition and age of Lau Basin and Ridge volcanic rocks: implications for evolution of an interarc basin and remnant arc. Geological Society America Bulletin. 87, 1384-1395.

Gill, J. B., 1987. Early geochemical evolution of an oceanic island arc and backarc: Fiji and the south Fiji basin. Journal of Geology. 95, 589-615.

Gorton, M. P., 1977. The geochemistry and origin of Quarternary volcanism in the New Hebrides. Geochimica et Cosmochimica Acta. 41, 1257-1270.

Graham, A. M., Thirlwall, M. F., 1981. Petrology of the 1979 eruption of Soufriere Volcano, St. Vincent, Lesser Antilles. Contributions to Mineralogy and Petrology. 76, 336-342.

Graham, I. J., Hackett, W. R., 1987. Petrology of calc-alkaline lavas from Ruapehu Volcano and related vents, Taupo Volcanic Zone, New Zealand. Journal of Petrology. 28, 531-567.

Graham, I. J., Cole, J. W., 1991. Petrogenesis of andesites and dacites of White Island Volcano, Bay of Plenty, New Zealand, In the light of new geochemical and isotopic data. New Zealand Journal of Geology and Geophysics. 34, 303-315.

Gust, D. A., Arculus, R. J., Kersting, A. B., 1997. Aspects of magma sources and processes in the Honshu arc. The Canadian Mineralogist. 35, 347-365.

Haase, K. M., Worthington, T. J., Stoffers, P., Garbe-Schonberg, C. D., Wright, I., 2002. Mantle dynamics, element recycling, and magma genesis beneath the Kermadec arc-Havre trough. Geochemistry Geophysics Geosystems. 3, 2002GC000335.

Hannah, R. S., Vogel, T. A., Patino, L. C., Alvarado, G. E., Perez, W., Smith, D. R., 2002. Origin of silicic volcanic rocks in central Costa Rica: A study of chemically variable ash-flow sheet in the Tiribi Tuff. Bulletin of Volcanology. 64, 117-133.

Hauff, F., Hoernle, K., Tilton, G., Graham, D., W., Kerr, A. C., 2000. Large volume recycling of oceanic Lithos.phere over short time scales: Geochemical constraints from the Caribbean Large Igneous Province. Earth and Planetary Science Letters. 174, 247-263.

Heath, E., MacDonald, R., Belkin, H., Hawkesworth, C., Sigurdsson, H., 1998. Magmagenesis at Soufriere Volcano, St Vincent, Lesser Antilles Arc. Journal of Petrology. 39, 1721-1764.

Hergt, J. M., Hawkesworth, C. J., 1994. Pb, Sr and Nd isotopic evolution of the Lau basin: Implications for mantle dynamics during backarc opening. Proceeding of the Ocean Drilling Program Scientific Results. 135, 505-517.

Hildreth, W., Fierstein, J., Siems, D. F., Budahn, J. R., Ruiz, J., 2004. Rear-arc vs. arc-front volcanoes in the Katmai reach of the Alaska Peninsula: a critical appraisal of across-arc compositional variation. Contributions to Mineralogy and Petrology. 147, 243-275.

Hildyard, S. C., Cole, J. W., Weaver, S. D., 2000. Tikorangi ignimbrite: A 0.89 Ma mixed andesite-rhyolite ignimbrite, Matahana basin, Taupo Volcanic Zone, New Zealand. New Zealand Journal of Geology and Geophysics. 43, 95-107.

Hoang, N., Uto, K., 2003. Geochemistry of Cenozoic basalts in the Fukuoka district (northern Kyushu, Japan): Implications for asthenosphere and Lithos.pheric mantle interaction. Chemical Geology.198, 249-268.

Hochstaedter, A. G., Kepezhinskas, P. K., Defant, M. J., 1996. Insights into the volcanic arc mantle wedge from magneian lavas from the Kamchatka arc. Journal of Geophysical Research. B101, 697-712.

Hole, M. J., Saunders, A. D., Marriner, G. F., Tarney, J., 1984. Subduction of pelagic sediments: implications for the origin of Ce-anomalous basalts from the Mariana Islands. Journal of the Geological Society London. 141, 453-472.

Hoogewerff, J., Van Bergen, M. J., Vroon, P. Z., Hertogen, J., Wordel, R., Sneyers, A., Nasution, A., Varekamp, J. C., Moens, H. L. E., Mouchel, D., 1997. U series, Sr-Nd-Pb isotope and trace element systematics across an active island arc-continent collision zone: Implications for element transfer at the slab-wedge interface. Geochimica et Cosmochimica Acta. 61, 1057-1072.

Huang, Y. M., Hawkesworth, C. J., Smith, I. E. M., Van Calsteren, P., Black, P. M., 2000. Geochemistry of late Cenozoic basaltic volcanism in Northland and Coromandel, New Zealand: Implications for mantle enrichment processes. Chemical Geology. 164, 219-238.

Ishizuka, O., Yuasa, M., 1999. Petrography and isotopic age of volcanic rocks dredged from the back-arc ridges and knolls at the north end of the Izu-Ogasawara arc. Geological Survey Japanese Cruise Report. 24, 171-190.

Ishiwatari, A., Ohama, H., 1997. Clinopyroxene basalt dikes in the Miocene Iwaine formation, Hokuriku Province, Japan: Various continental arc magmas including shoshonite series and origin of the clinopyroxene phenocrysts. Journal of the Geological Society of Japan. 103, 565-578.

Jaques, A. L., Chappell, B. W., 1980. Petrology and trace element geochemistry of the Papuan ultramafic belt. Contributions to Mineralogy and Petrology. 75, 55-70.

Jenner, G. A., 1981. Geochemistry of high-Mg andesites from Cape Vogel, Papua New Guinea. Chemical Geology. 33, 307-332.

Kagami, H., 1990. Sr and Nd isotopic ratios of volcanic rocks from Genbudo Area, Southwest, Japan. Journal of the Geological Society of Japan. 96, 471-474.

Kepezhinskas, P. K., McDermott, F., Defant, M. J., Hochstaedter, A. G., Drummond, M. S., Hawkesworth, C. J., Koloskov, A. V., Maury, R. C., Bellon, H., 1997. Trace element and Sr-Nd-Pb isotopic constraints on a three-component model of Kamchatka arc petrogenesis. Geochimica et Cosmochimica Acta. 61, 577-600.

Kita, I., Yamamoto, M., Asakawa, Y., Nakagawa, M., Taguchi, S., Hasegawa, H., 2001. Contemporaneous ascent of within-plate type and island-arc type magmas in the Beppu-Shimabara graben system, Kyushu island, Japan. Journal of Volcanology and Geothermal Research. 111, 99-109.

Kimura, J. I., Yoshida, T., Iizumi, S., 2002. Origin of low-K intermediate lavas at Nekoma volcano, NE Honshu arc, Japan: Geochemical constraints for lower-crustal melts. Journal of Petrology. 43, 631-661.

Knittel, U., Hegner, E., Bau, M., Satir, M., 1997. Enrichment processes in the sub-arc mantle: A Sr-Nd-Pb isotopic and REE study of primitive arc basalts from the Philippines. The Canadian Mineralogist. 35, 327-346.

Kobayashi, K., Nakamura, E., 2001. Geochemical evolution of Akagai Volcano, NE Japan: Implications for interaction between island-arc magma and lower crust, and generation of isotopically various magmas. Journal of Petrology. 42, 2303-2331.

Krippner, S. J. P., Briggs, R. M., Wilson, C. J. N., Cole, J. W., 1998. Petrography and geochemistry of lithic fragments in ignimbrites from the Mangakino volcanic center: Implications for the composition of the subvolcanic crust in western Taupo Volcanic Zone, New Zealand. New Zealand Journal of Geology and Geophysics. 41, 187-199.

Kuritani, T., Yokoyama, T., Kobayashi, K., Nakamura, E., 2003. Shift and rotation of composition trends by magma mixing: 1983 eruption at Miyake-Jima Volcano, Japan. Journal of Petrology. 44, 1895-1916.

Leonard, G. S., Cole, J. W., Nairn, I. A., Self, S., 2002. Basalt triggering of the C.AD 1305 Kaharoa rhyolite eruption, Tarawera volcanic complex, New Zealand. Journal of Volcanology and Geothermal Research. 115, 461-486.

Lidiak, E. G., Jolly, W. T., Lidiak, E. G., Larue, D. K. (1998) Geochemistry of intrusive igneous rocks, St. Croix, U. S. Virgin Islands. In: Tectonics and geochemistry of the northeastern Caribbean. pp. 133-153. Geological Society of America.

Lindsay, J. M., Worthington, T. J., Smith, I. E. M., Black, P. M., 1999. Geology, petrology and petrogenesis of Little Barrier island, Hauraki gulf, New Zealand. New Zealand Journal of Geology and Geophysics. 42, 155-168.

Luttinen, A. V., Furnes, H., 2000. Flood basalts of Vestfjella: Jurassic magnetism across an Archaean-Proterozoic Lithos.pheric boundary in Dronning Maud Land, Antarctica. Journal of Petrology. 41, 1271-1305.

Maillet, P., Monzier, M., Lefevre, C., 1986. Petrology of Matthew and Hunter Volcanoes, south New Hebrides island arc (southwest Pacific). Journal of Volcanology and Geothermal Research. 30, 1-27.

Maillet, P., Ruellan, E., Gerard, M., Person, A., Bellon, H., Cotten, J., Joron, J. L., Nakada, S., Price, R. C., 1995. Tectonics, magmatism, and evolution of the New Hebrides backarc troughs (southwest Pacific). Backarc basins: Tectonics and magmatism (Taylor, B.), Plenum Press, London, 177-235.

Marcelot, G., 1981. Geochemistry of the lavas of Erromango island (New Hebrides): Petrogenetic implications. Bulletin de la Société Géologique de France. 23, 367-376.

Marcelot, G., Dupuy, C., Girod, M., Maury, R. C., 1983. Petrology of Futuna island lavas (New Hebrides): An example of calc-alkaline magmatism associated with the initial stages of back-arc spreading. Chemical Geology. 38, 23-37.

Marsh, N. G., Saunders, A. D., Tarney, J., Dick, H. J. B., 1980. Geochemistry of basalts from the Shikoku and Daito Basins, Deep Sea Drilling Project Leg 58. In: G deVries Klein and K Kobayashi (eds.) Initial Reports of the Deep Sea Drilling Project. pp. 805-842. U.S. Government Printing Office: Washington.

Milner, D. M., Cole, J. W., Wood, C. P., 2003. Mamaku ignimbrite: A caldera-forming ignimbrite erupted from a compositionally zoned magma chamber in Taupo Volcanic Zone, New Zealand. Journal of Volcanology and Geothermal Research. 122, 243-264.

Monzier, M., Robin, C., Eissen, J. P., Cotten, J., 1997. Geochemistry vs seismo-tectonics along the volcanic New Hebrides central chain (southwest Pacific). Journal of Volcanology and Geothermal Research. 78, 1-29.

Morioka, K., Maury, R. C., Prouteau, G., Cotten, J., Schiano, P., Bellon, H., Fontaine, L., 2000. Slab melt as metasomatic agent in island arc magma mantle sources, Negros and Batan (Philippines). The Island Arc. 9, 472-486.

Morris, P. A., 1995. Slab Melting as an Explanation of Quaternary Volcanism and Aseismicity in Southwest Japan. Geology. 23, 395-398.

Nagao, T., Hase, Y., Nagamine, S., Kakabuchi, S., Sakaguchi, K., 1999. Late Miocene to middle Pleistocene Hisatsu volcanic rocks generated from heterogeneous magma sources: Evidence from temporal-spatial variation of distribution and chemistry of the rocks. J. Jpn. Assoc. Mineral. Petrol. Econ. Geol. (Ganseki Kobutsu Kosho Gakkai-Shi). 94, 461-481.

Nairn, I. A., 1992. The Te Rere and Okareka eruption episodes - Okataina Volcanic Centre, Taupo Volcanic Zone, New Zealand. New Zealand Journal of Geology and Geophysics. 35, 93-108.

Nairn, I. A., Shane, P. R., Cole, J. W., Leonard, G. S., Self, S., Pearson, N. J., 2004. Rhyolite magma processes of the ~AD 1315 Kaharoa eruption episode, Tarawera volcano, New Zealand. Journal of Volcanology and Geothermal Research. 131, 265-294.

Nakano, S., 1993. Ueno basaltic rocks I: Heterogeneous magmas at two monogenetic volcanoes. Journal of Japanese Association of Mineralogy Petrology and Economic Geology (Ganseki Kobutsu Kosho Gakkai-Shi). 88, 272-288.

Nakano, S., 1994. Ueno basaltic rocks II: Chemical variation in the Kiso Province, to the south of the Ontake volcano. Journal of Japanese Association of Mineralogy Petrology and Economic Geology (Ganseki Kobutsu Kosho Gakkai-Shi). 89, 115-130.

Nakagawa, M., Wada, K., Wood, C. P., 2002. Mixed Magmas, Mush Chambers and Eruption Triggers: Evidence from Zoned Clinopyroxene Phenocrysts in Andesitic Scoria from the 1995 Eruptions of Ruapehu Volcano, New Zealand. Journal of Petrology. 43, 2279-2303.

Nakashima, T., Shimoda, G., Tatsumi, Y., 2000. Porphyritic magnesian andesites in the Setouchi volcanic belt, SW Japan. Bulletin of Volcanological Society Japan. Ser. 2 45, 259-269.

Nicholls, I. A., Whitford, D. J., 1983. Potassium-rich volcanic rocks of the Muriah complex, Java, Indonesia: Products of multiple magma sources? Journal of Volcanology and Geothermal Research. 18, 337-359.

Nicholson, K. N., Black, P. M., Picard, C., 2000. Geochemistry and tectonic significance of the Tangihua Ophiolite Complex, New Zealand. Tectonophysics. 321, 1-15.

Nye, C. J., Reid, M. R., Avery, V. F., Francis, D. M., 1994. Geochemistry of the 1989-1990 eruption of Redoubt volcano part I: Whole-rock major and trace element chemistry. Journal of Volcanology and Geothermal Research. 62, 429-452.

O'Hara, Y., Fujioka, K., Ishizuka, O., Ishii, T., 2002. Peridotites and volcanics from the Yap arc system: Implications for tectonics of the southern Philippine sea plate. Chemical Geology. 189, 35-53.

Patino, L. C., Carr, M. J., Feigenson, M. D., 2000. Local and regional variations in Central American arc lavas controlled by variations in subducted sediment input. Contributions to Mineralogy and Petrology. 138, 265-283.

Pearce, J. A., Van Der Laan, S. R., Arculus, R. J., Murton, B. J., Ishii, T., Peate, D., Parkinson, I. J., 1992. Boninite and harzburgite from Leg 125 (Bonin-Mariana forearc): A case study of magma genesis during the initial stages of subduction. Proceeding of the Ocean Drilling Program Scientific Results. 125, 623-659.

Pearce, J. A., Kempton, P. D., Nowell, G. M., Noble, S. R., 1999. Hf-Nd Element and Isotope Perspective on the Nature and Provenance of Mantle and Subduction Components in Western Pacific Arc-Basin Systems. Journal of Petrology. 40, 1579-1611.

Peate, D. W., Pearce, J. A., Hawkesworth, C. J., Edwards, C. M. H., Hirose, K., 1997. Geochemical variations in Vanuatu arc lavas: The role of subducted material and a variable mantle wedge composition. Journal of Petrology. 38, 1331-1358.

Prouteau, G., Maury, R. C., Sajona, F. G., Cotten, J., Joron, J. L., 2000. Behavior of niobium, tantalum and other high field strength elements in adakites and related lavas from the Philippines. The Island Arc. 9, 487-498.

Price, R. C., Johnson, L. E., Crawford, A. J., 1990. Basalts of the North Fiji Basin: the generation of back arc basin magmas by mixing of depleted and enriched mantle sources. Contributions to Mineralogy and Petrology. 105, 106-121.

Price, R. C., Mcculloch, M. T., Smith, I. E. M., Stewart, R. B., 1992. Pb-Nd-Sr isotopic compositions and trace element characteristics of young volcanic rocks from Egmont Volcano and comparisons with basalts and andesites from the Taupo Volcanic Zone, New Zealand. Geochimica et Cosmochimica Acta. 56, 941-953.

Price, R. C., Stewart, R. B., Woodhead, J. D., Smith, I. E. M., 1999. Petrogenesis of High-K Arc Magmas: Evidence from Egmont Volcano, North Island, New Zealand. Journal of Petrology. 40, 167-197.

Puzankov. Y., 1994. Geochemistry of volcanic rocks of the Eocene-Oligocene island arc (Kamchatka). Geol Geofiz. 1, 89-97.

Reagan, M. K., Sims, K. W. W., Erich, J., Thomas, R. B., Cheng, H., Edwards, R. L., Layne, G. D., Ball, L., 2003. Time-scales of differentiation from mafic parents to rhyolite in North American continental arcs. Journal of Petrology. 44, 1703-1726.

Reubi, O., Nicholls, I. A., Kamenetsky, V. S., 2002. Early mixing and mingling in the evolution of basaltic magmas: Evidence from phenocryst assemblages, Slamet Volcano, Java, Indonesia. Journal of Volcanology and Geothermal Research. 119, 255-274.

Reubi, O., Nicholls, I. A., 2004. Magmatic evolution at Batur volcanic field, Bali, Indonesia: Petrological evidence for polybaric fractional crystallisation and

implications for caldera-forming eruptions. Journal of Volcanology and Geothermal Research. 138, 345-369.

Revillon, S., Arndt, N. T., Hallot, E., Kerr, A. C., Tarney, J., 1999. Petrogenesis of picrites from the Caribbean Plateau and the North Atlantic magmatic province. Lithos. 49, 1-21.

Rogers, N. W., Setterfield, T. N., 1994. Potassium and incompatible-element enrichment in shoshinitic lavas from the Tavua Volcano, Fiji. Chemical Geology. 118, 43-62.

Romick, J. D., Perfit, M. R., Swanson, S. E., Shuster, R. D., 1990. Magmatism in the eastern Aleutian Arc: temporal characteristic of igneous activity on Akutan Island. Contributions to Mineralogy and Petrology. 104, 700-721.

Raos, A. M., Crawford, A. J., 2004. Basalts from the Efate island group, central section of the Vanuatu arc, SW Pacific: Geochemistry and petrogenesis. Journal of Volcanology and Geothermal Research. 134, 35-56.

Sakuyama, M., Nesbitt, R. W., 1986. Geochemistry of Quaternary volcanic rocks of the northeast Japan arc. Journal of Volcanology and Geothermal Research. 29, 413-450.

Sasaki, Y., 1985. Res. Report Lab. Nuclear Sci. Tohoku Univ. 18, 175-188.

Schilling, J. G., Beget, J., Nye, C. J., Gardner, J. E., Devine, J. D., George, R. M., 2002. Geology and petrology of ejecta from the 1999 eruption of Shishaldin Volcano, Alaska. Bulletin of Volcanology. 64, 548-561.

Schmitz, M. D., Smith, I. E. M., 2004. The Petrology of the Rotoiti Eruption Sequence, Taupo Volcanic Zone: an Example of Fractionation and Mixing in a Rhyolitic System. Journal of Petrology. 45, 2045-2066.

Shinjo, R., Usami, K., Kato, Y., 1995. Geology and petrology of the Nishi and Fudenzaki formations of the Aguni group, Aguni island, the central Ryukyu arc: Petrogenetic relationship between the andesites and dacites. Bull. Coll. Sci. Univ. Ryukyu. 60, 27-50.

Shinjo, R., Chung, S. L., Kato, Y., Kimura, M., 1999. Geochemical and Sr-Nd isotopic characteristics of volcanic rocks from the Okinawa trough and Ryukyu arc: Implications for the evolution of a young, intracontinental back arc basin. Journal of Geophysical Research. B104, 10591-10608.

Shinjo, R., Woodhead, J. D., Hergt, J. M., 2000. Geochemical variation within the northern Ryukyu arc: Magma source compositions and geodynamic implications. Contributions to Mineralogy and Petrology. 140, 263-282.

Shinjo, R., Kato, Y., 2000. Geochemical constraints on the origin of bimodal magmatism at the Okinawa Trough, an incipient back-arc basin. Lithos. 54, 117-137.

Smellie, J. L., Pankhurst, R. J., Thomson, M. R. A., Davis, R. E. S., 1984. The geology of the South Shetland islands: VI. Stratigraphy, geochemistry and evolution. British Antarctic Survey Scientific Report. 87, 1-85.

Smith, I. E. M., Stewart, R. B., Price, R. C., 2003. The petrology of a large intra-oceanic silicic eruption: The Sandy Bay tephra, Kermadec arc, southwest Pacific. Journal of Volcanology and Geothermal Research. 124, 173-194.

Smith, T. E., Thirlwall, M. F., Macpherson, C., 1996. Trace element and isotope geochemistry of the volcanic rocks of Bequia, Grenadine Islands, Lesser Antilles arc: A study of subduction enrichment and intra-crustal contamination. Journal of Petrology. 37, 117-143.

Smith, V. C., Shane, P. R., Smith, I. E. M., 2002. Tephrostratigraphy and geochemical fingerprints of the Mangaone subgroup tephra beds, Okataina volcanic centre, New Zealand. New Zealand Journal of Geology and Geophysics. 45, 207-219.

Stern, R. J., Jackson, M. C., Fryer, P., Ito, E., 1993. O, Sr, Nd and Pb isotopic composition of the Kasuga cross-chain in the Mariana arc: a new perspective of the K-h relationship. Earth Planetary Science Letters. 119, 459-475.

Stolz, A. J., Varne, R., Davies, G. R., Wheller, G. E., Foden, J. D., 1990. Magma source components in an arc-continent collision zone: The Flores-Lembata sector, Sunda arc, Indonesia. Contributions to Mineralogy and Petrology. 105, 585-601.

Sutton, A. N., Blake, S., Wilson, C. J. N., 1995. An outline geochemistry of rhyolite eruptives from Taupo Volcanic Centre, New Zealand. Journal of Volcanology and Geothermal Research. 68, 153-175.

Tamura, Y., Yuhara, M., Ishii, T., 2000. Primary arc basalts from Daisen Volcano, Japan: Equilibrium crystal fractionation versus disequilibrium fractionation during supercooling. Journal of Petrology. 41, 431-448.

Tamura, Y., Yuhara, M., Ishii, T., Irino, N., Shukuno, H., 2003. Andesites and dacites from Daisen Volcano, Japan: Partial-to-total remelting of an andesite magma body. Journal of Petrology. 44, 2243-2260.

Taylor, R. N., Nesbitt, R. W., 1998. Isotopic characteristics of subduction fluids in an intra-oceanic setting, Izu-Bonin arc, Japan. Earth Planetary Science Letters. 164, 79-98.

Taylor, S. R., Capp, A. C., Graham, A. L., Blake, D. H., 1969. Trace element abundances in andesites, Saipan, Bougainville, and Fiji. Contributions to Mineralogy and Petrology. 23, 1-26.

Thirlwall, M. F., Graham, A. M., 1984. Evolution of high-Ca, high-Sr C-series basalts from Grenada, Lesser Antilles: Contamination in the arc crust. Journal of the Geological Society London. 141, 427-445.

Thirlwall, M. F., Graham, A. M., Arculus, R. J., Harmon, R. S., Macpherson, C. G., 1996. Resolution of the effects of crustal assimilation, sediment subduction and fluid transport in island arc magmas: Pb-Sr-Nd-O isotope geochemistry of Grenada, Lesser Antilles. Geochimica et Cosmochimica Acta. 60, 4785-4810.

Thomas, R. B., Hirschman, M. M., Cheng, H., Reagan, M. K., Mayfield, D. G., 2002. (^{231}Pa/^{235}U)-(^{230}Th/^{238}U) of young mafic volcanic rocks from Nicaragua and Costa Rica and the influence of flux melting on U-series systematics of arc lavas. Geochimica et Cosmochimica Acta. 66, 4287-4309.

Togashi, S., Tanaka, T., Yoshida, T., Ishikawa, K., Fujinawa, A., Kurasawa, H., 1992. Trace-elements and Nd-Sr isotopes of island arc tholeiites from frontal arc of northeast Japan. Geochemical Journal. 26, 261-277.

Tsuchiya, N., Suzuki, S., Kimura, J. I., Kagami, H., 2005. Evidence for slab melt/mantle reaction: Petrogenesis of early Cretaceous and Eocene high-Mg andesites from the Kitakami mountains, Japan. Lithos. 79, 179-206.

Tsukui, M., Hoshino, K., 2002. Magmatic differentiation of Hachijo-Nishiyama Volcano, Izu islands, Japan. Bulletin of the Volcanological Society Japan Ser 2. 47, 57-72.

Turner, S., Hawkesworth, C., Vancalsteren, P., Heath, E., Macdonald, R., Black, S., 1996. U-series isotopes and destructive plate margin magma genesis in the Lesser Antilles. Earth and Planetary Science Letters. 142, 191-207.

Turner, S. P., Hawkesworth, C. J., Rogers, N. W., Bartlett, J., Worthington, T. J., Hergt, J. M., Pearce, J. A., Smith, I. E. M., 1997. ^{238}U-^{230}Th disequilibria magma petrogenesis and flux rates beneath the depleted Tonga-Kermadec island arc. Geochimica et Cosmochimica Acta. 61, 4855-4884.

Turner, S. P., Mcdermott, F., Hawkesworth, C. J., Kepezhinskas, P. K., 1998. A U-series study of lavas from Kamchatka and the Aleutians: Constraints on source composition and melting processes. Contributions to Mineralogy and Petrology. 133, 217-234.

Turner, S. P., Peate, D. W., Hawkesworth, C. J., Eggins, S. M., Crawford, A. J., 1999. Two mantle domains and the time scales of fluid transfer beneath the Vanuatu arc. Geology. 27, 963-966.

Turner, S. P., Foden, J. D., 2001. U, Th and Ra disequilibria, Sr, Nd and Pb isotope and trace element variations in Sunda arc lavas: Predominance of a subducted sediment component. Contributions to Mineralogy and Petrology. 142, 43-57.

Turner, S. P., Foden, J. D., George, R. M., Evans, P., Varne, R., Elburg, M. A., Jenner, G. A., 2003. Rates and processes of potassic magma evolution beneath Sangeang Api Volcano, east Sunda arc, Indonesia. Journal of Petrology. 44, 491-515.

Ujike, O., Stix, J., 2000. Geochemistry and origins of Ueno and On-Take basaltic to andesitic rocks (<3 Ma) produced by distinct contributions of subduction components, central Japan. Journal of Volcanology and Geothermal Research. 95, 49-64.

Uto, K., Takahashi, E., Nakamura, E., Kaneoka, I., 1994. Geochronology of alkali volcanism in Oki-Dogo island, southwest Japan: Geochemical evolution of basalts related to the opening of the Japan sea. Geochemical Journal. 28, 431-449.

Varne, R., Foden, J. D., 1986. Geochemical and isotopic systematics of eastern Sunda arc volcanics: Implications for mantle sources and mantle mixing processes. The origin of arcs (Wezel, F. C), Elsevier, Amsterdam, 159-189.

Van Bergen, M. J., Vroon, P. Z., Varekamp, J. C., Poorter, R. P. E., 1992. The origin of the potassic rock suite from Batu Tara volcano (East Sunda Arc, Indonesia). Lithos. 28, 261-282.

Vidal, P., Le Guen de Kerneizon, M., Maury, R. C., Dupre, B., White, W. M., 1991. Large role of sediments in the genesis of some Lesser Antilles andesites and dacites (Soufriere, St. Lucia): Isotopic constraints. Bulletin de la Société Géologique de France. 162, 993-1002.

Volynets, O. N., 1994. Geochemical types, petrology, and genesis of late Cenozoic volcanic rocks from the Kurile-Kamchatka island arc system. International Geological Review. 36, 373-405.

Volynets, O. N., Karpenko, S. F., Kay, R. W., Gorring, M., 1997. Isotopic composition of late Neogene K-Na alkaline basalts of eastern Kamchatka: Indicators of the heterogeneity of the mantle magma sources. Geochemical International. 35, 884-896.

Vukadinovic, D., Sutamidjaja, I., 1995. Geology, mineralogy and magma evolution of Gunung Slamet Volcano, Java, Indonesia. Journal of Southeast Asian Earth Science. 11, 135-164.

Waight, T. E., Price, R. C., Stewart, R. B., Smith, I. E. M., Gamble, J. A., 1999. Stratigraphy and geochemistry of the Turoa area, with implications for andesite petrogenesis at Mt. Ruapehu, Taupo Volcanic Zone, New Zealand. New Zealand Journal of Geology and Geophysics. 42, 513-532.

Walker, J. A., Patino, L. C., Cameron, B. I., Carr, M. J., 2000. Petrogenetic insights provided by compositional transects across the Central American Arc: Southeastern Guatemala and Honduras. Journal of Geophysical Research., B, Solid Earth and Planets. 105, 18949-18963.

Wendt, J. I., Regelous, M., Collerson, K. D., Ewart, A., 1997. Evidence for a contribution from two mantle plumes to island-arc lavas from northern Tonga. Geology. 25, 611-614.

Wensink, H., Van Bergen, M. J., 1995. The tectonic emplacement of Sumba in the Sunda-Banda Arc: paleomagnetic and geochemical evidence from the early Miocene Jawila volcanics. Tectonophysics. 250, 15-30.

White, R. V., Tarney, J., Kerr, A. C., Saunders, A. D., Kempton, P. D., Pringle, M. S., Klaver, G. T., 1999. Modification of an oceanic plateau, Aruba, Dutch Caribbean: Implications for the generation of continental crust. Lithos. 46, 43-68.

Wood, D. A., Joron, J. L., Marsh, N. G., Tarney, J., Treuil, M., 1981. Major and trace element variations in basalts from the north Philippine sea drilled during DSDP Leg 58. Initial Reptort Deep Sea Drilling Program Project. 58, 873-894.

Woodland, S. J., Pearson, D. G., Thirlwall, M. F., 2002. A platinum group element and Re-Os isotope investigation of siderophile element recycling in subduction zones: Comparison of Grenada, Lesser Antilles arc, and the Izu-Bonin arc. Journal of Petrology. 43, 171-198.

Yokoyama, T., Kobayashi, K., Kuritani, T., Nakamura, E., 2003. Mantle metasomatism and rapid ascent of slab components beneath island arcs: Evidence from ^{238}U-^{230}Th-^{226}Ra disequilibria of Miyakejima Volcano, Izu arc, Japan. Journal of Geophysical Research. B108, EVC 1-1-EVC 1-25.

Zellmer, G. F., Hawkesworth, C. J., Sparks, R. S. J., Thomas, L. E., Harford, C. L., Brewer, T. S., Loughlin, S. C., 2003. Geochemical Evolution of the Soufrière Hills Volcano, Montserrat, Lesser Antilles Volcanic Arc Journal of Petrology. 44, 1349-1374.

B.2 The 1009 samples used to construct the Co vs Th diagram were taken from the references below:

Baker, P. E., 1984. Geochemical evolution of St. Kitts and Montserrat, Lesser Antilles. Journal of the Geological Society of London. 141, 401-411.

Bau, M., Knittel, U., 1993. Significance of slab-derived partial melts and aqueous fluids for the genesis of tholeiitic and calc-alkaline island-arc basalts: Evidence from Mt. Arayat, Philippines. Chemical Geology. 105, 233-251.

Bindeman, I. N., Bailey, J. C., 1994. A model of reverse differentiation at Dikii Greben` Volcano, Kamchatka: Progressive basic magma vesiculation in a silicic magma chamber. Contributions to Mineralogy and Petrology. 117, 263-278.

Bloomer, S. H., Ewart, A., Hergt, J. M., Bryan, W. B., 1996. Geochemistry and origin of igneous rocks from the outer Tonga forearc (Site 841). Proceeding of the Ocean Drilling Program Scientific Results. 135, 625-646.

Boespflug, X., Dosso, L., Bougault, H., Joron, J. L., 1990. Trace element and isotopic (Sr, Nd) geochemistry of volcanic rocks from the Lau Basin. Geologisches Jahrbuch. 92, 503-516.

Bougault, H., Maury, R. C., El Azzouzi, M., Joron, J. L., Cotten, J., Treuil, M., 1982. Tholeiites, basaltic andesites, and andesites from Leg 60 Sites: Geochemistry, mineralogy and low partition coefficient elements. Initial Report Deep Sea Drilling Program. 60, 657-677.

Briggs, R. M., Goles, G. G., 1984. Petrological and trace element geochemical features of the Okete Volcanics, western North Island, New Zealand. Contributions to Mineralogy and Petrology. 86, 77-88.

Briggs, R. M., 1986. Petrology and geochemistry of Maungatautari, a medium-K andesite-dacite volcano. New Zealand Journal of Geology and Geophysics. 29, 273-289.

Briggs, R. M., Fulton, B. W. J., 1990. Volcanism, structure and petrology of the Whiritoa-Whangamata coastal section, Coromandel Volcanic Zone, New Zealand: Facies model evidence for the Tunaiti caldera. New Zealand Journal of Geology and Geophysics. 33, 623-633.

Castillo, P. R., Newhall, C. G., 2004. Geochemical constraints on possible subduction components in lavas of Mayon and Taal volcanoes, southern Luzon, Philippines. Journal of Petrology. 45, 1089-1108.

Churikova, T., Dorendorf, F., Barman, T. R., 2001. Sources and fluids in the mantle wedge below Kamchatka, evidence from across-arc geochemical variation. Journal of Petrology. 42, 1567-1593.

Clark, S. K., Reagan, M. K., Plank, T., 1998. Trace element and U-series systematics for 1963-1965 tephras from Irazu volcano, Costa Rica: Implications for magma generation processes and transit times. Geochimica et Cosmochimica Acta. 62, 2689-2699.

Defant, M. J., Richerson, P. M., De Boer, J. Z., Stewart, R. H., Maury, R. C., Bellon, H., Drummond, M. S., Fergenson, M. D., Jackson, T. E., 1991. Dacite genesis via both differention and slab melting: Petrogenesis of La Yeguada volcanic complex. Journal of Petrology. 32, 1101-1142.

Dietrich, V. J., Emmerman, R., Oberhansli, R., Puchelt, H., 1978. Geochemistry of basaltic and gabbroic rocks from the west Mariana basin and the Marian trench. Earth Planetary Science Letters. 39, 127-144.

Dorendorf, F., Wiechert, U., Worner, G., 2000. Hydrated sub-arc mantle: A source for the Kluchevskoy Volcano, Kamchatka/Russia. Earth Planetary Science Letters. 175, 69-86.

Ewart, A., Bryan, W. B., Chappell, B. W., Rudnick, R. L., 1994. Regional geochemistry of the Lau-Tonga arc and back-arc systems. Proceeding of the Ocean Drilling Program Scientific Results. 135, 385-425.

Fedorov, P. I., Shapiro, M. N., 1998. Neogene volcanics of the Kamchatka isthmus and geodynamics of the Aleutian-Kamchatka junction. Geotectonics. 32, 122-137.

Gertisser, R., Keller, J., 2003. Trace element and Sr, Nd, Pb and O isotope variations in medium-K and high-K volcanic rocks from Merapi Volcano, Central Java, Indonesia: Evidence for the involvement of subducted sediments in Sunda arc magma genesis. Journal of Petrology. 44, 457-489.

Gill, J. B., 1976. Composition and age of Lau Basin and Ridge volcanic rocks: implications for evolution of an interarc basin and remnant arc. Geological Society America Bulletin. 87, 1384-1395.

Gill, J. B., 1987. Early geochemical evolution of an oceanic island arc and backarc: Fiji and the south Fiji basin. Journal of Geology. 95, 589-615.

Haase, K. M., Worthington, T. J., Stoffers, P., Garbe-Schonberg, C. D., Wright, I., 2002. Mantle dynamics, element recycling, and magma genesis beneath the Kermadec arc-Havre trough. Geochemistry Geophysics Geosystems. 3, 2002GC000335.

Hildreth, W., Fierstein, J., Siems, D. F., Budahn, J. R., Ruiz, J., 2004. Rear-arc vs. arc-front volcanoes in the Katmai reach of the Alaska Peninsula: a critical appraisal of across-arc compositional variation. Contributions to Mineralogy and Petrology. 147, 243-275.

Hoogewerff, J., Van Bergen, M. J., Vroon, P. Z., Hertogen, J., Wordel, R., Sneyers, A., Nasution, A., Varekamp, J. C., Moens, H. L. E., Mouchel, D., 1997. U series, Sr-Nd-Pb isotope and trace element systematics across an active island arc-continent collision zone: Implications for element transfer at the slab-wedge interface. Geochimica et Cosmochimica Acta. 61, 1057-1072.

Ishizuka, O., Yuasa, M., 1999. Petrography and isotopic age of volcanic rocks dredged from the back-arc ridges and knolls at the north end of the Izu-Ogasawara arc. Geological Survey Japanese Cruise Report. 24, 171-190.

Ishiwatari, A., Ohama, H., 1997. Clinopyroxene basalt dikes in the Miocene Iwaine formation, Hokuriku Province, Japan: Various continental arc magmas including shoshonite series and origin of the clinopyroxene phenocrysts. Journal of the Geological Society of Japan. 103, 565-578.

Kagami, H., 1990. Sr and Nd isotopic ratios of volcanic rocks from Genbudo Area, Southwest, Japan. Journal of the Geological Society of Japan. 96, 471-474.

Kimura, J. I., Yoshida, T., Iizumi, S., 2002. Origin of low-K intermediate lavas at Nekoma volcano, NE Honshu arc, Japan: Geochemical constraints for lower-crustal melts. Journal of Petrology. 43, 631-661.

Lidiak, E. G., Jolly, W. T., Lidiak, E. G., Larue, D. K. (1998) Geochemistry of intrusive igneous rocks, St. Croix, U. S. Virgin Islands. In: Tectonics and geochemistry of the northeastern Caribbean. pp. 133-153. Geological Society of America.

Maillet, P., Ruellan, E., Gerard, M., Person, A., Bellon, H., Cotten, J., Joron, J. L., Nakada, S., Price, R. C., 1995. Tectonics, magmatism, and evolution of the New Hebrides backarc troughs (southwest Pacific). Backarc basins: Tectonics and magmatism (Taylor, B.), Plenum Press, London, 177-235.

Marcelot, G., 1981. Geochemistry of the lavas of Erromango island (New Hebrides): Petrogenetic implications. Bulletin de la Société Géologique de France. 23, 367-376.

Marcelot, G., Dupuy, C., Girod, M., Maury, R. C., 1983. Petrology of Futuna island lavas (New Hebrides): An example of calc-alkaline magmatism associated with the initial stages of back-arc spreading. Chemical Geology. 38, 23-37.

Monzier, M., Robin, C., Eissen, J. P., Cotten, J., 1997. Geochemistry vs seismo-tectonics along the volcanic New Hebrides central chain (southwest Pacific). Journal of Volcanology and Geothermal Research. 78, 1-29.

Nagao, T., Hase, Y., Nagamine, S., Kakabuchi, S., Sakaguchi, K., 1999. Late Miocene to middle Pleistocene Hisatsu volcanic rocks generated from heterogeneous magma sources: Evidence from temporal-spatial variation of distribution and chemistry of the rocks. Journal of Japanese Association of

Mineralogy Petrology and Economic Geology (Ganseki Kobutsu Kosho Gakkai-Shi). 94, 461-481.

Nakano, S., 1993. Ueno basaltic rocks I: Heterogeneous magmas at two monogenetic volcanoes. Journal of Japanese Association of Mineralogy Petrology and Economic Geology (Ganseki Kobutsu Kosho Gakkai-Shi). 88, 272-288.

Nakano, S., 1994. Ueno basaltic rocks II: Chemical variation in the Kiso Province, to the south of the Ontake volcano. Journal of Japanese Association of Mineralogy Petrology and Economic Geology (Ganseki Kobutsu Kosho Gakkai-Shi). 89, 115-130.

Nicholls, I. A., Whitford, D. J., 1983. Potassium-rich volcanic rocks of the Muriah complex, Java, Indonesia: Products of multiple magma sources? Journal of Volcanology and Geothermal Research. 18, 337-359.

Nicholson, K. N., Black, P. M., Picard, C., 2000. Geochemistry and tectonic significance of the Tangihua Ophiolite Complex, New Zealand. Tectonophysics. 321, 1-15.

Pearce, J. A., Van Der Laan, S. R., Arculus, R. J., Murton, B. J., Ishii, T., Peate, D., Parkinson, I. J., 1992. Boninite and harzburgite from Leg 125 (Bonin-Mariana forearc): A case study of magma genesis during the initial stages of subduction. Proceeding of the Ocean Drilling Program Scientific Results. 125, 623-659.

Peate, D. W., Pearce, J. A., Hawkesworth, C. J., Edwards, C. M. H., Hirose, K., 1997. Geochemical variations in Vanuatu arc lavas: The role of subducted material and a variable mantle wedge composition. Journal of Petrology. 38, 1331-1358.

Puzankov. Y., 1994. Geochemistry of volcanic rocks of the Eocene-Oligocene island arc (Kamchatka). Geol Geofiz. 1, 89-97.

Reagan, M. K., Sims, K. W. W., Erich, J., Thomas, R. B., Cheng, H., Edwards, R. L., Layne, G. D., Ball, L., 2003. Time-scales of differentiation from mafic parents to rhyolite in North American continental arcs. Journal of Petrology. 44, 1703-1726.

Reubi, O., Nicholls, I. A., Kamenetsky, V. S., 2002. Early mixing and mingling in the evolution of basaltic magmas: Evidence from phenocryst assemblages, Slamet Volcano, Java, Indonesia. Journal of Volcanology and Geothermal Research. 119, 255-274.

Reubi, O., Nicholls, I. A., 2004. Magmatic evolution at Batur volcanic field, Bali, Indonesia: Petrological evidence for polybaric fractional crystallisation and implications for caldera-forming eruptions. Journal of Volcanology and Geothermal Research. 138, 345-369.

Revillon, S., Arndt, N. T., Hallot, E., Kerr, A. C., Tarney, J., 1999. Petrogenesis of picrites from the Caribbean Plateau and the North Atlantic magmatic province. Lithos. 49, 1-21.

Rogers, N. W., Setterfield, T. N., 1994. Potassium and incompatible-element enrichment in shoshinitic lavas from the Tavua Volcano, Fiji. Chemical Geology. 118, 43-62.

Romick, J. D., Perfit, M. R., Swanson, S. E., Shuster, R. D., 1990. Magmatism in the eastern Aleutian Arc: temporal characteristic of igneous activity on Akutan Island. Contributions to Mineralogy and Petrology. 104, 700-721.

Sasaki, Y., 1985. Res. Report Lab. Nuclear Sci. Tohoku Univ. 18, 175-188.

Shinjo, R., Usami, K., Kato, Y., 1995. Geology and petrology of the Nishi and Fudenzaki formations of the Aguni group, Aguni island, the central Ryukyu arc: Petrogenetic relationship between the andesites and dacites. Bull. Coll. Sci. Univ. Ryukyu. 60, 27-50.

Shinjo, R., Chung, S. L., Kato, Y., Kimura, M., 1999. Geochemical and Sr-Nd isotopic characteristics of volcanic rocks from the Okinawa trough and Ryukyu arc: Implications for the evolution of a young, intracontinental back arc basin. Journal of Geophysical Research. B104, 10591-10608.

Shinjo, R., Kato, Y., 2000. Geochemical constraints on the origin of bimodal magmatism at the Okinawa Trough, an incipient back-arc basin. Lithos. 54, 117-137.

Smith, I. E. M., Stewart, R. B., Price, R. C., 2003. The petrology of a large intra-oceanic silicic eruption: The Sandy Bay tephra, Kermadec arc, southwest Pacific. Journal of Volcanology and Geothermal Research. 124, 173-194.

Sutton, A. N., Blake, S., Wilson, C. J. N., 1995. An outline geochemistry of rhyolite eruptives from Taupo Volcanic Centre, New Zealand. Journal of Volcanology and Geothermal Research. 68, 153-175.

Tamura, Y., Yuhara, M., Ishii, T., Irino, N., Shukuno, H., 2003. Andesites and dacites from Daisen Volcano, Japan: Partial-to-total remelting of an andesite magma body. Journal of Petrology. 44, 2243-2260.

Taylor, R. N., Nesbitt, R. W., 1998. Isotopic characteristics of subduction fluids in an intra-oceanic setting, Izu-Bonin arc, Japan. Earth Planetary Science Letters. 164, 79-98.

Taylor, S. R., Capp, A. C., Graham, A. L., Blake, D. H., 1969. Trace element abundances in andesites, Saipan, Bougainville, and Fiji. Contributions to Mineralogy and Petrology. 23, 1-26.

Tsuchiya, N., Suzuki, S., Kimura, J. I., Kagami, H., 2005. Evidence for slab melt/mantle reaction: Petrogenesis of early Cretaceous and Eocene high-Mg andesites from the Kitakami mountains, Japan. Lithos. 79, 179-206.

Tsukui, M., Hoshino, K., 2002. Magmatic differentiation of Hachijo-Nishiyama Volcano, Izu islands, Japan. Bulletin of the Volcanological Society Japan Ser 2. 47, 57-72.

Turner, S., Hawkesworth, C., Vancalsteren, P., Heath, E., Macdonald, R., Black, S., 1996. U-series isotopes and destructive plate margin magma genesis in the Lesser Antilles. Earth and Planetary Science Letters. 142, 191-207.

Turner, S. P., Hawkesworth, C. J., Rogers, N. W., Bartlett, J., Worthington, T. J., Hergt, J. M., Pearce, J. A., Smith, I. E. M., 1997. ^{238}U-^{230}Th disequilibria magma petrogenesis and flux rates beneath the depleted Tonga-Kermadec island arc. Geochimica et Cosmochimica Acta. 61, 4855-4884.

Turner, S. P., Mcdermott, F., Hawkesworth, C. J., Kepezhinskas, P. K., 1998. A U-series study of lavas from Kamchatka and the Aleutians: Constraints on source composition and melting processes. Contributions to Mineralogy and Petrology. 133, 217-234.

Turner, S. P., Peate, D. W., Hawkesworth, C. J., Eggins, S. M., Crawford, A. J., 1999. Two mantle domains and the time scales of fluid transfer beneath the Vanuatu arc. Geology. 27, 963-966.

Turner, S. P., Foden, J. D., George, R. M., Evans, P., Varne, R., Elburg, M. A., Jenner, G. A., 2003. Rates and processes of potassic magma evolution beneath Sangeang Api Volcano, east Sunda arc, Indonesia. Journal of Petrology. 44, 491-515.

Ujike, O., Stix, J., 2000. Geochemistry and origins of Ueno and On-Take basaltic to andesitic rocks (<3 Ma) produced by distinct contributions of subduction components, central Japan. Journal of Volcanology and Geothermal Research. 95, 49-64.

Uto, K., Takahashi, E., Nakamura, E., Kaneoka, I., 1994. Geochronology of alkali volcanism in Oki-Dogo island, southwest Japan: Geochemical evolution of basalts related to the opening of the Japan sea. Geochemical Journal. 28, 431-449.

Van Bergen, M. J., Vroon, P. Z., Varekamp, J. C., Poorter, R. P. E., 1992. The origin of the potassic rock suite from Batu Tara volcano (East Sunda Arc, Indonesia). Lithos. 28, 261-282.

Volynets, O. N., 1994. Geochemical types, petrology, and genesis of late Cenozoic volcanic rocks from the Kurile-Kamchatka island arc system. International Geological Review. 36, 373-405.

Wendt, J. I., Regelous, M., Collerson, K. D., Ewart, A., 1997. Evidence for a contribution from two mantle plumes to island-arc lavas from northern Tonga. Geology. 25, 611-614.

Woodland, S. J., Pearson, D. G., Thirlwall, M. F., 2002. A platinum group element and Re-Os isotope investigation of siderophile element recycling in subduction zones: Comparison of Grenada, Lesser Antilles arc, and the Izu-Bonin arc. Journal of Petrology. 43, 171-198.

Zellmer, G. F., Hawkesworth, C. J., Sparks, R. S. J., Thomas, L. E., Harford, C. L., Brewer, T. S., Loughlin, S. C., 2003. Geochemical Evolution of the Soufrière Hills Volcano, Montserrat, Lesser Antilles Volcanic Arc Journal of Petrology. 44, 1349-1374.

B.3 The 121 samples from the Bismark and Kurile arcs used to test the Co vs Th diagram were taken from the references below:

Bailey, J. C., Frolova, T. I., Burikova, I. A., 1987. Mineralogy, geochemistry and petrogenesis of Kurile island-arc basalts. Contributions to Mineralogy and Petrology. 102, 265-280.

Blake, D. H., Ewart, A., 1974. Petrology and geochemistry of the Cape Hoskins volcanoes, New Britain, Papua New Guinea. Geological Society of Australia. 21, 319-331.

Frolova, T. I., Bindeman, I. N., Mahmoud, M., Bailey, J. C., 1992. Melanocratic inclusions in andesites and dacites of the Kurile-Kamchatka volcanic arc. International Geological Review. 34, 119-130.

Katsui, Y., Oba, Y., Ando, S., Nishimura, S., Masuda, Y., Kurasawa, H., Fujimaki, H., 1978. Petrochemistry of Quaternary volcanic rocks of Hokkaido, North Japan. Geological Minjnbouw. 18, 449-484.

Müller, D., Franz, L., Herzig, P. M., Hunt, S., 2001. Potassic igneous rocks from the vicinity of epithermal gold mineralization, Lihir Island, Papua New Guinea Lithos. 57, 163-186.

Taylor, S. R., Capp, A. C., Graham, A. L., Blake, D. H., 1969. Trace element abundances in andesites, Saipan, Bougainville, and Fiji. Contributions to Mineralogy and Petrology. 23, 1-26.

Volynets, O. N., 1994. Geochemical types, petrology, and genesis of late Cenozoic volcanic rocks from the Kurile-Kamchatka island arc system. International Geological Review. 36, 373-405.

Woodhead, J. D., Eggins, S. M., Johnson, R. W., 1998. Magma genesis in the New Britain island arc: Further insights into melting and mass transfer processes. Journal of Petrology. 39, 1641-1668.

B.4 The 280 samples from the Superior Province, Canada used to modify the Co vs Th diagram were taken from the references below:

Barrie, C. T., Corfu, F., Davis, P., Coutts, A. C., Maceachern, D., 1999. Geochemistry of the Dundonald komatiite-basalt suite and genesis of Dundeal Ni deposit, Abitibi Subprovince, Canada. Economic Geology. 94, 845-866.

Hollings, P., Kerrich, R., 1999. Trace element systematics of ultramafic and mafic volcanic rocks from the 3 Ga North Caribou greenstone belt, northwestern Superior Province. Precambrian Research. 93, 257-279.

Hollings, P., Wyman, D., Kerrich, R., 1999. Komatiite-basalt-rhyolite volcanic associations in Northern Superior Province greenstone belts: significance of plume-arc interaction in the generation of the proto continental Superior Province. Lithos. 46, 137-161.

Hollings, P., Kerrich, R., 2000. An Archean arc basalt-Nb-enriched basalt-adakite association: the 2.7 Ga Confederation assemblage of the Birch-Uchi greenstone belt, Superior Province. Contributions to Mineralogy and Petrology. 139, 208-226.

Hollings, P., Stott, G., Wyman, D., 2000. Trace element geochemistry of the Meen-Dempster greenstone belt, Uchi subprovince, Superior Province, Canada: back-arc development on the margins of an Archean protocontinent. Canadian Journal of Earth Sciences. 37, 1021-1038.

Hollings, P., 2002. Archean Nb-enriched basalts in the northern Superior Province. Lithos. 64, 1-14.

Kerrich, R., Polat, A., Wyman, D., Hollings, P., 1999. Trace element systematics of Mg-, to Fe-tholeiitic basalt suites of the Superior Province: implications for Archean mantle reservoirs and greenstone belt genesis. Lithos. 46, 163-187.

Polat, A., Kerrich, R., Wyman, D. A., 1998. The late Archean Schreiber-Hemlo and White River Dayohessarah greenstone belts, Superior Province: collages of oceanic plateaus, oceanic arcs, and subduction-accretion complexes. Tectonophysics. 289, 295-326.

Polat, A., Kerrich, R., Wyman, D. A., 1999. Geochemical diversity in oceanic komatiites and basalts from the late Archean Wawa greenstone belts, Superior Province, Canada: trace element and Nd isotope evidence for a heterogeneous mantle. Precambrian Research. 94, 139-173.

Polat, A., Kerrich, R., 2000. Archean greenstone belt magmatism and the continental growth- mantle evolution connection: constraints from Th-U-Nb-LREE

systematics of the 2.7 Ga Wawa subprovince, Superior Province, Canada. Earth and Planetary Science Letters. 175, 41-54.

Polat, A., Kerrich, R., 2001. Magnesian andesites, Nb-enriched basalt-andesites, and adakites from late-Archean 2.7 Ga Wawa greenstone belts, Superior Province, Canada: implications for late Archean subduction zone petrogenetic processes. Contributions to Mineralogy and Petrology. 141, 36-52.

Polat, A., Munker, C., 2004. Hf-Nd isotope evidence for contemporaneous subduction processes in the source of late Archean arc lavas from the Superior Province, Canada. Chemical Geology. 213, 403-429.

Sage, R. P., Lightfoot, P. C., Doherty, W., 1996. Bimodal cyclic Archean basalts and rhyolites from the Michipicoten (Wawa) greenstone belt, Ontario: Geochemical evidence for magma contributions from the asthenospheric mantle and ancient continental Lithos.phere near the southern margin of the Superior Province. Precambrian Research. 76, 119-153.

Wyman, D., Hollings, P., 1998. Long-lived mantle-plume influence on an Archean protocontinent: Geochemical evidence from the 3 Ga Lumby Lake greenstone belt, Ontario, Canada. Geology. 26, 719-722.

Wyman, D. A., 2000. High-precision exploration geochemistry: applications for volcanogenic massive sulfide deposits. Australian Journal of Earth Sciences. 47, 861-871.

Wyman, D. A., Ayer, J. A., Devaney, J. R., 2000. Niobium-enriched basalts from the Wabigoon subprovince, Canada: Evidence for adakitic metasomatism above an Archean subduction zone. Earth Planetary Science Letters. 179, 21-30.

B.5 The 62 samples from the Baltic Shield, Western Australian and Kaapvaal cratons used to test the Co vs Th diagram were taken from the references below:

Barley, M. E., Kerrich, R., Reudavy, I., Xie, Q., 2000. Late Archaean Ti-rich, Al-depleted komatiites and komaiitic volcaniclastic rocks from the Murchison Terrane in Western Australia. Australian Journal of Earth Sciences. 47, 873-883.

Bateman, R., Costa, S., Swe, T., Lambert, D., 2001. Archaean mafic magmatism in the Kalgoorlie area of the Yilgarn Craton, Western Australia: a geochemical and Nd isotopic study of the petrogenetic and tectonic evolution of a greenstone belt. Precambrian Research. 108, 75-112.

Bibikova, E., Slabunov, A. I., Bogdanova, S. V., Skiold, T., Stepanov, V. S., Borisova, E., 1999. Early magmatism of the Belomorian mobile belt, Baltic Shield: Lateral zoning and isotopic age. Petrology. 7, 123-146.

Bibikova, E. V., Samsonov, A. V., Shchipansky, A. A., Borina, M. M., Gracheva, T. V., Makarov, V. A., 2003. The Khizovaarskaya structure of the northern Karelian greenstone belt as an accretionary late Archean island arc: Isotopic-geochronological and petrological data. Petrologiya. 11, 289-320.

Maier, W. D., Barnes, S. J., Marsh, J. S., 2003. The concentrations of the noble metals in South African flood-type basalts and MORB: Implications for petrogenesis and magmatic sulphide exploration. Contributions to Mineralogy and Petrology. 146, 44-61.

Marsh, J. S., Bowen, M. P., Rogers, N. W., Bowen, T. B., 1992. Petrogenesis of late Archean flood-type basic lavas from the Klipriviersberg group, Ventersdorp supergroup, South Africa. Journal of Petrology. 33, 817-847.

O'Brien, H., Huhma, H., Sorjonen-Ward, P., 1993. Petrogenesis of the late Archean Hattu schist belt, Ilomantsi, eastern Finland: Geochemistry and Sr, Nd isotopic composition. Special Paper Geological Survey Finland. 17, 147-184.

Shchipansky, A. A., Samsonov, A. V., Borina, M. M., Slabunov, A. I., Bibikova, E. V., 1999. High-Mg, low Ti quartz amphibolites of greenstone belts from northern Karelia-metamorphosed Archean analogues of boninites? Dokl Akad Nauk SSSR. 365, 817-820.

Appendix C

Preparation of samples for analysis by Inductively-Coupled Plasma (ICP) Optical Emission Spectrometry (OES) and Mass Spectrometry (MS) and an evaluation of the accuracy and precision of the results

C.1 Preparation of sample powders

The Jamaican igneous samples were substantially altered and, as such, the weathered surfaces were removed using a saw. Approximately 100 ml of the freshest part of the sample was then crushed and powdered using a clean jaw crusher and an agate ball mill. An agate mill was used rather than a tungsten-carbide mill to minimise Nb and Ta contamination. Approximately 2g of each powdered sample were weighed into clean ceramic crucibles. The powders were ignited at 900°C for two hours to drive off any volatiles. Afterwards each vial was allowed to cool in a dessicator and re-weighed to obtain an accurate loss on lignition (LOI).

C.2 Preparation for ICP-OES and ICP-MS analysis

Major and trace element abundances were analysed using a JY Horiba Ultima 2 inductively coupled plasma optical emission spectrometer (ICP-OES) and a Thermo X7 series inductively coupled plasma mass spectrometer (ICP-MS) at Cardiff University, United Kingdom. The ignited powders can be prepared for

analysis by two methods: (1) HF-HNO_3 dissolution or (2) lithium tetraborate fusion. All the samples in this study were prepared by lithium tetraborate fusion and one batch were analysed by HF-HNO_3 dissolution to check the accuracy and precision of the fusion analysis. To prepare the samples by the fusion method 0.1g +/- 0.0005 of sample was mixed with 0.2-0.6g +/- 0.0005 Lithium tetraborate flux in an acid-washed platinum crucible. ~ 10 drops of lithium iodide non-wetting agent was added to the mixture, which was then fused on a Claisse Fluxy automated fusion system. The mixture was then dissolved in 30ml of 10% HNO_3 and 20ml of 18Ω de-ionised water. After the sample was fully dissolved 1ml of 100ppm Rh spike was added and the solution was made up to 100ml with de-ionised water. ~ 20ml of this solution was run on the ICP-OES to obtain the major element abundances. 1ml of the solution was added to 1ml of In and Tl and 8ml of 2% HNO_3 and analysed on the ICP-MS to obtain the trace element abundances.

For the acid digestion preparation, 0.1g +/- 0.0005 of sample was weighed into a nalgene vial. 0.5ml of concentrated HNO_3 and 4ml of concentrated HF were added to the vial. The vials were then heated for 24 hours on a hot plate at a temperature of 125°C. After the sample was dissolved the solution was evaporated until a clear gel could be identified in the bottom of the vial. 1ml of concentrated HNO_3 was added to the vial and left to evaporate, this procedure was then repeated. After the second evaporation 5ml of 5M HNO_3 was added to the vial to dissolve the residue. This solution was spiked with 1ml of 2500 ppb Rh-Re and made up to 50 ml with de-ionised water.

C.3 Evaluation of the accuracy and precision of the analysis

C.3.1 Standards

In order to assess the accuracy and precision of the whole rock and trace element data a number of external and internal standards were analysed. The external standards include JB-1a, BIR-1, W2, JA-2, MRG-1 and JG-3. JB-1a is a basalt from Nagasaki, Japan, BIR-1 is a basalt from Reykjavik, Iceland, W2 is a dolerite from Virginia USA, JA-2 is an andesite from Kamagawa, Japan, MRG-1 is a gabbro from

Montreal, Canada and JG-3 is a granodiorite from Mitoya-cho, Japan.

Eight batches of samples were run on the ICP-OES and ICP-MS over the course of this study. At least four external standards were analysed with each batch of samples run, in order for them to be used in determining the accuracy and precision of the analysis. At least three internal standards were also run during each batch. These standards are not used for accuracy because they can not be compared to any known composition unlike the external standards; however, they are useful in conjunction with the external standards in determining the precision of the analysis. Tables C.1 and C.2 contain the major and trace element data for the external and internal standards that were run in all 8 batches. The first internal standards used in batches one and two had to be changed for future analyses due to them not displaying adequate final totals (Tables C.1 and C.2). For future analyses the internal standards AHBD10, AHBD13 and AHBD14 were used. The external standard W2 was also analysed after every five samples during an analysis in order to correct for internal analytical drift.

C.3.2 Flux contamination

The samples were prepared for ICP-OES and ICP-MS analysis using the fusion method and not by the acid digestion method. There was a danger that the Li-metaborate flux used during the fusion process would contaminate the samples. To resolve this problem a number of blanks have been analysed containing the flux. The results show that the flux does not introduce significant contamination and that the fusion method should be accurate in measuring the trace elements within a sample. The usual amount of flux used in the analytical process is 0.4 to 0.6g.

However in an attempt to limit any possible contamination to an absolute minimum the first batches of samples were prepared using 0.2g of flux. The use of 0.2g of flux was extremely inefficient because the samples would not fuse properly, thus many samples failed to dissolve and had to be re-run. Even when it was thought that some of the samples had fused, the subsequent analysis showed that they had not and this resulted in many samples giving very low and high absolute totals. However not all the 0.2g samples failed, many worked and gave good totals. It was obvious that the later batches would have to be fused with 0.4g and then 0.6g of flux, which

		Batch 1 fused with 0.2g of flux							
		JB-1a st	BIR-1 st	JA-2 st	W2 st	AHBI06 st	AHBD12 st	AHBD29 st	AHBD10
Majors									
	SiO_2	52.43	48.14	57.67	51.94	88.14	78.15	48.91	45.96
	TiO_2	1.31	0.92	0.65	1.07	0.30	0.12	1.21	1.49
	Al_2O_3	14.79	15.43	14.90	15.37	9.70	2.20	12.78	13.26
	Fe_2O_3	9.15	11.11	6.68	11.19	1.28	0.94	11.94	13.81
	MnO	0.16	0.18	0.11	0.18	0.01	0.28	0.17	0.26
	MgO	7.79	9.36	7.55	6.60	0.17	0.42	7.51	6.61
	CaO	9.67	12.91	5.93	10.82	0.59	0.77	9.07	11.04
	NC2O	2.75	1.55	3.07	2.13	4.69	0.21	3.44	1.65
	K_2O	1.43	0.03	1.49	0.58	0.34	0.17	0.11	-0.03
	P_2O_5	0.27	0.03	0.15	0.12	0.05	0.10	0.10	0.11
	LOI	0.78	0.68	0.65	-0.31	0.69	3.14	3.21	4.46
	Total	100.52	100.33	98.85	99.68	105.97	86.51	98.44	98.61
Traces									
	Sc	31.1	44.4	18.9	38.0	6.9	3.4	48.8	54.3
	V	210.3	308.1	118.3	265.7	25.1	22.1	312.0	404.5
	Cr	453.2	376.1	400.6	112.6	29.2	7.6	219.9	163.9
	Co	46.4	56.8	31.7	50.5	4.8	4.9	53.3	62.7
	Ni	129.2	168.8	108.8	71.3	6.3	25.1	102.4	72.9
	Cu	161.5	350.0	146.9	128.1	222.9	205.5	387.5	97.2
	Zn	147.9	112.1	97.0	95.8	31.2	6.8	115.7	71.5
	Sr	437.1	101.1	241.6	198.1	51.9	154.5	178.8	206.7
	Y	25.74	14.63	17.63	23.87	23.83	11.01	25.74	31.29
	Zr	146.0	15.9	112.1	90.4	102.1	21.7	64.7	78.1
	Ba	515.4	6.0	322.4	181.4	214.1	664.7	75.5	43.4
		Batch 2 fused with 0.2g of flux							
		JB-1a st2	BIR-1 st2	JA-2 st2	W2 st2	AHBI06 st2	AHBD12 st2	AHBD29 st2	
Majors									
	SiO_2	52.36	47.50	57.19	52.14	79.38	89.62	48.48	
	TiO_2	1.28	0.96	0.68	1.09	0.28	0.10	1.23	
	Al_2O_3	14.79	15.55	15.65	15.85	10.40	2.61	13.53	
	Fe_2O_3	9.14	11.59	6.83	10.92	1.13	1.05	12.00	
	MnO	0.16	0.18	0.12	0.17	0.01	0.31	0.17	
	MgO	7.78	9.06	7.29	6.19	0.15	0.46	7.52	
	CaO	9.46	12.71	6.07	11.01	0.61	0.89	9.29	
	NC2O	2.75	1.62	3.15	2.16	5.44	0.28	3.57	
	K_2O	1.43	0.07	1.41	0.59	0.69	0.38	0.13	
	P_2O_5	0.27	0.03	0.16	0.12	0.05	0.11	0.11	
	LOI	0.78	0.68	0.65	-0.31	0.69	3.15	3.22	
	Total	100.64	99.95	99.21	99.93	98.84	98.95	99.25	
Traces									
	Sc	28.0	44.1	19.2	37.5	7.0	3.3	47.5	
	V	220.9	330.3	106.8	273.7	4.6	4.6	334.2	
	Cr	415.4	406.6	438.4	119.5	20.2	18.3	236.1	
	Co	39.7	50.9	28.6	46.6	3.4	5.8	46.7	
	Ni	140.5	176.1	112.6	74.5	6.9	22.3	103.1	
	Cu	55.7	75.9	20.6	55.4	38.9	30.8	56.7	
	Zn	82.3	80.2	57.2	89.6	29.0	63.8	70.4	
	Sr	444.7	110.6	274.1	194.7	63.5	177.4	201.8	
	Y	21.8	15.52	19.41	23.02	24.63	15.81	26.16	
	Zr	137.4	13.7	119.5	88.4	101.3	21.4	61.9	
	Ba	488.8	7.3	319.6	173.0	192.4	671.4	79.9	

Table C.1 – ICP-OES data for the external and internal standards in the 8 batches of samples analysed. Samples highlighted are the ones that gave erroneous totals.

		Batch 3 fused with 0.4g of flux							
		JB-1a st3	BIR-1 st4	JA-2 st3	W2 st3	MRG-1 st2	AHBD10 st	AHBD13 st	AHBD14 st
Majors									
	SiO_2	53.93	47.65	58.91	52.60	39.83	46.12	48.09	49.22
	TiO_2	1.33	0.98	0.71	1.05	3.89	1.41	1.42	1.33
	Al_2O_3	14.91	15.56	16.32	15.30	8.61	13.24	12.99	12.29
	Fe_2O_3	8.82	11.21	6.11	10.46	17.87	13.65	12.48	12.46
	MnO	0.15	0.17	0.11	0.17	0.17	0.22	0.25	0.22
	MgO	7.95	9.42	7.59	6.38	13.78	7.19	7.48	6.71
	CaO	9.47	13.24	6.50	10.84	14.95	10.39	8.46	9.07
	NC2O	2.01	1.11	2.26	1.58	0.47	1.75	3.38	2.03
	K_2O	0.33	0.03	0.44	0.10	0.03	0.03	0.03	0.02
	P_2O_5	0.26	0.01	0.16	0.12	0.06	0.12	0.10	0.11
	LOI	0.78	0.68	0.65	-0.31	1.02	4.46	4.39	4.87
	Total	99.94	100.06	99.76	98.30	100.67	98.57	99.08	98.32
Traces									
	Sc	27.6	44.1	19.7	35.2	55.9	46.5	51.5	43.9
	V	192.4	312.4	101.2	241.5	535.4	347.4	322.6	324.2
	Cr	417.5	385.3	430.5	90.1	449.9	177.2	138.5	168.0
	Co	34.3	42.5	25.4	36.5	87.5	44.5	45.7	42.2
	Ni	141.4	171.3	134.7	154.3	192.2	111.0	144.8	72.2
	Cu	4.9	69.3	23.1	34.3	95.1	103.2	90.8	150.9
	Zn	36.4	27.0	21.2	38.1	143.1	67.4	55.0	85.3
	Sr	449.0	106.9	260.1	203.2	278.5	193.0	60.1	380.2
	Y	23.18	16.37	19.36	21.35	13.76	28.70	28.63	26.88
	Zr	141.1	24.7	122.8	94.1	94.9	72.1	78.1	67.6
	Ba	493.0	7.4	318.6	166.2	48.0	42.1	27.4	126.5
		Batch 4 fused with 0.4g of flux							
		JB-1a st5	BIR-1 st5	JA-2 st5	W2 st4	JG-3 st2	AHBD10 st2	AHBD13 st2	AHBD14 st2
Majors									
	SiO_2	52.69	47.23	58.13	52.79	69.80	47.98	48.17	50.56
	TiO_2	1.34	0.95	0.70	1.08	0.49	1.43	1.35	1.38
	Al_2O_3	15.07	15.22	15.97	15.47	15.77	13.32	13.03	12.72
	Fe_2O_3	8.78	11.01	6.27	10.41	3.50	13.81	12.88	12.77
	MnO	0.15	0.21	0.12	0.17	0.07	0.23	0.26	0.23
	MgO	7.95	9.51	7.62	6.38	1.88	7.22	7.48	6.85
	CaO	9.67	13.13	7.31	11.01	3.88	10.59	8.56	9.39
	NC2O	2.80	1.54	2.31	1.91	3.06	1.68	3.29	2.16
	K_2O	1.23	0.05	0.02	0.52	0.77	0.01	0.01	0.01
	P_2O_5	0.28	0.03	0.18	0.13	0.12	0.11	0.12	0.11
	LOI	0.78	0.68	0.65	-0.31	0.46	4.46	4.39	4.87
	Total	100.73	99.56	99.30	99.55	99.79	100.85	99.55	101.04
Traces									
	Sc	29.1	41.8	18.7	34.5	8.4	49.0	47.7	47.6
	V	193.6	297.4	97.9	248.1	53.1	358.5	330.0	336.3
	Cr	423.2	461.3	448.4	136.1	31.4	161.5	162.9	153.6
	Co	36.2	43.0	25.3	39.2	13.9	48.1	43.7	44.4
	Ni	121.4	233.4	111.0	67.6	10.4	106.7	116.3	70.4
	Cu	93.6	87.4	34.8	42.9	32.0	110.8	124.3	58.3
	Zn	29.3	51.5	25.8	60.3	19.8	75.8	65.9	65.8
	Sr	454.4	111.8	262.2	189.3	372.9	200.5	59.4	389.8
	Y	22.73	16.18	18.37	22.09	15.76	27.29	25.48	27.05
	Zr	128.6	20.4	110.8	89.7	152.0	69.8	62.8	66.1
	Ba	503.1	19.4	326.3	162.2	448.1	43.1	32.2	123.8

Table C.1 – continued.

		Batch 6 fused with 0.4g of flux						
		JB-1a st6	BIR-1 st4	JA-2 st3	W2 st3	AHBD10 st	AHBD13 st	AHBD14 st
Majors								
	SiO_2	52.84	47.78	56.31	52.49	47.17	48.05	49.40
	TiO_2	1.24	0.92	0.66	1.01	1.35	1.30	1.27
	Al_2O_3	14.47	15.61	15.87	14.84	13.20	12.86	11.95
	Fe_2O_3	8.96	11.35	6.20	10.64	13.79	12.99	12.43
	MnO	0.15	0.18	0.11	0.17	0.24	0.26	0.23
	MgO	7.90	9.80	7.40	6.14	7.02	7.48	6.52
	CaO	9.35	13.65	6.35	11.10	10.68	8.52	9.27
	NC2O	2.53	1.36	2.80	2.00	2.02	3.72	2.41
	K_2O	0.48	0.03	1.61	0.59	0.00	0.00	0.04
	P_2O_5	0.27	0.03	0.16	0.14	0.11	0.11	0.11
	LOI	0.78	-0.68	0.65	-0.31	4.46	4.39	4.86
	Total	98.96	100.04	98.12	98.80	100.04	99.68	98.50
Traces								
	Sc	26.86	44.29	18.07	34.67	47.43	47.48	43.51
	V	192.7	320.7	85.6	249.2	384.1	348.3	347.0
	Cr	429.6	419.8	459.2	81.5	183.6	144.1	157.1
	Co	39.1	48.9	27.4	41.5	46.2	45.2	42.5
	Ni	140.2	163.6	140.3	75.9	115.5	177.3	74.2
	Cu	54.2	106.1	25.8	695.0	163.6	175.7	166.9
	Zn	67.6	48.0	65.1	69.4	90.5	89.9	95.1
	Sr	459.0	107.6	258.4	209.4	203.9	48.6	394.1
	Y	23.51	15.98	18.03	22.84	29.61	28.07	27.95
	Zr	125.2	18.5	113.6	92.3	70.6	69.2	67.5
	Ba	508.5	7.6	311.6	169.4	45.2	28.7	128.6
		Batch 7 fused with 0.4g of flux						
		JB-1a st7	BIR-1 st5	JA-2 st5	W2 st4	AHBD10 st2	AHBD13 st2	AHBD14 st2
Majors								
	SiO_2	53.09	48.13	56.77	52.73	46.57	47.94	50.22
	TiO_2	1.25	0.92	0.65	1.03	1.34	1.29	1.31
	Al_2O_3	14.60	15.31	15.83	15.32	13.17	12.95	12.58
	Fe_2O_3	8.84	11.23	6.12	10.48	13.85	12.99	12.74
	MnO	0.15	0.18	0.12	0.17	0.23	0.27	0.23
	MgO	8.00	9.75	7.61	6.45	7.12	7.49	6.85
	CaO	9.47	13.39	6.86	10.99	10.12	8.23	9.26
	NC2O	2.45	1.43	2.86	2.08	1.97	3.88	2.59
	K_2O	0.49	0.03	1.67	0.58	0.02	0.04	0.08
	P_2O_5	0.27	0.02	0.17	0.12	0.11	0.14	0.12
	LOI	0.78	-0.68	0.65	-0.31	4.46	4.40	4.86
	Total	99.38	99.71	99.31	99.65	98.97	99.61	100.84
Traces								
	Sc	27.64	43.02	18.23	35.04	46.99	46.50	44.23
	V	191.9	323.6	82.6	248.6	361.2	333.9	347.4
	Cr	445.8	511.5	466.5	127.9	159.6	136.9	156.5
	Co	37.9	47.4	28.1	42.5	43.1	43.5	42.7
	Ni	142.8	156.9	133.9	72.1	79.9	100.8	65.8
	Cu	50.5	121.1	21.3	94.8	136.2	84.3	94.5
	Zn	71.3	65.9	60.6	69.1	97.8	94.6	92.1
	Sr	465.0	110.5	247.3	204.5	206.8	56.4	414.5
	Y	23.73	16.59	18.17	22.45	30.27	27.89	28.76
	Zr	136.3	16.4	111.8	97.2	71.6	69.5	69.7
	Ba	511.2	12.4	315.9	171.5	44.3	30.6	131.1

Table C.1 – continued.

		Batch 8 fused with 0.6g of flux							
		JB-1a st8	BIR-1 st6	W2 st6	JA-2 st6	AHBD10 st4	AHBD13 st4	AHBD14 st4	
Majors									
	SiO_2	52.82	47.27	52.27	56.86	46.61	48.61	50.68	
	TiO_2	1.28	0.94	1.07	0.69	1.39	1.28	1.34	
	Al_2O_3	14.88	15.83	15.71	16.38	13.30	13.21	12.67	
	Fe_2O_3	8.97	11.06	10.67	6.36	13.74	12.61	12.61	
	MnO	0.15	0.17	0.17	0.11	0.22	0.25	0.23	
	MgO	8.01	9.70	6.56	7.71	7.05	7.56	6.83	
	CaO	9.66	13.55	11.29	6.51	10.67	8.27	9.39	
	NC2O	2.38	1.55	1.84	2.72	2.07	3.90	2.45	
	K_2O	0.69	0.03	0.26	0.89	0.07	0.06	0.13	
	P_2O_5	0.27	0.05	0.13	0.15	0.12	0.12	0.11	
	LOI	0.78	-0.65	-0.31	0.65	4.46	4.40	4.87	
	Total	99.88	99.49	99.67	99.04	99.70	100.27	101.30	
Traces									
	Sc	28.1	42.9	35.9	19.2	47.0	45.2	44.8	
	V	192.6	320.3	255.4	114.0	379.0	339.1	355.1	
	Cr	396.8	368.1	137.6	406.5	158.0	140.3	152.8	
	Co	39.7	50.9	49.3	26.3	64.0	58.0	58.8	
	Ni	159.7	176.3	116.9	139.7	92.8	95.1	89.7	
	Cu	80.4	179.5	108.4	49.7	133.3	184.1	153.1	
	Zn	86.1	84.7	80.4	70.0	99.9	91.9	97.0	
	Sr	446.0	104.3	196.3	257.0	196.8	48.7	386.9	
	Y	25.6	17.8	24.3	20.1	30.2	27.1	29.4	
	Zr	138.4	14.3	87.7	107.5	73.0	68.0	72.5	
	Ba	499.7	19.9	175.2	327.7	50.1	37.4	132.7	
		Batch 9 fused with 0.6g of flux							
		JB-1a st9	BIR-1 st7	W2 st7	JA-2 st7	JG-3 st3	AHBD10 st5	AHBD13 st5	AHBD14 st5
Majors									
	SiO_2	52.46	46.99	52.90	57.64	68.54	47.15	48.45	50.17
	TiO_2	1.25	0.95	1.04	0.66	0.47	1.43	1.32	1.30
	Al_2O_3	14.46	15.03	14.90	15.61	15.65	13.72	13.38	12.81
	Fe_2O_3	8.75	11.30	10.82	6.25	3.63	13.82	13.04	12.51
	MnO	0.14	0.17	0.17	0.11	0.07	0.23	0.26	0.22
	MgO	7.94	9.69	6.43	7.73	1.80	7.18	7.43	6.72
	CaO	9.91	13.50	11.23	6.49	3.78	10.67	8.38	9.48
	NC2O	2.32	1.51	1.80	2.64	3.31	1.85	3.89	2.49
	K_2O	0.70	0.02	0.25	0.81	1.02	0.05	0.04	0.10
	P_2O_5	0.27	0.03	0.13	0.16	0.14	0.13	0.12	0.12
	LOI	0.78	1.01	1.00	0.65	0.46	4.46	4.39	4.87
	Total	98.99	100.21	100.67	98.74	98.87	100.69	100.70	100.80
Traces									
	Sc	27.8	42.9	35.1	17.9	8.5	48.3	48.0	45.3
	V	187.4	303.3	248.7	108.6	73.2	377.7	345.8	346.3
	Cr	395.8	425.6	114.3	426.0	33.7	152.7	127.0	142.9
	Co	37.7	49.3	47.6	25.3	14.4	65.6	61.1	59.0
	Ni	152.5	194.1	86.7	141.2	42.0	89.5	83.7	82.0
	Cu	232.3	174.9	257.5	108.2	219.5	259.5	234.8	193.7
	Zn	111.6	77.8	91.6	71.4	67.8	105.6	82.6	107.6
	Sr	449.3	104.8	188.2	243.3	373.7	202.4	52.0	394.0
	Y	24.6	16.8	23.1	19.0	18.2	30.6	28.4	28.4
	Zr	123.6	14.5	81.6	104.7	140.7	74.4	72.3	69.0
	Ba	519.4	20.2	175.1	336.4	463.6	55.0	33.6	143.2

Table C.1 – continued.

		Batch 1 fused with 0.2g of flux							
		JB-1a st	BIR-1 st	JA-2 st	W2 st	AHBI06 st	AHBD12 st	AHBD29 st	AHBD10
Traces	Ti	1.31	0.94	0.68	1.08	0.30	0.11	1.21	1.49
	V	190.9	292.5	104.2	264.0	8.1	7.4	294.2	376.8
	^{52}Cr	422.3	375.3	422.2	93.1	33.1	10.9	219.8	163.3
	^{53}Cr	425.7	368.9	413.5	96.3	36.1	12.8	215.8	162.7
	Mn	0.15	0.16	0.10	0.18	0.01	0.28	0.15	0.23
	^{57}Fe	9.04	10.96	6.23	11.18	1.18	0.96	10.98	13.75
	Co	38.6	49.1	29.6	46.3	4.1	6.8	44.4	51.0
	^{60}Ni	140.1	175.3	115.6	82.4	-15.9	16.0	99.7	65.7
	^{62}Ni	151.0	177.3	124.7	82.0	-16.7	13.0	100.8	70.0
	Zn	106.8	22.7	58.0	47.4	24.8	18.8	30.7	32.4
	Ga	18.0	16.4	16.4	18.1	7.3	3.2	13.1	18.1
	Rb	23.9	0.0	28.6	3.0	1.0	3.0	0.3	0.0
	Sr	456.8	96.6	239.5	195.9	50.2	159.0	166.9	190.4
	Y	23.7	15.0	17.5	22.2	21.8	13.1	22.8	27.8
	Zr	132.4	12.8	110.7	92.7	97.6	18.3	58.5	81.8
	Nb	29.45	0.56	9.64	8.19	1.17	1.07	3.82	4.90
	Ba	507.7	1.9	313.2	169.5	195.9	631.2	68.7	40.1
	La	35.83	0.58	15.78	9.58	6.18	10.47	3.87	4.85
	Ce	65.79	1.93	33.55	24.13	12.82	21.75	10.18	11.43
	Pr	7.12	0.34	3.72	3.03	1.78	2.52	1.44	1.65
	Nd	25.48	2.20	13.92	12.64	8.14	10.18	7.29	8.19
	Sm	5.37	1.07	3.16	3.37	2.57	2.38	2.54	2.79
	Eu	1.47	0.46	0.89	1.11	0.60	0.62	0.85	1.05
	Gd	4.35	1.79	2.64	3.31	2.61	2.08	2.80	3.31
	Tb	0.69	0.31	0.44	0.58	0.48	0.34	0.55	0.66
	Dy	4.05	2.28	2.78	3.76	3.27	2.11	3.75	4.52
	Ho	0.74	0.48	0.53	0.72	0.65	0.39	0.74	0.89
	Er	2.12	1.47	1.58	2.03	1.98	1.12	2.22	2.71
	Tm	0.31	0.23	0.23	0.30	0.31	0.16	0.33	0.41
	Yb	2.13	1.56	1.66	2.02	2.15	1.10	2.28	2.75
	Lu	0.31	0.26	0.25	0.33	0.33	0.17	0.35	0.44
	Hf	3.48	0.43	2.53	2.20	2.51	0.41	1.49	1.90
	Ta	1.57	0.02	0.39	0.28	0.06	0.04	0.15	0.17
	Pb	3.11	2.44	4.34	1.07	0.57	4.76	2.99	1.23
	Th	9.42	0.04	5.02	2.29	0.74	0.58	0.25	0.30
	U	1.33	0.15	1.77	0.51	0.41	0.25	0.19	0.19

Table C.2 – ICP-MS data for the external and internal standards in the 8 batches of samples analysed. Samples highlighted are the ones that gave erroneous totals.

		Batch 2 fused with 0.2g of flux						
		JB-1a st2	BIR-1 st2	JA-2 st2	W2 st2	AHBI06 st2	AHBD12 st2	AHBD29 st2
Traces	Ti	1.30	0.96	0.72	1.15	0.28	0.11	1.28
	V	198.3	302.0	113.4	259.6	5.4	7.5	314.8
	^{52}Cr	427.9	403.4	471.4	113.6	17.3	10.5	250.5
	^{53}Cr	434.2	380.3	449.3	107.9	27.3	21.9	241.2
	Mn	0.15	0.17	0.12	0.17	0.01	0.30	0.17
	^{57}Fe	9.31	10.70	6.39	10.96	1.04	0.97	11.74
	Co	39.9	51.2	30.2	48.3	1.4	6.3	45.4
	^{60}Ni	137.9	191.7	124.8	73.2	7.1	22.5	100.7
	^{62}Ni	140.7	192.8	121.1	76.2	6.0	21.2	100.9
	Zn	100.4	26.6	58.9	50.4	24.6	17.8	35.1
	Ga	18.3	14.4	17.3	17.9	6.8	3.1	14.2
	Rb	8.3	0.0	24.4	3.4	1.1	3.5	0.3
	Sr	488.4	96.6	279.9	190.4	48.1	168.6	198.6
	Y	24.0	14.9	18.1	22.1	21.0	13.8	24.7
	Zr	135.2	13.0	114.6	87.7	90.0	20.1	60.1
	Nb	29.97	0.60	10.28	8.14	1.06	1.27	3.95
	Ba	521.1	2.0	329.1	166.1	190.0	669.8	79.8
	La	36.74	0.54	16.19	9.41	5.91	5.77	4.31
	Ce	67.33	1.94	34.18	23.58	12.22	12.57	10.75
	Pr	7.34	0.33	3.81	2.96	1.70	2.66	1.54
	Nd	26.01	2.08	14.25	12.52	7.92	10.88	7.76
	Sm	5.46	1.04	3.31	3.31	2.49	2.47	2.75
	Eu	1.50	0.46	0.93	1.11	0.57	0.64	0.90
	Gd	4.32	1.42	2.69	3.25	2.38	2.11	2.93
	Tb	0.67	0.31	0.47	0.59	0.46	0.35	0.57
	Dy	4.04	2.28	2.92	3.85	3.10	2.17	3.99
	Ho	0.75	0.48	0.56	0.73	0.61	0.42	0.78
	Er	2.07	1.41	1.62	2.09	1.88	1.15	2.38
	Tm	0.31	0.22	0.25	0.31	0.29	0.17	0.35
	Yb	2.06	1.44	1.68	2.06	1.99	1.15	2.39
	Lu	0.32	0.28	0.27	0.35	0.33	0.19	0.38
	Hf	2.96	0.45	2.66	2.16	2.31	0.47	1.49
	Ta	1.03	0.02	0.40	0.29	0.05	0.04	0.15
	Pb	0.84	1.30	3.18	0.86	1.27	3.01	1.50
	Th	9.07	0.03	5.02	2.22	0.69	0.62	0.25
	U	1.33	0.14	1.81	0.50	0.40	0.26	0.21

Table C.2 – continued.

		Batch 3 fused with 0.4g of flux							
		JB-1a st3	BIR-1 st4	JA-2 st3	W2 st3	MRG-1 st2	AHBD10 st	AHBD13 st	AHBD14 st
Traces	Ti	1.27	0.96	0.67	1.00	4.15	1.38	1.29	1.30
	V	193.9	321.8	110.7	248.0	540.1	366.5	337.4	343.8
	^{52}Cr	424.6	417.6	447.5	80.6	487.0	179.1	140.2	158.9
	^{53}Cr	414.9	405.5	425.6	82.2	461.2	174.0	137.0	156.2
	Mn	0.14	0.17	0.10	0.15	0.17	0.22	0.24	0.22
	^{57}Fe	8.69	11.30	5.99	10.23	17.89	13.32	12.40	12.19
	Co	40.3	54.0	31.1	43.6	98.9	53.7	51.8	50.8
	^{60}Ni	140.2	163.9	120.4	147.4	191.9	110.3	156.6	71.3
	^{62}Ni	140.0	163.5	129.3	161.4	237.0	127.4	173.8	84.6
	Zn	94.5	32.9	53.7	52.1	77.3	49.9	44.1	46.3
	Ga	17.5	15.6	16.8	17.1	18.3	17.5	14.8	13.3
	Rb	2.1	-0.1	3.9	0.9	0.3	0.0	0.0	0.1
	Sr	447.2	106.0	248.4	195.6	278.3	192.3	48.9	381.4
	Y	24.0	16.8	18.2	21.9	14.0	28.6	26.2	26.9
	Zr	138.2	15.6	114.9	90.9	104.0	70.9	68.3	67.5
	Nb	27.94	0.55	8.85	6.81	20.14	4.31	3.93	4.00
	Ba	497.0	3.3	317.6	162.1	47.4	41.2	26.3	125.0
	La	36.46	0.59	19.82	12.34	11.89	3.21	2.75	3.07
	Ce	66.14	1.91	33.90	22.38	26.09	10.40	9.30	9.68
	Pr	7.03	0.37	3.85	2.92	3.89	1.67	1.53	1.56
	Nd	26.60	2.43	14.77	12.57	18.80	8.70	7.94	8.24
	Sm	5.04	1.08	3.10	3.07	4.50	2.87	2.66	2.68
	Eu	1.52	0.51	0.93	1.03	1.41	1.04	0.97	0.98
	Gd	4.60	1.74	3.04	3.49	4.16	3.71	3.46	3.57
	Tb	0.65	0.33	0.45	0.55	0.54	0.64	0.60	0.62
	Dy	4.00	2.53	2.89	3.60	2.94	4.49	4.16	4.26
	Ho	0.71	0.51	0.54	0.67	0.46	0.87	0.81	0.82
	Er	2.19	1.64	1.71	2.09	1.20	2.82	2.59	2.65
	Tm	0.32	0.26	0.26	0.32	0.15	0.43	0.40	0.41
	Yb	2.01	1.65	1.67	1.96	0.84	2.77	2.54	2.63
	Lu	0.32	0.31	0.27	0.31	0.12	0.49	0.44	0.45
	Hf	3.36	0.56	2.88	2.36	3.60	1.82	1.82	1.79
	Ta	1.64	0.04	0.65	0.43	0.80	0.27	0.25	0.25
	Pb	2.77	2.62	3.13	2.70	8.14	4.70	3.50	6.76
	Th	8.46	0.04	4.73	1.97	0.73	0.27	0.26	0.26
	U	1.72	0.01	2.37	0.50	0.24	0.10	0.10	0.12

Table C.2 – continued.

		Batch 4 fused with 0.4g of flux							
		JB-1a st5	BIR-1 st5	JA-2 st5	W2 st4	JG-3 st2	AHBD10 st2	AHBD13 st2	AHBD14 st2
Traces	Ti	1.25	0.96	0.66	1.03	0.45	1.38	1.32	1.32
	V	189.4	322.1	111.1	252.8	57.1	371.6	346.5	348.5
	^{52}Cr	426.6	526.9	481.9	121.7	14.1	159.5	155.6	154.2
	^{53}Cr	426.9	508.0	444.4	119.4	16.8	172.6	153.8	148.6
	Mn	0.14	0.22	0.11	0.16	0.07	0.23	0.26	0.23
	^{57}Fe	8.37	11.37	5.88	10.39	3.32	13.39	12.66	12.43
	Co	38.0	54.1	28.8	43.8	11.6	49.4	45.9	46.2
	^{60}Ni	117.6	234.2	128.5	68.9	2.9	103.9	137.6	84.6
	^{62}Ni	129.9	240.8	127.9	78.9	3.2	105.8	161.7	95.9
	Zn	82.4	40.1	51.6	53.7	55.0	52.8	47.2	47.5
	Ga	17.2	15.6	16.5	16.8	15.6	17.6	14.7	13.4
	Rb	0.8	0.4	3.2	0.8	6.0	0.0	0.1	0.1
	Sr	443.3	114.6	260.5	188.0	363.3	194.9	54.3	386.5
	Y	23.5	16.8	18.1	22.3	16.8	29.0	26.6	27.3
	Zr	135.9	16.8	112.8	92.3	156.6	70.1	66.5	66.0
	Nb	26.70	0.62	8.83	6.95	5.56	4.31	3.87	4.02
	Ba	492.2	17.5	317.9	161.5	454.6	42.2	26.8	125.8
	La	38.40	0.59	15.66	9.13	24.65	4.78	4.46	4.29
	Ce	65.71	2.06	33.71	22.52	43.00	10.45	9.50	9.69
	Pr	6.99	0.38	3.82	2.91	4.74	1.67	1.53	1.57
	Nd	26.44	2.57	14.73	12.75	17.60	8.76	8.06	8.22
	Sm	4.92	1.09	3.02	3.11	3.24	2.82	2.62	2.67
	Eu	1.49	0.51	0.89	1.03	0.86	1.04	1.00	0.98
	Gd	4.66	1.77	2.97	3.44	2.84	3.72	3.44	3.50
	Tb	0.66	0.34	0.44	0.54	0.41	0.65	0.61	0.62
	Dy	4.02	2.54	2.89	3.63	2.56	4.55	4.26	4.29
	Ho	0.72	0.52	0.54	0.68	0.48	0.88	0.82	0.85
	Er	2.15	1.67	1.67	2.08	1.54	2.85	2.61	2.65
	Tm	0.32	0.26	0.25	0.31	0.25	0.44	0.40	0.41
	Yb	2.00	1.63	1.65	1.95	1.66	2.78	2.53	2.54
	Lu	0.36	0.30	0.31	0.34	0.28	0.45	0.41	0.41
	Hf	3.26	0.54	2.76	2.29	3.98	1.90	1.80	1.76
	Ta	1.65	0.04	0.64	0.41	0.54	0.26	0.25	0.25
	Pb	5.53	10.67	8.79	5.02	3.45	6.01	8.07	2.55
	Th	8.47	0.04	4.65	1.95	7.96	0.28	0.25	0.25
	U	1.67	0.03	2.42	0.52	2.50	0.09	0.10	0.12

Table C.2 – continued.

		Batch 6 fused with 0.6g of flux						
		JB-1a st6	BIR-1 st4	JA-2 st3	W2 st3	AHBD10 st	AHBD13 st	AHBD14 st
Traces	Ti	1.283	0.950	0.667	1.014	1.393	1.283	1.296
	V	195.820	312.870	85.543	258.970	366.522	326.932	335.013
	^{52}Cr	420.516	400.398	441.310	89.458	179.839	134.878	153.275
	^{53}Cr	413.606	391.036	439.148	89.407	165.809	127.390	143.160
	Mn	0.152	0.179	0.114	0.167	0.234	0.233	0.225
	^{57}Fe	9.354	11.935	6.473	10.903	14.214	11.707	12.904
	Co	38.367	52.213	28.672	42.559	49.219	47.175	45.977
	^{60}Ni	482.319	485.074	444.325	490.875	415.322	481.516	369.967
	^{62}Ni	427.401	428.631	390.212	439.569	369.840	475.275	351.036
	Ga	18.197	15.838	16.166	17.390	18.207	14.802	13.697
	Sr	459.502	118.149	263.192	209.707	207.189	61.472	386.387
	Y	24.591	17.420	18.271	22.854	29.600	26.524	27.487
	Zr	135.264	12.653	106.042	83.247	60.452	59.328	60.368
	Nb	27.272	0.487	9.231	6.268	3.576	3.418	3.616
	Ba	636.489	180.620	484.597	339.791	216.433	204.566	306.750
	La	40.731	0.786	16.425	11.735	5.081	4.625	4.956
	Ce	65.520	2.185	32.631	23.574	11.649	10.489	10.921
	Pr	7.337	0.576	4.092	3.154	1.893	1.724	1.793
	Nd	25.538	2.619	14.079	12.912	9.151	8.408	8.729
	Sm	5.094	1.217	3.349	3.380	3.095	2.876	2.898
	Eu	1.529	0.589	0.927	1.132	1.127	1.065	1.088
	Gd	4.714	1.952	3.171	3.603	3.799	3.617	3.734
	Tb	0.718	0.384	0.409	0.613	0.720	0.675	0.680
	Dy	4.181	2.743	3.113	3.845	4.781	4.406	4.459
	Ho	0.781	0.562	0.566	0.741	0.968	0.894	0.922
	Er	2.186	1.678	1.603	2.090	2.824	2.546	2.621
	Tm	0.327	0.265	0.268	0.324	0.449	0.405	0.418
	Yb	2.109	1.736	1.704	2.078	2.970	2.616	2.726
	Lu	0.279	0.266	0.280	0.282	0.470	0.400	0.411
	Hf	3.313	0.570	2.648	2.557	1.573	1.592	1.625
	Ta	1.607	0.032	0.583	1.372	0.209	0.202	0.212
	Pb	21.376	21.613	22.256	22.177	22.167	21.545	23.347
	Th	9.064	0.083	4.924	2.138	0.360	0.343	0.336
	U	1.693	0.054	2.513	0.558	0.183	0.180	0.202

Table C.2 – continued.

		Batch 7 fused with 0.6g of flux						
		JB-1a st7	BIR-1 st5	JA-2 st5	W2 st4	AHBD10 st2	AHBD13 st2	AHBD14 st2
Traces	Ti	1.287	0.950	0.665	1.029	1.402	1.287	1.318
	V	195.626	311.250	85.552	251.485	367.037	334.409	343.144
	^{52}Cr	430.039	396.799	447.635	92.194	157.385	130.094	155.231
	^{53}Cr	376.721	390.413	438.684	97.334	146.578	125.919	145.326
	Mn	0.146	0.214	0.113	0.164	0.226	0.252	0.226
	^{57}Fe	9.268	11.714	6.337	10.893	14.242	12.986	13.007
	Co	37.324	52.133	28.078	42.792	48.783	46.919	46.898
	^{60}Ni	228.405	361.564	197.891	93.998	112.113	142.323	93.942
	^{62}Ni	218.725	315.115	181.795	101.691	120.268	141.475	99.892
	Ga	18.085	15.548	16.750	17.412	18.003	14.824	13.571
	Sr	455.335	119.846	265.510	193.513	199.455	59.599	385.936
	Y	24.032	16.747	18.168	22.960	28.919	26.114	27.102
	Zr	127.940	14.475	108.339	87.359	67.186	61.266	61.943
	Nb	25.148	0.672	9.336	6.364	3.932	3.503	3.660
	Ba	540.508	80.981	371.478	220.035	101.933	85.955	181.270
	La	36.975	0.839	16.262	11.234	5.465	4.291	4.811
	Ce	65.334	2.062	33.710	23.740	10.713	9.628	9.940
	Pr	7.218	0.558	3.933	3.044	1.737	1.574	1.634
	Nd	25.610	2.885	14.192	13.409	8.535	7.775	8.070
	Sm	4.963	1.127	3.067	3.217	2.915	2.697	2.735
	Eu	1.500	0.535	0.940	1.062	1.081	1.007	1.020
	Gd	4.680	1.817	3.003	3.426	3.699	3.426	3.503
	Tb	0.701	0.371	0.429	0.596	0.699	0.637	0.653
	Dy	4.107	2.602	2.918	3.726	4.623	4.233	4.375
	Ho	0.759	0.548	0.581	0.727	0.939	0.862	0.892
	Er	2.141	1.635	1.581	2.067	2.802	2.517	2.584
	Tm	0.318	0.253	0.261	0.308	0.429	0.388	0.396
	Yb	2.048	1.682	1.708	2.022	2.883	2.596	2.648
	Lu	0.317	0.258	0.268	0.295	0.406	0.360	0.371
	Hf	3.300	0.578	2.717	2.438	1.605	1.592	1.696
	Ta	1.584	0.043	0.592	1.388	0.238	0.228	0.225
	Pb	8.674	12.558	12.856	10.773	11.596	11.358	8.835
	Th	8.799	0.087	4.941	2.185	0.340	0.321	0.339
	U	1.716	0.062	2.365	0.544	0.164	0.163	0.198

Table C.2 – continued.

		Batch 8 fused with 0.6g of flux						
		JB-1a st8	BIR-1 st6	W2 st6	JA-2 st6	AHBD10 st4	AHBD13 st4	AHBD14 st4
Traces	Ti	1.28	0.94	1.07	0.69	1.44	1.35	1.37
	V	196.00	312.60	259.20	116.50	377.60	347.60	355.80
	^{52}Cr	414.00	386.00	103.10	419.50	167.74	135.76	158.09
	^{53}Cr	410.80	390.10	105.50	419.20	169.90	137.05	161.38
	Mn	0.15	0.17	0.17	0.10	0.23	0.26	0.23
	^{57}Fe	8.98	11.28	10.90	6.09	13.79	12.96	12.85
	Co	36.79	50.93	43.70	28.46	50.38	48.57	47.46
	^{60}Ni	155.10	169.10	115.90	135.20	90.00	83.79	87.74
	^{62}Ni	146.60	162.20	107.90	125.10	91.58	88.95	114.94
	Ga	18.02	15.52	18.00	17.40	18.66	15.61	14.33
	Rb	10.01	0.07	3.70	17.50	0.72	0.50	0.54
	Sr	444.40	105.00	192.30	250.70	197.94	53.30	396.49
	Y	23.78	16.04	22.48	18.28	29.36	26.85	27.81
	Zr	133.30	14.68	95.47	117.10	72.76	69.19	69.24
	Nb	27.81	0.60	7.38	9.71	4.48	4.17	4.46
	Ba	493.30	7.46	169.70	324.50	45.25	28.60	130.18
	La	37.40	0.72	10.63	16.61	4.09	3.45	3.76
	Ce	65.39	1.85	23.02	34.17	10.48	9.45	9.75
	Pr	7.29	0.37	3.10	4.00	1.72	1.59	1.64
	Nd	25.73	2.36	12.75	14.83	8.68	7.99	8.26
	Sm	4.95	1.11	3.21	3.15	2.98	2.83	2.89
	Eu	1.46	0.51	1.08	0.94	1.06	1.00	1.02
	Gd	4.61	1.72	3.47	3.07	3.68	3.48	3.55
	Tb	0.67	0.34	0.58	0.48	0.69	0.64	0.66
	Dy	4.07	2.53	3.77	3.02	4.70	4.47	4.52
	Ho	0.74	0.52	0.72	0.56	0.94	0.87	0.89
	Er	2.06	1.58	2.03	1.67	2.76	2.56	2.59
	Tm	0.31	0.25	0.32	0.26	0.45	0.42	0.43
	Yb	2.07	1.67	2.08	1.75	2.83	2.62	2.69
	Lu	0.31	0.27	0.31	0.27	0.42	0.39	0.39
	Hf	3.43	0.58	2.54	3.05	2.05	1.90	1.95
	Ta	1.63	0.04	0.45	0.66	0.29	0.27	0.27
	Pb	11.58	13.41	8.92	10.88	8.23	7.46	5.46
	Th	8.91	0.04	2.17	5.13	0.31	0.29	0.30
	U	1.63	0.01	0.52	2.39	0.10	0.09	0.12

Table C.2 – continued.

		Batch 9 fused with 0.6g of flux							
		JB-1a st9	BIR-1 st7	W2 st7	JA-2 st7	JG-3 st3	AHBD10 st5	AHBD13 st5	AHBD14 st5
Traces	Ti	1.68	0.99	1.08	0.68	0.46	1.45	1.38	1.36
	V	201.61	328.19	259.78	117.90	65.14	382.34	356.40	350.73
	^{52}Cr	475.47	469.74	119.88	451.00	26.73	161.75	134.57	151.49
	^{53}Cr	436.87	494.35	122.12	477.47	22.92	168.02	136.80	157.43
	Mn	0.15	0.18	0.17	0.10	0.06	0.24	0.27	0.23
	^{57}Fe	8.83	11.73	10.92	5.51	3.12	14.05	13.31	12.63
	Co	36.97	53.39	44.30	28.98	11.21	50.21	50.12	47.03
	^{60}Ni	94.83	227.12	89.05	151.82	26.92	92.95	87.99	89.18
	^{62}Ni	112.09	237.96	93.63	161.41	27.11	99.69	101.15	102.75
	Ga	17.87	16.03	18.03	17.70	16.76	18.77	15.98	14.27
	Rb	10.77	0.62	4.87	17.61	12.24	0.12	0.10	0.30
	Sr	584.47	108.75	193.77	255.37	397.03	199.99	54.48	394.08
	Y	24.73	16.83	22.74	18.59	17.31	29.76	27.54	27.82
	Zr	151.13	15.51	90.81	116.26	154.46	73.59	72.26	68.14
	Nb	29.48	0.58	7.24	9.27	6.25	4.52	4.25	4.06
	Ba	516.08	7.24	168.81	326.55	464.90	45.76	29.12	127.27
	La	38.12	0.73	10.64	16.76	20.64	3.98	3.50	3.71
	Ce	68.54	1.91	22.96	34.45	41.68	10.60	9.74	9.68
	Pr	7.49	0.38	3.06	4.01	4.84	1.76	1.62	1.63
	Nd	25.61	2.33	12.58	14.44	16.76	8.67	7.95	8.19
	Sm	5.14	1.11	3.27	3.20	3.40	3.01	2.83	2.87
	Eu	1.49	0.51	1.09	0.93	0.87	1.10	1.03	1.01
	Gd	4.69	1.75	3.54	3.07	3.00	3.83	3.46	3.54
	Tb	0.71	0.35	0.61	0.49	0.45	0.71	0.66	0.65
	Dy	4.01	2.52	3.71	2.89	2.65	4.70	4.37	4.45
	Ho	0.74	0.52	0.71	0.57	0.51	0.94	0.88	0.87
	Er	2.08	1.60	2.05	1.65	1.53	2.83	2.60	2.58
	Tm	0.32	0.25	0.32	0.25	0.24	0.45	0.41	0.42
	Yb	2.05	1.64	2.02	1.68	1.74	2.91	2.65	2.66
	Lu	0.32	0.25	0.31	0.27	0.28	0.43	0.41	0.40
	Hf	3.50	0.60	2.44	3.01	4.06	2.13	2.04	1.95
	Ta	1.61	0.04	0.44	0.65	0.57	0.28	0.27	0.27
	Pb	8.43	10.59	12.29	15.25	7.87	5.79	5.24	6.55
	Th	8.66	0.04	2.09	4.95	8.61	0.30	0.27	0.28
	U	1.62	0.02	0.51	2.37	2.73	0.10	0.10	0.12

Table C.2 – continued.

subsequently solved the problems encountered with the 0.2g method. Some of the samples that had been successful in the 0.2g batches were re-run with 0.4g of flux. The results showed that the 0.2g samples had very similar compositions to the 0.4g samples and thus were reliable (Tables C.2, C.3 and C.4).

The analysis of samples with both the 0.2g and 0.4g method now presented an ideal opportunity to use the data to study the effects of any contamination that the flux may introduce to the sample. The ICP-MS trace element results for both the external and internal standards made with 0.2g and 0.4g of flux were plotted against one another to identify any contamination. The results are seen in Figures C.1, C.2 and C.3. The plots in Figures C.1 and C.2 have lines of best fit that have $y= \sim 1x+c$ and $R^2= \sim 1$. An x value of 1 would indicate a 45° line of best fit thus indicating that both sets of flux samples give identical results. Figure C.1 shows the bulk results for JB-1a and AHBD10 where all the elements are plotted for a correlation. Figure C.2 presents diagrams for JB-1a and AHBD10 that show the correlation of elements at different abundances. From the figures it is clear that the x values are very close to 1 and do not show any considerable variation. The R^2 values are also close to 1 thus showing that a high percentage of the total variance of the samples is represented by the trend line.

The R^2 information can then be utilised to determine the correlation coefficient (r) values, which are used to quantify a linear relationship. Figure C.3 shows the r values for different concentrations for JB-1a and AHBD10. The r values of the samples are very close to 1 thus indicating that the 0.2g and 0.4g samples show a very strong linear relationship with little scatter. From this statistical analysis it is obvious that the flux does not significantly contaminate the sample and that the results obtained with both 0.2g and 0.4g of flux are accurate and can be interpreted together. The last batches analysed used 0.6g of flux. It is assumed that because there is no contamination in increasing the flux content from 0.2g to 0.4g then further increasing the amount of flux to 0.6g should also not contaminate the sample.

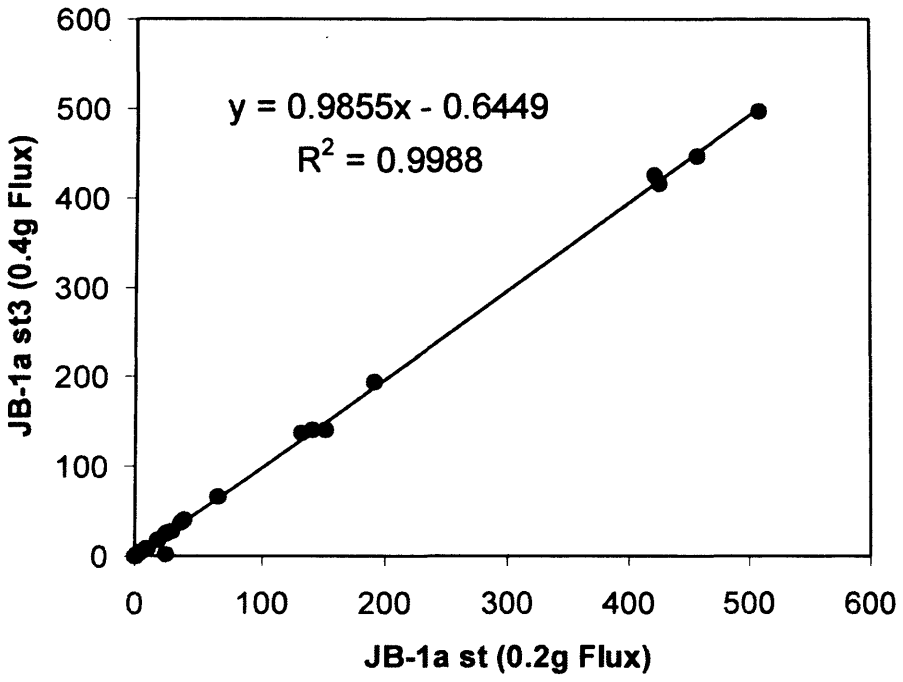

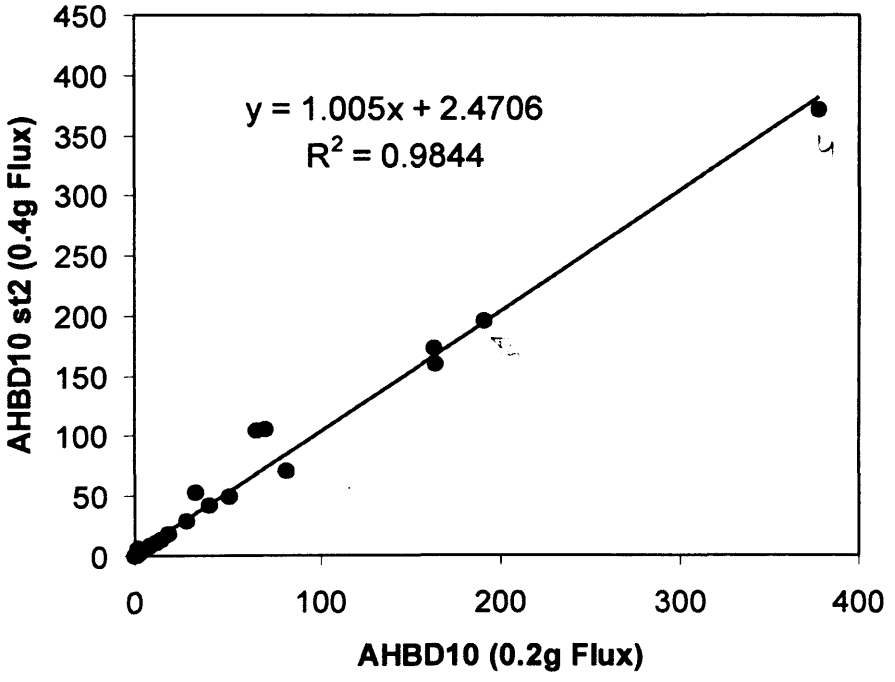

Figure C.1 – Variation diagrams showing (a) JB-1a st (0.2g flux) vs JB-1a st3 (0.4g flux); (b) AHBD10 (0.2g flux) vs AHBD10 st2 (0.4g flux). Both diagrams have a best of fit line of ~ 45° and an R^2 value of ~ 1, thus suggesting that the extra flux does not contaminate the samples.

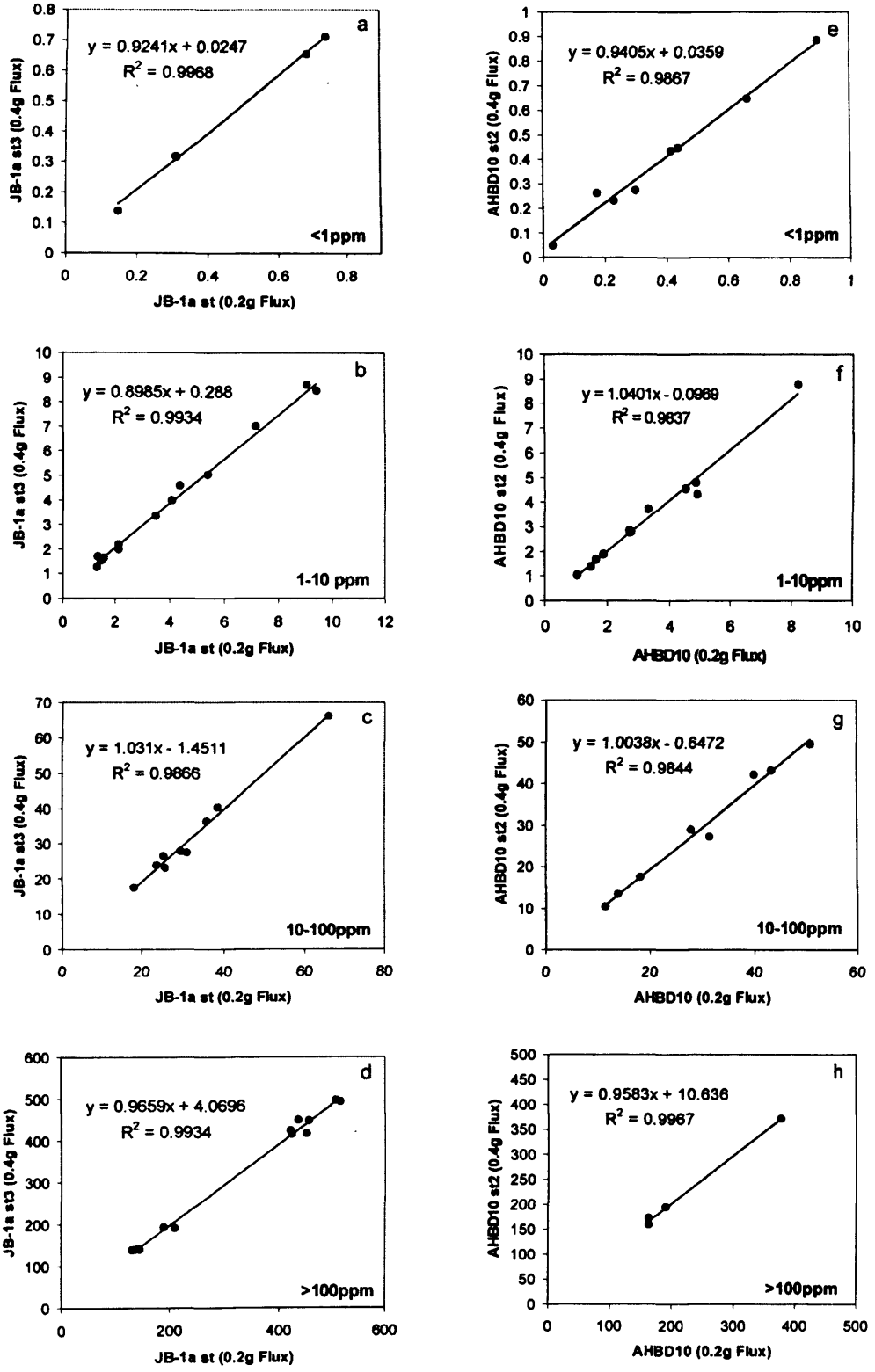

Figure C.2 – Variation diagrams showing the correlation of groups of elements at different abundances for JB-1a (a-d) and AHBD10 (e-h) when fused with 0.2g and 0.4g of flux. Note that m ~ 1 and R^2 ~ 1.

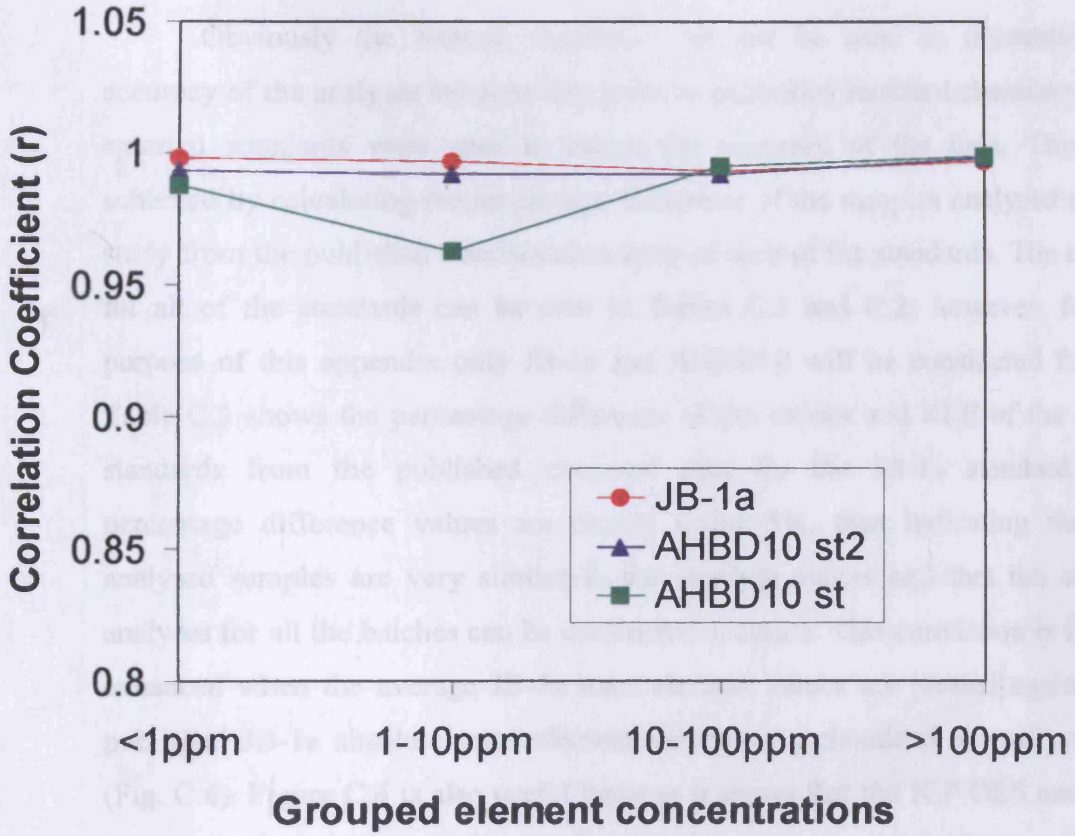

Figure C.3 - Concentration vs correlation coefficient (r) diagram showing the range of values for JB-1a, AHBD10 st2 and AHBD10 st.

C.3.3 Accuracy

Obviously the internal standards can not be used to determine the accuracy of the analyses because they have no published standard chemistry. The external standards were used to assess the accuracy of the data. This was achieved by calculating the percentage difference of the samples analysed in this study from the published standard chemistry of each of the standards. The results for all of the standards can be seen in Tables C.1 and C.2; however, for the purpose of this appendix only JB-1a and AHBD10 will be considered further. Table C.3 shows the percentage difference of the oxides and REE of the JB-1a standards from the published chemical data for the JB-1a standard. The percentage difference values are mostly under 5%, thus indicating that the analysed samples are very similar to the absolute values and that the sample analyses for all the batches can be considered accurate. This conviction is further enhanced when the average JB-1a trace element values are plotted against the published JB-1a absolute trace element values on a chondrite normalised plot (Fig. C.4). Figure C.4 is also useful because it shows that the ICP-OES and ICP-MS methods give very similar results thus indicating that both of the analytical machines produce relatively accurate data.

However it should be noted that not all of the ICP-OES and ICP-MS data displays such consistency. In some examples the ICP-OES and ICP-MS results can be slightly different and when this occurs it is the ICP-MS data that is considered to be the most accurate, due to the lower percentage difference totals, and it is these data that are used in the final interpretation. In summary, the similarity of the analysed standard samples to the published standard values suggests that the results obtained for this study are accurate.

	JB-1a published values		JB-1a st percentage difference	JB-1a st2 percentage difference	JB-1a st3 percentage difference	JB-1a st5 percentage difference	JB-1a st6 percentage difference	JB-1a st7 percentage difference	JB-1a st 8 percentage difference	JB-1a st 9 percentage difference	Average JB-1a	stdev (wt%/ppm)	rsd (%)
Oxides (wt %)													
SiO_2	**52.16**		0.5109	0.3866	3.3860	1.0125	1.3042	1.7736	1.2570	0.5717	52.8252	0.5081	0.9619
TiO_2	**1.3**		0.9361	1.4905	2.2610	2.8997	4.4795	3.8133	1.3752	3.4728	1.2861	0.0368	2.8608
Al_2O_3	**14.51**		1.9154	1.9250	2.7889	3.8924	0.2799	0.6082	2.5608	0.3215	14.7474	0.2193	1.4873
Fe_2O_3	**9.1**		0.5109	0.3866	3.0845	3.5413	1.5819	2.8246	1.4428	3.8395	8.9246	0.1540	1.7261
MnO	**0.15**		6.7425	6.6105	0.9752	0.6016	0.8043	2.0259	1.1808	3.5275	0.1508	0.0059	3.8858
MgO	**7.75**		0.5109	0.3866	2.5600	2.5431	1.9333	3.1856	3.3085	2.4427	7.9134	0.0862	1.0888
CaO	**9.23**		4.8133	2.5169	2.6479	4.7210	1.2519	2.6332	4.6483	7.3519	9.5829	0.1780	1.8575
Na_2O	**2.74**		0.5109	0.3866	26.6192	2.3144	7.6523	10.5441	13.1556	15.3444	2.4999	0.2697	10.7891
K_2O	**1.42**		0.5109	0.3866	77.0269	13.5192	66.0214	65.6618	51.4079	50.6564	0.8460	0.4465	52.7848
P_2O_5	**0.25**		6.3405	6.2090	5.7159	11.8282	7.0487	9.0421	6.7593	8.9281	0.2693	0.0051	1.9106
REE (ppm)													
La	**38.1**		5.9536	3.5635	4.2962	0.7775	6.9051	2.9516	1.8373	0.0656	37.5831	1.5257	4.0596
Ce	**66.10**		0.4731	1.8640	0.0567	0.5862	0.8777	1.1585	1.0741	3.6854	66.2187	1.1349	1.7139
Pr	**7.3**		2.4576	0.5876	3.6429	4.2836	0.5091	1.1187	0.1918	2.6315	7.2273	0.1713	2.3702
Nd	**25.5**		0.0735	1.9876	4.3049	3.6867	0.1504	0.4320	0.9020	0.4410	25.8771	0.4289	1.6573
Sm	**5.02**		7.0326	8.8361	0.3217	1.8996	1.4751	1.1265	1.3745	2.4855	5.1188	0.2006	3.9184
Eu	**1.47**		0.2606	1.9277	3.5000	1.6877	3.9858	2.0620	0.9524	1.1953	1.4951	0.0236	1.5770
Gd	**4.54**		4.1218	4.8979	1.3908	2.5474	3.8329	3.0756	1.5639	3.2128	4.5775	0.1543	3.3711
Tb	**0.69**		0.1465	3.4687	5.1983	3.7336	4.0304	1.5279	2.3188	2.7165	0.6843	0.0232	3.3856
Dy	**4.19**		3.2269	3.5140	4.5328	4.1285	0.2061	1.9813	2.9833	4.2442	4.0600	0.0598	1.4723
Ho	**0.72**		3.2735	3.9159	1.3897	0.1051	8.4670	5.3527	2.2222	2.7993	0.7421	0.0221	2.9760
Er	**2.18**		2.9734	4.8579	0.2683	1.3608	0.2660	1.7918	5.5505	4.7440	2.1235	0.0502	2.3656
Tm	**0.31**		0.5657	1.5064	3.1736	1.9442	5.4592	2.5685	0.9677	2.7062	0.3157	0.0068	2.1613
Yb	**2.1**		1.4079	2.0794	4.4973	4.6048	0.4324	2.4741	1.4286	2.1474	2.0596	0.0443	2.1487

Table C.3 – Shows the percentage difference of the oxide and REE analyses of the JB-1a standards from the published values, the average JB-1a value and the standard deviation (stdev) and relative standard deviation (rsd) of the JB-1a standards.

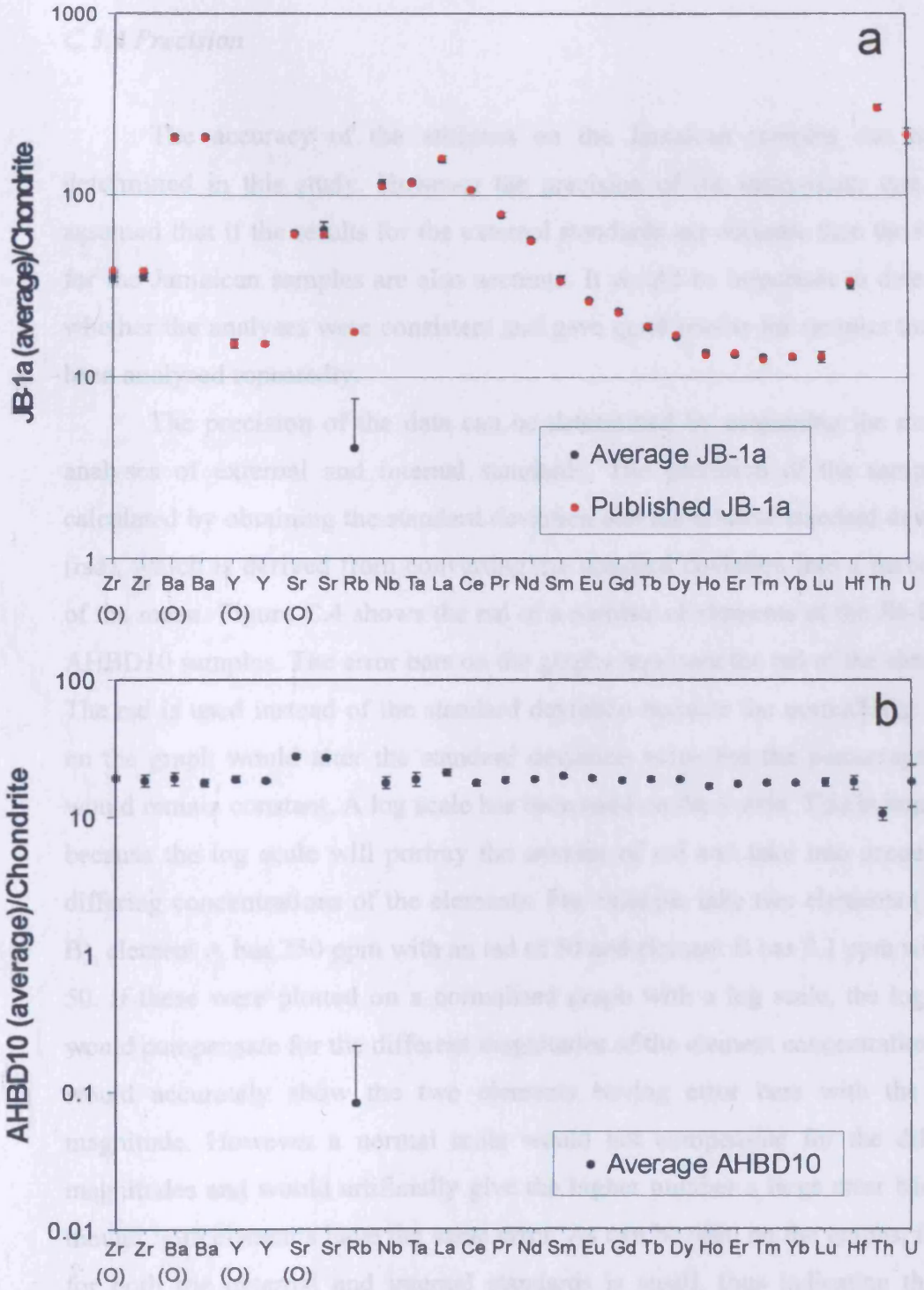

Figure C.4 – (a) JB-1a chondrite normalised plot showing data for averaged JB-1a data from this study and published JB-1a data; (b) AHBD10 chondrite normalised plot showing averaged data from this study. Elements with (O) beneath were analysed with ICP-OES, all other elements were analysed on the ICP-MS. The rsd values are represented by the error bars.

C.3.4 Precision

The accuracy of the analyses on the Jamaican samples can not be determined in this study. However the precision of the instruments can. It is assumed that if the results for the external standards are accurate then the results for the Jamaican samples are also accurate. It would be important to determine whether the analyses were consistent and gave good results for samples that had been analysed repeatedly.

The precision of the data can be determined by examining the multiple analyses of external and internal standards. The precision of the samples is calculated by obtaining the standard deviation and the relative standard deviation (rsd), which is derived from converting the standard deviation into a percentage of the mean. Figure C.4 shows the rsd of a number of elements of the JB-1a and AHBD10 samples. The error bars on the graphs represent the rsd of the elements. The rsd is used instead of the standard deviation because the normalising factor on the graph would alter the standard deviation value but the percentage (rsd) would remain constant. A log scale has been used on the y-axis. This is important because the log scale will portray the amount of rsd and take into account the differing concentrations of the elements. For example take two elements (A and B), element A has 250 ppm with an rsd of 50 and element B has 0.1 ppm with rsd 50. If these were plotted on a normalised graph with a log scale, the log scale would compensate for the different magnitudes of the element concentrations and would accurately show the two elements having error bars with the same magnitude. However a normal scale would not compensate for the different magnitudes and would artificially give the higher number a large error bar even though both elements have the same error. As can be seen on the graphs, the rsd for both the external and internal standards is small, thus indicating that the sample analyses are precise. The results also indicate that the ICP-OES results are just as precise as the ICP-MS results.

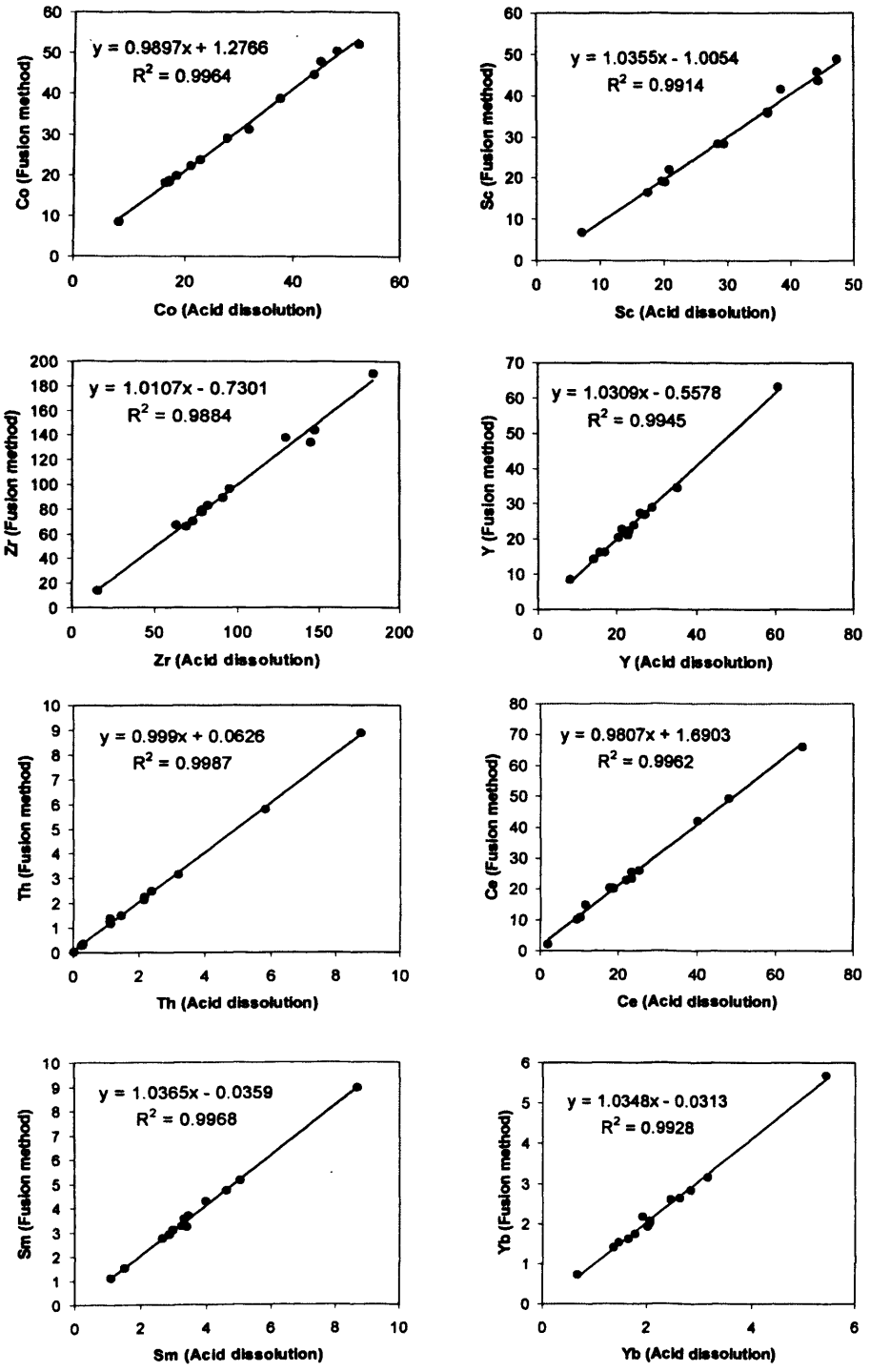

Figure C.5 – Variation diagrams plotting elements measured by both the acid dissolution and fusion methods against themselves. The ~ 45° slope of the lines of best fit and the R^2 ~ 1, indicate that samples prepared by both methods give the same results.

C.4 Fusion and acid dissolution comparison

A single batch of 14 standards and samples were prepared for analysis on the ICP-MS using the HF-HNO_3 dissolution method. This was done to: (a) provide further evidence to whether or not the flux contaminates the sample during the lithium tetraborate fusion method and (b) act as a second analytical technique to test whether the fusion results are accurate.

Variation diagrams were constructed plotting an element against itself by which it was measured using the acid dissolution and fusion methods (Figure C.5). The variation diagrams show that the elements analysed by both preparation methods have lines of best fit that have $y= \sim 1x+c$ and $R^2= \sim 1$. This indicates that the fusion method is accurate in determining the concentrations of all the elements analysed by the ICP-MS and provides further evidence that the flux does not contaminate the sample during fusion preparation.

C.5 Summary

The result of the statistical analysis performed on the analysed external and internal samples has shown that the data obtained is accurate and precise and can be relied upon during interpretation. The standards and HF-HNO3 analysis also indicate that the lithium tetraborate fusion preparation method does not contaminate the sample with any element analysed in this study.

Appendix D

Preparation and results of the radiogenic isotope (Sr, Nd, Hf and Pb) and geochronological (^{40}Ar-^{39}Ar) analysis

D.1 Sr, Nd, Hf and Pb isotope analysis

D.1.1 Sample selection

Care was taken in sample selection to choose the most unaltered samples representative of each locality and/or lithological type. The chosen samples were crushed and powdered using a clean jaw crusher and an agate ball mill at Cardiff University. The samples were then prepared for Sr, Nd, Pb and Hf isotope analysis at the NERC Isotope Geosciences Laboratories, Nottingham, UK under the supervision of Dr Ian Millar.

The samples were leached in hot 6M HCl prior to preparation in order to minimise the effects of alteration. It was hoped that the leaching would remove secondary phases and hence any potential "foreign" isotope ratio imparted into the rock. Unfortunately, the Jamaican samples are so altered that leaching was unsuccessful in some cases e.g. the Bath-Dunrobin lavas (Chapters 6 and 7). The isotopic results are presented in Table D.1 and D.2.

D.1.2 Sr, Nd and Pb preparation and analysis

Determinations of Sr, Nd and Pb isotopes followed the procedures of Kempton (1995) and Royse *et al.* (1998). Samples were leached in 6M HCl prior to analysis. $^{87}Sr/^{86}Sr$ ratios are normalised to $^{86}Sr/^{88}Sr = 0.1194$, and $^{143}Nd/^{144}Nd$ ratios are normalised to $^{146}Nd/^{144}Nd = 0.7219$. Sr was loaded on single Re filaments using a TaO activator, and run using static multicollection on Finnigan MAT262 (NBS987 = 0.710214 ± 0.000028, 2σ, n=14) and Triton (NBS987 = 0.710230 ± 0.000018, 2σ, n=40) mass spectrometers. All Sr isotope data are quoted relative to a value of 0.710240 for the NBS987 standard. Nd was run as the metal species using double Re-Ta filaments on a Finnigan Triton mass spectrometer. Replicate analysis of the in-house J&M standard gave a value of 0.511184 ± 0.000022, 2σ, n=24); Nd isotope data are reported relative to a value of 0.511123 for this standard, equivalent to a value of 0.511864 for La Jolla.

Pb isotopes were analysed on a VG Axiom MC-ICP-MS, with mass fractionation corrected within-run using a Tl-doping method (Thirlwall, 2002), using a $^{203}Tl/^{205}Tl$ value of 0.41876, which was determined empirically by cross calibration with NBS 981. On the basis of repeated runs of NBS981, the reproducibility of whole rock Pb isotope measurements is better than 0.02% (2σ). Blank contribution was less than 100 pg.

D.1.3 Hf preparation and analysis

For Hf isotope analysis, samples were fused with Li-metaborate flux, and dissolved in 3M HCl. Hf was separated using a single column procedure using LN-Spec resin, following Münker *et al.* 2001, and run on a Nu-Plasma multicollector ICP-MS. Hf blanks are < 100pg. Correction for Lu and Yb was carried out using reverse-mass-bias correction of empirically predetermined $^{176}Yb/^{173}Yb$ (0.7950) and $^{176}Lu/^{175}Lu$ (0.02653). Replicate analyses of the JMC475 standard across the period of analysis gave $^{176}Hf/^{177}Hf = 0.282174 \pm 0.000010$ (2σ, n=37); reported data are

	Age (Ma)	Lu ppm	Hf ppm	$^{176}Lu/^{177}Hf$	$^{176}Hf/^{177}Hf$ measured	$^{176}Hf/^{177}Hf$ initial	εHf(i)	Sm ppm	Nd ppm	$^{147}Sm/^{144}Nd$	$^{143}Nd/^{144}Nd$ measured	$^{143}Nd/^{144}Nd$ initial	εNd(i)
AHAR02	64	0.24	4.27	0.0080	0.28307	0.28306	11.64	3.08	17.46	0.107	0.51290	0.51286	5.92
AHAR16	70.5	0.35	1.95	0.0255	0.28310	0.28306	11.86	3.82	16.31	0.141	0.51293	0.51286	6.15
AHAR18	70.5	0.24	1.97	0.0172	0.28310	0.28308	12.34	2.93	13.46	0.132	0.51294	0.51288	6.40
AHBD10	88.5	0.46	1.87	0.0347	0.28314	0.28308	12.77	2.83	8.55	0.200	0.51310	0.51298	8.97
AHBD16	88.5	0.39	1.79	0.0294	-	-	-	2.55	7.82	0.197	0.51305	0.51294	8.06
AHBD18	88.5	0.49	2.02	0.0327	-	-	-	2.99	9.02	0.201	0.51303	0.51291	7.56
AHBD19	88.5	0.32	1.68	0.0271	0.28311	0.28307	12.44	2.63	7.61	0.209	0.51309	0.51296	8.60
AHBD23	88.5	0.30	1.40	0.0303	0.28312	0.28307	12.63	1.95	6.00	0.196	0.51308	0.51297	8.72
AHBD28	88.5	0.36	1.63	0.0317	0.28311	0.28305	11.99	2.50	7.75	0.195	0.51305	0.51293	8.01
AHBI01	120	0.49	2.16	0.0324	0.28318	0.28311	14.65	3.56	10.41	0.207	0.51311	0.51295	9.03
AHBI03	120	0.51	2.22	0.0323	0.28319	0.28312	14.97	3.41	9.86	0.209	0.51309	0.51293	8.64
AHBI13	120	0.45	2.07	0.0308	0.28316	0.28309	13.80	5.50	23.31	0.143	0.51301	0.51290	8.12
AHBI27	120	0.74	4.14	0.0254	0.28313	0.28307	13.22	4.62	14.47	0.193	0.51307	0.51292	8.50
AHCI21	79.5	0.98	5.36	0.0260	0.28315	0.28211	13.66	8.95	33.69	0.161	0.51301	0.51293	7.68
AHCI37	79.5	0.20	1.83	0.0152	0.28313	0.28311	13.60	3.18	14.12	0.136	0.51298	0.51291	7.21
AHCI43	79.5	0.34	2.07	0.0233	0.28312	0.28309	12.97	3.66	13.87	0.160	0.51302	0.51294	7.90
AHCI56	79.5	0.33	1.80	0.0258	0.28314	0.28310	13.31	3.07	10.43	0.178	0.51307	0.51298	8.57
AHCI72	79.5	0.35	1.79	0.0274	0.28317	0.28312	14.27	3.01	9.15	-	-	-	-
AHCI74	79.5	0.36	2.12	0.0243	0.28315	0.28311	13.92	3.56	12.03	0.179	0.51305	0.51296	8.29
AHHB03	51.65	0.26	2.80	0.0134	0.28307	0.28306	11.35	4.75	17.07	0.168	0.51298	0.51292	6.80
AHHB07	51.65	0.26	3.15	0.0116	0.28308	0.28307	11.54	5.35	21.24	0.152	0.51297	0.51292	6.77
AHSUN105	70.5	0.28	1.82	0.0220	0.28313	0.28310	13.14	5.27	22.91	0.139	0.51298	0.51292	7.24
AHWG12	51.65	0.13	3.23	0.0056	0.28309	0.28308	12.23	1.22	5.95	0.124	0.51294	0.51289	6.31
AHWG19	51.65	0.15	3.22	0.0064	0.28309	0.28308	12.03	1.75	9.39	0.113	0.51292	0.51288	6.05
AHWG21	51.65	0.13	3.21	0.0058	0.28309	0.28309	12.34	1.54	7.49	0.125	0.51293	0.51289	6.17
AHWG32	51.65	0.10	3.13	0.0046	0.28310	0.28309	12.48	1.68	9.71	0.104	0.51297	0.51293	7.02
AHWG33	51.65	0.11	3.28	0.0047	0.28309	0.28309	12.26	1.64	9.20	0.108	0.51296	0.51292	6.78

Table D.1 – Nd and Hf isotopic data for the Jamaican igneous rocks.

	Age	Rb ppm	Sr ppm	$^{87}Sr/^{86}Sr$ measured	$^{87}Sr/^{86}Sr$ initial	Th ppm	U ppm	Pb ppm	$^{206}Pb/^{204}Pb$ measured	$^{207}Pb/^{204}Pb$ measured	$^{208}Pb/^{204}Pb$ measured	$^{206}Pb/^{204}Pb$ initial	$^{207}Pb/^{204}Pb$ initial	$^{208}Pb/^{204}Pb$ initial
AHAR02	64	7.34	745.88	0.70770	0.70768	6.27	2.65	3.32	19.334	15.617	39.015	18.818	15.593	38.614
AHAR16	70.5	54.12	761.58	0.70362	0.70341	1.81	0.64	17.43	19.088	15.597	38.819	19.062	15.596	38.794
AHAR18	70.5	40.57	672.19	0.70372	0.70355	2.48	0.92	17.48	18.988	15.603	38.726	18.951	15.601	38.694
AHBD10	88.5	0.03	192.56	0.70348	0.70345	0.28	0.13	3.98	19.093	15.557	38.661	19.065	15.556	38.640
AHBD16	88.5	0.03	74.33	0.70379	0.70370	0.24	0.10	2.75	19.854	15.567	39.055	19.822	15.566	39.028
AHBD18	88.5	1.56	30.07	0.70460	0.70437	0.31	0.16	1.05	19.170	15.574	38.761	19.037	15.568	38.674
AHBD19	88.5	1.90	1030.94	0.70513	0.70512	0.29	0.14	8.27	19.685	15.587	38.852	19.670	15.586	38.841
AHBD23	88.5	0.58	48.93	0.70574	0.70560	0.19	0.11	3.46	19.394	15.604	38.876	19.364	15.603	38.860
AHBD28	88.5	0.12	57.96	0.70553	0.70541	0.24	0.11	4.79	19.688	15.542	38.960	19.668	15.541	38.945
AHBI01	120	3.75	116.57	0.70455	0.70439	0.35	0.28	1.41	18.703	15.558	38.158	18.467	15.547	38.061
AHBI03	120	3.19	138.40	0.70452	0.70441	0.34	0.28	1.90	18.704	15.559	38.177	18.528	15.550	38.108
AHBI13	120	2.27	524.62	0.70428	0.70426	1.43	1.10	0.54	18.977	15.573	38.240	16.515	15.454	37.188
AHBI27	120	0.64	28.42	0.70456	0.70445	0.79	0.78	7.44	18.877	15.566	38.227	18.752	15.560	38.186
AHCI21	79.5	0.27	324.26	0.70331	0.70325	1.51	0.84	2.90	18.713	15.580	38.285	18.485	15.569	38.150
AHCI37	79.5	14.08	609.83	0.70341	0.70337	2.20	0.79	1.68	18.716	15.582	38.316	18.343	15.564	37.978
AHCI43	79.5	6.39	605.44	0.70330	0.70326	1.30	0.48	4.66	18.652	15.572	38.316	18.571	15.568	38.244
AHCI56	79.5	6.39	538.21	0.70350	0.70346	0.69	0.36	4.34	18.610	15.576	38.286	18.545	15.573	38.244
AHCI72	79.5	2.48	383.82	0.70355	0.70350	0.44	0.20	5.24	18.593	15.581	38.247	18.563	15.580	38.225
AHCI74	79.5	5.70	570.87	0.70344	0.70341	0.47	0.27	14.12	18.619	15.567	38.217	18.603	15.567	38.209
AHHB03	51.65	0.21	97.22	0.70485	0.70484	2.32	0.57	4.67	19.504	15.627	39.272	19.440	15.624	39.186
AHHB07	51.65	0.68	167.20	0.70460	0.70459	2.53	0.72	6.17	19.017	15.608	38.721	18.956	15.605	38.651
AHSUN105	70.5	13.95	1910.26	0.70404	0.70402	3.02	1.13	5.30	18.862	15.591	38.620	18.711	15.584	38.488
AHWG12	51.65	9.56	160.30	0.70431	0.70418	2.68	0.39	5.09	19.402	15.614	39.043	19.362	15.613	38.953
AHWG19	51.65	6.00	96.96	0.70481	0.70468	3.04	0.98	5.35	20.183	15.647	39.945	20.085	15.643	39.846
AHWG21	51.65	2.13	75.51	0.70485	0.70479	2.75	0.90	4.20	21.355	15.709	41.259	21.237	15.704	41.141
AHWG32	51.65	3.74	141.19	0.70482	0.70476	3.03	0.94	8.44	19.629	15.614	39.138	19.570	15.612	39.076
AHWG33	51.65	2.22	137.69	0.70452	0.70448	2.91	0.88	7.33	23.586	15.790	42.961	23.516	15.786	42.885

Table D.2 – Sr and Pb isotopic data for the Jamaican igneous rocks.

normalised to a preferred value of 0.282160 (Nowell & Parrish, 2001). Replicate analyses of BCR-1 gave a mean value of 0.282872 ± 0.000009 (2σ, n=4), comparable to previously reported values 0.282879 ± 0.000008 (Blichert-Toft, 2001). Replicate analyses of the in-house standard PK-g-D12 gave 0.283050 ± 0.000005 (2σ, n=5), comparable to previously reported values of 0.283049 ± 0.000018 (2σ, n=27; Kempton *et al.*, 2002) and 0.283046 ± 0.000016 (2σ, n=9; Nowell *et al.*, 1998).

D.2 ^{40}Ar - ^{39}Ar geochronological analysis

D.2.1 The argon method

Argon dating is a radiometric dating technique which is similar to the potassium-argon (K-Ar) radiometric dating method, where ^{40}K decays to stable ^{40}Ar over time. The K-Ar method assumes that all of the ^{40}Ar is derived from the radioactive decay of ^{40}K and that no ^{40}Ar has been added or removed. This assumption may not be feasible for the Jamaican samples because (i) ^{40}Ar is a gaseous element and (ii) the samples in this study have been modified by post-eruption alteration processes. Additionally, K and Ar abundances are needed for K-Ar age determinations; however, the abundances of each element are analysed from different aliquots of sample, therefore, sample heterogeneity could produce significant errors in the dating technique.

With the argon technique ^{39}K is converted to ^{39}Ar by bombarding the sample with neutrons in a nuclear reactor (irradiating). The sample is then degassed in a high-vacuum mass spectrometer by using a laser or resistance furnace to obtain the $^{39}Ar/^{40}Ar$ ratio. This negates the need for determining elemental abundances and reduces analytical error because isotopic ratios are more accurately determined than absolute abundances. During the analysis the argon gas can be extracted from the sample in two ways. Incremental step heating releases argon from different reservoirs within the sample by gradually increasing the temperature in a series of steps until total fusion is achieved. An age can be obtained from each step which

enables alteration and magmatic ages to be identified. The second method involves total fusion which fuses the sample in one step to release all of the argon thus obtaining the total fusion age. The step heating method is useful in aging altered igneous rocks because the alteration age can be identified and discounted from the magmatic age.

D.2.2. Sample selection

K-rich mineral phases, such as feldspar and biotite, and rock groundmasses are used for the argon dating analysis. It is advantageous to use samples which lack secondary K-rich phases, such as sericite, because they would contain excess argon and give younger ages. All of the Jamaican igneous rocks are variably altered; consequently, the samples chosen for analysis include AHAR02, AHAR14, AHBD07, AHBD10, AHCI37, AHCI39 and AHWG03, which were some of the least altered samples (Table D.3).

D.2.3. Mineral separation

Feldspar, biotite and groundmass separates were used in the Jamaican argon analysis. To obtain the groundmass the sample was firstly crushed in a jaw crusher so that the sample grain size was not less than ~ 2000 μm. The sample was then sieved to obtain material which was > 100 μm. This removes the fines and dust because after irradiation very fine-grained (<100 μm) separates become radioactive powder and present serious concerns for contamination and health hazard in the laboratory. The sample is then ground in an agate tema mill to reduce the remainder of the sample to < 500 μm. The sample is further sieved to split the sample up into 200-300 μm and 300-500 μm aliquots. The Jamaican lavas were not particularly coarse; therefore, the 200-300 aliquots were used for the analysis.

To remove altered material the samples are leached in 3N HNO_3 for 20 minutes in an ultrasonic bath at ~ 50°C and this is repeated until the solution becomes clear. The separates are then rinsed in de-ionised water and placed in an ultrasonic bath for ~ 10 minutes. This process is again repeated until the water

becomes clear. The samples are then dried and handpicked to remove any altered grains. 200-300 mg of sample was obtained for the analysis.

The aforementioned process is used for the plagioclase and biotite preparation. However, a Frantz Isodynamic Separator (FIS) is used prior to removing the altered material. The FIS magnetically separates the samples into aliquots of differing minerals. This enables the plagioclase and biotite to be separated from the other minerals. After the HNO_3 acid rinsing the plagioclase separates are also leached in 7% HF for 5 minutes to remove the secondary alteration products.

D.2.4 Irradiation and analysis

Approximately 20-90 handpicked mineral grains per sample were wrapped in copper foil and placed in quartz vials. The vials were irradiated for 18 hours at 1 MW in the cadmium-shielded CLICIT facility at the Oregon State University TRIGA reactor. The samples were then left to cool for ~ 3 months before any further preparation.

At the Scottish Universities Environmental Research Centre (SUERC) Dr Dan Barfod loaded the samples into a resistance furnace and laser for step heating analysis. All the data were acquired with an Argus multi-collector mass spectrometer in static collection mode.

D.2.5 Results

The results of the argon dating analysis can be seen in Table D.3. Unfortunately data for samples AHBD07, AHBD10 and AHCI37 are not available because of a mistake by the staff at SUERC. ^{37}Ar is required to correct for excess ^{36}Ar which is produced by irradiation of Ca in the nuclear reactor. Unfortunately ^{37}Ar only has a half life of 35.1 days and the samples for this study were analysed at such a late stage that the aforementioned samples lacked enough ^{37}Ar for the correction.

Sample	Run	material	rock type	extraction method	mass (mg) or [no. of grains]	J	total fusion age (Ma)	1s	%^{40}Ar ATM (total)
AHAR02	G	biotite	granodiorite	laser	[~20]	0.003152	63.5	0.7	4.2
	K	biotite	granodiorite	laser	[~20]	0.003152	63.2	2.5	6.3
AHAR14		plagioclase	andesite	furnace	69	0.003153	69.0	0.8	
AHBD07		plagioclase	microgranite	furnace	66	0.003155	25.2	0.3	
AHBD10	C	groundmass	basalt	furnace	59	0.003157	150.5	1.9	67.0
	D	groundmass			48		113.8	1.3	58.4
AHCI37		plagioclase	andesite	furnace	91	0.003158	-	-	
AHCI39		plagioclase	basaltic andesite	furnace	61	0.003160	79.7	0.9	
AHWG03	8A	groundmass	adakite	furnace	38	0.003163	51.1	0.6	
	8B	groundmass	adakite		22	0.003163	51.5	0.6	7.7

Table D.3 – ^{40}Ar – ^{39}Ar geochronological data for the Jamaican igneous rocks.

Sample	Run	plateau age (Ma)	1s	% of ^{39}Ar	MSWD	N	isochron age (Ma)	1s	$^{40}Ar/^{36}Ar$ (i)	1s	MSWD	N
AHAR02	G	64.3	0.53	66	0.9		63.7	1.0	162	350	32	6
	K	-	-	-	-		66.3	0.7	8	37	27	11
AHAR14		68.9	0.42	62	1.7	10	70.5	2.1	274	37	29	23
AHBD07		-	-	-	-		-	-	-	-	-	
AHBD10	C	-	-	-	-		-	-	-	-	-	
	D	-	-	-	-		-	-	-	-	-	
AHCI37		-	-	-	-		-	-	-	-	-	
AHCI39		80.3	0.5	75	0.7	13	79.5	2.7	406	77	35	20
AHWG03	8A	53.0	0.35	61	0.5	7	51.7	1.0	292	12	19	18
	8B	52.6	0.32	65	1.1	10	51.6	1.1	278	22	37	23

Table D.3 continued.

Appendix E

Major and trace element data for the Cretaceous and Tertiary Jamaican igneous rocks and their variation diagrams

E.1 Introduction

8 batches of samples were run on the ICP-OES and ICP-MS at Cardiff University, United Kingdom. A full list of external and internal standards used in the analyses can be found in Appendix C. For each batch approximately 25 Jamaican samples were analysed. Problems associated with the preparation method meant that not all of the Jamaican samples gave publishable totals (Appendix C). However, 155 Cretaceous and Tertiary Jamaican igneous rocks were analysed successfully. The number of rocks analysed from each area include:

- 60 from the Central Inlier.
- 24 from the Benbow Inlier.
- 19 from the Above Rocks Inlier.
- 20 from the Bath-Dunrobin Formation.
- 19 from the Newcastle Volcanic Formation.
- 11 from the Halberstadt Volcanic Formation.
- 2 from the Sunning Hill Inlier.

The location from which each sample was collected can be found in detailed locality maps and grid references in Appendix A. A detailed petrogenesis for each sample

and its associated suite can be found in Chapters 4, 6, 7 and 8. This appendix lists the raw major element, trace element and isotopic data for each of the samples analysed.

Sections E.2 – E.8 list the raw ICP-MS and ICP-OES data obtained by analysing the igneous rocks from the Benbow, Central, Above Rocks, Sunning Hill inliers and the Bath-Dunrobin, Newcastle Volcanic and Halberstadt Volcanic Formations. The oxides and LOI for each sample are within 1.5% of a 100% total, any sample which was outside this 1.5% value was either re-run or removed from the data. Sc, V, Cr, Co, Ni, Cu, Zn, Sr, Y, Zr and Ba are analysed by the ICP-MS and ICP-OES, however, during the interpretation of the data in Chapters 5, 6 and 7 only the ICP-MS data is used due to it being statistically more accurate and precise (Appendix C).

Sections E.9 – E.14 are composed of major and trace element variation diagrams for the igneous rocks from the Benbow, Central, Above Rocks, Sunning Hill inliers and the Bath-Dunrobin, Newcastle Volcanic and Halberstadt Volcanic Formations. Zr is used as the abscissa in all of the variation diagrams apart from those of the Newcastle Volcanic Formation where Nb is used due to Zr being buffered in the adakitic magmas. Zr and Nb are utilised because they are immobile elements and can be analysed accurately and precisely by ICP-MS. If an element produces a good correlation with Zr or Nb on these variation diagrams it is considered immobile. A correlation can be a straight or curved line depending on whether the element is incompatible and/or compatible during fractional crystallisation. A poor correlation suggests that either there are several different rock suites with different mantle or crustal sources and/or the element in question has been mobilised (Chapters 6 and 7).

E.2 Central Inlier samples

		AHCI03	AHCI04	AHCI05	AHCI06	AHCI07	AHCI08	AHCI09	AHCI09a	AHCI10	AHCI11	AHCI12
ICP-OES analysis	Majors (wt %)											
	SiO_2	52.64	51.45	52.09	55.59	56.93	59.00	57.52	53.54	49.91	50.51	56.45
	TiO_2	0.87	0.63	0.86	0.67	0.64	0.64	0.39	0.39	0.53	0.62	0.51
	Al_2O_3	18.21	17.93	19.08	17.95	18.88	18.51	18.40	17.02	19.42	20.36	17.86
	Fe_2O_3	9.69	8.09	9.31	8.35	7.19	6.52	3.89	4.39	8.12	6.85	5.18
	MnO	0.17	0.14	0.15	0.16	0.21	0.23	0.09	0.14	0.18	0.16	0.14
	MgO	2.58	3.24	3.83	3.66	3.09	3.12	2.86	3.32	3.44	2.19	3.38
	CaO	8.44	8.10	7.65	6.30	7.97	7.09	5.63	8.54	5.54	5.95	3.95
	Na_2O	2.65	3.94	1.82	3.06	2.71	2.65	2.76	2.73	6.12	6.49	3.26
	K_2O	0.13	0.12	0.06	0.42	0.27	0.20	2.05	2.31	1.43	1.52	1.82
	P_2O_5	0.23	0.16	0.19	0.15	0.17	0.18	0.14	0.14	0.47	0.30	0.14
	LOI	4.73	5.42	3.88	3.76	2.26	2.04	5.95	5.95	3.53	5.32	5.66
	Total	100.32	99.22	98.93	100.09	100.32	100.18	99.68	98.46	98.68	100.26	98.35
	Traces (ppm)											
	Sc	22.20	15.85	24.97	18.43	19.97	18.65	10.36	10.65	12.61	16.23	13.39
	V	137.59	167.80	208.21	146.33	186.28	147.36	86.94	90.40	151.44	146.04	103.12
	Cr	15.28	11.42	11.64	20.37	8.37	15.92	13.73	7.78	10.81	3.05	12.10
	Co	22.68	19.84	24.78	20.75	20.54	18.31	12.95	16.08	21.40	17.11	17.69
	Ni	7.04	11.21	15.52	14.72	17.16	20.88	2.17	6.55	22.23	13.34	3.06
	Cu	10.85	19.78	39.65	161.17	63.85	13.71	37.63	21.36	56.76	55.31	30.48
	Zn	12.45	72.08	45.65	16.25	30.54	15.24	78.72	98.38	107.39	94.14	79.09
	Sr	591.51	391.37	480.91	564.01	668.22	631.60	703.82	655.36	820.85	1102.06	593.88
	Y	21.32	20.05	19.90	20.77	16.39	14.54	14.52	15.12	19.63	20.10	21.44
	Zr	85.67	67.24	78.52	71.86	95.02	71.30	104.61	84.43	121.36	106.58	116.46
	Ba	783.11	24.70	304.28	442.01	646.21	602.88	1168.38	1086.34	470.24	253.81	1181.15
ICP-MS analysis	Traces (ppm)											
	Ti	0.82	0.66	0.82	0.64	0.62	0.59	0.40	0.40	0.54	0.68	0.52
	V	148.90	176.74	213.00	161.64	198.25	158.15	86.40	91.85	139.61	140.77	111.49
	^{52}Cr	12.53	11.89	6.35	4.06	6.91	13.33	11.51	6.76	9.72	1.96	10.34
	^{53}Cr	15.60	19.44	11.15	5.10	11.58	16.02	18.98	14.99	10.35	2.99	17.20
	Mn	0.16	0.14	0.15	0.16	0.21	0.23	0.09	0.13	0.17	0.16	0.14
	^{57}Fe	9.73	8.61	9.08	8.15	7.28	6.45	4.04	4.54	7.35	6.72	5.32
	Co	24.56	23.25	25.68	22.68	22.31	18.44	15.11	18.18	20.07	16.61	20.21
	^{60}Ni	8.82	339.00	0.16	19.02	25.34	6.41	-23.58	-12.68	20.30	14.23	-29.33
	^{62}Ni	13.24	280.74	4.26	22.00	27.30	9.34	-11.88	-4.50	20.60	13.18	-18.15
	Zn	44.35	-	48.43	40.30	58.31	50.17	-	-	93.01	88.08	-
	Ga	16.95	21.37	19.01	16.19	18.77	17.62	18.47	18.10	19.53	21.26	17.68
	Rb	0.38	-	0.17	3.46	1.71	0.86	-	-	5.05	4.43	-
	Sr	586.21	388.39	480.43	571.39	677.69	605.96	665.39	612.80	861.20	1295.21	572.21
	Y	22.60	19.97	21.23	21.10	17.27	15.15	14.47	14.95	17.53	18.17	21.13
	Zr	82.93	62.93	81.67	70.99	94.98	70.47	100.12	80.63	107.92	99.87	114.01
	Nb	1.98	1.56	1.58	1.55	2.08	1.53	7.12	7.38	3.25	2.38	9.37
	Ba	774.64	24.70	297.51	448.03	651.29	601.45	1168.38	1086.34	458.33	251.14	1181.15
	La	7.43	7.91	6.40	7.02	15.28	10.55	36.34	29.81	32.65	21.21	26.87
	Ce	18.37	18.59	16.38	14.12	32.96	24.25	47.41	43.05	66.83	46.97	42.26
	Pr	2.79	2.80	2.49	2.20	4.45	3.36	6.85	5.49	8.51	6.12	5.21
	Nd	13.27	12.26	12.16	10.52	19.18	14.66	23.28	19.08	32.73	24.44	18.83
	Sm	3.29	3.21	3.15	2.74	3.90	3.12	4.26	3.52	6.17	5.01	3.95
	Eu	1.19	1.04	1.05	0.96	1.23	1.08	1.39	1.13	1.72	1.39	1.30
	Gd	3.42	3.11	3.31	2.97	3.46	2.79	3.36	2.99	4.00	3.63	3.52
	Tb	0.53	0.51	0.51	0.48	0.46	0.39	0.47	0.42	0.55	0.53	0.53
	Dy	3.50	3.21	3.31	3.15	2.74	2.44	2.59	2.41	3.03	3.09	3.30
	Ho	0.67	0.64	0.62	0.61	0.49	0.45	0.47	0.46	0.53	0.57	0.64
	Er	2.18	1.92	2.01	2.01	1.58	1.39	1.32	1.30	1.50	1.60	1.84
	Tm	0.33	0.29	0.31	0.31	0.24	0.20	0.20	0.21	0.22	0.23	0.30
	Yb	2.14	1.97	2.00	2.01	1.57	1.36	1.34	1.37	1.46	1.62	1.99
	Lu	0.37	0.31	0.35	0.33	0.28	0.27	0.17	0.18	0.24	0.26	0.28
	Hf	2.19	1.68	2.20	1.97	2.50	1.88	2.49	2.09	2.14	2.36	3.00
	Ta	0.11	0.08	0.10	0.09	0.12	0.10	0.47	0.49	0.08	0.07	0.62
	Pb	2.57	17.41	3.06	3.67	9.32	5.92	8.17	8.21	4.02	0.67	8.32
	Th	0.90	0.72	0.89	0.68	3.39	2.06	6.56	6.35	3.66	3.29	6.93
	U	0.36	0.33	0.34	0.35	1.38	0.92	1.26	0.94	1.04	1.05	1.37

Appendix E: Major and trace element data for the Cretaceous and Tertiary Jamaican igneous rocks and their variation diagrams

		AHCI13	AHCI14	AHCI15	AHCI16	AHCI18	AHCI19	AHCI20	AHCI21	AHCI22	AHCI23	AHCI24
ICP-OES analysis	Majors (wt %)											
	SiO_2	55.72	52.11	47.02	50.93	62.18	45.55	45.14	54.13	48.35	56.09	48.88
	TiO_2	0.52	1.65	1.18	1.78	0.40	1.27	1.25	2.02	1.16	0.62	1.33
	Al_2O_3	18.08	14.37	17.53	14.76	16.63	18.45	19.06	15.39	17.66	17.09	19.22
	Fe_2O_3	5.55	10.85	9.75	12.36	4.64	10.03	11.02	11.76	10.26	7.35	11.50
	MnO	0.12	0.20	0.22	0.25	0.06	0.21	0.15	0.15	0.15	0.21	0.15
	MgO	4.01	3.40	3.91	3.89	1.28	5.27	4.96	3.71	4.17	2.24	4.80
	CaO	4.80	7.83	9.48	5.75	3.13	7.05	10.69	6.24	10.43	5.07	10.40
	Na_2O	3.18	2.74	2.91	4.73	5.90	4.28	2.37	4.42	2.89	3.50	2.17
	K_2O	1.91	0.09	0.79	0.40	0.63	1.87	0.22	0.10	0.13	1.60	0.12
	P_2O_5	0.13	0.52	0.21	0.47	0.29	0.19	0.22	0.56	0.22	0.17	0.24
	LOI	4.69	6.12	5.89	4.54	3.38	6.14	5.00	1.87	4.34	5.07	2.56
	Total	98.71	99.88	99.88	99.86	98.53	100.33	100.08	100.33	99.76	99.02	101.37
	Traces (ppm)											
	Sc	13.23	38.78	35.11	38.79	8.27	34.39	36.83	43.65	33.77	18.46	36.52
	V	110.45	345.74	265.09	387.57	17.63	301.32	346.26	381.04	324.46	75.95	343.21
	Cr	13.41	9.12	13.45	10.04	2.83	12.93	17.59	6.22	19.27	4.02	21.90
	Co	17.87	19.37	37.64	28.09	7.47	31.58	25.61	27.50	23.87	15.11	27.53
	Ni	1.46	23.23	28.48	20.14	27.06	21.20	15.20	12.15	18.60	12.02	23.29
	Cu	133.51	321.24	139.66	192.47	43.27	19.24	22.23	365.91	85.99	42.08	48.42
	Zn	96.14	79.50	74.77	100.48	64.28	96.81	43.67	2.48	26.40	112.10	7.53
	Sr	706.02	456.75	613.73	397.45	399.60	381.95	533.53	331.92	657.41	495.63	586.62
	Y	28.14	58.38	27.56	55.53	25.64	30.09	26.65	61.83	26.78	27.47	27.75
	Zr	118.91	154.04	89.27	165.22	92.78	94.65	87.95	176.07	88.69	75.29	99.87
	Ba	1285.14	125.50	368.54	151.76	336.13	277.70	183.22	84.69	168.61	605.76	297.55
ICP-MS analysis	Traces (ppm)											
	Ti	0.52	1.76	1.17	1.87	0.44	1.33	1.28	1.96	1.20	0.64	1.29
	V	113.20	335.26	251.63	359.56	21.96	286.82	331.06	387.99	322.85	71.79	356.43
	^{52}Cr	11.19	8.07	19.70	18.74	0.41	15.19	18.91	5.36	20.47	2.03	18.43
	^{53}Cr	18.13	16.17	24.24	18.23	1.93	16.18	27.47	4.63	29.82	1.44	23.93
	Mn	0.12	0.20	0.21	0.24	0.05	0.21	0.15	0.14	0.14	0.20	0.15
	^{57}Fe	5.51	11.51	9.45	11.69	4.57	9.74	11.67	11.96	10.62	7.03	11.76
	Co	18.64	11.87	35.94	17.71	6.15	28.41	24.85	18.21	23.64	14.08	25.27
	^{60}Ni	-25.91	358.45	198.81	19.70	25.14	23.72	349.18	9.70	363.35	9.45	7.00
	^{62}Ni	-6.90	309.78	172.73	17.95	26.37	22.03	303.11	12.45	303.43	10.12	20.65
	Zn	-	-	50.23	73.79	42.18	64.51	-	69.24	-	45.03	40.24
	Ga	18.84	19.52	15.23	18.78	17.52	18.75	22.51	14.81	20.23	17.02	19.60
	Rb	-	-	4.59	1.93	2.73	9.18	-	0.27	-	5.60	0.18
	Sr	658.31	450.44	587.93	397.01	419.31	394.16	520.44	324.26	633.78	520.12	583.39
	Y	27.42	56.04	25.26	50.73	24.36	28.30	26.42	63.09	25.92	25.50	28.39
	Zr	114.10	156.15	80.03	153.50	87.69	89.30	84.13	190.31	81.92	71.86	101.64
	Nb	9.24	3.51	2.47	3.69	1.92	2.93	2.51	4.16	2.58	1.57	3.03
	Ba	1285.14	125.50	368.54	143.02	334.46	275.30	183.22	82.78	168.61	607.54	283.07
	La	40.28	15.17	10.05	14.57	7.50	10.75	10.35	16.05	10.09	6.65	6.50
	Ce	43.13	37.06	23.72	36.61	19.35	27.18	23.66	41.99	23.42	17.05	17.89
	Pr	8.19	5.94	3.59	5.74	2.91	3.93	3.53	6.71	3.51	2.51	3.04
	Nd	29.18	27.24	16.09	26.95	13.50	17.83	15.28	33.69	15.37	11.87	15.64
	Sm	5.11	7.77	4.36	7.54	3.62	4.77	4.08	8.95	4.15	3.38	4.30
	Eu	1.66	1.92	1.30	1.87	1.09	1.39	1.30	2.38	1.36	1.09	1.46
	Gd	4.82	8.29	4.03	7.19	3.23	4.13	4.14	9.68	4.19	3.30	4.50
	Tb	0.65	1.42	0.66	1.23	0.55	0.70	0.69	1.49	0.68	0.58	0.69
	Dy	3.79	9.00	4.17	8.16	3.68	4.64	4.30	10.01	4.35	3.96	4.56
	Ho	0.73	1.79	0.81	1.60	0.72	0.87	0.86	1.89	0.84	0.79	0.86
	Er	2.02	5.21	2.30	4.65	2.22	2.59	2.44	5.89	2.42	2.36	2.67
	Tm	0.30	0.79	0.35	0.69	0.35	0.38	0.37	0.89	0.36	0.37	0.40
	Yb	1.93	5.23	2.29	4.80	2.55	2.56	2.44	5.68	2.37	2.61	2.54
	Lu	0.26	0.84	0.36	0.77	0.41	0.39	0.38	0.98	0.39	0.43	0.48
	Hf	2.94	4.41	1.95	3.97	2.12	2.08	2.03	5.36	2.07	1.92	2.57
	Ta	0.59	0.19	0.11	0.12	0.06	0.10	0.13	0.24	0.12	0.05	0.18
	Pb	8.87	23.20	9.77	2.29	0.57	2.22	17.56	2.90	17.45	0.48	2.92
	Th	6.69	1.44	1.13	1.33	0.64	1.32	1.33	1.51	1.23	0.84	1.30
	U	1.77	0.79	0.41	0.65	0.37	0.48	0.50	0.84	0.61	0.42	0.61

Appendix E: Major and trace element data for the Cretaceous and Tertiary Jamaican igneous rocks and their variation diagrams

		AHCI25	AHCI26	AHCI27	AHCI28	AHCI29	AHCI30	AHCI31	AHCI33	AHCI35	AHCI36	AHCI37
ICP-OES analysis	Majors (wt %)											
	SiO_2	57.86	45.61	49.38	47.49	50.41	52.05	49.56	45.95	54.74	54.41	55.66
	TiO_2	0.62	1.24	0.96	0.98	0.71	0.83	0.83	1.18	0.53	0.61	0.59
	Al_2O_3	16.97	18.88	19.53	18.49	19.70	17.70	16.95	20.10	17.27	18.50	17.96
	Fe_2O_3	7.06	11.14	9.86	10.17	8.49	8.81	9.62	10.55	6.14	6.22	6.36
	MnO	0.21	0.14	0.22	0.21	0.17	0.16	0.18	0.13	0.13	0.18	0.13
	MgO	2.01	3.80	4.60	5.14	3.30	3.91	4.57	3.52	3.09	2.76	2.11
	CaO	3.26	11.08	10.77	8.18	9.59	5.84	6.98	8.18	4.42	6.69	6.26
	Na_2O	5.42	2.44	2.66	3.15	2.73	5.37	3.28	3.77	2.95	4.20	4.13
	K_2O	1.21	0.19	0.15	0.51	0.47	0.39	0.25	0.78	0.60	1.94	2.29
	P_2O_5	0.18	0.24	0.17	0.19	0.14	0.17	0.16	0.12	0.18	0.17	0.17
	LOI	4.07	5.10	1.71	5.64	4.67	4.49	7.01	5.45	8.93	3.98	2.49
	Total	98.86	99.85	100.02	100.16	100.39	99.72	99.40	99.73	98.99	99.66	98.15
	Traces (ppm)											
	Sc	17.71	32.41	30.78	21.10	24.14	23.69	26.39	31.40	14.61	19.18	18.58
	V	67.01	314.64	312.97	284.40	216.12	218.60	229.39	285.18	128.84	159.04	158.55
	Cr	13.84	18.07	35.27	20.96	8.28	19.64	35.36	13.84	13.45	22.75	16.74
	Co	13.94	25.12	27.41	29.01	20.18	22.32	27.31	24.91	15.88	18.29	17.58
	Ni	32.25	14.41	33.27	9.94	59.01	11.35	8.86	9.95	2.68	24.22	31.42
	Cu	33.95	51.26	113.78	14.25	118.25	7.32	51.39	129.50	36.19	51.10	58.49
	Zn	121.41	33.54	61.14	90.48	83.73	63.49	75.23	70.91	54.11	86.55	83.13
	Sr	373.70	459.98	702.34	601.92	657.10	574.77	459.57	597.61	483.93	596.32	563.80
	Y	29.58	28.29	22.12	25.65	18.23	23.33	20.00	21.05	14.96	14.83	13.31
	Zr	85.57	91.38	66.10	88.47	48.16	77.27	64.74	49.50	86.37	78.22	76.69
	Ba	498.42	146.91	126.64	338.58	262.34	224.27	200.01	357.92	590.41	586.28	560.45
ICP-MS analysis	Traces (ppm)											
	Ti	0.63	1.22	1.01	1.01	0.72	0.87	0.86	1.29	0.55	0.67	0.66
	V	58.72	304.17	304.61	280.16	209.81	221.49	248.88	363.15	148.00	165.62	163.12
	^{52}Cr	14.57	14.80	36.94	21.64	9.39	20.34	33.93		11.41	23.13	17.72
	^{53}Cr	16.44	22.08	44.16	29.68	20.50	29.68	41.51	15.34	21.91	24.38	19.19
	Mn	0.20	0.13	0.22	0.21	0.16	0.16	0.17	0.13	0.13	0.18	0.13
	^{57}Fe	6.59	11.07	10.41	10.68	8.76	9.17	9.99	10.85	6.49	6.35	6.38
	Co	12.11	21.29	29.76	31.83	21.80	23.72	29.70	28.82	18.14	19.83	17.62
	^{60}Ni	24.47	-157.72	404.33	343.64	430.66	6.31	-153.79	10.24	-176.20	24.38	25.01
	^{62}Ni	23.82	-109.56	345.87	311.34	362.02	13.52	-112.77	8.75	-134.46	25.60	26.34
	Zn	48.49	-	-	-	-	-	-	-	-	56.19	50.11
	Ga	15.48	19.17	20.04	19.46	18.47	17.87	18.53	17.17	17.60	19.18	18.44
	Rb	2.58	-	-	-	-	-	-	7.33	-	4.92	14.08
	Sr	383.57	432.85	684.71	587.01	640.92	565.86	436.87	600.02	459.53	646.59	609.83
	Y	27.84	27.61	22.24	25.08	18.09	22.91	20.57	21.82	15.52	14.27	13.70
	Zr	78.20	95.32	62.81	81.36	44.87	74.88	59.77	46.94	81.95	78.12	75.59
	Nb	1.82	3.09	1.48	2.11	1.08	1.76	1.43	0.71	2.00	1.97	1.86
	Ba	490.81	146.91	126.64	338.58	262.34	224.27	200.01	368.72	590.41	620.42	584.98
	La	7.73	13.08	7.20	10.23	5.08	7.48	9.89	3.70	12.74	11.00	11.00
	Ce	18.77	23.62	18.07	23.47	12.45	17.97	15.25	10.72	24.04	25.58	25.72
	Pr	2.76	3.68	2.80	3.54	1.99	2.82	2.39	1.78	3.37	3.39	3.47
	Nd	12.98	16.45	12.36	15.04	9.03	12.56	10.78	9.29	13.42	14.07	14.12
	Sm	3.67	4.37	3.28	3.95	2.51	3.34	2.93	2.95	2.92	3.10	3.18
	Eu	1.16	1.62	1.08	1.33	0.95	1.09	1.02	1.07	1.05	1.04	1.01
	Gd	3.53	4.38	3.48	4.08	2.76	3.46	3.03	3.28	2.64	2.46	2.42
	Tb	0.64	0.73	0.58	0.65	0.46	0.57	0.51	0.55	0.41	0.38	0.36
	Dy	4.31	4.61	3.70	4.16	2.94	3.66	3.28	3.48	2.42	2.43	2.30
	Ho	0.85	0.90	0.72	0.81	0.58	0.73	0.65	0.67	0.48	0.44	0.43
	Er	2.59	2.58	2.12	2.34	1.73	2.10	1.91	2.11	1.40	1.31	1.23
	Tm	0.40	0.41	0.33	0.36	0.27	0.32	0.30	0.31	0.21	0.20	0.18
	Yb	2.86	2.67	2.18	2.38	1.81	2.18	2.05	2.02	1.43	1.40	1.25
	Lu	0.51	0.37	0.34	0.43	0.30	0.35	0.28	0.32	0.20	0.23	0.20
	Hf	2.17	2.47	1.74	2.07	1.26	2.00	1.62	1.44	2.24	1.88	1.83
	Ta	0.06	0.17	0.07	0.11	0.05	0.09	0.08	0.05	0.12	0.07	0.07
	Pb	2.29	5.09	18.73	17.97	17.94	9.71	4.76	1.53	4.71	2.08	1.68
	Th	0.95	1.32	1.22	1.96	0.50	0.89	1.05	0.36	2.61	2.24	2.20
	U	0.47	0.62	0.63	0.63	0.29	0.40	0.36	0.27	0.83	0.78	0.79

Appendix E: Major and trace element data for the Cretaceous and Tertiary Jamaican igneous rocks and their variation diagrams

		AHCI39	AHCI40	AHCI42	AHCI43	AHCI45	AHCI46	AHCI47	AHCI48	AHCI49	AHCI50	AHCI51
ICP-OES analysis	Majors (wt %)											
	SiO_2	48.02	47.42	48.53	46.79	55.66	49.14	56.97	58.41	46.56	61.91	53.90
	TiO_2	1.27	1.16	0.71	1.03	0.71	0.95	0.71	0.67	0.94	0.38	0.72
	Al_2O_3	18.61	17.92	19.02	19.26	18.12	18.30	18.27	17.61	18.11	16.08	18.45
	Fe_2O_3	11.18	11.42	8.29	10.46	7.13	10.38	6.37	6.77	9.42	4.80	7.48
	MnO	0.13	0.22	0.19	0.22	0.13	0.17	0.15	0.14	0.21	0.09	0.16
	MgO	4.13	5.07	3.25	3.97	3.22	4.90	2.26	2.72	4.35	1.44	2.96
	CaO	9.66	7.80	9.22	8.39	3.06	7.25	5.13	4.84	8.66	4.41	4.54
	Na_2O	3.23	3.69	2.75	3.04	7.12	2.42	5.78	4.27	2.92	4.68	6.78
	K_2O	0.33	0.53	0.07	0.25	0.47	0.22	0.98	0.31	0.74	1.63	1.01
	P_2O_5	0.25	0.19	0.16	0.17	0.15	0.18	0.15	0.16	0.19	0.29	0.16
	LOI	3.51	5.54	6.37	5.94	3.52	5.43	3.33	3.33	6.95	3.36	4.10
	Total	100.33	100.95	98.56	99.52	99.30	99.33	100.10	99.22	99.06	99.07	100.24
	Traces (ppm)											
	Sc	36.10	33.45	22.81	19.04	18.62	21.86	19.67	18.81	23.47	8.15	21.13
	V	360.65	301.88	182.99	236.07	145.11	222.66	124.11	116.60	189.52	25.09	131.10
	Cr	21.97	30.15	15.47	14.47	7.49	31.32	16.72	6.59	28.24	15.27	41.97
	Co	25.48	29.69	18.58	27.58	20.75	28.86	17.28	16.32	25.60	9.87	20.59
	Ni	28.98	22.38	2.28	3.10	30.15	13.13	29.58	13.93	24.52	15.02	42.64
	Cu	42.11	9.24	95.66	14.46	137.11	8.18	233.77	58.85	53.46	32.18	232.26
	Zn	46.96	77.20	64.84	66.92	103.38	55.96	88.56	63.66	81.78	69.24	125.92
	Sr	699.01	446.38	598.17	618.95	411.98	666.34	464.66	470.02	587.19	458.97	442.25
	Y	27.76	22.76	18.32	23.15	36.07	22.49	34.72	35.13	22.37	25.55	37.50
	Zr	104.90	90.64	51.11	86.66	127.10	79.49	126.88	124.86	74.60	92.84	139.34
	Ba	204.59	241.97	209.88	210.31	95.90	265.46	335.29	338.11	673.09	317.10	222.87
ICP-MS analysis	Traces (ppm)											
	Ti	1.30	1.20	0.74	1.09	0.67	0.98	0.77	0.70	0.97	0.42	0.77
	V	369.15	312.18	204.38	257.39	124.21	224.83	125.97	128.19	194.76	27.13	127.27
	^{52}Cr	19.42	28.02	14.38	12.93	5.11	29.14	16.96	3.94	26.48	15.13	43.31
	^{53}Cr	28.28	34.20	20.28	19.77	7.74	34.52	18.22	13.31	31.35	17.57	42.10
	Mn	0.13	0.21	0.19	0.21	0.11	0.17	0.15	0.14	0.21	0.09	0.16
	^{57}Fe	11.71	12.01	8.69	11.11	6.12	10.77	6.37	7.12	9.92	4.72	7.31
	Co	23.61	30.42	21.07	28.95	19.01	31.52	16.66	17.43	27.15	10.39	18.55
	^{60}Ni	-127.84	-143.78	-194.73	-175.82	30.70	-160.72	27.17	-160.73	-133.79	17.96	37.97
	^{62}Ni	-86.21	-98.59	-141.52	-126.40	30.18	-117.05	25.31	-112.92	-88.79	14.01	37.58
	Zn	-	-	-	-	47.39	-	49.24	-	-	41.03	58.84
	Ga	20.25	18.78	19.35	21.15	16.97	18.72	18.70	18.89	16.96	16.84	19.08
	Rb	-	-	-	-	1.51	-	5.07	-	-	9.29	5.86
	Sr	657.94	418.24	566.67	605.44	380.32	630.57	482.26	449.90	553.00	489.75	452.00
	Y	27.33	23.06	18.21	22.80	30.71	21.21	33.28	33.64	21.63	24.50	35.31
	Zr	96.34	79.10	50.02	79.29	104.94	74.74	119.93	120.33	74.03	88.38	123.30
	Nb	2.95	2.33	1.18	2.19	2.46	2.11	2.80	2.63	2.01	1.97	2.87
	Ba	204.59	241.97	209.88	210.31	84.01	265.46	350.51	338.11	673.09	334.62	231.45
	La	8.03	9.63	6.11	8.45	9.32	9.13	10.00	10.17	12.25	8.50	10.00
	Ce	20.35	22.44	12.34	20.04	22.96	21.37	24.93	23.93	21.02	21.56	25.61
	Pr	3.31	3.41	1.97	3.11	3.39	3.16	3.70	3.72	3.16	3.23	3.85
	Nd	15.21	14.87	9.01	13.87	15.57	13.70	16.60	16.45	13.42	14.59	17.49
	Sm	4.27	3.78	2.52	3.66	4.36	3.40	4.88	4.67	3.52	3.94	5.01
	Eu	1.39	1.22	0.95	1.21	1.06	1.16	1.26	1.20	1.19	1.18	1.17
	Gd	4.36	3.85	2.60	3.73	4.00	3.42	4.48	4.80	3.54	3.31	4.48
	Tb	0.73	0.62	0.44	0.60	0.72	0.56	0.80	0.81	0.56	0.58	0.80
	Dy	4.62	3.92	2.92	3.81	4.76	3.58	5.22	5.24	3.53	3.76	5.26
	Ho	0.91	0.76	0.59	0.75	0.92	0.69	1.02	1.04	0.70	0.74	1.02
	Er	2.64	2.21	1.75	2.23	2.80	2.07	3.11	3.08	2.02	2.33	3.11
	Tm	0.41	0.34	0.28	0.34	0.42	0.31	0.47	0.50	0.31	0.36	0.49
	Yb	2.61	2.21	1.85	2.18	2.92	2.07	3.27	3.39	2.06	2.45	3.28
	Lu	0.42	0.37	0.26	0.34	0.49	0.31	0.55	0.53	0.27	0.43	0.54
	Hf	2.56	2.06	1.38	2.07	2.76	2.01	3.18	3.47	1.99	2.17	3.17
	Ta	0.18	0.14	0.06	0.13	0.09	0.13	0.11	0.17	0.11	0.06	0.11
	Pb	5.23	4.66	4.64	4.66	3.17	4.33	0.85	4.79	4.15	2.45	1.18
	Th	1.40	1.31	0.49	1.30	1.08	1.02	1.22	1.20	1.05	0.65	1.22
	U	0.64	0.44	0.25	0.48	0.55	0.64	0.60	0.68	0.52	0.36	0.60

Appendix E: Major and trace element data for the Cretaceous and Tertiary Jamaican igneous rocks and their variation diagrams

		AHCI52	AHCI53	AHCI55	AHCI56	AHCI59	AHCI62	AHCI63	AHCI64	AHCI65	AHCI72
ICP-OES analysis	Majors (wt %)										
	SiO_2	59.37	55.76	49.94	49.85	54.83	55.55	60.30	48.72	53.25	45.69
	TiO_2	0.65	0.72	0.84	0.79	0.85	0.69	0.57	1.05	0.87	1.13
	Al_2O_3	17.15	18.64	19.57	20.48	18.16	15.71	16.49	20.33	18.82	17.49
	Fe_2O_3	6.14	6.87	9.05	8.28	11.57	8.59	5.44	11.00	9.48	9.81
	MnO	0.15	0.15	0.23	0.23	0.06	0.26	0.20	0.21	0.23	0.20
	MgO	2.13	2.73	3.01	3.70	1.81	5.82	3.03	3.50	2.77	3.16
	CaO	6.21	3.98	7.12	8.20	6.44	5.70	3.94	8.01	5.40	8.65
	Na_2O	4.06	6.54	5.14	2.82	3.74	3.55	4.49	4.32	5.19	3.83
	K_2O	0.58	0.58	2.21	0.42	0.78	1.26	2.68	0.90	0.79	0.30
	P_2O_5	0.15	0.15	0.23	0.23	0.17	0.21	0.17	0.21	0.22	0.13
	LOI	3.49	3.54	2.42	5.63	1.97	2.32	1.96	2.17	2.05	8.73
	Total	100.08	99.66	99.75	100.63	100.39	99.65	99.27	100.42	99.11	99.11
	Traces (ppm)										
	Sc	19.60	20.70	22.09	19.05	20.86	26.79	17.93	24.36	19.50	29.18
	V	118.34	132.41	181.47	132.86	129.31	209.27	159.15	217.04	186.53	216.64
	Cr	43.13	39.28	16.34	32.43	19.63	153.17	43.23	16.38	13.60	43.85
	Co	17.82	19.58	21.43	19.34	15.34	22.74	12.56	25.45	23.14	46.54
	Ni	16.44	20.13	99.93	23.20	5.28	41.46	33.27	27.30	22.67	37.08
	Cu	76.14	130.37	438.56	3.69	23.98	6.35	29.92	44.64	36.63	143.71
	Zn	81.30	67.15	1001.92	110.65	51.16	64.42	383.48	73.36	124.41	103.44
	Sr	407.68	442.96	604.24	579.44	469.04	478.06	406.06	511.17	442.31	384.51
	Y	33.34	36.50	23.98	21.79	26.66	14.13	16.78	24.60	24.70	25.28
	Zr	123.34	135.90	67.43	76.89	85.69	83.24	113.94	78.96	97.22	52.07
	Ba	240.49	193.81	571.64	250.53	646.06	970.45	899.11	109.80	277.47	318.01
ICP-MS analysis	Traces (ppm)										
	Ti	0.72	0.77	0.87	0.79	0.87	0.70	0.62	1.16	0.91	1.15
	V	115.92	127.64	172.43	141.35	140.86	214.94	156.39	212.89	175.90	225.26
	^{52}Cr	47.75	40.87	9.56	30.38	17.75	149.48	45.51	15.94	11.56	40.63
	^{53}Cr	48.05	42.59	12.09	35.22	25.02	138.75	47.53	18.50	13.68	40.43
	Mn	0.14	0.14	0.20	0.22	0.05	0.25	0.19	0.21	0.22	0.21
	^{57}Fe	6.06	6.75	8.46	8.42	11.91	8.94	5.35	11.40	9.23	10.10
	Co	16.29	18.49	18.17	19.13	14.13	25.43	11.50	19.89	21.45	30.52
	^{60}Ni	12.68	20.99	23.66	-140.31	-182.44	-121.93	31.50	29.72	24.15	33.73
	^{62}Ni	15.02	19.53	19.58	-93.27	-131.90	-88.56	32.23	26.84	22.45	49.65
	Zn	50.34	46.44	40.30	-	-	-	115.66	44.91	46.61	-
	Ga	17.59	19.51	16.44	17.79	15.48	17.18	17.04	18.66	16.56	16.65
	Rb	3.97	2.72	6.83	-	-	-	16.69	7.19	5.09	2.48
	Sr	434.59	471.13	609.60	538.21	445.45	463.91	423.40	543.37	450.07	383.82
	Y	32.05	34.61	21.48	20.65	25.47	14.79	16.31	22.88	23.07	23.76
	Zr	115.96	125.74	66.28	70.57	82.94	73.10	106.97	72.87	83.13	57.14
	Nb	2.68	2.93	1.51	1.50	1.90	1.77	2.63	1.68	1.95	1.01
	Ba	248.22	198.26	526.09	250.53	646.06	970.45	899.11	110.39	256.20	312.86
	La	10.00	10.50	7.45	4.07	6.93	10.76	16.99	6.60	6.70	4.07
	Ce	24.55	26.07	17.68	12.33	14.05	23.30	35.40	16.28	16.83	10.28
	Pr	3.71	3.88	2.66	2.17	2.39	3.43	4.51	2.45	2.45	1.84
	Nd	16.46	17.44	12.39	10.43	10.87	14.34	17.53	11.58	11.39	9.15
	Sm	4.78	5.09	3.45	3.07	3.18	3.35	3.71	3.27	3.24	3.01
	Eu	1.17	1.24	1.18	1.05	1.22	1.10	1.08	1.11	1.06	1.04
	Gd	4.15	4.55	3.01	3.16	3.61	2.90	2.68	3.08	3.08	3.30
	Tb	0.76	0.81	0.52	0.52	0.61	0.42	0.41	0.53	0.53	0.57
	Dy	4.96	5.23	3.38	3.32	3.95	2.45	2.50	3.47	3.54	3.83
	Ho	0.97	1.04	0.66	0.66	0.81	0.46	0.47	0.69	0.69	0.74
	Er	2.96	3.11	1.93	1.92	2.36	1.32	1.37	2.00	2.04	2.15
	Tm	0.45	0.49	0.29	0.30	0.37	0.20	0.21	0.32	0.31	0.35
	Yb	3.08	3.32	2.03	2.09	2.49	1.36	1.47	2.06	2.11	2.25
	Lu	0.52	0.55	0.33	0.33	0.35	0.20	0.24	0.34	0.35	0.35
	Hf	2.98	3.19	1.60	1.80	2.23	1.99	2.65	1.72	1.92	1.79
	Ta	0.10	0.11	0.05	0.08	0.11	0.12	0.11	0.05	0.07	0.05
	Pb	1.40	0.22	3.56	4.34	4.47	4.69	2.33	0.45	3.97	5.24
	Th	1.16	1.23	0.63	0.69	1.01	2.02	3.42	0.43	0.51	0.44
	U	0.58	0.60	0.38	0.36	0.35	0.88	1.07	0.29	0.30	0.20

Appendix E: Major and trace element data for the Cretaceous and Tertiary Jamaican igneous rocks and their variation diagrams

		AHCI73	AHCI74	AHCI75	AHCI76	AHCI77	AHCI78	AHCI79
ICP-OES analysis	Majors (wt %)							
	SiO_2	49.04	49.45	49.54	41.44	43.51	43.22	49.91
	TiO_2	1.04	1.07	1.47	1.14	1.14	1.33	0.93
	Al_2O_3	20.48	21.02	20.01	16.82	17.04	17.22	21.12
	Fe_2O_3	11.39	9.88	11.61	9.22	11.27	10.66	9.01
	MnO	0.17	0.13	0.34	0.17	0.12	0.13	0.15
	MgO	4.45	3.91	6.09	2.18	3.93	3.02	3.69
	CaO	8.28	9.04	2.36	14.51	9.65	9.11	9.52
	Na_2O	3.03	3.52	2.36	1.84	2.01	1.53	2.80
	K_2O	0.27	0.19	2.01	0.05	0.06	0.31	0.24
	P_2O_5	0.22	0.21	0.33	0.24	0.24	0.36	0.17
	LOI	1.56	1.22	4.79	13.09	11.83	12.95	2.26
	Total	99.93	99.64	100.89	100.69	100.80	99.84	99.79
	Traces (ppm)							
	Sc	23.54	24.81	35.99	40.99	41.85	37.35	29.51
	V	251.10	216.39	296.94	637.48	401.47	334.59	261.47
	Cr	28.30	200.49	35.94	46.73	20.50	32.74	20.11
	Co	56.10	47.39	56.13	44.88	55.63	53.54	41.56
	Ni	41.62	138.08	31.02	45.99	35.69	33.13	21.46
	Cu	197.09	100.15	264.41	127.70	212.06	233.64	166.60
	Zn	87.43	66.19	331.46	114.22	101.48	120.09	75.08
	Sr	511.15	570.67	304.43	712.69	712.35	380.32	719.71
	Y	23.77	27.30	49.01	29.62	27.24	35.11	23.75
	Zr	67.45	71.39	162.20	58.92	56.49	74.00	41.64
	Ba	111.70	103.56	4545.37	250.98	277.78	498.80	350.19
ICP-MS analysis	Traces (ppm)							
	Ti	1.05	1.09	1.41	1.14	1.13	1.32	0.94
	V	253.72	220.45	279.33	637.63	396.78	322.63	261.14
	^{52}Cr	24.09	225.60	31.72	46.60	15.57	31.36	15.11
	^{53}Cr	21.45	237.02	27.27	45.02	11.85	29.81	9.59
	Mn	0.17	0.14	0.35	0.18	0.12	0.14	0.17
	^{57}Fe	11.76	10.45	11.44	9.65	11.55	11.09	9.54
	Co	31.19	23.59	35.95	44.09	33.19	23.55	26.20
	^{60}Ni	28.27	186.14	17.86	49.85	36.06	23.53	8.24
	^{62}Ni	47.57	184.56	39.58	54.06	35.33	35.70	9.48
	Zn	-	-	-	-	-	-	-
	Ga	19.73	18.92	17.76	18.21	19.17	21.04	19.75
	Rb	3.45	5.70	11.31	0.33	0.26	1.99	0.85
	Sr	531.76	570.87	298.18	865.00	851.45	361.98	896.69
	Y	21.94	25.25	44.57	27.51	24.72	33.13	22.44
	Zr	76.73	77.83	169.65	63.01	60.78	79.74	45.80
	Nb	1.67	1.88	3.52	1.88	1.80	2.20	1.47
	Ba	99.61	103.42	5808.59	258.09	279.51	498.04	358.64
	La	7.34	5.83	12.97	9.24	8.17	11.76	5.81
	Ce	17.67	14.26	30.83	20.66	19.28	27.24	13.73
	Pr	2.84	2.45	5.07	3.31	3.11	4.39	2.31
	Nd	13.07	12.03	23.09	15.42	14.63	20.85	11.26
	Sm	3.43	3.56	6.52	4.31	4.24	5.93	3.31
	Eu	1.13	1.16	1.82	1.29	1.24	1.72	1.12
	Gd	3.40	3.72	6.65	4.33	4.11	5.72	3.41
	Tb	0.55	0.63	1.13	0.70	0.67	0.91	0.56
	Dy	3.52	4.11	7.26	4.41	4.24	5.76	3.63
	Ho	0.68	0.81	1.39	0.86	0.81	1.09	0.70
	Er	1.99	2.34	4.02	2.48	2.25	3.13	2.04
	Tm	0.32	0.37	0.65	0.39	0.36	0.51	0.33
	Yb	2.11	2.44	4.11	2.50	2.31	3.27	2.12
	Lu	0.33	0.36	0.58	0.37	0.34	0.49	0.32
	Hf	2.10	2.12	4.77	2.01	1.90	2.52	1.51
	Ta	0.09	0.09	0.21	0.09	0.09	0.11	0.06
	Pb	5.11	14.12	7.50	4.96	7.80	6.70	6.03
	Th	0.45	0.47	2.82	1.38	1.38	1.72	0.67
	U	0.24	0.27	1.29	0.65	0.64	0.71	0.29

E.3 Benbow Inlier samples

		AHBI01	AHBI03	AHBI05	AHBI06	AHBI07	AHBI09	AHBI10	AHBI11	AHBI12	AHBI13	AHBI14
ICP-OES analysis	Majors (wt %)											
	SiO_2	59.07	58.98	81.08	82.63	76.98	50.02	53.85	48.87	45.69	52.49	46.12
	TiO_2	0.86	0.86	0.39	0.30	0.64	1.22	1.17	1.10	1.15	1.20	1.17
	Al_2O_3	15.07	15.04	10.99	10.07	12.62	17.02	16.23	16.96	15.47	16.11	14.69
	Fe_2O_3	8.36	8.39	1.91	0.92	0.91	11.37	7.11	11.14	10.53	11.12	13.83
	MnO	0.14	0.15	0.03	0.01	0.03	0.15	0.11	0.18	0.18	0.13	0.24
	MgO	2.55	2.60	0.84	0.15	2.55	2.96	0.95	3.60	3.66	2.65	2.49
	CaO	2.13	2.40	0.35	0.58	0.39	3.80	6.88	10.66	9.46	3.85	6.81
	Na_2O	7.37	7.10	3.68	3.59	4.39	2.54	5.37	2.79	2.00	5.75	4.28
	K_2O	0.45	0.40	0.16	0.08	0.23	0.61	0.09	0.54	0.31	0.25	1.53
	P_2O_5	0.13	0.12	0.06	0.05	0.14	0.62	0.29	0.16	0.25	0.24	0.24
	LOI	2.24	2.31	1.05	0.69	2.01	7.86	6.99	2.43	9.98	5.81	6.95
	Total	98.38	98.34	100.54	99.07	100.90	98.18	99.03	98.43	98.67	99.59	98.35
	Traces (ppm)											
	Sc	28.22	29.38	8.67	6.78	16.41	34.70	31.70	41.58	33.51	36.47	35.42
	V	155.39	152.38	46.76	47.16	48.13	272.47	240.99	416.08	362.99	416.09	413.95
	Cr	6.51	14.85	33.97	78.58	22.01	17.76	20.55	25.99	44.81	6.93	121.38
	Co	22.68	25.32	6.31	5.42	8.82	24.75	21.66	39.33	26.58	39.24	33.60
	Ni	20.29	67.70	9.20	124.51	7.46	7.32	56.13	16.07	7.74	16.42	39.74
	Cu	263.41	1503.21	125.17	15.34	43.37	27.39	31.50	450.53	-2.08	342.60	85.84
	Zn	142.11	1013.39	4.25	-0.62	78.17	94.38	79.40	173.78	55.21	164.74	207.37
	Sr	116.96	138.63	48.64	54.06	61.89	439.26	398.15	583.39	472.12	544.71	512.82
	Y	38.86	35.61	25.80	25.57	33.16	39.29	23.58	23.59	24.44	40.80	24.42
	Zr	85.05	83.88	113.25	91.78	113.10	90.83	85.75	68.02	76.92	86.75	81.01
	Ba	368.91	245.33	411.49	195.43	175.77	469.07	81.87	348.28	670.77	353.18	501.96
ICP-MS analysis	Traces (ppm)											
	Ti	0.91	0.91	0.35	0.27	0.62	1.16	1.10	1.07	1.10	1.24	1.19
	V	151.36	148.72	14.84	10.46	0.73	275.15	250.73	399.30	361.85	387.29	373.99
	^{53}Cr	10.04	14.34	20.06	69.24	15.77	1.97	5.73	28.95	30.62	10.38	124.72
	^{53}Cr	13.62	17.40	21.51	68.97	18.00	5.09	8.98	31.08	33.33	14.61	125.09
	Mn	0.14	0.15	0.03	0.01	0.03	0.13	0.11	0.16	0.17	0.12	0.22
	^{57}Fe	8.45	8.36	1.92	1.04	1.04	10.77	6.79	10.18	9.98	10.23	12.97
	Co	18.68	18.89	3.75	3.69	2.00	23.44	19.93	31.20	24.27	30.43	25.00
	^{60}Ni	6.67	39.49	5.52	109.29	0.05	4.75	53.41	3.55	7.16	2.73	28.01
	^{62}Ni	11.27	44.09	4.81	112.70	3.74	10.40	62.76	6.38	13.55	7.48	31.22
	Zn	34.61	33.84	27.45	24.03	37.07	71.83	46.95	49.83	51.44	55.47	60.69
	Ga	15.54	15.65	9.75	7.00	12.64	18.94	11.47	18.07	15.53	16.08	17.94
	Rb	3.75	3.19	0.38	0.20	1.50	2.38	0.28	4.97	0.90	2.27	14.48
	Sr	116.57	138.40	43.23	48.83	57.51	435.41	386.78	545.08	467.45	524.62	490.15
	Y	34.49	31.78	25.67	22.15	34.78	38.64	23.91	21.07	23.78	34.88	22.87
	Zr	82.92	82.06	113.19	96.23	123.27	91.55	86.22	67.10	77.69	89.40	84.27
	Nb	1.86	1.85	1.16	0.93	1.58	2.33	2.17	1.72	1.77	2.14	2.00
	Ba	347.70	219.34	413.78	196.33	182.66	469.49	80.34	300.66	657.14	305.59	432.72
	La	6.25	5.10	6.80	4.80	5.75	23.00	11.00	8.70	9.10	14.50	11.00
	Ce	14.92	12.91	16.92	11.79	16.53	48.31	27.94	20.20	23.78	35.43	25.90
	Pr	2.06	1.98	2.47	1.76	2.85	5.33	4.12	2.82	3.65	5.30	3.52
	Nd	10.41	9.86	11.38	8.66	14.40	23.90	18.12	12.43	16.59	23.31	15.24
	Sm	3.56	3.41	3.00	2.49	4.27	5.40	4.09	3.24	3.94	5.50	3.76
	Eu	1.15	1.13	0.78	0.60	1.05	1.70	1.17	1.12	1.35	1.74	1.30
	Gd	3.93	3.85	3.44	2.82	4.83	5.52	4.02	3.05	3.99	4.99	3.51
	Tb	0.73	0.72	0.56	0.48	0.81	0.82	0.60	0.52	0.59	0.83	0.62
	Dy	5.02	5.01	3.84	3.29	5.70	5.46	3.95	3.41	3.87	5.32	3.90
	Ho	1.02	1.02	0.75	0.64	1.11	1.06	0.75	0.64	0.72	1.01	0.75
	Er	3.04	3.06	2.41	2.11	3.65	3.37	2.39	1.85	2.27	2.95	2.25
	Tm	0.46	0.45	0.38	0.33	0.60	0.51	0.37	0.28	0.35	0.43	0.34
	Yb	3.15	3.23	2.55	2.14	3.94	3.26	2.39	1.92	2.17	2.81	2.24
	Lu	0.49	0.51	0.46	0.40	0.65	0.54	0.40	0.30	0.42	0.45	0.35
	Hf	2.16	2.22	3.12	2.65	3.38	2.63	2.37	1.52	2.14	2.07	2.03
	Ta	0.07	0.08	0.11	0.09	0.11	0.14	0.12	0.06	0.11	0.07	0.07
	Pb	1.41	1.90	3.19	3.00	3.31	3.18	3.47	1.18	2.61	0.54	2.28
	Th	0.35	0.34	0.83	0.69	0.65	1.71	1.62	1.17	1.31	1.43	1.41
	U	0.28	0.28	0.50	0.40	0.57	0.48	0.96	0.62	0.59	1.10	0.51

Appendix E: Major and trace element data for the Cretaceous and Tertiary Jamaican igneous rocks and their variation diagrams

		AHBI15	AHBI16	AHBI17	AHBI18	AHBI19	AHBI20	AHBI21	AHBI22	AHBI23	AHBI26	AHBI27
ICP-OES analysis	Majors (wt %)											
	SiO_2	42.01	53.98	59.44	64.80	65.82	75.73	77.01	81.42	56.99	77.67	73.22
	TiO_2	1.11	1.17	0.97	1.27	0.77	0.39	0.40	0.31	1.02	0.43	0.53
	Al_2O_3	17.53	16.37	14.67	11.57	15.67	11.33	9.51	8.16	14.59	10.57	12.79
	Fe_2O_3	9.16	12.03	9.39	9.85	6.69	3.41	4.56	1.49	10.22	2.88	4.76
	MnO	0.15	0.16	0.20	0.25	0.13	0.03	0.08	0.02	0.12	0.05	0.04
	MgO	3.07	3.35	0.39	2.29	2.28	0.69	1.10	0.36	1.92	0.43	0.90
	CaO	9.86	4.95	4.68	2.27	0.33	1.53	0.50	0.85	7.45	1.14	0.20
	Na_2O	4.12	4.65	5.12	4.53	5.24	1.93	3.32	2.54	4.47	3.99	5.18
	K_2O	0.48	0.18	0.19	0.06	0.05	2.13	0.05	0.29	0.03	0.06	0.06
	P_2O_5	0.24	0.15	0.17	0.25	0.13	0.05	0.08	0.05	0.12	0.09	0.09
	LOI	11.20	2.97	3.54	2.48	2.62	1.96	2.33	0.98	3.03	1.68	1.98
	Total	98.92	99.96	98.75	99.63	99.72	99.18	98.93	96.47	99.95	98.99	99.77
	Traces (ppm)											
	Sc	32.28	38.43	34.87	30.31	28.66	9.90	12.23	7.52	34.18	10.83	15.29
	V	342.22	374.09	342.96	321.25	86.92	66.27	24.33	63.17	316.74	18.06	17.57
	Cr	58.55	25.20	23.16	28.87	31.82	35.43	22.57	47.50	46.35	22.52	41.23
	Co	22.80	54.62	41.74	44.21	28.85	13.72	18.64	5.04	46.31	10.87	18.95
	Ni	17.71	43.10	36.51	17.35	38.51	35.09	36.05	62.47	17.51	31.29	67.29
	Cu	153.71	100.15	78.26	86.56	122.01	69.02	61.50	60.13	88.12	56.59	67.13
	Zn	93.73	99.57	97.59	91.67	85.75	49.96	74.76	34.96	78.04	97.81	74.59
	Sr	704.42	325.93	384.39	107.84	60.07	96.03	27.43	43.90	75.10	51.66	24.73
	Y	27.73	26.13	22.64	34.81	35.43	44.74	41.49	23.78	23.85	40.86	51.62
	Zr	74.41	43.57	25.63	51.32	67.34	168.49	93.55	102.38	32.29	95.50	130.07
	Ba	143.33	192.04	74.20	106.31	66.18	671.00	35.71	208.97	19.47	265.78	48.77
ICP-MS analysis	Traces (ppm)											
	Ti	1.15	1.18	0.99	1.28	0.76	0.38	0.39	0.31	0.99	0.42	0.52
	V	325.44	370.18	340.79	319.87	83.82	33.16	15.39	25.60	306.81	7.75	5.55
	^{52}Cr	58.10	22.42	20.52	25.99	29.86	35.17	18.43	47.18	44.66	19.29	40.48
	^{53}Cr	58.37	23.51	18.48	24.41	28.17	32.44	15.21	42.64	43.19	16.19	37.99
	Mn	0.14	0.16	0.21	0.26	0.13	0.02	0.07	0.02	0.12	0.04	0.04
	^{57}Fe	9.62	12.01	9.58	10.17	6.38	2.98	4.05	1.24	10.26	2.46	4.10
	Co	21.68	31.11	10.16	22.88	9.64	3.54	4.71	2.40	18.87	2.38	4.02
	^{60}Ni	163.25	41.87	32.85	14.32	39.37	29.72	30.60	58.16	15.02	21.67	63.58
	^{62}Ni	146.61	45.01	36.14	20.72	39.45	34.18	32.47	76.07	47.56	23.44	68.81
	Zn	-	-	-	-	-	-	-	-	-	-	-
	Ga	20.52	18.64	11.64	10.79	16.86	10.69	12.81	6.15	24.21	12.02	17.58
	Rb	-	1.04	1.22	0.52	0.51	10.29	0.12	1.04	0.43	0.25	0.64
	Sr	689.04	328.14	389.37	111.81	62.47	97.55	31.76	49.71	77.51	55.69	28.42
	Y	27.12	25.14	21.37	33.73	33.30	42.43	39.69	22.75	22.10	40.39	49.51
	Zr	69.73	49.87	28.87	59.21	74.12	188.16	103.25	97.15	33.28	108.71	145.71
	Nb	1.78	1.25	0.96	1.56	1.56	4.57	1.87	1.34	0.97	2.09	2.71
	Ba	143.33	190.68	70.97	99.27	57.93	665.21	29.04	211.44	8.41	264.29	42.61
	La	13.25	3.08	3.70	4.24	4.17	9.39	6.54	4.35	2.80	6.73	7.31
	Ce	26.01	7.86	8.24	10.53	10.33	22.12	15.53	9.25	6.60	16.02	17.48
	Pr	4.01	1.46	1.10	1.92	1.86	3.58	2.62	1.49	1.17	2.82	3.11
	Nd	16.98	7.56	5.78	9.58	9.06	16.03	12.64	6.70	6.10	13.78	14.47
	Sm	4.17	2.60	2.00	3.16	2.99	4.73	3.92	2.09	2.14	4.17	4.62
	Eu	1.39	1.00	0.80	1.13	0.92	1.01	1.00	0.55	0.91	1.11	1.29
	Gd	4.20	3.24	2.71	3.95	3.66	5.09	4.55	2.45	2.75	4.88	5.65
	Tb	0.67	0.59	0.47	0.72	0.67	0.94	0.84	0.48	0.49	0.90	1.09
	Dy	4.17	3.89	3.16	4.73	4.52	6.35	5.58	3.24	3.29	5.96	7.39
	Ho	0.84	0.78	0.64	0.95	0.96	1.31	1.18	0.70	0.68	1.23	1.53
	Er	2.41	2.29	1.87	2.79	2.91	4.03	3.59	2.17	1.99	3.67	4.64
	Tm	0.36	0.37	0.30	0.45	0.46	0.67	0.59	0.36	0.31	0.57	0.77
	Yb	2.38	2.38	1.90	2.81	3.03	4.64	4.01	2.51	2.04	3.69	5.10
	Lu	0.37	0.35	0.32	0.43	0.47	0.73	0.61	0.41	0.32	0.53	0.74
	Hf	1.84	1.54	0.91	1.68	2.26	5.42	2.90	2.68	1.07	3.28	4.14
	Ta	0.10	0.07	0.05	0.09	0.11	0.33	0.13	0.10	0.06	0.15	0.17
	Pb	12.59	10.41	6.04	4.71	5.87	7.83	6.64	7.18	5.51	9.19	7.44
	Th	1.44	0.17	0.09	0.22	0.32	1.50	0.59	0.74	0.11	0.64	0.79
	U	0.75	0.13	0.10	0.15	0.24	0.70	0.50	0.37	0.12	0.51	0.78

Appendix E: Major and trace element data for the Cretaceous and Tertiary Jamaican igneous rocks and their variation diagrams

		AHBI28	AHBI30
ICP-OES analysis	Majors (wt %)		
	SiO_2	76.34	66.09
	TiO_2	0.44	0.50
	Al_2O_3	10.59	15.33
	Fe_2O_3	4.14	5.40
	MnO	0.07	0.09
	MgO	0.65	2.44
	CaO	0.24	3.11
	Na_2O	4.73	2.90
	K_2O	0.04	0.72
	P_2O_5	0.09	0.10
	LOI	1.55	2.73
	Total	98.89	99.40
	Traces (ppm)		
	Sc	12.51	15.99
	V	13.49	103.86
	Cr	42.58	15.43
	Co	16.64	22.37
	Ni	26.08	28.51
	Cu	73.22	93.47
	Zn	78.10	81.76
	Sr	20.16	133.23
	Y	36.68	20.13
	Zr	106.83	66.51
	Ba	24.23	715.50
ICP-MS analysis	Traces (ppm)		
	Ti	0.44	0.49
	V	4.66	104.37
	^{52}Cr	40.92	11.42
	^{53}Cr	38.02	6.56
	Mn	0.06	0.08
	^{57}Fe	3.61	4.75
	Co	3.42	10.37
	^{60}Ni	19.32	20.06
	^{62}Ni	16.61	21.13
	Zn	-	-
	Ga	13.12	14.88
	Rb	0.48	2.94
	Sr	24.41	135.72
	Y	34.60	18.47
	Zr	117.89	74.20
	Nb	2.08	1.71
	Ba	19.22	700.46
	La	5.84	4.55
	Ce	15.14	10.07
	Pr	2.63	1.52
	Nd	12.77	6.59
	Sm	3.98	1.86
	Eu	0.86	0.67
	Gd	4.56	2.08
	Tb	0.82	0.39
	Dy	5.47	2.65
	Ho	1.11	0.55
	Er	3.37	1.73
	Tm	0.55	0.30
	Yb	3.63	2.02
	Lu	0.59	0.33
	Hf	3.43	2.04
	Ta	0.15	0.13
	Pb	8.30	7.82
	Th	0.66	0.76
	U	0.48	0.46

E.4 Above Rocks Inlier samples

		AHAR01	AHAR02	AHAR03	AHAR04	AHAR05	AHAR06	AHAR07	AHAR08	AHAR09	AHAR10
ICP-OES analysis	Majors (wt %)										
	SiO_2	70.65	65.93	64.87	53.56	61.30	66.20	62.06	64.14	63.42	63.70
	TiO_2	0.38	0.75	0.75	1.02	0.78	0.93	0.64	0.74	0.69	0.72
	Al_2O_3	16.19	16.75	17.08	15.91	18.14	15.98	16.26	16.31	16.14	16.66
	Fe_2O_3	2.68	5.17	5.56	9.58	6.70	4.75	5.76	5.40	5.72	5.85
	MnO	0.07	0.10	0.11	0.23	0.14	0.12	0.13	0.10	0.09	0.11
	MgO	1.01	2.38	2.50	5.45	3.02	2.43	2.89	2.38	2.25	2.61
	CaO	2.85	4.84	5.15	8.29	6.20	3.98	5.84	4.92	4.75	5.15
	Na_2O	2.98	2.89	2.60	2.97	3.38	3.13	3.73	2.99	3.48	2.84
	K_2O	0.80	0.85	0.64	0.37	0.83	1.25	1.16	0.86	1.30	0.68
	P_2O_5	0.11	0.20	0.21	0.27	0.23	0.27	0.23	0.26	0.26	0.21
	LOI	1.27	0.58	0.75	0.93	0.61	0.45	0.66	0.75	0.89	1.02
	Total	98.99	100.45	100.23	98.57	101.32	99.49	99.36	98.87	98.97	99.55
	Traces (ppm)										
	Sc	4.60	13.21	13.97	30.02	16.48	15.10	15.75	11.71	11.21	14.00
	V	54.38	107.80	121.06	227.77	138.99	113.54	141.18	102.01	121.80	113.71
	Cr	15.29	3.78	8.51	32.03	15.76	16.41	66.08	72.18	44.97	61.49
	Co	8.91	14.35	15.30	26.42	16.67	13.90	13.84	15.19	12.72	15.98
	Ni	14.71	0.82	6.45	43.14	3.43	5.30	13.23	16.70	30.94	81.45
	Cu	42.76	172.40	99.46	2.85	212.29	64.84	5.90	90.42	8.95	732.01
	Zn	6.85	16.80	20.11	53.43	32.25	28.52	34.61	39.83	40.12	835.16
	Sr	764.61	752.80	772.09	630.91	796.86	370.29	910.74	827.65	883.21	799.20
	Y	12.42	15.34	17.64	22.40	19.53	25.04	16.68	17.26	17.43	19.13
	Zr	153.49	168.34	116.28	67.46	133.20	294.28	161.79	178.27	183.12	139.43
	Ba	1542.78	1200.24	1167.22	369.96	848.14	1058.06	1123.90	1281.76	1361.74	1111.89
ICP-MS analysis	Traces (ppm)										
	Ti	0.33	0.66	0.66	0.93	0.68	0.85	0.65	0.66	0.70	0.65
	V	39.56	117.66	125.96	233.56	140.00	125.94	143.40	107.80	121.89	125.16
	^{52}Cr	12.24	3.22	6.23	14.21	13.23	16.53	62.27	54.34	44.39	44.45
	^{53}Cr	16.73	6.57	9.47	20.53	16.65	20.31	64.74	57.16	48.46	46.78
	Mn	0.07	0.09	0.10	0.23	0.12	0.11	0.13	0.09	0.09	0.10
	^{57}Fe	2.58	4.94	5.09	9.15	5.93	4.46	5.96	5.00	5.84	5.43
	Co	8.14	14.00	14.08	26.30	15.80	11.47	14.77	12.43	12.89	14.33
	^{60}Ni	10.52	0.19	4.85	39.60	2.04	9.70	1.52	-1.07	362.09	2.89
	^{62}Ni	11.09	2.84	8.90	43.88	5.75	16.01	7.83	2.93	309.82	4.10
	Zn	50.68	56.01	57.38	57.41	63.57	82.75	-	71.00	-	62.42
	Ga	15.36	17.15	16.95	16.86	18.63	16.60	18.05	17.12	18.63	17.99
	Rb	5.58	7.34	4.12	4.51	6.58	5.69	-	5.43	-	4.95
	Sr	754.23	745.88	726.10	617.86	752.36	356.55	880.21	805.98	856.68	788.97
	Y	12.81	15.07	17.53	23.79	18.64	25.55	16.46	17.16	17.36	19.28
	Zr	160.31	171.85	112.29	67.23	132.95	301.50	153.81	184.31	180.53	164.51
	Nb	8.83	11.58	11.40	4.64	11.04	16.61	8.35	13.78	14.26	10.57
	Ba	1499.70	1132.60	1106.53	351.77	798.87	1006.22	1123.90	1225.94	1361.74	1066.84
	La	26.22	27.52	27.64	20.74	28.80	33.13	18.96	30.76	34.02	24.31
	Ce	38.36	41.80	44.88	34.88	44.21	57.03	36.18	51.98	64.00	45.35
	Pr	4.36	4.70	5.36	4.43	5.29	6.97	4.58	6.07	7.50	5.50
	Nd	15.81	17.46	20.47	18.49	20.62	27.53	17.04	23.26	26.02	21.60
	Sm	2.68	3.08	3.86	4.11	3.90	5.33	3.45	4.08	4.55	4.02
	Eu	0.94	1.15	1.17	1.06	1.14	1.42	1.17	1.34	1.48	1.22
	Gd	2.34	2.74	3.31	4.13	3.48	4.73	3.09	3.46	3.76	3.67
	Tb	0.32	0.37	0.46	0.62	0.48	0.66	0.46	0.46	0.52	0.50
	Dy	1.92	2.26	2.81	3.92	3.01	4.11	2.66	2.71	2.82	3.05
	Ho	0.35	0.42	0.51	0.74	0.55	0.75	0.51	0.49	0.54	0.57
	Er	1.17	1.35	1.58	2.25	1.70	2.40	1.50	1.53	1.52	1.76
	Tm	0.19	0.22	0.25	0.33	0.26	0.36	0.24	0.23	0.24	0.27
	Yb	1.28	1.39	1.58	2.12	1.60	2.34	1.59	1.55	1.60	1.78
	Lu	0.21	0.24	0.25	0.34	0.27	0.40	0.25	0.26	0.25	0.33
	Hf	3.94	4.27	2.80	1.70	3.28	7.37	3.90	4.39	4.28	3.92
	Ta	0.60	0.63	0.70	0.20	0.60	0.98	0.49	0.90	0.75	0.69
	Pb	3.85	3.32	4.17	2.97	11.92	4.92	8.59	5.02	18.21	17.85
	Th	6.28	6.27	7.41	1.02	13.62	5.65	5.15	6.48	7.35	6.57
	U	2.11	2.65	2.50	0.52	3.02	2.12	2.10	2.09	2.45	2.61

Appendix E: Major and trace element data for the Cretaceous and Tertiary Jamaican igneous rocks and their variation diagrams

		AHAR11	AHAR12	AHAR13	AHAR14	AHAR15	AHAR16	AHAR17	AHAR18	AHAR19
ICP-OES analysis	Majors (wt %)									
	SiO_2	65.50	53.88	68.56	61.51	60.10	47.42	57.06	57.54	63.97
	TiO_2	0.72	0.83	0.36	0.83	0.76	0.92	0.90	0.57	0.74
	Al_2O_3	15.68	15.25	16.68	17.63	16.50	18.00	17.49	16.42	15.65
	Fe_2O_3	4.64	10.45	3.80	6.30	6.33	10.33	7.53	6.62	6.46
	MnO	0.09	0.26	0.10	0.20	0.15	0.14	0.17	0.12	0.06
	MgO	1.47	4.27	1.59	2.32	1.38	4.24	4.47	2.09	1.24
	CaO	3.52	10.49	4.90	4.20	6.50	7.27	5.91	5.63	4.52
	Na_2O	3.48	2.63	2.91	3.32	3.49	3.69	2.60	3.68	3.04
	K_2O	2.62	0.26	0.38	0.80	1.18	0.13	0.69	0.86	0.63
	P_2O_5	0.20	0.20	0.14	0.28	0.27	0.23	0.28	0.18	0.15
	LOI	0.49	0.72	0.96	1.80	3.11	7.00	3.48	6.05	3.73
	Total	98.40	99.23	100.39	99.19	99.78	99.38	100.58	99.74	100.19
	Traces (ppm)									
	Sc	10.72	33.82	9.08	15.95	15.40	24.92	21.99	16.52	19.53
	V	97.48	244.56	58.76	202.11	172.30	221.22	190.69	129.42	147.52
	Cr	22.68	324.15	24.96	22.99	11.20	79.35	28.56	10.41	63.51
	Co	11.44	18.34	9.68	19.12	17.91	22.38	23.49	15.88	22.48
	Ni	10.88	30.12	2.59	1.72	3.74	155.48	2.74	18.71	18.02
	Cu	27.99	32.13	44.65	56.29	2.06	19.03	25.18	3.48	44.32
	Zn	62.10	62.11	18.92	47.15	58.67	77.54	48.52	57.36	24.71
	Sr	510.05	507.27	723.78	1005.61	950.62	790.82	869.92	686.58	576.93
	Y	25.21	28.13	12.66	25.98	32.79	23.82	18.42	15.97	15.55
	Zr	336.45	66.05	106.16	150.03	145.95	89.84	139.00	81.48	111.59
	Ba	1575.69	1125.39	942.53	1479.75	1305.62	271.03	1263.62	656.66	954.01
ICP-MS analysis	Traces (ppm)									
	Ti	0.73	0.79	0.31	0.77	0.78	0.92	0.82	0.60	0.76
	V	89.28	245.44	63.53	208.10	171.03	214.50	188.64	132.22	150.92
	^{52}Cr	23.35	329.37	8.25	6.36	12.30	77.72	12.06	10.80	61.59
	^{53}Cr	30.53	331.17	11.21	8.25	19.75	74.99	14.34	19.05	62.49
	Mn	0.09	0.26	0.09	0.19	0.15	0.14	0.15	0.11	0.06
	^{57}Fe	4.75	9.97	3.56	6.07	6.50	10.65	6.82	6.72	6.58
	Co	10.90	17.74	8.92	18.03	18.56	23.53	22.15	18.06	24.75
	^{60}Ni	325.64	25.96	3.46	3.98	302.65	497.90	1.19	314.14	352.99
	^{62}Ni	289.40	29.47	4.09	2.13	260.32	419.56	0.99	269.72	293.43
	Zn	-	63.42	53.53	79.81	-	-	73.74	-	-
	Ga	17.13	16.43	16.19	18.70	19.40	19.43	19.00	14.80	17.38
	Rb	-	2.09	2.40	5.10	-	-	3.74	-	-
	Sr	487.80	510.86	723.88	997.02	931.36	761.58	842.47	672.19	554.53
	Y	23.65	28.91	13.08	26.09	31.39	22.87	20.59	16.16	15.59
	Zr	325.58	66.83	104.82	158.55	140.71	79.93	143.94	77.61	105.88
	Nb	17.20	2.36	4.72	10.97	10.12	5.41	10.20	4.04	8.46
	Ba	1575.69	1108.44	925.64	1448.46	1305.62	271.03	1241.53	656.66	954.01
	La	28.02	15.77	16.70	26.50	29.92	14.64	25.50	12.86	13.62
	Ce	53.16	30.99	33.27	55.24	53.11	28.54	49.31	25.89	26.78
	Pr	6.57	4.53	3.85	6.80	7.17	4.01	6.04	3.46	3.45
	Nd	23.74	20.18	14.72	27.20	27.29	16.31	24.48	13.46	13.30
	Sm	4.77	4.59	2.62	5.25	5.70	3.82	4.73	2.93	3.10
	Eu	1.26	1.47	0.95	1.68	1.78	1.27	1.48	1.00	1.07
	Gd	4.23	4.63	2.26	4.75	5.54	3.90	4.15	2.77	2.90
	Tb	0.65	0.71	0.32	0.65	0.81	0.62	0.57	0.43	0.46
	Dy	3.76	4.53	1.94	3.99	4.62	3.71	3.36	2.57	2.73
	Ho	0.73	0.87	0.38	0.75	0.90	0.74	0.62	0.51	0.52
	Er	2.18	2.72	1.19	2.23	2.51	2.14	1.86	1.49	1.43
	Tm	0.33	0.42	0.19	0.34	0.36	0.32	0.28	0.23	0.21
	Yb	2.32	2.60	1.33	2.13	2.33	2.17	1.74	1.52	1.47
	Lu	0.38	0.42	0.24	0.35	0.39	0.35	0.29	0.24	0.22
	Hf	7.63	1.79	2.58	3.83	3.41	1.95	3.54	1.97	2.58
	Ta	1.00	0.12	0.31	0.66	0.57	0.27	0.62	0.22	0.54
	Pb	19.06	7.03	5.34	7.14	18.03	17.43	4.10	17.48	17.27
	Th	9.19	1.41	3.54	5.80	5.88	1.81	5.77	2.48	2.01
	U	3.50	1.83	1.28	2.05	2.00	0.64	1.91	0.92	0.86

E.5 Bath-Dunrobin Formation samples

		AHBD07	AHBD09	AHBD10	AHBD11	AHBD12	AHBD13	AHBD14	AHBD16	AHBD18	AHBD19
ICP-OES analysis	Majors (wt %)										
	SiO_2	73.13	46.39	46.76	44.09	89.62	47.86	49.70	49.55	48.10	47.77
	TiO_2	0.23	1.36	1.40	0.98	0.10	1.35	1.34	1.29	1.56	1.21
	Al_2O_3	15.15	13.17	13.24	12.75	2.61	12.94	12.43	12.45	12.98	12.50
	Fe_2O_3	1.29	13.05	13.78	10.32	1.05	12.89	12.69	12.61	14.10	11.83
	MnO	0.02	0.21	0.24	0.41	0.31	0.26	0.23	0.35	0.21	0.23
	MgO	0.71	6.35	7.03	8.41	0.40	7.40	6.67	7.55	6.49	6.72
	CaO	1.14	10.73	10.56	9.18	0.89	8.49	9.32	8.75	7.22	8.85
	Na_2O	7.07	2.67	1.81	3.93	0.28	3.61	2.39	2.51	4.35	2.42
	K_2O	0.49	0.05	0.02	0.05	0.38	0.03	0.04	0.00	0.40	0.04
	P_2O_5	0.05	0.11	0.11	0.10	0.11	0.12	0.11	0.10	0.12	0.10
	LOI	0.31	5.25	4.46	9.08	3.15	4.39	4.87	4.83	5.70	8.45
	Total	99.59	99.36	99.42	99.31	98.90	99.31	99.31	99.98	101.21	100.12
	Traces (ppm)										
	Sc	2.98	45.84	48.85	40.72	3.30	49.10	45.93	45.27	49.41	41.32
	V	48.99	360.58	371.15	264.61	4.63	342.62	346.61	326.33	393.39	313.27
	Cr	71.29	174.13	169.14	404.88	18.32	143.56	157.80	140.99	130.80	90.76
	Co	5.22	45.14	45.49	37.48	5.80	44.54	42.98	42.97	50.91	41.94
	Ni	7.79	106.74	97.19	97.78	22.33	125.42	73.31	76.88	56.55	71.68
	Cu	318.60	136.75	122.19	124.84	30.77	135.05	184.28	57.00	230.22	76.89
	Zn	7.92	98.52	80.59	79.90	63.75	92.20	104.88	44.49	112.69	74.44
	Sr	274.94	392.80	202.17	120.08	177.42	55.54	397.55	76.60	34.35	1045.88
	Y	3.78	30.07	29.43	20.82	15.81	28.00	28.17	22.62	32.42	25.52
	Zr	99.09	69.51	72.43	45.48	21.44	70.33	68.46	69.23	79.04	64.33
	Ba	331.77	48.82	43.61	220.74	671.42	29.24	130.59	43.70	43.50	934.79
ICP-MS analysis	Traces (ppm)										
	Tl	0.20	1.42	1.41	1.02	0.11	1.32	1.33	1.26	1.51	1.25
	V	13.20	363.39	369.69	257.20	7.45	337.34	344.98	340.90	376.12	314.93
	^{52}Cr	61.06	172.40	167.81	390.71	10.54	138.83	154.45	138.04	97.66	92.10
	^{53}Cr	61.62	160.06	164.33	344.55	21.85	135.20	148.76	136.42	98.31	87.86
	Mn	0.02	0.21	0.23	0.37	0.30	0.25	0.23	0.35	0.20	0.22
	^{57}Fe	1.36	13.97	13.78	9.86	0.97	12.48	12.67	12.35	13.38	12.30
	Co	3.71	50.19	50.42	42.07	6.31	48.30	47.86	48.60	46.30	47.86
	^{60}Ni	9.04	287.85	107.14	393.51	22.49	147.10	137.86	74.35	52.70	104.44
	^{62}Ni	6.81	276.81	116.63	385.42	21.21	167.76	142.30	82.75	63.28	106.38
	Zn	18.82	-	51.34	-	17.81	42.97	44.35	44.69	49.36	-
	Ga	15.50	18.37	17.87	14.71	3.11	14.82	13.53	14.21	15.82	15.23
	Rb	5.21	-	0.03	-	3.46	0.12	0.59	0.03	1.56	-
	Sr	275.93	386.98	196.86	128.73	168.64	54.73	383.79	74.33	30.07	1030.94
	Y	3.43	29.94	28.77	21.03	13.85	26.19	26.98	26.06	30.27	24.96
	Zr	102.53	65.64	70.07	42.13	20.12	66.26	65.95	64.19	80.49	64.03
	Nb	1.85	3.85	4.21	2.47	1.27	3.79	3.90	3.85	4.64	3.88
	Ba	326.71	48.82	41.16	220.74	669.80	25.86	123.94	42.82	40.75	934.79
	La	9.93	4.90	4.91	3.52	5.77	4.47	4.86	3.50	4.79	4.67
	Ce	13.73	11.56	10.93	8.81	12.57	9.90	10.20	9.27	11.47	9.64
	Pr	1.56	1.89	1.72	1.45	2.66	1.58	1.61	1.48	1.74	1.55
	Nd	5.96	9.14	8.67	6.97	10.88	7.96	8.19	7.82	9.02	7.61
	Sm	1.19	3.06	2.90	2.31	2.47	2.71	2.74	2.55	2.99	2.63
	Eu	0.51	1.13	1.07	0.88	0.64	1.00	1.01	0.99	1.09	1.08
	Gd	1.04	3.88	3.65	2.87	2.11	3.40	3.49	3.39	3.74	3.28
	Tb	0.13	0.73	0.67	0.53	0.35	0.63	0.64	0.59	0.69	0.60
	Dy	0.65	4.79	4.59	3.43	2.17	4.26	4.35	4.13	4.86	4.00
	Ho	0.10	0.98	0.91	0.69	0.42	0.84	0.87	0.81	0.96	0.82
	Er	0.28	2.83	2.80	1.95	1.15	2.54	2.60	2.51	2.93	2.32
	Tm	0.04	0.44	0.43	0.30	0.17	0.39	0.40	0.39	0.45	0.36
	Yb	0.22	2.94	2.83	1.97	1.15	2.57	2.63	2.50	3.01	2.32
	Lu	0.03	0.45	0.45	0.30	0.19	0.40	0.41	0.39	0.49	0.32
	Hf	2.51	1.72	1.76	1.14	0.47	1.71	1.71	1.79	2.02	1.68
	Ta	0.12	0.22	0.27	0.15	0.04	0.23	0.22	0.24	0.24	0.23
	Pb	3.40	15.38	9.14	21.43	3.01	8.98	8.33	2.75	1.05	8.27
	Th	1.58	0.36	0.31	0.33	0.62	0.29	0.29	0.24	0.31	0.29
	U	0.72	0.17	0.15	0.18	0.26	0.15	0.17	0.10	0.16	0.14

Appendix E: Major and trace element data for the Cretaceous and Tertiary Jamaican igneous rocks and their variation diagrams

		AHBD20	AHBD22	AHBD23	AHBD24	AHBD25	AHBD26	AHBD27	AHBD28	AHBD29	AHBD30
ICP-OES analysis	Majors (wt %)										
	SiO_2	48.70	76.50	46.95	47.07	44.79	47.19	48.72	50.03	49.04	42.98
	TiO_2	1.17	0.34	1.01	1.33	1.21	1.30	0.99	1.23	1.23	1.55
	Al_2O_3	11.92	6.51	13.39	12.40	12.96	12.31	13.42	13.31	13.20	14.19
	Fe_2O_3	11.03	4.36	10.80	12.95	12.07	11.59	10.68	11.47	11.93	18.33
	MnO	0.38	0.85	0.71	0.29	0.25	0.24	0.14	0.18	0.17	0.21
	MgO	7.31	2.04	8.38	7.23	7.56	6.22	6.90	7.39	7.63	5.81
	CaO	9.32	1.49	7.87	8.70	10.89	8.54	9.52	7.33	9.28	8.17
	Na_2O	1.62	0.43	3.34	2.31	2.74	3.06	2.58	3.74	3.24	5.21
	K_2O	0.15	0.30	0.10	0.24	0.00	0.04	0.03	0.06	0.11	0.20
	P_2O_5	0.09	0.10	0.08	0.11	0.08	0.10	0.14	0.09	0.10	0.12
	LOI	7.14	6.32	7.47	7.34	7.09	7.67	7.30	4.44	3.22	3.12
	Total	98.83	99.25	100.10	99.97	99.65	98.27	100.41	99.28	99.14	99.88
	Traces (ppm)										
	Sc	40.94	8.21	40.16	46.15	49.13	46.21	41.59	45.60	47.78	41.90
	V	278.19	55.82	245.04	356.55	346.51	333.87	182.76	307.85	312.71	355.80
	Cr	122.56	38.27	328.39	154.79	231.29	81.50	258.00	234.52	235.22	37.79
	Co	37.72	12.68	39.00	50.20	54.77	52.86	36.47	39.56	47.57	54.78
	Ni	67.17	19.61	167.50	66.69	109.31	74.14	107.40	95.21	131.30	57.93
	Cu	91.48	78.26	14.30	245.09	371.13	388.27	133.65	128.15	351.66	324.03
	Zn	43.85	22.79	45.20	111.73	149.82	158.89	51.02	38.54	330.60	148.68
	Sr	374.12	217.08	51.79	819.10	211.05	174.30	193.82	63.85	188.68	148.13
	Y	21.71	16.60	18.01	26.95	26.54	26.86	30.97	24.63	25.18	32.91
	Zr	56.81	55.55	47.93	69.34	60.30	67.07	83.55	60.19	62.18	84.68
	Ba	1753.93	941.87	152.84	912.32	13.21	146.51	34.46	2214.79	80.20	511.88
ICP-MS analysis	Traces (ppm)										
	Ti	1.10	0.32	0.96	1.34	1.23	1.32	0.96	1.17	1.24	1.70
	V	284.40	61.47	254.92	350.06	317.99	318.38	196.52	303.27	307.73	361.88
	^{52}Cr	111.43	25.70	336.14	156.02	232.91	84.11	255.78	229.32	242.41	41.92
	^{53}Cr	110.51	28.32	322.19	156.38	227.83	87.74	248.76	231.74	239.81	45.94
	Mn	0.38	0.85	0.70	0.28	0.23	0.23	0.14	0.18	0.16	0.21
	^{57}Fe	10.67	4.18	10.15	12.74	11.83	11.62	10.43	11.11	11.49	13.37
	Co	40.65	14.07	41.94	48.15	45.97	42.52	39.02	43.29	44.84	45.53
	^{60}Ni	65.75	7.03	155.67	64.33	112.62	71.12	101.93	82.62	112.46	50.40
	^{62}Ni	72.65	9.07	162.93	72.09	120.21	83.91	107.92	91.98	114.93	59.53
	Zn	40.01	36.76	42.52	41.99	37.54	35.88	49.52	36.84	34.91	39.07
	Ga	12.86	7.86	12.91	15.29	17.52	13.85	15.16	11.01	13.67	17.83
	Rb	0.36	3.63	0.58	1.42	0.42	0.73	0.21	0.12	0.22	3.05
	Sr	374.04	216.06	48.93	837.30	192.43	166.40	187.13	57.96	182.58	149.54
	Y	23.13	17.71	19.00	26.63	23.21	24.40	34.34	24.55	24.16	30.30
	Zr	56.53	57.00	49.20	71.40	63.40	71.60	88.11	62.14	61.03	91.95
	Nb	3.35	2.43	2.79	4.08	3.46	4.00	5.29	3.77	3.80	5.46
	Ba	1794.74	951.06	153.05	848.10	14.01	134.93	32.49	2214.80	74.63	478.95
	La	3.15	10.23	2.20	4.00	4.00	4.30	5.35	3.25	3.82	4.60
	Ce	8.44	19.88	6.89	10.13	9.78	10.23	13.90	8.89	10.18	11.71
	Pr	1.35	3.05	1.15	1.52	1.35	1.42	2.19	1.43	1.51	1.67
	Nd	7.09	12.60	6.00	7.88	6.85	7.24	11.23	7.75	7.72	8.42
	Sm	2.30	2.66	1.95	2.68	2.45	2.58	3.44	2.50	2.64	3.13
	Eu	1.14	0.82	0.72	1.11	0.90	0.95	1.28	1.08	0.89	1.23
	Gd	3.00	2.74	2.56	3.40	2.87	3.08	4.47	3.26	3.01	3.67
	Tb	0.53	0.43	0.45	0.63	0.57	0.60	0.77	0.57	0.57	0.71
	Dy	3.71	2.69	3.05	4.41	3.85	4.25	5.39	3.90	3.92	4.88
	Ho	0.72	0.51	0.59	0.87	0.75	0.83	1.05	0.75	0.77	1.01
	Er	2.25	1.60	1.86	2.62	2.21	2.41	3.31	2.35	2.36	2.95
	Tm	0.34	0.24	0.29	0.41	0.34	0.37	0.51	0.36	0.36	0.45
	Yb	2.20	1.51	1.83	2.67	2.29	2.53	3.17	2.29	2.37	3.04
	Lu	0.35	0.23	0.30	0.43	0.34	0.39	0.55	0.36	0.39	0.46
	Hf	1.58	1.48	1.40	1.82	1.41	1.66	2.35	1.63	1.57	2.08
	Ta	0.22	0.19	0.18	0.21	0.14	0.16	0.34	0.24	0.15	0.20
	Pb	3.74	3.86	3.46	1.08	1.10	1.50	4.21	4.79	6.27	1.40
	Th	0.22	1.64	0.19	0.27	0.26	0.28	0.38	0.24	0.25	0.34
	U	0.08	0.66	0.11	0.16	0.18	0.19	0.14	0.11	0.17	0.22

E.6 Newcastle Volcanic samples

		AHWG11	AHWG12	AHWG14	AHWG16	AHWG17	AHWG18	AHWG19	AHWG20	AHWG21
ICP-OES analysis	Majors (wt %)									
	SiO_2	71.66	69.63	68.05	68.99	68.97	69.31	69.38	68.75	70.58
	TiO_2	0.32	0.30	0.37	0.31	0.35	0.35	0.36	0.35	0.34
	Al_2O_3	15.76	15.21	14.95	15.32	15.32	15.16	15.28	15.26	15.75
	Fe_2O_3	2.29	3.27	2.32	3.00	3.08	3.28	3.32	3.02	3.11
	MnO	0.02	0.05	0.03	0.02	0.05	0.04	0.03	0.04	0.05
	MgO	0.41	1.42	0.61	1.39	1.92	2.09	2.08	1.93	1.78
	CaO	1.20	1.46	2.89	0.99	0.81	0.56	0.34	1.11	0.34
	Na_2O	5.16	5.13	4.86	6.23	6.06	5.65	6.56	5.54	6.25
	K_2O	0.42	0.67	0.51	0.31	0.32	0.75	0.50	0.43	0.18
	P_2O_5	0.04	0.08	0.13	0.08	0.10	0.10	0.11	0.10	0.11
	LOI	1.88	2.12	3.94	2.07	2.15	1.92	2.11	2.73	1.68
	Total	97.28	99.34	98.66	98.73	99.14	99.21	100.05	99.26	100.17
	Traces (ppm)									
	Sc	5.63	5.65	5.33	5.93	6.99	6.39	6.48	6.87	5.81
	V	62.25	48.88	63.86	42.24	65.22	63.80	66.12	64.85	64.61
	Cr	36.70	36.44	29.38	48.35	36.70	43.94	53.75	41.83	27.05
	Co	5.27	13.11	8.89	12.00	12.20	12.98	13.57	12.08	12.60
	Ni	32.61	29.26	23.84	21.69	35.17	31.05	42.17	42.92	11.94
	Cu	103.80	144.27	89.49	108.63	102.44	147.69	256.61	98.91	61.87
	Zn	13.61	25.40	23.69	20.70	50.54	43.54	68.45	41.28	50.18
	Sr	147.79	171.77	79.68	143.01	92.61	125.63	104.54	97.67	75.35
	Y	13.63	9.71	11.75	9.16	10.60	11.21	11.31	9.31	10.06
	Zr	133.07	124.72	147.07	132.72	137.75	122.64	124.38	122.03	122.77
	Ba	216.64	365.84	54.55	153.22	117.46	318.60	129.43	123.58	105.97
ICP-MS analysis	Traces (ppm)									
	Ti	0.29	0.29	0.35	0.29	0.34	0.34	0.34	0.33	0.31
	V	34.38	36.00	34.92	36.28	41.31	42.44	39.44	41.83	37.31
	^{52}Cr	28.77	33.40	24.99	47.38	32.73	41.99	54.11	39.92	23.20
	^{53}Cr	27.33	28.93	18.36	42.90	28.53	35.25	50.54	34.58	17.60
	Mn	0.02	0.05	0.02	0.02	0.05	0.03	0.03	0.04	0.05
	^{57}Fe	1.97	2.86	1.91	2.54	2.59	2.81	2.86	2.60	2.67
	Co	2.73	7.68	4.52	6.56	7.60	8.28	8.84	7.56	7.84
	^{60}Ni	27.52	12.07	-2.31	-6.84	19.08	7.16	25.81	29.72	-22.65
	^{62}Ni	22.19	13.54	4.22	-2.71	36.87	12.12	35.12	45.18	-21.07
	Ga	15.04	15.22	15.80	15.09	15.19	14.98	14.85	15.13	15.31
	Rb	5.17	9.56	7.12	3.62	2.70	6.62	6.00	6.13	2.13
	Sr	149.77	160.30	73.73	131.00	86.12	117.40	96.96	91.83	75.51
	Y	12.78	8.18	10.12	7.39	8.89	9.67	9.69	7.71	8.12
	Zr	138.81	138.60	155.67	145.03	134.80	134.17	133.54	134.06	133.96
	Nb	4.98	4.92	7.35	5.37	6.87	6.90	6.93	6.85	6.09
	Ba	210.39	378.08	50.77	151.72	120.09	321.36	127.77	124.49	63.96
	La	4.55	11.28	15.10	12.47	17.78	13.67	15.25	13.08	9.61
	Ce	9.40	15.70	27.88	18.79	29.51	22.17	23.78	20.04	16.73
	Pr	1.67	1.74	3.27	1.99	3.29	2.54	2.67	2.21	2.02
	Nd	6.17	5.95	11.39	6.62	11.17	9.01	9.39	7.64	7.49
	Sm	1.43	1.22	2.29	1.30	2.08	1.80	1.75	1.50	1.54
	Eu	0.75	0.46	0.62	0.43	0.58	0.66	0.49	0.50	0.38
	Gd	1.72	1.27	2.01	1.16	1.81	1.78	1.66	1.37	1.45
	Tb	0.28	0.20	0.30	0.19	0.25	0.25	0.24	0.22	0.22
	Dy	1.73	1.24	1.70	1.21	1.44	1.52	1.44	1.27	1.32
	Ho	0.33	0.24	0.29	0.23	0.26	0.27	0.27	0.23	0.24
	Er	0.92	0.68	0.75	0.69	0.76	0.77	0.77	0.66	0.68
	Tm	0.13	0.11	0.11	0.11	0.12	0.12	0.12	0.11	0.11
	Yb	0.85	0.72	0.74	0.73	0.78	0.80	0.78	0.74	0.70
	Lu	0.15	0.13	0.16	0.14	0.14	0.16	0.15	0.14	0.13
	Hf	3.25	3.23	3.60	3.41	3.14	3.23	3.22	3.17	3.21
	Ta	0.47	0.41	0.63	0.45	0.55	0.56	0.56	0.54	0.50
	Pb	10.07	5.09	6.35	4.70	4.22	5.71	5.35	4.68	4.20
	Th	3.26	2.68	3.19	3.15	2.98	3.04	3.04	2.97	2.75
	U	0.59	0.39	1.03	0.86	0.97	0.95	0.98	0.91	0.90

Appendix E: Major and trace element data for the Cretaceous and Tertiary Jamaican igneous rocks and their variation diagrams

		AHWG22	AHWG23	AHWG24	AHWG25	AHWG26	AHWG27	AHWG30	AHWG32	AHWG33
ICP-OES analysis	Majors (wt %)									
	SiO_2	66.24	71.00	69.01	70.14	70.48	71.12	67.10	71.81	70.45
	TiO_2	0.29	0.35	0.31	0.33	0.34	0.33	0.33	0.33	0.33
	Al_2O_3	14.49	15.93	15.23	15.29	15.31	15.27	14.88	15.83	15.58
	Fe_2O_3	2.92	4.40	3.35	3.43	3.57	2.82	2.81	3.22	2.08
	MnO	0.06	0.02	0.02	0.05	0.05	0.05	0.04	0.03	0.02
	MgO	0.48	0.82	0.82	1.67	1.22	1.69	1.24	1.37	0.93
	CaO	3.95	0.32	0.28	0.34	0.85	0.47	2.35	0.31	0.41
	Na_2O	6.19	7.04	8.23	6.44	5.81	6.45	5.74	5.02	7.55
	K_2O	1.14	0.11	0.20	0.16	0.75	0.36	0.87	0.67	0.21
	P_2O_5	0.12	0.11	0.10	0.10	0.10	0.10	0.12	0.10	0.10
	LOI	4.24	1.26	0.98	1.52	1.64	1.74	3.62	1.52	1.66
	Total	100.14	101.36	98.54	99.46	100.11	100.40	99.09	100.21	99.33
	Traces (ppm)									
	Sc	5.22	6.17	4.53	6.09	5.31	5.94	6.33	5.87	5.04
	V	29.37	26.76	23.16	65.52	49.66	66.43	44.97	64.73	63.50
	Cr	6.73	31.51	16.49	41.80	37.33	32.26	25.28	97.71	28.97
	Co	1.98	18.79	10.01	14.06	6.71	11.20	8.08	12.93	7.95
	Ni	11.23	9.70	12.40	23.97	16.81	16.56	20.17	68.15	20.29
	Cu	42.31	48.49	149.37	53.11	101.55	105.78	87.65	90.64	147.79
	Zn	7.55	20.47	18.66	39.77	50.32	42.18	5.01	24.54	47.16
	Sr	100.06	81.30	77.88	106.86	132.46	149.92	114.76	146.71	138.95
	Y	8.48	10.83	8.21	9.07	6.54	10.05	7.66	8.38	7.17
	Zr	143.89	129.81	148.02	122.43	138.22	121.62	143.57	123.87	132.64
	Ba	117.21	58.63	49.77	45.67	287.70	103.57	281.64	452.10	85.95
ICP-MS analysis	Traces (ppm)									
	Ti	0.26	0.32	0.27	0.31	0.29	0.31	0.28	0.31	0.31
	V	36.25	26.67	25.54	38.24	32.41	44.13	42.66	37.32	31.62
	^{52}Cr	8.62	26.15	16.61	40.56	29.32	28.39	30.86	101.72	24.37
	^{53}Cr	-	21.37	-	37.00	-	21.67	-	106.33	16.09
	Mn	0.06	0.02	0.02	0.05	0.05	0.04	0.04	0.03	0.02
	^{57}Fe	2.96	3.76	3.38	2.92	3.34	2.37	2.78	2.69	1.68
	Co	3.38	8.11	8.76	6.77	7.94	7.21	6.82	7.59	4.33
	^{60}Ni	10.89	-27.67	6.73	-9.02	16.91	-20.34	19.95	61.37	-16.08
	^{62}Ni	9.52	-9.45	8.96	17.37	15.84	30.03	18.26	62.19	-12.42
	Ga	14.61	16.26	14.44	15.79	15.21	15.07	14.89	16.54	16.99
	Rb	32.23	0.98	6.05	1.94	10.86	5.09	23.35	3.74	2.22
	Sr	92.69	79.40	65.79	107.10	130.79	146.55	108.77	141.19	137.69
	Y	8.54	8.97	8.15	7.97	6.71	8.29	7.87	6.27	5.44
	Zr	134.23	136.92	144.91	133.86	137.30	132.91	136.53	134.28	142.22
	Nb	6.17	6.52	7.21	6.39	5.32	6.52	5.20	3.57	3.30
	Ba	116.09	57.03	44.09	42.88	275.35	90.80	284.27	447.57	74.47
	La	20.65	13.56	11.07	14.68	13.25	12.97	12.47	17.55	13.77
	Ce	24.09	21.48	19.98	22.35	22.79	19.94	18.65	26.81	23.56
	Pr	2.56	2.54	2.16	2.47	2.35	2.24	1.97	2.90	2.70
	Nd	9.12	9.04	8.13	8.48	8.12	7.84	7.09	9.71	9.20
	Sm	1.75	1.74	1.63	1.60	1.47	1.55	1.45	1.68	1.64
	Eu	0.64	0.55	0.59	0.57	0.48	0.56	0.51	0.54	0.44
	Gd	1.66	1.59	1.46	1.46	1.36	1.47	1.41	1.45	1.35
	Tb	0.23	0.24	0.22	0.21	0.19	0.22	0.21	0.20	0.18
	Dy	1.36	1.46	1.32	1.22	1.16	1.31	1.29	1.08	0.96
	Ho	0.24	0.28	0.24	0.23	0.21	0.25	0.23	0.19	0.17
	Er	0.75	0.80	0.76	0.65	0.62	0.69	0.70	0.53	0.50
	Tm	0.12	0.13	0.11	0.10	0.10	0.12	0.10	0.08	0.08
	Yb	0.75	0.84	0.74	0.66	0.63	0.75	0.67	0.56	0.53
	Lu	0.13	0.16	0.12	0.13	0.10	0.11	0.10	0.10	0.11
	Hf	3.05	3.26	3.23	3.21	3.15	3.18	3.02	3.13	3.28
	Ta	0.62	0.54	0.55	0.51	0.45	0.54	0.38	0.32	0.27
	Pb	1.35	4.03	-0.10	12.58	5.14	5.48	-0.40	8.44	7.33
	Th	2.62	3.06	2.97	2.82	2.99	2.98	2.18	3.03	2.91
	U	0.95	1.84	1.61	0.98	0.85	1.31	0.72	0.94	0.88

Appendix E: Major and trace element data for the Cretaceous and Tertiary Jamaican igneous rocks and their variation diagrams

		AHWG34	AHWG01	AHWG02	AHWG03
ICP-OES analysis	Majors (wt %)				
	SiO_2	64.61	72.16	70.25	70.95
	TiO_2	0.30	0.35	0.35	0.34
	Al_2O_3	14.64	15.88	15.54	15.54
	Fe_2O_3	2.82	3.02	3.84	2.86
	MnO	0.06	0.03	0.03	0.03
	MgO	1.75	1.50	0.81	1.39
	CaO	3.44	1.40	1.39	1.01
	Na_2O	5.71	4.20	3.81	4.24
	K_2O	0.23	0.60	0.45	0.58
	P_2O_5	0.12	0.11	0.10	0.10
	LOI	4.79	1.68	2.08	1.78
	Total	98.47	100.91	98.64	98.82
	Traces (ppm)				
	Sc	6.52	6.81	6.47	7.20
	V	55.10	21.41	46.45	50.45
	Cr	39.31	35.78	32.03	36.79
	Co	11.09	9.05	9.13	10.44
	Ni	22.44	19.37	10.69	20.17
	Cu	327.10	18.47	23.75	165.12
	Zn	94.57	7.09	4.62	3.46
	Sr	402.53	175.08	153.18	148.54
	Y	8.49	8.38	8.42	8.11
	Zr	83.33	128.39	133.54	130.68
	Ba	170.76	599.03	537.43	602.99
ICP-MS analysis	Traces (ppm)				
	Ti	0.29	0.31	0.31	0.29
	V	52.91	23.12	26.18	22.68
	^{52}Cr	39.08	18.94	18.26	19.17
	^{53}Cr	32.81	20.70	20.20	20.41
	Mn	0.05	0.03	0.03	0.03
	^{57}Fe	2.34	2.84	3.74	2.72
	Co	7.63	8.55	8.83	8.47
	^{60}Ni	-13.97	22.07	23.79	14.93
	^{62}Ni	7.90	23.35	22.05	13.89
	Ga	14.93	14.55	15.14	14.10
	Rb	2.76	3.49	3.25	2.84
	Sr	405.60	165.70	147.46	136.14
	Y	6.85	8.62	7.81	8.41
	Zr	82.70	137.57	144.49	130.97
	Nb	3.45	7.75	8.06	7.31
	Ba	164.13	583.72	526.25	580.90
	La	8.04	19.45	17.94	17.07
	Ce	15.02	22.80	21.03	20.49
	Pr	1.92	2.43	2.24	2.33
	Nd	7.23	8.71	7.99	8.44
	Sm	1.44	1.53	1.45	1.51
	Eu	0.41	0.62	0.60	0.61
	Gd	1.27	1.48	1.40	1.50
	Tb	0.18	0.22	0.20	0.21
	Dy	1.05	1.31	1.22	1.29
	Ho	0.19	0.24	0.22	0.23
	Er	0.57	0.74	0.70	0.74
	Tm	0.09	0.12	0.10	0.11
	Yb	0.63	0.73	0.68	0.70
	Lu	0.11	0.12	0.11	0.11
	Hf	2.15	3.04	3.27	2.93
	Ta	0.23	0.63	0.65	0.62
	Pb	4.93	3.14	2.12	2.68
	Th	1.60	3.15	3.22	3.06
	U	0.77	0.97	0.94	0.88

E.7 Halberstadt Volcanic samples

		AHHB01	AHHB02	AHHB03	AHHB04	AHHB05	AHHB07	AHHB08
ICP-OES analysis	Majors (wt %)							
	SiO_2	49.64	48.53	53.53	51.29	45.99	50.94	48.67
	TiO_2	2.17	2.56	2.21	2.03	2.87	2.50	2.80
	Al_2O_3	12.94	14.83	13.55	12.15	14.15	15.04	13.93
	Fe_2O_3	9.01	11.62	9.42	7.75	9.66	8.72	7.71
	MnO	0.11	0.05	0.04	0.07	0.09	0.04	0.06
	MgO	7.65	10.28	8.04	7.72	8.04	7.75	6.68
	CaO	6.21	1.26	3.04	5.94	5.62	2.40	5.45
	Na_2O	2.61	2.80	2.13	2.52	3.09	3.37	3.83
	K_2O	0.07	0.03	0.05	0.02	0.10	0.09	0.09
	P_2O_5	0.27	0.31	0.38	0.32	0.67	0.30	0.67
	LOI	10.06	8.74	8.33	10.08	9.19	8.06	9.28
	Total	100.74	101.00	100.71	99.90	99.48	99.21	99.18
	Traces (ppm)							
	Sc	20.71	23.50	21.53	18.74	18.06	24.25	18.01
	V	210.84	228.79	196.99	168.93	199.80	232.12	194.77
	Cr	120.41	119.91	120.99	105.79	156.39	152.03	156.09
	Co	39.72	51.56	42.14	32.43	42.77	37.63	34.12
	Ni	149.91	94.77	96.96	95.95	116.69	133.72	99.43
	Cu	153.63	123.49	103.41	140.48	95.74	61.39	93.21
	Zn	62.99	58.07	47.50	56.31	86.71	71.40	100.21
	Sr	178.67	143.03	95.25	104.32	160.45	163.58	168.46
	Y	21.83	19.40	25.22	23.07	21.48	28.32	22.46
	Zr	92.90	102.48	92.39	84.59	160.21	127.75	133.09
	Ba	97.67	46.29	89.37	397.97	129.53	136.82	151.86
ICP-MS analysis	Traces (ppm)							
	Ti	2.21	2.79	2.30	2.14	3.44	2.56	3.47
	V	198.90	229.10	200.43	183.73	194.80	228.50	196.11
	^{52}Cr	112.43	123.29	125.15	115.84	162.18	167.23	165.01
	^{53}Cr	113.33	126.61	129.25	116.35	168.34	171.57	170.53
	Mn	0.11	0.05	0.04	0.07	0.08	0.04	0.05
	^{57}Fe	8.90	11.38	9.44	7.92	9.57	8.78	8.03
	Co	33.07	38.36	30.21	29.65	35.48	34.05	27.17
	^{60}Ni	126.56	89.95	93.63	103.97	119.03	135.05	101.47
	^{62}Ni	136.16	104.03	98.89	108.60	126.38	137.88	112.86
	Ga	16.18	18.92	16.82	15.01	19.33	16.36	17.27
	Rb	0.29	0.12	0.21	0.10	0.45	0.68	0.47
	Sr	177.48	146.18	97.22	110.14	160.52	167.20	170.75
	Y	20.13	17.94	23.53	22.31	19.91	26.46	21.29
	Zr	100.89	116.82	104.09	97.34	168.84	117.30	147.01
	Nb	28.82	33.36	29.50	27.56	45.97	33.69	43.36
	Ba	88.90	39.47	78.94	382.07	123.87	133.62	152.60
	La	17.91	11.76	13.87	13.54	27.61	19.31	24.11
	Ce	33.03	22.79	27.67	26.73	63.87	38.51	55.72
	Pr	4.28	3.08	3.84	3.65	8.93	5.09	7.74
	Nd	17.84	13.54	17.07	15.82	36.73	21.24	30.59
	Sm	4.40	3.79	4.75	4.32	7.71	5.35	6.21
	Eu	1.51	1.18	1.63	1.52	2.47	1.84	1.73
	Gd	4.32	3.72	4.91	4.43	6.39	5.41	5.02
	Tb	0.66	0.60	0.78	0.71	0.82	0.85	0.70
	Dy	3.89	3.58	4.48	4.13	4.13	4.99	3.82
	Ho	0.66	0.63	0.78	0.71	0.65	0.87	0.66
	Er	1.72	1.66	2.02	1.90	1.63	2.29	1.80
	Tm	0.25	0.26	0.28	0.27	0.22	0.32	0.27
	Yb	1.47	1.50	1.65	1.60	1.28	1.91	1.66
	Lu	0.22	0.21	0.26	0.23	0.18	0.26	0.25
	Hf	2.70	3.22	2.80	2.58	4.01	3.15	3.35
	Ta	1.68	1.99	1.70	1.56	2.42	1.88	2.37
	Pb	5.26	6.50	4.67	7.25	4.87	6.17	7.40
	Th	2.30	2.73	2.32	2.14	2.60	2.53	2.52
	U	0.61	0.74	0.57	0.52	0.72	0.72	0.69

Appendix E: Major and trace element data for the Cretaceous and Tertiary Jamaican igneous rocks and their variation diagrams

		AHHB09	AHWG08	AHWG09	AHWG10
ICP-OES analysis	Majors (wt %)				
	SiO_2	45.70	47.93	48.17	42.13
	TiO_2	2.84	2.85	2.97	2.57
	Al_2O_3	13.54	15.65	16.18	14.06
	Fe_2O_3	7.78	8.50	8.15	9.56
	MnO	0.10	0.14	0.15	0.21
	MgO	7.14	3.94	3.79	5.44
	CaO	7.39	8.48	8.00	10.92
	Na_2O	3.18	4.34	4.35	3.29
	K_2O	0.10	0.58	0.75	0.70
	P_2O_5	0.72	0.72	0.72	0.60
	LOI	10.56	6.85	6.90	10.00
	Total	99.03	99.98	100.14	99.48
	Traces (ppm)				
	Sc	17.80	17.00	18.15	15.47
	V	196.70	206.25	196.92	79.25
	Cr	212.62	61.82	77.41	85.48
	Co	34.78	38.44	37.36	45.42
	Ni	105.76	57.62	58.09	36.58
	Cu	46.82	176.64	170.77	66.76
	Zn	117.93	93.70	95.80	65.93
	Sr	211.43	496.96	479.90	235.07
	Y	23.40	23.55	24.43	21.06
	Zr	120.74	142.43	159.87	80.50
	Ba	135.17	817.23	978.72	519.68
ICP-MS analysis	Traces (ppm)				
	Ti	3.45	3.31	3.35	2.60
	V	198.52	203.57	200.49	77.92
	^{52}Cr	225.71	61.68	75.48	86.67
	^{53}Cr	231.56	61.48	74.47	88.82
	Mn	0.10	0.14	0.15	0.22
	^{57}Fe	8.11	8.68	8.13	9.71
	Co	27.96	20.99	21.20	24.98
	^{60}Ni	110.33	57.48	56.03	31.62
	^{62}Ni	121.06	82.77	82.37	54.81
	Ga	17.43	20.94	20.26	17.27
	Rb	1.03	2.69	4.04	4.88
	Sr	215.60	488.79	487.52	224.03
	Y	22.43	22.22	22.28	19.42
	Zr	144.45	153.48	160.98	90.60
	Nb	41.83	47.21	48.62	35.56
	Ba	131.38	822.66	956.73	513.55
	La	34.71	35.97	35.38	28.56
	Ce	75.75	77.74	77.21	65.87
	Pr	10.27	10.42	10.28	8.86
	Nd	40.27	41.36	40.80	35.55
	Sm	7.85	8.32	8.23	7.32
	Eu	2.31	2.52	2.54	2.27
	Gd	6.57	6.59	6.57	5.91
	Tb	0.86	0.88	0.88	0.78
	Dy	4.30	4.37	4.46	3.90
	Ho	0.70	0.70	0.71	0.61
	Er	1.74	1.78	1.78	1.52
	Tm	0.24	0.25	0.24	0.21
	Yb	1.35	1.44	1.42	1.27
	Lu	0.20	0.21	0.21	0.21
	Hf	3.25	3.39	3.62	1.87
	Ta	2.34	2.73	2.80	2.31
	Pb	6.67	4.94	4.91	4.14
	Th	2.51	3.37	3.48	2.79
	U	1.09	0.88	0.89	0.70

E.8 Sunning Hill Inlier samples

		AHSUN102	AHSUN105
ICP-OES analysis	Majors (wt %)		
	SiO_2	63.56	50.73
	TiO_2	0.63	0.93
	Al_2O_3	19.32	20.01
	Fe_2O_3	4.34	9.41
	MnO	0.14	0.18
	MgO	1.05	3.82
	CaO	1.16	7.50
	Na_2O	4.68	2.57
	K_2O	3.55	1.72
	P_2O_5	0.28	0.89
	LOI	1.57	2.61
	Total	100.27	100.37
	Traces (ppm)		
	Sc	3.15	15.97
	V	112.74	349.21
	Cr	16.57	15.66
	Co	17.30	42.15
	Ni	50.55	56.19
	Cu	53.80	144.39
	Zn	121.39	98.97
	Sr	621.57	1517.94
	Y	27.93	23.25
	Zr	121.28	62.90
	Ba	1011.50	1060.57
ICP-MS analysis	Traces (ppm)		
	Ti	0.59	0.92
	V	109.06	339.35
	^{52}Cr	11.86	12.83
	^{53}Cr	7.61	7.83
	Mn	0.14	0.19
	^{57}Fe	3.58	9.47
	Co	5.75	26.26
	^{60}Ni	38.11	49.11
	^{62}Ni	52.70	54.12
	Ga	18.34	19.26
	Rb	26.64	13.95
	Sr	708.27	1910.26
	Y	25.72	21.69
	Zr	132.04	70.21
	Nb	5.46	3.88
	Ba	974.74	1062.52
	La	33.64	21.56
	Ce	65.76	41.60
	Pr	8.39	5.63
	Nd	31.26	22.91
	Sm	6.58	5.27
	Eu	1.86	1.72
	Gd	5.32	4.78
	Tb	0.75	0.67
	Dy	4.15	3.67
	Ho	0.74	0.65
	Er	2.17	1.82
	Tm	0.34	0.28
	Yb	2.31	1.78
	Lu	0.35	0.28
	Hf	3.31	1.82
	Ta	0.28	0.20
	Pb	6.22	5.30
	Th	7.01	3.02
	U	2.23	1.13

E.9 Major and trace element variation diagrams for the Bath-Dunrobin lavas and tuffs

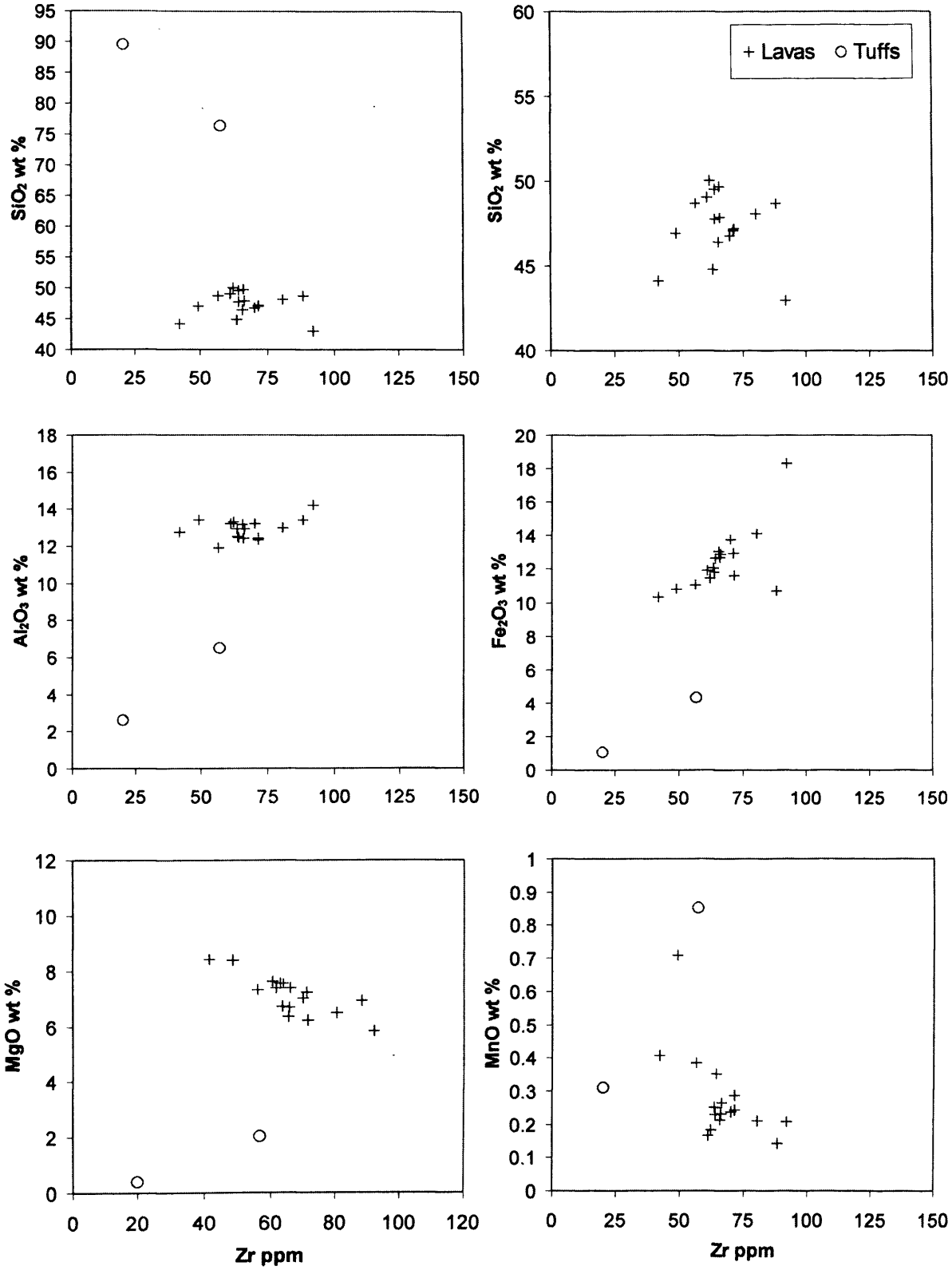

Appendix E: Major and trace element data for the Cretaceous and Tertiary Jamaican igneous rocks and their variation diagrams

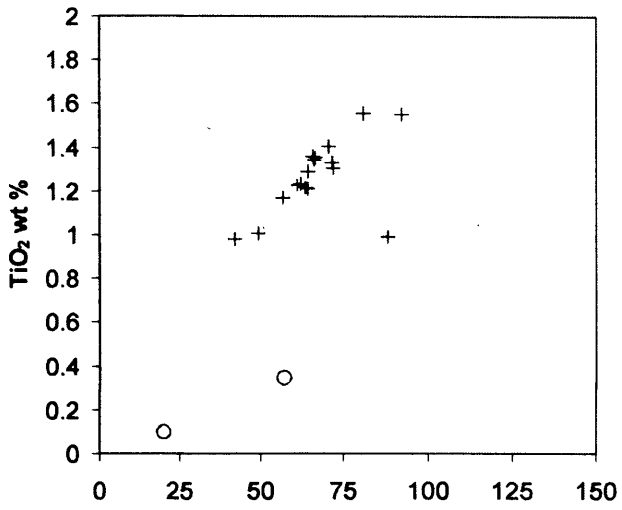

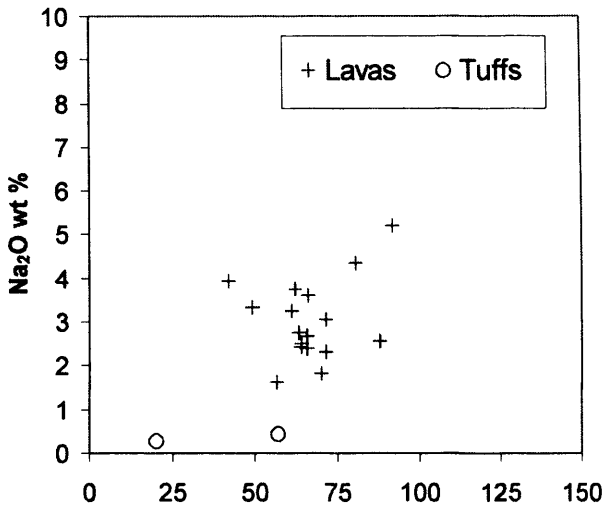

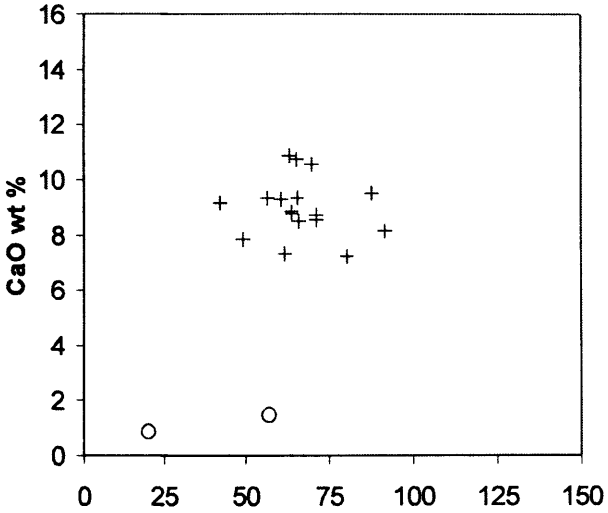

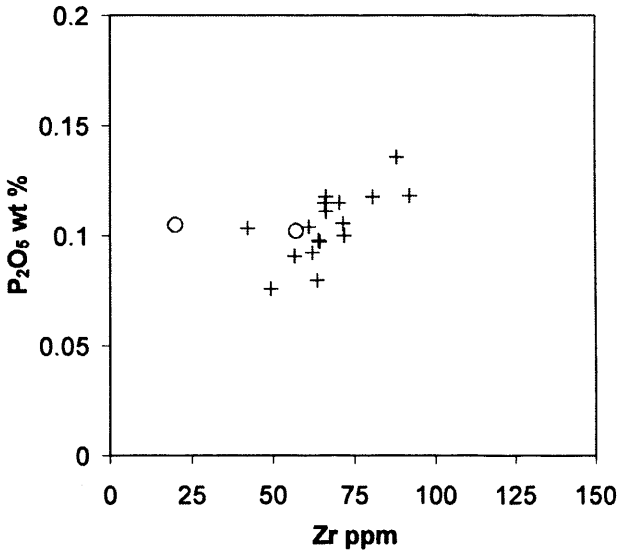

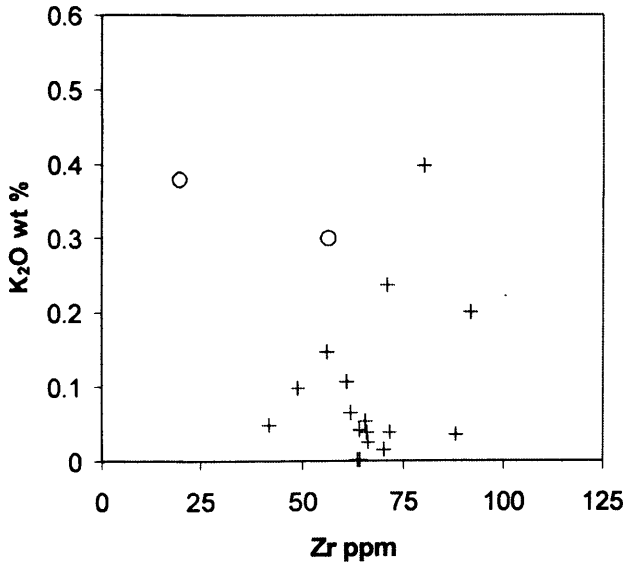

Appendix E: Major and trace element data for the Cretaceous and Tertiary Jamaican igneous rocks and their variation diagrams

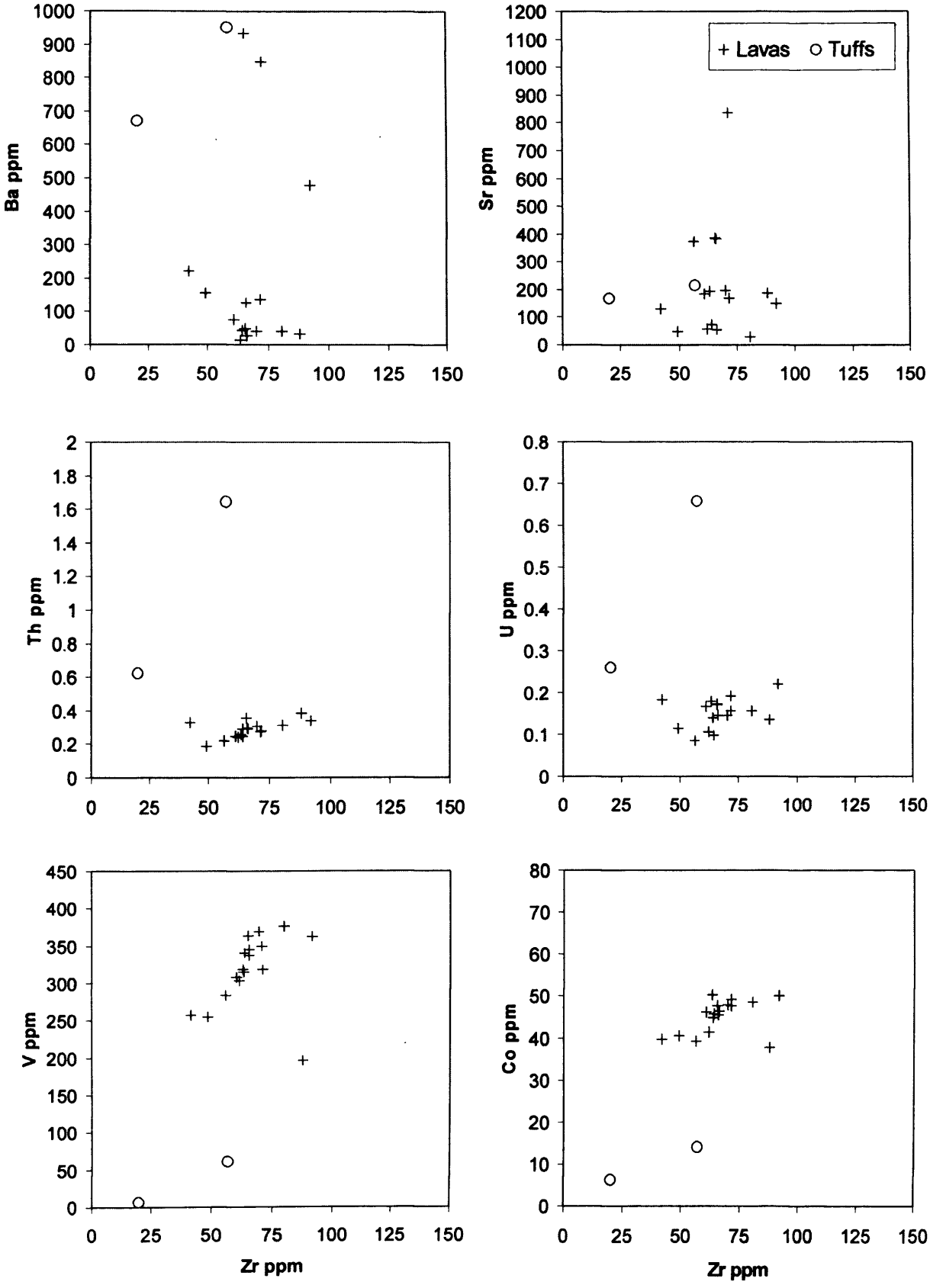

Appendix E: Major and trace element data for the Cretaceous and Tertiary Jamaican igneous rocks and their variation diagrams

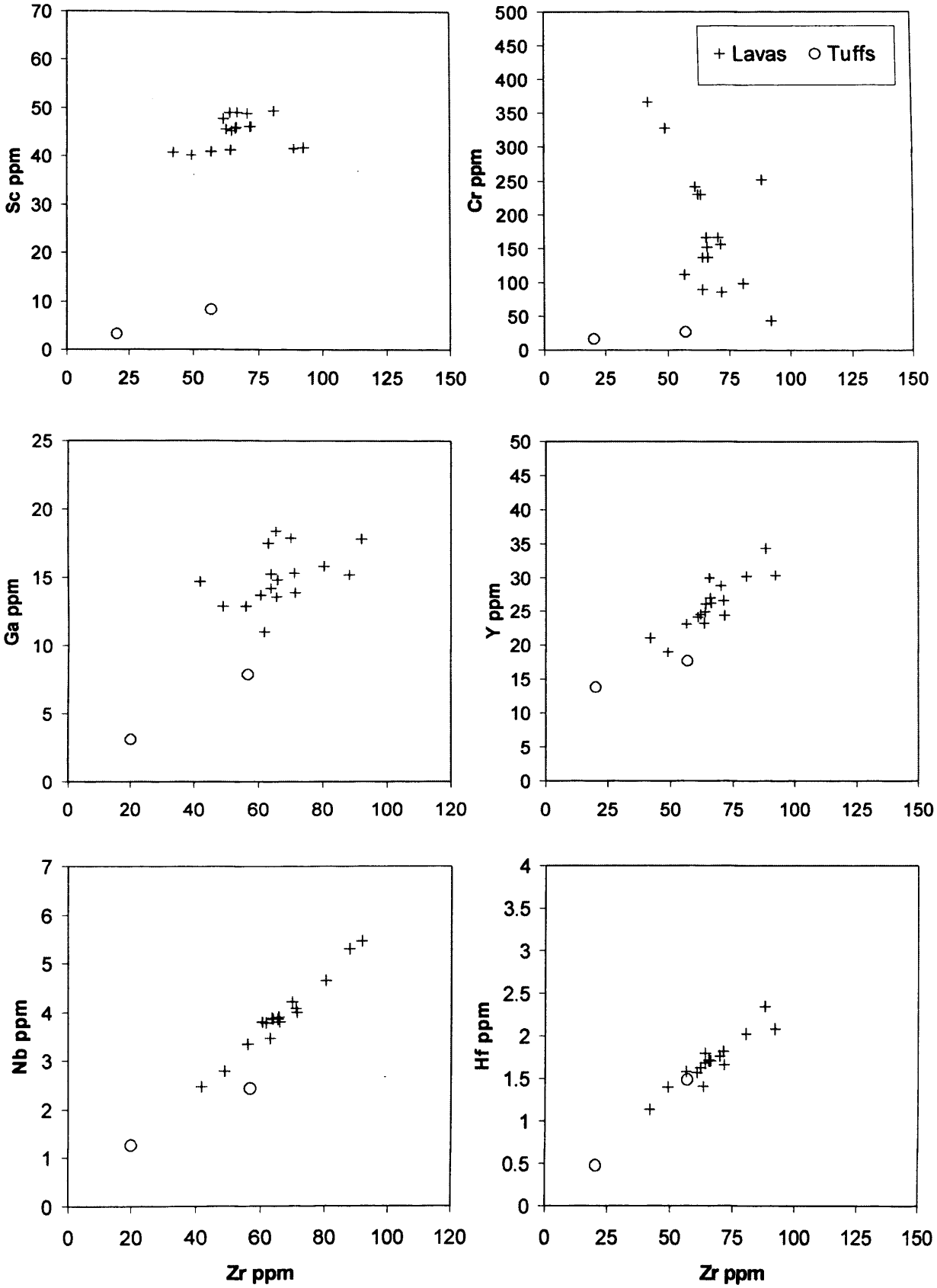

Appendix E: Major and trace element data for the Cretaceous and Tertiary Jamaican igneous rocks and their variation diagrams

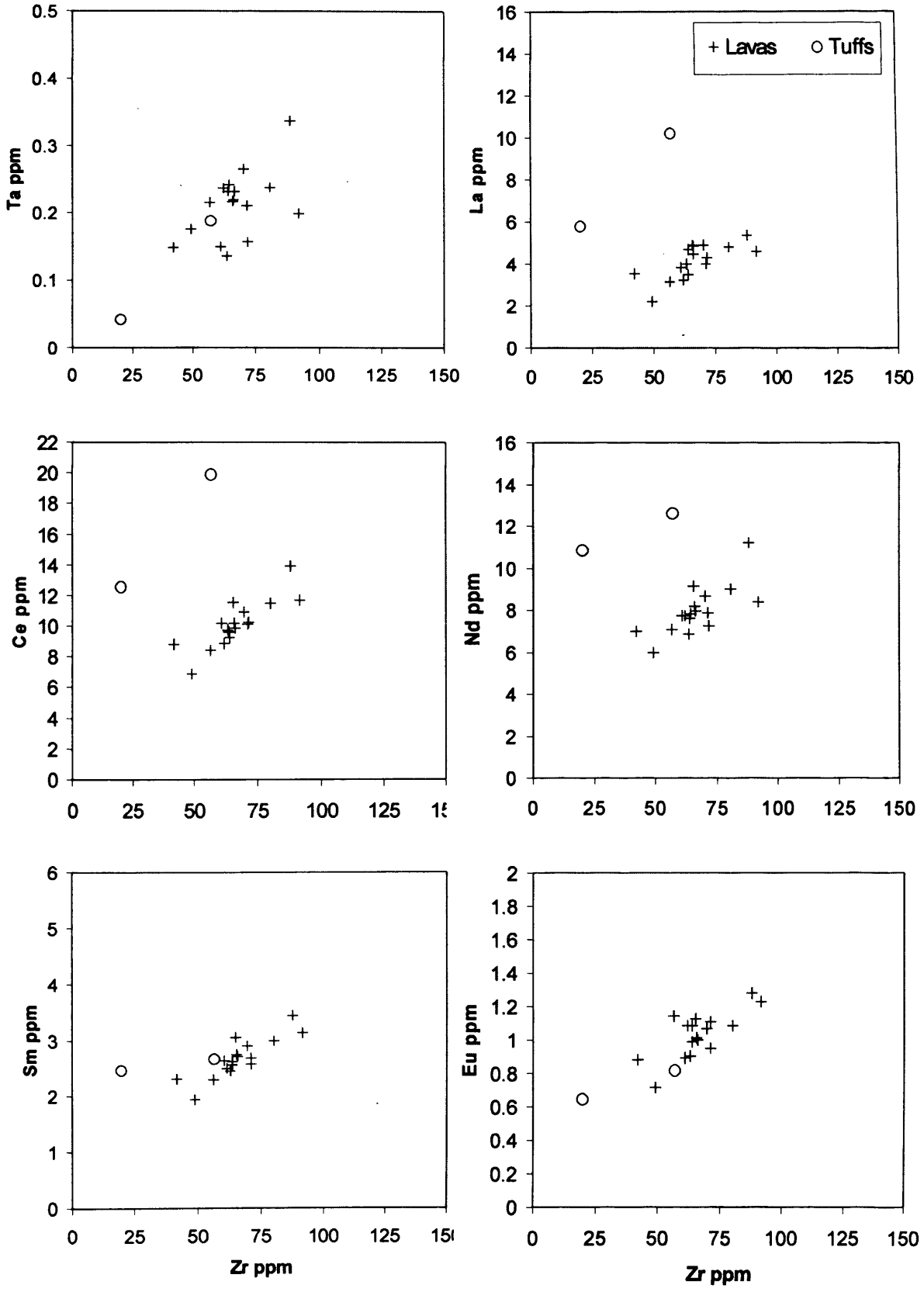

Appendix E: Major and trace element data for the Cretaceous and Tertiary Jamaican igneous rocks and their variation diagrams

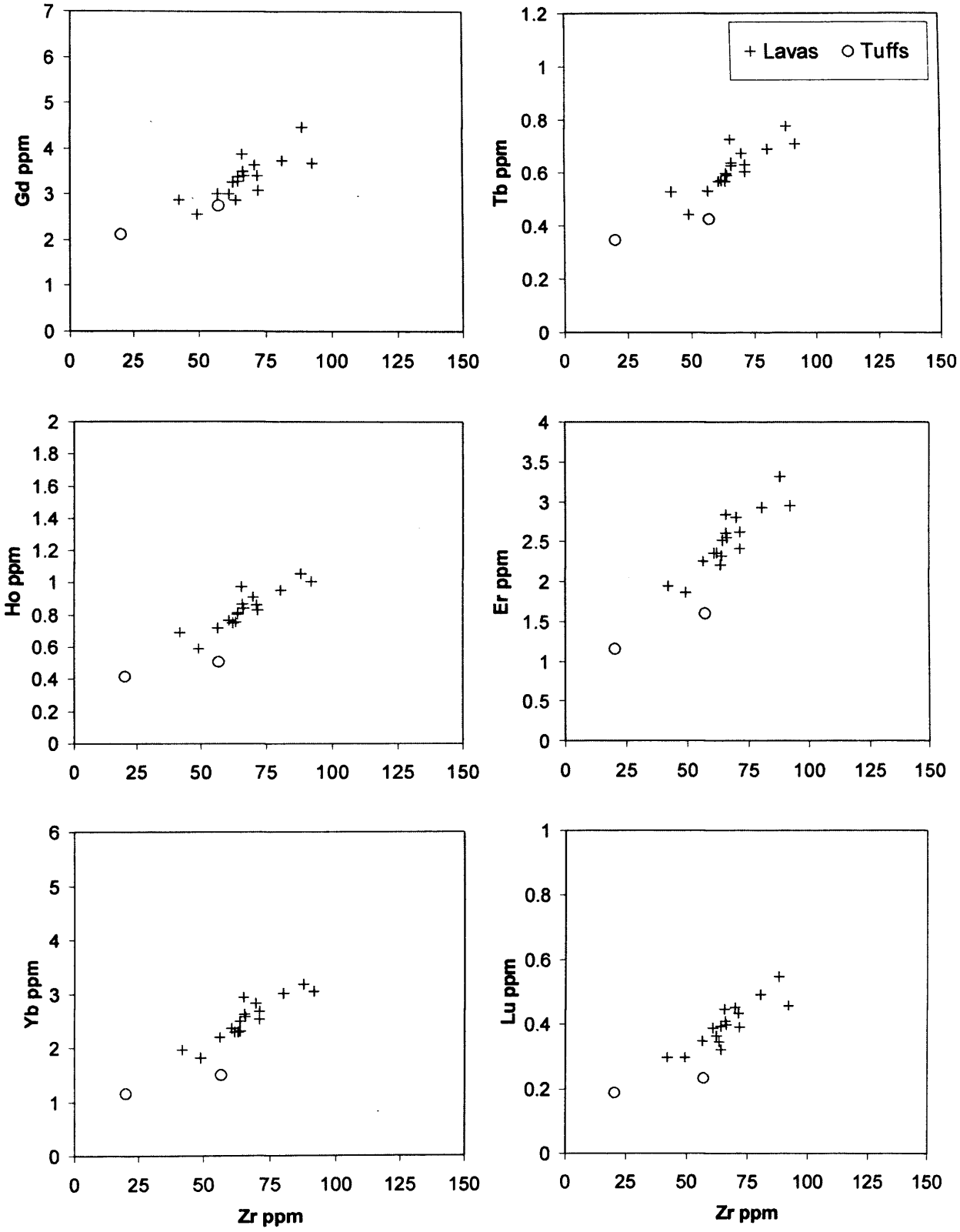

E.10 Major and trace element variation diagrams for the Devils Racecourse lavas, Benbow Inlier

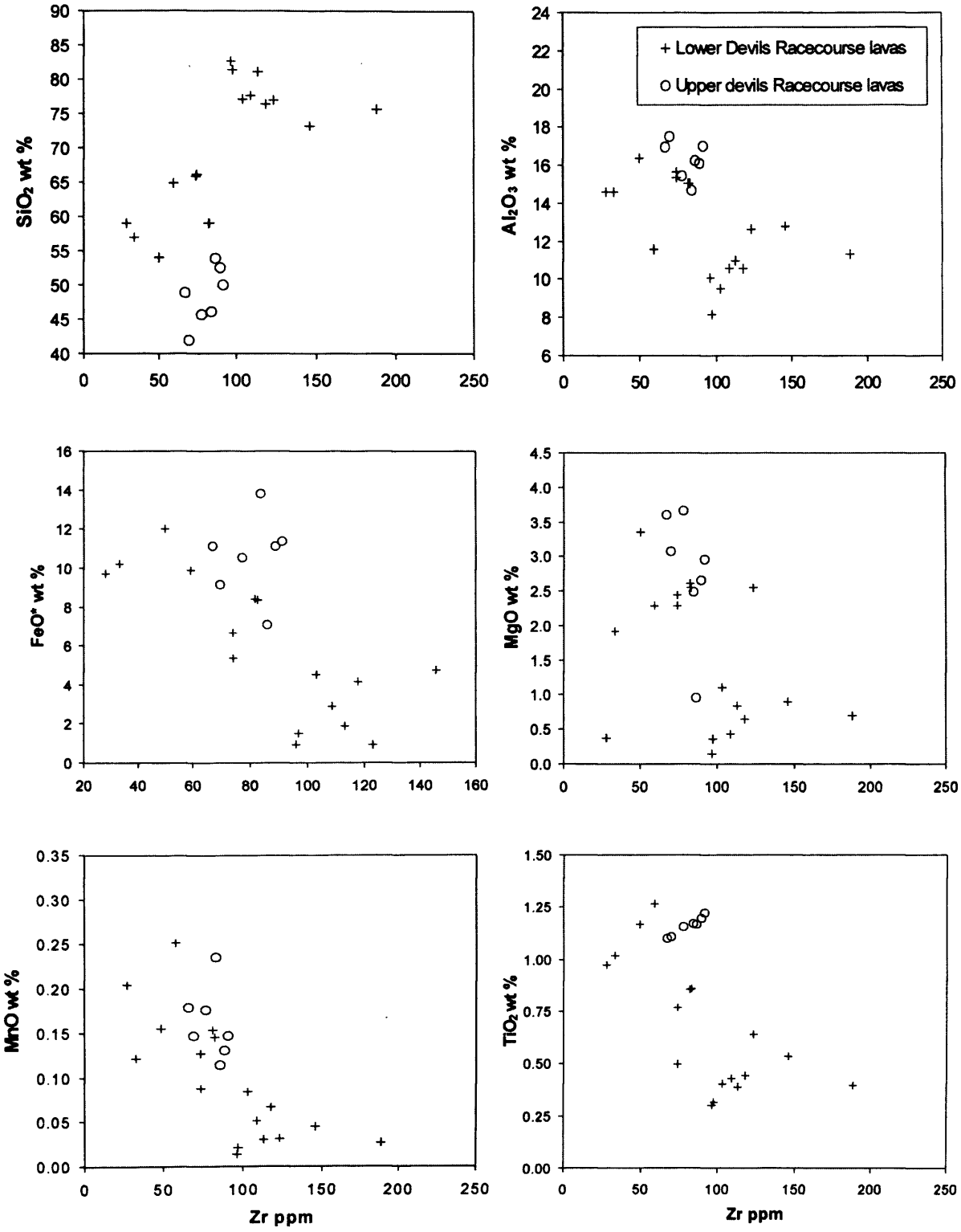

Appendix E: Major and trace element data for the Cretaceous and Tertiary Jamaican igneous rocks and their variation diagrams

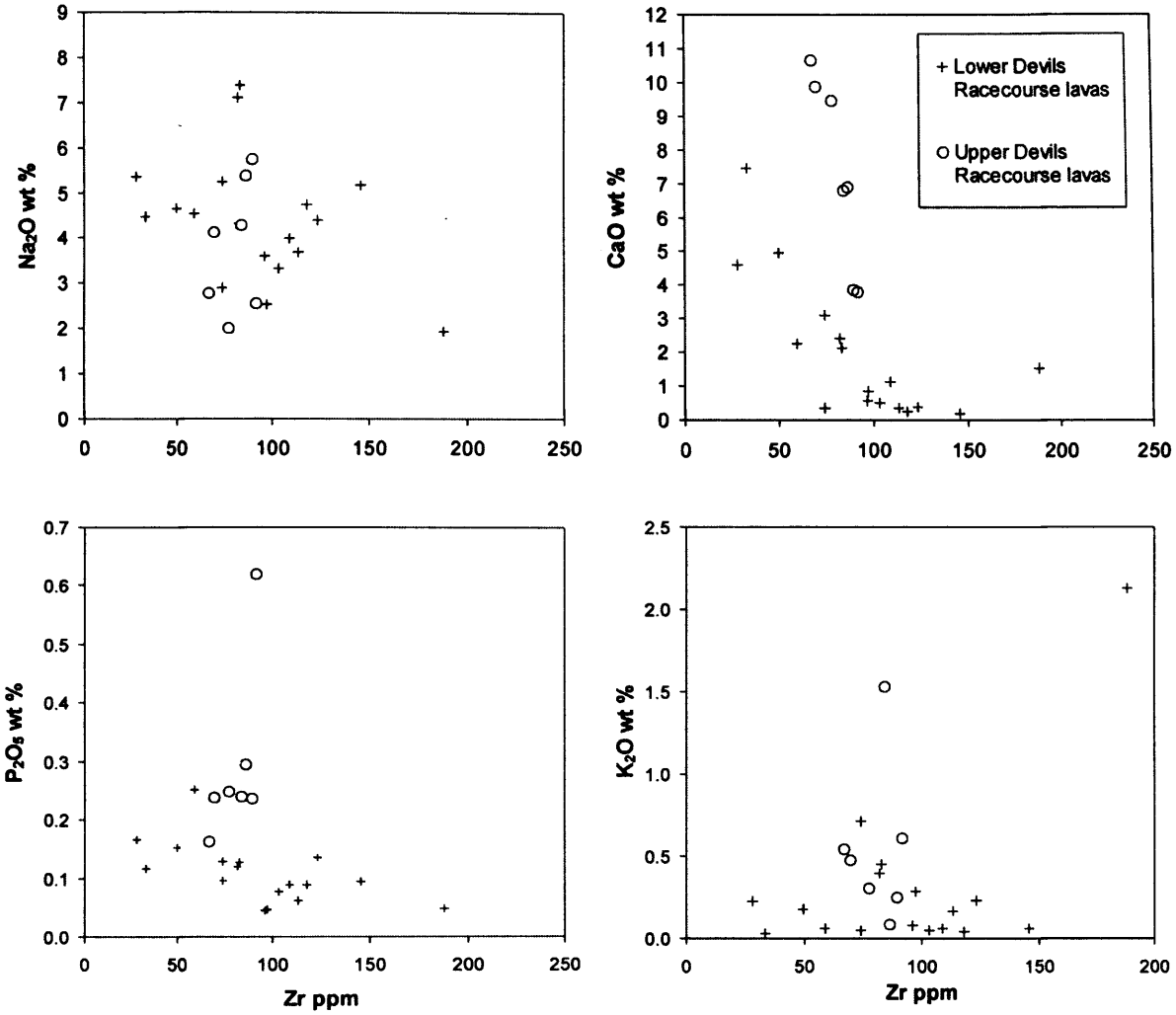

Appendix E: Major and trace element data for the Cretaceous and Tertiary Jamaican igneous rocks and their variation diagrams

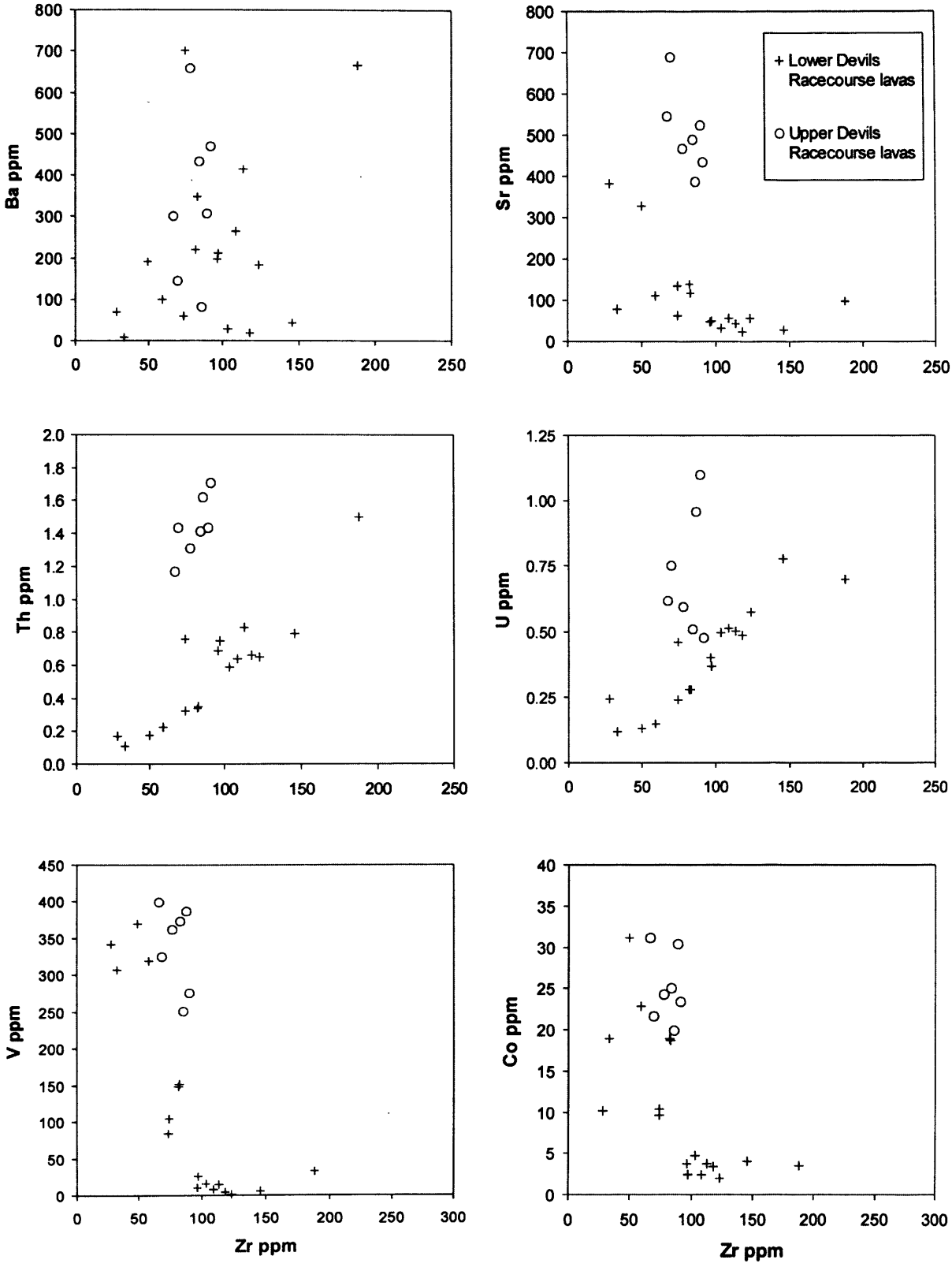

Appendix E: Major and trace element data for the Cretaceous and Tertiary Jamaican igneous rocks and their variation diagrams

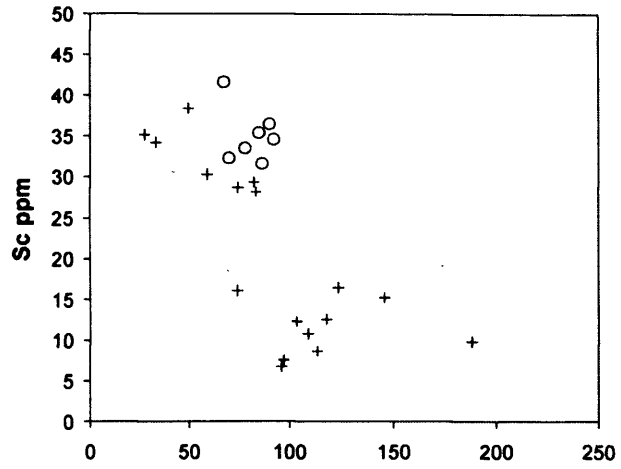

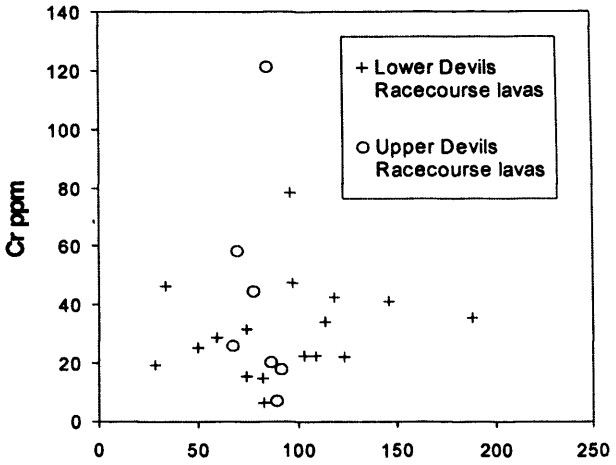

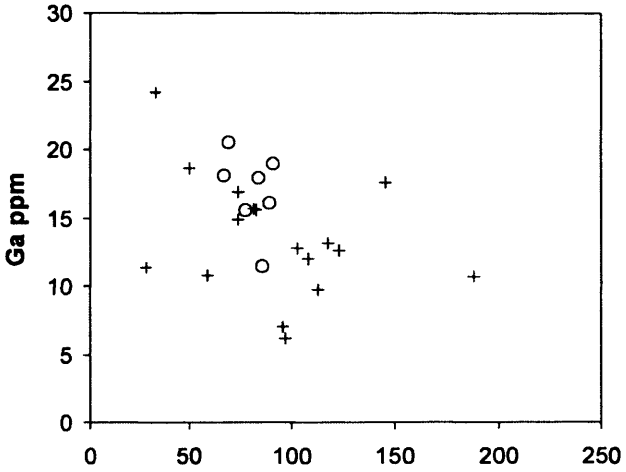

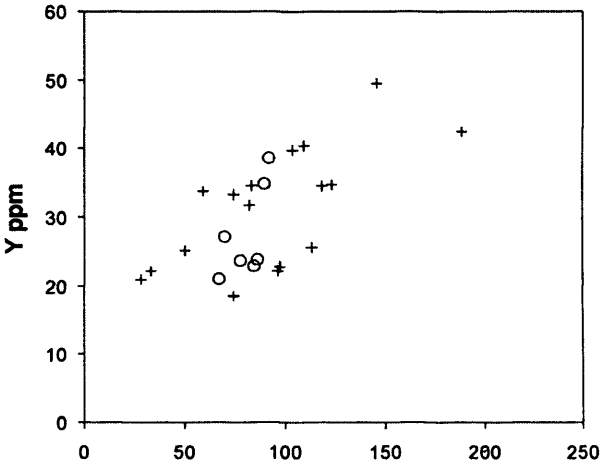

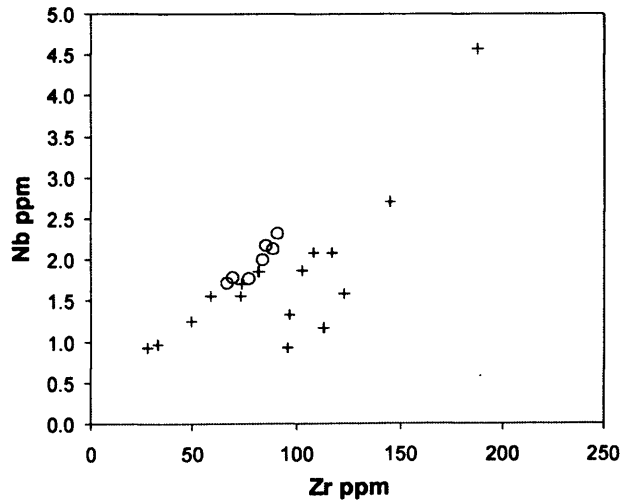

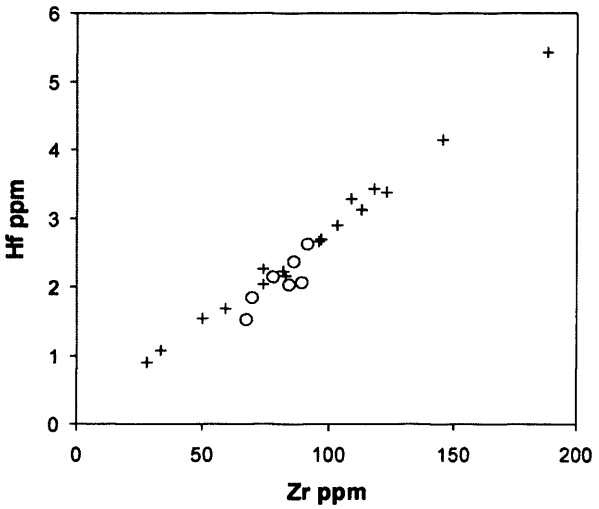

Appendix E: Major and trace element data for the Cretaceous and Tertiary Jamaican igneous rocks and their variation diagrams

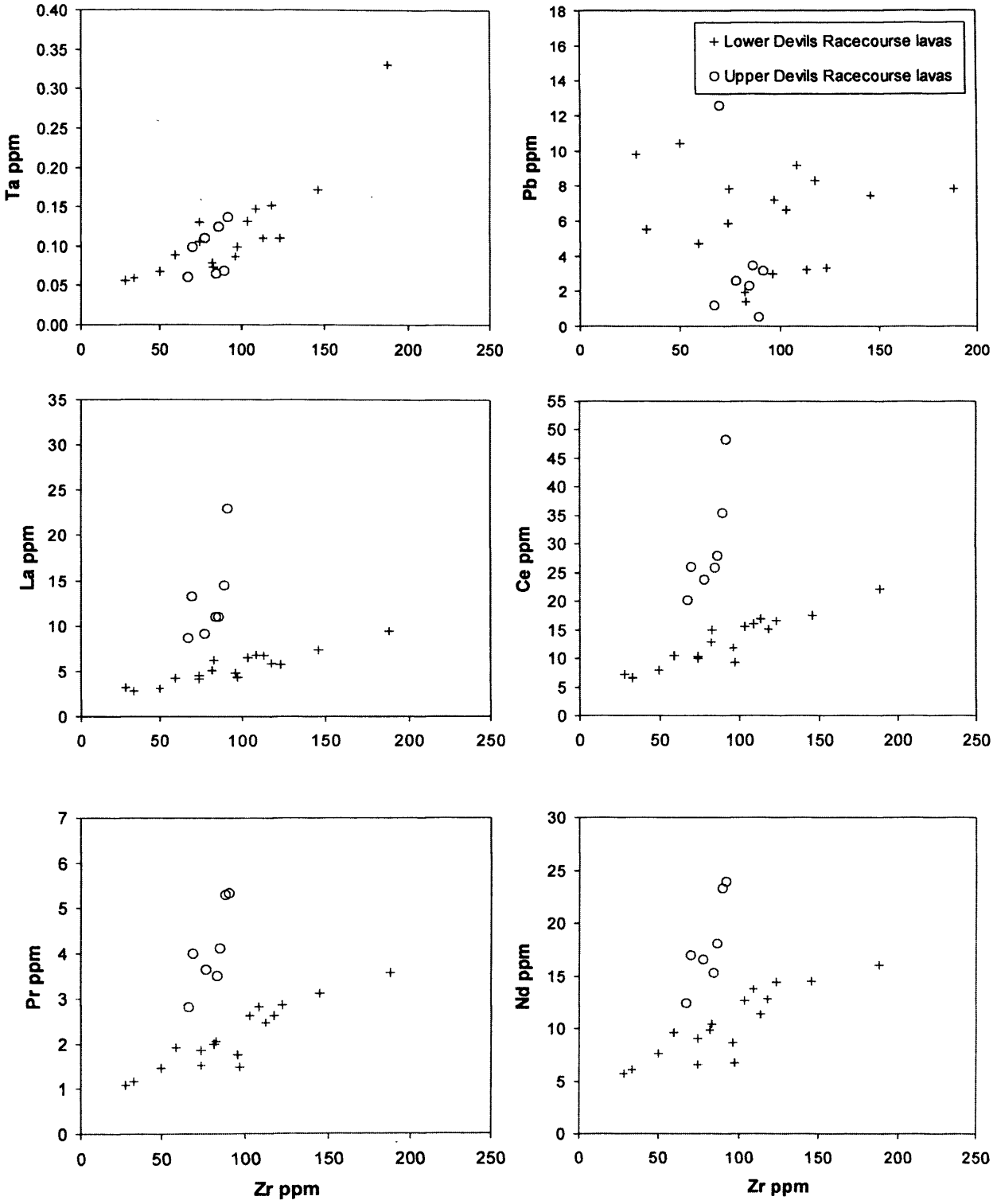

Appendix E: Major and trace element data for the Cretaceous and Tertiary Jamaican igneous rocks and their variation diagrams

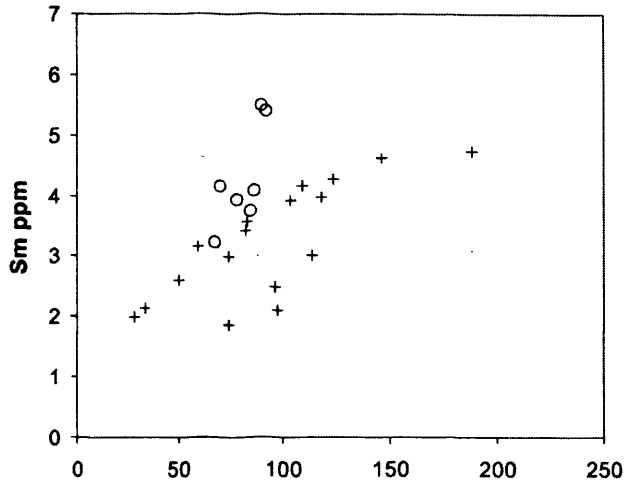

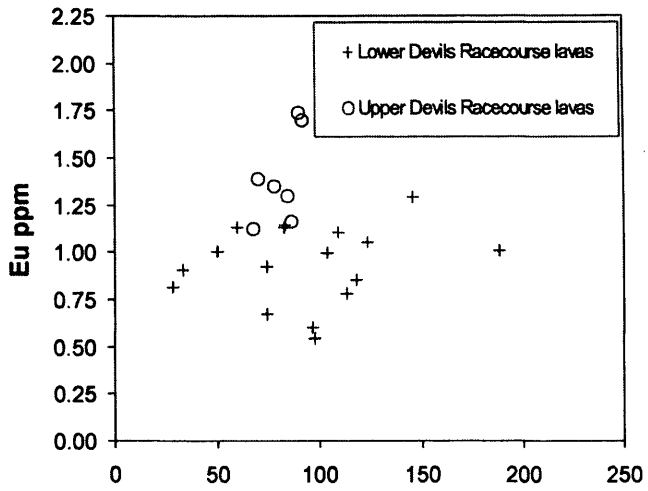

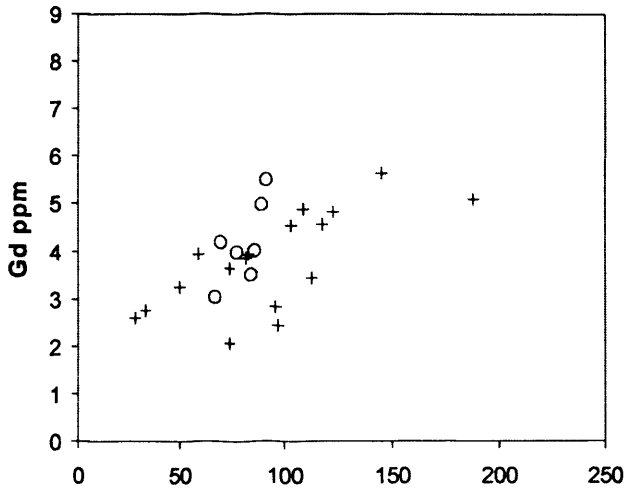

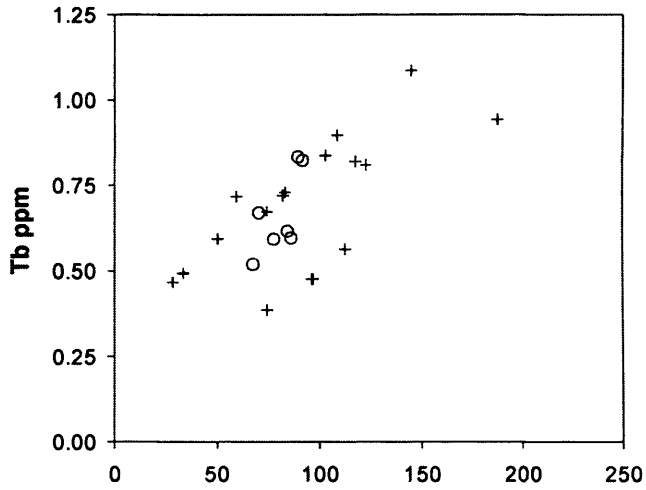

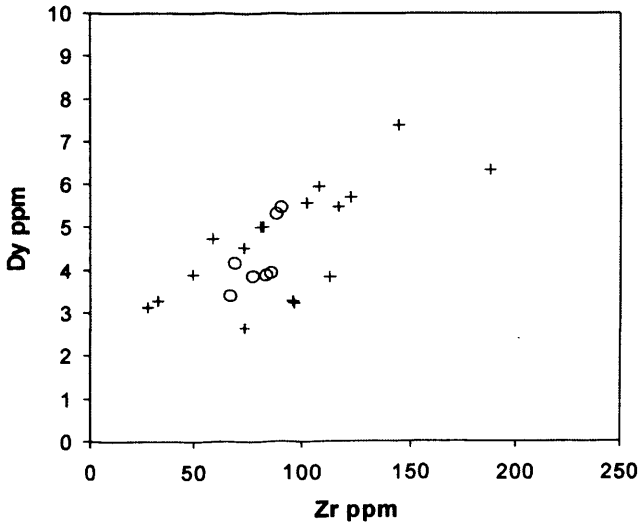

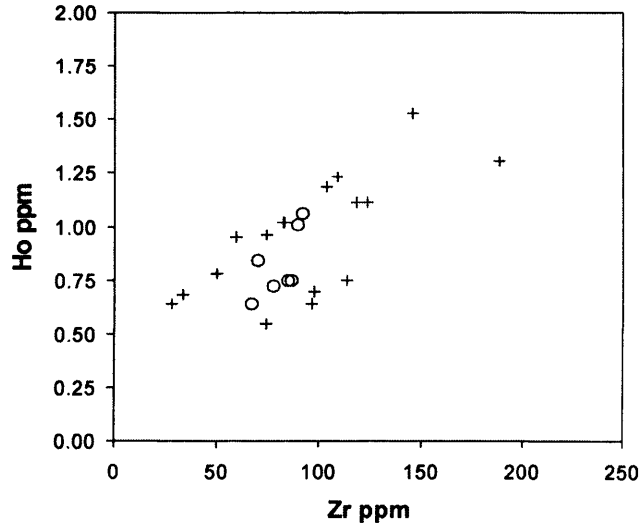

Appendix E: Major and trace element data for the Cretaceous and Tertiary Jamaican igneous rocks and their variation diagrams

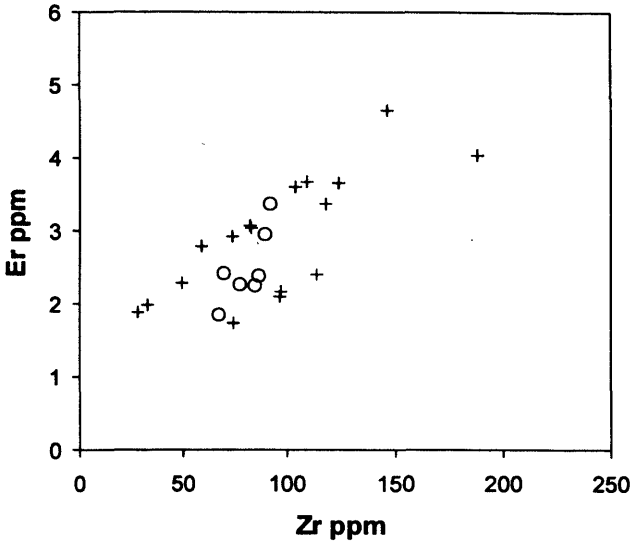

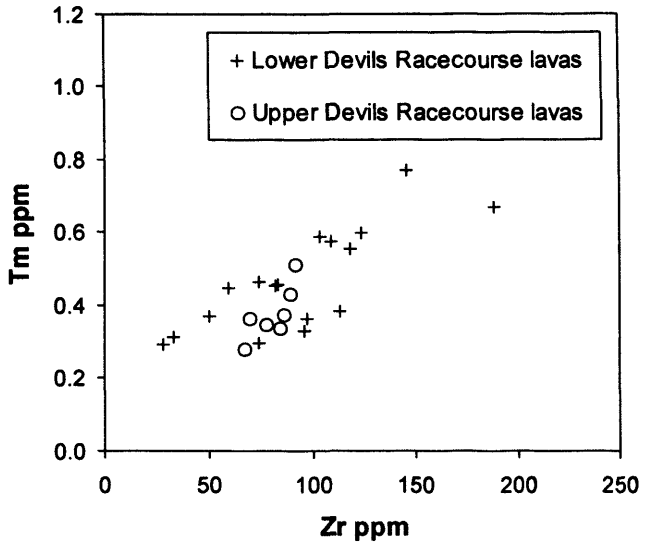

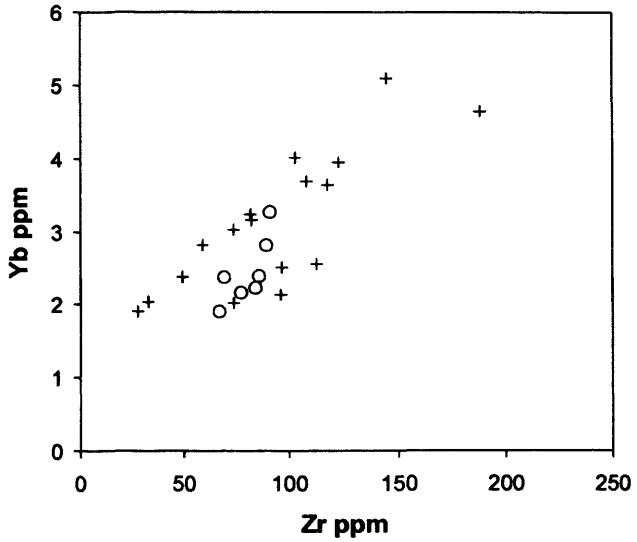

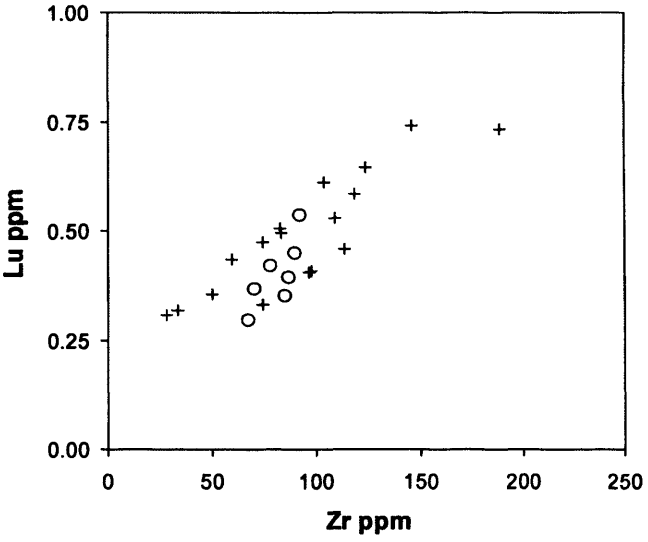

E.11 Major and trace element variation diagrams for the Above Rocks and Sunning Hill inlier samples

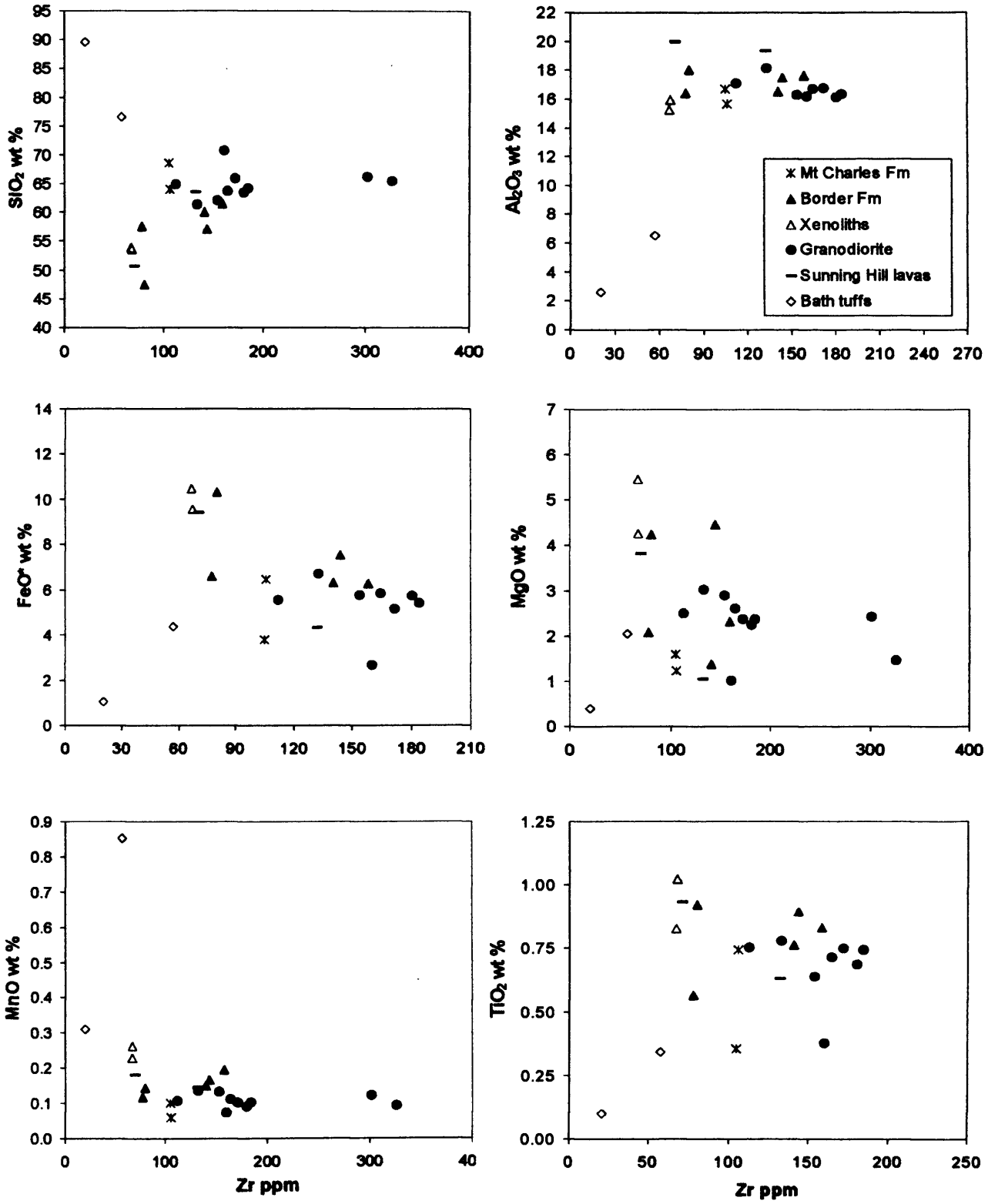

Appendix E: Major and trace element data for the Cretaceous and Tertiary Jamaican igneous rocks and their variation diagrams

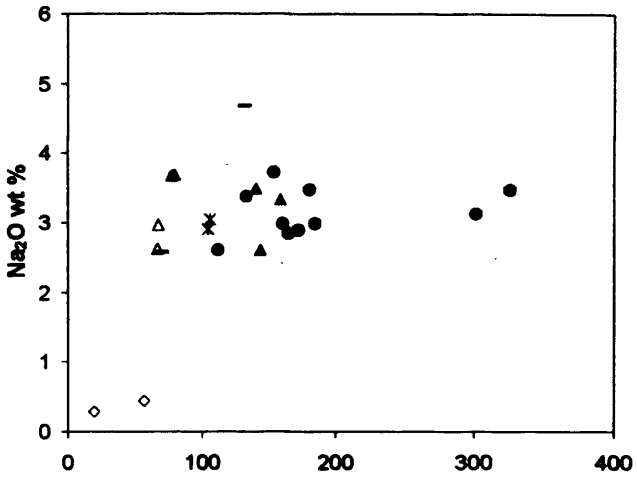

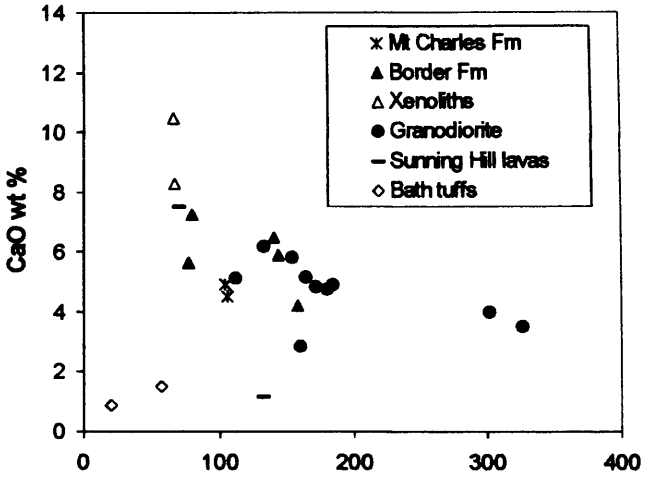

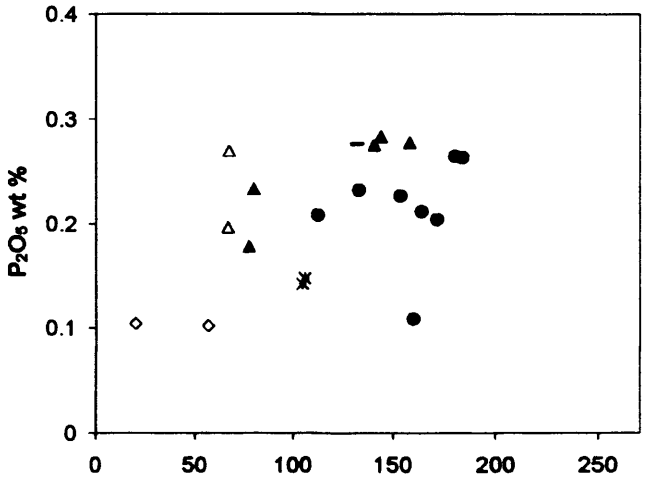

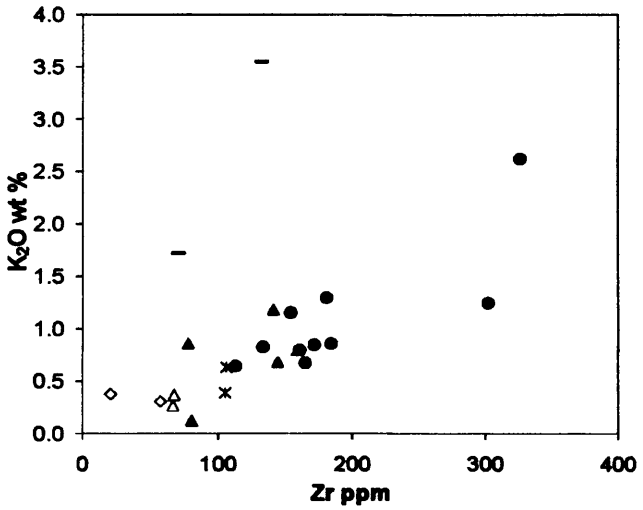

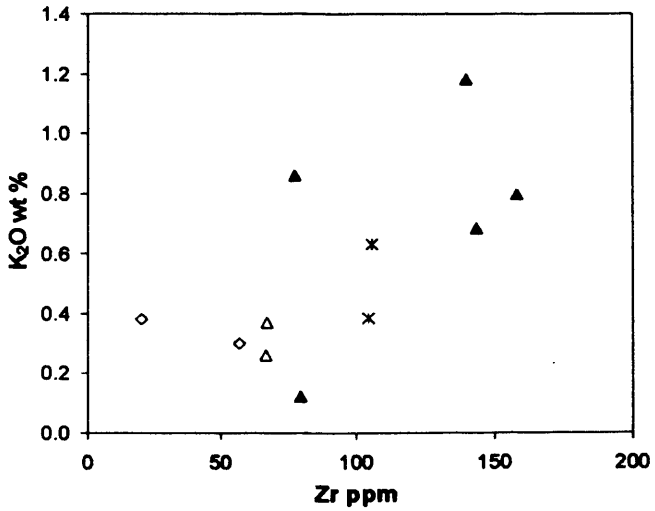

Appendix E: Major and trace element data for the Cretaceous and Tertiary Jamaican igneous rocks and their variation diagrams

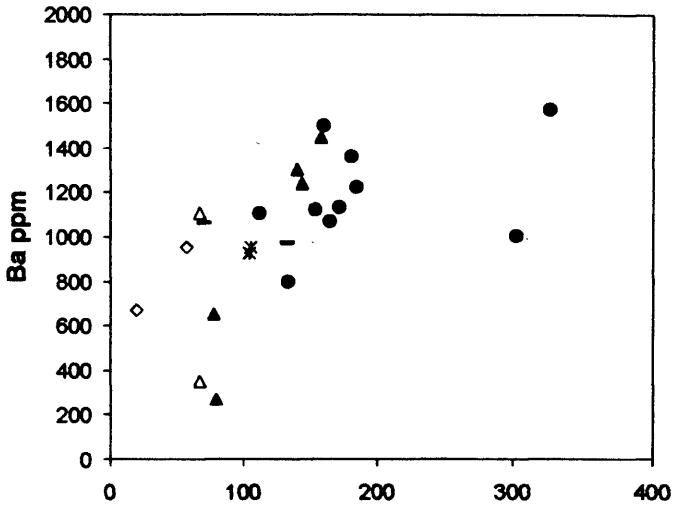

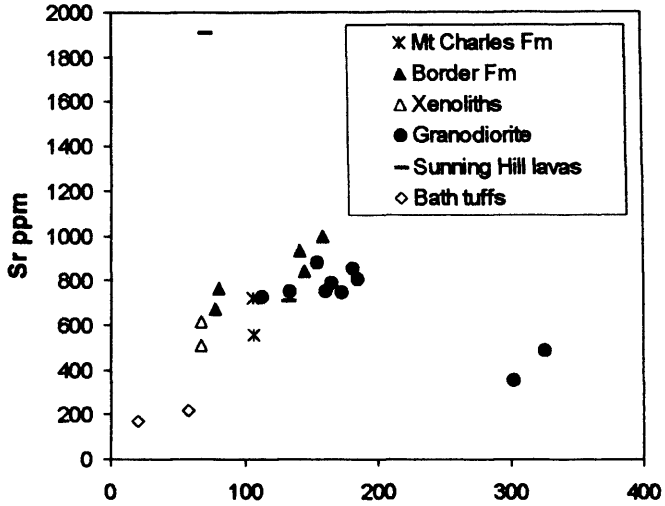

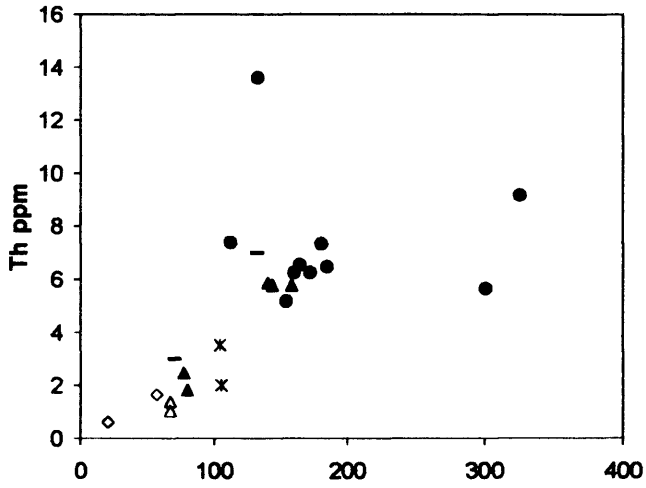

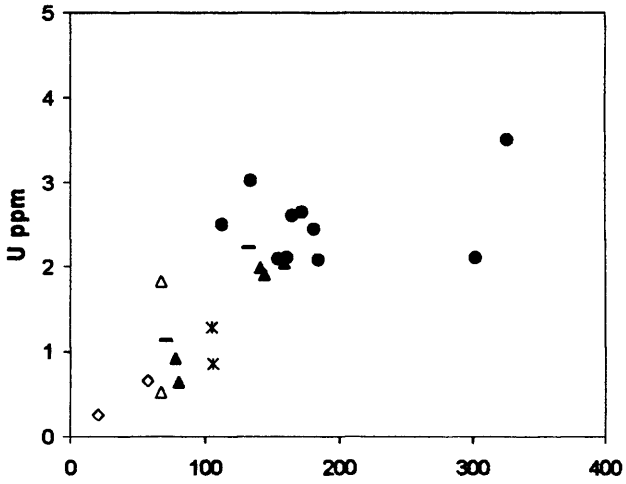

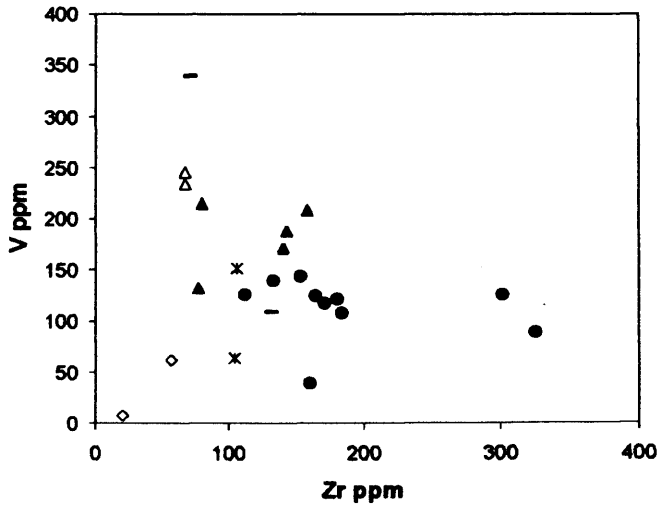

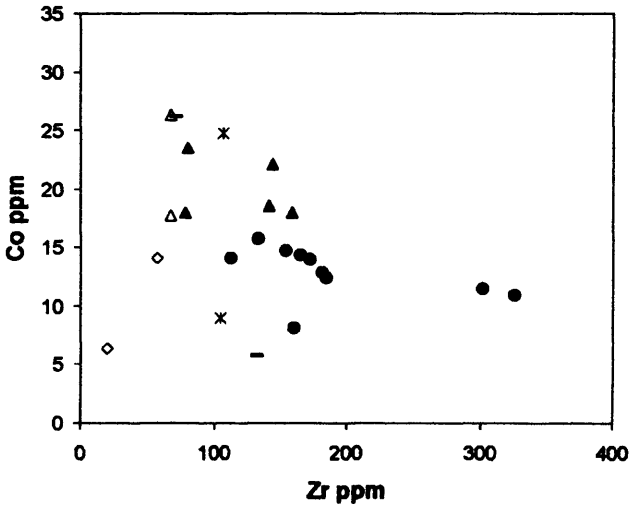

Appendix E: Major and trace element data for the Cretaceous and Tertiary Jamaican igneous rocks and their variation diagrams

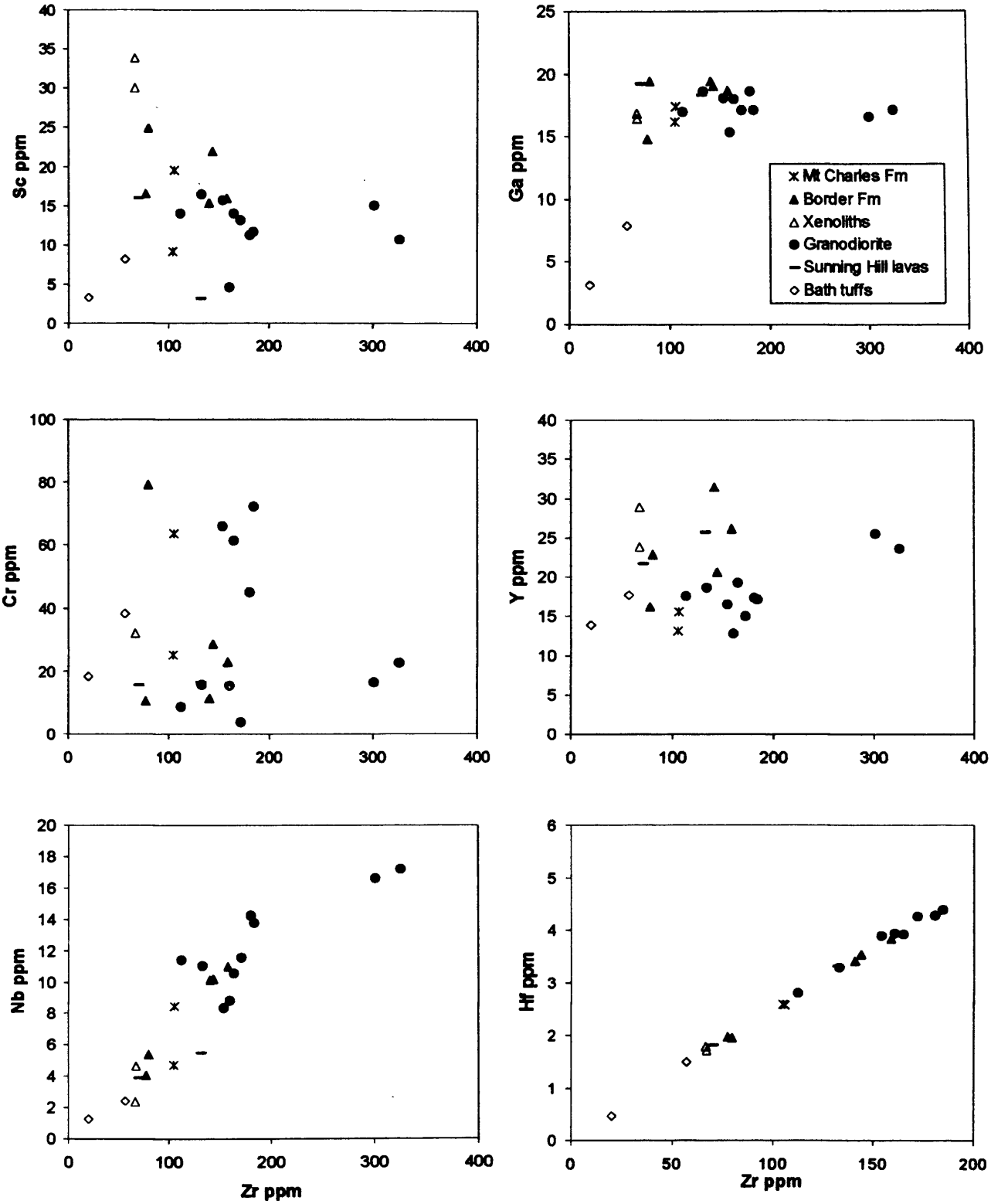

Appendix E: Major and trace element data for the Cretaceous and Tertiary Jamaican igneous rocks and their variation diagrams

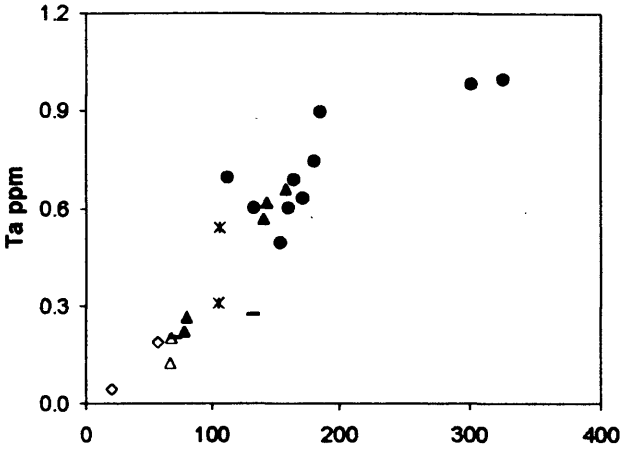

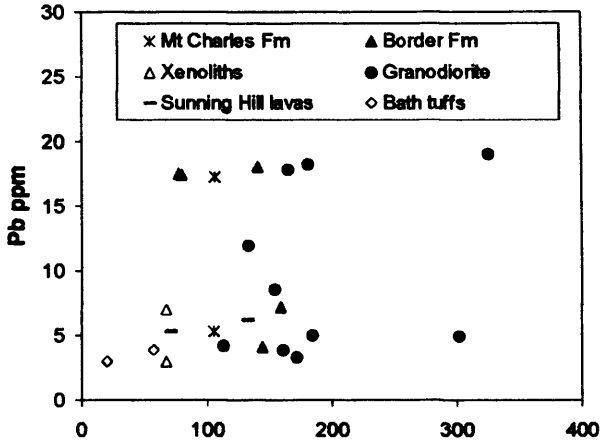

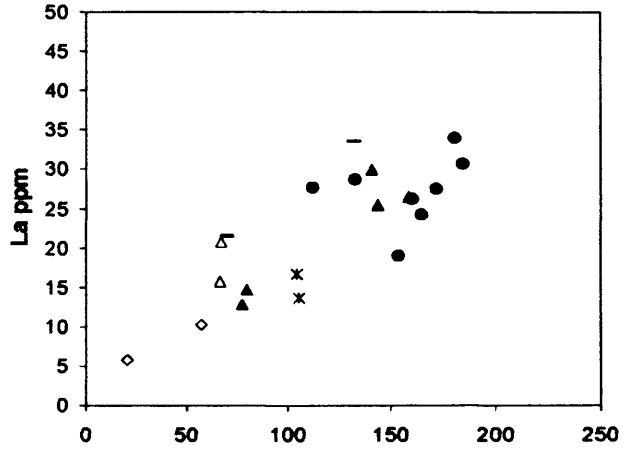

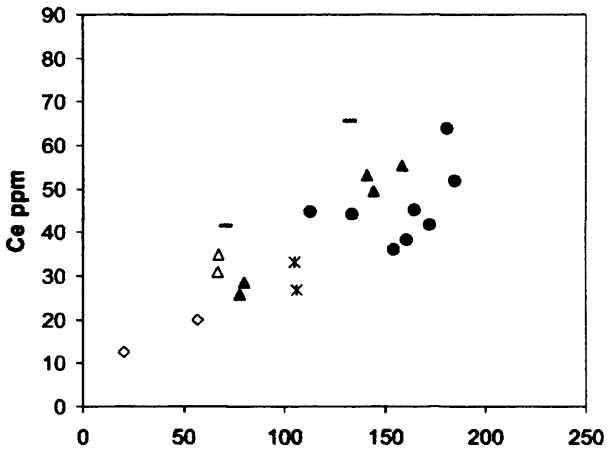

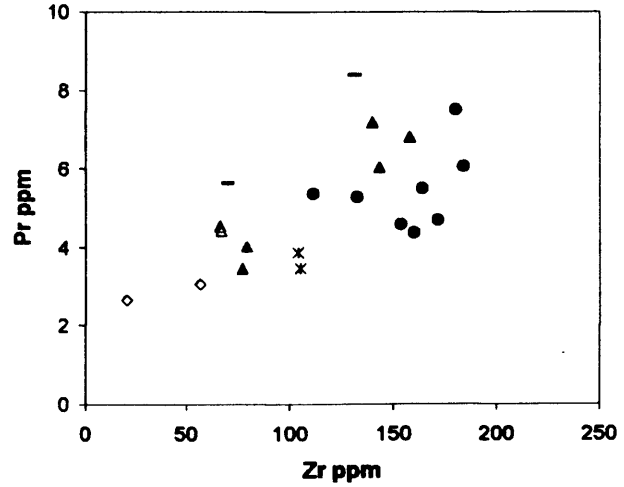

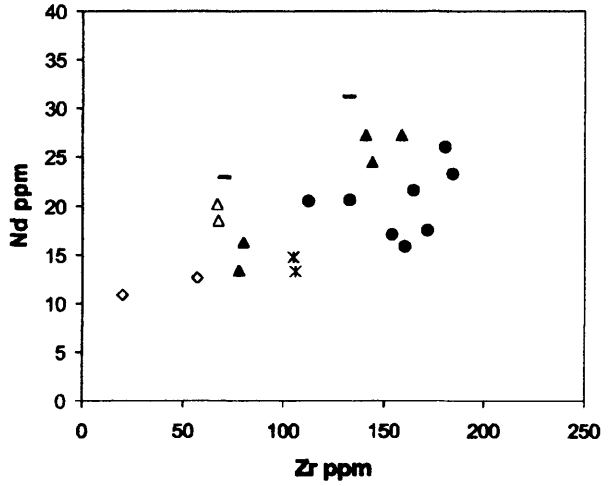

Appendix E: Major and trace element data for the Cretaceous and Tertiary Jamaican igneous rocks and their variation diagrams

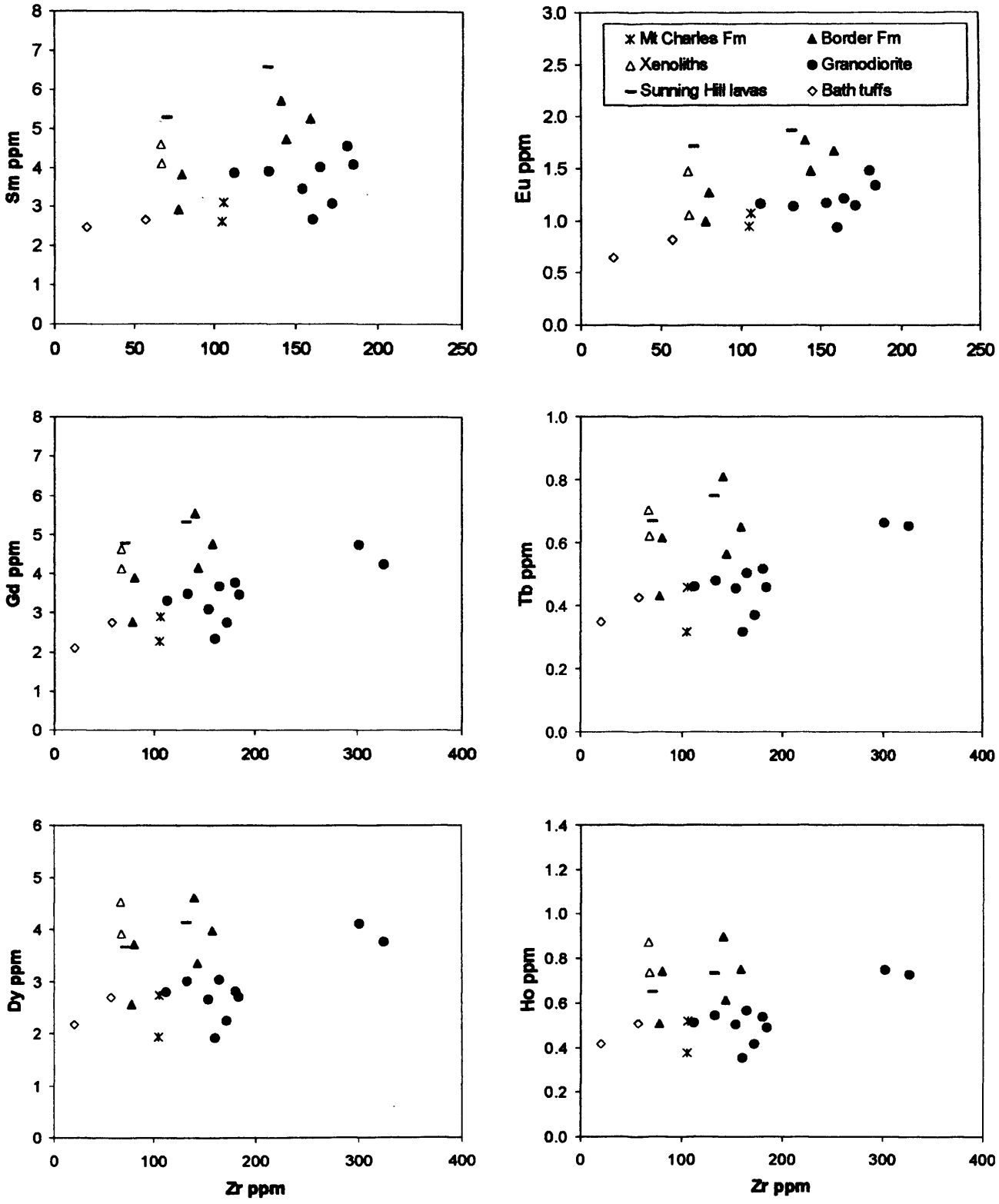

Appendix E: Major and trace element data for the Cretaceous and Tertiary Jamaican igneous rocks and their variation diagrams

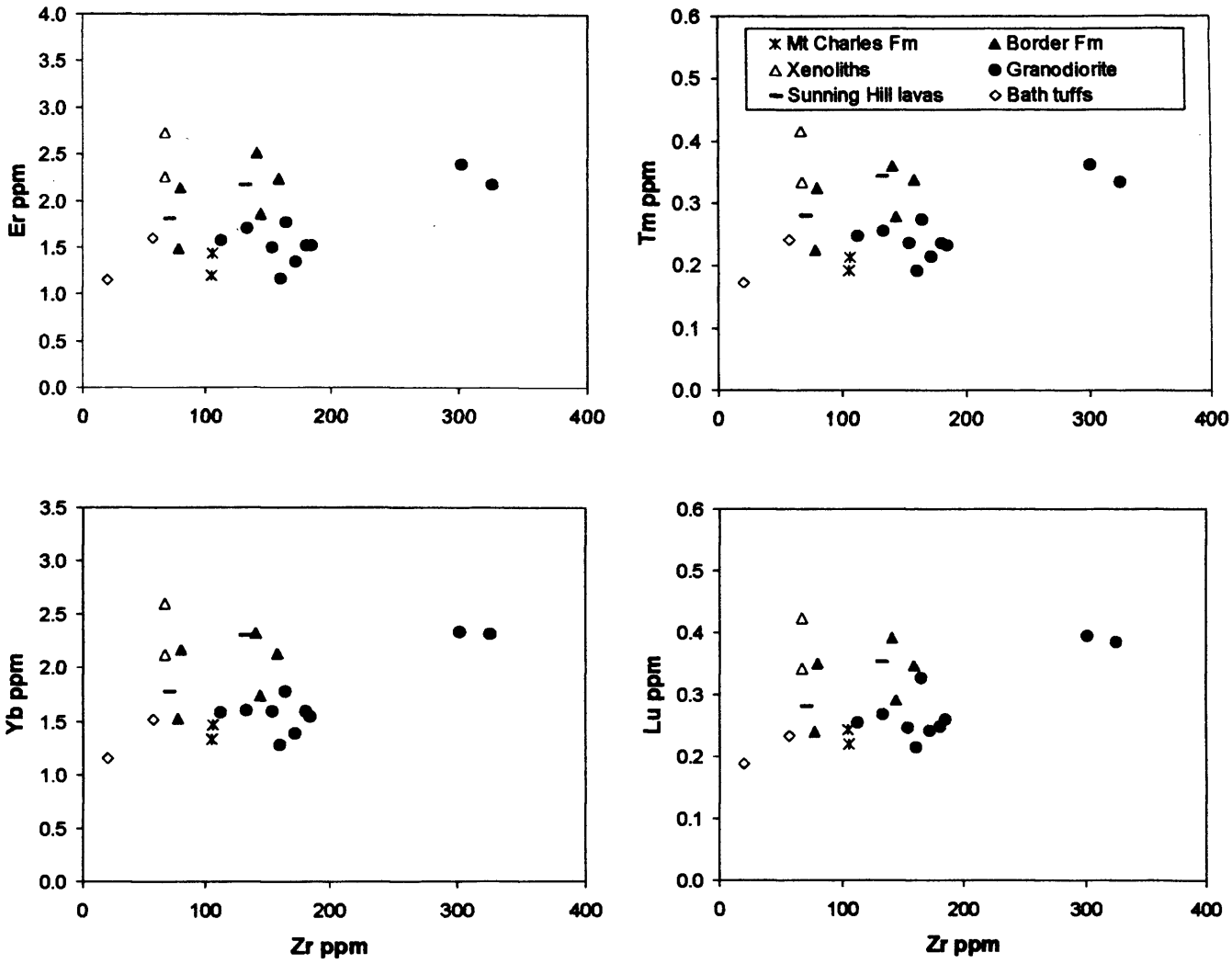

E.12 Major and trace element variation diagrams for the igneous rocks of the Central Inlier.

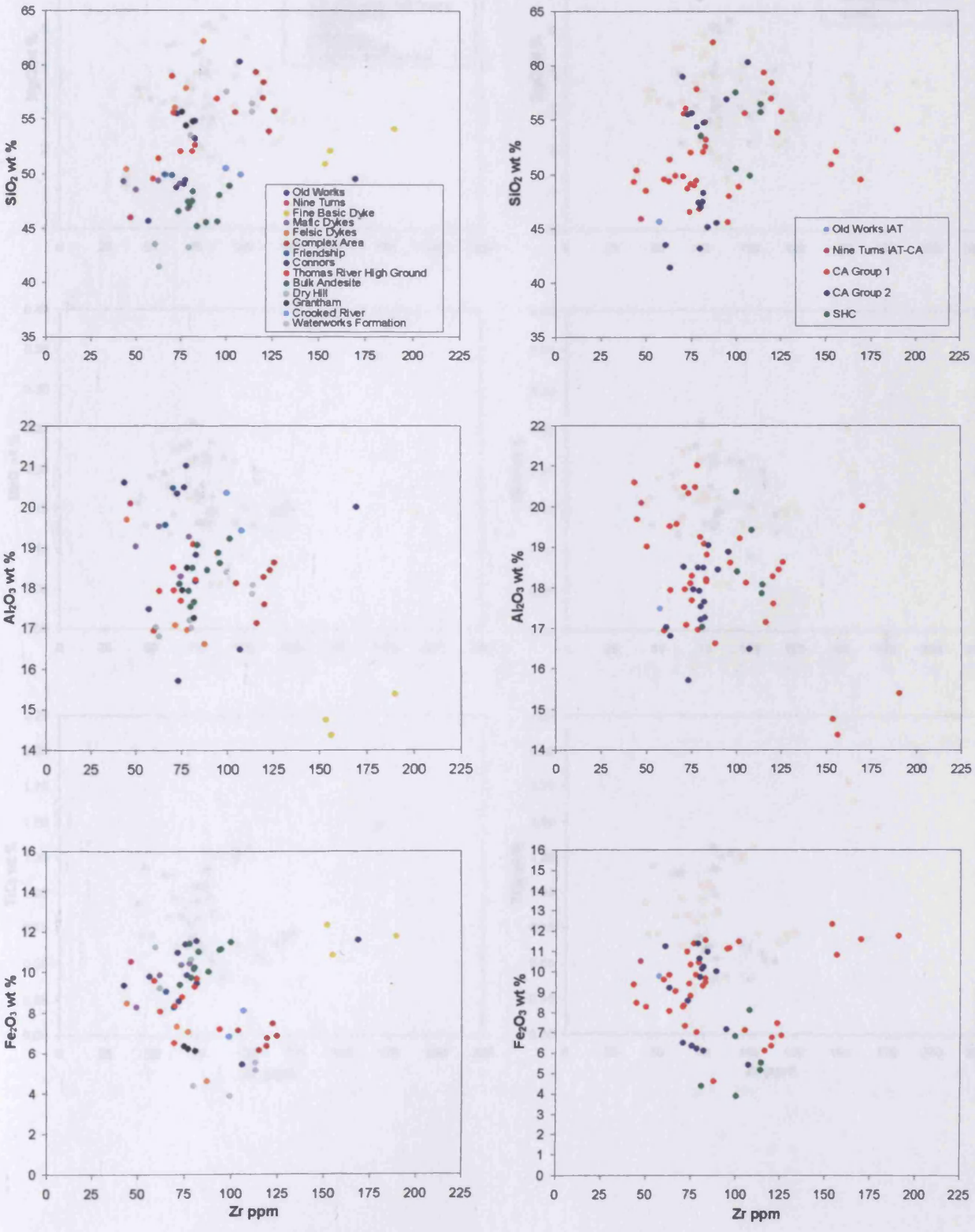

Appendix E: Major and trace element data for the Cretaceous and Tertiary Jamaican igneous rocks and their variation diagrams

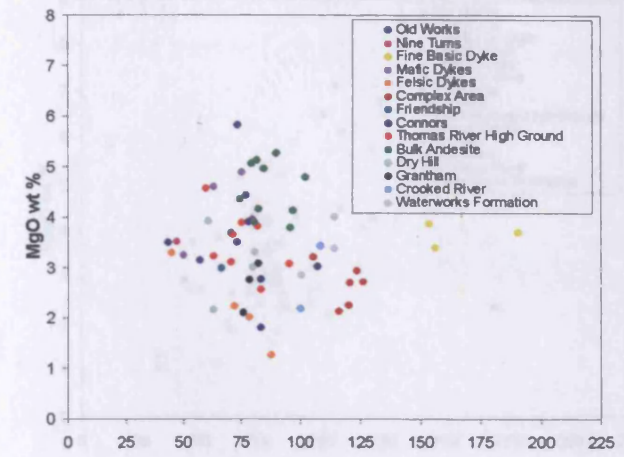

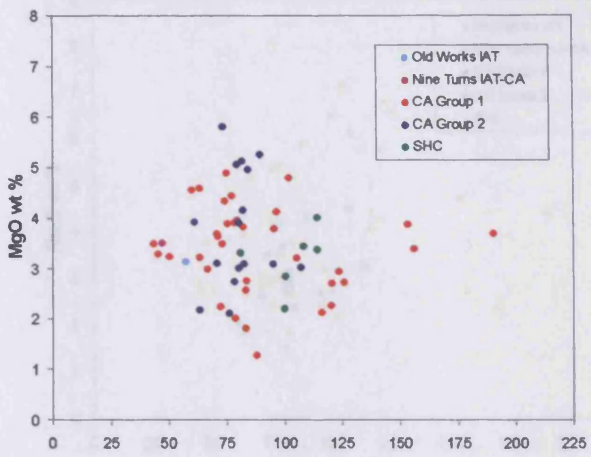

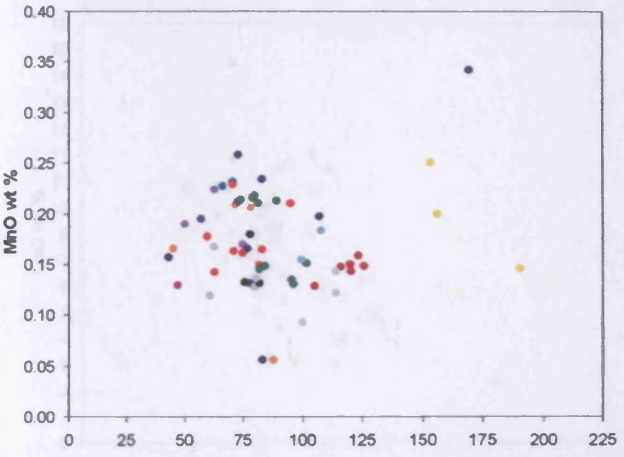

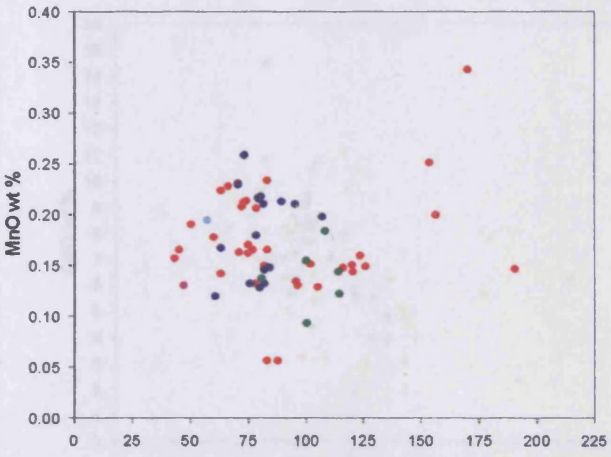

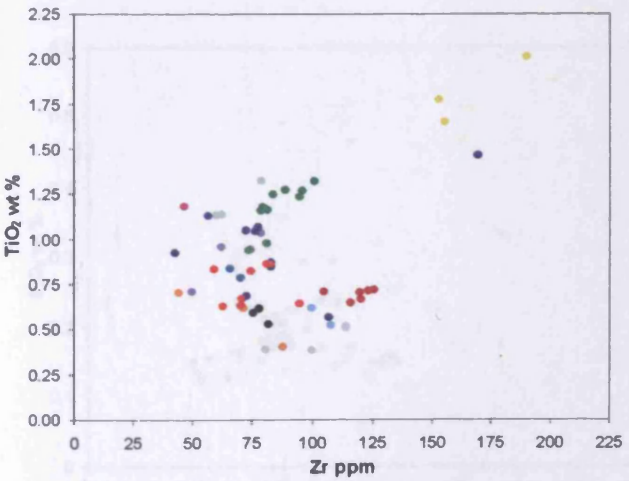

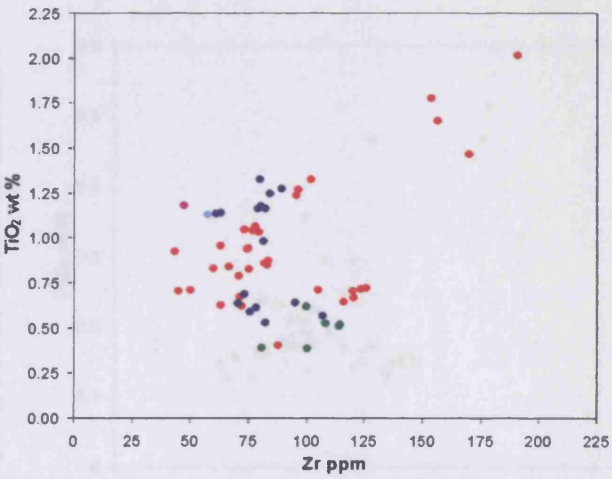

Appendix E: Major and trace element data for the Cretaceous and Tertiary Jamaican igneous rocks and their variation diagrams

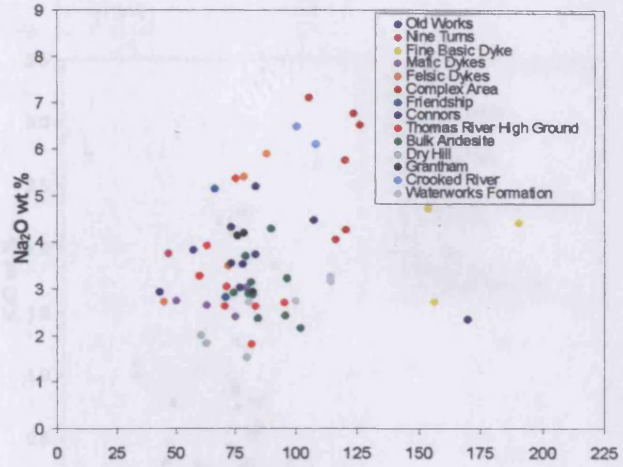

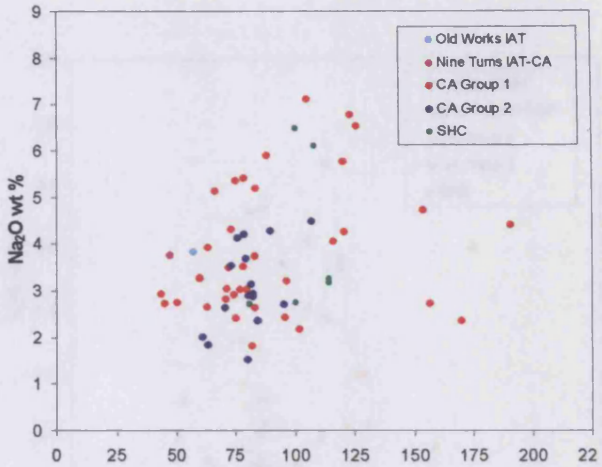

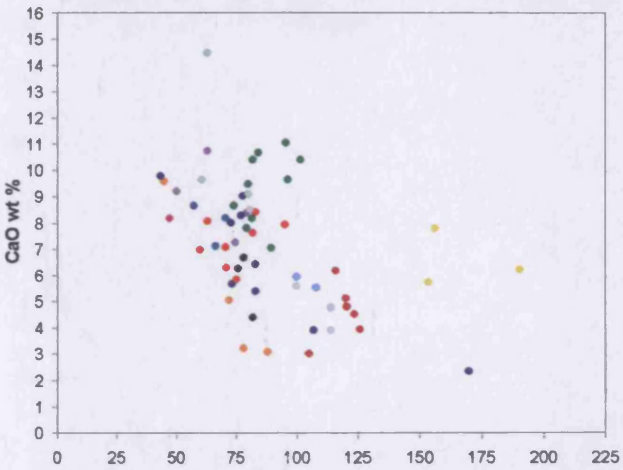

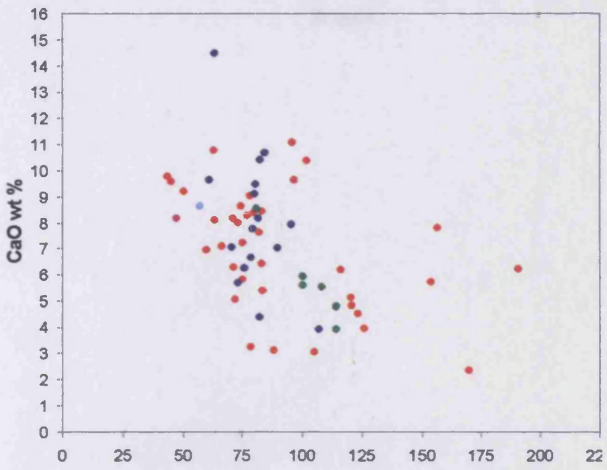

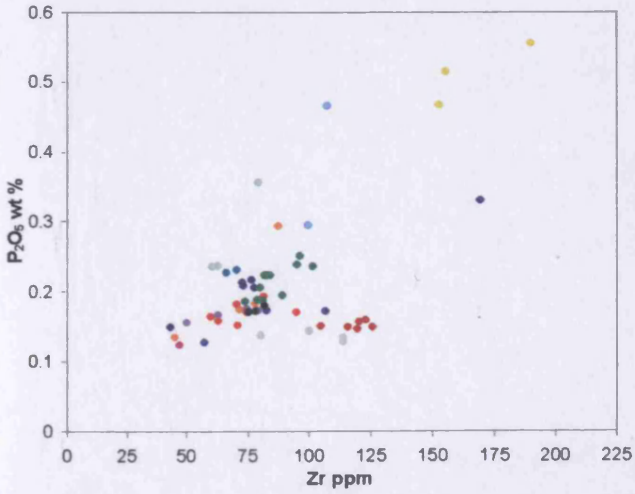

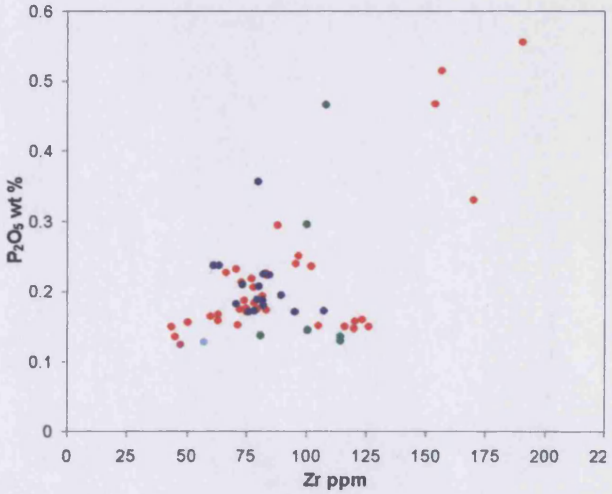

Appendix E: Major and trace element data for the Cretaceous and Tertiary Jamaican igneous rocks and their variation diagrams

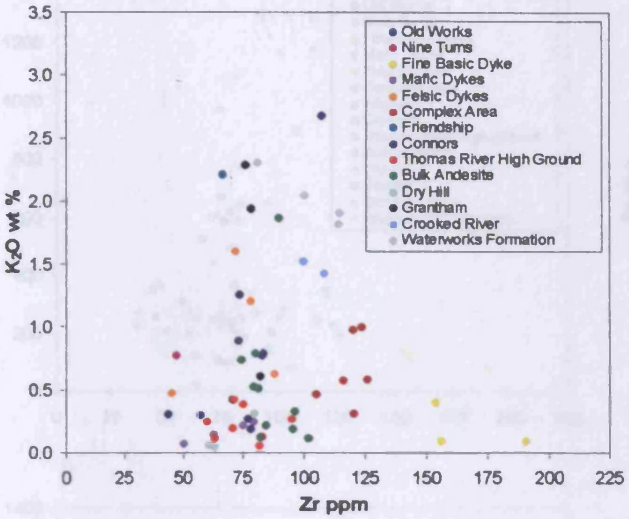

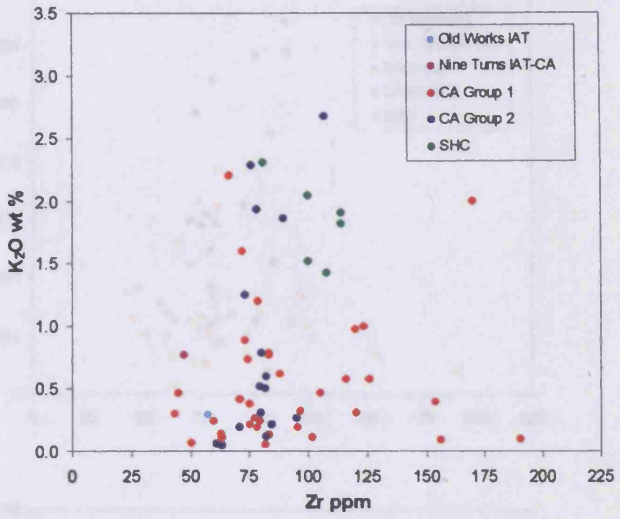

Appendix E: Major and trace element data for the Cretaceous and Tertiary Jamaican igneous rocks and their variation diagrams

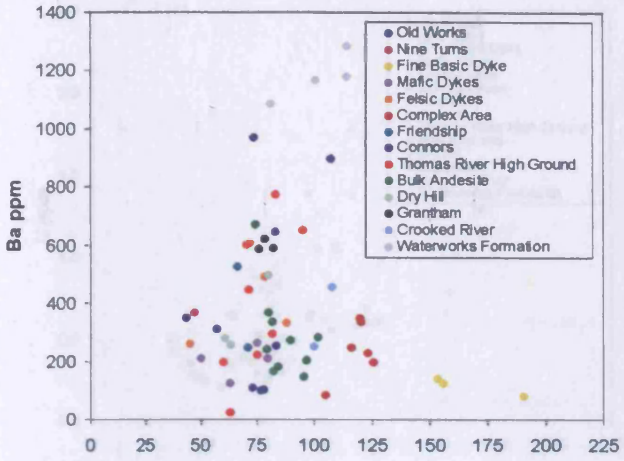

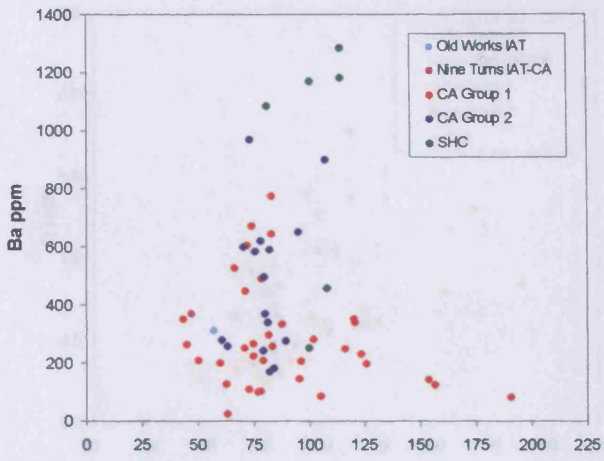

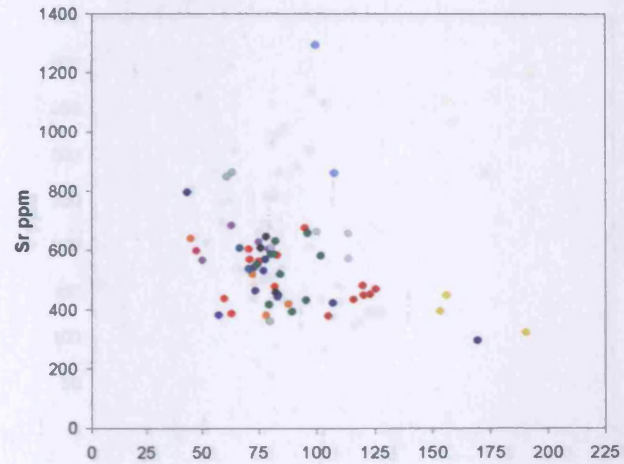

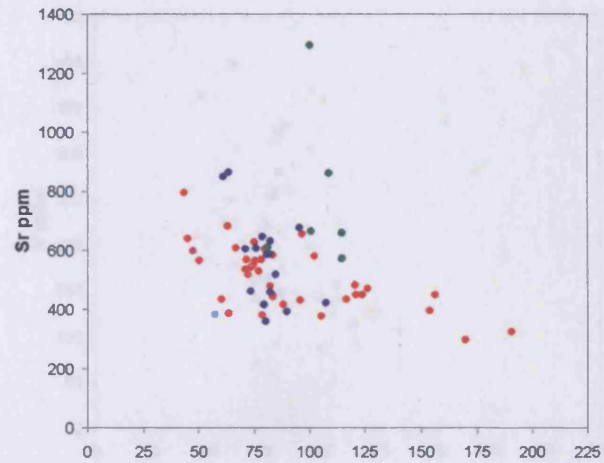

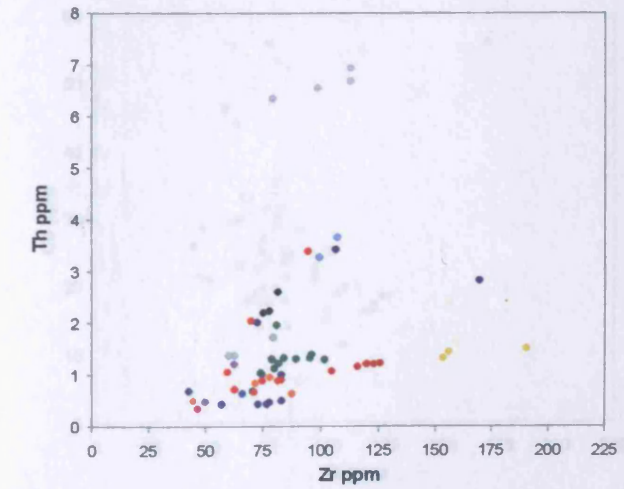

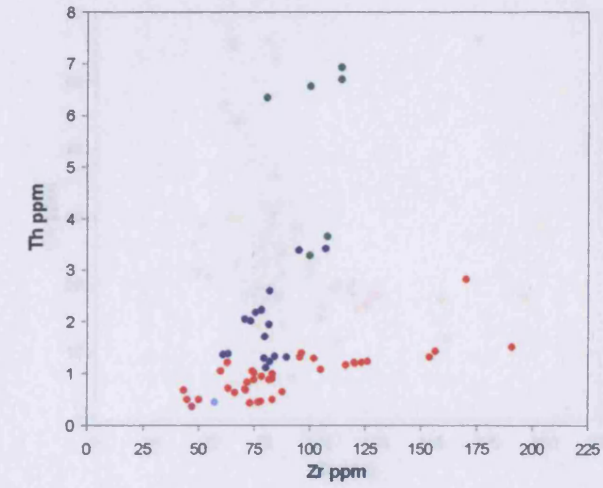

Appendix E: Major and trace element data for the Cretaceous and Tertiary Jamaican igneous rocks and their variation diagrams

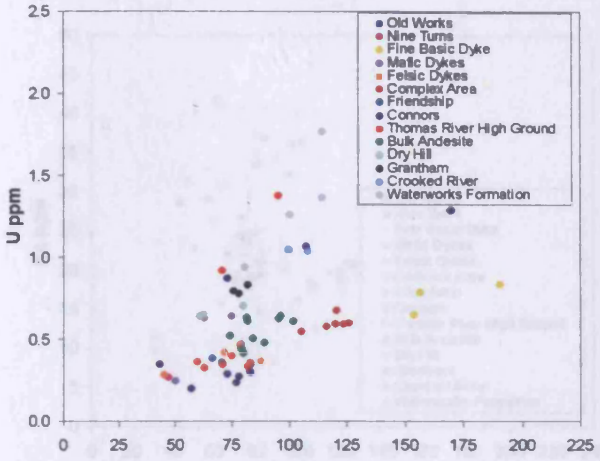

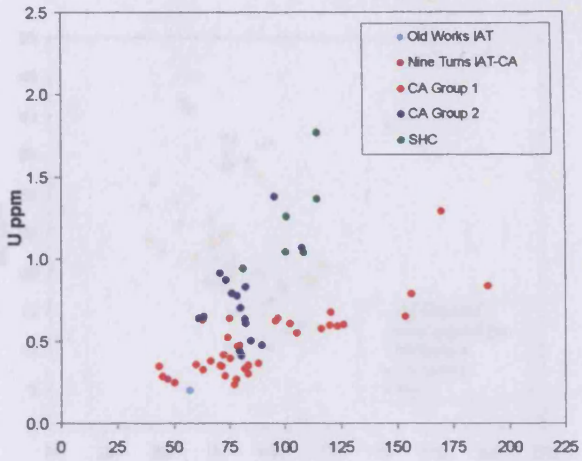

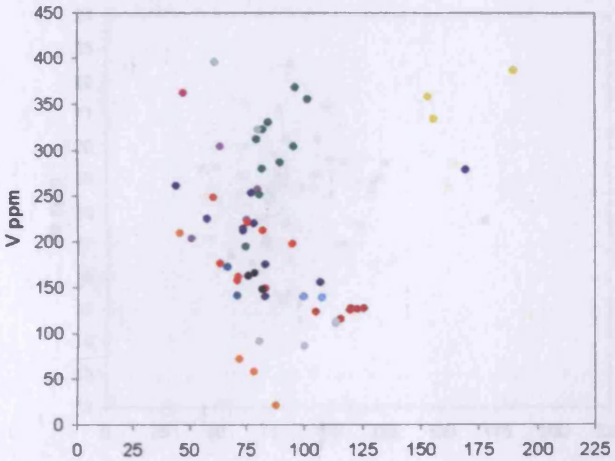

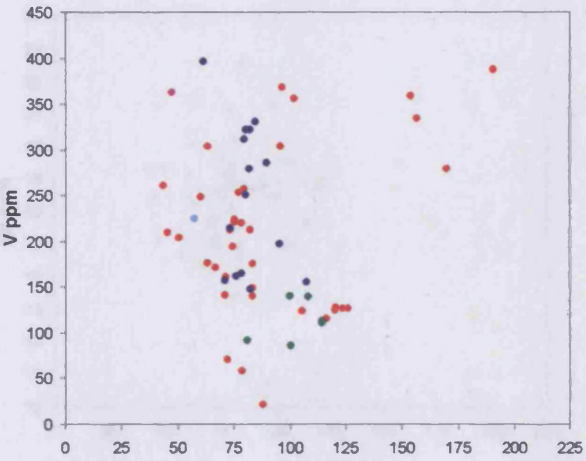

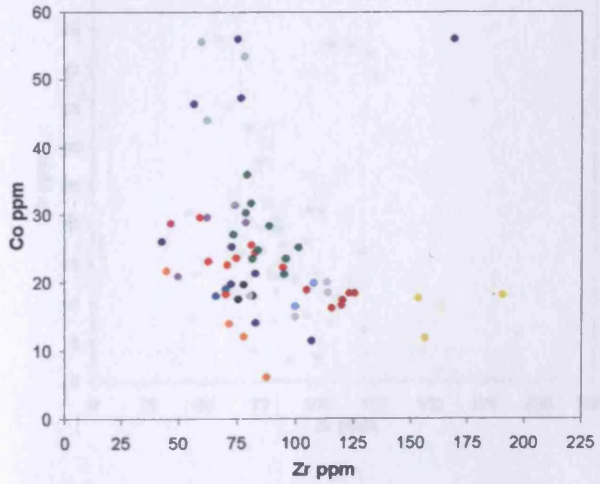

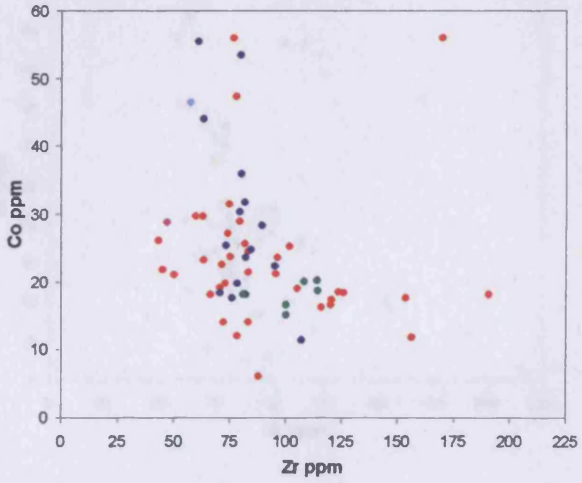

Appendix E: Major and trace element data for the Cretaceous and Tertiary Jamaican igneous rocks and their variation diagrams

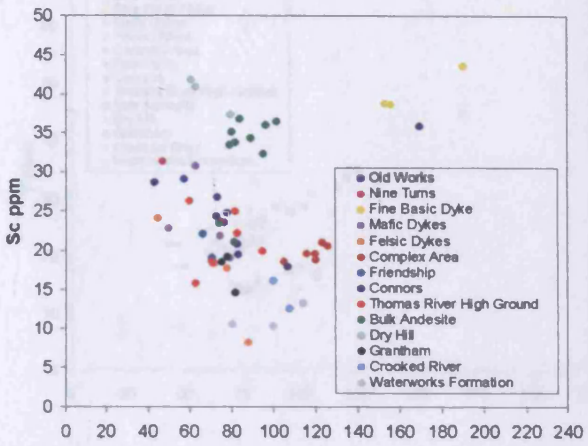

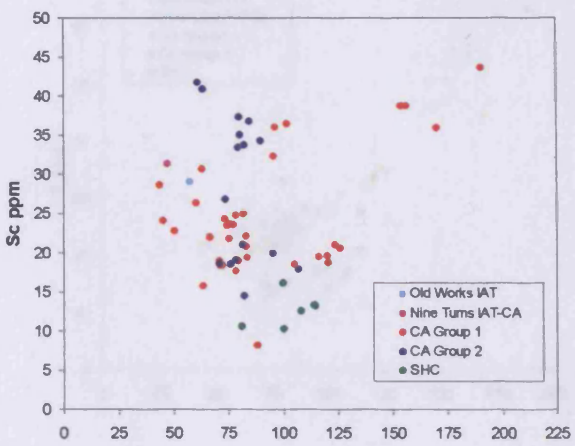

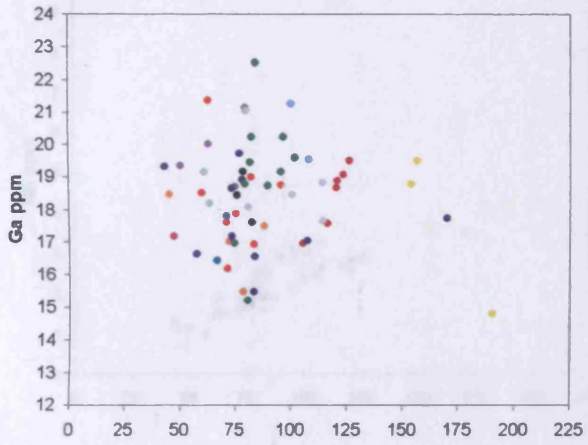

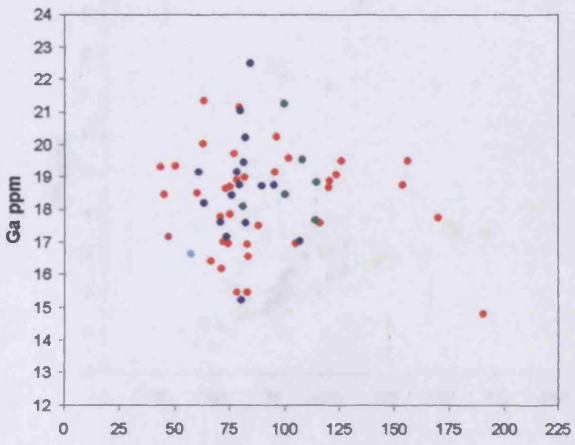

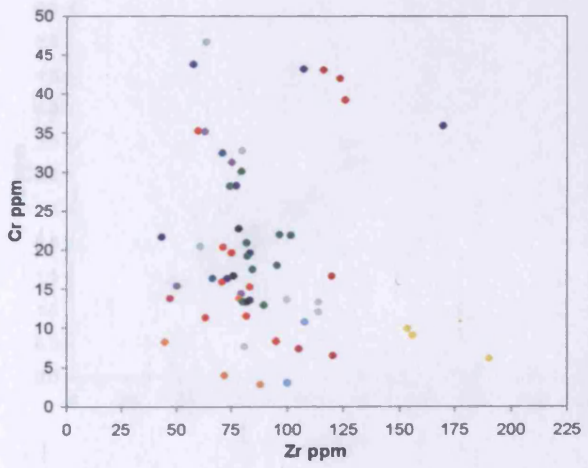

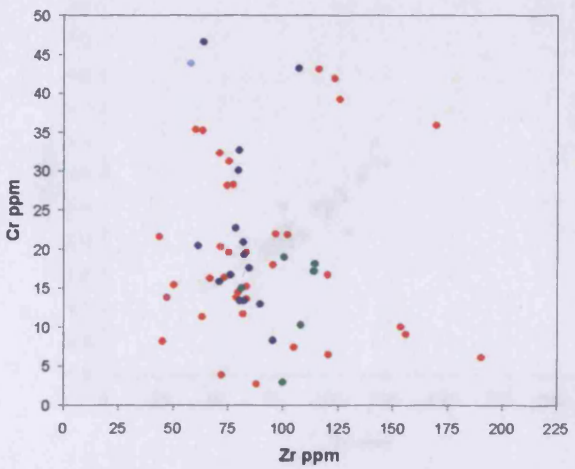

Appendix E: Major and trace element data for the Cretaceous and Tertiary Jamaican igneous rocks and their variation diagrams

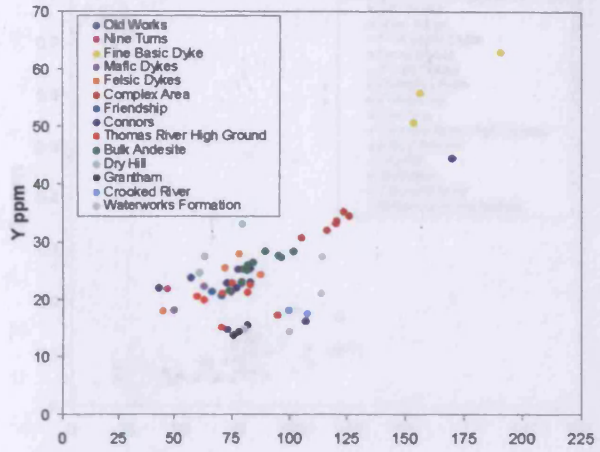

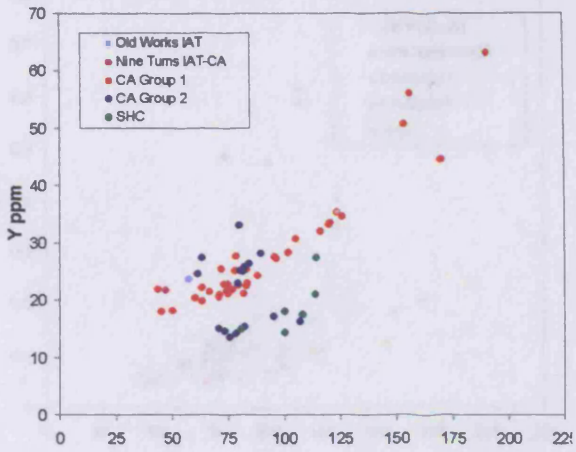

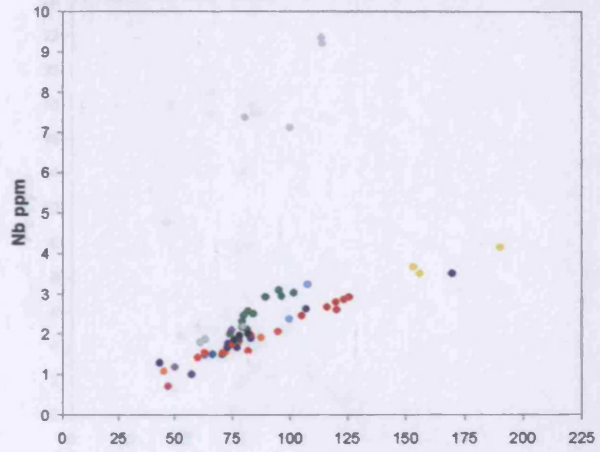

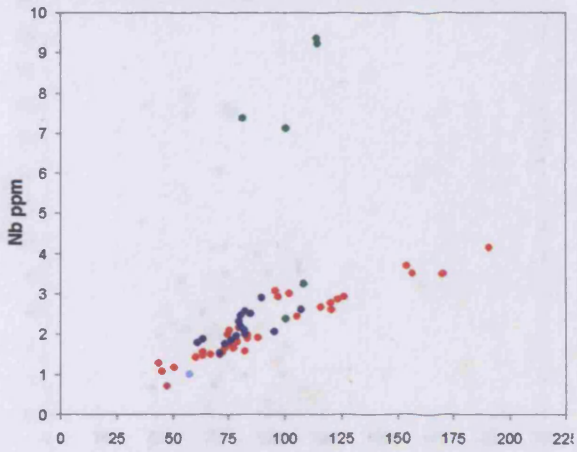

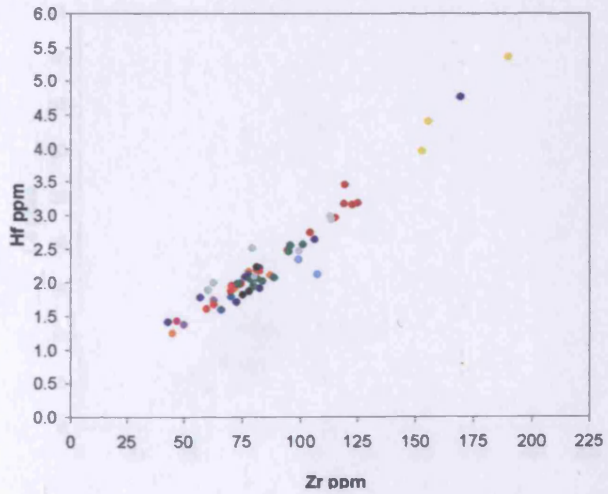

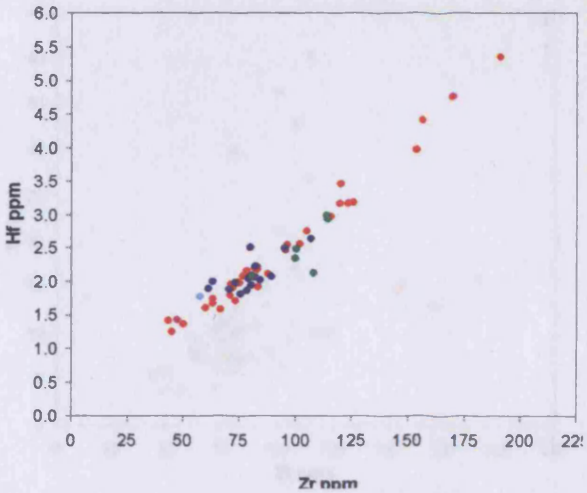

Appendix E: Major and trace element data for the Cretaceous and Tertiary Jamaican igneous rocks and their variation diagrams

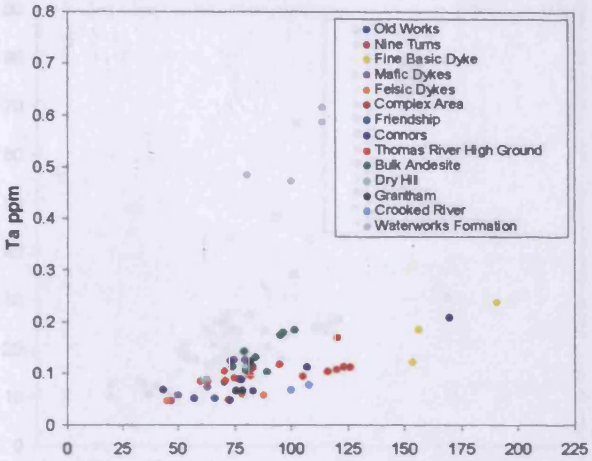

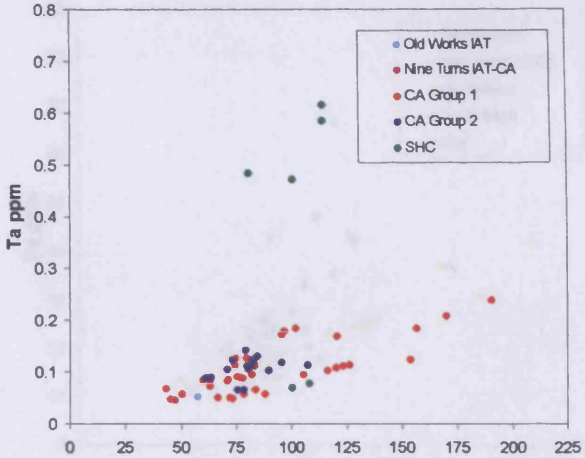

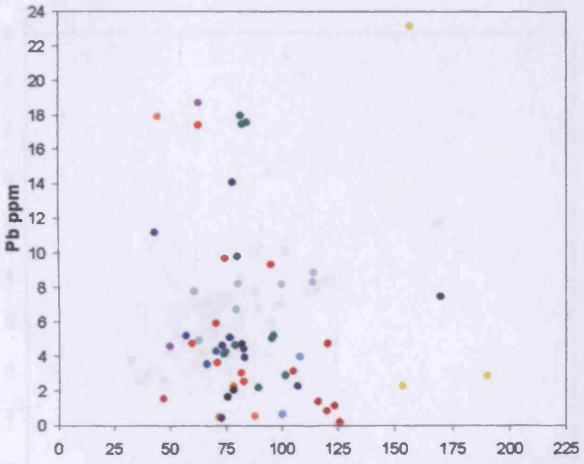

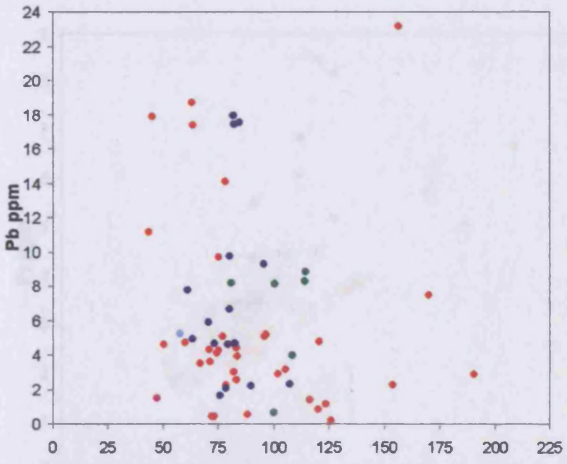

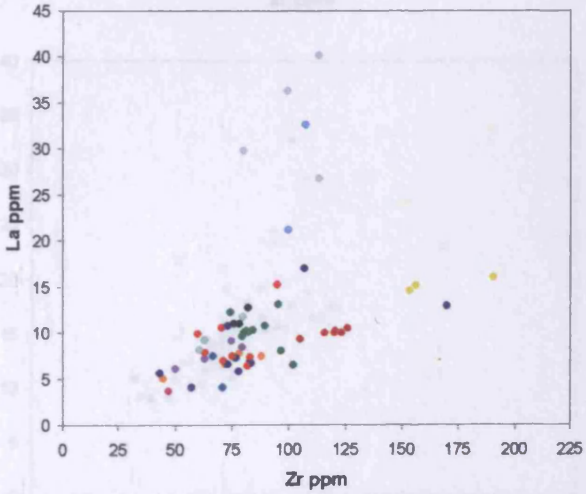

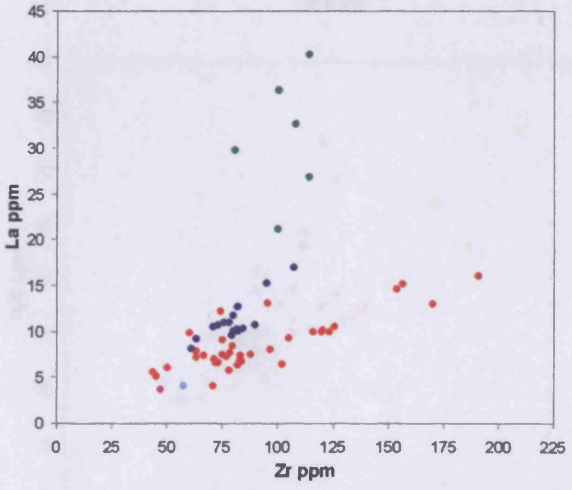

Appendix E: Major and trace element data for the Cretaceous and Tertiary Jamaican igneous rocks and their variation diagrams

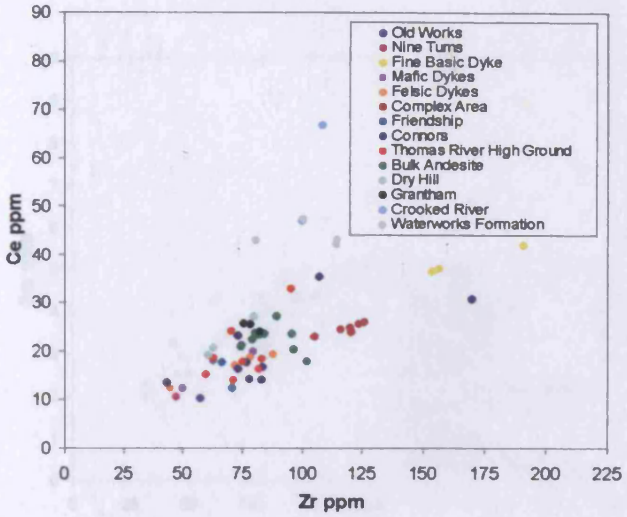

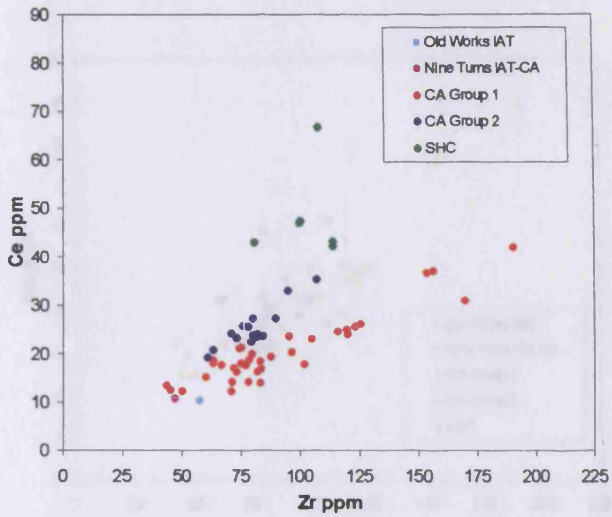

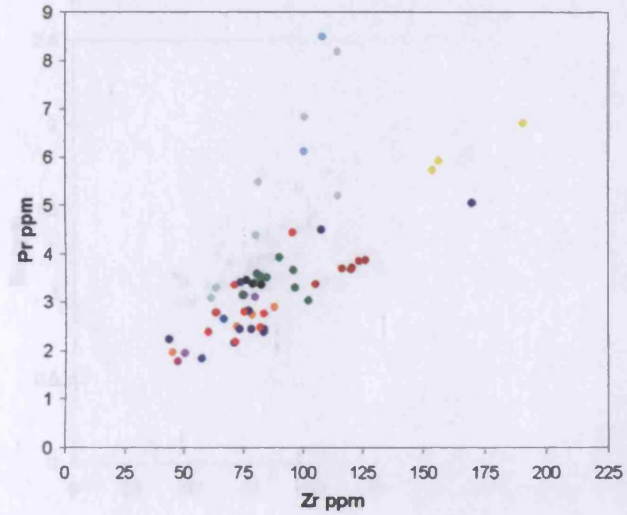

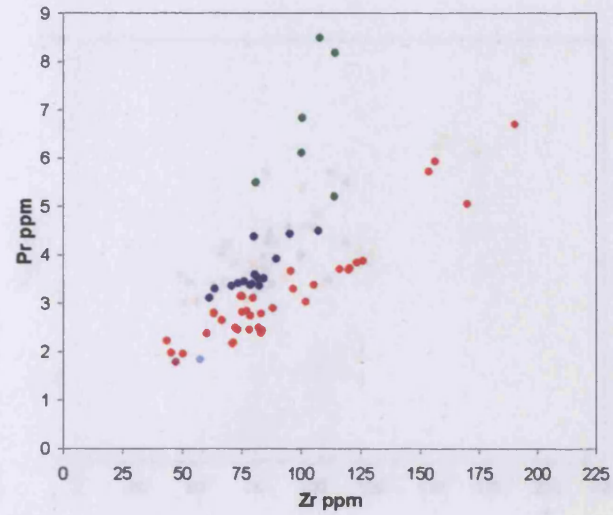

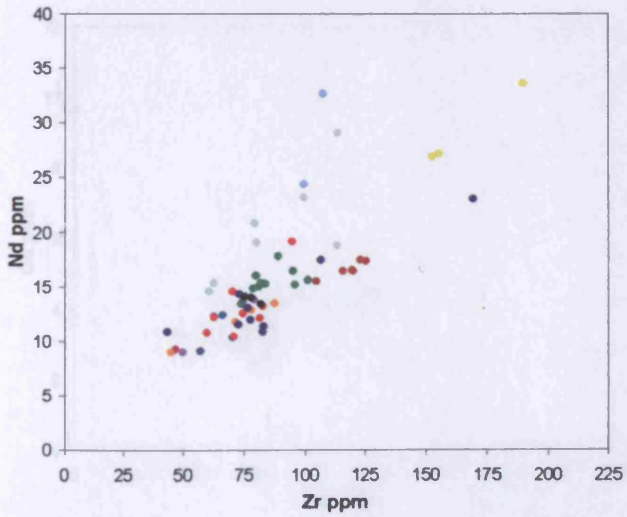

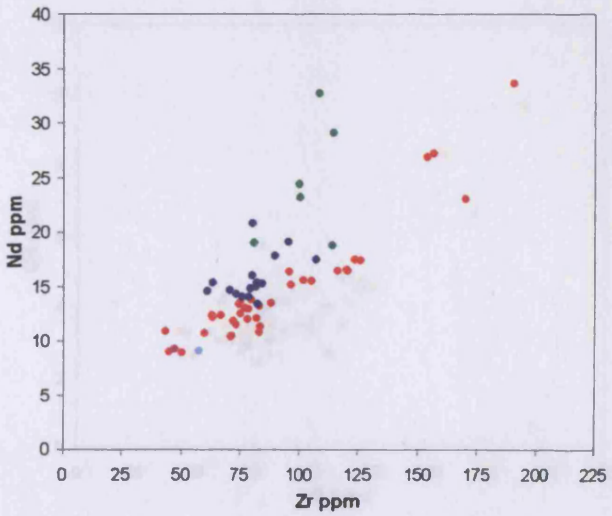

Appendix E: Major and trace element data for the Cretaceous and Tertiary Jamaican igneous rocks and their variation diagrams

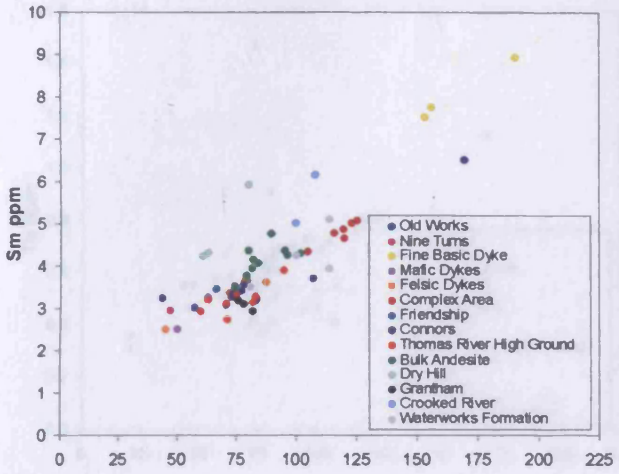

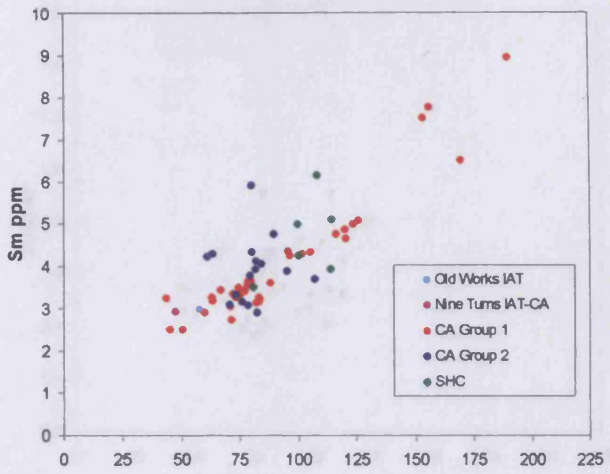

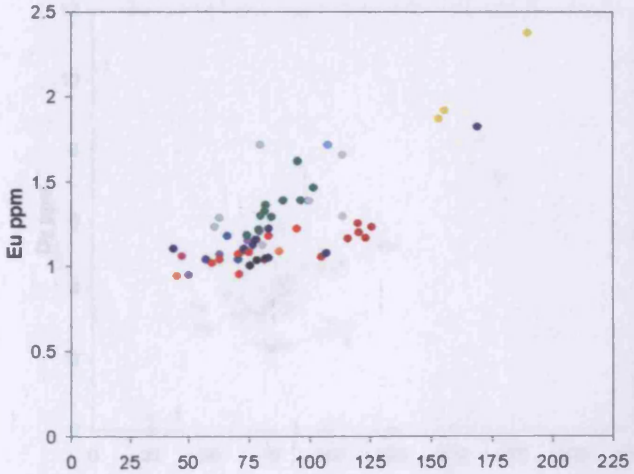

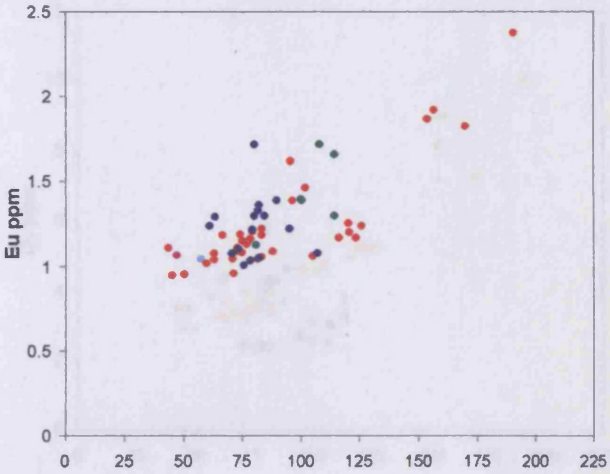

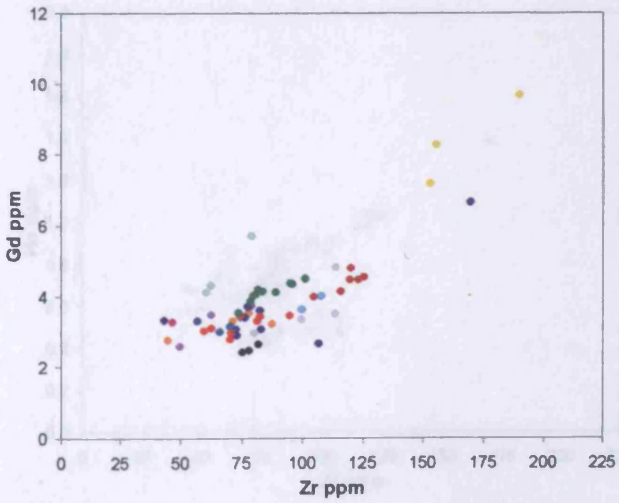

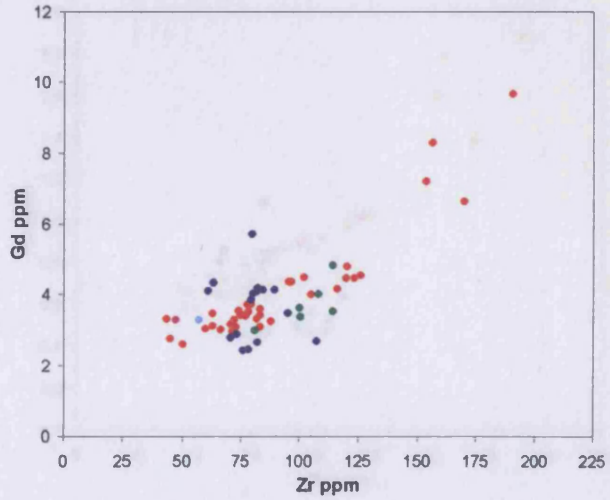

Appendix E: Major and trace element data for the Cretaceous and Tertiary Jamaican igneous rocks and their variation diagrams

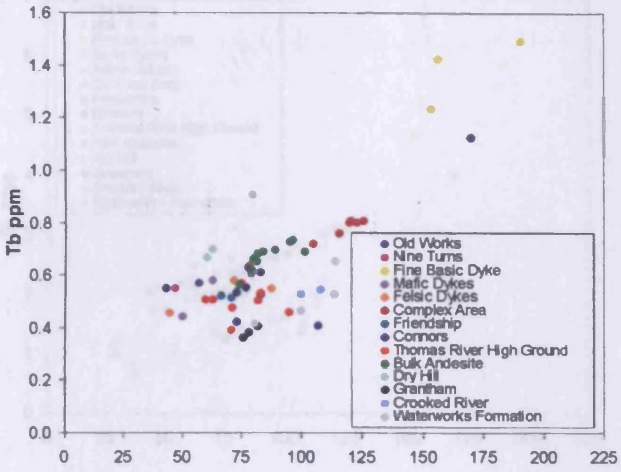

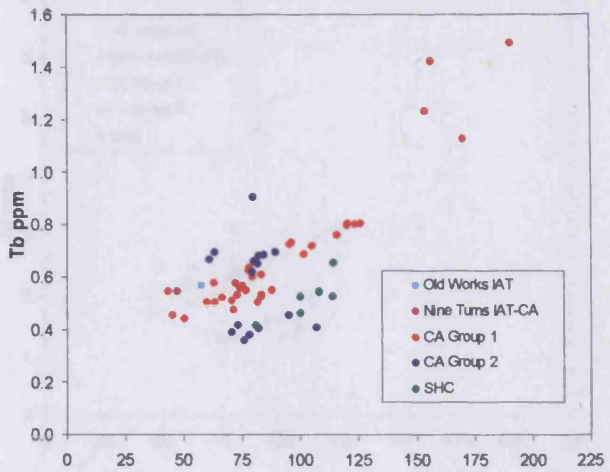

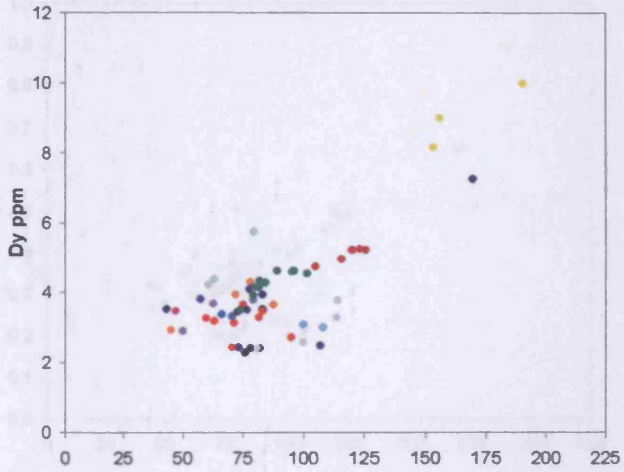

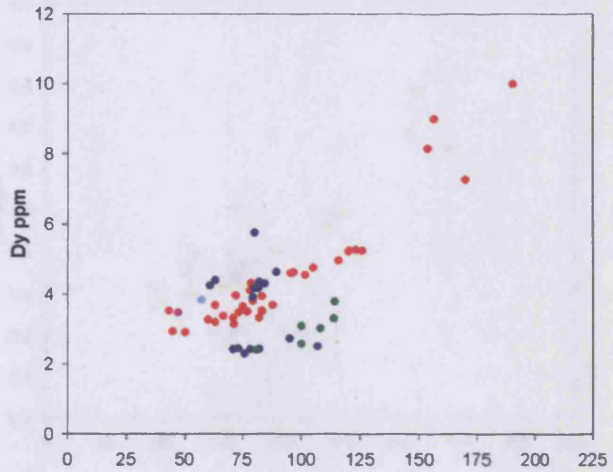

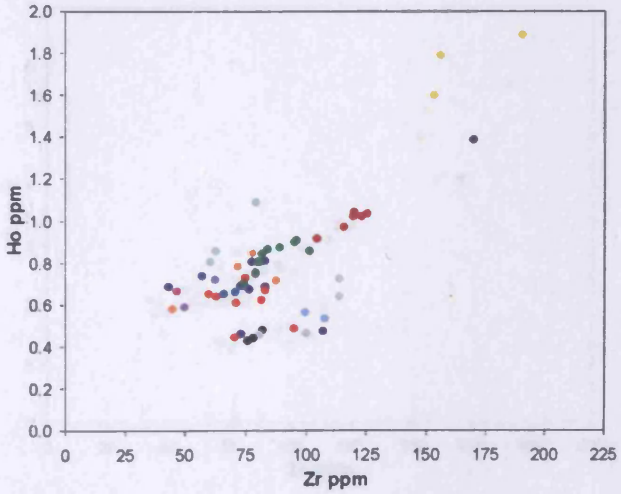

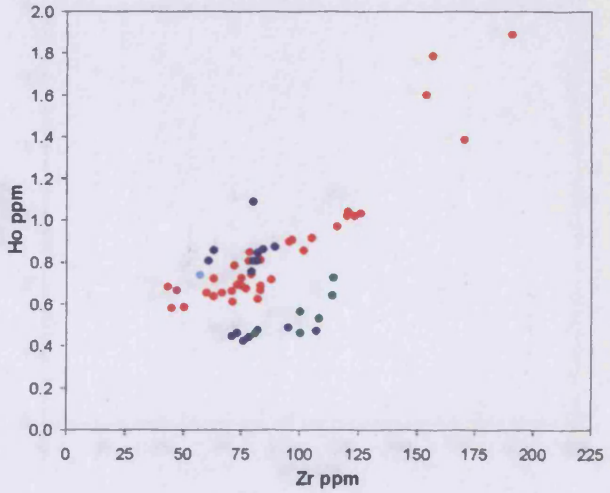

Appendix E: Major and trace element data for the Cretaceous and Tertiary Jamaican igneous rocks and their variation diagrams

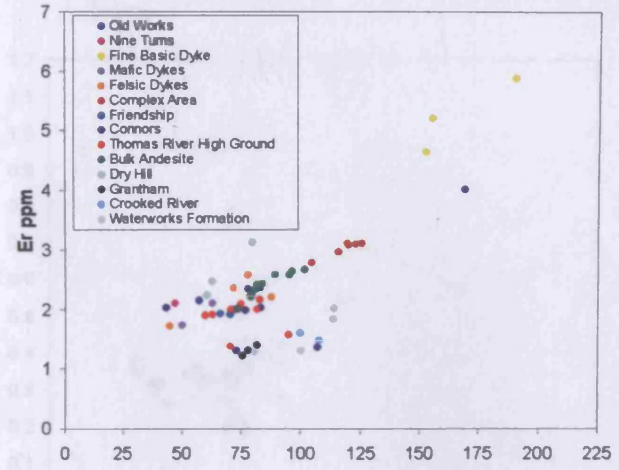

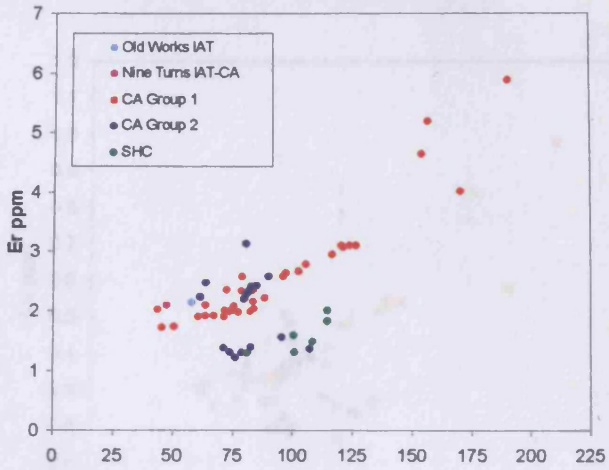

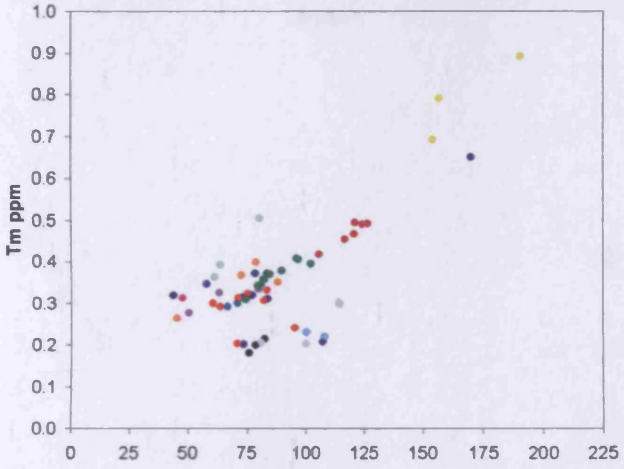

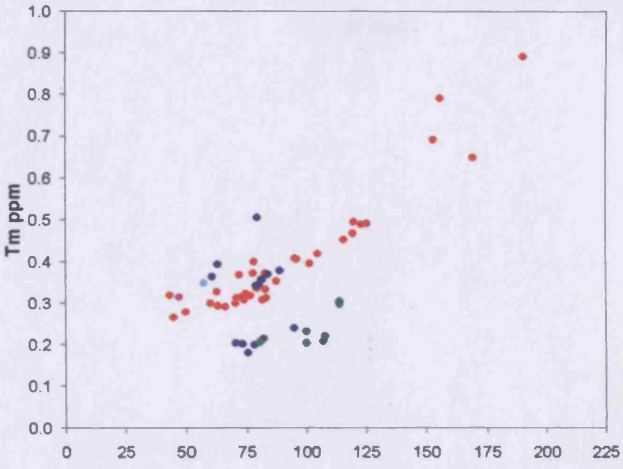

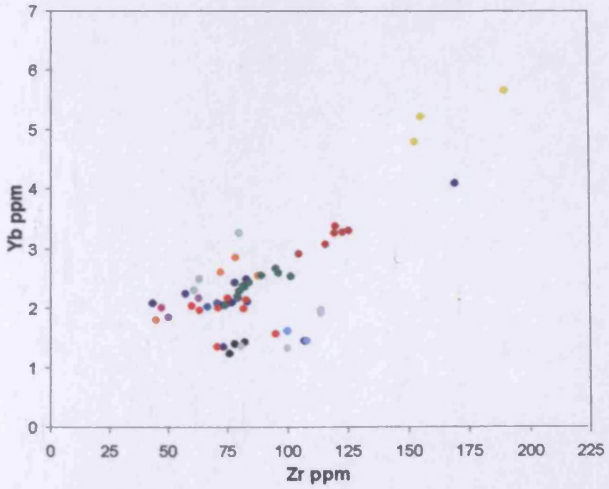

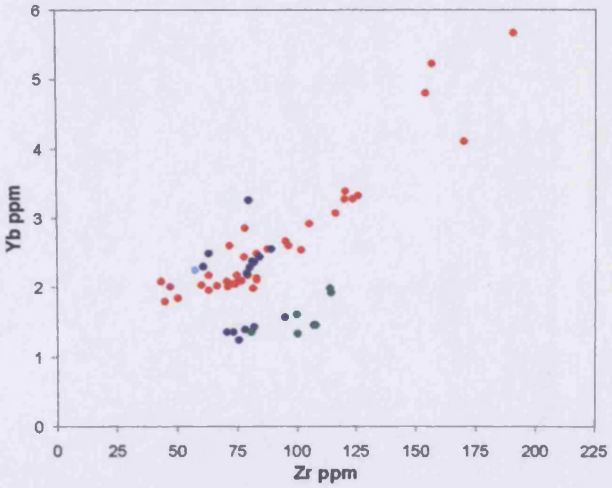

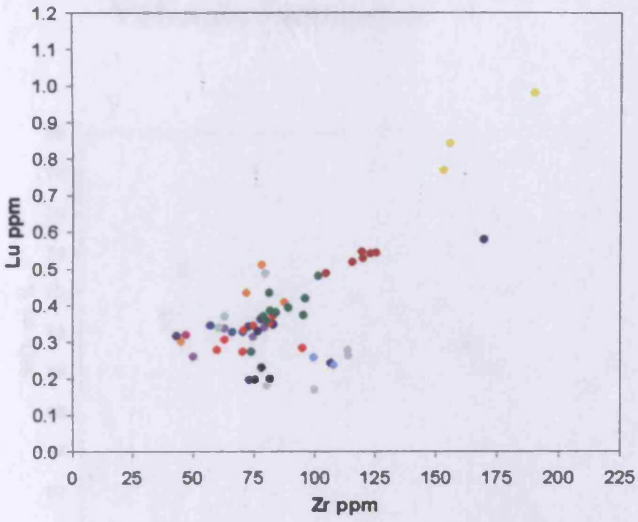
Lu ppm
Zr ppm
0.0
0.1
0.2
0.3
0.4
0.5
0.6
0.7
0.8
0.9
1.0
1.1
1.2
0
25
50
75
100
125
150
175
200
225

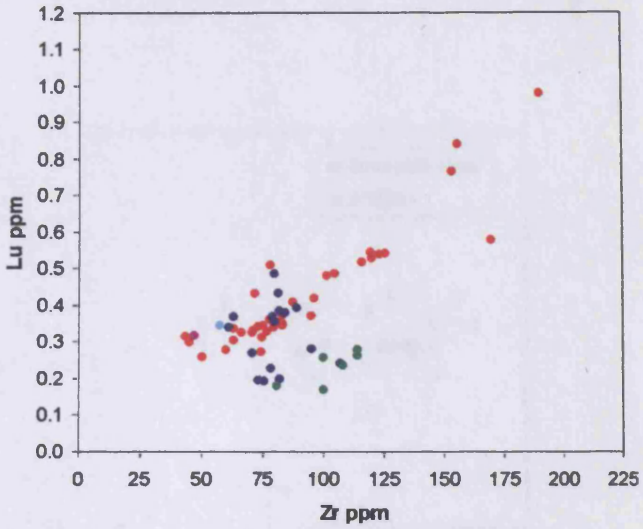
Lu ppm
Zr ppm
0.0
0.1
0.2
0.3
0.4
0.5
0.6
0.7
0.8
0.9
1.0
1.1
1.2
0
25
50
75
100
125
150
175
200
225

E.13 Major and trace element variation diagrams for the Newcastle Volcanic Formation

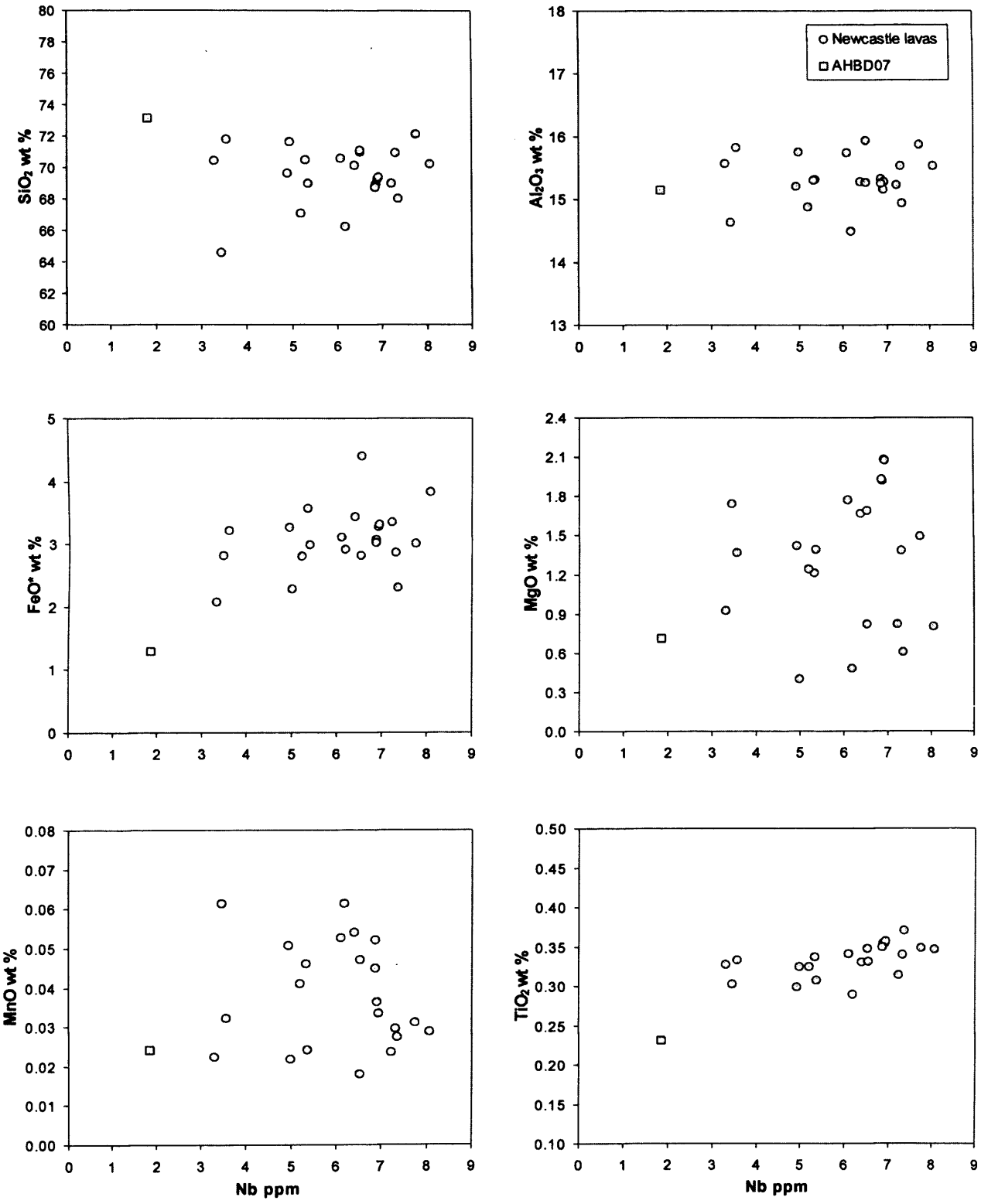

Appendix E: Major and trace element data for the Cretaceous and Tertiary Jamaican igneous rocks and their variation diagrams

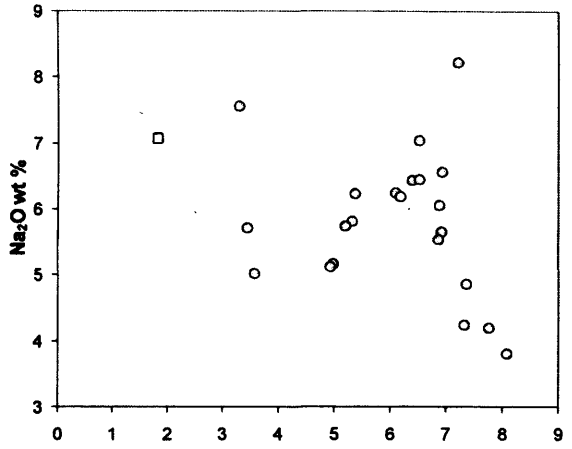

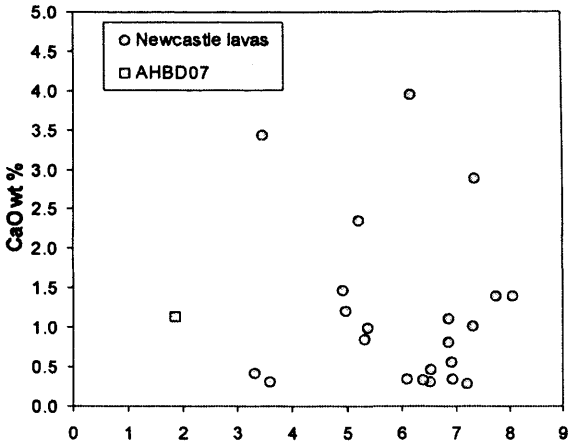

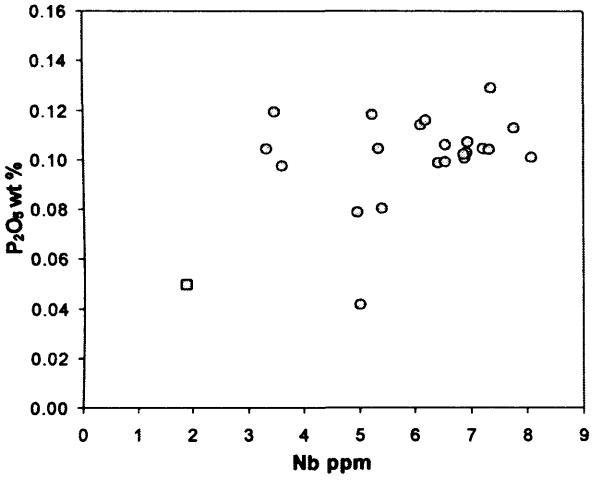

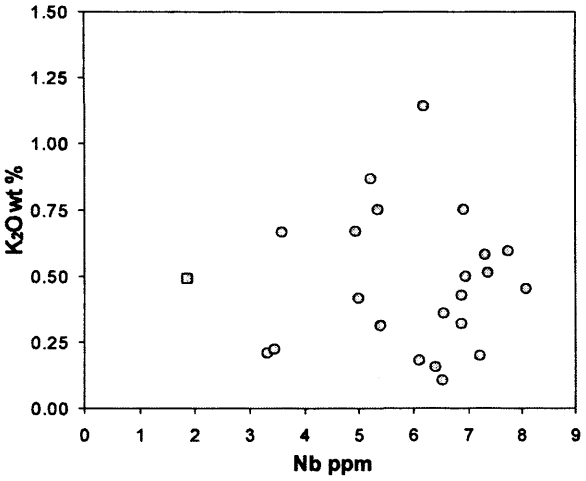

Appendix E: Major and trace element data for the Cretaceous and Tertiary Jamaican igneous rocks and their variation diagrams

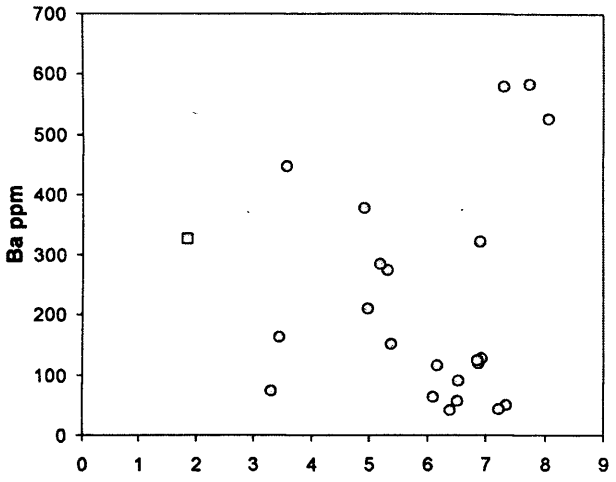

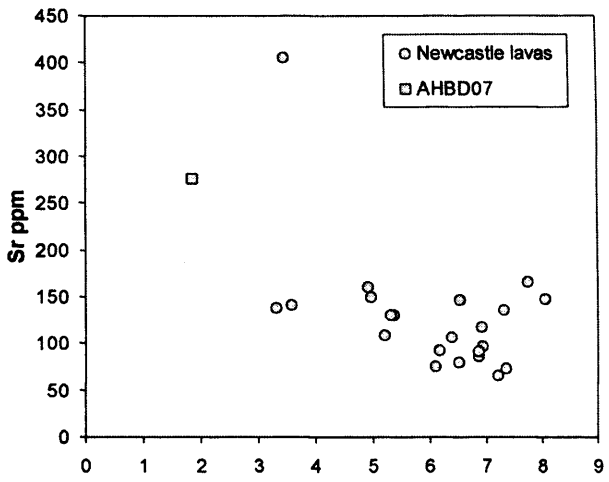

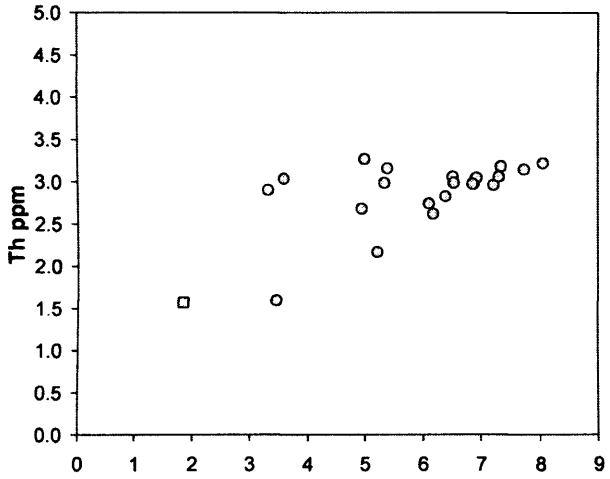

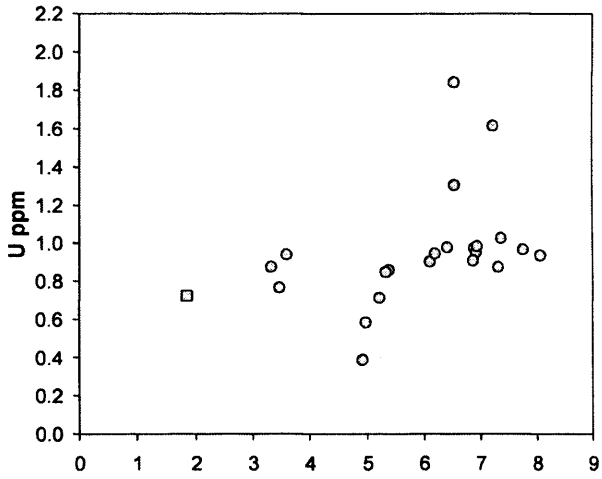

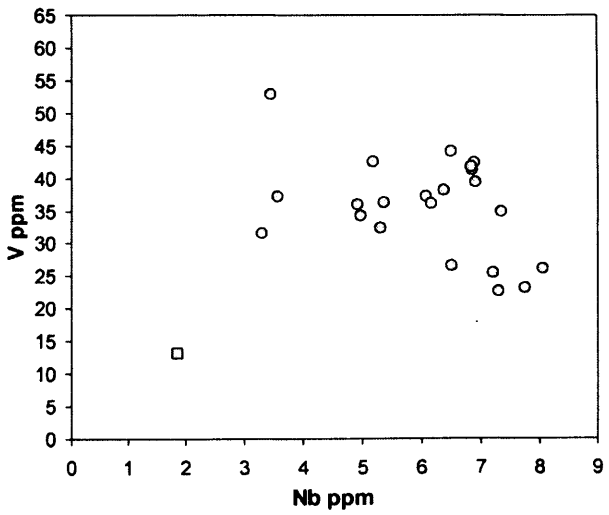

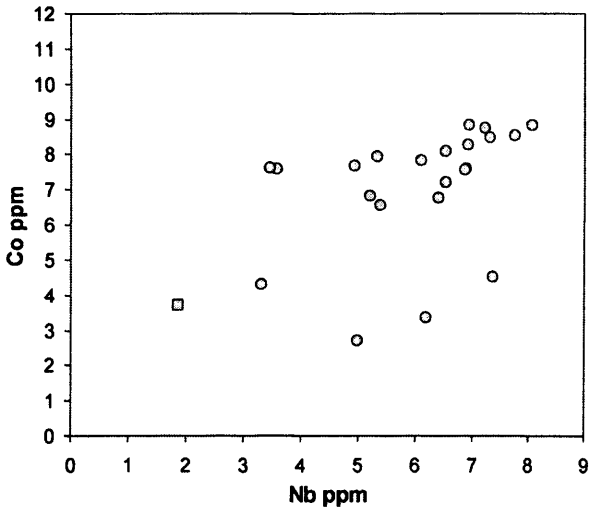

Appendix E: Major and trace element data for the Cretaceous and Tertiary Jamaican igneous rocks and their variation diagrams

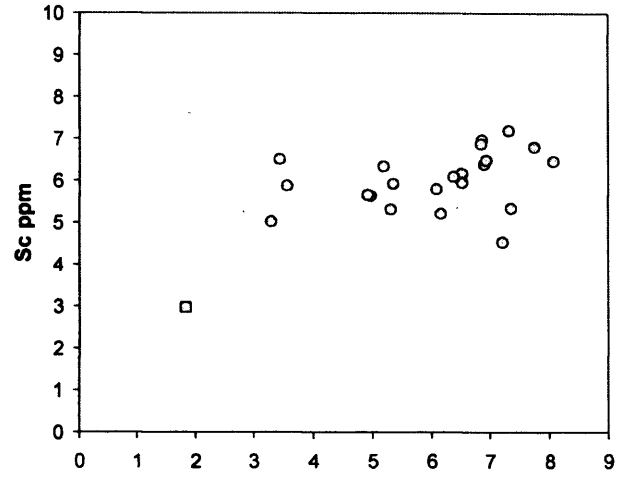

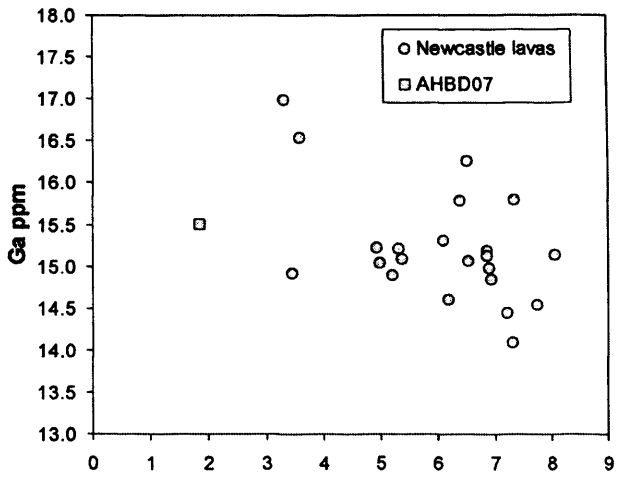

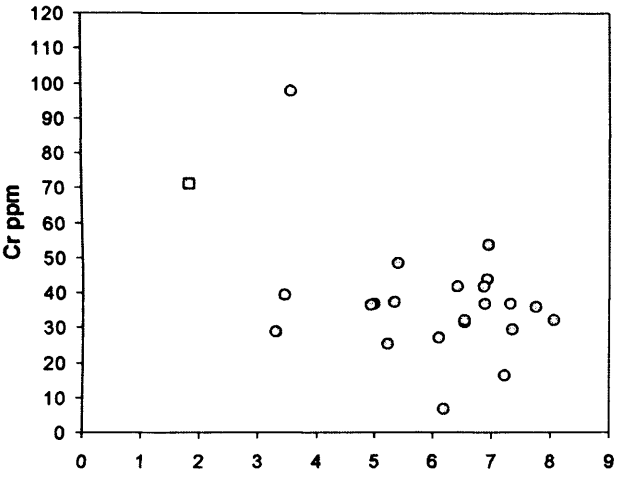

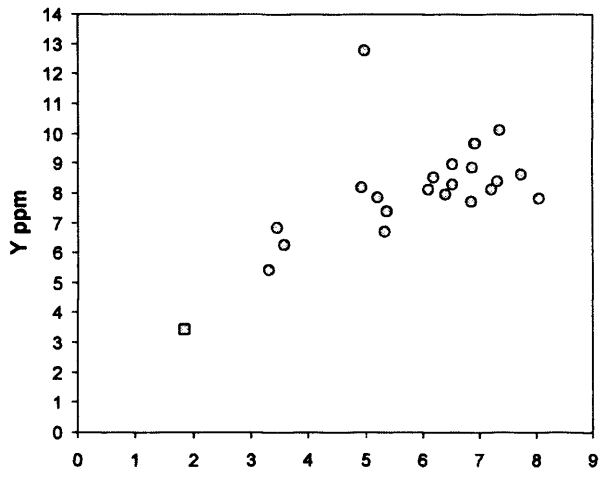

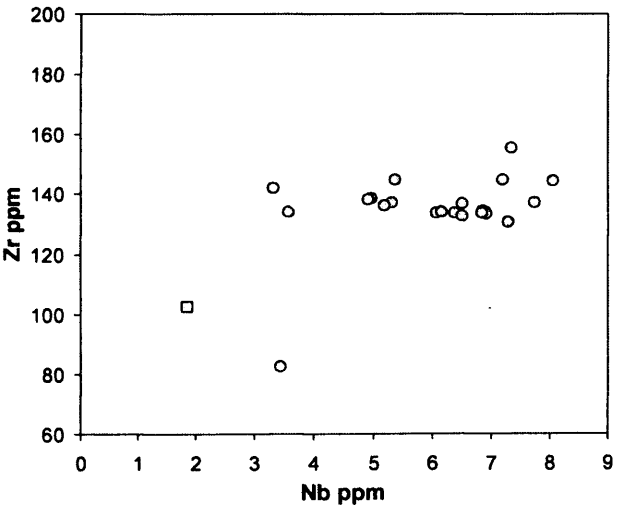

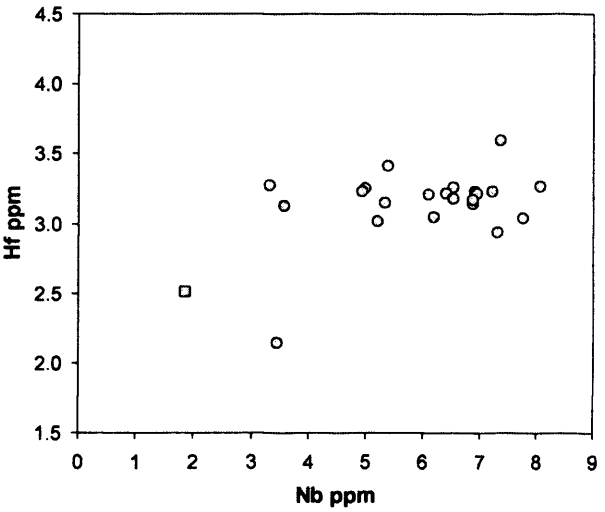

Appendix E: Major and trace element data for the Cretaceous and Tertiary Jamaican igneous rocks and their variation diagrams

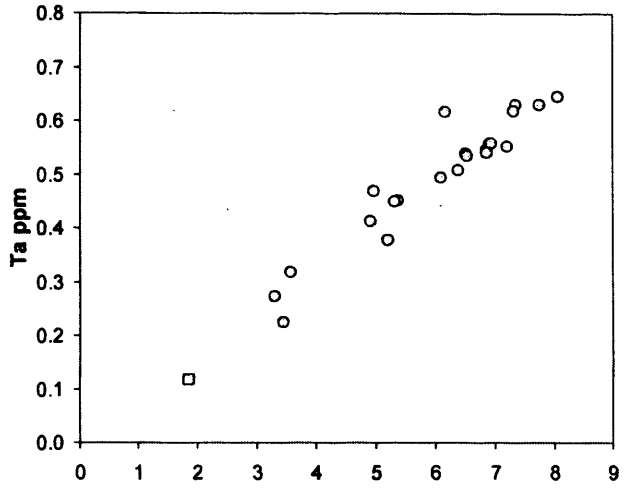

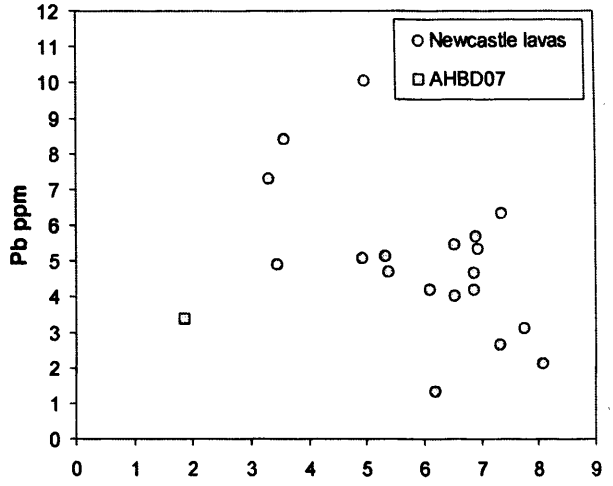

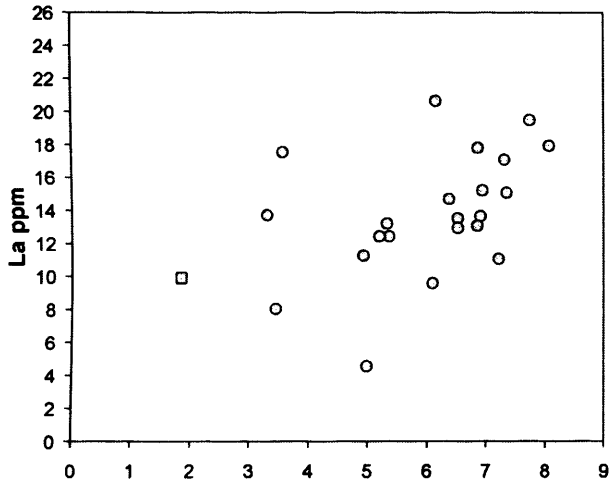

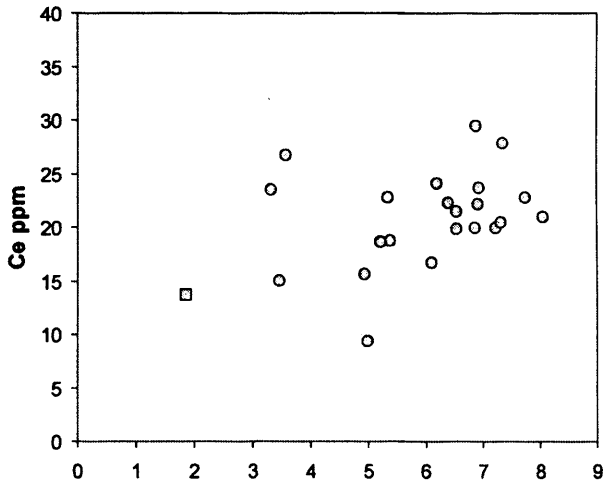

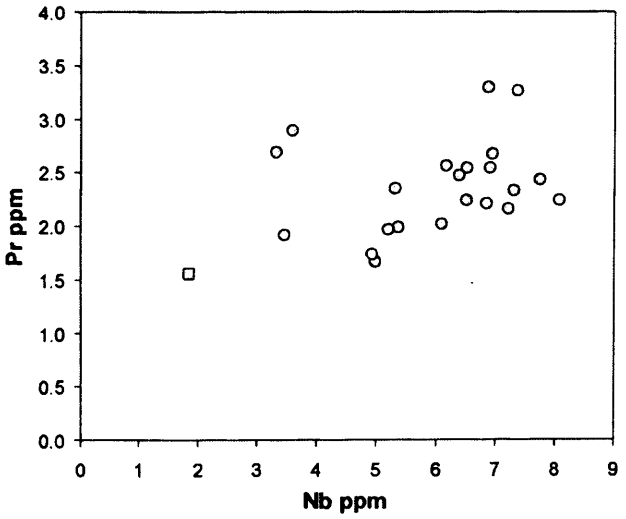

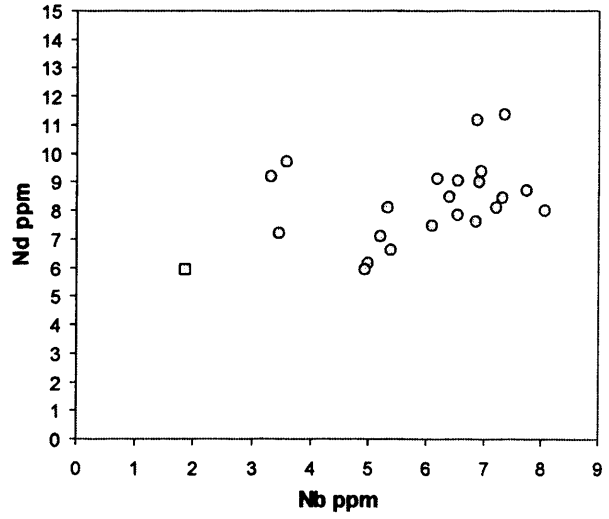

Appendix E: Major and trace element data for the Cretaceous and Tertiary Jamaican igneous rocks and their variation diagrams

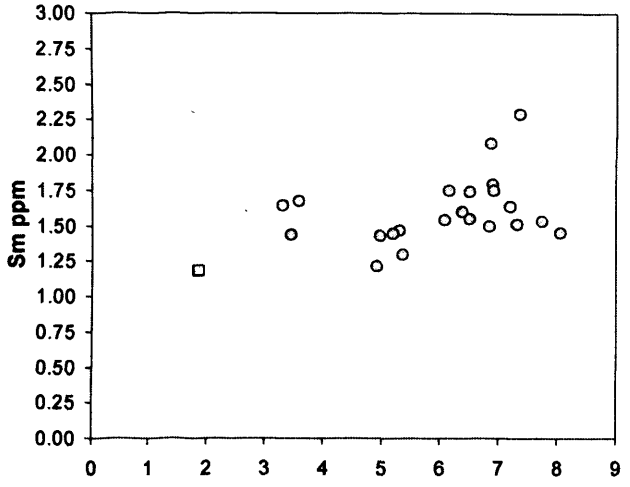

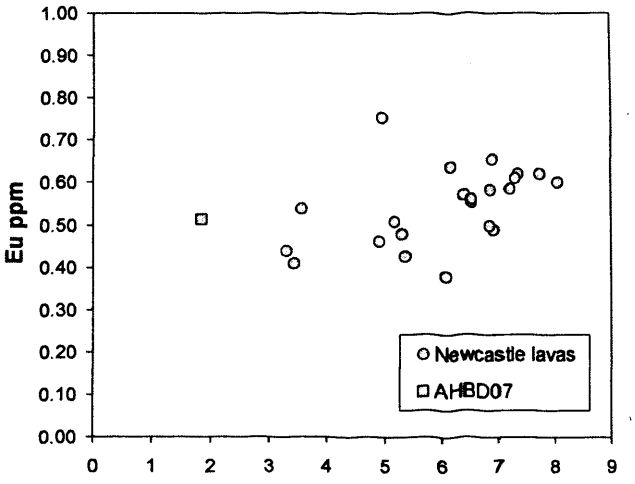

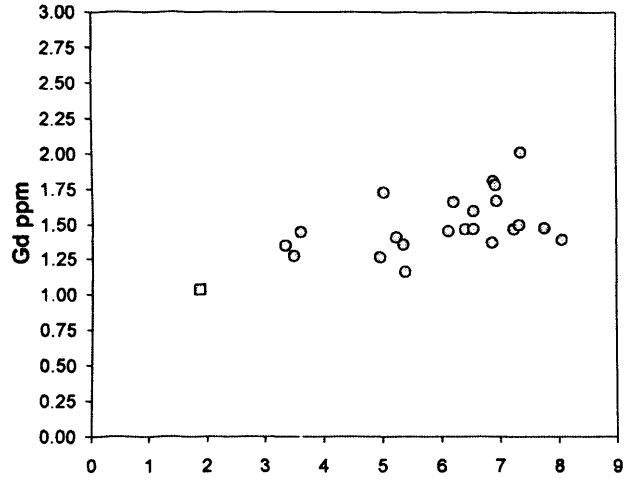

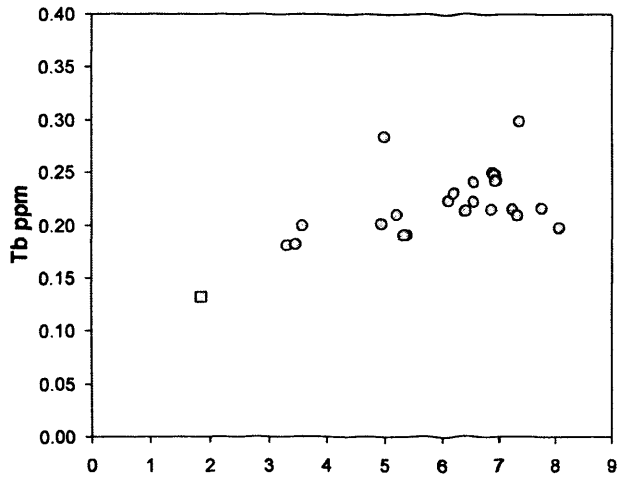

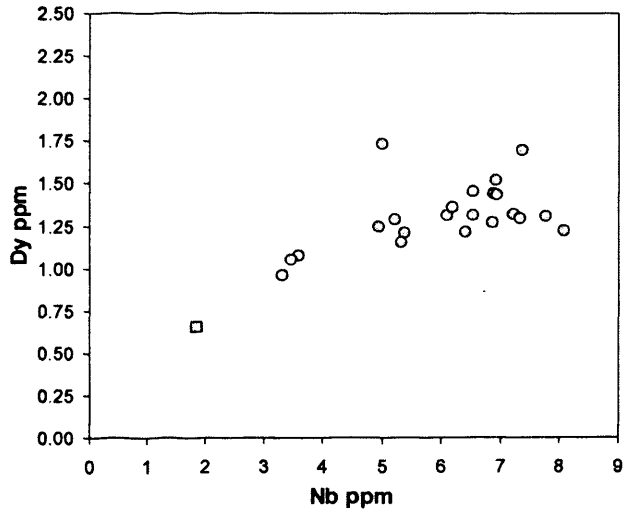

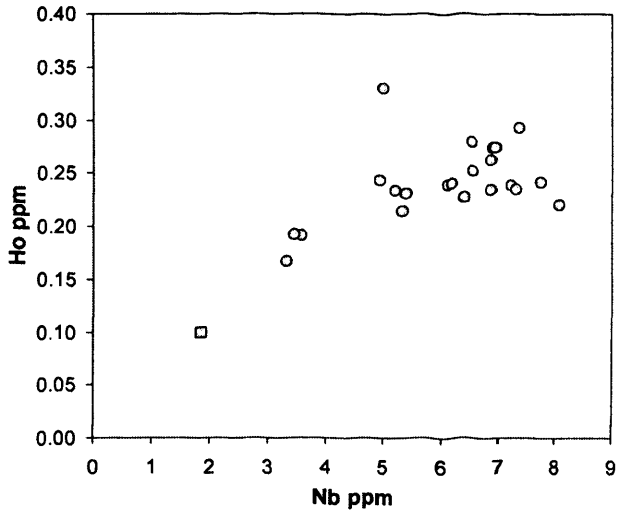

Appendix E: Major and trace element data for the Cretaceous and Tertiary Jamaican igneous rocks and their variation diagrams

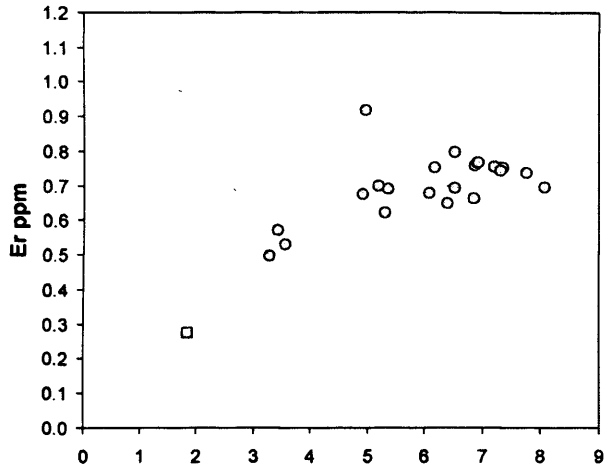

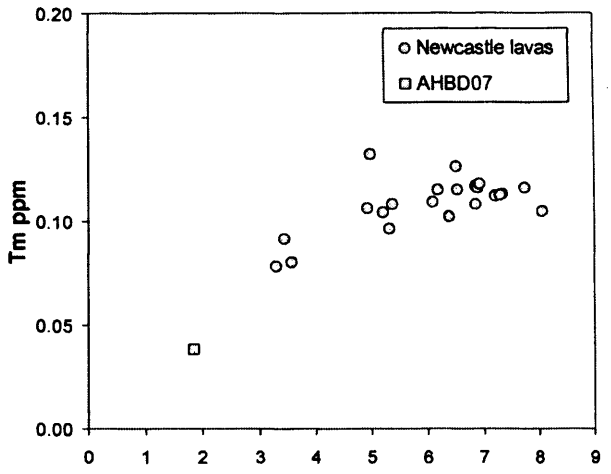

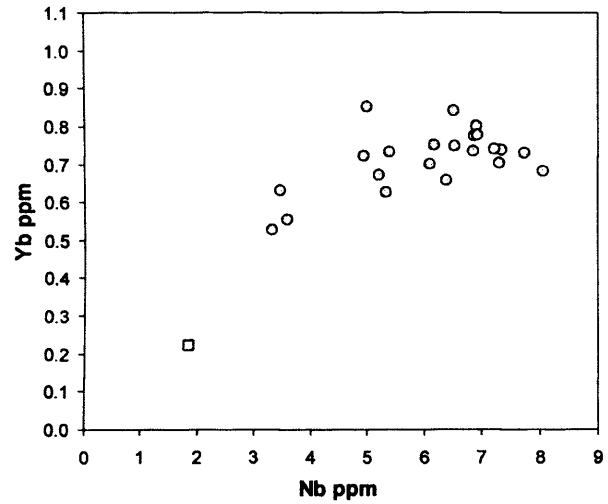

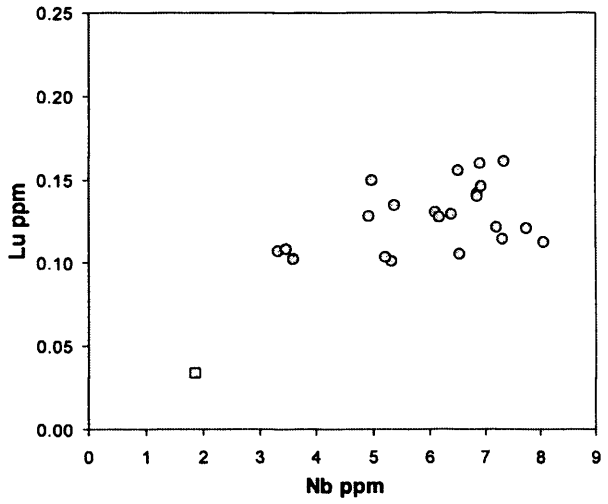

E.14 Major and trace element variation diagrams for the Halberstadt Volcanic Formation

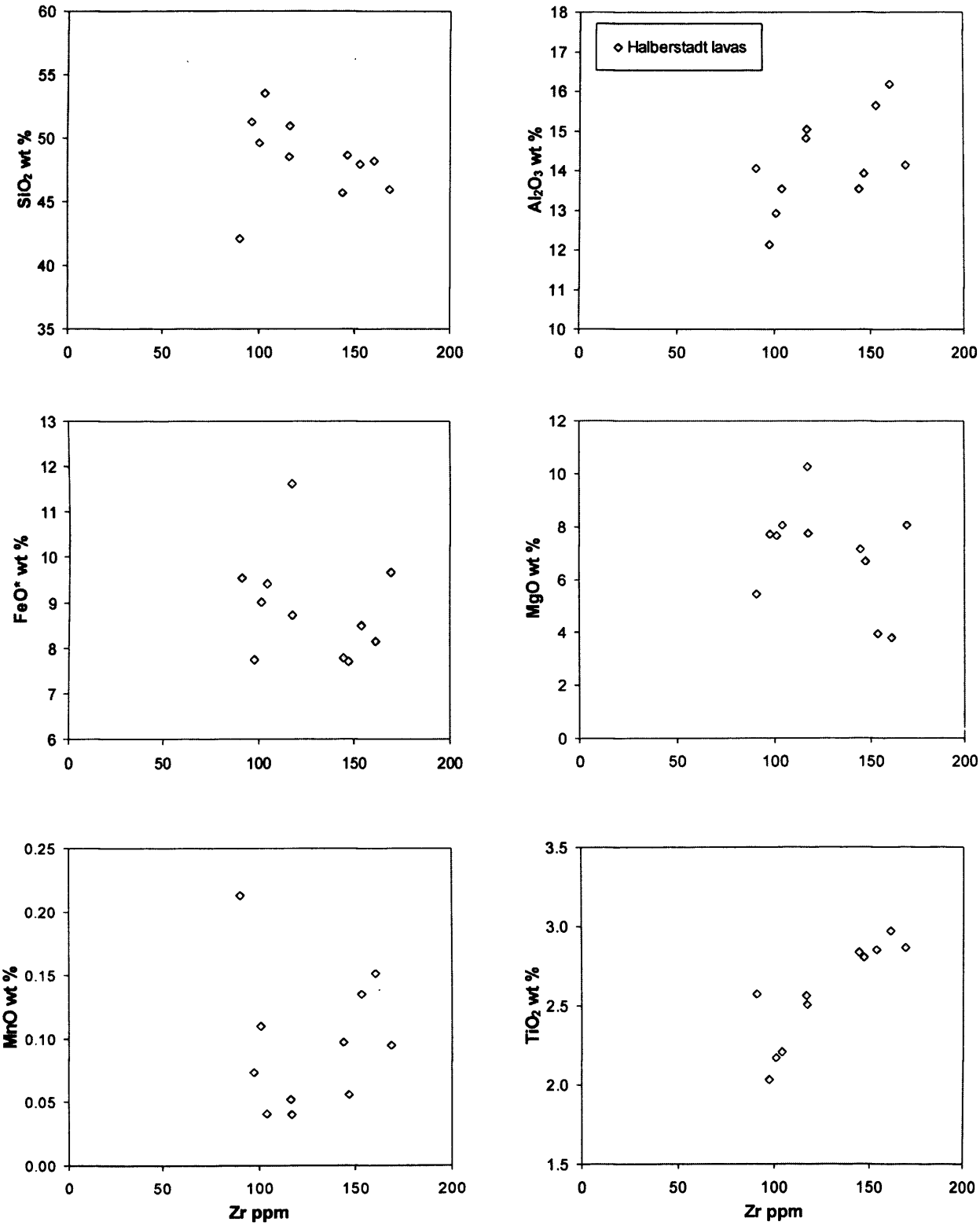

Appendix E: Major and trace element data for the Cretaceous and Tertiary Jamaican igneous rocks and their variation diagrams

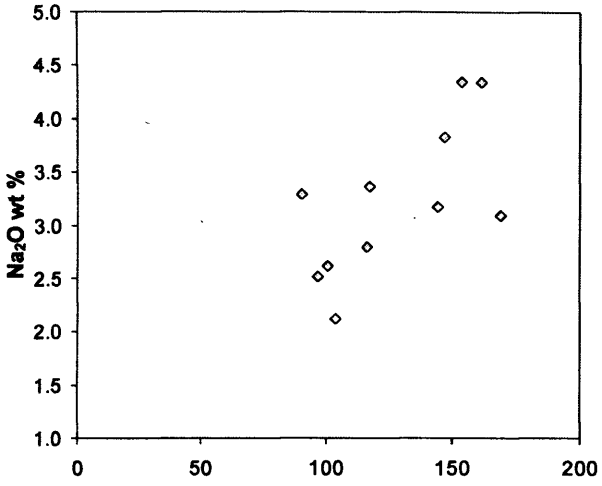

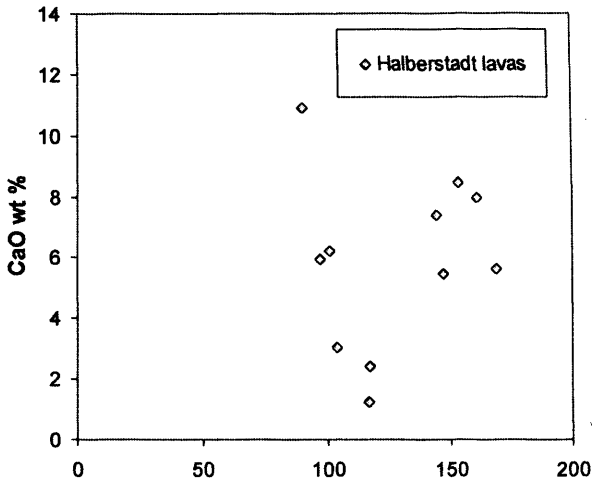

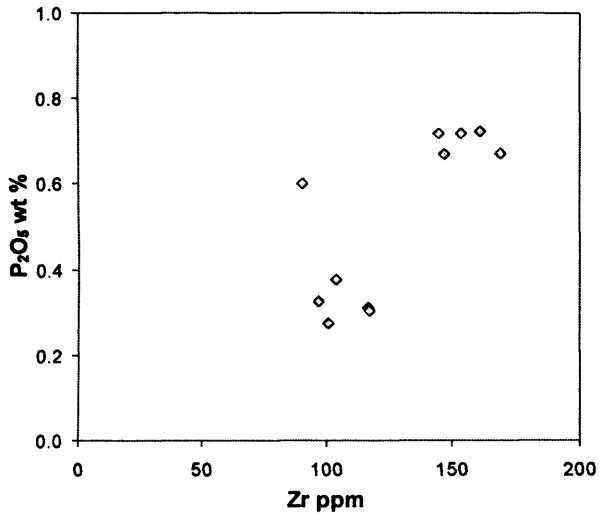

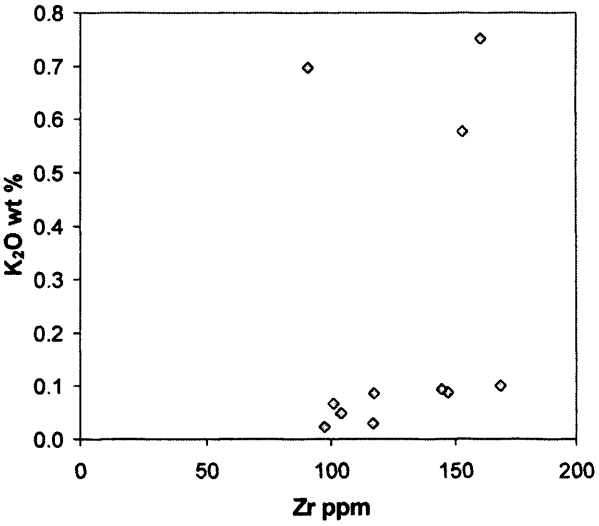

Appendix E: Major and trace element data for the Cretaceous and Tertiary Jamaican igneous rocks and their variation diagrams

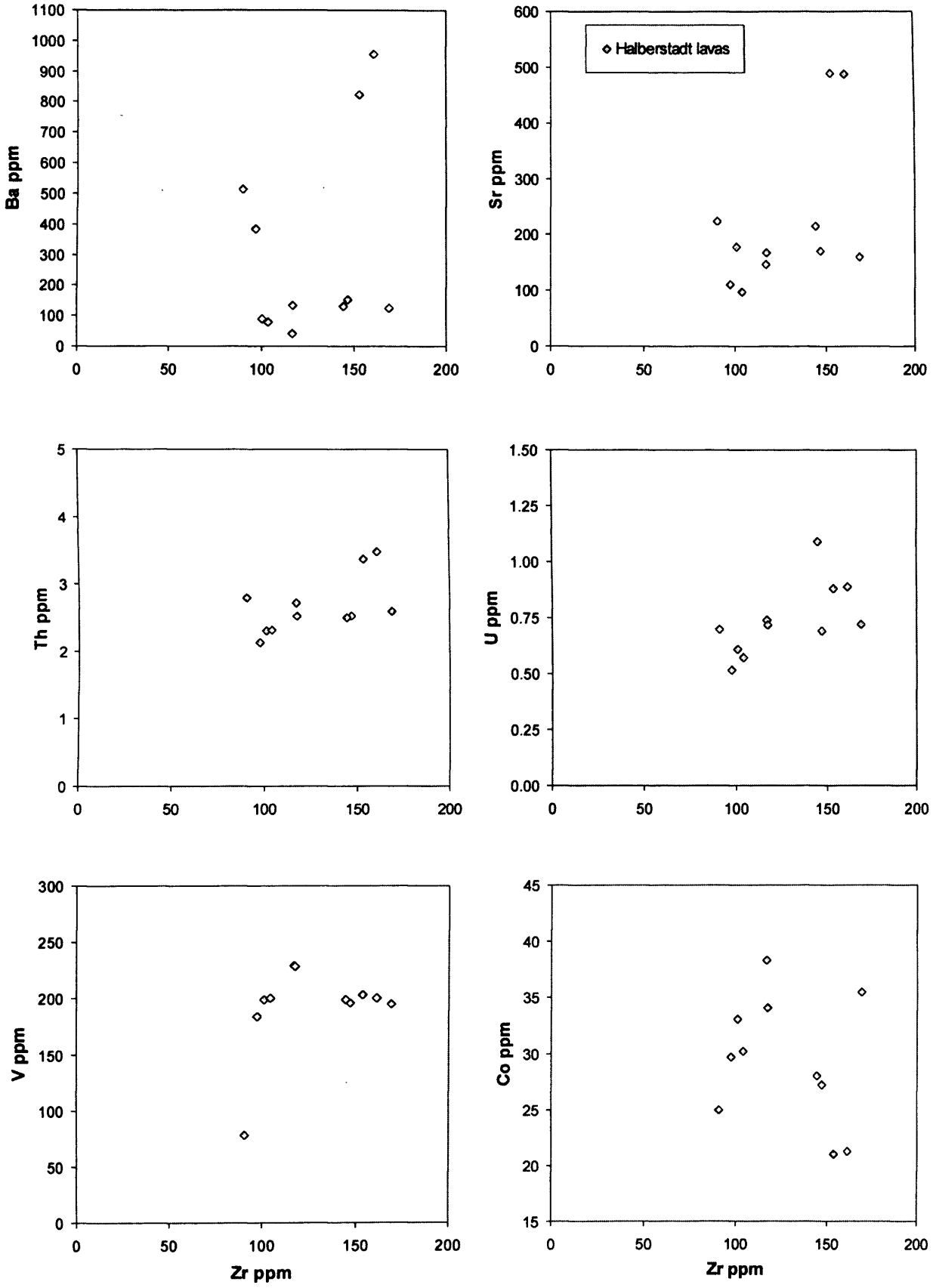

Appendix E: Major and trace element data for the Cretaceous and Tertiary Jamaican igneous rocks and their variation diagrams

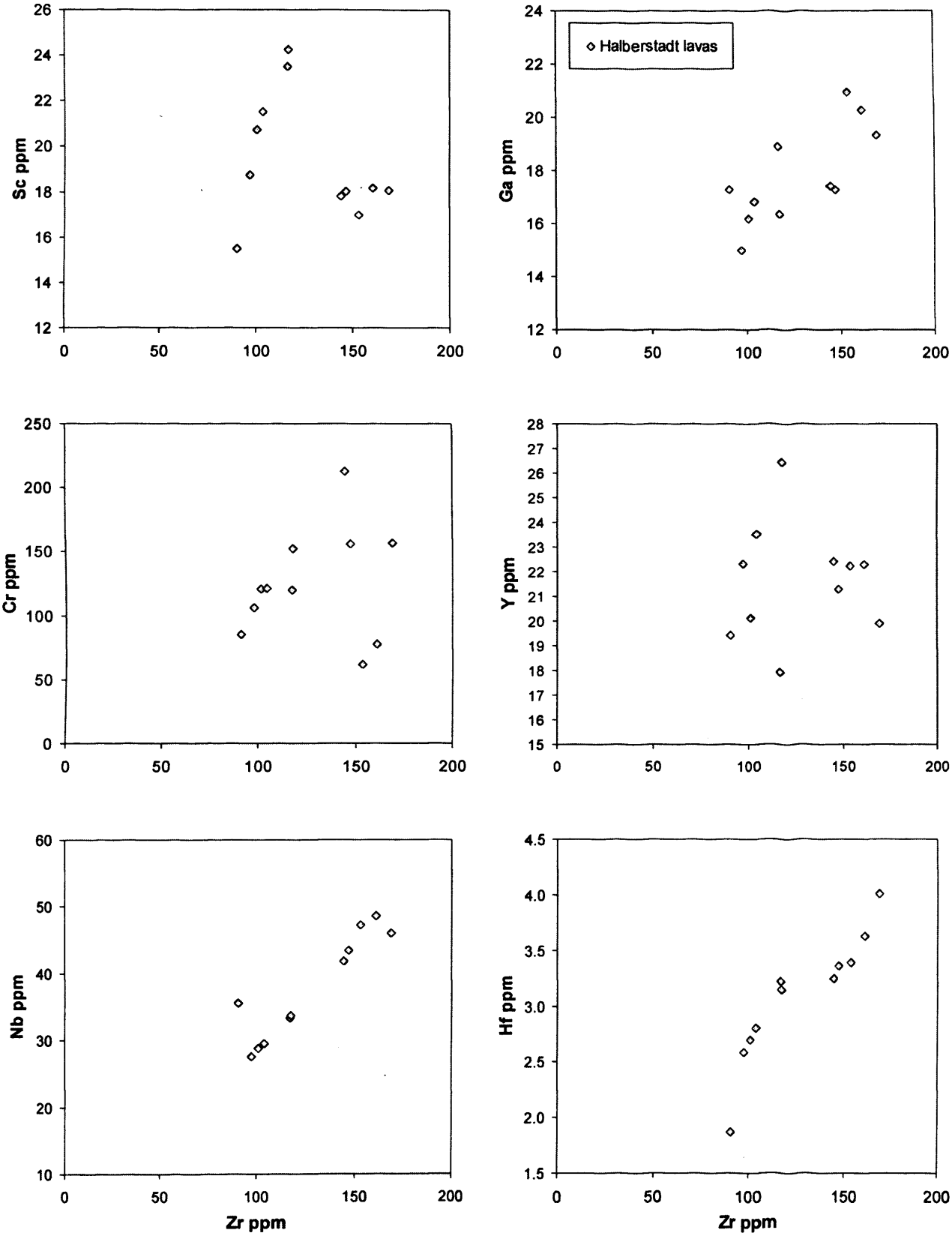

Appendix E: Major and trace element data for the Cretaceous and Tertiary Jamaican igneous rocks and their variation diagrams

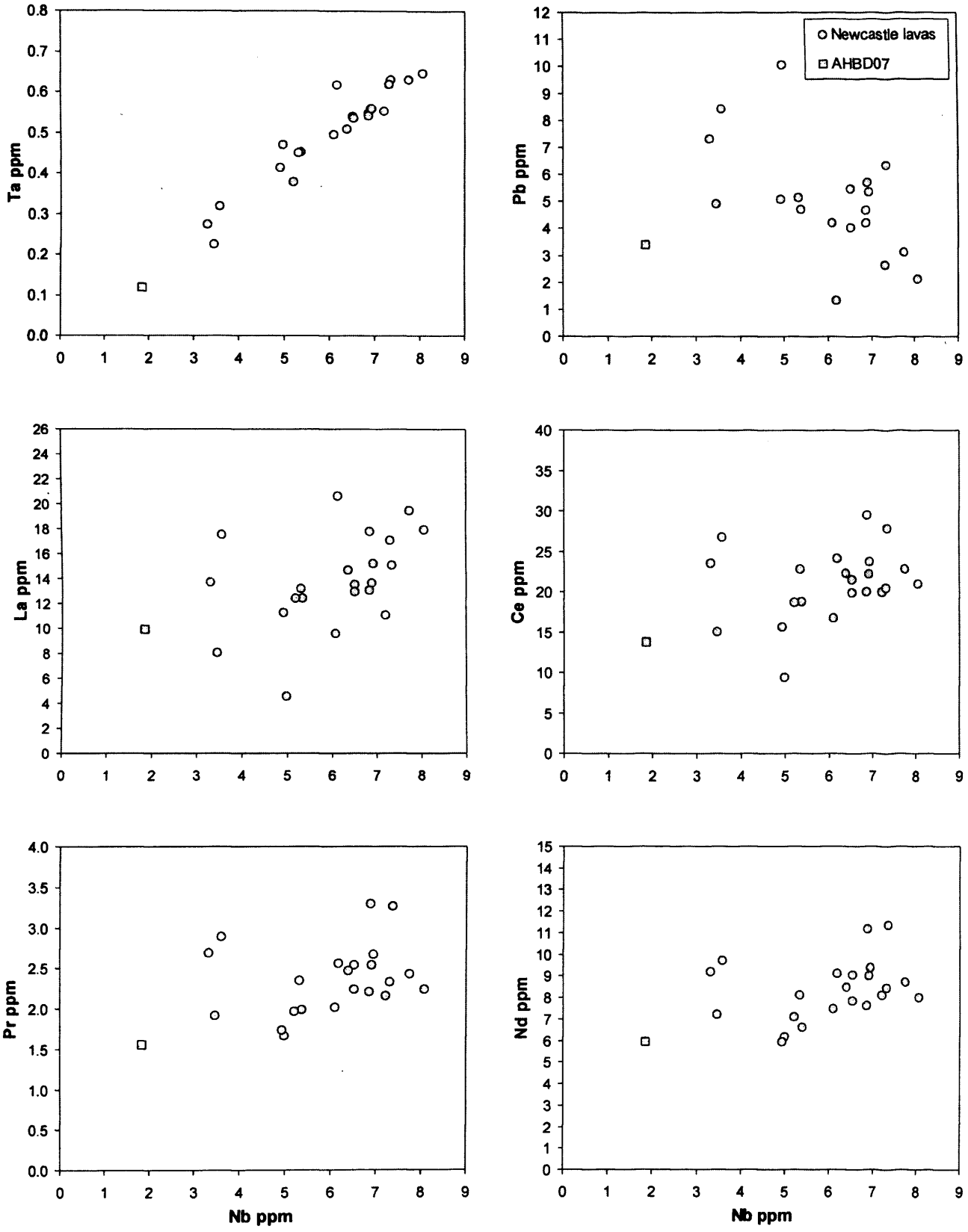

Appendix E: Major and trace element data for the Cretaceous and Tertiary Jamaican igneous rocks and their variation diagrams

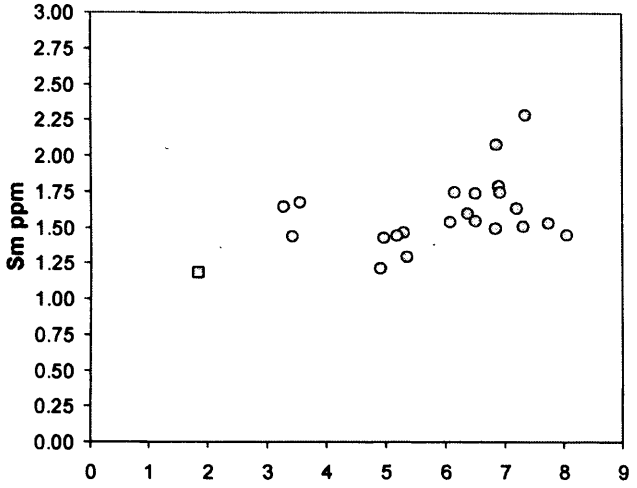

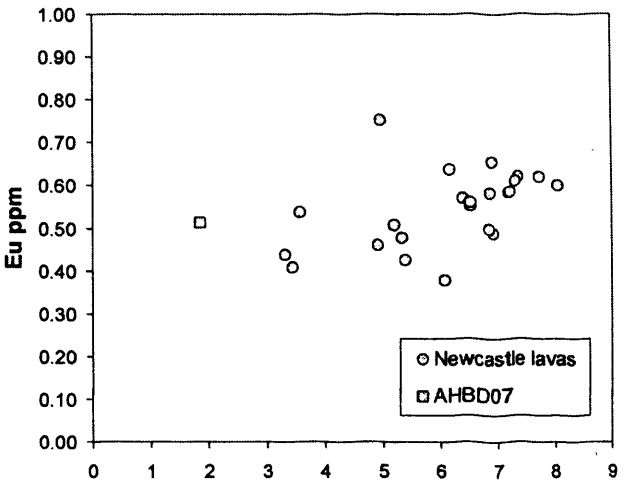

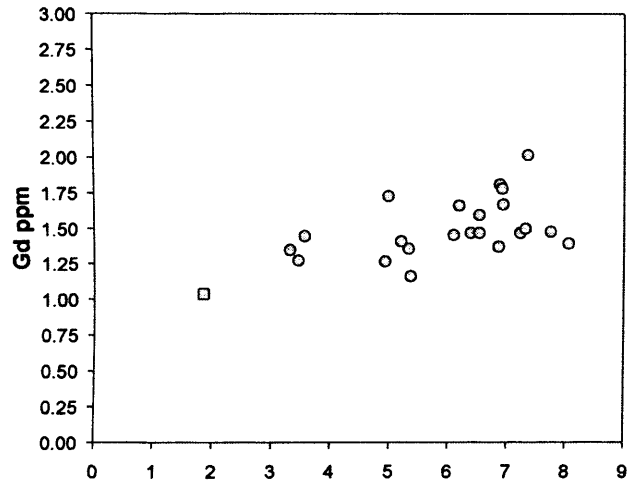

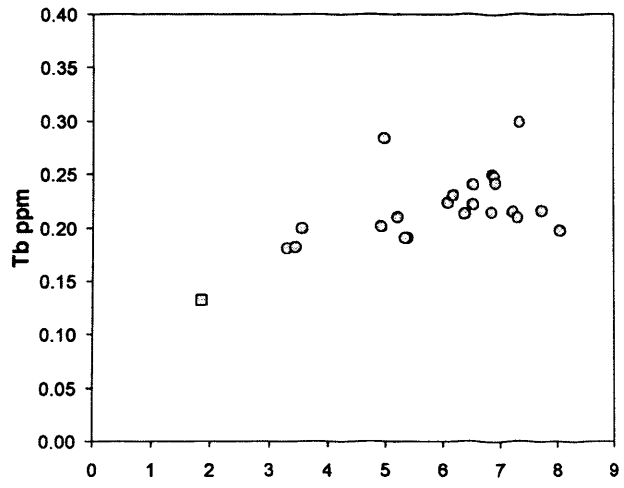

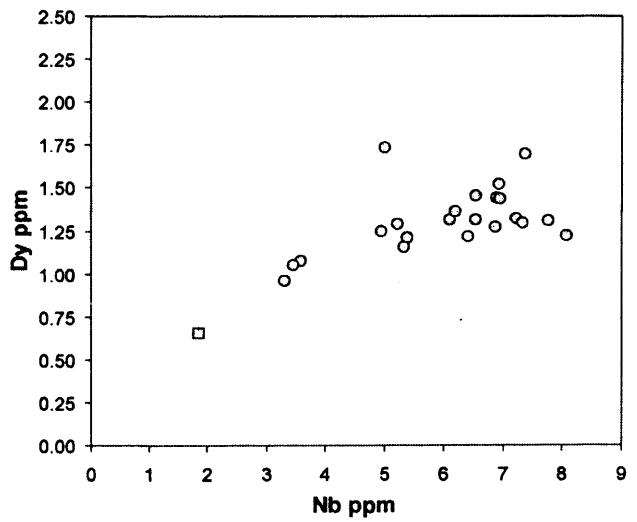

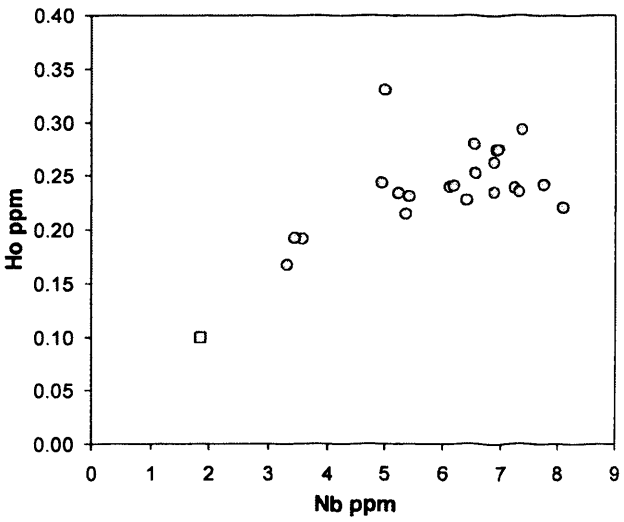

Appendix E: Major and trace element data for the Cretaceous and Tertiary Jamaican igneous rocks and their variation diagrams

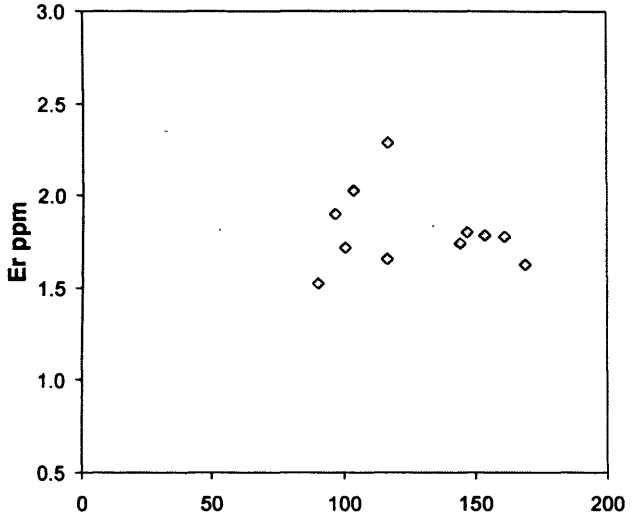

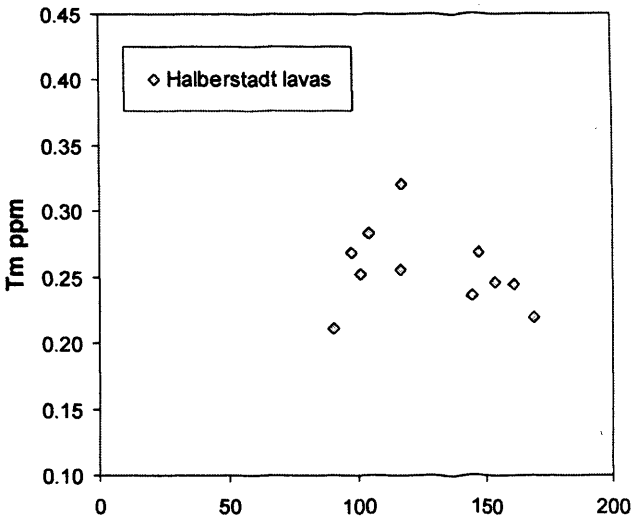

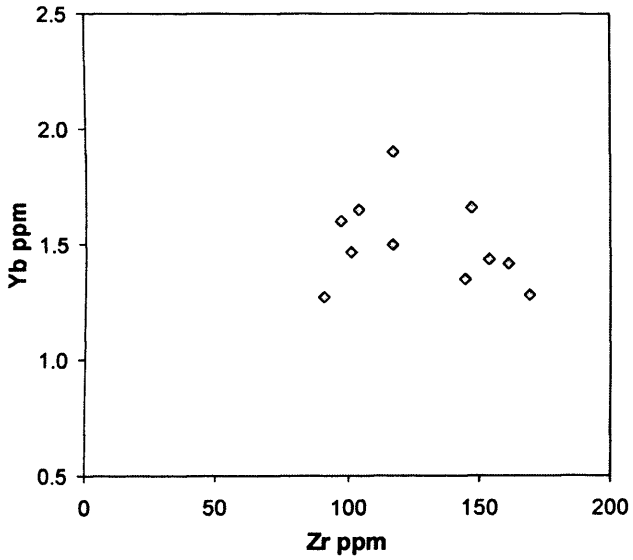

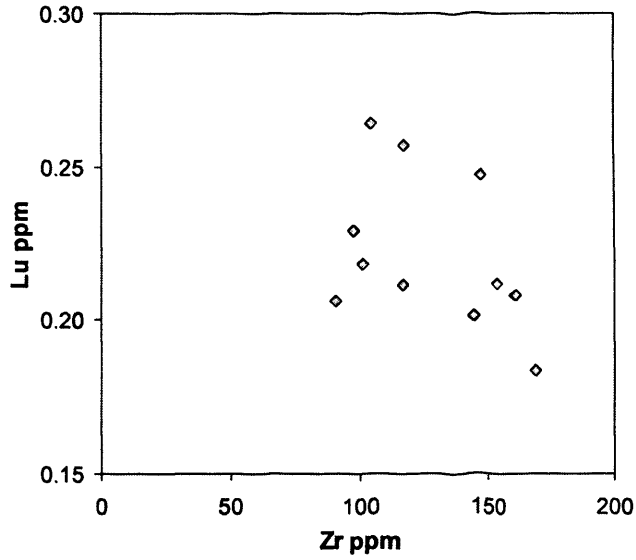

Appendix F

References for data sources used in the discrimination diagrams in Chapters 6 and 7.

Data used in the trace element and isotope diagrams in Chapters 6 and 7 were taken from the papers listed below:

F.1 Ontong Java Plateau

Mahoney, J.J., 1987. An isotopic survey of Pacific oceanic plateaus: Implications for their nature and origin. In. Keating, B., Fryer, P., Batiza, R., Bochlert, G, (Eds.) Seamounts, Islands, and Atolls. American Geophysical Union Monograph. 43, 207-220.

Mahoney, J.J., Spencer, K.J., 1991. Isotopic evidence for the origin of the Manihiki and Ontong Java oceanic plateaus. Earth and Planetary Science Letters. 104, 196-210.

Mahoney, J.J., Storey, M., Duncan, R.A., Spencer, K.J., Pringle, M., 1993. Geochemistry and age of the Ontong Java Plateau. In: M.S. Pringle (Editor.) The Mesozoic Pacific: Geology, Tectonics and Volcanism. American Geophysical Union. pp. 233-261.

Mahoney, J.J., Storey, M., Duncan, R.A., Spencer, K.J., Pringle, M., 1993. Geochemistry and geochronology of Leg 130 basement lavas: nature and origin of the Ontong Java Plateau. In: W.H. Berger, L.W. Kroenke and L.A. Mayer (Editors.) Proceedings of the Ocean Drilling Program, Scientific Results. Ocean Drilling Program, Texas and University: College Station, TX. pp. 3-22.

Tejada, M.L.G., Mahoney, J.J., Duncan, R.A., Hawkins, M.P., 1996. Age and geochemistry of basement and alkalic rocks of Maliata and Santa Isabel, Solomon Islands, southern margin of Ontong Java Plateau. Journal of Petrology. 37, 361-394.

Tejada, M.L.G., Mahoney, J.J., Neal, C.R., Duncan, R.A., Petterson, M.G., 2002. Basement geochemistry and geochronology of central Malaita, Solomon islands, with implications for the origin and evolution of the Ontong Java Plateau. Journal of Petrology. 43, 449-484.

Tejada, M.L.G., Mahoney, J.J., Castillo, P.R., Ingle, S.P., Sheth, H.C., and Weis, D., 2004. Pin-pricking the elephant: evidence on the origin of the Ontong Java Plateau from Pb-Sr-Hf-Nd isotopic characteristics of ODP Leg 192 basalts. In: Fitton, J. G., Mahoney, J. J., Wallace, P. J., and Saunders, A. D., (Editors.), Origin and Evolution of the Ontong Java Plateau, Geological Society of London, Special Publication. 229, 275-306.

F.2 Curaçao, Colombia and DSDP Leg 15

Bence, A.E., Papike, J.J., Ayuso, R.A., 1975. Petrology of submarine basalts from the Central Caribbean: DSDP Leg 15. Journal of Geophysical Research. 80, 4775-4804.

Hauff, F., Hoernle, K., Tilton, G., Graham, D.W., Kerr, A.C., 2000. Large volume recycling of oceanic lithosphere over short time scales: geochemical constraints from the Caribbean Large Igneous Province. Earth Planetary Science Letters. 174, 247-263.

Geldmacher, J., Hanan, B.B., Blichert-Toft, J., Harpp, K., Hoernle, K., Hauff, F., Werner, R., Kerr, A.C., 2003. Hafnium isotopic variations in volcanic rocks from the Caribbean Large Igneous Province and Galapagos hot spot tracks. Geochemistry Geophysics Geosystems 4, paper number 2002GC000477.

Kerr, A.C., Tarney, J., Marriner, G.F., Nivia, A., Saunders, A.D., Klaver, G.T., 1996. The geochemistry and tectonic setting of late Cretaceous Caribbean and Colombian volcanism. Journal of South American Earth Science. 9, 111-120.

Kerr, A.C., Tarney, J., Marriner, G.F., Klaver, G.T., Saunders, A.D., Thirlwall, M.F., 1996. The geochemistry and petrogenesis of the late-Cretaceous picrites and basalts of Curacao, Netherlands Antilles: A remnant of an oceanic plateau. Contributions to Mineralogy and Petrology. 124, 29-43.

Kerr, A.C., Tarney, J., Kempton, P.D., Spadea, P., Nivia, A., Marriner, G.F., Duncan, R.A., 2002. Pervasive mantle plume head heterogeneity: Evidence from the late Cretaceous Caribbean-Colombian oceanic plateau. Journal of Geophysical Research-Solid Earth 107, DOI 10.1029, 2001JB000790.

Spadea, P., Espinosa, A., 1996. Petrology and chemistry of late Cretaceous volcanic rocks from the southernmost segment of the Western Cordillera of Colombia (South America). Journal of South American Earth Sciences. 9, 79-90.

Thompson, P.M.E., Kempton, P.D., White, R.V., Kerr, A.C., Tarney, J., Saunders, A. D., Fitton, J.G., 2003. Hf-Nd isotope constraints on the origin of the Cretaceous

Caribbean plateau and its relationship to the Galapagos plume. Earth and Planetary Science Letters. 217, 59-75.

F.3 Galapagos, Gorgona and Costa Rica

Hauff, F., Hoernle, K., Tilton, G., Graham, D.W., Kerr, A.C., 2000a. Large volume recycling of oceanic lithosphere over short time scales: Geochemical constraints from the Caribbean Large Igneous Province. Earth and Planetary Science Letters 174, 247-263.

Hauff, F., Hoernle, K., van den Bogaard, P., Alvarado, G.E., Garbe-Schonberg, C.D., 2000b. Age and geochemistry of basaltic complexes in western Costa Rica: Contributions to the geotectonic evolution of Central America. Geochemistry Geophysics Geosystems 1, paper number 1999GC000020.

Geldmacher, J., Hanan, B.B., Blichert-Toft, J., Harpp, K., Hoernle, K., Hauff, F., Werner, R., Kerr, A.C., 2003. Hafnium isotopic variations in volcanic rocks from the Caribbean Large Igneous Province and Galapagos hot spot tracks. Geochemistry Geophysics Geosystems 4, paper number 2002GC000477.

Kerr, A.C., 2005. La Isla de Gorgona, Colombia: A petrological enigma? Lithos. 84, 77-101.

Thompson, P.M.E., Kempton, P.D., White, R.V., Kerr, A.C., Tarney, J., Saunders, A. D., Fitton, J.G., 2003. Hf-Nd isotope constraints on the origin of the Cretaceous Caribbean plateau and its relationship to he Galapagos plume. Earth and Planetary Science Letters. 217, 59-75.

F.4 Iceland and N-MORB

Kempton, P.D., Fitton, J.G., Saunders, A.D., Nowell, G.M., Taylor, R.N., Hardarson, B.S., Pearson, G., 2000. The Iceland plume in space and time: a Sr-Nd-Pb-Hf study of the North Atlantic rifted margin. Earth and Planetary Science Letters. 177, 255-271.

Nowell, G.M., Kempton, P.D., Noble, S.R., 1998. High precision Hf isotope measurements of MORB and OIB by thermal ionisation mass spectrometry: insights into the depleted mantle. Chemical Geology. 149, 211-233.

O'Nions, R.K., Hamilton, P.J., Evenson, N.M., 1977. Variations in $^{143}Nd/^{144}Nd$ and $^{87}Sr/^{86}Sr$ in oceanic basalts. Earth and Planetary Science Letters. 34, 13-22.

Rollinson, H., 1993. Using geochemical data: evaluation, presentation, interpretation, Longman Group Limited.

Salters, V.J.M., Hart, S.R., 1991. The mantle sources of ocean ridges, islands and arcs: the Hf-isotope connection. Earth and Planetary Science Letters. 104, 364-380.

Salters, V.J.M., 1996. The generation of mid-ocean ridge basalts from the Hf and Nd isotope perspective. Earth and Planetary Science Letters. 141, 109-123.

Salters, V.J. M., White, W.M., 1998. Hf isotope constraints on mantle evolution. Chemical Geology. 145, 447-460.

White, W.M., Hofmann, A.W., 1982. Sr and Nd isotope geochemistry of oceanic basalts and mantle evolution. Nature. 296, 821-825.

F.5 E-MORB

Andres, M., Blichert-Toft, J., Schilling., 2002. Hafnium isotopes in basalts from the southern Mid-Atlantic Ridge from 40°S to 55°S: Discovery and Shona plume-ridge interactions and the role of recycled sediments. Geochemistry Geophysics Geosystems. 3.

Andres, M., Blichert-Toft, J., Schilling., 2004. Nature of depleted upper mantle beneath the Atlantic: evidence from Hf isotopes in normal mid-ocean ridge basalts from 79°N to 55°S. Earth and Planetary Science Letters. 225, 89-103.

Debaille, V., Blichert-Toft, J., Agranier, A., Doucelance, R., Schiano, P., Albarede., 2006. Geochemical component relationships in MORB from the Mid-Atlantic Ridge, 22-35°N. Earth and Planetary Science Letters. 241, 844-862.

F.6 DMM

Workman, R.K., Hart, S.R., 2005. Major and trace element composition of the depleted MORB mantle (DMM). Earth and Planetary Science Letters. 231, 53-72.

F.7 Jamaica, Benbow Inlier – island arc rocks

Hastie, A.R., Kerr, A.C. Pearce, J.A., Mitchell, S.F. 2007, Classification of altered volcanic island arc rocks using immobile trace elements: Development of the Co-Th discrimination diagram. Journal of Petrology. in press.

F.8 Bonaire island arc rocks

Thompson, P.M.E., 2002. Petrology and geochronology of an arc sequence, Bonaire, Dutch Antilles, and its relationship to the Caribbean Plateau. PhD thesis, University of Leicester.

Thompson, P.M.E., Kempton, P.D., White, R.V., Saunders, A.D., Kerr, A.C., Tarney, J., Pringle, M.S., 2004. Elemental, Hf-Nd isotopic and geochronological constraints on an island arc sequence associated with the Cretaceous Caribbean plateau: Bonaire, Dutch Antilles. Lithos. 74, 91-116.

F.9 Vanuatu, Tonga, Mariana, Lesser Antilles, Izu-Bonin and Aleutian intra-oceanic island arcs

Ewart, A., Collerson., K.D., Regelous, M., Wendt, J.I., Niu, Y., 1998. Geochemical evolution within the Tonga-Kermadec-Lau arc-back-arc systems: The role of varying mantle wedge composition in space and time. Journal of Petrology. 39, 331-368.

Regelous, M., Collerson, K.D., Ewart, A., Wendt, J., 1997. Trace element transport rates in subduction zones: evidence from Th, Sr and Pb isotope data for Tonga-Kermadec arc lavas. Earth and Planetary Science Letters. 150, 291-302.

Turner, S.P., Hawkesworth, C.J., Van Calsteren, P.W., Heath, E., MacDonald, R., Black, S., 1996. U-series isotopes and destructive plate margin magma genesis in the Lesser Antilles. Earth and Planetary Science Letters. 142, 191-207.

Turner, S.P., Peate, D.W., Hawkesworth, C.J., Eggins, S.M., Crawford, J.A., 1999. Two mantle domains and the time scales of fluid transfer beneath the Vanuatu arc. Geology. 27, 963-966.

White W.M., Patchett, P.J., 1984. Hf-Nd-Sr isotopes and incompatible element abundances in island arcs: implications for magma genesis and crust-mantle evolution. Earth and Planetary Science Letters. 67, 167-185.

Woodhead, J.D., Hergt, J.M., Davidson, J.P., Eggins, S.M., 2001. Hafnium isotope evidence for "conservative" element mobility during subduction zone processes. Earth and Planetary Science Letters. 192, 331-346.

F.10 Pelagic and terrigenous sediments

Ewart, A., Collerson., K.D., Regelous, M., Wendt, J.I., Niu, Y., 1998. Geochemical evolution within the Tonga-Kermadec-Lau arc-back-arc systems: The role of varying mantle wedge composition in space and time. Journal of Petrology. 39, 331-368.

Pearce, J.A., Kempton, P.D., Nowell, G.M., Noble, S.R., 1999. Hf-Nd elemental and isotope perspective on the nature and provenance of mantle and subduction components in western Pacific arc-basin systems. Journal of Petrology. 40, 1579-1611

Plank, T., Langmuir, C.H., 1998. The chemical composition of subducting sediment and its consequences for the crust and mantle. Chemical Geology. 145, 325-394

Turner, S.P., Hawkesworth, C.J., Rogers, N.W., Bartlett, J., Worthington, T.J., Hergt, J.M., Pearce, J.A., Smith, I.E.M., 1997. ^{238}U-^{230}Th disequilibria magma petrogenesis and flux rates beneath the depleted Tonga-Kermadec island arc. Geochimica et Cosmochimica Acta. 61, 4855-4884

Woodhead, J.D., Hergt, J.M., Davidson, J.P., Eggins, S.M., 2001., Hafnium isotope evidence for "conservative" element mobility during subduction zone processes. Earth and Planetary Science Letters. 192, 331-346.

F.11 Adakites

Beate, B., Monzier, M., Spikings, R., Cotton, J., Silva, J., Bourdon, E., Eissen, J. P., 2001. Mio-Pliocene adakite generation related to flat subduction in southern Ecuador: the Quimsacocha volcanic centre. Earth and Planetary Science Letters. 192, 561-570.

Kepezhinskas, P.K., Defant, M.J., Drummond, M.S., 1997. Progressive enrichment of island arc mantle by melt-peridotite interaction inferred from Kamchatka xenoliths. Geochimica et Cosmochimica Acta. 60, 1217-1229.

Mahlburg Kay, S., Ramos, V.A., Marquez, M., 1993. Evidence in Cerro Pampa volcanic rocks for slab-melting prior to ridge-trench collision in southern South America. Journal of Geology. 101, 703-714.

Polat, A., Kerrich, R., 2000. Archean greenstone belt magmatism and the continental growth- mantle evolution connection: constraints from Th-U-Nb-LREE systematics of the 2.7 Ga Wawa subprovince, Superior Province, Canada. Earth and Planetary Science Letters. 175, 41-54.

Polat, A., Kerrich, R., 2001. Magnesian andesites, Nb-enriched basalt-andesites, and adakites from late-Archean 2.7 Ga Wawa greenstone belts, Superior Province, Canada: implications for late Archean subduction zone petrogenetic processes. Contributions to Mineralogy and Petrology. 141, 36-52.

Polat, A., Munker, C., 2004. Hf-Nd isotope evidence for contemporaneous subduction processes in the source of late Archean arc lavas from the Superior Province, Canada. Chemical Geology. 213, 403-429.

Puchtel, I.S., Hofmann, A.W., Amelin Yu, V., Garbe-Schonberg, C.D., Samsonov, A. V., Shchipansky, A.A., 1999. Combined mantle plume-island arc model for the formation of the 2.9 Ga Sumozero-Kenozero greenstone belt, S.E. Baltic Shield: Isotope and trace element constraints. Geochimica et Cosmochimica Acta. 63, 3579-3595

Stern, C.R., Kilian, R., 1996. Role of the subducted slab, mantle wedge and continental crust in the generation of adakites from the Andean Austral Volcanic Zone. Contributions to Mineralogy and Petrology. 123, 263-281

F.12 OIB - Austral-Cook, Hawaii, St Helena, Samoa, Society and Walvis Ridge

Chaffey, D.J., Cliff, R.A., Wilson, B.M., 1989. Characterization of the St Helena magma source. In: A. D. Saunders and M. J. Norry (Editors.) Magmatism in the Ocean Basins. Geological Society of London Special Publication. Blackwell Scientific Publications: Oxford. pp. 257-276.

Chauvel, C., Hofmann, A.W., Vidal, P., 1992. HIMU-EM - the French-Polynesian Connection. Earth and Planetary Science Letters.110, 99-119.

Chauvel, C., McDonough, W., Guille, G., Maury, R., Duncan, R., 1997. Contrasting old and young volcanism in Rurutu Island, Austral chain. Chemical Geology. 139, 125-143.

Cheng, Q.C., MacDougall, J.D., Lugmair, G.W., 1993. Geochemical studies of Tahiti, Teahitia and Mehetia, Society Island chain. Journal of Volcanological and Geothermal Research. 55, 155-184.

Cohen, R.S., O'Nions, R.K., 1982. Identification of recycled continental material in the mantle from Sr, Nd and Pb isotope investigations. Earth and Planetary Science Letters. 61, 73-84.

Devey, C.W., Albarede, F., Cheminée, J.L., Michard, A., Mühe, R., Stoffers, P., 1990. Active Submarine volcanism on the Society hotspot swell (West Pacific): a geochemical study. Journal of Geophysical Research. 95, 5049-5066.

Hart, S.R., Coetzee, M., Workman, R.K., Blusztajn, J., Johnson, K.T.M., Sinton, J. M., Steinberger, B., Hawkins, J. W., 2004. Genesis of the western Samoa seamount province: age, geochemical fingerprint and tectonics. Earth and Planetary Science Letters. 227, 37-56.

Lassiter, J.C., Blichert-Toft, J., Hauri, E.H., Barsczus, H.G., 2004. Isotope and trace element variations in lavas from Raivavae and Rapa, Cook-Austral Islands: constraints on the nature of HIMU and EM mantle and the origin of mid-plate volcanism in French Polynesia. Chemical Geology. 202, 115-138.

Nakamura, Y., Tatsumoto, M., 1988. Pb, Nd and Sr isotopic evidence for a multicomponent source for rocks of Cook-Austral Islands and heterogeneities of mantle plumes. Geochimica et Cosmochimica Acta. 52, 2909-2924.

Newsom, H.E., White, W.M., Jochum, K.P., Hofmann, A., 1986. Siderophile and chalcophile element abundances in oceanic basalts, Pb isotope evolution and growth of the Earth's core. Earth and Planetary Science Letters. 80, 299-313.

Palacz, Z.A., Saunders, A.D., 1986. Coupled trace element and isotope enrichment in the Cook-Austral-Samoa islands, southwest Pacific. Earth and Planetary Science Letters. 79, 270-280.

Richardson, S.H., Erlank, A.J., Duncan, A.R., Reid, D.L., 1982. Correlated Nd, Sr, and Pb isotopic variation in Walvis Ridge basalts and implications for the evolution of their mantle source. Earth and Planetary Science Letters. 59, 327-342.

Salters, V.J.M., Hart, S.R., 1991. The mantle sources of ocean ridges, islands and arcs: the Hf-isotope connection. Earth and Planetary Science Letters. 104, 364-380.

Salters, V.J.M., White, W.M., 1998. Hf isotope constraints on mantle evolution. Chemical Geology. 145, 447-460.

White , W.M., Duncan, R.A., 1996. Geochemistry and geochronology of the Society Islands: new evidence for deep mantle recycling Earth processes, reading the isotopic code (Basu, A and Hart, S.R.). AGU, Washington DC, 183-206.

Workman, R.K., Hart, S.R., Jackson, M.G., Regelous, M., Farley, K.A., Blusztajn, J., Kurz, M., Staudigel, H., 2004. Recycled metasomatised lithosphere as the origin of the enriched mantle II (EM2) end-member: evidence from the Samoan volcanic chain. Geochemistry Geophysics Geosystems. 5, 2003GC000623.

Wright, E., White, W.M., 1987. The origin of Samoa: new evidence from Sr, Nd and Pb isotopes. Earth and Planetary Science Letters. 81, 151-162.

F.13 High-Nb Basalts (HNB)

Defant, M.J., Jackson, T.E., Drummond, M.S., De Boer, J.Z., Bellon, H., Feigenson, M.D., Maury, R.C., Stewart, R.H., 1992. The geochemistry of young volcanism throughout western Panama and southeastern Costa Rica: an overview. Journal of the Geological Society, London. 149, 569-579.

Castillo, P.R., Rigby, S.J., Solidum, R.U., 2007. Origin of high field strength element enrichment in volcanic arcs: Geochemical evidence from the Sulu Arc, southern Philippines. Lithos. Doi: 10.1016/j.lithos.2006.12.012

Appendix G

Values for the fractional crystallisation and partial melting equations in Chapters 6 and 7

G.1 Fractionation data

Partition coefficient data for modelling the fractional crystallisation of the Bath-Dunrobin plateau, Benbow, Above Rocks, Sunning Hill, Central and Halberstadt igneous rocks in a mafic melt.

G.1.1 List of references from where the partition coefficient data were obtained

Agee, C.B., 1990. A New Look at Differentiation of the Earth from Melting Experiments on the Allende Meteorite. Nature. 346, 834-837.

Beattie, P., 1993. The effect of partial melting of spinel peridotite on uranium series disequilibria: constraints from partitioning studies. Earth and Planetary Science Letters. 177, 379-391.

Ewart, A., Griffin, W.L., 1994. Application of Proton-Microprobe Data to Trace-Element Partitioning in Volcanic-Rocks. Chemical Geology. 117, 251-284.

Fujimaki, H., Tatsumoto, M., Aoki, K., 1984. Partition coefficients of Hf, Zr and REE between phenocrysts and groundmasses. Proceedings of the fourteenth lunar and planetary science conference Part 2. Journal of Geophysical Research. 89, B662-B672.

Hauri, E.H., Wagner, T.P., Grove, T.L., 1994. Experimental and natural partitioning of Th, U, Pb and other trace elements between garnet, clinopyroxene and basaltic melts. Chemical Geology. 117, 149-166.

Appendix G: Values for the fractional crystallisation and partial melting equations in Chapter 7

Irving, A.J., Frey, F.A., 1978. Distribution of Trace-Elements between Garnet Megacrysts and Host Volcanic Liquids of Kimberlitic to Rhyolitic Composition. Geochimica et Cosmochimica Acta. 42, 771-787.

Kravuchuk, I.K., Chernysheva, I., Urosov, S., 1981. Element distribution between plagioclase and groundmass as an indicator for crystallization conditions of the basalts in the southern vent of Tolbachik. Geochemistry International. 17, 18-24.

Larsen, L.M., 1979. Distribution of REE and Other Trace-Elements between Phenocrysts and Peralkaline Undersaturated Magmas, Exemplified by Rocks from the Gardar Igneous Province, South Greenland. Lithos. 12, 303-315.

Latourrette, T., Hervig, R.L., Holloway, J.R., 1995. Trace-Element Partitioning between Amphibole, Phlogopite, and Basanite Melt. Earth and Planetary Science Letters. 135, 13-30.

Luhr, J.F., Carmichael, I.S.E., Varekamp, J.C., 1984. The 1982 eruptions of El Chichon volcano, Chiapas, Mexico: mineralogy and petrology of the anhydrite-bearing pumices. Journal of Volcanology and Geothermal Research. 23, 69-108.

Mahood, G.A., Hildreth, E.W., 1983. Large partition coefficients for trace elements in high-silica rhyolites. Geochimica et Cosmochimica Acta. 47, 11-30.

Matsui, Y., Onuma, N., Nagasawa, H., Higuchi, H., Banno, S., 1977. Crystal structure control in trace element partition between crystal and magma. Tectonics. 100, 315-324.

McCallum, I.S., Charette, M.P., 1978. Zr and Nb partition coefficients: implications for the genesis of mare basalts, kreep, and sea floor basalts. Geochimica et Cosmochimica Acta. 42, 859-869.

McKenzie, D., O'Nions, R.K., 1991. Partial melt distributions from inversion of rare Earth element concentrations. Journal of Petrology. 32, 1021-1091.

Nagasawa, H., Schnetzler, C.C., 1971. Partitioning of rare Earth, alkali, and alkaline Earth elements between phenocrysts and acidic igneous magmas. Geochimica et Cosmochimica Acta. 35, 953-968.

Paster, T.P., Schauwecker, D.S., Haskin, L.A., 1974. The behavior of some trace elements during solidification of the Skaergaard layered series. Geochimica et Cosmochimica Acta. 38, 1549-1577.

Schwandt, C.S., McKay, G.A., 1998. Rare earth element partition coefficients from enstatite/melt synthesis experiments. Geochimica et Cosmochimica Acta. 62, 2845-2848.

Appendix G: Values for the fractional crystallisation and partial melting equations in Chapter 7

Shimizu, N., Kushiro, I., 1975. Partitioning of Rare-Earth Elements between Garnet and Liquid at High-Pressures - Preliminary Experiments. Geophysical Research Letters. 2, 413-416.

Sisson, T.W., 1991. Pyroxene-High Silica Rhyolite Trace-Element Partition-Coefficients Measured by Ion Microprobe. Geochimica et Cosmochimica Acta. 55, 1,575-1,585.

Villemant, B., Jaffrezic, H., Joron, J.L., Treuil, M. 1981. Distribution Coefficients of Major and Trace-Elements - Fractional Crystallization in the Alkali Basalt Series of Chaine-Des-Puys (Massif Central, France). Geochimica et Cosmochimica Acta. 45, 1997-2016.

Watson, E.B., Green, T.H., 1981. Apatite/liquid partition coefficients for the rare earth elements and strontium. Earth and Planetary Science Letters. 56, 405-421.

Zack, T., Brumm, R., 1998. Ilmenite/liquid partition coefficients of 26 trace elements determined through ilmenite/clinopyroxene partitioning in garnet pyroxene. In: 7th International Kimberlite Conference. Gurney, J.J., Gurney, J.L., Pascoe, M.D., Richardson, S.H. (Editors). Red Roof Design. Cape Town, 986-988.

G.1.2 Table of partition coefficients for the selected elements and minerals in a mafic melt.

	Co	Ba	Sr	Th	U	Nb	La	Gd	Yb	Zr
Amphibole	1.35	0.436	1.02	0.5	0.15	0.8	0.5442	2.0165	1.642	1.2
K-feldpar	0.58	3.409	2.3	0.01	0.017	0.01	0.19	0.071	0.056	0.13
Plagioclase	0.58	0.26	1.8	0.01	0.1	0.01	0.19	0.071	0.056	0.13
Quartz	0	0	0	0	0	0	0	0	0	0
Ilmenite	2.2	0.00034	0	0.00055	0.0082	0.8	0.098	0.14	0.17	0.28
Apatite	0.03	0.05	1.3	17.1	1.82	0	8.6	15.8	8.1	0.636
Magnetite	3.4	0.028	0.11	0.05	0.11	0.01	0.015	0.018	0.018	0.02
Biotite	23	10	0.7	0.12	0.13	0.088	0.7	0.016	0.0484	2.5
Clinopyroxene	1.02	0.04	0.16	0.03	0.05	0.005	0.056	0.556	0.542	0.27
Olivine	3.1	0.03	0.0000154	0.0000024	0.0000056	0.009	0.0004	0.0069	0.0015	0.06
Garnet	0.97	0.0007	0.0099	0.0017	0.015	0.0538	0.01	0.68	3.88	0.9

Plagioclase values; red, alkali basalt values; green, andesite values; blue and trachyte; purple.

Appendix G: Values for the fractional crystallisation and partial melting equations in Chapter 7

G.2 Fractionation data

Partition coefficient data for modelling the fractional crystallisation of the Newcastle adakites in an andesitic melt.

G.2.1 List of references from where the partition coefficient data were obtained

Bacon, C.R., Druitt, T.H., 1988. Compositional Evolution of the Zoned Calcalkaline Magma Chamber of Mount-Mazama, Crater Lake, Oregon. Contributions to Mineralogy and Petrology. 98, 224-256.

Beattie, P., 1993. The effect of partial melting of spinel peridotite on uranium series disequilibria: constraints from partitioning studies. Earth and Planetary Science Letters. 177, 379-391.

Brenan, J.M., Shaw, H.F., Ryerson, F.J., Phinney, D.L., 1995. Experimental-Determination of Trace-Element Partitioning between Pargasite and a Synthetic Hydrous Andesitic Melt. Earth and Planetary Science Letters. 135, 1-11.

Dostal, J., Dupuy, C., Carron, J.P., Dekerneizon, M.L., Maury, R.C., 1983. Partition-Coefficients of Trace-Elements - Application to Volcanic-Rocks of St-Vincent, West-Indies. Geochimica et Cosmochimica Acta. 47, 525-533.

Esperanca, S., Carlson, R.W., Shirey, S.B., Smith, D., 1997. Dating crust-mantle separation: Re-Os isotopic study of mafic xenoliths from central Arizona. Geology. 25, 651-654.

Ewart, A., Griffin, W.L., 1994. Application of Proton-Microprobe Data to Trace-Element Partitioning in Volcanic-Rocks. Chemical Geology. 117, 251-284.

Fujimaki, H., 1986. Partition-Coefficients of Hf, Zr, and REE between Zircon, Apatite, and Liquid. Contributions to Mineralogy and Petrology. 94, 42-45.

Gaetani, G.A., Grove, T.L., 1997. Partitioning of moderately siderophile elements among olivine, silicate melt, and sulfide melt: Constraints on core formation in the Earth and Mars. Geochimica et Cosmochimica Acta. 61, 1829-1846.

Green, T.H., Pearson, N.J., 1985a. Experimental determination of REE partition coefficients between amphibole and basaltic liquids at high pressure. Geochimica et Cosmochimica Acta. 49, 1465-1468.

Haskin, L.A., Frey, F.A., Schmitt, R.A., Smith, R.H., 1966. Meteoritic, solar and terrestrial rare-earth distributions. Physical and Chemical Earth. 7, 167-321.

Higuchi, H., Nagasawa, H., 1969. Partition of trace elements between rock-forming minerals and the host volcanic rocks. Earth and Planetary Science Letters. 7, 281-287.

Irving, A.J., Frey, F.A., 1978. Distribution of Trace-Elements between Garnet Megacrysts and Host Volcanic Liquids of Kimberlitic to Rhyolitic Composition. Geochimica et Cosmochimica Acta. 42, 771-787.

Larsen, L.M., 1979. Distribution of REE and Other Trace-Elements between Phenocrysts and Peralkaline Undersaturated Magmas, Exemplified by Rocks from the Gardar Igneous Province, South Greenland. Lithos. 12, 303-315.

Luhr, J.F., Carmichael, I.S.E., Varekamp, J.C., 1984. The 1982 eruptions of El Chichon volcano, Chiapas, Mexico: mineralogy and petrology of the anhydrite-bearing pumices. Journal of Volcanology and Geothermal Research. 23, 69-108.

Mahood, G.A., Hildreth, E.W., 1983. Large partition coefficients for trace elements in high-silica rhyolites. Geochimica et Cosmochimica Acta. 47, 11-30.

Matsui, Y., Onuma, N., Nagasawa, H., Higuchi, H., Banno, S., 1977. Crystal structure control in trace element partition between crystal and magma. Tectonics. 100, 315-324.

Nash, W.P., Crecraft, H.R., 1985. Partition coefficients for trace elements in silicic magmas. Geochimica et Cosmochimica Acta. 49, 2309-2322.

Nielsen, R.L., Gallahan, W.E., Newberger, F., 1992. Experimentally determined mineral-melt partition coefficients for Sc, Y and REE for olivine, orthopyroxene, pigeonite, magnetite and ilmenite. Contributions to Mineralogy and Petrology. 110, 488-499.

Philpotts, J.A., Schnetzler, C.C., 1970. Phenocryst-matrix partition coefficients for K, Rb, Sr and Ba with applications to anorthosite and basalt genesis. Geochimica et Cosmochimica Acta. 34, 307-322.

Rollinson, H., 1993. Using geochemical data: evaluation, presentation, interpretation. Pearson education limited 102-170.

Schwandt, C.S., McKay, G.A., 1998. Rare earth element partition coefficients from enstatite/melt synthesis experiments. Geochimica et Cosmochimica Acta. 62, 2845-2848.

Sisson, T.W., Bacon, C.R., 1992. Garnet High-Silica Rhyolite Trace-Element Partition-Coefficients Measured by Ion Microprobe. Geochimica et Cosmochimica Acta. 56, 2133-2136.

Stix, J., Gorton, M.P., 1990. Variations in Trace-Element Partition-Coefficients in Sanidine in the Cerro Toledo Rhyolite, Jemez Mountains, New-Mexico -

Effects of Composition, Temperature, and Volatiles. Geochimica et Cosmochimica Acta. 54, 2697-2708.

Sweeney, R.J., Green, D.H., Sie, S.H., 1992. Trace and Minor Element Partitioning between Garnet and Amphibole and Carbonatitic Melt. Earth and Planetary Science Letters. 113, 1-14.

Villemant, B., Jaffrezic, H., Joron, J.L., Treuil, M. 1981. Distribution Coefficients of Major and Trace-Elements - Fractional Crystallization in the Alkali Basalt Series of Chaine-Des-Puys (Massif Central, France). Geochimica et Cosmochimica Acta. 45, 1997-2016.

Watson, E.B., Green, T.H., 1981. Apatite/liquid partition coefficients for the rare earth elements and strontium. Earth and Planetary Science Letters. 56, 405-421.

G.2.2 Table of partition coefficients for the selected elements and minerals in an andesitic melt.

	Co	Ba	Sr	Th	U	Nb	La	Gd	Yb	Zr
Amphibole	6.1	0.3	0.28	0.017	0.008	0.2	0.31	1.72	1.25	0.23
K-feldpar	0.09	6.12	3.87	0.02	0.017	0.004	0.052	0.023	0.028	0.003
Plagioclase	0.07	0.27	5.28	0.01	0.01	0.06	0.18	0.017	0.1	0.15
Quartz	0	0	0	0	0	0	0	0	0	0
Ilmenite	26	0	0.034	7.5	3.2	4.6	0.0072	0.0077	4.1	0.49
Apatite	0.6	0.3	1.3	17.1	1.82	0	14.5	43.9	15.4	0.636
Magnetite	7.4	0.12	0.11	0.05	0.21	0.7	0.22	0.3	0.24	0.38
Biotite	28.5	13.9	0.12	0.31	0.46	7.5	0.272	0.282	0.44	0.59
Clinopyroxene	5.5	0.1	0.28	0.1	0.04	2.1	0.28	0.095	2	0.33
Olivine	1.81	0.02	0.07	0.03	0.01	0.11	0.0028	0.0069	0.0313	0.0047
Garnet	1.8	0.0172	0.0154	0	0	0	0.076	5.2	53	0.4

Basaltic andesite values; red, dacite values; green, trachyte values; blue, rhyolite values; purple.

G.3 Fractionation data

Nb, Ce, Dy and Y partition coefficient data for modelling the fractional crystallisation of the Newcastle adakites in an andesitic melt.

G.3.1 List of references from where the partition coefficient data were obtained

Bacon, C.R., Druitt, T.H., 1988. Compositional Evolution of the Zoned Calcalkaline Magma Chamber of Mount-Mazama, Crater Lake, Oregon. Contributions to Mineralogy and Petrology. 98, 224-256.

Beattie, P., 1993. The effect of partial melting of spinel peridotite on uranium series disequilibria: constraints from partitioning studies. Earth and Planetary Science Letters. 177, 379-391.

Brenan, J.M., Shaw, H.F., Ryerson, F.J., Phinney, D.L., 1995. Experimental-Determination of Trace-Element Partitioning between Pargasite and a Synthetic Hydrous Andesitic Melt. Earth and Planetary Science Letters. 135, 1-11.

Ewart, A., Griffin, W.L., 1994. Application of Proton-Microprobe Data to Trace-Element Partitioning in Volcanic-Rocks. Chemical Geology. 117, 251-284.

Fujimaki, H., 1986. Partition-Coefficients of Hf, Zr, and REE between Zircon, Apatite, and Liquid. Contributions to Mineralogy and Petrology. 94, 42-45.

Green, T.H., Pearson, N.J., 1985a. Experimental determination of REE partition coefficients between amphibole and basaltic liquids at high pressure. Geochimica et Cosmochimica Acta. 49, 1465-1468.

Haskin, L.A., Frey, F.A., Schmitt, R.A., Smith, R.H., 1966. Meteoritic, solar and terrestrial rare-earth distributions. Physical and Chemical Earth. 7, 167-321.

Larsen, L.M., 1979. Distribution of REE and Other Trace-Elements between Phenocrysts and Peralkaline Undersaturated Magmas, Exemplified by Rocks from the Gardar Igneous Province, South Greenland. Lithos. 12, 303-315.

Luhr, J.F., Carmichael, I.S.E., 1980. The Colima volcanic complex, Mexico. I: post-caldera andesites from Volcan Colima. Contributions to Mineralogy and Petrology. 71, 343-372.

Nash, W.P., Crecraft, H.R., 1985. Partition coefficients for trace elements in silicic magmas. Geochimica et Cosmochimica Acta. 49, 2309-2322.

Nielsen, R.L., Gallahan, W.E., Newberger, F., 1992. Experimentally determined mineral-melt partition coefficients for Sc, Y and REE for olivine, orthopyroxene, pigeonite, magnetite and ilmenite. Contributions to Mineralogy and Petrology. 110, 488-499.

Philpotts, J.A., Schnetzler, C.C., 1970. Phenocryst-matrix partition coefficients for K, Rb, Sr and Ba with applications to anorthosite and basalt genesis. Geochimica et Cosmochimica Acta. 34, 307-322.

Rollinson, H., 1993. Using geochemical data: evaluation, presentation, interpretation. Pearson education limited 102-170.

Sisson, T.W., 1994. Hornblende-Melt Trace-Element Partitioning Measured by Ion Microprobe. Chemical Geology. 117, 331-344.

G.3.2 Table of partition coefficients for the selected elements and minerals in an andesitic melt.

	Nb	Y	Ce	Dy
Amphibole	0.2	2.46	0.22	1.7
K-feldpar	0.004	0.017	0.039	0.025
Plagioclase	0.06	0.066	0.12	0.03
Quartz	0	0	0	0
Ilmenite	4.6	0.0045	7.8	4.9
Apatite	0.1	40	21.1	34.8
Magnetite	0.7	0.64	0.12	0.44
Biotite	7.5	0.6	0.037	0.097
Clinopyroxene	2.1	2.4	0.47	1.2

Dacite values; red, rhyolite values; green.

Appendix G: Values for the fractional crystallisation and partial melting equations in Chapter 7

G.4 Forming an adakite by partially melting the Benbow Inlier lavas

G.4.1 Estimated mineral proportions for an IAT/CA Devils Racecourse succession which has been metamorphosed to at least amphibolite facies

	Mineral proportions
Feldspar	0.45
Amphibole	0.472
Clinopyroxene	0.05
Garnet	0.025
Sphene	0.003
SUM	1

G.4.2 Table of partition coefficients for an andesitic melt.

	Feldspar	Amphibole	Clinopyroxene	Garnet	Sphene
Th	0.01	0.017	0.1	0.00137	17.1
Nb	0.06	0.2	2.1	0.22	6.1
Ta	0.03	0.59	0.43	0.22	17
La	0.18	0.31	0.28	0.076	46
Ce	0.028	0.53	0.084	0.076	46
Pr	0.028	0.53	0.183	0.076	46
Nd	0.028	1.2	0.183	1.25	25*
Sm	0.028	1.2	0.377	1.25	25*
Eu	0.028	1.9	0.583	1.52	10
Gd	0.017	1.72	0.095	5.2	10
Tb	0.076	2	0.774	5.5	10
Dy	0.076	2	0.774	5.5	10
Ho	0.153	2	0.708	5.5	10
Er	0.153	2	0.708	5.5	6
Tm	0.254	2.1	0.633	5.5	6
Yb	0.254	2.1	0.633	5.5	6

* Values estimated due to a lack of published data.

Appendix G: Values for the fractional crystallisation and partial melting equations in Chapter 7

Mineral partition coefficients were obtained from the references listed below:

Arth, J.G., 1976. Behaviour of trace elements during magmatic processes-a summary of theoretical models and their applications. Journal of Research U. S. Geological Survey. 4, 41-47.

Bacon, C.R., Druitt, T.H., 1988. Compositional Evolution of the Zoned Calcalkaline Magma Chamber of Mount-Mazama, Crater Lake, Oregon. Contributions to Mineralogy and Petrology. 98, 224-256.

Brenan, J.M., Shaw, H.F., Ryerson, F.J., Phinney, D.L., 1995. Experimental-Determination of Trace-Element Partitioning between Pargasite and a Synthetic Hydrous Andesitic Melt. Earth and Planetary Science Letters. 135, 1-11.

Fujimaki, H., Tatsumoto, M., Aoki, K., 1984. Partition coefficients of Hf, Zr and REE between phenocrysts and groundmasses. Proceedings of the fourteenth lunar and planetary science conference Part 2. Journal of Geophysical Research. 89, B662-B672.

Gill, J.B., 1981. Orogenic andesites and plate tectonics. Springer. Berlin.

Green, T.H., Pearson, N.J., 1983. Effect of pressure on rare earth element partition coefficients in common magmas. Nature. 305, 414-416.

Green, T. H., Pearson, N. J., 1985a. Experimental determination of REE partition coefficients between amphibole and basaltic liquids at high pressure. Geochimica et Cosmochimica Acta. 49, 1465-1468.

Green, T.H., Sie, S.H., Ryan, C.G., Cousens, D.R., 1989. Proton microprobe-determined partitioning of Nb, Ta, Zr, Sr and Y between garnet, clinopyroxene and basaltic magma at high pressure and temperature. Chemical Geology. 74, 201-216.

Hauri, E.H., Wagner, T.P., Grove, T.L., 1994. Experimental and natural partitioning of Th, U, Pb and other trace elements between garnet, clinopyroxene and basaltic melts. Chemical Geology. 117, 149-166.

Irving, A.J., Frey, F.A., 1978. Distribution of trace elements between garnet megacrysts and host volcanic liquids of kimberlitic to rhyolitic composition. Geochimica et Cosmochimica Acta. 42, 771-787.

Jenner, G.A., Foley, S.F., Jackson, S.E., Green, T.H., Fryer, B.J., Longerich, H.P., 1993. Determination of partition coefficients for trace elements in high pressure-temperature experimental run products by laser ablation microprobe-inductively coupled plasma-mass spectrometry (LAM-ICP-MS). Geochimica et Cosmochimica Acta. 57, 5099-5103.

Lynton, S.J., Candela, P.A., Piccoli, P.M., 1993. An experimental study of the partitioning of copper between pyrhotite and a high silica rhyolitic melt. Economic Geology and the Bulletin of the Society of Economic Geologists. 88, 901-915.

Matsui, Y., Onuma, N., Nagasawa, H., Higuchi, H., Banno, S., 1977. Crystal structure control in trace element partition between crystal and magma. Tectonics. 100, 315-324.

Nicholls, I.A., Harris, K.L., 1980. Experimental rare Earth element partition coefficients for garnet, clinopyroxene and amphibole coexisting with andesitic and basaltic liquids. Geochimica et Cosmochimica Acta. 44, 287-308.

Pearce, J.A., Norry, M.J., 1979. Petrogenetic implications of Ti, Zr, Y and Nb variations in volcanic rocks. Contributions to Mineralogy and Petrology. 69, 33-47.

Philpotts, J.A., Schnetzler, C.C., 1970. Phenocryst-matrix partition coefficients for K, Rb, Sr and Ba with applications to anorthosite and basalt genesis. Geochimica et Cosmochimica Acta. 34, 307-322.

Schnetzler, C.C., Philpotts, J.A., 1970. Partition coefficients of rare earth elements between igneous matrix material and rock-forming mineral phenocrysts-II. Geochimica et Cosmochimica Acta. 34, 331-340.

G.5 Forming an adakite by partially melting the Above Rocks lavas

G.5.1 Estimated mineral proportions for a succession of Above Rocks lavas which has been metamorphosed to at least upper greenschist facies.

	Mineral Proportions			
	Model 2	**Model 3**	**Model 4**	**Model 5**
Feldspar	0.475	0.44	0.5	0.6
Amphibole	0.4	0.405	0.34	0.35
Clinopyroxene	0	0.025	0.14	0.025
Garnet	0.01	0.005	0.005	0.01
Sphene	0.015	0.015	0.012	0.01
Biotite	0.1	0.11	0	0
Apatite			0.003	0.005
SUM	1	1	1	1

Appendix G: Values for the fractional crystallisation and partial melting equations in Chapter 7

G.5.2 Table of partition coefficients for an andesitic melt.

	Feldspar	Amphibole	Clinopyroxene	Garnet	Sphene	Biotite	Apatite
Th	0.01	0.017	0.1	0.00137	17.1	0.31	17.1
Nb	0.06	0.2	2.1	0.22	6.1	7.5	142
Ta	0.03	0.59	0.43	0.22	17	1.2	142
La	0.18	0.31	0.28	0.076	46	0.272	14.5
Ce	0.028	0.53	0.084	0.076	46	0.318	21.1
Pr	0.028	0.53	0.183	0.076	46	0.044	32.8
Nd	0.028	1.2	0.183	1.25	25*	0.044	32.8
Sm	0.028	1.2	0.377	1.25	25*	0.058	46
Eu	0.028	1.9	0.583	1.52	10	0.145	25.5
Gd	0.017	1.72	0.095	5.2	10	0.282	43.9
Tb	0.076	2	0.774	5.5	10	0.258	34.8
Dy	0.076	2	0.774	5.5	10	0.097	34.8
Ho	0.153	2	0.708	5.5	10	0.162	22.7
Er	0.153	2	0.708	5.5	6	0.162	22.7
Tm	0.254	2.1	0.633	5.5	6	0.176	15.4
Yb	0.254	2.1	0.633	5.5	6	0.176	15.4

* Values estimated due to a lack of published data.

Mineral partition coefficients were obtained from the references listed below:

Arth, J.G., 1976. Behaviour of trace elements during magmatic processes-a summary of theoretical models and their applications. Journal of Research U. S. Geological Survey. 4, 41-47.

Bacon, C.R., Druitt, T.H., 1988. Compositional Evolution of the Zoned Calcalkaline Magma Chamber of Mount-Mazama, Crater Lake, Oregon. Contributions to Mineralogy and Petrology. 98, 224-256.

Brenan, J.M., Shaw, H.F., Ryerson, F.J., Phinney, D.L., 1995. Experimental-Determination of Trace-Element Partitioning between Pargasite and a Synthetic Hydrous Andesitic Melt. Earth and Planetary Science Letters. 135, 1-11.

Ewart, A., Griffin, W.L., 1994. Application of Proton-Microprobe Data to Trace-Element Partitioning in Volcanic-Rocks. Chemical Geology. 117, 251-284.

Fujimaki, H., Tatsumoto, M., Aoki, K., 1984. Partition coefficients of Hf, Zr and REE between phenocrysts and groundmasses. Proceedings of the fourteenth lunar and planetary science conference Part 2. Journal of Geophysical Research. 89, B662-B672.

Gill, J. B., 1981. Orogenic andesites and plate tectonics. Springer. Berlin.

Green, T.H., Pearson, N.J., 1983. Effect of pressure on rare earth element partition coefficients in common magmas. Nature. 305, 414-416.

Green, T.H., Pearson, N.J., 1985a. Experimental determination of REE partition coefficients between amphibole and basaltic liquids at high pressure. Geochimica et Cosmochimica Acta. 49, 1465-1468.

Green, T.H., Sie, S.H., Ryan, C.G., Cousens, D.R., 1989. Proton microprobe-determined partitioning of Nb, Ta, Zr, Sr and Y between garnet, clinopyroxene and basaltic magma at high pressure and temperature. Chemical Geology. 74, 201-216.

Hauri, E.H., Wagner, T.P., Grove, T.L., 1994. Experimental and natural partitioning of Th, U, Pb and other trace elements between garnet, clinopyroxene and basaltic melts. Chemical Geology. 117, 149-166.

Higuchi, H., Nagasawa, H., 1969. Partition of trace elements between rock-forming minerals and the host volcanic rocks. Earth and Planetary Science Letters. 7, 281-287.

Irving, A.J., Frey, F. A., 1978. Distribution of trace elements between garnet megacrysts and host volcanic liquids of kimberlitic to rhyolitic composition. Geochimica et Cosmochimica Acta. 42, 771-787.

Jenner, G.A., Foley, S.F., Jackson, S.E., Green, T.H., Fryer, B.J., Longerich, H.P., 1993. Determination of partition coefficients for trace elements in high pressure-temperature experimental run products by laser ablation microprobe-inductively coupled plasma-mass spectrometry (LAM-ICP-MS). Geochimica et Cosmochimica Acta. 57, 5099-5103.

Lynton, S.J., Candela, P.A., Piccoli, P.M., 1993. An experimental study of the partitioning of copper between pyrhotite and a high silica rhyolitic melt. Economic Geology and the Bulletin of the Society of Economic Geologists. 88, 901-915.

Matsui, Y., Onuma, N., Nagasawa, H., Higuchi, H., Banno, S., 1977. Crystal structure control in trace element partition between crystal and magma. Tectonics. 100, 315-324.

Nash, W.P., Crecraft, H.R., 1985. Partition coefficients for trace elements in silicic magmas. Geochimica et Cosmochimica Acta. 49, 2309-2322.

Nicholls, I.A., Harris, K.L., 1980. Experimental rare Earth element partition coefficients for garnet, clinopyroxene and amphibole coexisting with andesitic and basaltic liquids. Geochimica et Cosmochimica Acta. 44, 287-308.

Pearce, J.A., Norry, M.J., 1979. Petrogenetic implications of Ti, Zr, Y and Nb variations in volcanic rocks. Contributions to Mineralogy and Petrology. 69, 33-47.

Philpotts, J.A., Schnetzler, C.C., 1970. Phenocryst-matrix partition coefficients for K, Rb, Sr and Ba with applications to anorthosite and basalt genesis. Geochimica et Cosmochimica Acta. 34, 307-322.

Schnetzler, C.C., Philpotts, J.A., 1970. Partition coefficients of rare earth elements between igneous matrix material and rock-forming mineral phenocrysts-II. Geochimica et Cosmochimica Acta. 34, 331-340.

G.6. Forming a HNB by partially melting DMM/N-MORB/Primitive Mantle source regions

G.6.1 Estimated mineral proportions for a HNB mantle source region

	Mineral Proportions	
	Model 1	Model 2
Olivine	0.6	0.6
Clinopyroxene	0.08	0.05
Orthopyroxene	0.3	0.28
Amphibole	0	0.05
Garnet	0.02	0.02
SUM	1	1

G.6.2 Table of partition coefficients for an ultramafic melt

	Th	Nb	Ta	La	Ce	Pr	Nd	Sm	Eu	Gd	Tb	Dy	Ho	Er	Tm	Yb
Olivine	0.0000024	0.001	0.001	0.0004	0.0005	0.001	0.001	0.0013	0.0016	0.0015	0.0017	0.0017	0.0015	0.0015	0.0015	0.0015
Amphibole	0.006	0.032	0.032	0.17	0.26	0.44	0.44	0.76	0.88	0.86	0.78	0.78	0.68	0.68	0.59	0.59
Clinopyroxene	0.04	0.012	0.012	0.054	0.098	0.21	0.21	0.26	0.31	0.3	0.33	0.33	0.3	0.3	0.28	0.28
Orthopyroxene	0.04	0.01	0.01	0.002	0.003	0.0068	0.0068	0.01	0.013	0.016	0.022	0.022	0.03	0.03	0.049	0.049
Garnet	0.0017	0.01	0.01	0.01	0.021	0.087	0.087	0.217	0.32	0.498	1.06	1.9	3.95	3.95	4.03	6.6

Basaltic values; red.

G.6.2 Table of partition coefficients for an ultramafic melt

	Th	Nb	Ta	La	Ce	Pr	Nd	Sm	Eu	Gd	Tb	Dy	Ho	Er	Tm	Yb
Olivine	0.0000024	0.001	0.001	0.0004	0.0005	0.001	0.001	0.0013	0.0016	0.0015	0.0017	0.0017	0.0015	0.0015	0.0015	0.0015
Amphibole	0.006	0.032	0.032	0.17	0.26	0.44	0.44	0.76	0.88	0.86	0.78	0.78	0.68	0.68	0.59	0.59
Clinopyroxene	0.04	0.012	0.012	0.054	0.098	0.21	0.21	0.26	0.31	0.3	0.33	0.33	0.3	0.3	0.28	0.28
Orthopyroxene	0.04	0.01	0.01	0.002	0.003	0.0068	0.0068	0.01	0.013	0.016	0.022	0.022	0.03	0.03	0.049	0.049
Garnet	0.0017	0.01	0.01	0.01	0.021	0.087	0.087	0.217	0.32	0.498	1.06	1.9	3.95	3.95	4.03	6.6

Basaltic values; red.

Appendix G: Values for the fractional crystallisation and partial melting equations in Chapter 7

G.6.3 List of references from where the partition coefficient data were obtained

Beattie, P., 1993. The effect of partial melting of spinel peridotite on uranium series disequilibria: constraints from partitioning studies. Earth and Planetary Science Letters. 177, 379-391.

Chazot, G., Menzies, M.A., Harte, B., 1996. Determination of partition coefficients between apatite, clinopyroxene, amphibole, and melt in natural spinel lherzolites from Yemen: Implications for wet melting of the lithospheric mantle. Geochimica et Cosmochimica Acta. 60, 423-437.

Hauri, E.H., Wagner, T.P., Grove, T.L., 1994. Experimental and natural partitioning of Th, U, Pb and other trace elements between garnet, clinopyroxene and basaltic melts. Chemical Geology. 117, 149-166.

Irving, A.J., Frey, F.A., 1978. Distribution of Trace-Elements between Garnet Megacrysts and Host Volcanic Liquids of Kimberlitic to Rhyolitic Composition. Geochimica et Cosmochimica Acta. 42, 771-787.

Jenner, G.A., Foley, S.F., Jackson, S.E., Green, T.H., Fryer, B.J., Longerich, H.P., 1993. Determination of partition coefficients for trace elements in high pressure-temperature experimental run products by laser ablation microprobe-inductively coupled plasma-mass spectrometry (LAM-ICP-MS). Geochimica et Cosmochimica Acta. 57, 5099-5103.

Johnson, K.T.M., 1994. Experimental cpx/ and garnet/melt partitioning of REE and other trace elements at high pressures; petrogenetic implications. Mineralogical Magazine. 58, 454-455.

Latourrette, T.Z., Kennedy, A.K., Wasserburg, G.J., 1993. Thorium-Uranium Fractionation by Garnet - Evidence for a Deep Source and Rapid Rise of Oceanic Basalts. Science. 261, 739-742.

Pearce, J.A., Parkinson, I.J., 1993. Trace element models for mantle melting: application to volcanic arc petrogenesis. Geological Society of London Special Publication. 76, 373-403.

Rollinson, H., 1993. Using geochemical data: evaluation, presentation, interpretation. Pearson education limited 102-170.

Villemant, B., Jaffrezic, H., Joron, J.L., Treuil, M., 1981. Distribution Coefficients of Major and Trace-Elements - Fractional Crystallization in the Alkali Basalt Series of Chaine-Des-Puys (Massif Central, France). Geochimica et Cosmochimica Acta. 45, 1997-2016.